THE PHASE EQUILIBRIUM OF ALKANES AND SUPERCRITICAL FLUIDS

by

Cara Elsbeth Schwarz

Thesis Submitted in Partial Fulfilment
of the Requirements for the Degree
of

MASTER OF SCIENCE IN ENGINEERING (CHEMICAL ENGINEERING)

In the Department of Chemical Engineering
at the University of Stellenbosch

Supervised by

Prof. Izak Nieuwoudt

Stellenbosch
December 2001

DECLARATION

I, the undersigned, hereby declare that the work contained in this thesis is my own original work and that I have not previously in its entirety or in part submitted it at any university for a degree

Cara Elsbeth Schwarz

10 October 2001

ABSTRACT

Current methods for wax fractionation result in products with large polydispersity, and due to the high temperatures required, thermal degradation of the wax is often incurred. The need for an alternative process thus exists. The purpose of this project is to investigate the technical viability of supercritical fluid processing as an alternative wax fractionation technology.

The main aims of this project are to select a suitable supercritical solvent, to conduct binary phase equilibrium experiments, to determine if the process is technically viable and to investigate the ability of various equations of state to correlate the phase equilibrium data.

Based on limited data from the literature, propane and a propane rich LPG (Liquefied Petroleum Gas) were selected as suitable solvents. Literature data for propane and high molecular weight alkanes is scares and incomplete, thus necessitating experimental measurements. A phase equilibrium cell was designed, constructed and commissioned. The cell was designed for pressures up to 500 bar and temperatures to 200 $^{\circ}$C, and with the aid of an endoscope, the phase transitions were detected visually. The measurements correspond well to literature values from reliable research groups.

Phase equilibrium data sets for propane with nC32, nC36, nC38, nC40, nC44, nC46, nC54 and nC60 as well as LP Gas with nC36 were measured. At temperatures just above the melting point of the alkanes, the phase transition pressures can be considered to be moderate, which will positively impact the economics of the process. The phase transition pressure increases with increasing carbon number, the relationship being found to be linear when the pressure is plotted as a function of carbon number at constant mass fractions and temperature. The increase in phase transition pressure with increasing carbon number indicates that the solvent will be able to selectively fractionate the wax. At higher temperatures the gradient of the line is larger and may thus lead to improved selectivity. The higher temperatures will also lead to better mass transfer. The linear relationship indicates that limited extrapolation to higher carbon numbers may be possible. However, this needs to be verified experimentally.

The inability to measure the critical point and vapour pressure curves of the higher molecular weight normal alkanes, as well as the inability of cubic equations of state to predict liquid volumes and to capture the chain specific effects such as internal rotations, results in cubic equations of state requiring large interaction parameters to fit the data. The alternative, statistical mechanical equations of state, have difficulty in predicting the critical point of the solvent correctly and thus overpredicts the mixture critical point, yet require smaller interaction parameters to fit the data. Further work is required to improve the predictability of these non-cubic equations of state.

This project has proven that wax fractionation by supercritical extraction with propane is technically feasible

OPSOMMING

Huidige metodes vir wasfraksioneering produseer produkte met 'n hoë polidispersiteit en as gevolg van die hoë temperatuur wat benodig word, kan termiese degradering voorkom. Daar bestaan dus 'n behoefte vir 'n alternatiewe proses. Die doel van hierdie projek is om die tegniese lewensvatbaarheid van superkritiese ekstraksie as 'n alternatiewe fraksioneringstegnologie te ondersoek.

Die hoofdoelwitte van hierdie projek is om: 'n geskikte oplosmiddel te vind; binêre fase-ewewigseksperimente uit te voer, te bepaal of die proses tegnies lewensvatbaar is en die geskiktheid van verskeie toestansvergelykings te ondersoek.

Gebaseer op beperkte inligting beskikbaar in die literatuur is propaan en 'n propaan-ryke VPG as geskikte oplosmiddels gekies. Literatuurdata vir propaan en hoë molekulêre massa alkane is skaars en dus is eksperimentele werk nodig. 'n Fase-ewewigsel is ontwerp, gebou en in gebruik geneem. Die sel is ontwerp vir drukke tot 500 bar en temperature tot 200 $^{\circ}$C. Die fase oorgang is met behulp van 'n endoskoop opties waargeneem. Die metings vergelyk goed met literatuur data van betroubare navorsingsgroepe.

Fase-ewewigsdatastelle vir propaan met nC32, nC36, nC38, nC40, nC44, nC46, nC54 en nC60 sowel as VPG met nC36 is gemeet. By temperature net bokant die smeltingstemperatuur van die was is matige fase oorgangsdrukke gemeet. Die matige drukke sal 'n positiewe effek op die ekonomie van die proses hê. Die fase ewewigsdruk styg met toenemende koolstofgetal en 'n lineêre verband is gevind wanneer druk as 'n funksie van koolstofgetal by konstante massafraksie en temperatuur geplot word. 'n Verhoging in faseoorgangsdruk met 'n verhoging in koolstofgetal dui daarop dat die oplosmiddel moontlik die was selektief sal kan fraktioneer. By hoër temperature is die helling van die lyn groter en sal dit dus moontlik tot 'n verbetering in selektiwiteit lei. Hoër temperature sal ook die massa-oordrag verbeter. Die lineêre verband dui aan dat 'n beperkte mate van ekstrapolasie tot hoër koolstofgetalle moontlik is, maar dit sal eksperimenteel getoets moet word.

Vir hoë molekulêre massa normale alkane kan die kritieke punt en dampdrukkurwes nie bepaal word nie. Dit, saam met die onvermoë van kubiese toestandsvergelykings om die vloeistofvolumes te voorspel en die feit dat die kubiese toestandsvergelykings nie kettingeffekte soos interne rotasies in berekening kan bring nie, lei daartoe dat groot interaksieparameters benodig word om die data te pas. Die alternatief, statistiese meganiese toestandsvergelykings, sukkel om die kritieke punt van die oplosmiddel korrek te voorspel en as gevolg hiervan word die mengsel kritieke druk te hoog voorspel, maar die interaksieparameters is kleiner vir hierdie toestandsvergelykings. Verdere werk word benodig om die voorspellende aard van nie-kubiese toestandsvergelykings te verbeter.

Die projek het bewys dat wasfraksionering met superkritiese ekstraksie met propaan tegnies haalbaar is .

ACKNOWLEDGEMENTS

TABLE OF CONTENTS

LIST OF FIGURES

LIST OF TABLES

1. FRACTIONATION OF SYNTHETIC WAXES

In the early days of the petrochemical industry, only crudes with a desired composition were processed. As time passed, mankind has had to use all available resources and has even developed synthetic methods in the production of petroleum products, often resulting in large quantities of by-products. Previously by-products were simply dumped due to either the technical inability to reprocess these products, or the fact that reprocessing was not economically viable.

Yet, mainly due to dwindling resources, the beneficiation of by-products had to be tackled. Ironically, with time these products have, in many cases, become significant economic contributors in the petrochemical industry.

This project entails the measurement of the phase equilibrium data for the processing of one of these 'by-products', namely synthetic or hard waxes.

1.1. SYNTHETIC / HARD WAXES

1.1.1. DEFINITION

Synthetic waxes obtain their name from their origin: they are generally not found in abundance in nature but are man-made. Synthetic waxes constitute mainly high molecular weight normal alkanes produced as by-products in the Fisher-Tropsch petroleum synthesis and the production of polyethylene.

The alternate name for synthetic waxes is hard waxes. This can be attributed to the characteristics of synthetic waxes: They are usually harder, more brittle and less ductile than traditional paraffin waxes.

In general, synthetic waxes are long chain normal alkanes with 30 or more carbon atoms.

1.1.2. SOURCES

Synthetic or hard waxes have two main sources, namely Fisher-Tropsch wax and polyethylene wax. Although resulting from two totally different sources, the final products are similar in chemical structure, the main difference being the length of the paraffin chain and the degree of branching.

Firstly, consider the production of Fisher-Tropsch wax: In the slurry or bubble column reactor a finely divided iron or cobalt catalyst is suspended in a Fisher Tropsch wax that has a low viscosity at the reaction temperature, and synthesis gas is bubbled through. At reaction temperatures of 220 – 240 ^{o}C and pressures of up to 4 MPa, normal alkanes and alkenes are preferentially formed. The crude wax is separated from the other products by fractional condensation. Distillation under atmospheric pressures removed the other low boiling point constituents such as gasoline and diesel fuel, and a last step of vacuum distillation is used to remove the soft waxes. The remainder in the bottoms stream contains n-alkanes as well as alkenes, hydrocarbons with hydroxyl and carboxyl groups, and coloured components. For purification and stabilization the bottoms stream is subjected to hydrofining over a nickel catalyst to produce a hard white wax that is practically free of alkenes, aromatics, functionalized hydrocarbons and sulphur compounds. This can be defined as a Fisher-Tropsch wax.

The exact yield of wax varies with the ratio of hydrogen to carbon monoxide, the process temperature and pressures as well as other process variables. The range of the waxes produced can thus not be clearly defined as the range and maximum molecular weight differ with different reaction parameters. It is possible that the range may extend as far as from 24 to 150 carbon atoms, or molar masses of 340 – 2140 g/mol.

Secondly, consider polyethylene wax: Polyethylene is produced by the polymerization of ethylene where purified ethylene gas reacts in a suitable vessel under conditions of combined high temperatures and pressures. With a basic structure of CH_3-$(-CH_2-)_n$-CH_3 is it is not far different from high molecular weight paraffins. Polyethylenes of molecular weight less than 6000 is said to have wax like properties while polyethylene with a molecular weight less than 4000 can be defined as a wax.

The low molecular weight end of the polyethylene cut often overlaps with the high molecular weight end of the Fisher Tropsch waxes. The polyethylene wax can thus be treated in a similar manner, the only difference being that the polyethylene wax has a higher molecular weight and may have slightly more methyl branches.

1.1.3. PROPERTIES

Waxes are hard, translucent in colour, tasteless, odourless and non-toxic. They are insoluble in water and many chemicals and are only slightly soluble in turpentine, naphtha, xylene, toluene and carbon disulphide. The melting point range of synthetic waxes ranges between 68 and about 120 ^{o}C, depending on the composition of the wax.

1.1.4. USES

Synthetic waxes have the following uses (from Schümann-Sasol website [166]):

- To the lay man, the most well known use of wax is in the candle industry.

- In the printing industry, waxes are used in inks and coatings. The addition of wax allows for slip in inks, coatings and powder coatings. In coatings, the waxes aid in the protective layer of the coating and provide efficient gloss reduction when a matt appearance is required.

- A wax coating on paper is often used so that the quality of the contents remains stable during transport and storage, thus preventing the adoption of unwanted odours or loss of flavour or aroma. Wax coated paper is used to pack bread, fruit, vegetables, fish, meat, poultry and other products.

- Fruit, such as oranges, are often coated with wax to preserve their quality during transportation.

- In the cable industry, waxes are used as lubricants, filling the hollow spaces in the inner cable and providing a protective layer on the outside.

- In the polish industry, which includes shoe, leather, floor, automobile and furniture polish, waxes are used to provide protection against abrasion, marring of the produce, restores gloss and are required to improve the 'feel' of the surface while simultaneously improving its resistance to weather.

- They can be used as corrosion protection, especially in the automotive industry.

- In the timber industry, waxes are used in chip- and fibreboard, matches, fire logs and in the treating and smoothing of wooden surfaces.

- In the rubber and tire industry, waxes are used as ozone protectors and processing aids. Additionally, waxes are used in mould and die release applications.

- Hot Melt Adhesives contain between 15 and 30 percent wax. The wax is added to reduce the viscosity of the polymer and thus allow for efficient mixing. The wax also allows for adequate wetting of the surface when applied.

- During the extrusion of rigid PVC pipes and profiles, wax lubricants play an essential role in the optimization of the operation of the extruder and ensuring the quality of the finished article.

- Narrow boiling range waxes can be used as thermostats in applications such as the automotive industry.

- Waxes have a high heat capacity and can thus be used as heat insulators.

- In the construction industry, waxes are used to improve the insulation properties of the construction materials for houses. Additionally, waxes are used in prefabricated concrete so that constant temperature is attained during construction of ready-made parts.

- In the textile and leather industry waxes are used to improve lubrication and thus reducing the possibility of damage by means of friction.

- Other uses of waxes include carriers for rodent poison, the smoothing of wood surfaces for toys and kitchen appliances, pencil and lead casting as well as conditioners for fertilizers.

1.2. STATE OF THE ART IN WAX FRACTIONATION METHODS

Synthetic waxes are produced with a wide carbon number range, but for application in the above-mentioned uses, these waxes need to be fractionated into narrower melting range cuts. Before considering a new process the current processes need to be investigated and the shortcomings need to be highlighted.

1.2.1. CURRENT FRACTIONATION METHODS

Due to the high boiling points of the waxes, the traditional method of distillation cannot be applied. Additionally, liquid extraction solvents, such as toluene and xylene are not selective enough and may result in a solvent residue difficult to remove from the wax.

Currently wax is fractionated using deep vacuum distillation. The waxes have boiling points that differ according to the molecular weight of the molecule and therefore, under vacuum the wax can be fractionated into various cut with this method.

1.2.2. PROBLEMS WITH CURRENT METHODS

Currently, short path distillation is the most widely used method to fractionate waxes. It does, however, have many problems and the main shortcomings are listed below:

- The cut that is obtained is not very sharp, i.e. the carbon number range is not as narrow as desired.

- The temperatures required for the process, especially the higher molecular weight fractions, approach the decomposition temperatures of the waxes. This may therefore lead to discolouration and eventually coking of the product.

- Additionally, due to the temperatures and the type of process used, the bottoms product often takes on a yellowish colour.

- Synthetic waxes obtained from polyethylene wax will not easily be able to be fractionated with this method due to the fact that the boiling point of the compounds, even at extreme vacuum conditions, are above their decomposition temperatures.

1.3. AN ALTERNATIVE: SUPERCRITICAL FLUID PROCESSING

Brennecke et al rightfully stated that supercritical fluid processing should not be the first separation technique investigated as traditional methods such as liquid-liquid separation and distillation are cheaper (Brennecke et al., 1989). Yet, should these processes not produce satisfactory results, supercritical extraction is an alternative well worth investigating. From the discussion in paragraph 1.2 above, it can be seen that an alternative process for the fractionation of wax merits investigation.

Supercritical fluid processing is proposed as an attractive alternative technique to obtain fractions with a narrow molecular weight distribution without the use of hazardous solvents. Fluids near their critical points have dissolving powers comparable to that of liquids and have transport properties intermediate between liquids and gasses. It is this unusual combination of properties of supercritical fluids that are proposed to be used here to fractionate hard waxes. Supercritical fluid extraction is said to have the following advantages (Brunner, 1990):

- High mass transfer rates

- Ease of phase separation

- Easy solvent recovery

With specific reference to this project, supercritical fluid processing may also have the following advantages:

- Lower operating temperature, thus reducing the possibility of coking.

- Sharper cuts may be obtained with this method.

- A finely powdered wax can possibly be produced.

- The solvent residue in the wax will be low, if not negligible, due to the fact that at atmospheric conditions the wax is a solid and the solvent a gas.

1.4. AIM OF PROJECT

The ultimate aim is to develop a process that enables the separation of wax into various fractions. Figure 1-1 shows how this aim can be achieved:

```
┌─────────────────────────────────────────────────────┐
│        Select a suitable solvent to fractionate the wax        │
└─────────────────────────────────────────────────────┘
                           ⇩
┌─────────────────────────────────────────────────────┐
│          Measure the Required Phase Equilibrium Data          │
└─────────────────────────────────────────────────────┘
                           ⇩
┌─────────────────────────────────────────────────────┐
│           Obtain an accurate Thermodynamic Model            │
└─────────────────────────────────────────────────────┘
                           ⇩
┌─────────────────────────────────────────────────────┐
│           Model the Fractionation Columns Required           │
└─────────────────────────────────────────────────────┘
                           ⇩
┌─────────────────────────────────────────────────────┐
│              Design the Fractionation Process               │
└─────────────────────────────────────────────────────┘
```
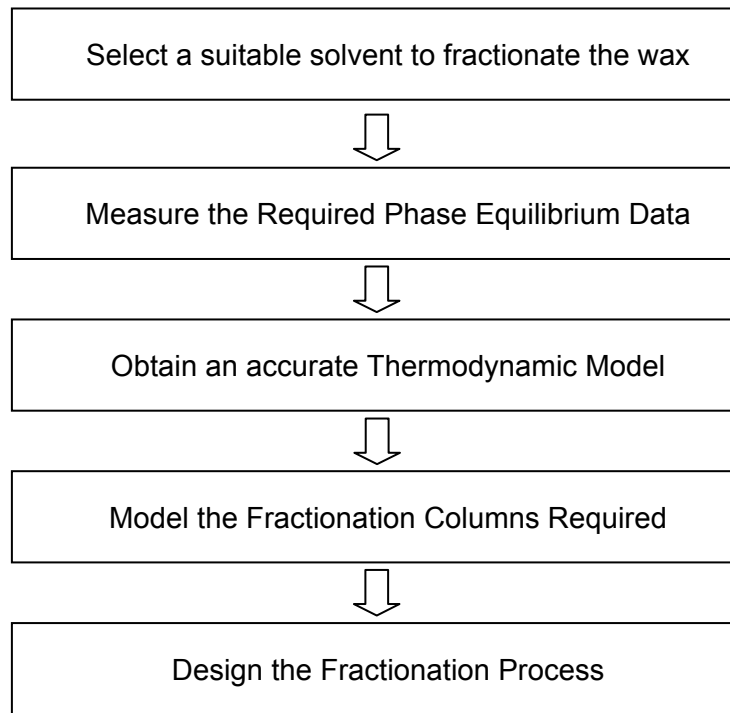
Figure 1-1:Schematic Representation of Methodology to Design Supercritical Fractionation Process

However, the aim of this project is not to design a detailed process for the fractionation of synthetic waxes with supercritical fluids but rather to do a preliminary investigation as the technical viability of the process and to obtain the required data to facilitate a detailed design. The first three steps shown in Figure 1.1 will thus be investigated and the aims of this project are thus:

- A literature study to reveal relevant processes already studied, the data available, the possible solvents and ultimately the selection of a suitable solvent.

- The design and construction of a high-pressure phase equilibrium cell for the measurement of the required phase equilibrium data.

- Phase equilibrium and density data measurements for selected systems and the prediction of data for systems not studied.

- Thermodynamic modelling of the data generated to predict the phase equilibrium of various systems.

2. THEORY OF SUPERCRITICAL FLUIDS AND SUPERCRITICAL FLUID PROCESSING

2.1. DEFINITION OF A SUPERCRITICAL FLUID

The critical temperature is defined as a temperature above which a liquid-vapour meniscus cannot be formed by increasing the pressure at constant temperature. Similarly, the critical pressure is defined as the pressure above which a liquid-vapour meniscus cannot be formed by increasing the temperature at constant pressure. Figure 2-1 illustrates the region of a supercritical fluid.
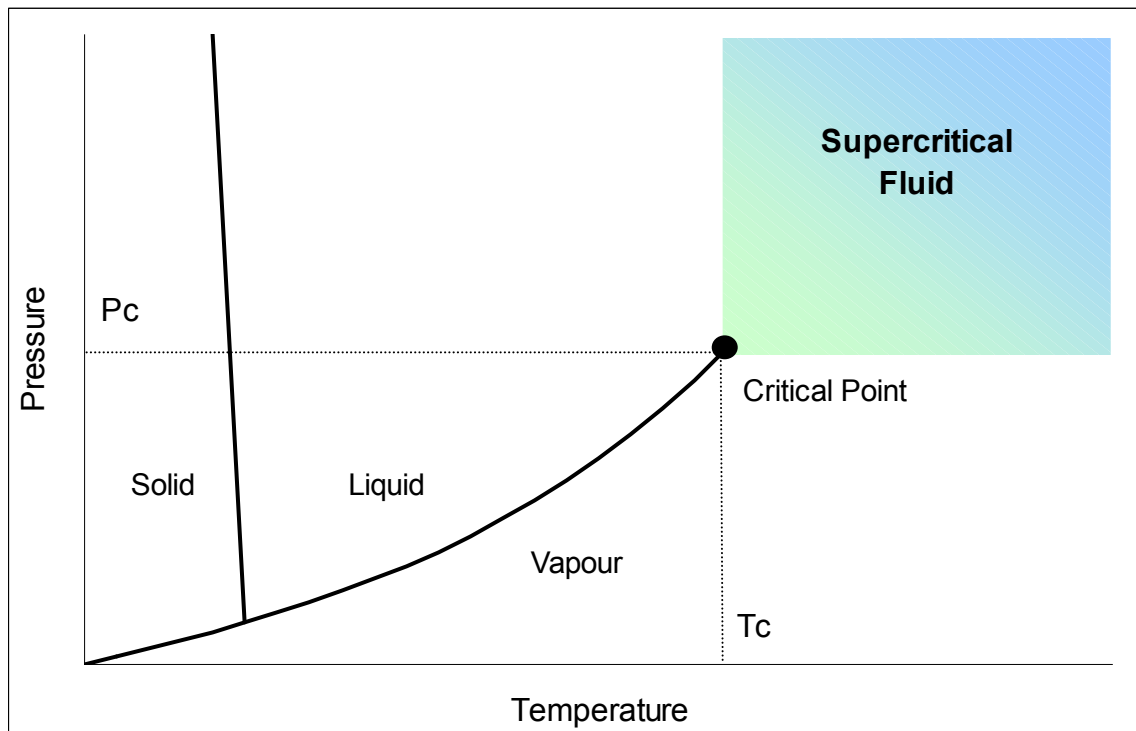
Figure 2-1: Temperature-Pressure phase diagram showing the critical region.

It must be noted that below and to the left of the supercritical region there are no distinct boundaries and the transition from a single phase liquid or gas to a supercritical fluid is not dramatic but a rather gradual change.

Mathematically the critical point can be defined as the temperature and the pressure where the following is true:

$$\left(\frac{\partial P}{\partial v}\right)_T = 0 \quad .... 2.1$$

$$\left(\frac{\partial P^2}{\partial v^2}\right)_T = 0 \quad .... 2.2$$

The critical density is the density of the fluid at the critical temperature and pressure. From equations 2.1 and 2.2 it can be seen that the density, which is the inverse of the specific volume, changes dramatically around the critical point.

The transition from a vapour in equilibrium with a liquid to a supercritical fluid, can be described as follows:

As temperature increases, the density of the liquid decreases due to thermal expansion, while the density of the gas increases due to the pressure rise. The interface between the two phases thus becomes less noticeable due to the smaller difference in density and the refractive index. At the critical point the refractive indices become the same.

2.2.   TRANSPORT PROPERTIES

2.2.1. DIFFUSIVITY

Diffusion is the transport of components along a concentration gradient. In general, faster diffusion gives rise to faster extraction and separation.

The diffusion in a supercritical fluid lies between that of a liquid and a gas, therefore diffusion of a solute in a supercritical fluid is thus always higher than the diffusion in an ordinary liquid solvent. The value of the diffusion coefficient approaches that of a liquid at very high pressure.

2.2.2. VISCOSITY

Viscosity is a measure of the transport of momentum along a transverse velocity gradient. The viscosity of a supercritical fluid lies between that of a liquid and a gas, therefore allowing more favourable hydrodynamic properties than for liquids. The value of the viscosity approaches that of a liquid at very high pressures. Unlike in a gas, for a supercritical fluid, an increase in temperature will lead to a decrease in viscosity.

2.2.3. THERMAL CONDUCTIVITY

Thermal conductivity is a measure of the transport of energy along a temperature gradient. The thermal conductivity shows enhancement in the critical region, which, in turn, decreases the heat capacity at constant pressure.

2.2.4. DENSITY

Although the density of a supercritical fluid is between that of a liquid and a gas, the value tends towards that of a liquid at high pressures.

The density of a supercritical fluid is dependent on the pressure and the temperature. The temperature and pressure relationship is typically non-linear and can be obtained from an equation of state. As in liquids and gasses, the density increases with increasing pressure and decreases with increasing temperature.

It is important to note that just above the critical point for reduced temperatures 1.0 to 1.2 a very small increase in pressure results in a dramatic increase in density. From equation 2.1 it can be seen that at the critical point, the gradient of the density with respect to pressure is infinitively large. For reduced temperatures above 1.5 the density change is much smaller for the same pressure change.

2.2.5. INTERFACIAL TENSION

The interfacial tension between the two phases in a supercritical phase equilibrium situation depends strongly on the system conditions, such as the temperature, pressure and composition. Near the mixture critical point the interfacial tension will be low while far away from the mixture critical point the interfacial tension may be large.

Gasem et al published data for the interfacial tension between carbon dioxide and n-tetradecane at 344 K (Gasem et al., 1989b). Values for the interfacial tension varies between 4.03 mN/m far away from the mixture critical point, to virtually zero close to the mixture critical point.

2.2.6. EFFECT OF PROPERTIES MASS TRANSFER

According to Saito et al the diffusion coefficient of a supercritical fluid is higher than that of a liquid by a factor of several hundreds (Saito et al., 1994). This implies that the mass transfer rate in a supercritical fluid is higher than that in a liquid by the same factor.

The dynamic viscosity of a supercritical fluid is about 100 times lower than that of a liquid, although the density is similar. By implication, the kinematic viscosity is therefore a lot lower due to the definition:

$$\nu = \frac{\eta}{\rho} \quad \text{.. 2.3}$$

This in turn results in a higher Reynolds number allowing turbulent flow to develop preventing laminar flow dispersion of separated bands.

The properties of supercritical fluids therefore favour mass transfer in extraction using supercritical fluids. This is another justification of a study into a separation process with these fluids.

2.3.   SUPERCRITICAL FLUID PROCESSING

2.3.1.   PRINCIPLES OF SUPERCRITICAL PROCESSING

As in all separation processes with an auxiliary medium, separation with supercritical fluids requires two basic steps. In the first step the desirable extraction is achieved while in the second step the supercritical fluid is removed from the feed, regenerated and recycled.

The removal of the supercritical fluid from the solute is generally a relatively simple procedure, usually conducted by a decrease in pressure, and often accompanied by a decrease in temperature. An alternative would be to raise the temperature isobarically.

This project will concentrate on the extraction aspect of the process. Supercritical separation processes can be divided into three main categories. The aim of the discussion below is to illustrate the concepts and not to provide detailed flow diagrams.

The most simple supercritical separation process is a single stage process (See Figure 2-2). Extraction from solids belongs to this category but this category is not limited to solids. Single stage extraction from a liquid also belongs to this category and can be equated with a single flash. For separation in this category to occur with success, the separation factors need to be very high.

Compressed Gas + Product

Feed → Extractor → Separator → Product

Rafinate   Compressed Gas
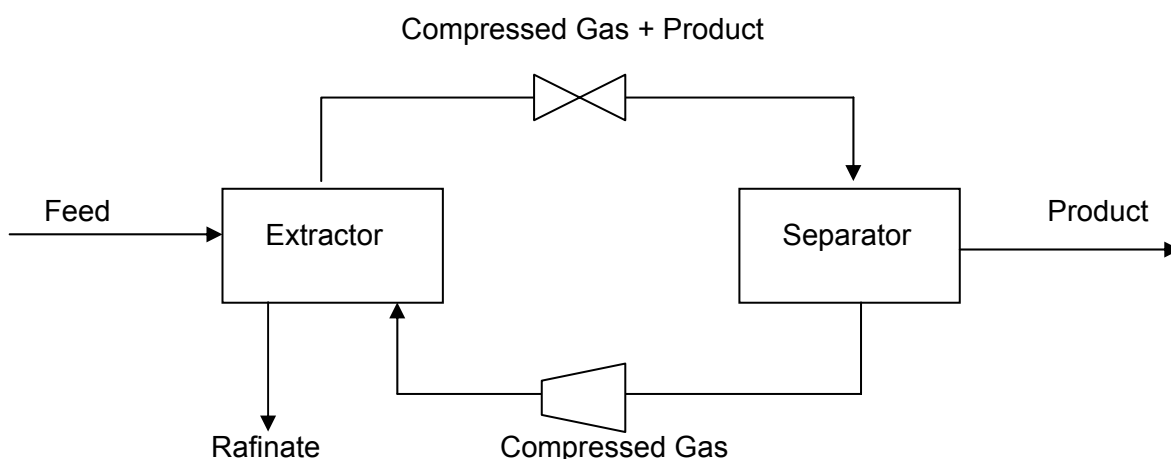
Figure 2-2: Schematic Representation of a Single Stage Process

Common industrial application examples of single stage processes include the extraction of edible oils, spices and alkaloids from solids and the de-oiling of lecithin (Brunner, 1990).

A multistage process can also be used for extraction (See Figure 2-3). This category of extraction is similar to single stage extraction but can be applied when the single stage separation factors are not high enough. Additionally, in a multistage process the extraction and/or separation conditions can be varied for optimal extraction.
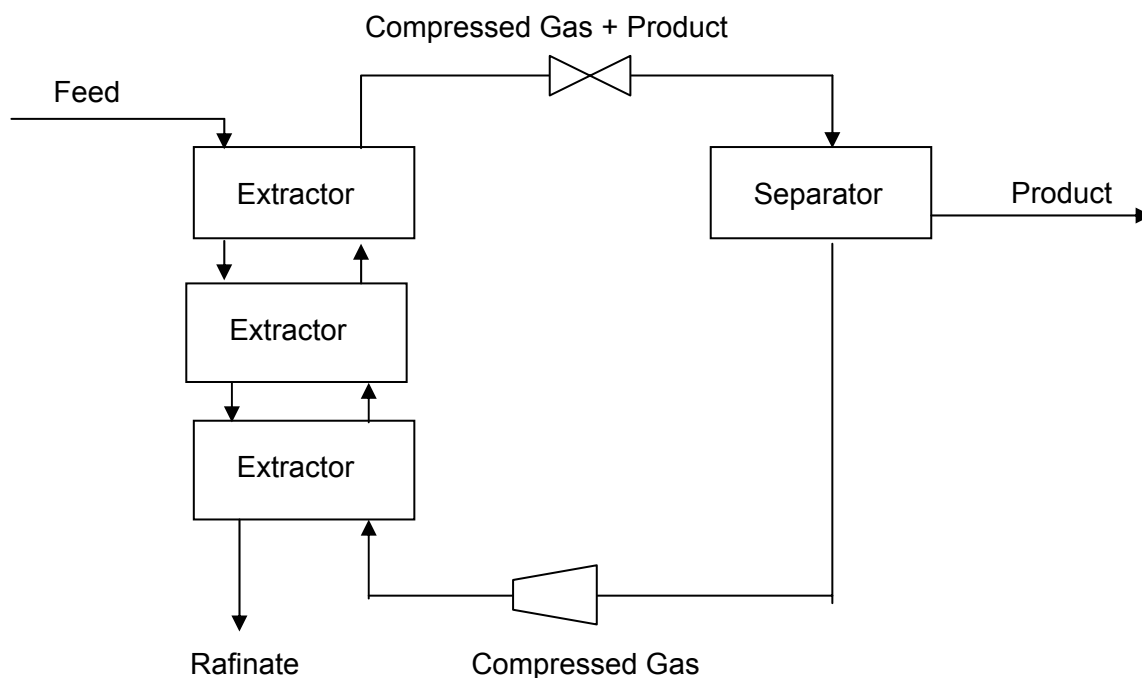
Figure 2-3: Schematic Representation of a Multistage Process

Examples of multistage processes include the refining of used oils, the fractionation of edible oils and the deasphalting (Brunner, 1990).

The last category of supercritical extraction is continuous counter-current operation (See Figure 2-4). This type of separation can be compared to liquid-liquid extraction and is treated in a similar manner. Examples of continuous counter-current operation include the enrichment of ethanol from dilute aqueous solutions, the separation of mono- and diglycerides and the separation of fatty acids (Brunner, 1990).
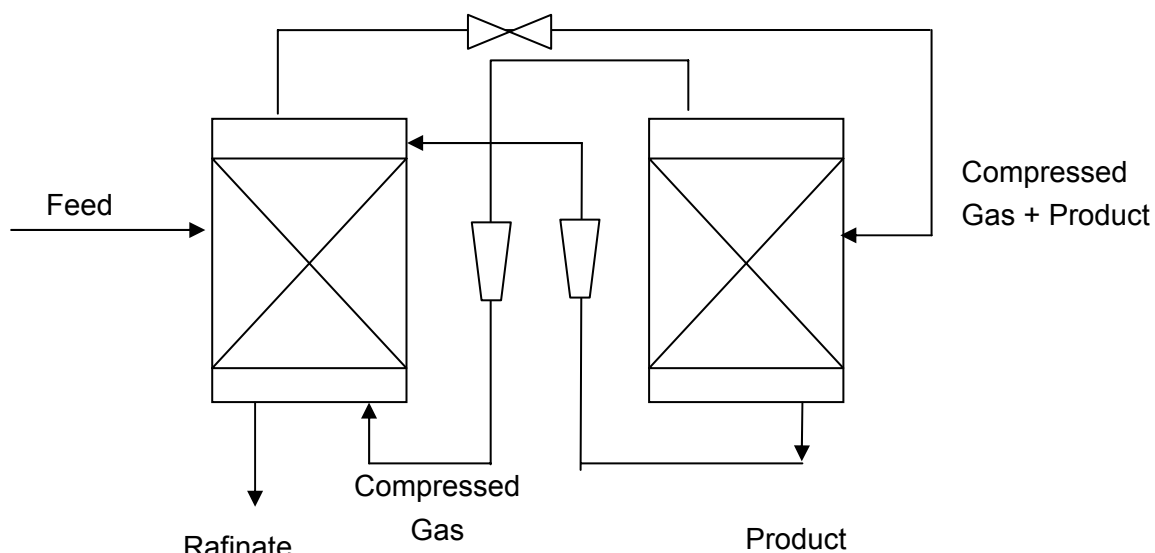
Figure 2-4: Schematic Representation of Counter Current Process

2.3.2. ADVANTAGES AND DISADVANTAGES

Supercritical fluid processing holds the following advantages:

- Supercritical fluids show good solvating power that depends strongly on the temperature and pressure.

- The solvating power can be varied so that the dissolved material can be removed from the solvent and allow regeneration of the solvent with low solvent residue in the product.

- The solvating power depends strongly on pressure and in some cases also on temperature.

- The operating temperature is determined by the critical temperature of the solvent and is usually considerably lower than the boiling temperature of the material of lower volatility. This allows the processing of temperature sensitive materials.

- Supercritical fluids offer an alternative to liquid solvents. Liquid solvents are often hazardous in terms of toxicity and flamability and conducive to solvent residue problems. Supercritical fluids often do not pose these all problems.

- Many of the supercritical fluids used, such as carbon dioxide, are inert, non-toxic and inexpensive. Although these characteristics are not necessary all true for all solvents, a large number of solvents have many of these advantages.

As in all processes, disadvantages also exist:

- Supercritical processes operate at much higher pressures than traditional processes.

- The phase behaviour of supercritical processes is complicated due to the fact that the systems are highly non-ideal in both the liquid and the vapour phase.

- Due to an unfamiliarity with high pressures, especially in the food industry, there has been little tendency to come to terms with the high operating pressures (Basta et al., 1985). This is, however, changing with plants going up in China and France.

It has been postulated than supercritical processes are less energy intensive than traditional processes, yet conflicting reports exist in this regard (Perrut, 2000).

2.3.3. COST OF SUPERCRITICAL PROCESSING

A perception exists that supercritical processing is expensive and not financially viable due to the high investment cost in comparison to classical low-pressure equipment.

When considering the investment costs of supercritical processes, Perrut suggests that large capacity processes are financially viable. It is stated that the investment cost grows slowly with increasing capacity and large plant are thus not excessively expensive. Additionally, it is true that the equipment costs, and thus the initial capital outlay, is high, yet these figures may change drastically with the type of equipment used. (Perrut, 2000)

It is also suggested that the operating costs are low due to the fact that the process can operate continuously. However, optimisation in this regard may be required. The operating costs can also vary from process to process and thus the cost of supercritical processes cannot be defined in general but rather depend on the specific details of the process being investigated.

Nieuwoudt conducted a study on the economics of the supercritical fractionation of high molecular alkane mixtures. He found that economically the process compares well to short path distillation yet the supercritical process yields a better product. (Nieuwoudt, 1994)

Nieuwoudt et al studied the economic viability of supercritical fractionation of paraffin waxes. They compared supercritical fractionation to recrystallization and short path distillation. The analysis showed that supercritical fractionation can be more economically viable, yet depends strongly on the design of the auxiliary equipment. Contrary to other studies and general belief, the capital cost for a supercritical fractionation plant is less than the recrystallization plant. The utility costs depend on the amount of energy integration and with correct equipment choice and energy integration the utility costs are similar to the recrystallization and short path distillation plants. (Nieuwoudt et al., 2001)

Although a vital factor, for the purpose of this project, economics of the process will take a backseat to the technical viability of the process.

2.4.   HISTORY, CURRENT APPLICATIONS AND THE FUTURE OF SUPERCRITICAL FLUIDS

2.4.1.   HISTORY AND FUTURE OF SUPERCRITICAL FLUIDS

The principles of supercritical fluids have been known for over a hundred years but have not received much attention until recently. The ability of supercritical fluids to dissolve solids was reported as early as 1879 by Hannay and Hogarth. In 1896 Villard published a review on supercritical solubility phenomenon describing the ability of methane, ethylene, carbon dioxide, and nitrous oxide to dissolve a number of liquid and solids hydrocarbons, including amongst others, paraffin waxes (McHugh et al., 1994).

The most widely investigated supercritical fluid phase diagram is that of supercritical solvents and naphthalene. Research started as early as 1906 with Brüchner doing studies of primarily a qualitative nature. As with the naphthalene system, early studies mainly concentrated on the solubility in supercritical fluids. (McHugh et al., 1994)

One of the first reports on the solubility of non-volatile substances in supercritical fluids was made by Todd et al in 1955 (Todd et al., 1955). He proposed three types of systems, depending on the ability of the solvent to dissolve the component.

The above-mentioned studies continued, concentrating mainly on laboratory scale experiments, with no extensive industrial use. Yet, in the late 1970's and early 1980's much hype existed regarding this 'magical' substance (Kohn et al., 1979). In 1981 Worthy stated that it is 'About Time' that supercritical fluids should arouse more interest. It was believed that supercritical processes would result in lower energy costs. (Worthy, 1981)

Yet the hype was short-lived, as this 'magical' substance did not seem so 'magical' after all. By 1985 questions were asked regarding this 'magical' process that had not yet been fully implemented (Basta et al., 1985). Yet, Denis Peaver, venture manager at Air product and Chemical Company, Allentown, PA, USA stated the following with regard to supercritical Fluids (Basta et al., 1985):

"We think as the manufacturers get more comfortable with it [SCFE] and the basic understanding of it rises, it will succeed."

The problem at this stage was, that although the advantages of supercritical fluids were already known, very little was understood regarding the thermodynamics of supercritical processes. The problem with the thermodynamics was that the phase diagrams were complex showing many discontinuities. Additionally it was found that the equipment required was up to 50 percent more expensive than conventional units due to the high operating pressures and the fact that the solvents may be extremely corrosive or erosive (Basta et al., 1985).

Yet, by the late 1980s the interest in supercritical engineering had a revival and by October 1998 the first International Symposium on Supercritical fluids was held (Nice, France, 17-19 October 1988).

On an industrial scale, with exception of fossil fuel processing, supercritical fluid technology was first developed and implemented industrially in Germany in the food industry such as tea and coffee decaffeination and hops resin extraction (Perrut, 1998). Most of these supercritical plants operated on a batch scale extracting from solids.

Without much competition from other countries during the 1980's, the industry extended to new areas, including small-scale food processing and pharmaceutical applications. By the late 1980's and in the 1990's, many other players started to impact on the supercritical fluid processing industry introducing countries such as France, Italy, The USA, Japan, Korea, China, India and others.

Currently the industrial and scientific interest can be attributed to:

- The capability of supercritical fluids to replace toxic industrial solvents.

- Ability to synthesise new materials under mild temperatures in the presence of supercritical fluids.

- The possibility of tuning the properties of a solvent for application in highly specific reactions or separations.

In the future, supercritical fluids may become more widely used. This can be attributed to the following:

- In a growing number of countries the use of many organic solvents have been banned. Supercritical fluids offer solvents that are relatively cheap, yet still environmentally friendly and the process results in low solvent residues in the products.

- Supercritical fluids have the ability to produce products of a higher quality than traditional products. This can be attributed to the fact that the processes are often at lower operating temperatures and may have a lower solvent residue.

- Many 'new' products can now be developed due to improved reaction and/or separation conditions.

However, supercritical fluids should be used with caution. They are not a magical cure to a problem and should not be used blindly as a first option but rather as an alternative where traditional methods are not successful.

2.4.2. GENERAL APPLICATIONS

As will be discussed below, supercritical fluids have great potential. Supercritical fluids are currently used in industrial, analytical, waste detoxification and other applications.

The well-known applications of supercritical fluids are in the field of extraction. Supercritical fluids are used for foodstuffs such as the decaffeinating of coffee beans and tea (Zosel, 1978), and the extraction of flavours (Hubert et al., 1978), scents, drugs and oils and fats. Additionally supercritical fluids have been used to remove alcohol from raw materials like cider and wine fermentation broth without the use of excessive heat (Perrut, 2000).

Supercritical fluids have been applied in the petrochemical and polymer industry. Although well studied on laboratory and pilot plant scale, industrial applications have been limited. Examples of industrial applications include the ROSE (Gearhart et al., 1976) and DEMEX (1985) processes. Supercritical fluids are also used in polymer synthesis, impurity removal and polymer precipitation. Other industrial uses include coal distillation and the regeneration of used car oils.

Analytical applications include supercritical fluid chromatography and extraction. In supercritical chromatography, the supercritical fluid is used as the mobile phase. These applications allow for the analysis of low volatility and/or thermally unstable substances at relatively low temperatures (Perrut, 2000).

Supercritical fluids can be used to oxidize organic materials in water. Supercritical fluids have also been used to decontaminate soils from industrial wastes and fuels without the disadvantage of toxic residues in the soil.

In the last few years a rapid increase in the use of supercritical fluids to produce fine particles has occurred. It has been aimed to produce particles of micron and sub-micron size with a narrow particle size distribution range.

2.4.3. PREVIOUS APPLICATIONS OF SUPERCRITICAL FLUIDS IN PETROCHEMICAL AND POLYMER FIELD

A brief overview of the application of supercritical fluids in relevant fields will be given below. All the studies conducted were either on laboratory or pilot plant scale and commercial application in this field have not been realised yet.

Wax Fractionation

De Haan studied the supercritical fluid extraction of liquid hydrocarbon mixtures. Both aliphatic and aromatic compounds were studied. For the normal alkanes, ethane and carbon dioxide were found to give reasonable solubilities, yet monochlorotrifloromethane

and trifloromethane were not as good solvents due the fact that these compounds had larger dipole moments. A supercritical fractionation process was designed where a 25 weight percent of each tetradecane, hexadecane, octadecane and eicosane were fractionated with carbon dioxide into a purity of 99 percent. However, no experimental work was done to back up or verify this design. The molecular weight of the compounds are also too low to be of any commercial interest. (de Haan, 1991)

Nieuwoudt studied the fractionation of high molecular weight alkanes with supercritical butane or LPG (Liquefied Petroleum Gas) (Nieuwoudt, 1994). A detailed design was conducted and the process was found to be highly feasible. Pilot plant experiments were done to confirm these results.

The fractionation of low molecular weight paraffin waxes with supercritical carbon dioxide or ethane has already been proven on experimental scale by Crause et al. (Crause et al., 2000). From the experimental results, carbon dioxide or ethane as a supercritical solvent, produces products with a narrower carbon number distribution than those obtained from short path distillation. The main difference in the carbon dioxide and ethane work is that for the ethane case the pressure is markedly lower.

Extraction and Fractionation of Heavy Petroleum Fractions

In addition to wax fractionation, supercritical fluids have already been used to extract and fractionate petroleum residue. The following examples of extraction and fractionation of petroleum residue are merely a few examples found in the literature:

- The ROSE (Residuum Oil Supercritical Extraction) process has been developed by Gearhart et al (Gearhart et al., 1976). Here oil is separated from residuum resulting in an asphaltene resin. The process entails the extraction of the oil with the aid of near critical butane.

- The DEMEX (Demetallization by Extraction) process, developed by UOP (1985) separates a vacuum residue into an asphaltene-free, low metal content oil and a high metal and asphaltene content pitch. A near critical solvent is used in the separation process.

- Shi et al stated that the use of supercritical fluids provides the advantage of low operating temperatures and high extraction yield (Shi et al., 1997). Supercritical fluid fractionation and extraction was employed to separate four Chinese vacuum residua each into 15 – 17 narrow fractions. It was also found that compared to carbon dioxide, light hydrocarbons provided higher yields and the higher the carbon number of the hydrocarbon, the higher the yield.

- Yang et al fractionated heavy oils and petroleum residue (Yang et al., 1999). They found that a much deeper cut could be accomplished with supercritical fluids than with traditional methods.

- Cheng at al fractionated a Sheig-Bei wax-bearing residue (Cheng et al., 1994). Their results show that fractions of increasing molecular weight can be produced. In addition, the solvent showed a higher affinity for the aromatics than the aliphatic compounds, with an increasing amount of poly-aromatics occurring in the fractions as the pressure increased.

- Peng et al. fractionated petroleum residue into 14 and 10 fractions for the iso-butane and pentane solvents respectively (Peng et al., 1988). The pressures used for the iso-butane fractionation were higher yet the temperatures were lower.

- Chung et al fractionated a heavy petroleum feedstock with the aid of normal pentane. (Chung et al., 1997)

- Jennings et al fractionated a vacuum gas oil with propane and butane (Jennings et al., 1994). The vacuum gas constituted 58.9 % saturated paraffins and naphtha's, with an average molecular weight of 30 to 34 carbon atoms. The remainder of the vacuum gas constituted 39.8 % Aromatics and 1.3 % resin. The vacuum gas had a melting point of about 60 $^{\circ}$C and the results are thus applicable to this project. Phase equilibria with propane resulted in data similar to that of Peters et al (Peters et al., 1992). For propane a three-phase region occurred while for butane no three-phase region was found. For both solvents a small amount of the solute did not dissolve in the solvent.

- Huang et al. studied the solubility of hydrogen and carbon monoxide in n-C20, n-C28 and n-C36 as well as in a Mobil Fisher Tropsch Wax (Huang et al., 1988a). Additionally, for the paraffins, a mixture of the synthesis gasses was also studied. It was found that at the temperatures (373 – 573 K) and pressures (up to 50 atm) in their study, very low concentrations of the paraffins were measured in the vapour phase. The work of Huang only published bubble point data and no dew point data was given.

- Radosz studied the behaviour of supercritical propane and butane in oil solutions (Radosz, 1987a). Oil solutions often contain medium length hydrocarbons with a certain amount of waxes dissolved in the oils. The study conducted here is purely qualitative giving an indication of the phase diagram that can be expected. Here the phase diagrams are compiled by the fact that the heavy phase is not a single component but rather a poorly defined mixture. A three-phase region is observed, appearing at n-C18 for ethane as the supercritical solvent and in the region of n-C40 to n-C50 for propane.

- Radosz et al studied the phase equilibria of propane and two oil systems with temperatures between 374.4 K and 413.5 K and pressures up to 55 bar (Radosz et

al., 1987b). The first oil system studied is rich in saturated hydrocarbons while the second system is rich in aromatics. It is the first system that is of interest here and results show that an increase in pressure leads to an increase in the propane content of the oil rich phase and the oil content in the propane rich phase. However, no numerical values were given so as to indicate if the oil in the propane rich phase differs at all from the oil in the oil rich phase.

Fractionation of Polymers

Low molecular weight polyethylene borders on being a high molecular weight wax. Polyethylene is a long chained alkane, thus having a similar structure as a Fisher-Tropsch wax and studies of supercritical fluid behaviour with polymers thus warrants further investigation.

Various studies concerning the fractionation of polymers have been done. McHugh et al gives an extensive discussion of polymer fractionation (McHugh et al., 1994). The techniques of either isothermally decreasing the pressure from one column to another as well as isothermally increasing the pressure were illustrated. Whereas the isothermal decrease in pressure results in products from the bottoms of the columns, the isothermal increase in pressure results in products from the distillate. Industrial processes typically use a degreasing in pressure profile from one column to another, while laboratory experiments are often easier with an increasing pressure profile from one column to another.

The fractionation of polyethylene, a polyethylene based co-polymer, polisiloxane, polymer binders and other polymers were discussed both in a qualitative and a quantitative manner. In addition the extraction of oligmers from polymers was discussed.

For the purpose of polyethylene McHugh et al states that fractionation in terms of molecular weight is readily accomplished by isothermally increasing the pressure profile while fractionation in terms of backbone structure is obtained by isobarically increasing the temperature. A combination of these two methods may lead to polymer fractions that are fractionated by both molecular weight and backbone structure.

Other discussion on the fractionation of polymers include:

- Meilchen et al studied various polymer and copolymer systems and found that propane is a much better solvent than carbon dioxide. (Meilchen et al., 1990)

- Radosz and Huang discussed the fractionation of polymers with more than one supercritical component. This, together with the fact that the heavy component is not a single component but rather a mixture, allows for study of more realistic systems which would more closely resemble the process conditions encountered in industry. (Radosz et al., 1990)

- Clifford et al fractionated poly-isobutene and polydimethylsiloxane and compared the experimental results to computer-simulated predictions. From the experimental results it can be seen that the fractionation was possible but the polymers are not very soluble in carbon dioxide. (Clifford et al., 1998)

- Britto et al studied the fractionation of high-density polyethylene at isothermal as well as isobaric conditions. They found that isothermal conditions lead to fractionation by molecular weight and reduced the polydispersity of the wax from 5.06 in the unfractionated resin to between 1.47 and 3.14 in the fractions, the higher values occurring in the higher molecular weight fractions. The higher molecular weight fractions have broader molecular weight distributions. Their study of fractionation at isobaric conditions resulted in fractions having similar molecular weight distributions and only a slightly lower polydispersity than the parent resin. Isobaric fractionation is thus not controlled by molecular weight. However, a crystallization temperature analysis shows that the crystallization temperature increases with increasing fractionation temperature. (Britto et al., 1999)

2.5. SUMMARY

On pilot plant scale supercritical fluid applications in the petrochemical industry has proven to be successful. From these studies it is likely that the application proposed here can be implemented successfully.

3. PHASE DIAGRAMS IN THE CRITICAL REGION

For a clear understanding of the fundamentals of processing with supercritical fluids, an understanding of phase behaviour of the mixtures involved is necessary. From this knowledge a qualitative prediction of the phase behaviour outside the experimental region can be made, thus assisting in full understanding of the system under investigation.

3.1. PHASE RULE

A point of departure in the understanding of the phase behaviour is the Gibbs Phase Rule and the resulting degrees of freedom. The phase rule can be defined as follows:

A system with N components and Π phases in equilibrium with one another can be fully described by V variables:

$$V = 2 + \Pi(N-1) \quad \text{...} 3.1$$

From the Gibbs Phase Rule the degree of freedom, F, can be defined as the difference between the number of variables and the number of equilibrium conditions and expressed mathematically as follows:

$$F = N - \Pi + 2 - \phi \quad \text{...} 3.2$$

In equation 3.2, the symbol ϕ represents additional relations. The additional relations allow for incorporation of azeotropes. For each azeotrope or critical point one needs to be added to ϕ. For all other systems, ϕ should be taken as zero. This is explained in more detail in the book edited by Kiran et al. (Kiran et al., 1994)

The phase rule and the number of degrees of freedom will be applied to the experimental measurements to ensure that the system is fully defined.

3.2. GENERAL PHASE DIAGRAMS

Phase behaviour of fluids at moderate to high pressures show that the phase diagrams are very complex and difficult to understand.

The binary solvent solute phase diagram in Figure 3-1 can be considered to show desirable characteristics due to the fact that the phase behaviour is simple without a three

phase region. Additionally these types of systems can usually produce a high vapour loading at moderate pressure.
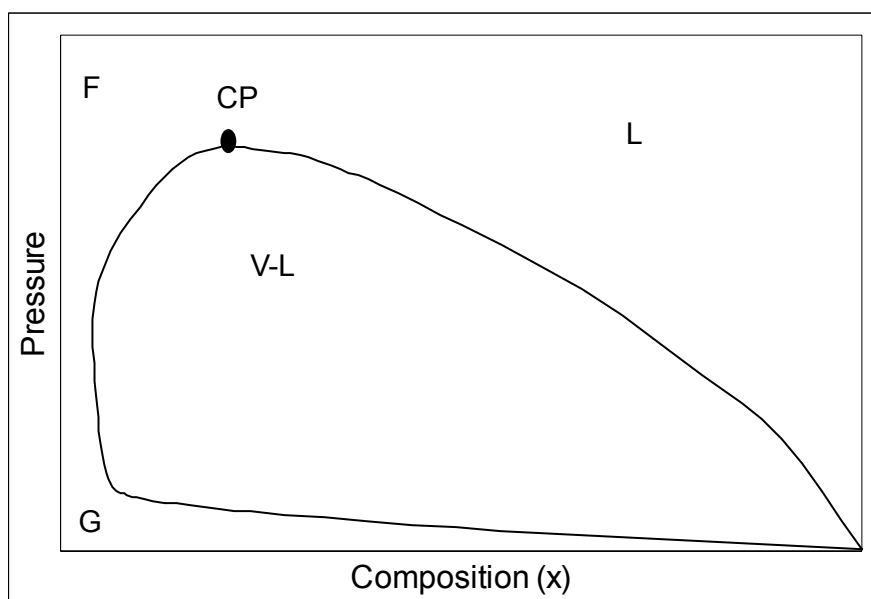
Figure 3-1: Phase diagram for a desirable solvent in a solvent-solute system.

The phase diagram shown in Figure 3-2 shows some less desirable characteristics. It can be seen that two liquid phases can occur, and at a specific point, three phases may occur.
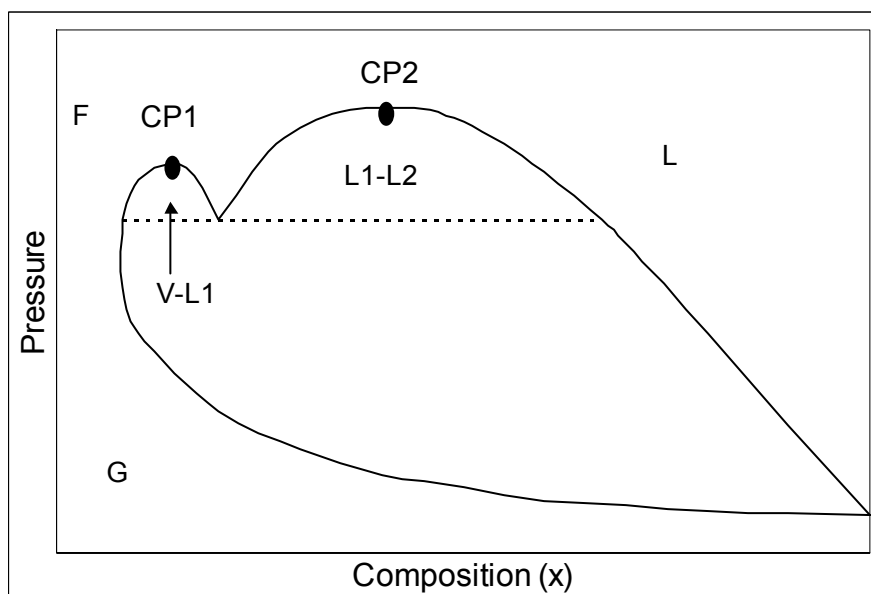
Figure 3-2: Phase diagram for a less desirable solvent in a solvent-solute system.

The phase diagram may also exhibit the characteristics shown in Figure 3-3. Under certain conditions these characteristics may be less desirable due to the fact that a high solute loading of the solvent may not be attained. Additionally, for hydrodynamic considerations, a single phase region may not easily be attained.
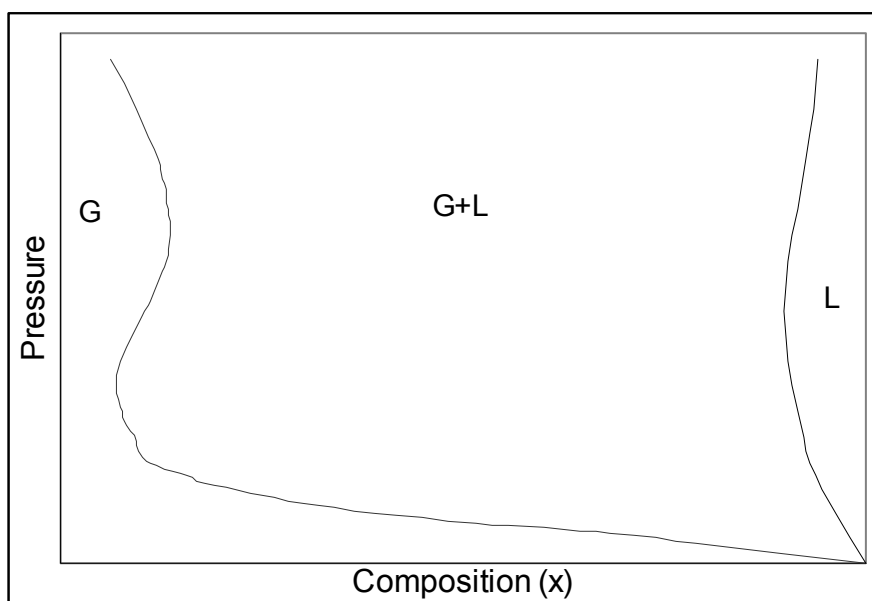
Figure 3-3: Phase diagram for an undesirable solvent in a solvent-solute system.

3.3.   BINARY PHASE DIAGRAM CLASSIFICATION BY CLASS

Binary mixtures of supercritical fluids fall into two main classes, depending on the critical temperature and the molar mass of the solute with respect to that of the solvent.

Class 1: Fluid – Modifier Mixtures

In the first class, the solute has a molar mass mostly above, but not far above the first component. In this class the solute is added to modify the solvent characteristics or, alternatively, added as a reactant.

Class 2: Fluid – Solute Mixtures

In the second class, the solute has a molar mass and critical temperature much higher than that of the solvent. In this class the solvent is used to dissolve the solute, which usually is a non-volatile liquid or a solid. This class of phase behaviour is usually used in extraction or separation processes as well as reactions in a desired phase.

3.4.   BINARY PHASE DIAGRAM CLASSIFICATION BY TYPE

The two classes discussed in paragraph 3.3 can further be divided into the six different types. This classification is currently widely accepted based on the work of van Konynenburg et al. (van Konynenburg et al., 1980) Classification can be done into six principle types (Type I to Type VI) according to the nature of their temperature-pressure diagrams. The first five types can be qualitatively predicted by the van der Waals equation of state while type VI cannot be predicted by this equation of state. However, with the aid

of a simple Carnahan-Starling type equation of state type VI can be predicted (Wei et al., 2000). Type VI is only found in aqueous mixtures and complex interactions may play a significant role in this type of system. The classification given in this work is the same as that given by van Konynenburg et al.

The six types of phase diagrams can be summarised by Figure 3-4:
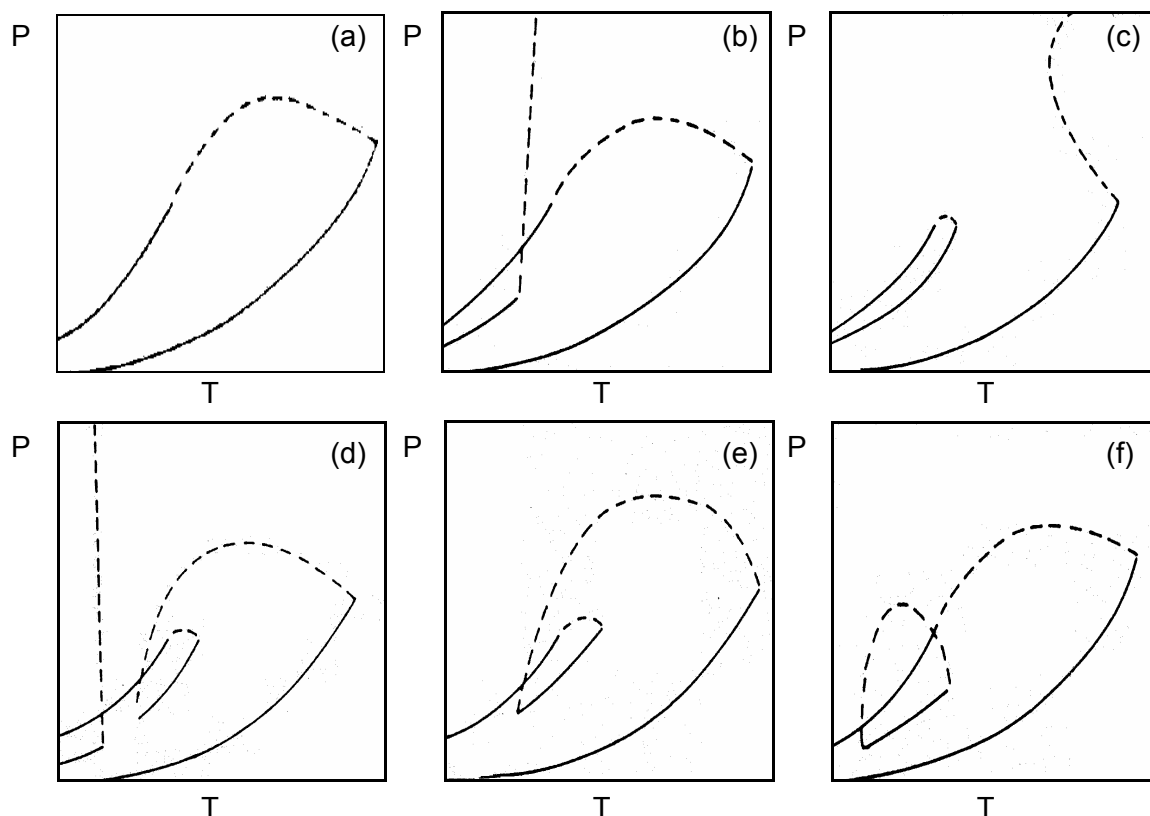
Figure 3-4: Pressure-temperature plots at constant composition of the six main types of possible binary phase diagrams for fluids. (a) Type I, (b) Type II, (c) Type III, (d) Type IV, (e) Type V, (f) Type VI (Rowlinson et al., 1982)

In Figure 3-4 the dashed curve is the mixture critical curve. The above figures will be discussed in more detail below as the different types are discussed.

Before the types are discussed in detail, the following terms need to be defined. Consider a type VI phase behaviour. In Figure 3-5 the location of the definitions on the phase diagrams are illustrated.
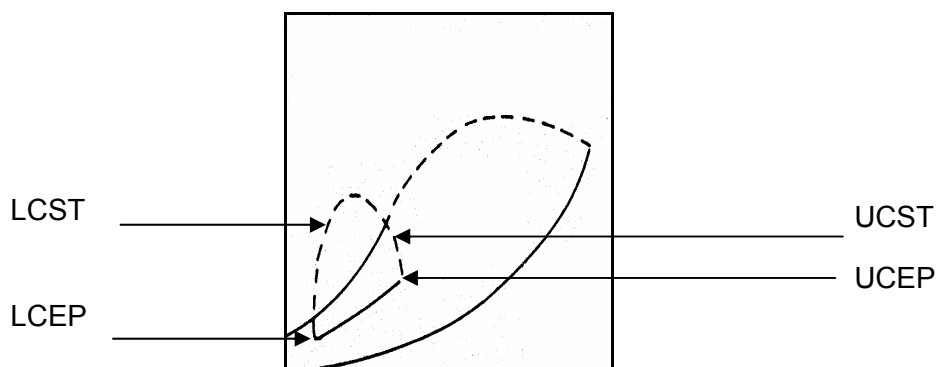
Figure 3-5: Type VI phase behaviour illustrating the definitions discussed.

Definition: Lower Critical Solution Temperature (LCST)

The lower critical solution temperature at a set pressure is the temperature at which two liquids critically merge to form a single liquid phase as the system temperature is isobarically lowered. This may occur in the presence of a gas phase. The LCST forms a continuous line on the PT diagram.

Definition: Upper Critical Solution Temperature (UCST)

The upper critical solution temperature at a set pressure is temperature at which two liquids critically merge to form a single liquid phase as the system temperature is isobarically raised. The UCST forms a continuous line on the PT diagram.

Definition: Critical End Point (CEP)

At the critical endpoint, two phases in a three-phase equilibrium become identical and the two corresponding curves in the P-T-x space merge into one point. The critical end point is also the end point of the critical solution temperature line.

Definition: Upper Critical End Point (UCEP)

The upper critical end point is the upper temperature limit of the three-phase equilibrium where two liquid phases become identical. The UCEP is also the end point of the USCT line.

Definition: Lower Critical End Point (LCEP)

The lower critical end point is the lower temperature limit of the three-phase equilibrium where the two liquid phases become identical. The LCEP is also the end point of the LCST line.

Definition: Tricritical Point

When the UCEP and LCEP temperatures are plotted as a function of temperature, the tricritical point is the point where the LCEP and UCEP merge. The tricritical point is thus not a point on a phase diagram but rather the point where a homologous series changes from one type of phase diagram to another. To illustrate the concept of the tricritical point, the UCEP and LCEP temperatures of the homologous series of propane with normal alkanes are plotted in Figure 3-6.
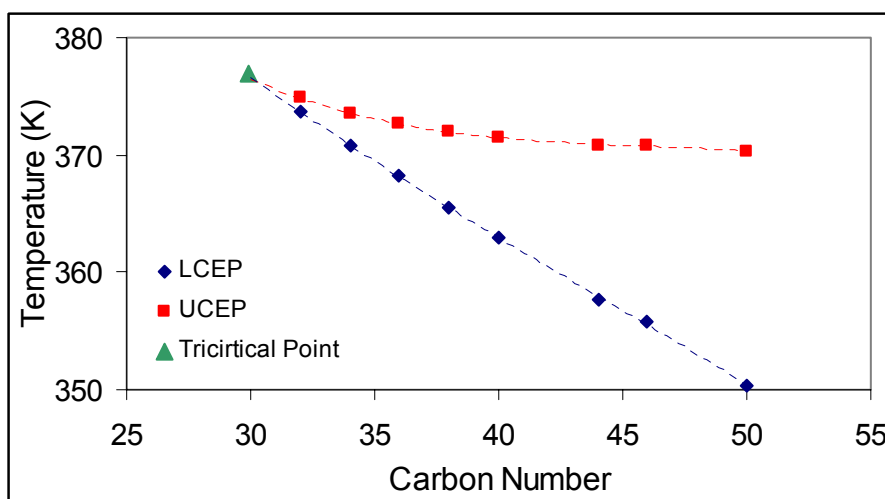
Figure 3-6: Illustration of Tricritical Point of normal alkanes homologous series with near critical propane (Peters et al., 1989)

Definition: Mixture Critical Point

The mixture critical point for a set temperature can be defined as the composition and pressure where the properties of the liquid and the vapour phase are identical. These properties include density, composition, viscosity and other thermodynamic properties. Graphically, the mixture critical point can be represented as follows:
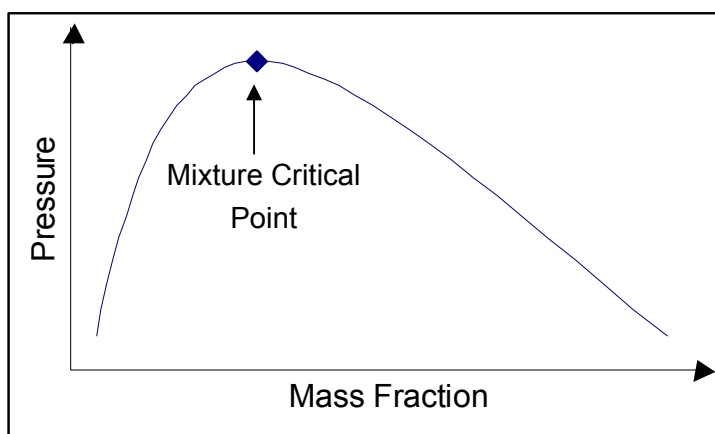
Figure 3-7: Mixture Critical Point

More complicated phase diagrams may have more than one mixture critical point.

3.4.1. TYPE I

Type I is the simplest possible phase behaviour for a binary mixture. A pressure-temperature composition phase diagram is given in Figure 3-8. This type of phase diagram is distinguished by the fact that only one liquid phase exists throughout the phase diagram and that the critical curve runs continuously from the critical point of the more volatile component to the critical point of the less volatile component. A typical type I PTx diagram is shown in Figure 3-8.
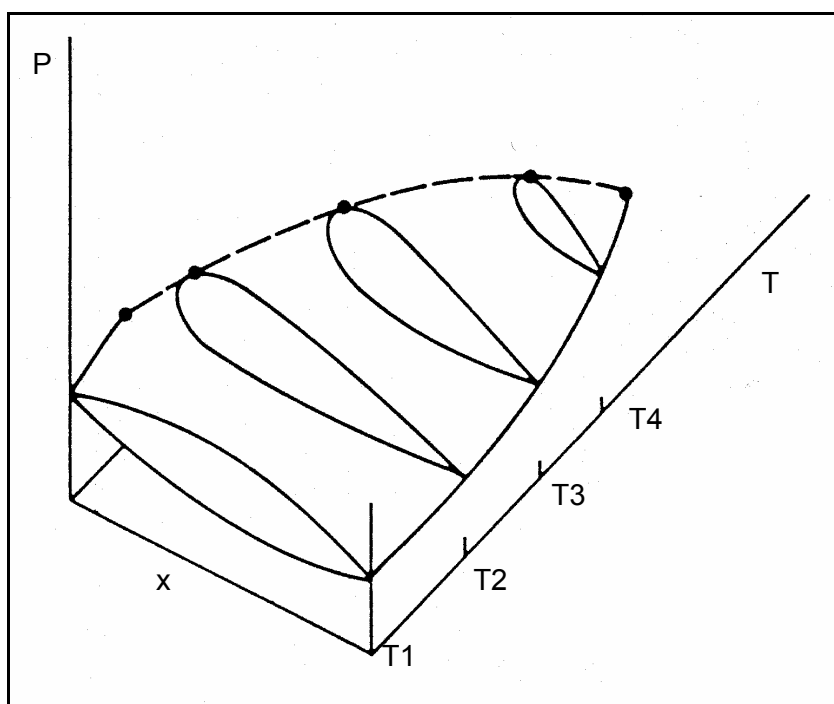
Figure 3-8: P-T-x Phase Diagram for Type I Binary Mixtures (McHugh et al., 1994)

This type of phase diagram usually occurs when the components have similar molecular size or diameters and similar interaction strengths, or have critical properties of comparable magnitude. Examples of this type of phase behaviour is methane + ethane, carbon dioxide + oxygen, benzene + cyclohexane (Rowlinson et al., 1982), carbon dioxide + ethane and carbon dioxide + propane (Brunner, 1994).

Components of a particular homologous series, such as normal paraffins (as studied in this project) will show this type of trend, unless the size difference exceeds a particular value. For this project it is expected that the size difference will exceed this value. This will be explained in more detail in subsequent sections.

It must be mentioned that azeotropes may occur for this type of system and are also classified as Type I, provided that the phase behaviour is associated with a continuous critical line.

3.4.2. TYPE II

Type II phase behaviour is similar to that of Type I, with the exception of the existence of two liquid phases at specific temperatures and pressures. This phase behaviour can be seen in Figure 3-9:
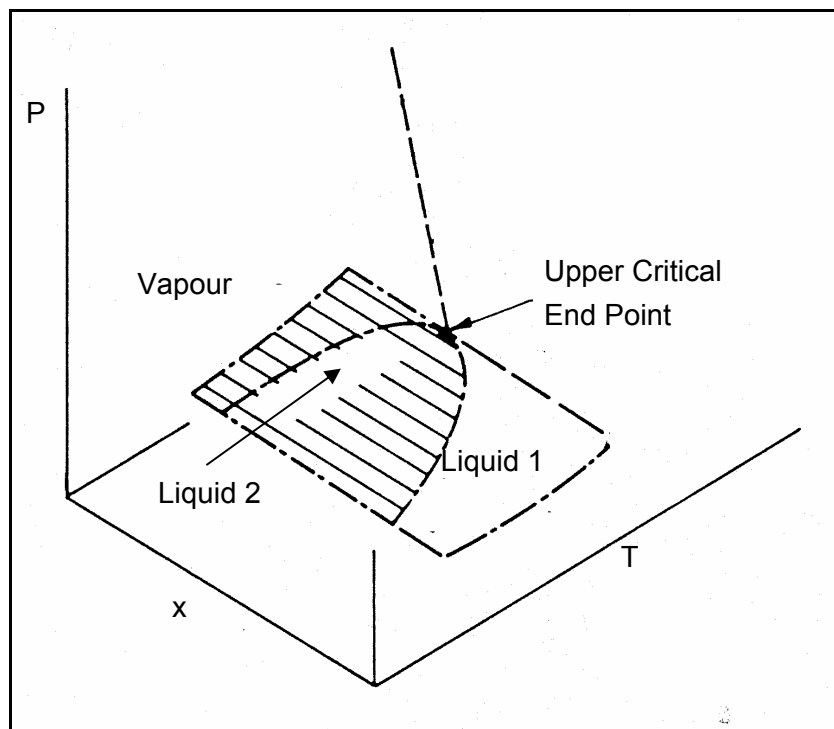
Figure 3-9: P-T-x Phase Diagram for Type II Binary Mixtures

From Figure 3-9 it can be seen that the two liquids become critically identical in the presence of a gas phase at the UCEP. As in the case of type I, the phase diagram may be complicated by the presence of an azeotrope. Examples of type II phase behaviour include n-octane + carbon dioxide and n-hexane + nitrobenzene (Brunner, 1994).

3.4.3. TYPE III

Type III systems are systems with a divided gas-liquid critical curve. One part of the critical curve starts at the critical point of the less volatile component, while the other part starts at the critical point of the more volatile component and ends on the three phase liquid-liquid-vapour line.

A three dimensional representation of a type III system is given in Figure 3-10. To clarify the above diagram a series of points at 4 different temperatures is given in Figure 3-11:

:
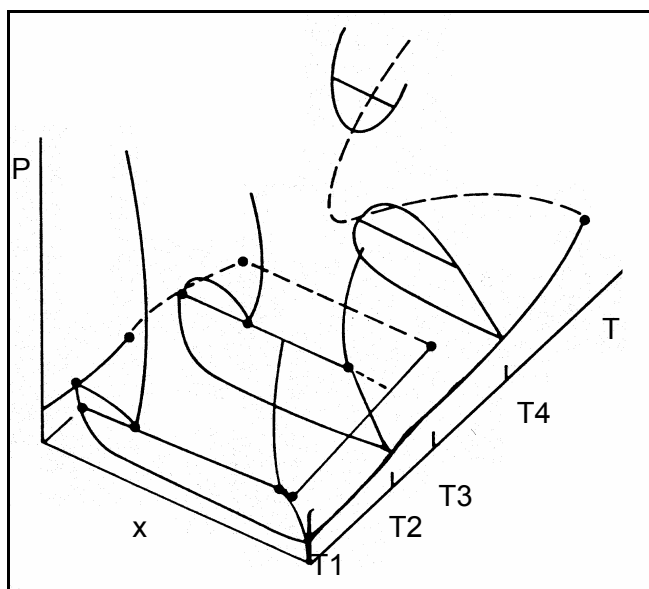
Figure 3-10: P-T-x Phase Diagram for Type III Binary Mixtures (McHugh et al., 1994)
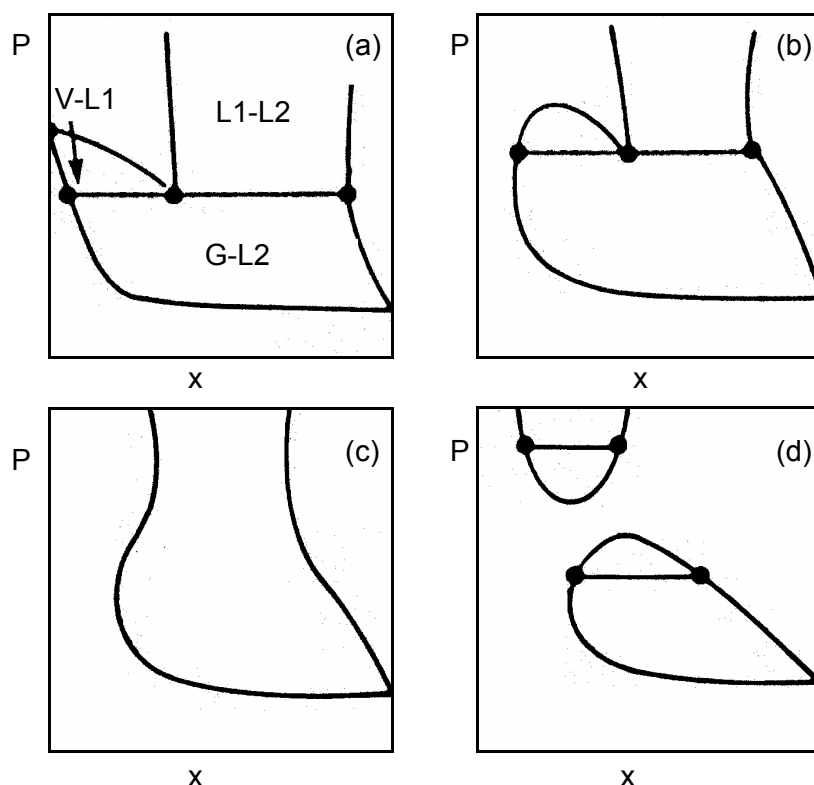
Figure 3-11: P-x Phase Diagrams for Type III for Binary Mixtures at various Temperatures (McHugh et al., 1994) (a) Temperature below critical temperature of more volatile compound (T2 - Figure 3-10). (b) Temperature slightly above critical temperature of more volatile compound (T3 - Figure 3-10). (c) Temperature well above critical temperature of more volatile compound (T4 - Figure 3-10). (d) Temperature even higher above critical temperature of more volatile compound (T5 - Figure 3-10).

Examples of type III systems include carbon dioxide + nC24 (du Rand, 2000), carbon dioxide + nC16 and carbon dioxide + squalene. (Schneider et al., 1967)

3.4.4. TYPE IV

The distinguishing characteristic of type IV phase diagram is that a liquid-liquid-vapour region exists very close to the critical point of the more volatile compound. As the temperature increases, this region of liquid-liquid immiscibility will become smaller and later disappear. This phenomenon can be seen in Figure 3-12 but it should be noted that the illustration exaggerates this region of immiscibility.
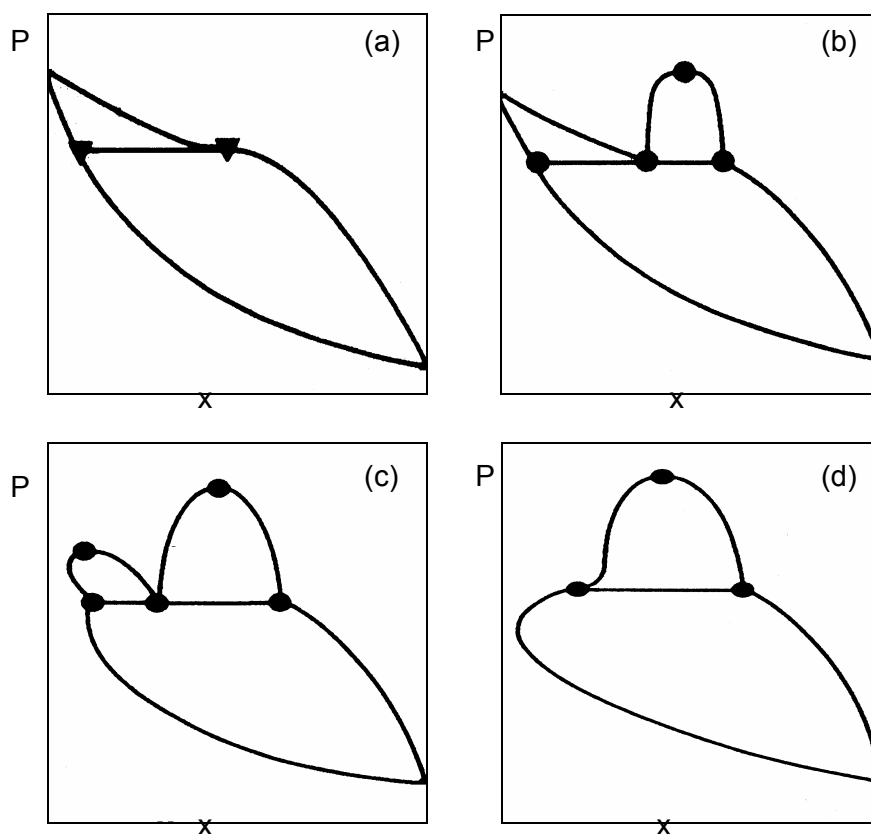
Figure 3-12: P-x sections at constant temperature (Kiran et al., 1994). (a) Temperature where second liquid phase appears (b) At Lower Critical Solution Temperature (c) Temperature slightly above critical temperature of more volatile component (d) Temperature well above critical temperature of more volatile component.

Type IV behaviour is very similar to that of Type V (see paragraph 3.4.5) but, as can be seen in Figure 3-4, liquid-liquid immiscibility occurs at temperatures below the LCST. This is further illustrated in Figure 3-12.

Examples of type IV phase behaviour include ethylene + nitromethane, methane + n-hexene (Kiran et al., 1994) and carbon dioxide + n-tridecane (Schneider et al., 1967). For the carbon dioxide + n-paraffin homologous series the transition from type IV to type III seems to occur between the carbon number of 13 and 16.

3.4.5. TYPE V

Type V is the same as Type IV, but no low temperature liquid-liquid critical curve is observed. Figure 3-13 shows the general PTx diagram for Type V systems.
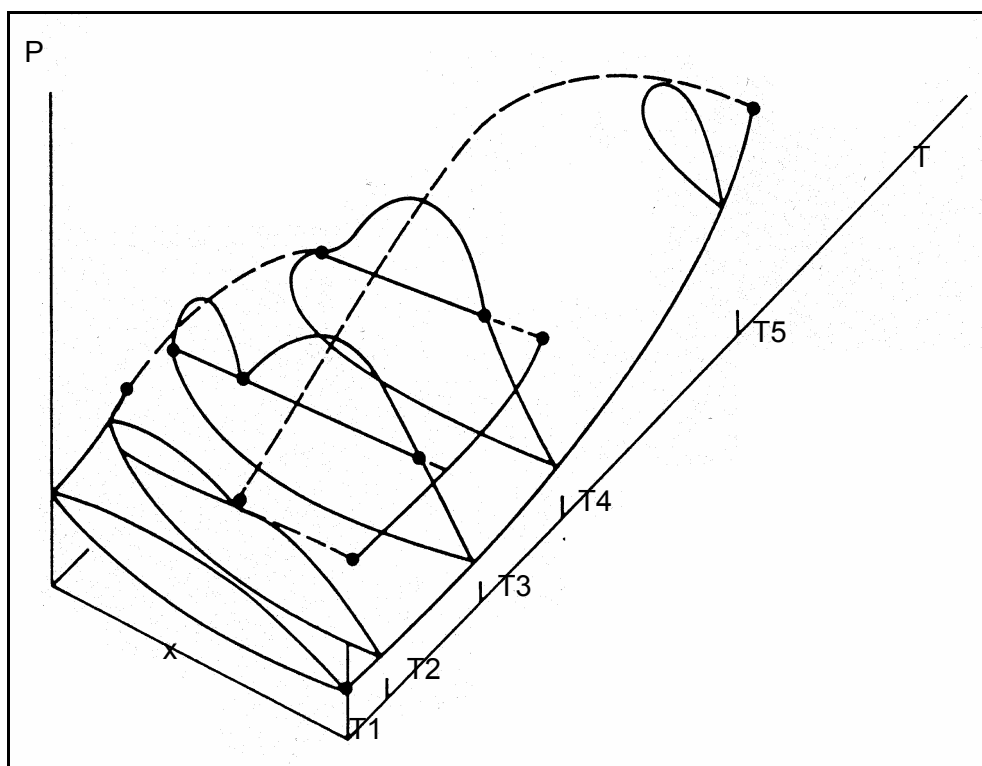
Figure 3-13: P-T-x Phase Diagram for Type V Binary Mixtures (McHugh et al., 1994)
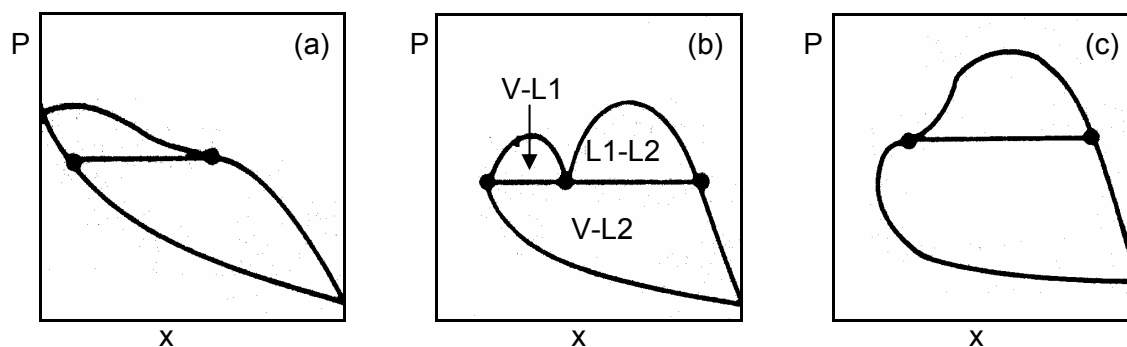
Figure 3-14: P-x Phase Diagrams for Type V for Binary Mixtures at various Temperatures (McHugh et al., 1994) (a) Temperature below critical temperature of more volatile compound (T2 - Figure 3-13). (b) Temperature slightly above critical temperature of more volatile compound (T3 - Figure 3-13). (c) Temperature well above critical temperature of more volatile compound (T4 - Figure 3-13).

Type V phase behaviour usually occurs when the critical properties of the two components differ significantly or if the species differs considerably in the strength of the intermolecular potential. The latter will not be discussed here, as it is not applicable to this project.

When examining the homologous series of normal alkanes type V behaviour occurs when the ratio of the carbon atoms exceeds a certain value. For methane – normal alkane systems type V phase behaviour occurs when the ratio exceeds 5 (McHugh et al., 1994), i.e. in systems with more than 5 carbon numbers type III occurs. For ethane the ratio was found to be 9.5 (McHugh et al., 1994), therefore systems with 19 or more carbon atoms show type V behaviour.

It can be argued that some systems can be incorrectly classified as type V when they are in fact type IV with the liquid-liquid critical curve being hidden by the solidification of one of the components. Although of academic interest, it is of no practical importance if a system is classified as type IV with the liquid-liquid critical curve hidden by solidification or a type V with no liquid-liquid critical curve. In various publications Peters and co-workers did not report a liquid-liquid critical curve and by implication thus classified these systems into type V (Peters et al., 1987a), (Peters et al., 1987b), (Peters et al., 1986), (Peters et al., 1988b). For the purpose of this project it will be assumed that if the liquid-liquid critical curve cannot be observed, a system will be classified as type V.

For propane Leder et al found no region of immiscibility for propane-hexatriacontane and stated that heptatriacontane is likely to be the lowest possible normal paraffin that could display liquid-liquid immiscibility (Leder et al., 1976). McHugh et al. published this ratio as 13.5, resulting in systems with 40 or more carbon atoms showing type V behaviour (McHugh et al., 1994). Peters et al conducted experiments and found that regions of immiscibility occur for the C3 - C32, C3 - C34, C3 - C36, C3 - C38, C3 - C40, C3 - C44, C3 - C46 and C3 - C50 systems and classified all these systems as type V (Peters et al., 1989). Extrapolation from the lower and the upper critical solution temperatures leads to a prediction that the transition may occur hydrocarbons with 29 or 30 carbon atoms (See Figure 3-6). Jennings et al found a three-phase liquid-liquid-vapour region near the critical point of propane for the systems vacuum gas oil and propane where the vacuum oil gas has an average carbon number of 30 to 34 (Jennings et al., 1994). Jennings et al found no three phase region for butane with vacuum gas oil.

For the purpose of this project it is not important to measure exactly the form of the phase in the region of immiscibility or at which carbon number immiscibility first occurs, but to rather note that if immiscibility occurs, where the region is and to ensure that any process is designed well away from this region, by either adjusting the temperature or pressure or both.

3.4.6. TYPE VI

Type VI is type I with the addition of a liquid-liquid immiscibility region. This can be seen in Figure 3-15:
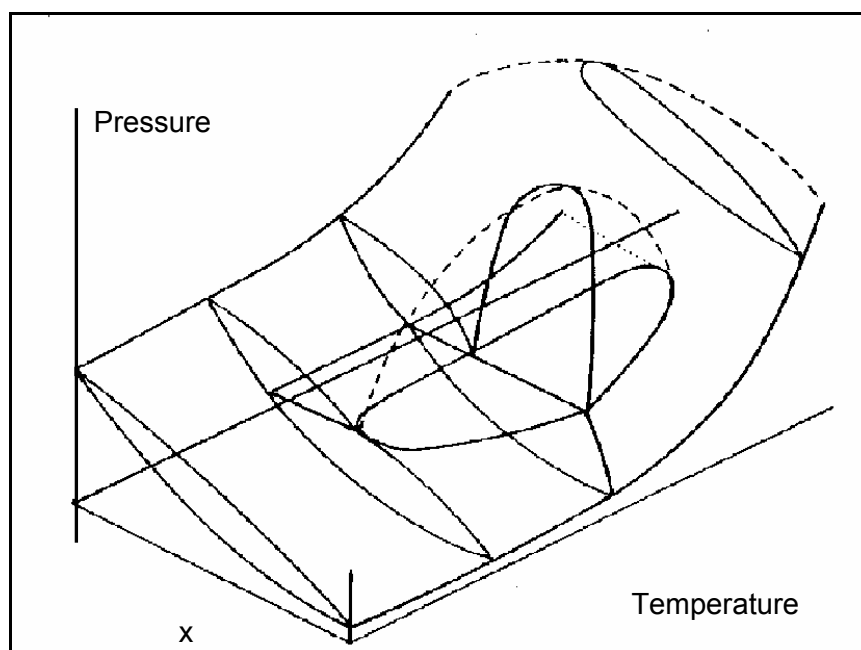
Figure 3-15: P-T-x Phase Diagram for Type VI Binary Mixtures (Rowlinson et al., 1982)

To clarify the above diagram a series of points at 3 different temperatures is given in Figure 3-16:
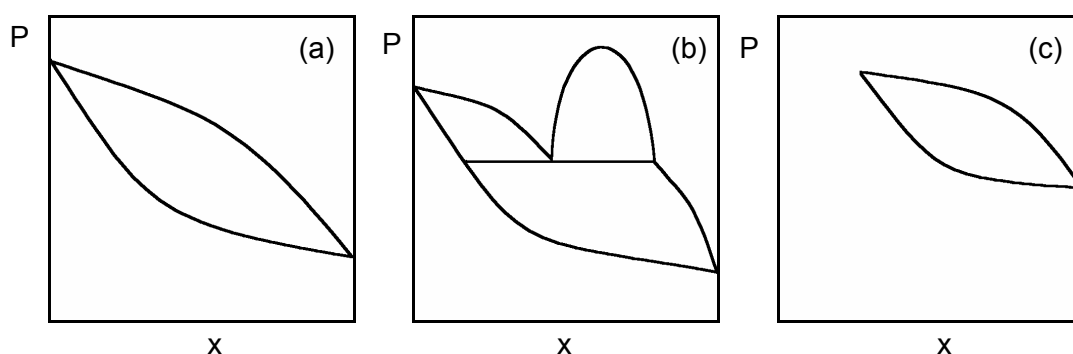
Figure 3-16: P-x Phase Diagrams for Type VI or Binary Mixtures at various Temperatures (a) Temperature below the immiscibility critical region. (b) Temperature in the immiscibility region. (c) Temperature above the immiscibility region.

For type VI a region of liquid-liquid immiscibility occurs. This region of liquid-liquid immiscibility is, however, limited to a limited temperature range. Below the LCST and above the UCST the system is miscible. As in the case of types I and II, the phase diagram may be complicated by the presence of an azeotrope.

Type VI system is only found in mixtures with chemically complex substances where one or more of the pure components exhibit self association due to hydrogen bonding and in the mixture self there is the added complication of strong inter-component hydrogen bonding. Water is almost always one of the components. Examples may include water + n-butanol and water + 2-butanol.

3.5. SOLID-SUPERCRITICAL FLUID PHASE DIAGRAMS

The six types of phase diagrams discussed in section 3.4 explain phase behaviour for the liquid, vapour and fluid states. However, solid phases are also part of the total phase diagram. Various studies have been conducted on the solid-liquid-vapour phase equilibria. For methane-tetracosane Flötter et al conducted a study of the solid-fluid equilibrium (Floeter et al., 1997). For Ethane with various n-alkanes, Garcia et al conducted a solid-liquid equilibrium study (Garcia et al., 1999).

In this project all experiments will be conducted at temperatures above the normal melting point of the waxes. Solid-Supercritical Fluid Phase Equilibria will thus not be considered further in this study.

3.6. CRITICAL OPALESCENCE

In the region around the critical point, a supercritical fluid scatters visible light. This phenomenon is known as critical opalescence.

Critical opalescence can be attributed to long range concentration fluctuations that occur in the solution when sufficient number of molecules group together for a long enough time to form a correlated structure that has dimensions large enough to scatter visible light. The effect shows that there are intermolecular density fluctuations in the distance equal to the visible light wavelength.

On a microscopic scale, critical opalescence can be explained as follows (de Podesta, 1997): The molecular randomness causes a liquid near the critical temperature to constantly fluctuate into nearly vapour-like volumes and back again. As the critical temperature is approached, the length scale of the fluctuations grows as the energy required for the fluctuations into the vapour state becomes smaller as one approaches the critical temperature. Eventually the fluctuations occur on the scale of a fraction of a micron, i.e. of the same order of the wavelength of light. Should there be a difference in the refractive index of the vapour and the liquid phases, and there generally is a small difference, then the light will be strongly scattered and the mixture of the phases appears cloudy. The solution will appear as a bluish white colour when light is reflected through the solution while it will appear a reddish-orange colour if light is transmitted through the solution.

Should the pressure-composition curve of the phase boundary be quite flat, critical opalescence is often found for the range of compositions where the curve is nearly flat.

3.7. SUMMARY

When considering the binary phase diagrams studied above, it can be seen that the phase equilibria the various systems are expected to display are complicated and non-ideal. Due to the non-ideality, experimental results are required to facilitate the design process.

4. LITERATURE DATA AND SOLVENT SELECTION

Before extensive, time-consuming experiments are conducted, a literature survey will be done to determine if any applicable systems have already been studied and to aid in the selection of a suitable solvent.

It is imperative that the optimum solvent is selected. For the purpose of this project suitable solvents will be investigated by consulting the literature. Additionally, the literature data available will indicate for which systems experimental data is required.

4.1. VARIOUS SUPERCRITICAL FLUIDS

Various possibilities exist for supercritical fluid solvents and many factors need to be considered. The various options are discussed below.

Carbon Dioxide

Carbon dioxide is the most widely used supercritical fluid due to its convenient critical parameters, its cheapness, non-flammability and non-toxicity. The CO_2 used is usually obtained as a by-product from fermentation or combustion.

Although carbon dioxide is a non-polar molecule, it may be applied as a weak polar solvent due to its large quadruple moment. Carbon dioxide can be used for many organic compounds and has a particular affinity for fluorinated compounds.

Carbon dioxide is not such a good solvent for polymers and high molar mass hydrocarbons. This can be justified against the work of du Rand who studied the interaction of carbon dioxide with alkanes with 12 to 36 carbon numbers (du Rand, 2000).

Methane, Ethane, Ethylene, Propane, Propylene and other Hydrocarbons and Monomers of Polymers

These compounds have good solvating power for hydrocarbon polymers and high molecular mass hydrocarbons due to their similarity in structure. This can be seen in paragraph 2.4.

Methane, ethane, propane and other alkanes have the same functional structure and are thus expected to perform well. Ethylene, propylene and other monomers of polymers are

also expected to perform well due to the fact that the solvent is the building block of the solute.

These compounds have the disadvantage that they are flammable.

Other compounds

- Ammonia behaves similar to carbon dioxide but is often not used due to environmental problems.

- Halocarbons have the disadvantage of cost and environmental problems.

- Xenon may be used on small scale but is very expensive.

Supercritical Fluids for Investigation

For the purpose of this investigation, the following compounds will be investigated further as possible solvent for the fractionation of waxes:

- Carbon Dioxide

- Methane

- Ethane

- Propane

- Normal- and iso-Butane

- LPG (Mixture of normal- and iso-Butane and Propane)

- Other alkanes and alkane mixtures

Following from an investigation of the above-mentioned solvents and their estimated ability to fractionate the required paraffins, a selection of the most suitable solvents will be made.

4.2. COMPOSITION OF WAXES

Various references refer to Fisher Tropsch and low molecular weight, high density polyethylene waxes. Yet very little reliable detail regarding the exact composition of a typical wax can be found in the literature.

Mobil Fisher Tropsch wax was approximated as a long chained alkane with 61 carbon atoms by Tsai et al and Huang et al (Tsai et al., 1988),(Huang et al., 1988a). Both approximations were done by calculating the average molecular weight of the wax.

Marano characterised the vapour and liquid streams of the product stream from the Fisher-Tropsch reactor (Marano et al., 1997). It is expected that the liquid fraction of the product stream has a composition similar to that of a Fisher-Tropsch wax due to the fact that at the operating conditions these components are still in the liquid phase. No indication was given as to the fraction that the liquid stream comprises of the total stream.
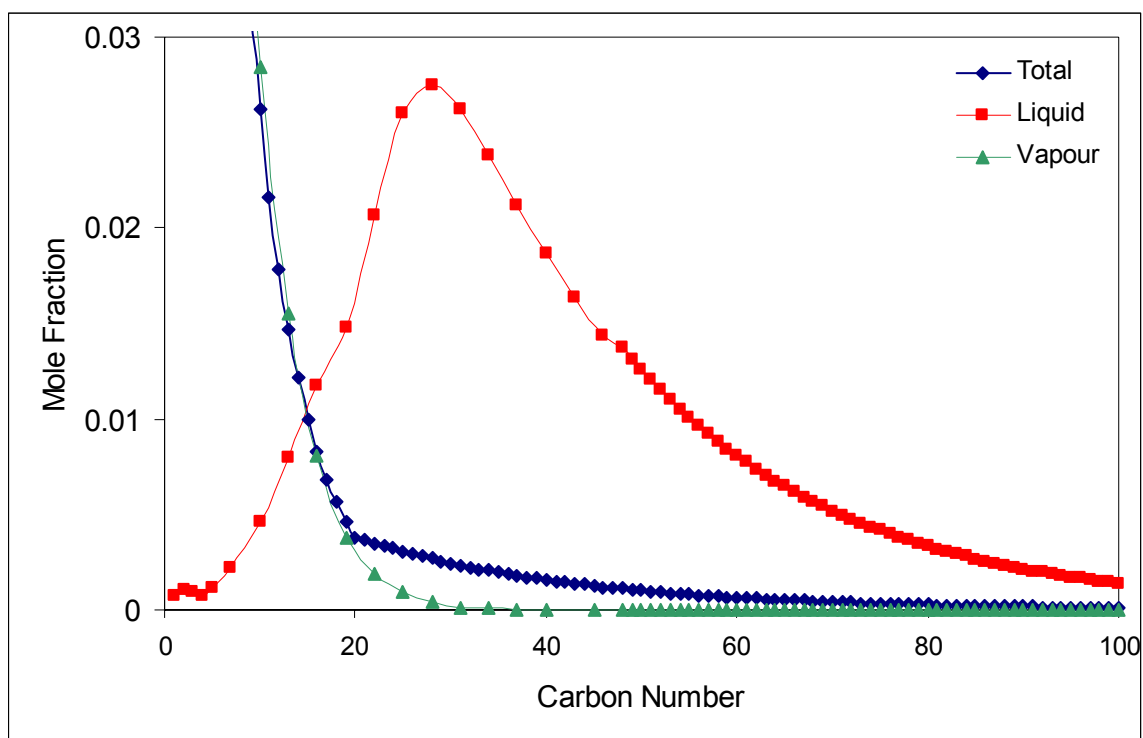
Figure 4-1: Feed, Vapour and Liquid Compositions for the Product Stream from a Fisher-Tropsch Reactor.

Stenger et al published results on the molecular weight distribution of the heavy wax fraction of the Fischer-Tropsch synthesis (Stenger et al., 1984). They found that the liquid phase of the outlet of the Fisher-Tropsch reactors had a peak molecular weight between 22 and 25 carbon atoms. A plot of the weight fraction divided by the carbon number versus the carbon number on a log-linear scale results in a straight-line graph with a negative gradient as seen in Figure 4-2 (Taken from Stenger et al)
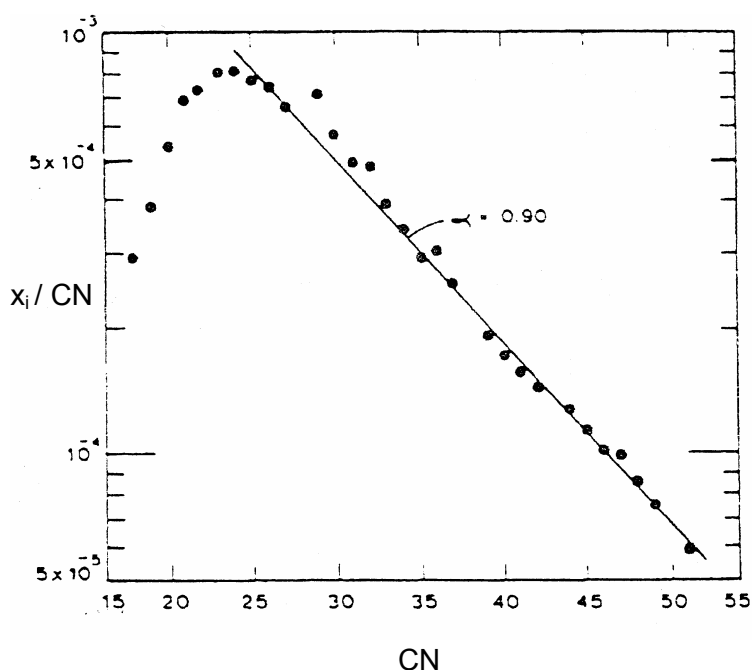
Figure 4-2: Relationship between weight fraction and carbon number (From Stenger et al)

4.3.   LITERATURE DATA

A literature survey was conducted for applicable high-pressure phase-equilibria measurements as well as fractionation and extraction of long chain normal alkanes with various solvents. In addition to alkanes, data of the above-mentioned supercritical solvents with polymers such as polyethylene and wax mixtures are also included. This data will be used for the compilation of trends and will give an idea of the operating temperature and pressure of the proposed process.

A wide range of relevant data sets is available. The data sets have been sorted by the solvent used and are give in Table 4-1 to Table 4-7. Only data for paraffins with 24 or more carbon atoms will be considered. High density polyethylene can also be regarded as a wax as it is almost entirely a saturated linear chain of carbon atoms. For completeness polypropylene will also be included, although polypropylene is a saturated highly branched alkane chain.

Table 4-1: Literature Phase Equilibrium Data with Carbon Dioxide as solvent

Solute	Type of Study	Temperature and Pressure Range	Source
n-C24	VLE – Liquid and vapour side, also densities	Temp: 329.7 – 357.1 K Pres: Up to 300 bar	(du Rand, 2000)
n-C28	Solubility – Liquid Side	Temp: 348.2 – 423.2 K Pres: Up to 96.04 bar	(Gasem et al., 1985)
n-C28	VLE – Liquid and vapour side, also densities	Temp: 338.5 – 366.4 K Pres: Up to 300 bar	(du Rand, 2000)
n-C28	Solubility and VLE - Liquid and Vapour side at 573.45 K	Temp: 373.35 – 573.45 K Pres: Up to 50.61 bar	(Huang et al., 1988b)
n-C28	VLE – Liquid and vapour side (Calculated)	Temp: 397.9 – 519.4 K Pres: 18.67 – 24.95 bar	(Breman et al., 1994)
n-C36	Solubility – Liquid Side	Temp: 373.2 – 423.2 K Pres: Up to 86.32 bar	(Gasem et al., 1985)
n-C36	VLE – Liquid and vapour side, also densities	Temp: 338.5 – 366.4 K Pres: Up to 300 bar	(du Rand, 2000)
n-C28	Solubility – Liquid Side	Temp: 373.2 – 423.2 K Pres: Up to 70.81 bar	(Gasem et al., 1985)
SASOL Wax	Solubility – Liquid Side	Temp: 473 – 573 K Pres: Up to 50 bar	(Chou et al., 1992)
Mobil Fisher-Tropsch Wax	Solubility – Liquid Side	Temp: 200 – 300 $^{\circ}$C Pres: Up to 51 bar	(Tsai et al., 1988)
PE Wax	Fractionation	Temp: 373 K Pres: Up to 415 bar	(Via et al., 1994)

Table 4-2: Literature Phase Equilibrium Data with Methane as solvent

Solute	Type of Study	Temperature and Pressure Range	Source
n-C24	VLE – Liquid and vapour side	Temp: 315 – 450 K Pres: Up to 2000 bar	(Floeter et al., 1997)
n-C28	Solubility and VLE - Liquid and Vapour side at 573.25 K	Temp: 373.25 – 573.25 K Pres: Up to 50.77 bar	(Huang et al., 1988b)
n-C7 to n-C36	Solubility (n-C16 to n-C36 extrapolated) – Vapour Side	Temp: 293.2 – 423.2 K Pres: 120 – 240 bar	(Suleiman et al., 1995a)
Mobil Fisher-Tropsch Wax	Solubility – Liquid Side	Temp: 473 – 573 K Pres: Up to 51 bar	(Tsai et al., 1988)
SASOL Wax	Solubility – Liquid Side	Temp: 473 – 573 K Pres: Up to 50 bar	(Chou et al., 1992)

Table 4-3: Literature Phase Equilibrium Data with Ethane as solvent

Solute	Type of Study	Temperature and Pressure Range	Source
n-C24	VLE – Liquid and vapour side, also densities	Temp: 332.8 – 352.7 K Pres: Up to 145 bar	(du Rand, 2000)
n-C24	Solubility – Vapour Side	Temp: 328.2 – 348.2 K Pres: 80 – 240 bar	(Suleiman et al., 1995b)
n-C25	Solubility – Vapour Side	Temp: 328.2 – 348.2 K Pres: 80 – 240 bar	(Suleiman et al., 1995b)
n-C28	Solubility – Vapour Side	Temp: 333.2 – 348.2 K Pres: 80 – 240 bar	(Suleiman et al., 1995b)

TTable 4-3 continued

Solute	Type of Study	Temperature and Pressure Range	Source
n-C28	VLE – Liquid and vapour side, also densities	Temp: 337.8 – 352.6 K Pres: Up to 165 bar	(du Rand, 2000)
n-C28	Solubility – Liquid Side	Temp: 348.2 – 423.2 K Pres: Up to 37.88 bar	(Gasem et al., 1989a)
n-C28	Solubility and VLE - Liquid and Vapour side at 573.15 K	Temp: 373.25 – 573.15 K Pres: Up to 40.71 bar	(Huang et al., 1988b)
n-C28	VLE – Liquid and Vapour Side	Temp: 424.0 – 518.6 K Pres: 24.66 – 30.67	(Breman et al., 1994)
n-C29	Solubility – Vapour Side	Temp: 333.2 – 348.2 K Pres: 80 – 240 bar	(Suleiman et al., 1995b)
n-C32	Solubility – Vapour Side	Temp: 348.2 K Pres: 80 – 240 bar	(Suleiman et al., 1995b)
n-C33	Solubility – Vapour Side	Temp: 348.2 K Pres: 80 – 240 bar	(Suleiman et al., 1995b)
n-C36	Solubility – Liquid Side	Temp: 348.2 – 423.2 K Pres: Up to 47.60 bar	(Gasem et al., 1989a)
n-C36	Solubility – Vapour Side	Temp: 348.2 K Pres: 80 – 240 bar	(Suleiman et al., 1995b)
n-C44	Solubility – Liquid Side	Temp: 348.2 – 423.2 K Pres: Up to 31.07 bar	(Gasem et al., 1989a)
SASOL Wax	Solubility – Liquid Side	Temp: 473 – 573 K Pres: Up to 40 bar	(Chou et al., 1992)
Mobil Fisher-Tropsch Wax	Solubility – Liquid Side	Temp: 473 – 573 K Pres: Up to 51 bar	(Tsai et al., 1988)

Table 4-4: Literature Phase Equilibrium Data with Propane as solvent

Solute	Type of Study	Temperature and Pressure Range	Source
n-C28	VLE – Vapour and liquid side	Temp: 423.8 – 518.7 K Pres: 4.46 – 6.19 bar	(Breman et al., 1994)
n-C30	VLE – Sub-critical liquid side only, also densities	Temp: 353.0 – 373.2 K Pres: 31.59 – 44.88 bar	(Aalto et al., 1996)
Squalane (C30 isomer)	VLE – Sub-critical liquid side only, also densities	Temp: 353.1 – 373.1 K Pres: 31.55 – 45.09 bar	(Aalto et al., 1996)
n-C34	VLE – Liquid and vapour side	Temp: 350 – 420 K Pres: Up to 100 bar	(Peters et al., 1992)
n-C36	VLE – Sub-critical liquid side only, also densities	Temp: 353.1 – 373.1 K Pres: 31.55 – 45.09 bar	(Aalto et al., 1996)
n-C40	VLE – Vapour side only	Temp: 368 – 433 K Pres: Up to 110 bar	(Chan et al., 2000)
n-C40	VLE – Sub-critical liquid side only, also densities	Temp: 353.0 – 363.0 K Pres: 31.53 – 37.87 bar	(Aalto et al., 1996)
n-C50	VLE – Sub-critical liquid side only, also densities	Temp: 353.0 – 363.1 K Pres: 31.53 – 39.73 bar	(Aalto et al., 1996)
n-C60	VLE – Liquid side only	Temp: 310 – 420 K Pres: Up to 150 bar	(Peters et al., 1993)
Vacuum Gas Oil	VLE – Liquid and vapour side	Temp: 313 – 393 K Pres: Up to 220 bar	(Jennings et al., 1994)
PE Wax	Fractionation	Temp: 373 K Pres: Up to 280 bar	(Via et al., 1994)

Table 4-4 continued

Solute	Type of Study	Temperature and Pressure Range	Source
Poly Ethylene	Isothermal fractionation	Temp: 423 K Pressure not stated	(Britto et al., 1999)
Poly Ethylene	Isobaric fractionation	Temp: 358 – 433 K	(Britto et al., 1999)

		Pressure not stated	
Poly Propylene	VLE – Liquid and vapour side	Temp: 368 – 406 K Pres: 190 – 265 bar	(Vladimir Oliviera et al., 2000)

Table 4-5: Literature Phase Equilibrium Data with Butane as solvent

Solute	Type of Study	Temperature and Pressure Range	Source
n-C44	VLE – Vapour and liquid side, also densities	Temp: 443.15 – 453.15 K Pres: Up to 80bar	(Nieuwoudt, 1994)
n-C54	VLE – Vapour and liquid side, also densities	Temp: 443.15 – 453.15 K Pres: Up to 80bar	(Nieuwoudt, 1994)
n-C60	VLE – Vapour and liquid side, also densities	Temp: 443.15 – 453.15 K Pres: Up to 87 bar	(Nieuwoudt, 1996)
Vacuum Gas Oil	VLE – Vapour and liquid side	Temp: 333 – 433 K Pres: Up to 100 bar	(Jennings et al., 1994)
Poly Propylene	VLLE – Liquid and vapour side	Temp: 358 – 423 K Pres: 12 – 115 bar	(Vladimir Oliviera et al., 2000)

Table 4-6: Literature Phase Equilibrium Data with Hexane as solvent

Solute	Type of Study	Temperature and Pressure Range	Source
n-C24	VLE – Liquid and vapour side	Temp: 473.0 – 622.9 K Pres: Up to 52 bar	(Joyce et al., 2000)
n-C28	VLE – Liquid and vapour side (calculated)	Temp: 372.4 – 518.6 K Pres: 0.28 – 1.62 bar	(Breman et al., 1994)
n-C36	VLE – Liquid and vapour side	Temp: 521.7 – 621.8 K Pres: Up to 65 bar	(Joyce et al., 2000)

Table 4-7: Literature Phase Equilibrium Data with Other Solvents

Solvents	Solute	Type of Study	Temperature and Pressure Range	Source
LPG	n-C54	VLE – Vapour and liquid side and densities	Temp: 354 – 393 K Pres: Up to 120 bar	(Nieuwoudt, 2001)
LPG	n-C60	VLE – Vapour and liquid side, also densities	Temp: 413 – 453 K Pres: Up to 87 bar	(Nieuwoudt, 1994)
CO, H_2 and CO-H_2 Mixtures	n-C20, n-C28, n-C36, and Fisher Tropsch Wax	Solubility – Liquid Side	Temp: 373 – 573 K Pres: Up to 50 bar	(Huang et al., 1988a)
Propane and CO_2	PE Wax	Fractionation	Temp: 373 K Pres: Up to 430 bar	(Via et al., 1994)

4.4. EVALUATION OF LITERATURE DATA

From the literature survey it is evident that for most of the data sets not enough data is available for design purposes. Especially in the category of vapour-liquid phase equilibrium data, it can be seen that more data is required. Phase equilibrium data will thus have to be measured for the solvent of choice.

The experimental data cited above will now be evaluated critically to choose a solvent.

4.4.1. CARBON DIOXIDE

A large amount of the data cited above is solubility data where the solubility of the supercritical fluid in the alkane is investigated. Although this data is useful, in most sets only the liquid phase was analysed or it was assumed that the paraffin does not dissolve in the supercritical solvent. Additionally, the pressures used here are very low and can generally not be used in supercritical extraction processes.

Du Rand measured phase equilibrium data for carbon dioxide and normal alkanes with up to 36 carbon atoms (du Rand, 2000). The data is consistent with the literature and can be used for design purposes in the range of measurement (du Rand et al., 2001). When considering the temperature and the pressure of operation used here, it can be seen that carbon dioxide may not be a very good solvent. This can be justified by the data

generated by du Rand is plotted in Figure 4-3. As seen, the solubility of the various components in the vapour phase does not differ significantly.
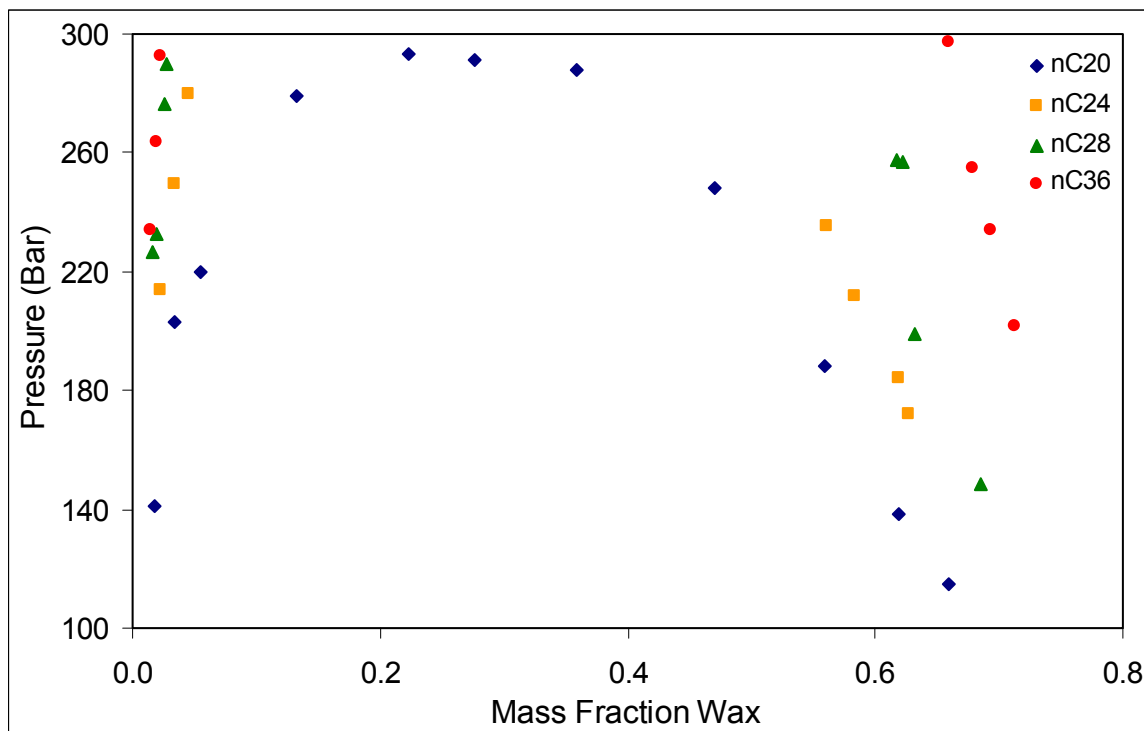
Figure 4-3: Effect of Molecular Weight by Comparison of Phase Boundaries of n-alkanes in Carbon Dioxide at 74.9°C (du Rand, 2000)

As can be seen above, an increase in the molecular weight of the wax, leads to a dramatic increase in the phase transition pressure. The phase transition pressure has been increased to such an extent that the higher carbon number curves may not even close. Considering the fact that the heavier alkanes used in the study of du Rand are the lighter alkanes to be used in this study, it can be expected that the phase transition pressures will be even higher. Additionally, the temperatures used by Du Rand are lower than the melting point of some of the alkanes to be in this study. This will result in an additional increase in phase transition pressure.

4.4.2. METHANE

Considerably less data, especially useful data, is available where methane is the solvent. A single set of vapour-liquid equilibrium data is available while the remaining data is either solubility data at relatively low pressures or data generated by means of extrapolation. From the data it can be seen that the operating pressures required are high due to the fact that there is such large difference in the molar mass of the solvent and the solute, and the fact that operation occurs well away from the critical temperature of the solvent.

4.4.3. ETHANE

A relatively large amount of data is available for the phase equilibria between ethane and normal alkanes. Du Rand measured phase equilibrium data (du Rand, 2000) and compared the measured values to data found in the literature (du Rand et al., 2001). The data measured by du Rand compares well to most sets in the literature and can thus be regarded as of good quality. Some of the data measured by du Rand is given in Figure 4-4:
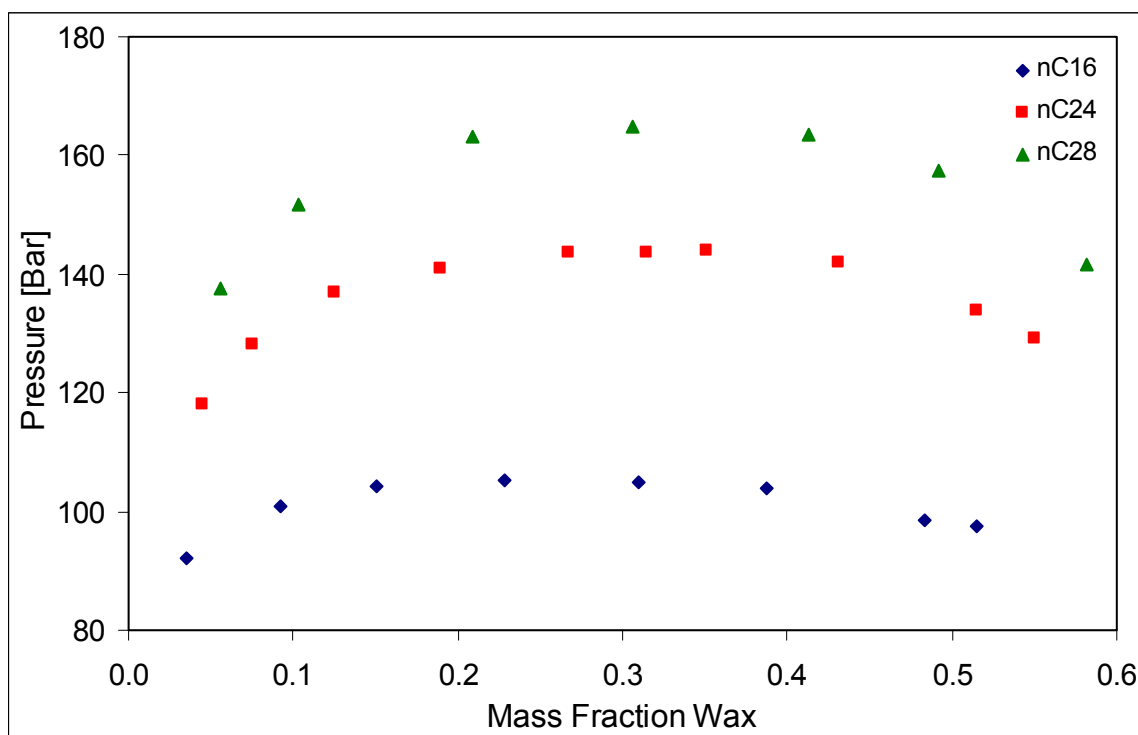
Figure 4-4: Effect of Molecular Weight by Comparison of Phase Boundaries of n-alkanes in Ethane at 79.6^{o}C (du Rand, 2000)

The above data indicates that phase equilibrium boundary curves may close for higher alkanes yet indicated that the pressures required may exceed 200 bar. Peters et al published phase equilibrium data for ethane and docosane (Peters et al., 1988b). Unfortunately a direct comparison with data measured by du Rand can not be made due to the fact that the measurements made by Peters et al are at larger mass fractions than those measured by du Rand, and in the region where the mass fractions do overlap, the temperature ranges differ (du Rand, 2000).

When considering the various data sets available, it can be seen that once again most of the data falls out of the range of alkanes to be used in this work. The data sets where the alkanes are applicable are mostly out of the temperature or pressure range and can thus not be directly used for design purposes.

4.4.4. PROPANE

For propane as solvent it is evident that very little relevant data is available. Most of the data available is for sub-critical propane and thus not in the temperature and pressure range applicable to this study.

Yet, three data sets exist in the temperature range just above the melting point of the paraffins. A comparison of the n-C34, n-C40 and n-C60 literature data is shown in Figure 4-5. The data given for these data sets is not isothermal data but over a limited temperature range, the pressure and temperature have a linear relationship. This linear relationship is used for the temperature corrections in the data and a detailed description of the method used can be found in paragraph 6.1.1. A comparison of the propane vapour liquid data available is given in Figure 4-5:
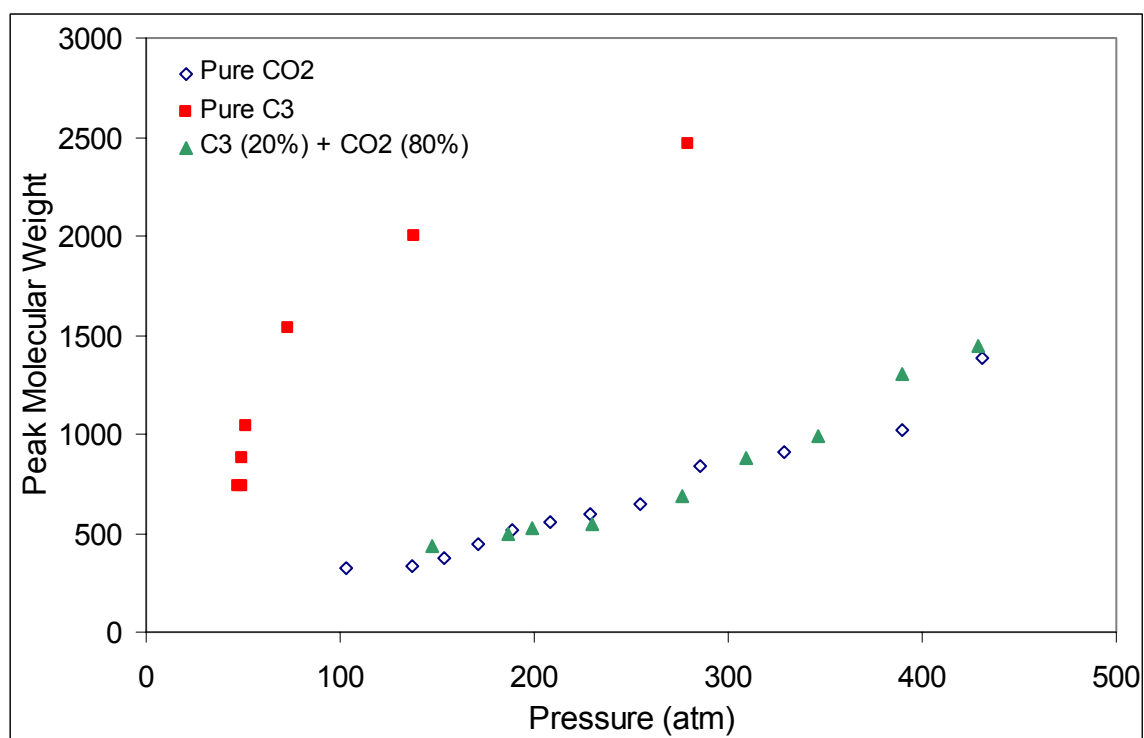
Figure 4-5: Effect of Molecular Weight by Comparison of Phase Boundaries of n-alkanes in Propane at 393.15 K (Chan et al., 2000), (Peters et al., 1992), (Peters et al., 1993)

The importance of these plots at this point in the study does not lie so much in the exact location of the phase equilibrium boundary but rather, by means of extrapolation, the magnitude of the expected pressure. From the above data it can be seen that for 393.15 K the maximum pressure for the system propane-nC60 should not exceed 130 bar. In the same manner, it can be estimated that the maximum pressure for 408.15 K should not exceed 150 bar. It can thus be seen that the phase equilibrium pressure is considerably less than required for ethane. Additionally, these plots show that significant amounts of high molecular weight material can be dissolved in the vapour phase.

4.4.5. BUTANE

Various studies by Nieuwoudt were conducted to investigate the phase equilibrium of normal alkanes with butane. The results show similar patterns to that of ethane and propane, yet the pressure is lower due to better solubility of the alkane in the solvent, while the temperature is higher due to a higher critical temperature of the solvent.

However, the butane will be a less selective solvent than propane as the mixture critical point will be at a lower mass fraction. Additionally the temperature of the system will be higher and thus increase the utility costs and the risk of thermal degradation. Although butane is a gas at environmental conditions, traces of the solvent may remain in the paraffins due to the higher boiling point in comparison to to propane.

4.4.6. HEXANE

Data available for hexane is scarce and currently limited to two sets. It can be seen that the operating pressure is a lot lower at the cost of a higher operating temperature. As in the case of butane, hexane will be even less selective, have even higher temperatures of operation and the risk of a significant solvent residue is high.

4.4.7. OTHER SOLVENTS AND SOLVENT MIXTURES

Various mixtures of solvents have been investigated. LPG shows similar results to propane and butane, depending on the composition of the gas.

4.5. COMPARISON OF SOLVENTS

To be able to select a suitable solvent, various solvents need to be compared. Due to the fact that the range of operation is usually just above the critical temperature of the solvent, a comparison at the same reduced temperatures will be done.

A direct comparison of the effect of solvents for tetracosane will be done by comparing the phase behaviour of carbon dioxide, ethane and methane, as shown in Figure 4-6.
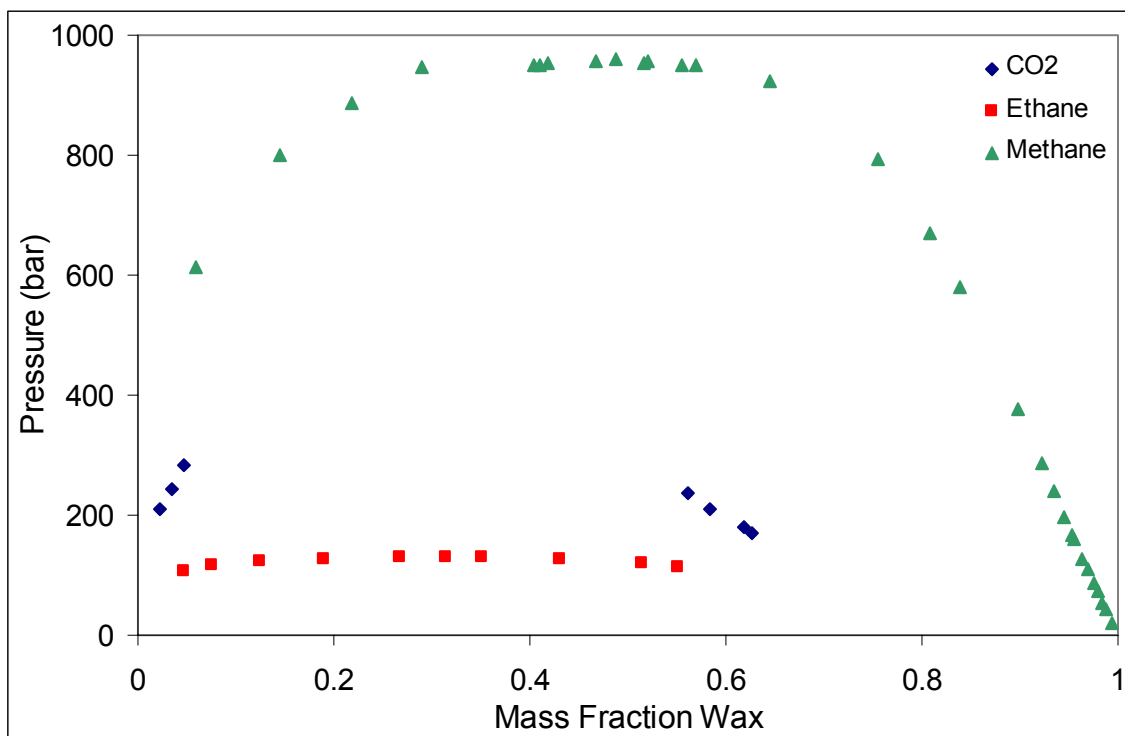
Figure 4-6: Effect of Solvent by Comparison of Tetracosane phase equilibria for carbon dioxide (du Rand, 2000), methane (Floeter et al., 1997) and ethane (du Rand, 2000) at 70.5 °C.

In the Figure 4-6 it can be seen that the methane phase equilibrium pressures are very high. These can be attributed to two factors: Firstly, the reduced temperature of the methane is a lot higher and secondly, the ethane and carbon dioxide are much better solvents.

The second comparison of the solubility of tetracosane in supercritical solvents will be done at a reduced temperature of 1.1 comparing carbon dioxide, ethane and hexane as shown in Figure 4-7.

In Figure 4-7 it can be seen that the hexane is a much better solvent than ethane or carbon dioxide but it must be remembered that the operating temperature of the hexane system is a lot higher (approximately 558 K). The higher operating temperature may result in decomposition of the wax. Additionally, larger energy inputs may be required.
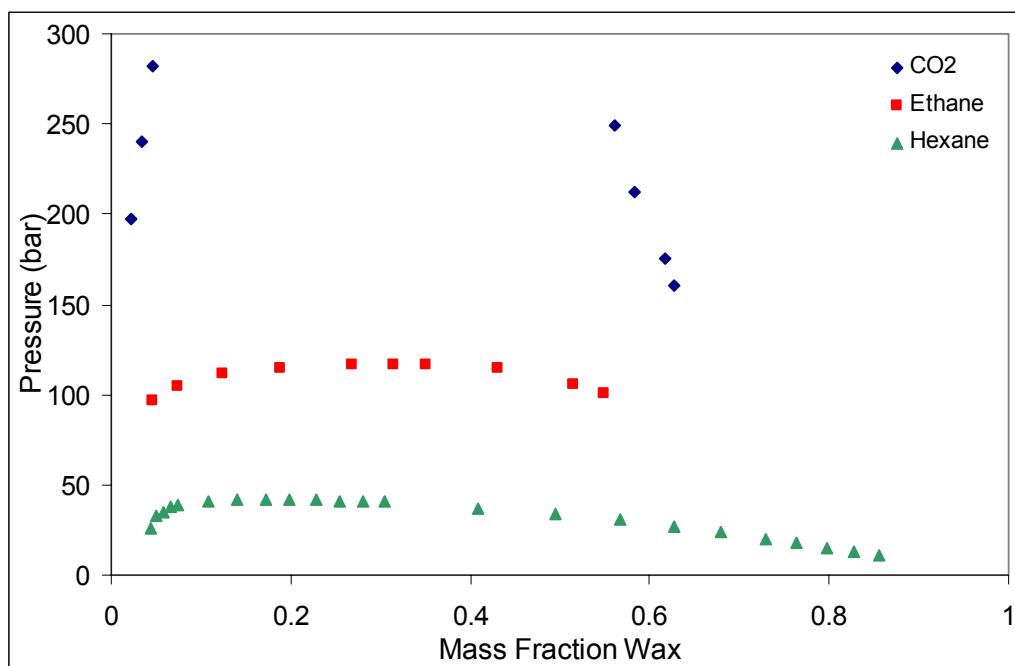
Figure 4-7: Effect of Solvent by Comparison of Tetracosane phase equilibria for carbon dioxide (du Rand, 2000), ethane (du Rand, 2000) and hexane (Joyce et al., 2000) at a reduced temperature of 1.1.

Via et al. fractionated low molecular weight, high density polyethylene (Via et al., 1994). A comparison of propane, carbon dioxide and a mixture of the two gases were done and the results are displayed in Figure 4-8:
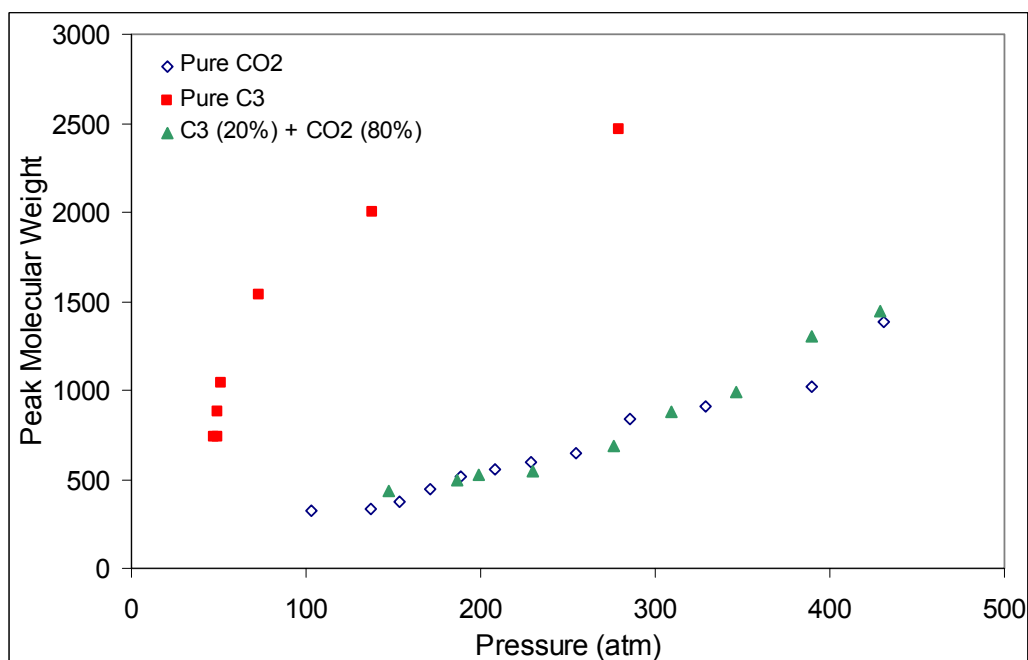
Figure 4-8: Comparison peak molecular weights of extract with propane, propane modified carbon dioxide and carbon dioxide as solvents for the fractionation of low molecular weight, high density polyethylene wax (T = 373.15 K)

Table 4-8: Total recovery of polyethylene for the three solvents used

Solvent	Total Recovery
Carbon Dioxide	30 %
Propane	96 %
Carbon Dioxide (80%) and Propane (20%)	54 %

From Figure 4-8 it can be seen that propane had the ability to dissolve material of higher molecular weight. Carbon dioxide and the propane-modified carbon dioxide will require more solvent to dissolve the wax due to a lower solubility of the extract in the solvent.

For the purpose of this project the above data is significant due the difference in the pressures required for the extraction of the various fractions and the interaction of the various solvents.

4.6.   SOLVENT SELECTION

When considering a solvent, the operating temperature and pressure as well as the solvating ability of the solvent needs to be determined.

When considering the operating temperature, the limits of operation are set by the critical temperature of the solvent and the decomposition and melting temperatures of the solute. When considering supercritical extraction, the most effective region for extraction is just above the critical temperature. In this region the density of the supercritical fluid changes significantly with a small change in pressure. Due to the density changes, the solubility of the paraffin in the solvent can be manipulated with ease. The operating temperature therefore needs to be a few degrees above the critical temperature of the solvent, yet low enough so that decomposition does not occur.

In Table 4-9 the critical temperature and pressure of the solvents suggested are given:

Considering the various solvents, carbon dioxide should not be favoured as high solubilities will not be achieved, not even at pressures around 350 bar.

When considering the critical temperature of the solvent, together with the fact that extraction from a liquid phase is favoured and the fact that the operating temperature should be just above the critical temperature of the solvent, methane and ethane are not recommended. The melting points of the waxes are well above the critical temperature of the solvents.

Table 4-9: Critical Properties of Solvents

Solvent	Critical Temperature (^{o}C)	Critical Pressure (bar)
Carbon Dioxide	31.0	73.8
Methane	-82.7	46.0
Ethane	31.4	48.8
Propane	96.7	42.5
n-Butane	152.1	38.0
iso-Butane	135.1	36.5
LPG	96.7 < T_c < 152.1 [*]	42.5 < P_c < 36.5 [*]
n-Hexane	234.4	30.1

[*] Exact values depend on composition of LPG

On the other end of the paraffin spectrum, hexane has the advantage that the operating pressure will be low, yet the temperature is higher. The higher temperature and energy costs as well as the possibility of thermal decomposition and the fact that hexane is a liquid at ambient conditions, thus possibly resulting in a liquid residue in the final product, leads to the elimination of hexane as a suitable solvent.

By elimination, propane, butane, iso-butane and LPG remain. All four of these solvents are suitable. When considering the operating temperatures, propane will have the lowest operating temperatures. Propane has the advantage that just above the critical point of the solvent, the waxes will be in the molten state, just above their solidification temperature.

By selecting propane as the optimal solvent, the operation will be conducted at the lowest possible temperature near the critical point of the solvent. A propane rich LPG will be considered as an industrial alternative but will not be investigated extensively.

4.7.   CONCLUSIONS

The following conclusion can thus be made:

- By a process of elimination and selection according to the solubility and critical parameters, propane and a propane rich LPG are selected as possible solvents for this process.

- A literature survey revealed that data for propane and paraffins are scarce and incomplete. Phase equilibrium measurements are thus required.

5. EXPERIMENTAL DESIGN, SETUP AND PROCEDURE

From the experimental data available it can be seen that a demand exists for reliable data for the supercritical fractionation of waxes. The purpose of the experiments is thus to generate the data required for the process design of the fractionation of hard or synthetic waxes with supercritical propane.

Before highly complex multiphase data can be generated, binary data of propane and the various paraffins is required. A two-component system was thus used and according to the phase rule (see paragraph 3.1), by measuring the temperature and the pressure as well as the specific volume at a known composition, the system is fully defined. No analytical work is therefore required.

The experimental set-up and the operating procedure will follow a brief discussion of current measurement techniques and equipment described in the literature.

5.1. MEASUREMENT TECHNIQUES

High pressure phase equilibrium measurement techniques can either be dynamic or static. In a dynamic technique the solute is continuously swept with the supercritical fluid while in static measurement techniques the solute and solvent are loaded together in a high-pressure cell. While static methods are favoured to obtain P-T-x data, dynamic methods are used to determine the solubility of solids in a supercritical fluid and for stripping measurements.

The two measurement techniques will be discussed briefly and the advantages and disadvantages of each will be listed. For more information, the reader is referred to Dohrn et al and Fornari et al who published review articles on experimental methods and the type of systems investigated in high-pressure fluid phase equilibria. Detailed explanations of the various techniques used are given. The surveys include reference to high-pressure phase equilibrium measurements for publications from 1978 to 1987 (Fornari et al., 1990) and 1988 to 1993 (Dohrn et al., 1995) respectively. For each of the systems investigated, the type of measurement technique used is stated.

5.1.1. DYNAMIC MEASUREMENT

A simple, yet typical, dynamic flow apparatus is shown in Figure 5-1:
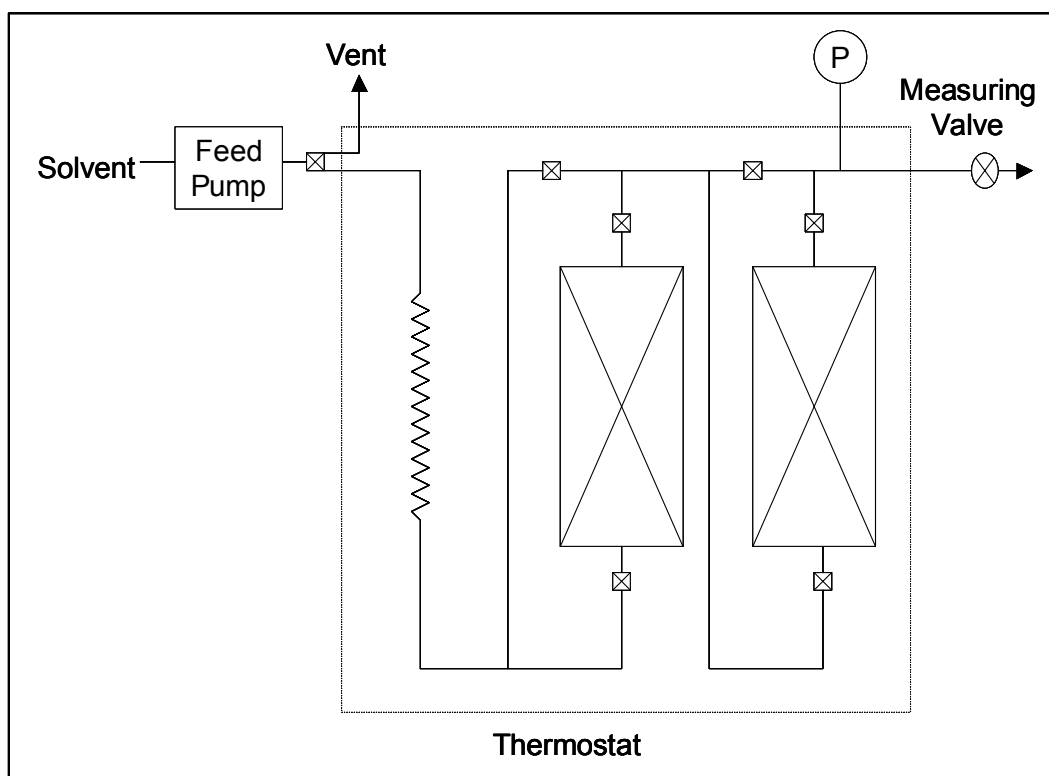
Figure 5-1: Schematic Representation of a Typical Simple Dynamic Flow Apparatus (McHugh et al., 1994)

For this type of system the supercritical fluid is introduced into the system with a high-pressure pump. After exiting the pump, the supercritical fluid is preheated in either a heating coil or a preheating column within the constant temperature bath. The supercritical fluid is then fed to the column that is packed with the non-volatile solute, either in the liquid or the solid phase. After the supercritical fluid, rich in solute, exits the column, it is expanded to atmospheric pressure where the non-volatile component precipitates.

This type of system has the following advantages:

- Reasonably large amounts of data can be collected quickly.

- Equilibrium, stripping or fractionation data can be obtained.

- The sampling procedure may be simple.

This type of system has the following disadvantages:

- Phase inversion can occur resulting in the liquid phase being pushed out of the column.

- Undetected phase changes can occur such a solid to liquid, and liquid to two liquid phases.

- Only the lighter phase can be sampled.

- Entrainment of the liquid phase may occur at high flow rates.

- Heavy solid or liquids can clog the metering valve.

- Multi-component solutes may give problems due to depletion of one or more of the components.

- Attaining true equilibrium may be problematic with this type of equipment.

- Densities cannot easily be measured.

An alternative to the above set-up can be seen in Figure 5-2:
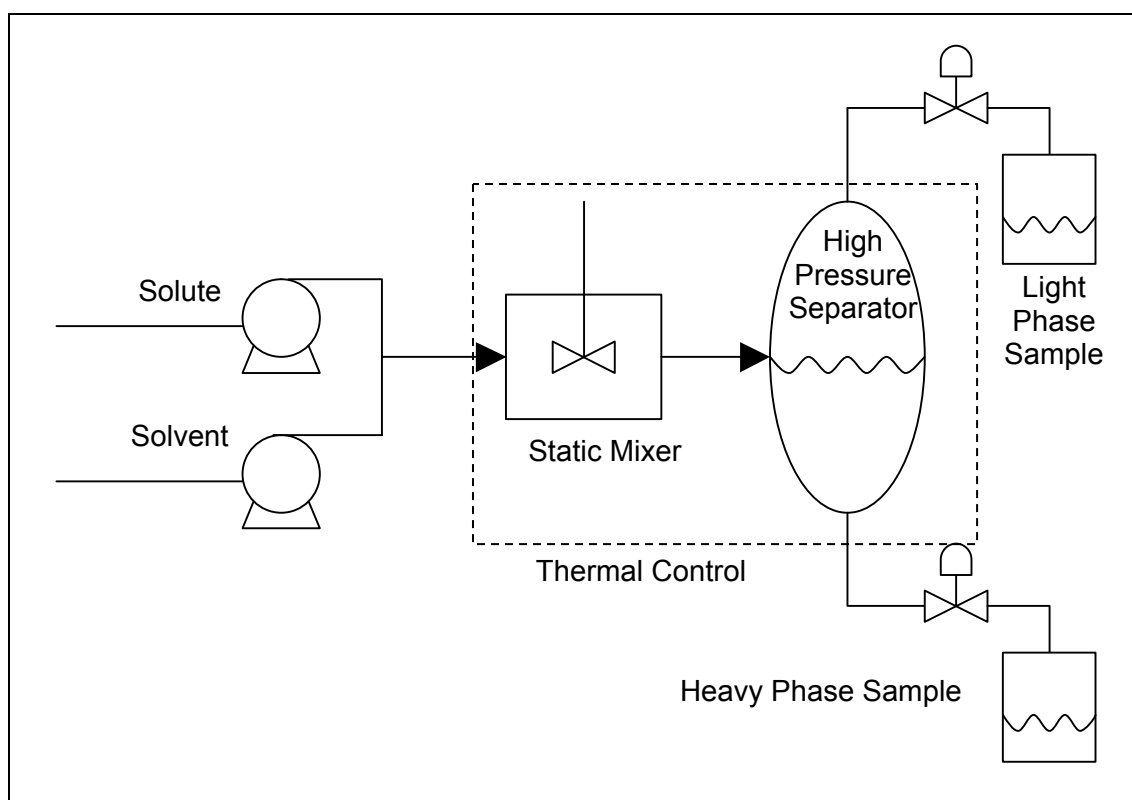
Figure 5-2: Alternative Continuous Flow Apparatus (McHugh et al., 1994)

This type of apparatus can be used for multi-component mixtures as well as mixtures where both phases need to be analysed.

5.1.2. STATIC MEASUREMENT

A typical static measurement device can be seen as a piston-and-cylinder set-up where the volume of the cell can be varied. A typical static view can be seen in Figure 5-3:
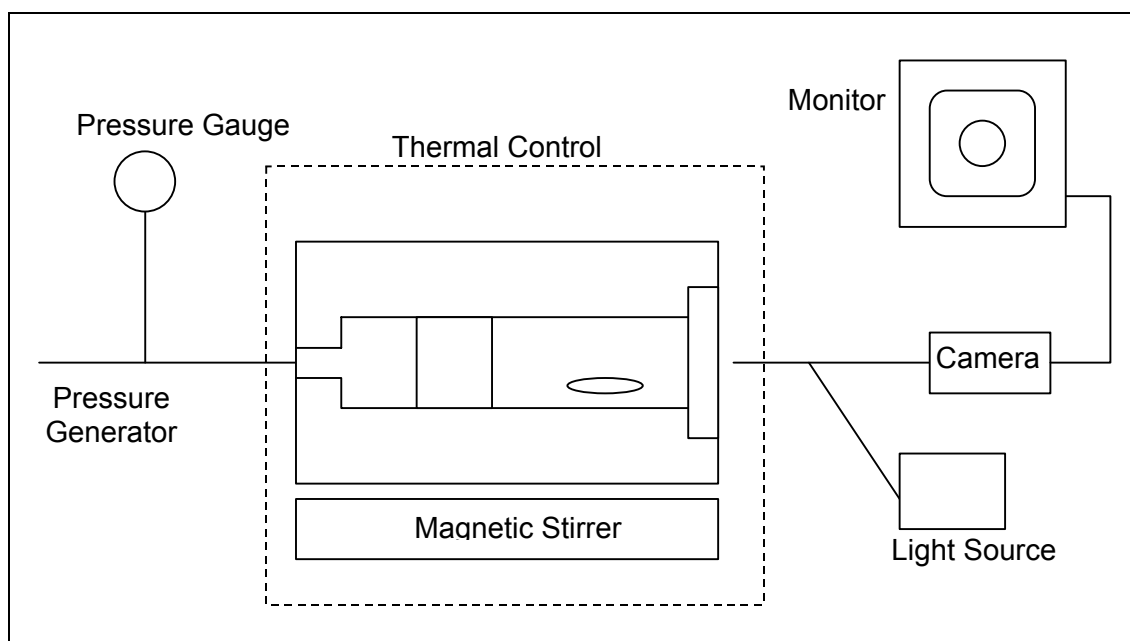
Figure 5-3: Typical Static View System (McHugh et al., 1994)

The cell is initially loaded with a measured amount of solute and purged numerous times with the supercritical solvent to remove any air. The cell is heated to a set temperature and the contents compressed into the single phase region. The pressure is slowly decreased in small increments, leaving time for equilibrium to be attained. This is done until a second phase appears. A typical measurement technique is to project the image onto a television screen with a borescope. Typically, the pressure is measured from the outer piston pressure and calculated via the area ratio of the piston. Previous applications of this type of variable volume cell include studies by Li et al and Chan et al. (Li et al., 1981), (Chan et al., 2000)

This type of set-up has the following advantages:

- The phase transitions are observed visually and phase inversions can easily be detected.

- Solubilities of binary mixtures are obtained easily without sampling.

- Only a small amount of heavy components is used in a single experiment.

- Multi-component mixtures can be measured and samples can be drawn.

- Densities can be calculated from the cell volume.

- At a constant composition, the pressure and temperature can be varied without unloading the cell.

The main disadvantages of this type of system are:

- Stripping or fractionation data is not obtained

- Only one very small sample can be obtained per loading

- The set-up used in Figure 5-3 has an indirect method for pressure measurement. This may result in inaccuracies in the pressure measurement due to friction losses and inertia of the system.

5.2. PREVIOUS EXPERIMENTAL PROCEDURES FOR HIGH PRESSURE VAPOUR-LIQUID-EQUILIBRIUM MEASUREMENT

Before the cell was designed, a study was done regarding the type of equipment previously used on similar or the same type of systems. The advantages and disadvantages of each piece of equipment are listed so as to incorporate these in the cell designed for this project.

5.2.1. HIGH PRESSURE CAILLETET EQUIPMENT

This apparatus was used by Peters et as well as Gregorowicz et al. to determine the phase equilibrium of propane-hexacontane , propane-tetratriacontane and propane-eicosane al (Peters et al., 1987a), (Peters et al., 1992), (Peters et al., 1993), (Gregorowicz et al., 1992). This apparatus can be used for pressures up to 15 MPa (150 bar) and temperatures between 250K and 450K.

Description of Apparatus

This apparatus consists of a Pyrex tube of about 500 mm and an inner and outer diameter of 3 and 10 mm respectively. The one end of the tube is closed, the other open. Mercury is used as a sealing agent on the open end and also functions as a pressure-transmitting fluid.

A detailed schematic representation and description is given in Peters et al (Peters et al., 1993).

Advantages

- The phase transitions can be observed visually, which at this point is still the most accurate method for determining the phase transition.

Disadvantages

- The volume of the cell is very small, therefore introducing the possibility of inaccuracies in the mass fraction determination.

- No direct inlet and outlet valve is present therefore possibly resulting in a tedious washing and cleaning process.

- Peters et al. only used this type of equipment to 140 bar and higher pressures may be required for the data to be measured in this work (Peters et al., 1987a) (Peters et al., 1992) (Peters et al., 1993).

5.2.2. APPARATUS USED BY DIMITRELIS ET AL.

Dimitrelis et al used a packed bed system for their equilibrium measurements. A schematic representation is given by Dimitrelis et al. (Dimitrelis et al., 1989).

Experimental Procedure

Here high-pressure propane is passed through a packed bed containing the hydrocarbons. The propane and the hydrocarbons reach equilibrium and the resultant saturated fluid is analysed. The pressure of the equipment and the temperature at absorption can be regulated.

Disadvantages

Obvious disadvantages include the fact that extreme care needs to be taken to prevent condensation of the saturated fluid, it is often difficult to attain equilibrium, phase inversions may not be measured and a large amount of wax and solvent may be required for this type of set-up.

5.2.3. APPARATUS USED BY CHAN ET AL.

Chan et al used a high-pressure cell to measure phase transitions. The apparatus is similar to the one illustrated in Figure 5-3 (Chan et al., 2000).

Although the solid-liquid transition as well as the spinodal pressure is also measured in this equipment, it will not be discussed here as this project entails the measurement of liquid-fluid phase equilibrium.

Experimental Procedure and Phase Transition Measurement

A know amount of solvent and solute is loaded into the cell. The cell is compressed, heated and mixed to become homogenous. The pressure is controlled with a floating piston.

The phase transition is measured by measuring the intensity of light transmitted as a function of pressure at constant temperature. As the phase transition is reached, the solution becomes cloudy and this transition can be measured. Figure 5-4 (Chan et al., 2000) gives a schematic representation of the measurement of the phase transition.
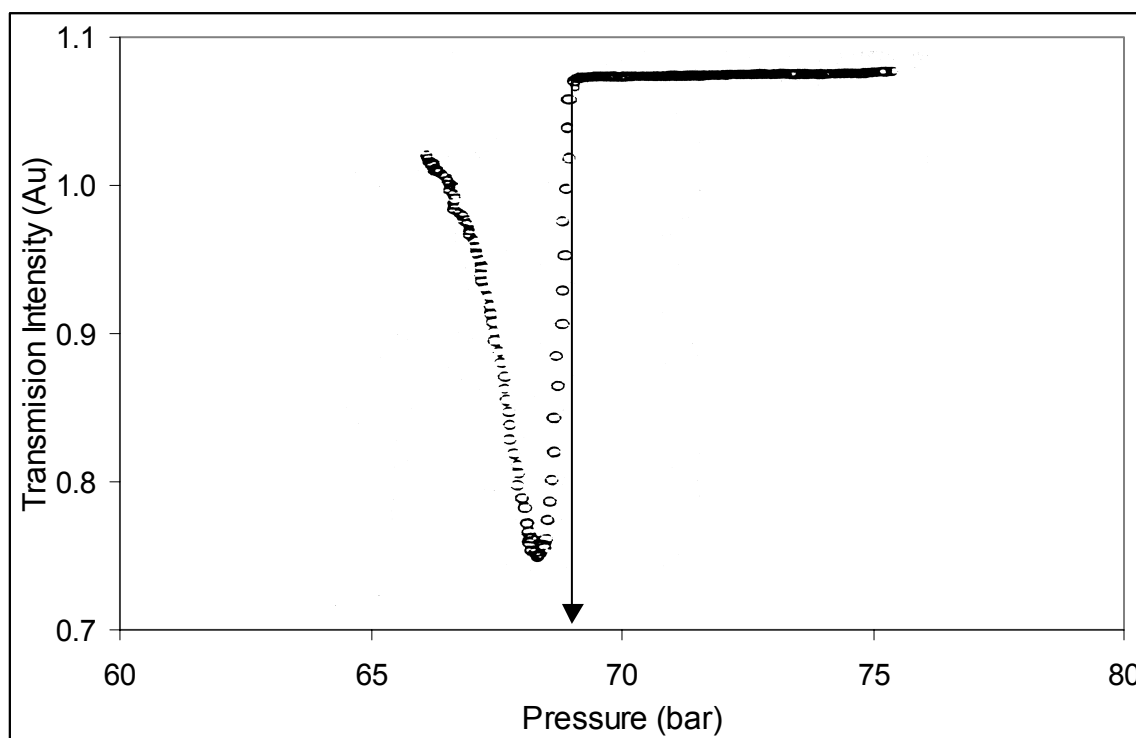
Figure 5-4: Plot of transmitted intensity as a function of pressure for the determination of the fluid-liquid phase transition pressure. From Chan et al. (Chan et al., 2000) measured for propane-tetracontane at X = 0.079, T = 110ºC.

In Figure 5-4 the transition point is measured as follows: The pressure is lowered from the one phase region to the two-phase region and the light intensity is measured. The phase transition is the pressure where the light intensity starts to change. For the above point the phase transition was measured at a pressure of 69 bar. No indication is given if the pressure is increased to determine if the same answer is obtained. The systems may display meta-stability if this is not done and the results may thus be inaccurate.

Advantages

- The equipment is simple in design.

- The fluid mixture is mixed well with the aid of a magnetic stirrer.

Disadvantages

- From the set-up, as shown above, it is not clear if the temperature is measured directly or indirectly. It is essential to measure the temperature directly in the cell.

- In the set-up used here, the pressure is measured indirectly, resulting in errors due to inertia and friction.

- Although this method of measurement of the phase transition can be used, it does contain flaws. Often the first sign of two phases is just a small vapour-bubble or liquid

drop. Even with rigorous stirring, the light sensor may not detect these and the phase transition pressure may be recorded lower than in reality. In addition, near the mixture critical point it may occur that the refractive index in the two phases is very close or even the same, therefore allowing very little change in the light intensity. In addition, this equipment may become costly.

5.2.4. APPARATUS USED BY NIEUWOUDT

Nieuwoudt used a variable volume static cell constructed by Sitec-Sieber AG. The pressure in the cell was controlled by a counter balance piston thus changing the volume of the cell while the temperature was regulated with heating elements. A schematic representation of the cell is given by Nieuwoudt. (Nieuwoudt, 1996)

Advantages

- The pressure is measured directly.

- Due to the small volume of the cell, phase equilibria can be measured for systems where one component is expensive. This can be accomplished due to the fact that very little material is required.

- A visual method for phase transition determination is used.

- Densities can be measured.

Disadvantages

- The window of the cell was placed in a position where the entire cell contents was not visible.

- There were small stagnant zones in the cell.

- The electrical elements used may have caused temperature gradients.

5.3.   EQUIPMENT AND SETUP

A high pressure vapour liquid equilibrium cell with a variable volume is required for the experiments. The reason for selecting this type of apparatus is given below.

5.3.1. DESIGN DECISIONS

To be able to construct the optimal equipment for the phase measurements required, design decisions had to be made. These were primarily based on previous experimental set-ups and the applicability to this system. The main decisions are discussed below:

Type of High Pressure Cell

Although the dynamic type of set-up has advantages, a static cell set-up will be used here. This decision is based on the following reasons:

- Only a small amount of the very expensive pure paraffins is required for the static cell. For the purpose of this project, this is probably the most important factor favouring the static cell.

- In the dynamic set-up the phases need to be sampled. This may result in problems due to the fact that at ambient temperatures the one component is a vapour and the other a solid. Additionally, traditional analytical methods cannot be used due to the fact that the waxes have such a high boiling point.

- In a dynamic cell often only one of the two phases in equilibrium can be measured. On the other hand, a static cell may allow the measurement of both the liquid and the vapour phase through the manipulation of the concentration in the cell.

- In a dynamic set-up with all the piping concerned, solidification of the wax may occur, resulting in problems. These problems can be avoided in the static set-up.

- Phase inversions can be detected in the static cell provided a window is used.

- Densities are easily measured in a static cell.

Temperature and Pressure Measurement

Although previous set-ups have used indirect pressure measurement, direct pressure and temperature measurement will be used here. Indirect temperature measurement may not take heat losses and environmental conditions into account. Indirect pressure measurement results in incorrect measurements due to friction on the piston and inertia of the system. This has been observed experimentally in this work. By changing he pressure of the pressurising gas slightly, no change in the pressure in the cell was measured.

Phase Transition Measurement

Three main methods can be used for phase transition measurement:

- Light intensity measurement

- Density measurement

- Visual method

Light intensity measurement was discussed above and although the method has its merits, the equipment is expensive and inaccuracies may occur. This method will therefore not be used.

An alternative method for phase transition measurement is to measure the density changes with pressure changes. This method of phase transition works on the principle of a compressibility difference between the liquid and the vapour phase. The density versus pressure line in the two-phase region will have a different slope than in the one phase region.

As the density is measured with the piston position, the piston position can be used to determine the phase transition. An arbitrary selection of 36 phase transition points were chosen to test the validity of this method. These points represent the entire temperature range and are from both the liquid and the vapour side. In Figure 5-5 a typical diagram for the phase transition detection by density can be seen. Complete data can be seen in Appendix E.3.
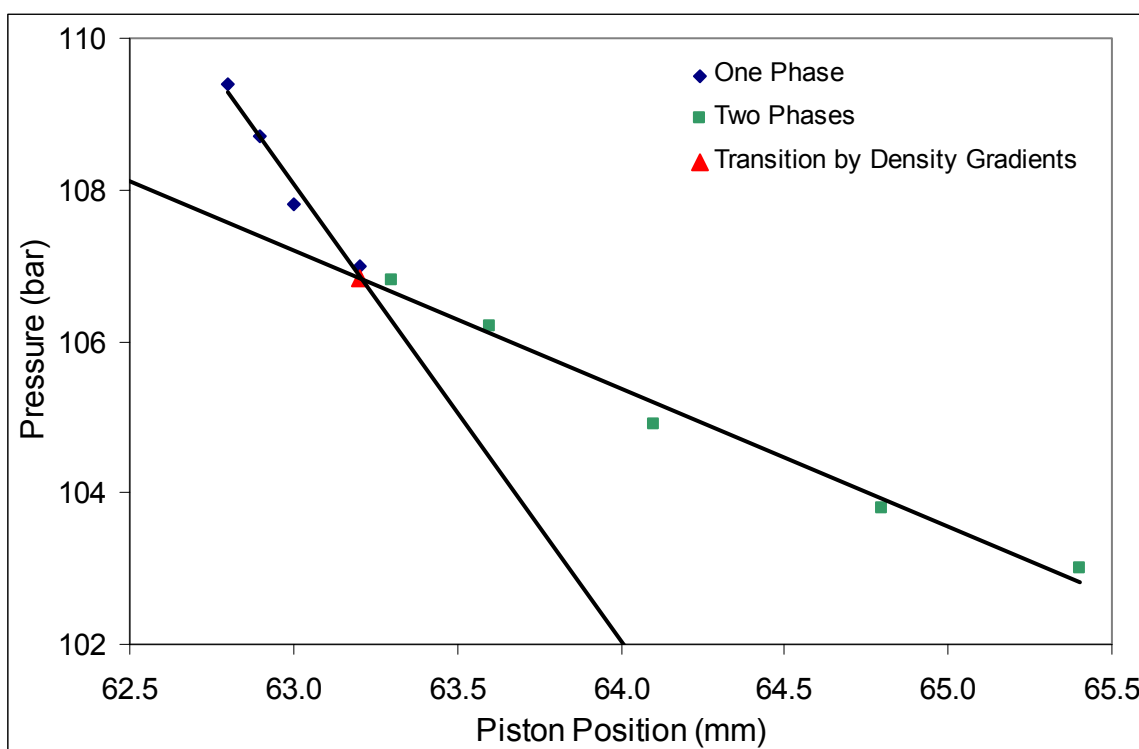
Figure 5-5: Representative Diagram of Phase Transition Detection by Density Measurement for C3-C40 at x = 0.309 and 407.15 K

For the composition and temperature shown in Figure 5-5, the gradients differ significantly and therefore the phase transition point can be determined with ease using this method. The measured transition point at the highest pressure where two phases are in equilibrium and the transition point measured from density changes differ within the accuracy of the measurements.

However, close to the critical composition where the densities and compressibilities of the liquid and the vapour phase are very close, phase transition measurement with this method is difficult. This is illustrated in Figure 5-6 and it can be seen that here this method would result in difficulties in the detection of the phase transition point, especially if the user had no idea where the transition point was.
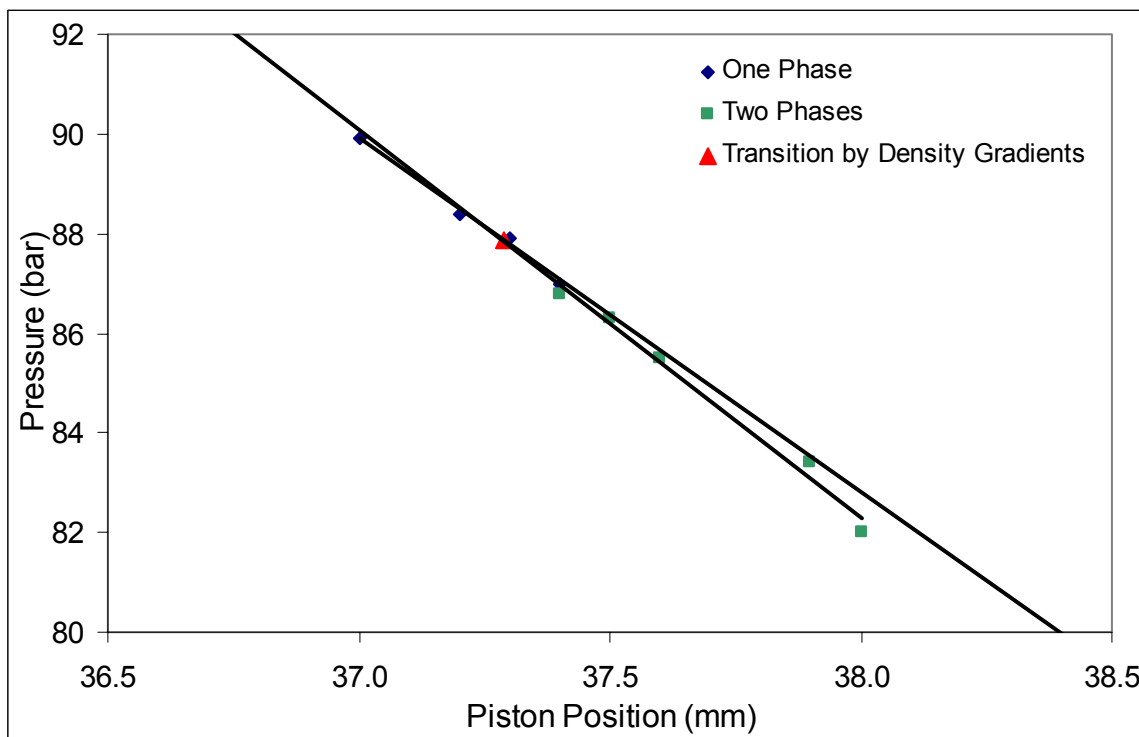
Figure 5-6: Phase Transition Detection by Density Measurement near the Mixture Critical Point for C3-C54 at x = 0.264 and 378.05 K

In addition to measurements near the critical point, phase transition detection for very low concentrations of wax may also become problematic as the contribution of the liquid to the average density becomes negligible. This is illustrated in Figure 5-7.
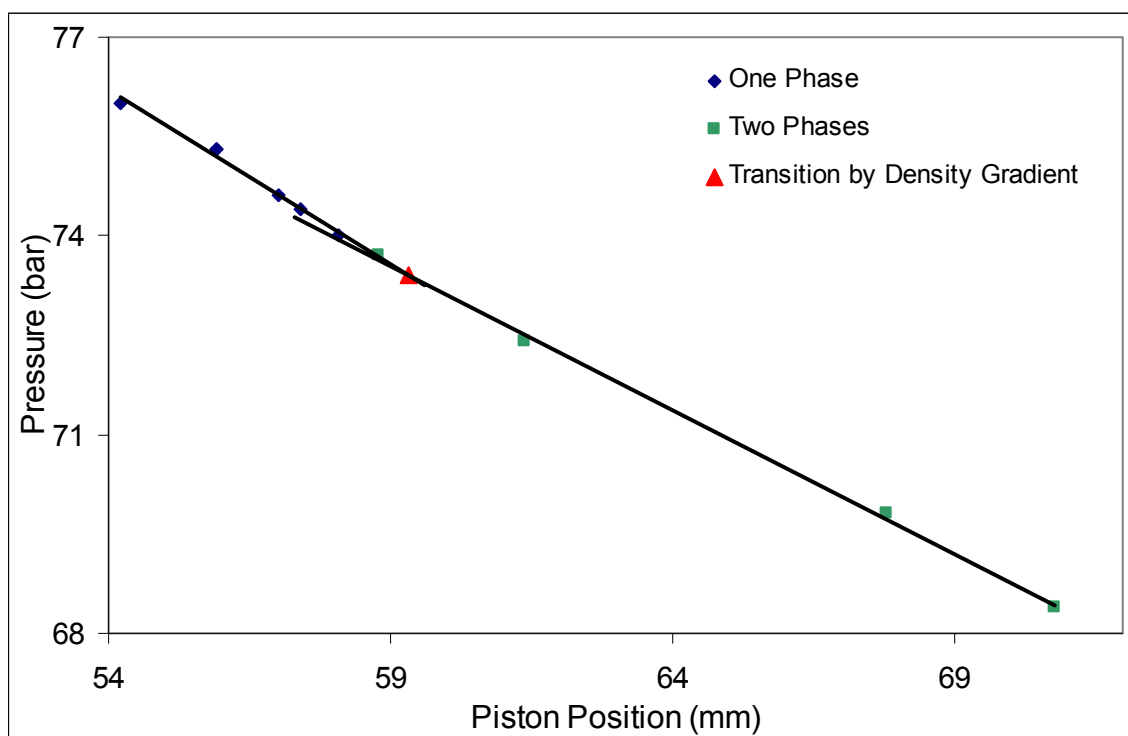
Figure 5-7: Phase Transition Detection by Density Measurement for very low paraffin concentrations for C3-C36 at x = 0.0188 and 405.85 K

Although the above methods still provided good transition points, it may prove difficult to determine which points are in the one phase region and which are in the two phase region as only slight changes in the gradient is observed.

An additional problem with the detection of the phase transition by means of density is that enough of the wax solvent mixture is required. If too little wax-solvent mixture is loaded into the cell, the change in the piston position does not change enough so that a wide enough density range can be covered. Using the visual method, the amount of waxes used in this work is enough for mass fractions over 0.5. However, when using the density method, the same amount of wax is only enough for mass fractions up to 0.3.

A summary of error in the phase transition measurement by density can be seen in Figure 5-8. Assuming that the visual method is correct, the accuracy of the phase transition measurement by density as well as the piston position calculated from the gradients is calculated. The error of these calculated points are shown in Figure 5-8.
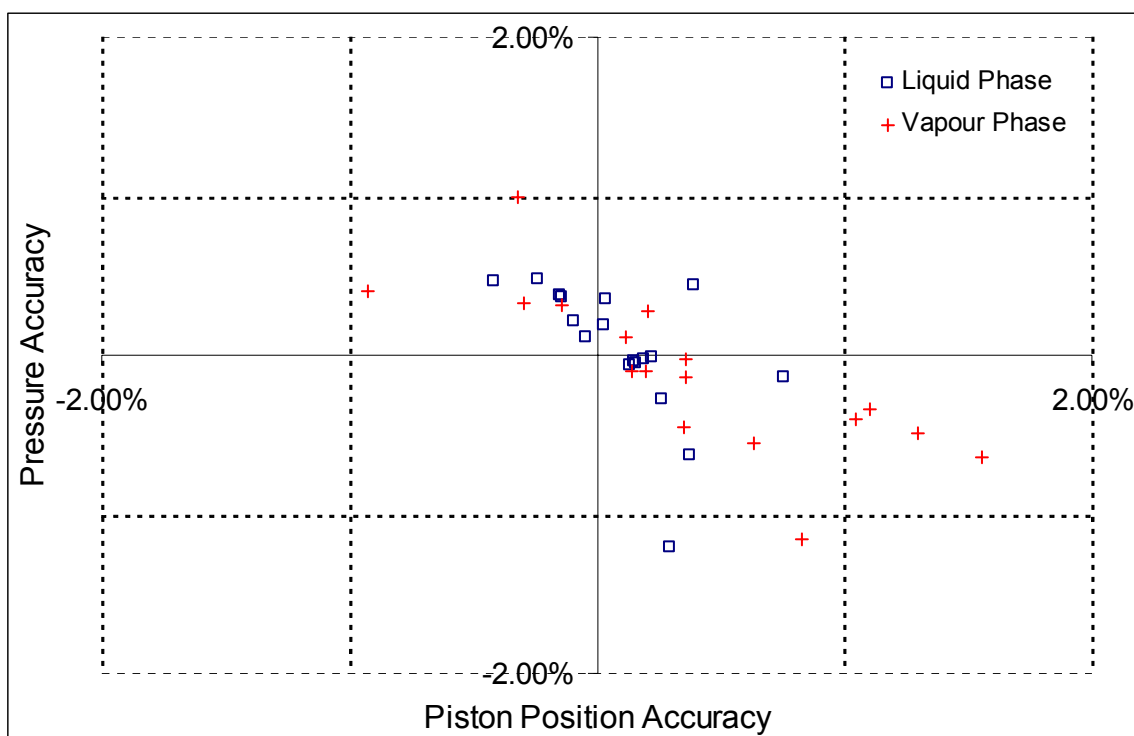
Figure 5-8: Error in Phase Transition Measurement via Density Measurement

All measurements, with exception of one vapour side density measurement fall into the accuracy of $\pm$ 2.00% accuracy in both the piston position and the pressure. As can be seen, the liquid phase transition can be determined with more accuracy. This can be attributed to the fact that the liquid phase density changes between the one phase and the two-phase region is more pronounced.

From the above discussion it can therefore be seen that the visual method is the most accurate method and can be used with confidence to determine the phase transition point.

5.3.2. REQUIREMENTS FOR CELL

The requirements in the design procedure of the cell can be listed as follows:

Cell Volume and Dimensions

- The cell has to have a volume large enough for accurate measurements. However, the pure paraffins used are extremely costly. The volume of the cell is therefore a compromise between the above two factors.

- The cell needs to be wide enough so that the contents of the cell can be mixed properly, yet the narrower the cell, the more accurate the volume measurement.

A maximum cell volume of about 40 cm^3 was decided upon with a minimum volume of 20 cm^3. It was decided that the diameter of the cell should be 22 mm, taking into account the dimensions for the sight glass.

Cell Pressure and Temperature and Regulation thereof

- The maximum operating pressure of the cell has to be 500 Bar Abs.

- The cell needs to withstand temperatures high enough so that the measurements can be made. A maximum temperature of 200 °C will be used, the temperature limit being imposed by the sight glass.

- The pressure and the temperature in the cell need to be regulated. To regulate the temperature, the cell is jacketed and heating oil is used. To regulate the pressure the volume of the cell is changed, necessitating in a piston-cylinder set-up.

- Temperature and pressure measurements are required. The design must allow for a pressure and temperature sensor for direct measurements. Indirect measurements may result in unacceptable inaccuracies.

Phase Transition Measurement

A window is required so that phase change can be observed. Due to the high pressures, the operator cannot look directly into the cell. For this reason an endoscope attached to a light source is used and attached to a television monitor from where the phase transition can be observed visually.

Mixing of Cell Contents

The content of the cell needs to be mixed. To enable this, a magnetic stirrer is used. To ensure the magnetic stirrer can withstand the temperatures of the system, a magnetic stirrer with a hotplate is required. Additionally the temperature of the hotplate can be set and thus aiding in preventing heat loss.

5.3.3. DESIGN SPECIFICATIONS

The following specifications were used for the cell design:

- The inner diameter of the cylinder is 22.00 mm.

- A maximum temperature of 200 °C and a maximum pressure of 500 barA.

- The inner diameter of the head of the piston was determined from the pressure ratio. The pressure ratio was based on the fact that a pressure of 500 bar in the cell is required with 15 barA nitrogen pressure.

- The cylinder length was calculated on the basis of a maximum volume of about 40 cm^3.

All calculations for the design of the cell are given in Appendix E.1 while detailed mechanical drawings are given in Appendix F.

5.3.4. PRESSURE AND TEMPERATURE MEASUREMENT AND CONTROL

The phase equilibrium measurements are only useful if the temperature and the pressure can both be measured at the phase transition point.

Temperature Control and Measurement

The temperature in the cell is controlled with an oil bath where the temperature can be set to an accuracy of 0.1K.

The temperature in the cell is measure with a high accuracy 4 wire PT-100 probe, which is inserted into the temperature sensor well in the cell. The thermocouple has an accuracy of better than 0.1K. The calibration data is given in appendix C.1.

Pressure Measurement and Control and Pressure Gauge Calibration

The pressure in the cell is controlled with the aid of the piston position. The piston position is controlled by varying the pressure of the nitrogen in the head of the cell.

Before any experiments were conducted, the pressure gauge had to be calibrated. Additionally calibrations were conducted at regular intervals. A dead weight tester was used to calibrate the pressure gauge. The pressure was read from the pressure indicator and corrections were done from the calibration curves. The calibration data and curves are given in appendix C.2.

The pressure measurements are accurate to $\pm$ 0.2 bar.

5.3.5. PHASE TRANSITION MEASUREMENT

As stated above, a visual method for phase transition was decided upon. An endoscope coupled to a light source and a television monitor was used to make the phase transition measurements.

The window unit was obtained from SITEC and has a lens diameter of 18 mm and is rated to withstand 200 ^{o}C and 500 bar. A non-flexible endoscope was used and the endoscope and light source were both obtained from WOLF. A television monitor was used for projection of the images.

5.3.6. EXPERIMENTAL SET-UP

The experimental set-up for phase equilibrium measurement is shown in Figure 5-9. A detailed description of the experimental procedure is given in paragraph 5.4.
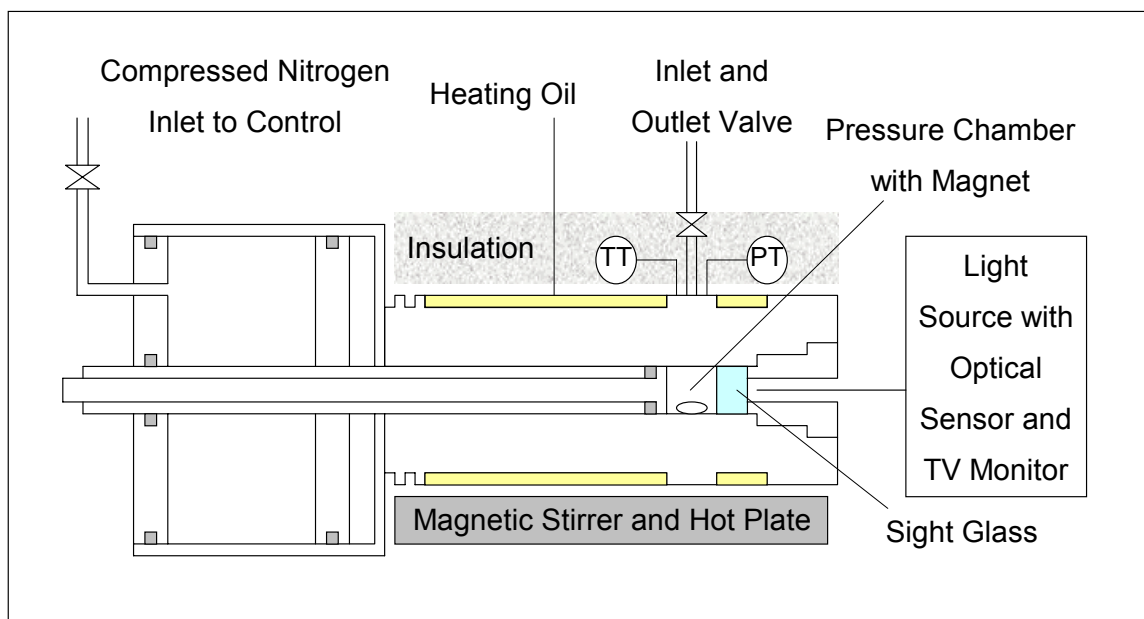
Figure 5-9: Schematic Representation of Experimental Set-up

5.3.7. SEALING MECHANISMS

Due to the fact that high pressures are used and the cell is required to seal properly, the mechanism for sealing and the type of seals used is discussed below.

Sealing of Piston to Cylinder

The seal used here is designed to operate well at high pressures but should be able to seal at atmospheric pressures. The piston consists of two parts, an outer rod and an inner rod. Between the two parts of the rod, a teflon seal and a brass ring are used to accomplish sealing. The two parts of the piston are kept together with the nut and bolt principle, the inner rod forming the bolt. The nut is tightened to allow the Teflon to compress axially and expand in the radial direction.

Pressure is used to improve sealing in the system and the mechanism used is illustrated in Figure 5-10 below:
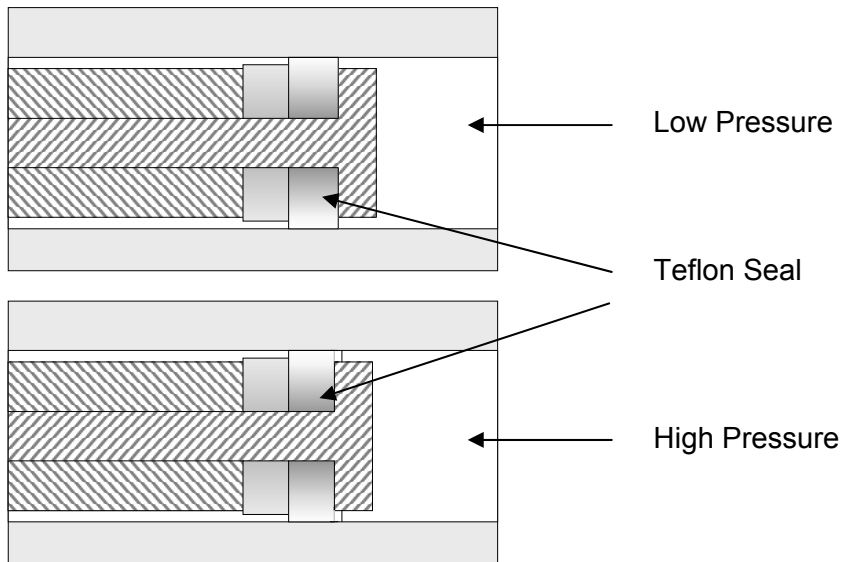
Figure 5-10: Sealing Mechanism for Piston.

As can be seen above, an increase in the system pressure caused the teflon seal to compress in an axial manner, resulting in an expansion in the radial direction. This in turn will increase the sealing effect of the teflon seal. In Figure 5-11 the final dimensions of the piston and inner part of the cylinder relevant to sealing are given. With these dimensions the piston was found to be virtually leak proof.
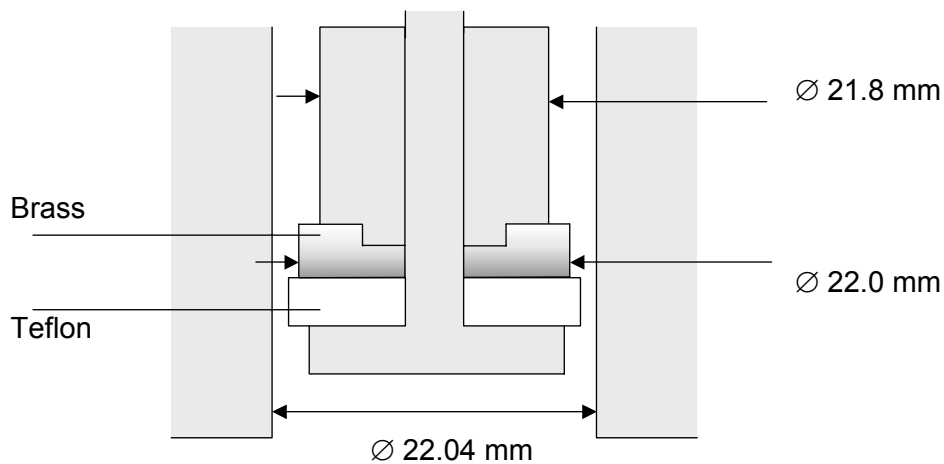
Figure 5-11: Dimensions for Piston in Cylinder.

Sealing of Sight Glass

A Bridgeman type of seal is used to seal the sight glass. The same type teflon seal with a backing that was used to seal the piston, was used here.

Sealing of Upper Chamber.

Sealing is required here to prevent nitrogen leaking from the upper chamber to the environment between the piston and the upper disc part of the head, the piston and the

piston disc, and the upper disc and the upper chamber. In all cases, viton o-rings were used for the sealing due to the ability of viton to withstand the required temperatures.
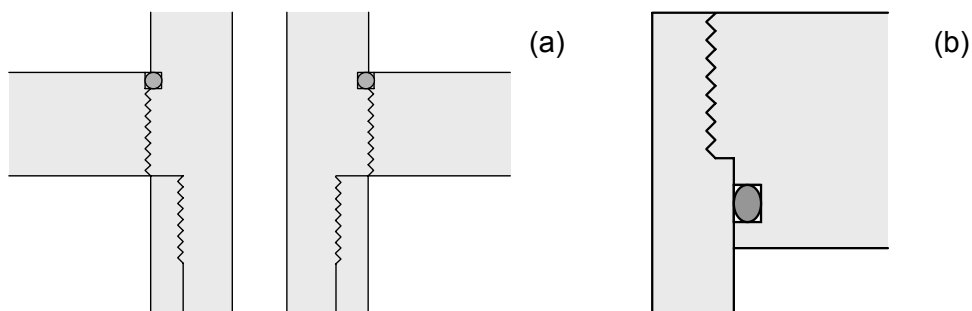
Figure 5-12: Schematic Representation of Sealing of (a) Piston Disc to Piston and (b) Upper Disc and Upper Chamber.

To prevent nitrogen leaking to the atmosphere, the following mechanism was used to seal the piston to the piston disc. After construction, a part of the screw thread on the piston disc was removed and a grove was made at the relevant place on the outer rod - upper part. A schematic representation can be seen in Figure 5-12 (a).

The upper chamber and the upper disc need to be sealed to prevent nitrogen loss to the atmosphere. In addition, mechanical strength is require to ensure that the disc does not come loose when the head is pressurised. A combination of screw thread is used with an o-ring to accomplish both functions. A schematic representation of the design decided upon is shown in Figure 5-12 (b). The indentation is used so as to prevent damage to the o-rings.

Sealing during Loading

The loading procedure is illustrated in Figure G-1. Sealing is required between the evacuation pump, the gas cylinder and the cell so as to prevent any solvent from exiting the set-up and air from entering. Sealing is accomplished with viton o-rings.

5.4.   EXPERIMENTAL PROCEDURE, MAINTENANCE AND SAFETY

The experimental procedure can be divided into four main procedures:

Firstly the experiment needs to be set up. This step entails the loading of an accurate amount of solvent and solute in such a manner that the exact composition is known and the amount of air in the cell is negligible.

Secondly the experimental data is obtained. For each mass fraction the phase transition pressure is measured at three different temperatures.

Thirdly, on conclusion of the experimental measurements, the cell contents needs to be removed from the cell. This needs to be conducted in such a manner that the maximum amount of wax is recycled.

Lastly, the cell needs to be cleaned thoroughly to remove all the wax.

Due to the limitations on the amount of wax available and the wax lost in the unloading process, in some runs only the solvent will be removed from the cell between consecutive runs. A slightly modified loading and unloading procedure is required for these runs.

The equipment used is expensive and is operated at high pressures and moderate temperatures. It is of utmost importance that the operator is safe when using the equipment. The following were taken into account to ensure safety:

- The chemicals used in operation and for cleaning.

- The pressure of the system.

- The temperature of the system.

Additionally regular maintenance is required on the cell.

Details of experimental procedure, the maintenance required on the cell and the safety precautions are given in Appendix G.

5.5. TESTING OF CELL AGAINST LITERATURE DATA

It is important to test results obtained from the equipment against reliable published data. The following criteria is required:

1. The data sets have to include both dew point and bubble point measurements.

2. The data needs to be in the same pressure and temperature range as the experiments to be done.

3. The system chosen should be similar to the systems to be studied.

For the systems to be studied, the following possibilities for testing data exist:

1. In this project propane-nC32 and propane-nC36 data will be generated. Published data of propane-nC34 exists. The accuracy of the cell can be determined by plotting the data of the nC32, nC34 and nC36 at the same temperature and determining if the nC34 data lies between the nC32 and nC36 data.

2. Additionally the cell can be tested with ethane – nC24 data. The data has been produced by Peters et al and du Rand and show consistency with one another (Peters et al., 1987a), (du Rand, 2000).

Additionally the vapour pressure of propane near its critical point will also be measured and compared to experimental data.

Comparison with n-C34 Published Data

A comparison of the nC32 – propane and nC36 – propane data with published nC34 – propane data was done once the nC32 and nC36 runs with propane were completed. The comparison is given in paragraph 6.3.1.

Comparison of Ethane – n-C24 data

Two different sets of published data of Ethane and nC24 exist and agree with one another (du Rand, 2000), (Peters et al., 1987a). A vapour and a liquid side data point was measured on the cell and yielded the following result:
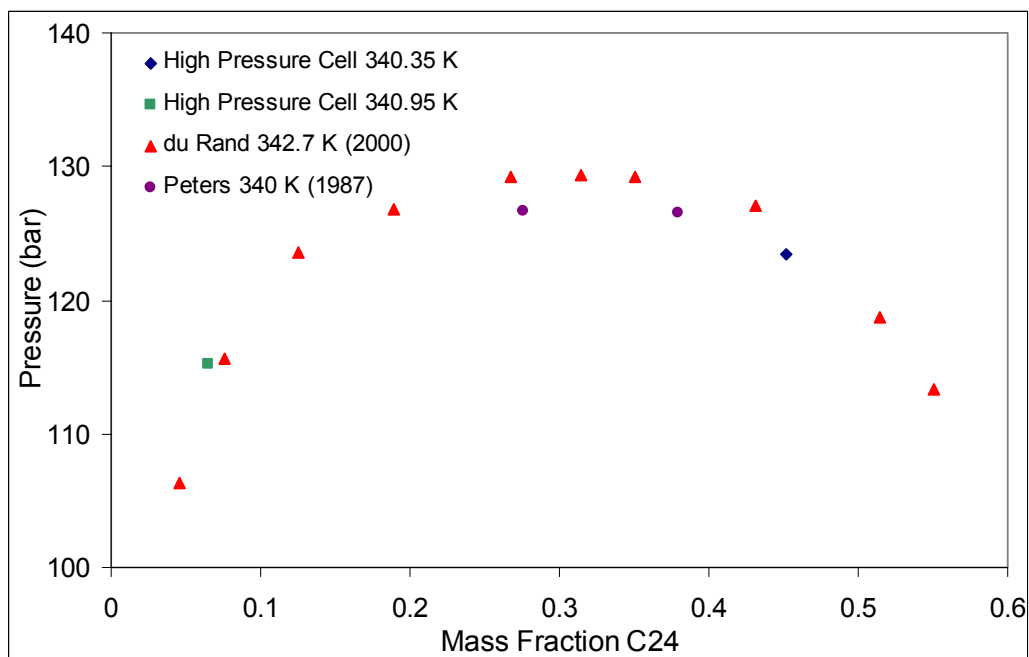
Figure 5-13: Comparison of published data with data measured on cell for ethane Tetracosane system.

As can be seen from the above figure, the data measured here agrees well with both published sets of data. It can thus be concluded that the cell produces accurate high pressure phase equilibrium data.

Vapour Pressure Data

The vapour pressure of propane is measured near the critical point. In Table 5-1 the measured data is reported and compared to experimental data from the literature As can be seen the data measured is within the pressure and temperature accuracy of the experimental set-up.

Table 5-1: Vapour measurement data and comparison with literature data (Reid et al., 1987)

Temperature (K)	Experimental Data (bar)	Literature Data (bar)	Pressure Difference (bar)
369.25	41.6	42.1	-0.5
366.35	40.2	39.9	0.3
363.45	37.6	37.8	-0.2

5.6.   CHEMICALS USED

The chemicals used, their purity as well as their suppliers are given. This information is important so as to analyse the accuracy of the results obtained. All materials were used without further purification.

Solvents

Propane is supplied by Mossgas. The ethane used for the testing of the cell is the same used by du Rand (du Rand, 2000) The supplier, Messer Griesheim, certified that the ethane has a purity of greater than 99.5 percent. Both the propane and the LPG were analysed with GC-FID and GC-MS in a PONA capillary column and resulted in the following compositions.

Table 5-2: Propane Gas Composition

Component	Percentage
Propane	99.95%
Iso-Butane	0.0323%
n-Butane	0.0151%

Table 5-3: LP Gas Composition

Component	Percentage
Propane	87.78 %
Iso-Butane	6.70 %
n-Butane	5.52 %

Wax / Normal Paraffins

A compromise between accuracy due to component purity and cost had to be made in the selection of the wax purity. In addition, where possible, similar purity of chemicals were used throughout the project. The normal paraffins used together with their purity and the supplier is given in Table 5-4. Gas chromatograph tests were not conducted, as the heavier components could not be analysed due to their high boiling points. The given purities are thus as stated by their suppliers.

Table 5-4: List of normal paraffins with purity and suppliers

Component	Purity	Supplier
Tetracosane (nC24)	> 99 %	Fluka
Dotriacontane (nC32)	97 %	Aldrich
Hexatriacontane (nC36)	≈ 98 %	Fluka
Octatriacontane (nC38)	≥ 98 %	Fluka
Tetracontane (nC40)	98 %	Aldrich
	≈ 97 %	Fluka
Tetratetracontane (nC44)	99 %	Aldrich
Hexatetracontane (nC46)	≥ 98 %	Fluka
Tetrapentacontane (nC54)	≈ 99 %	Fluka
Hexacontane (nC60)	≥ 98 %	Fluka

5.7.   CONCLUSIONS

A high pressure cell has been designed, constructed, tested and results obtained on the cell compared well with literature data. The high pressure cell can now be used to measure the required data.

6.   EXPERIMENTAL RESULTS

In this chapter the results of the experiments and the discussion thereof will be given. In addition, the various data sets will be compared with one another and with literature data so as to determine the effect of temperature, mass fraction and the solvent used on the phase equilibrium pressure and density.

All experimental measurements are given in Appendix A.1.

6.1.   BINARY PHASE EQUILIBRIUM DATA

Binary phase equilibrium experiments were conducted in the phase equilibrium equipment designed as described in chapter 5. The following data sets were measured and the binary phase equilibrium pressure results will be presented in this section:

- Propane-Dotriacontane

- Propane-Hexatriacontane

- Propane-Octatriacontane

- Propane-Tetracontane

- Propane-Tetratetracontane

- Propane-Hexatetracontane

- Propane-Tetrapentacontane

- Propane-Hexacontane

- LPG-Hexatriacontane

6.1.1.   PHASE EQUILIBRIUM MEASUREMENTS

Phase Equilibrium measurements were made in accordance with the procedures as set out in paragraph 5.4. The pressure sensor was calibrated regularly and the calibration equations are given in Appendix C.1.

Temperature Correction of Data

The data points that were measured were not all obtained at exactly the same temperature and thus the data is not isothermal. This can be attributed to environmental conditions that were not identical during the entire experimental time.

To represent the data in a useful manner, isothermal data is required. Temperature corrections are thus required for the data. From the literature it is evident that various methods have previously been used to make temperature corrections to data:

- Nieuwoudt found that when the bubble and dew point pressures at constant composition are plotted as a function of temperature, a virtually linear relationship was found. This allows for linear interpolation and limited extrapolation (Nieuwoudt, 1996).

- The same linear relationship was found by du Rand for ethane – n-alkane systems (du Rand, 2000).

- For their study of the systems propane-tetratriacontane and propane-hexacontane data Peters et al did state that an interpolation method was used but did not give any details of the method (Peters et al., 1992), (Peters et al., 1993).

- In their study of propane-eicosane, Gregorowicz et al. used a third degree polynomial to describe the same pressure temperature relationship. It must, however, be noted that a much larger temperature range was studied (Gregorowicz et al., 1992).

From the above studies it can be seen that simple methods were used. Due to the fact that only three data points were measured for each composition and that the temperature range is not very large, linear interpolation and limited extrapolation will be used.

For the system propane-tetrapentacontane selected linearized lines are shown in Figure 6-1 The type of plot shown in Figure 6-1 was used to do temperature corrections for all data points. An average R^2 value of 0.9983 was found for the correlation of the all the experimental data.

:
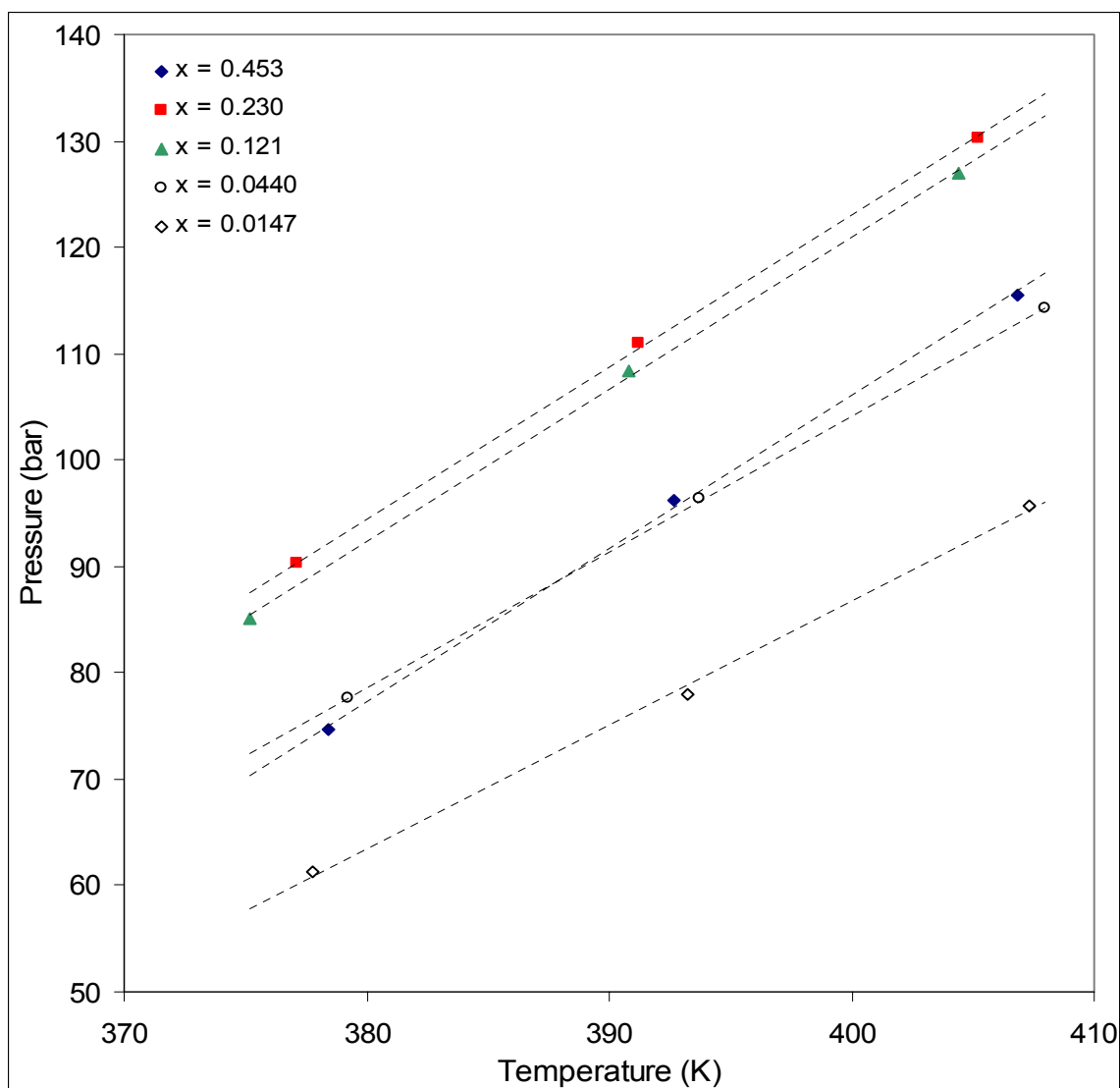
Figure 6-1: Temperature Correction of Phase Equilibrium Data by Linear Interpolation: Pressure-Temperature plot of Experimental Data at Constant Mass Fraction: C3-C54

Accuracy of Data

The accuracy of the experiments depends on the accuracy of the wax and solvent loaded, the thermocouple, the pressure gauge and the accuracy of the determination of the phase equilibrium detection. The experiments were conducted at the following accuracy:

- The amount of wax in the cell was accurate to $\pm$ 0.01 grams for masses larger than 1.5 grams and $\pm$ 0.001 grams for masses less than 1.5 grams.

- The solvent was measured off accurate to $\pm$ 0.01 grams.

- The pressure gauge is accurate to $\pm$ 0.2 bar.

- The temperature is measured accurate to $\pm$ 0.1 K.

- The phase transitions were made visually and this in itself may cause some inaccuracies. It can comfortably be assumed that the phase transitions are measured with an accuracy of 0.5 bar.

Reproducibility of Data

It is important that the data measured is reproducible.

When measuring the phase equilibrium pressure, a bisection method was used. This allowed for the user to move through the phase equilibrium a number of times, thus ensuring that the pressure measured is the correct pressure.

To prove that the same data point can be measured from different loadings and from different pressure calibrations, the data points measured for propane-octatriacontane at mass fractions of 0.0989 and 0.0949 are compared. These two points were measured from different pressure calibrations (See Appendix A).
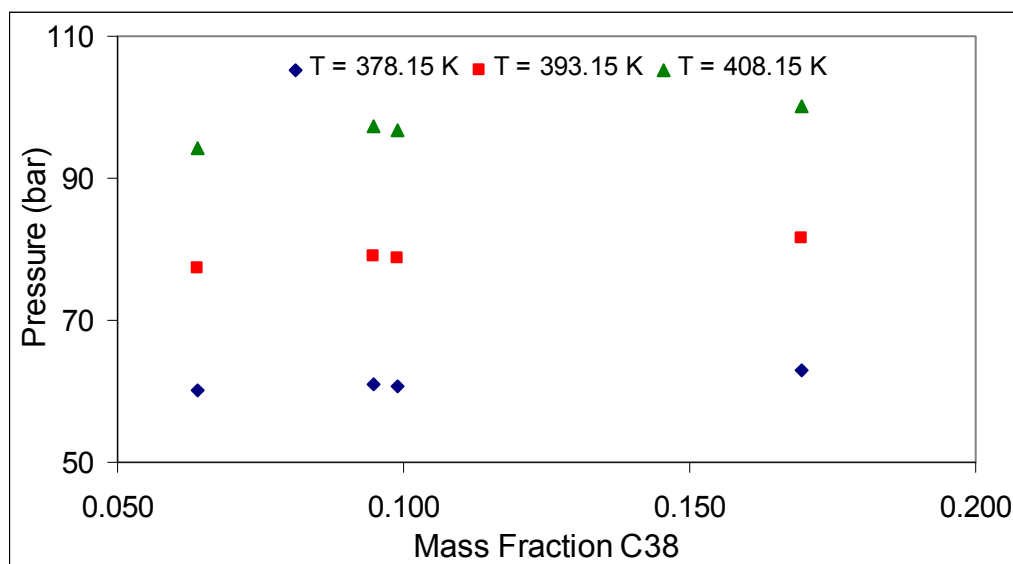
Figure 6-2: Pressure-Composition Plot for Propane-Octatriacontane for proof of reproducibility.

As can be seen in Figure 6-2 the difference in the pressure measured is minimal.

6.1.2. PRESSURE COMPOSITION PLOT

The temperature corrected data is plotted in Figure 6-3 to Figure 6-11 as a pressure-composition plot at constant temperature. The temperature corrected data used to generate the graphs, is given in Appendix B.
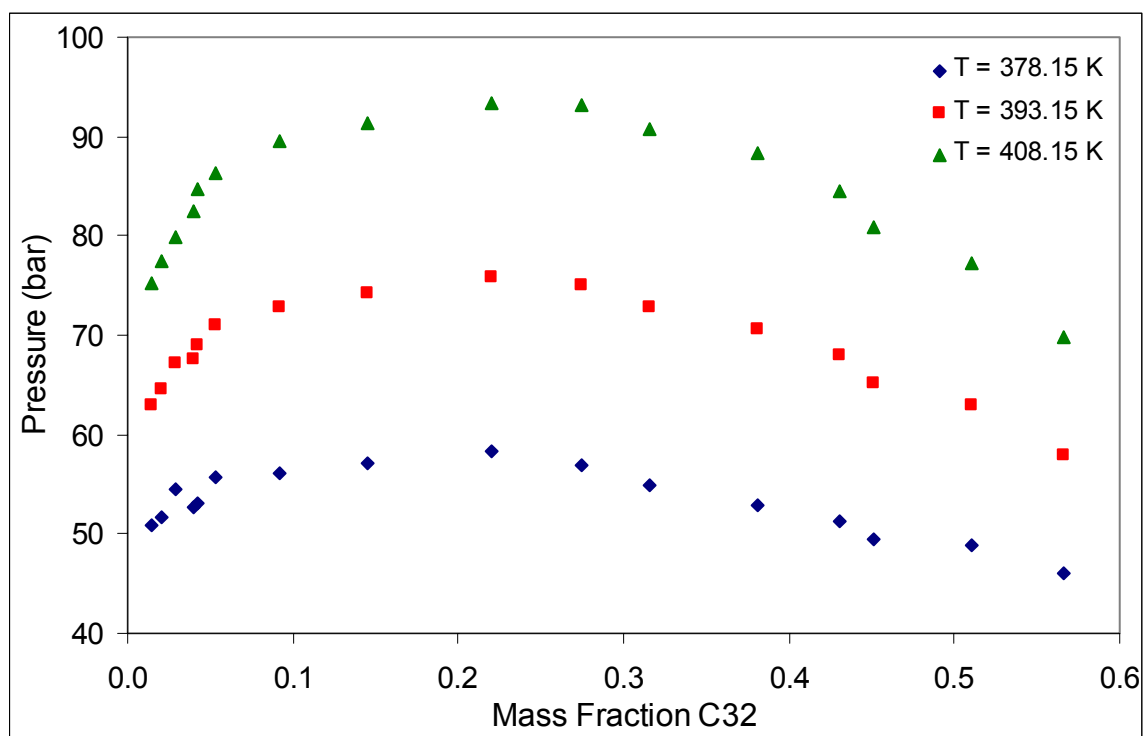
Figure 6-3: Isothermal Pressure-Composition Plot of Phase Boundary Plot for Propane-Dotriacontane system.
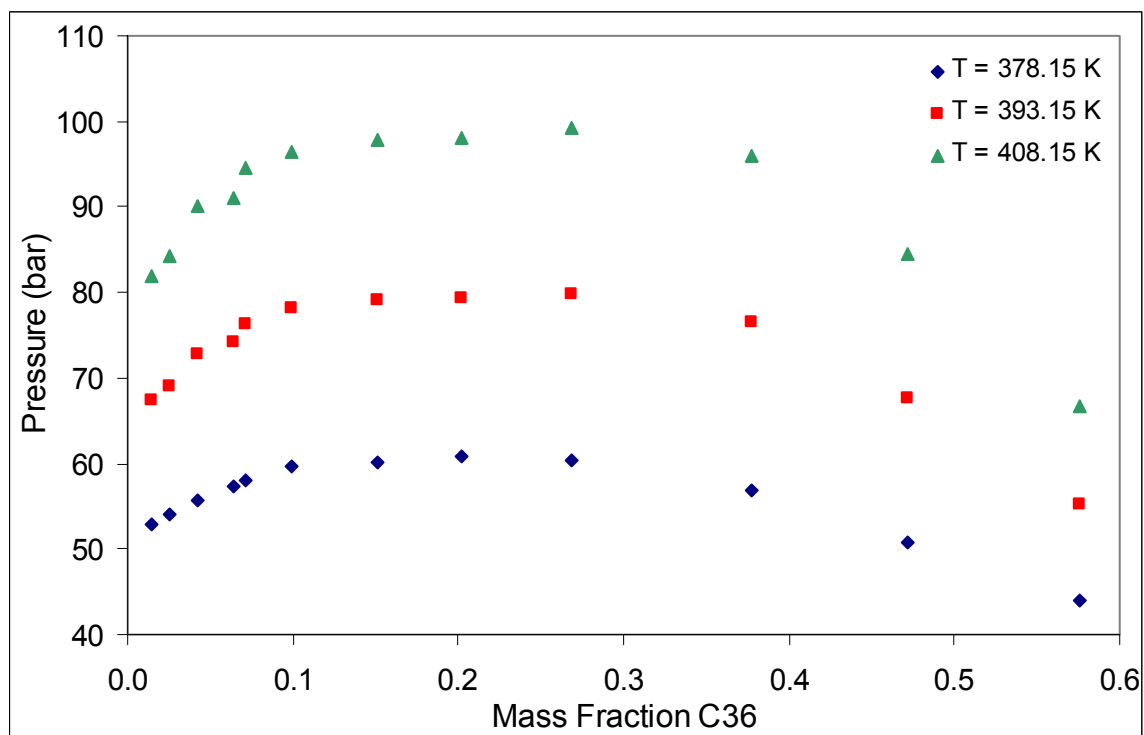
Figure 6-4: Isothermal Pressure-Composition Plot of Phase Boundary Plot for Propane-Hexatriacontane system.
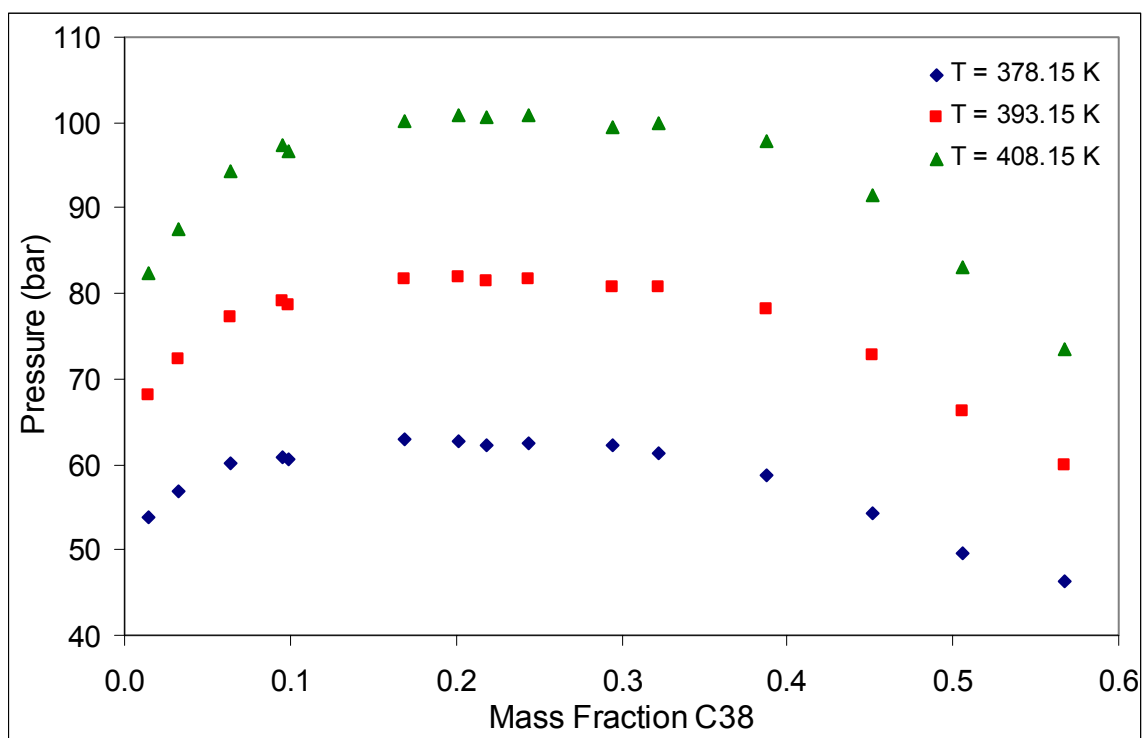
Figure 6-5: Isothermal Pressure-Composition Plot of Phase Boundary Plot for Propane-Octatriacontane system.
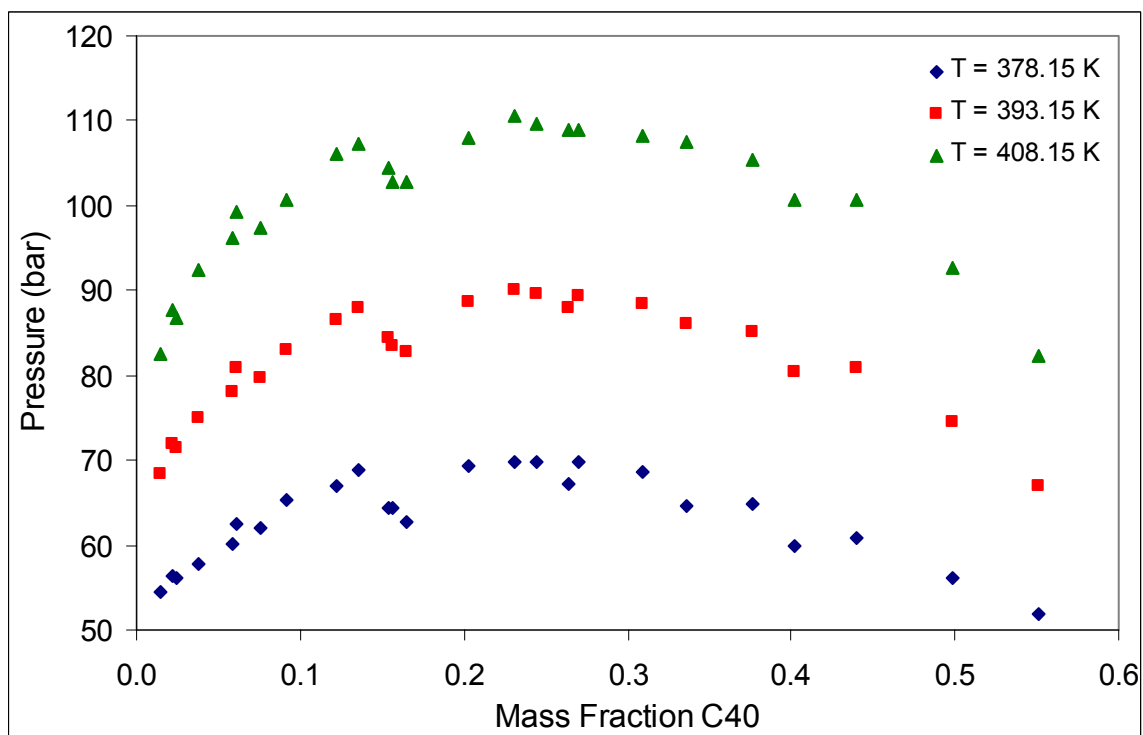
Figure 6-6: Isothermal Pressure-Composition Plot of Phase Boundary Plot for Propane-Tetracontane system.
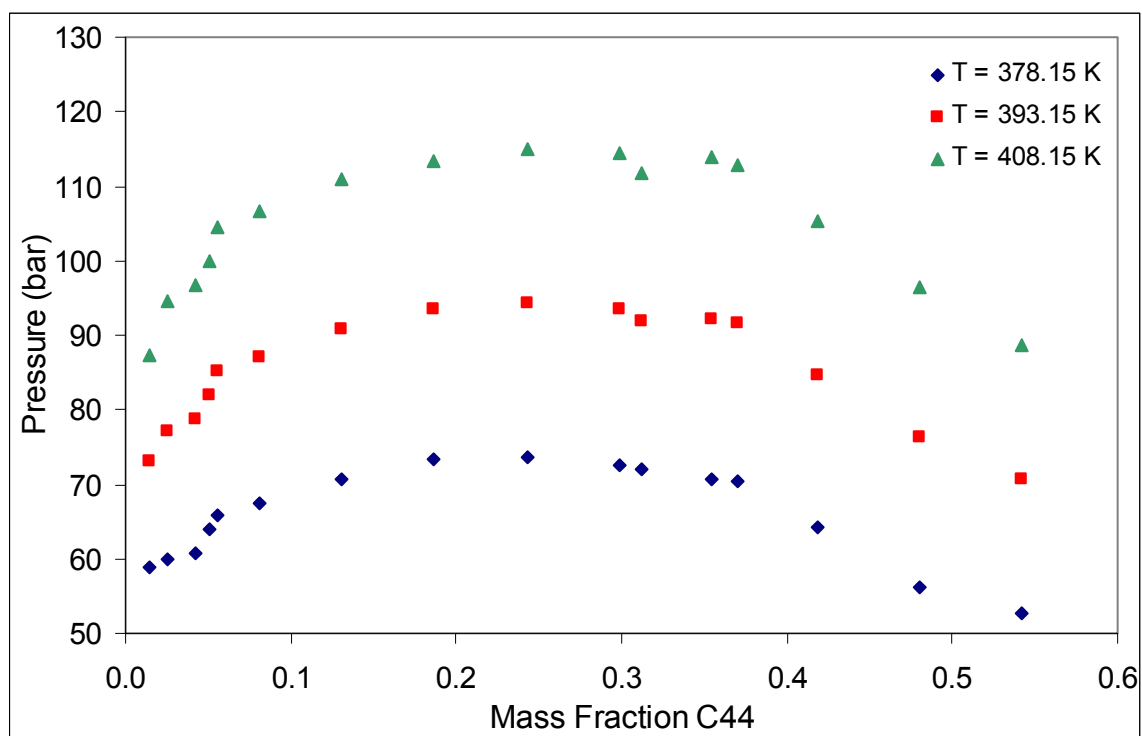
Figure 6-7: Isothermal Pressure – Composition Plot of Phase Boundary Plot for Propane-Tetratetracontane system.
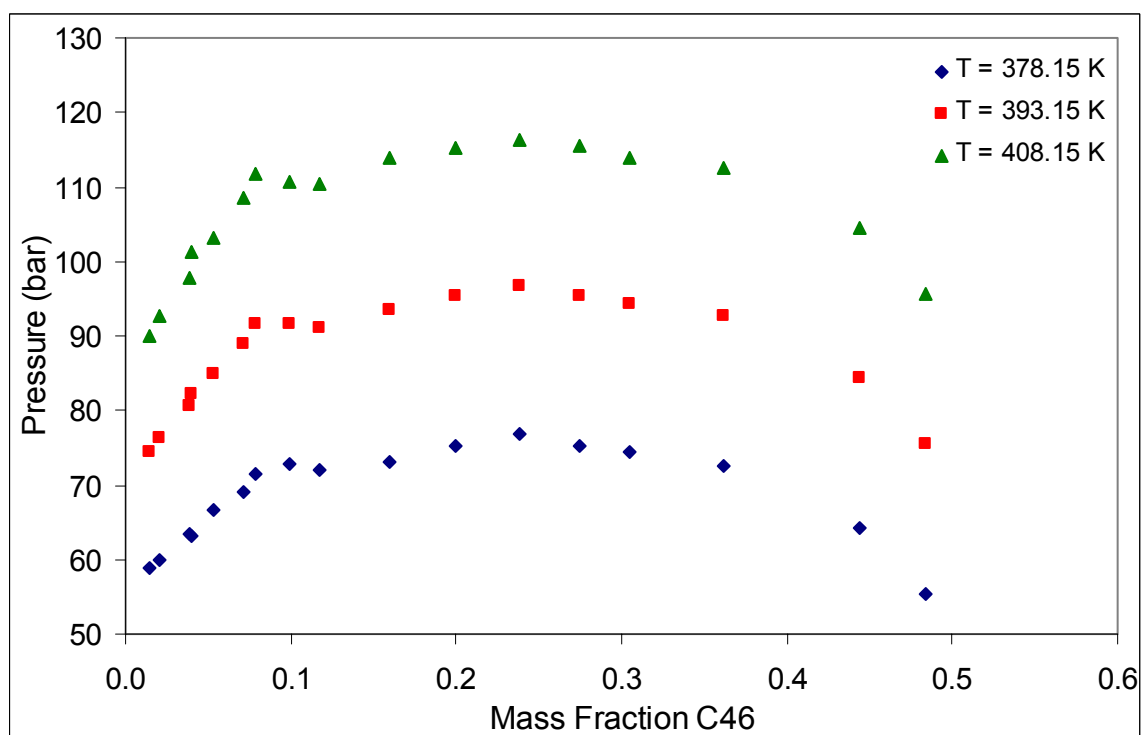
Figure 6-8: Isothermal Pressure-Composition Plot of Phase Boundary Plot for Propane-Hexatetracontane system.
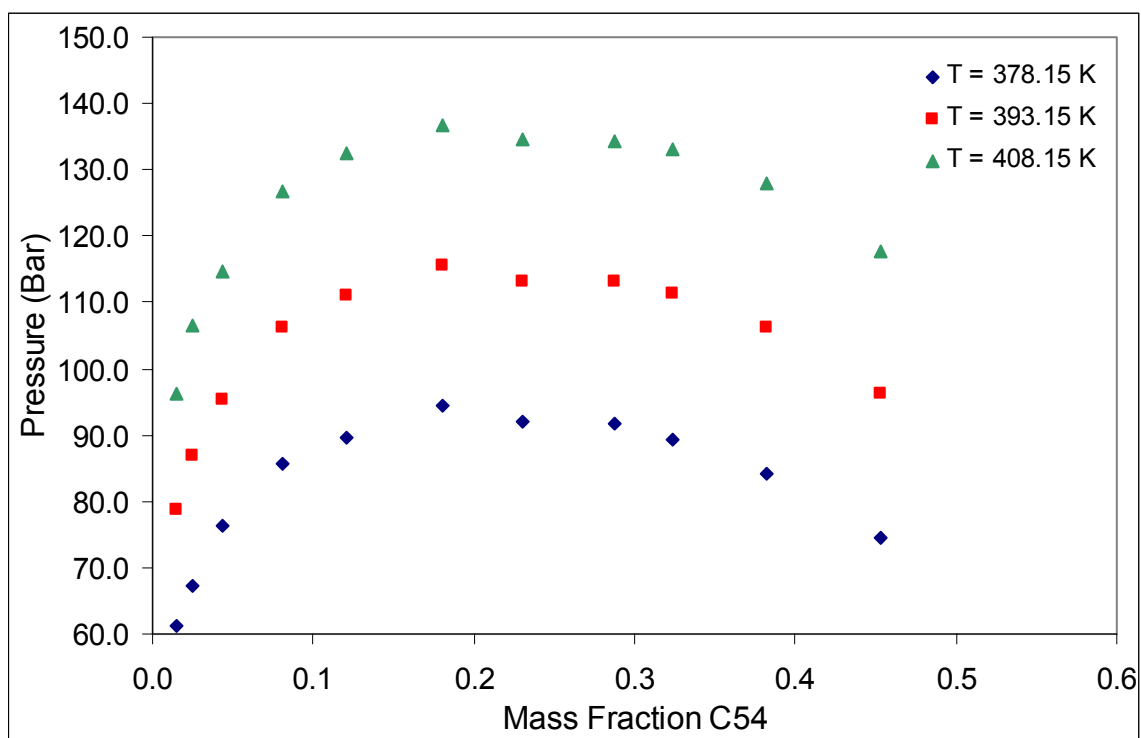
Figure 6-9: Isothermal Pressure-Composition Plot of Phase Boundary Plot for Propane-Tetrapentacontane system.
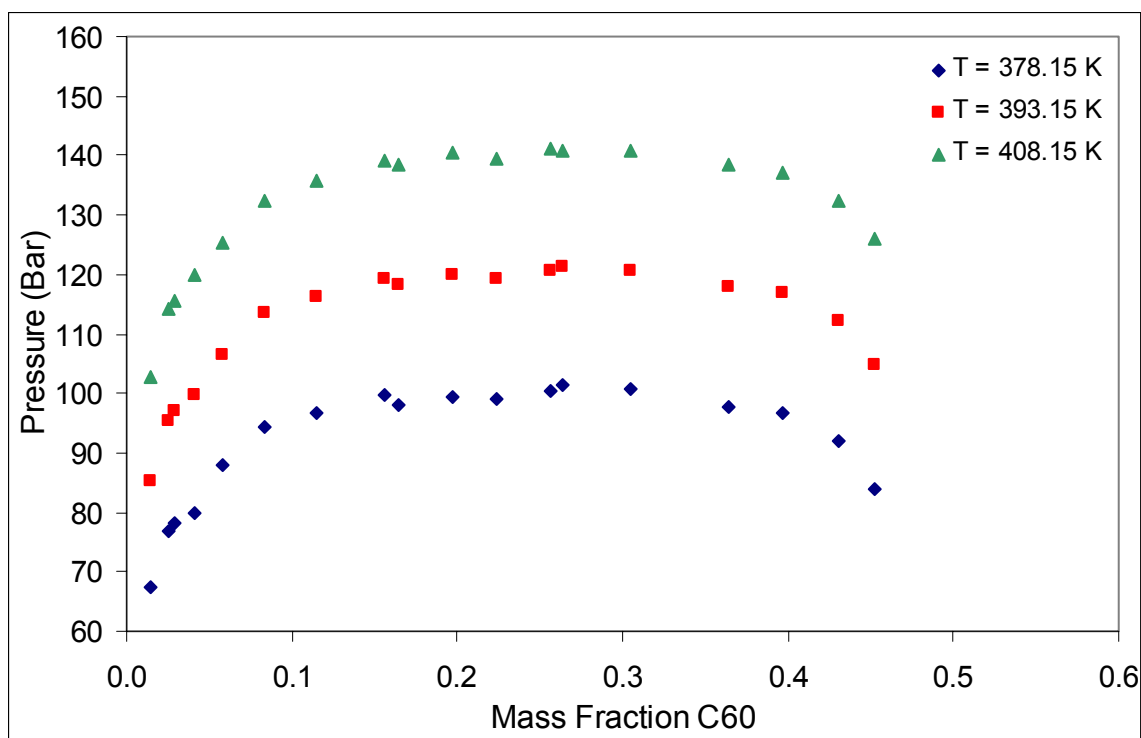
Figure 6-10: Isothermal Pressure-Composition Plot of Phase Boundary Plot for Propane-Hexacontane system.
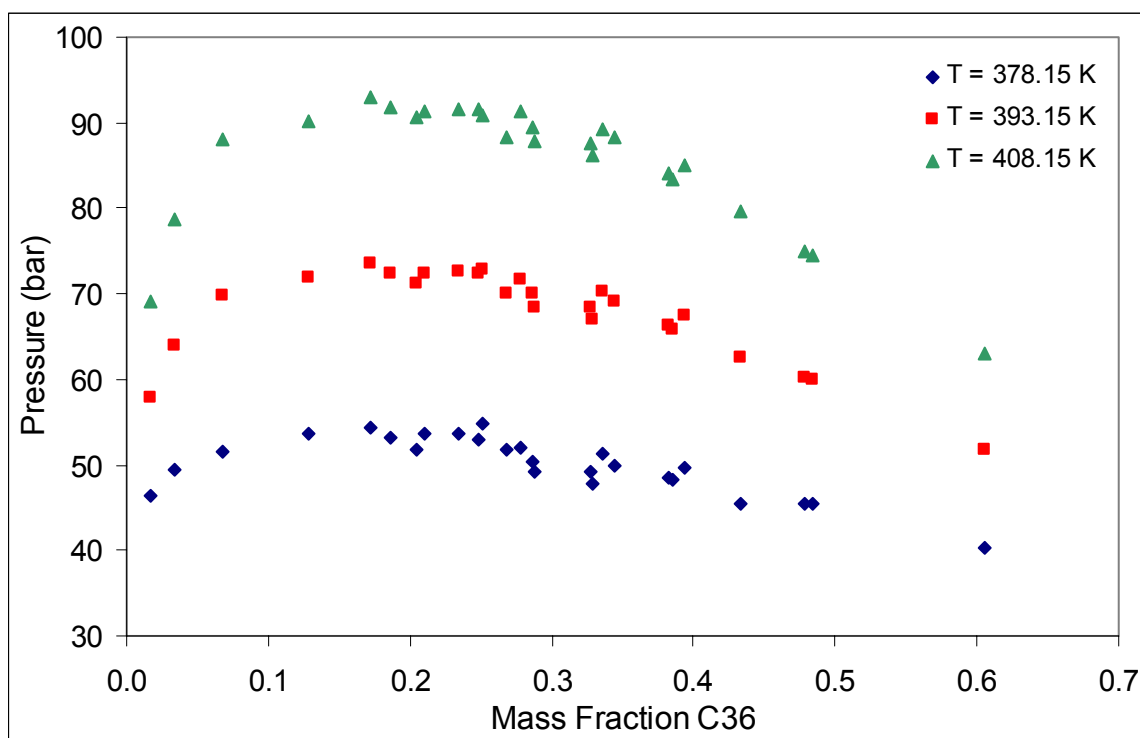
Figure 6-11: Isothermal Pressure-Composition Plot of Phase Boundary Plot for LPG-Hexatriacontane system.

6.1.3. DISCUSSION OF DATA

A detailed comparison of the above data with literature data is given in paragraph 6.3 while the different data sets are compared in paragraph 6.4. It must be noted that the large amount of scattering that occurs in the LPG-Hexatriacontane data can be attributed to the fact that the measurements were made without the aid of the endoscope and the phase transition could thus not be seen as easily.

Effect of Temperature

From the plots above it can be seen that the temperature has a profound effect on the phase transition pressure. An increase in temperature results in an marked increase in phase transition pressure.

Flash Considerations

The main aim of this project is to determine if fractionation of synthetic waxes by supercritical fluid extraction is possible. The first step is to consider the phase equilibrium between the solvent and a single paraffin. A necessary but not sufficient requirement is that the vapour phase has a significant loading so that wax can be selectively absorbed into the light phase.

The results in paragraph 6.1.2 show that this criterion is fulfilled. For example, consider the C3-C54 system at 408.15 K.
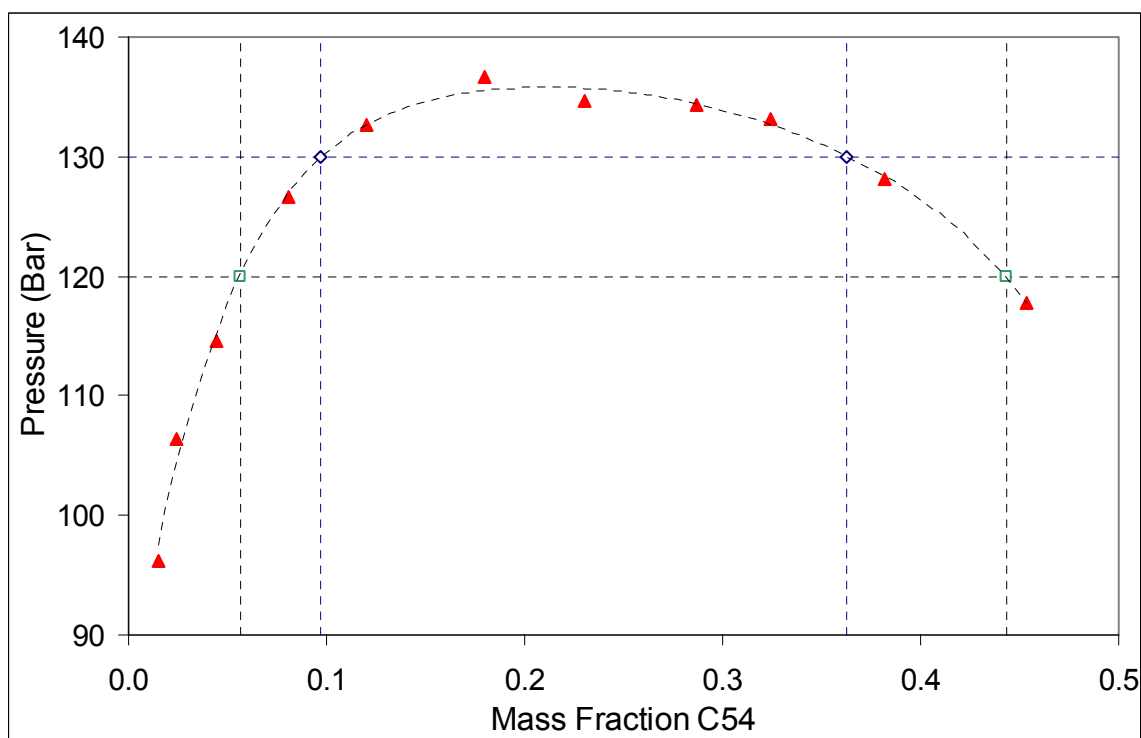
Figure 6-12: Isothermal (408.15 K) Pressure-Composition plot for Propane-Tetrapentacontane for use in Flash Calculations

As can be seen above, at a pressure of 130 bar and 408.15 K a bubble point flash would result in a light phase with a mass fraction of about 0.0965. Similarly a flash at 120 bar would result in vapour phase mass fractions of about 0.057. Significant amounts of the wax are present in the light phase.

Classification of Systems

The transition from completely miscible phase behavior (Type I) to phase behavior with a region of liquid-liquid immiscibility (Type V) for propane systems has been a source of debate. (See paragraph 3.4 for description of phase behavior). Peters et al predicted that this transition may occur for hydrocarbons with carbon numbers between 29 and 30 carbon atoms (Peters et al., 1989). Additionally, pressures and temperature measurements of the upper and lower critical solution temperatures were made. These measurements are presented in Table 6-1:

Table 6-1: Pressures and Temperatures of the Lower and Upper Critical End Points for Propane Binaries with Long Chain Alkanes from Peters et al (Peters et al., 1989)

Binary Mixture	Lower Critical End Point		Upper Critical End Point	
	Temperature	Pressure	Temperature	Pressure
C3 – C32	373.66 K	44.79 bar	374.90 K	45.69 bar
C3 – C34	370.80 K	42.71 bar	373.44 K	44.91 bar
C3 – C36	368.24 K	40.82 bar	372.64 K	44.32 bar
C3 – C38	365.52 K	38.91 bar	372.00 K	43.83 bar
C3 – C40	362.92 K	37.10 bar	371.52 K	43.50 bar
C3 – C44	357.63 K	33.80 bar	370.80 K	43.13 bar
C3 – C46	355.85 K	32.78 bar	370.81 K	43.14 bar
C3 – C50	350.40 K	29.58 bar	370.33 K	42.80 bar

From the temperature and the pressure ranges given above, it can be seen that no region of immiscibility can be expected for the studies conducted here. This was confirmed by the experimental results. At most two phases were observed.

From the experiments conducted in this work it cannot be said with certainty if type I or type V phase behaviour occurs but with the aid of the results of Peters et al it can be predicted that the phase behaviour is of type V and that the operating temperatures used in this study are above the region of immiscibility. This will allow a process to be designed at these operating conditions with confidence that no region liquid-liquid immiscibility will occur.

6.2. DENSITY DATA

Although not the primary aim of the experiments, a secondary aim was to obtain the densities of the co-existing phases. Densities were measured at the same time as the measurement of the phase transition pressure.

6.2.1. PURE COMPONENT DENSITIES

To obtain values for the limits of the densities, the pure component density values are required.

Heavy Components

At the temperatures used in this project, the waxes are all liquids. Fisher published a method to calculate the pure component densities. From the method of Fisher the following values for the pure component densities were obtained at the stated temperatures (Fisher, 1989):

Table 6-2: Pure Component Densities of Heavy Components

Alkane	Density (kg/m^3) at T = 378.15 K	Density (kg/m^3) at T = 393.15 K	Density (kg/m^3) at T = 408.15 K
n-C32	758	749	740
n-C36	763	755	746
n-C38	765	757	748
n-C40	767	759	750
n-C44	771	762	753
n-C46	772	764	755
n-C54	777	768	760
n-C60	780	771	763

These values are included in the Density-Composition and Pressure-Composition Plots in paragraphs 6.2.3 and 6.2.4. They also constitute the maximum values of the density of the mixture.

Propane and LPG

At the operating conditions propane and LPG are supercritical fluids and would be in the single phase. Therefore both the temperature and the pressure are required to calculate the density. For the operating region described here, the pure component densities are between 200 and 400 kg/m^3 for propane.

Younglove et al. published detailed density data for propane (Younglove et al., 1987). Stewart et al. published data for, amongst others, propane, normal butane and iso-butane (Stewart et al., 1986). Additionally, data was obtained from the National Institute for Standards and Technology (NIST) website [165]. The pure component densities for propane on the NIST website were used to calibrate the relationship between the piston position and the volume of the cell. (See appendix C.3.)

6.2.2. DENSITY MEASUREMENTS

Densities were measured in conjunction with the phase transition pressures in the method described below:

Method of Measurement

Due to the fact that the system is closed and of constant mass, the density can be determined if the volume of the cell at the phase transition pressure is known. The diameter of the cell remains constant and only the length changes as the piston moved in and out. Thus by measuring the length of the piston and correlating the volume and the piston position, the density of the mixture in the cell can be determined. The correlations used for the density measurement is given in Appendix C.3.

Temperature Correction of Data

As with the phase transition pressures measurement, the densities are not all measured at the same temperature. To be able to compare the values on a quantitative basis, corrections need to be made.

When consulting the literature, it was found that very little data was available for the densities at the phase boundaries, and none of these studies suggested any method for density correlation. Aalto et al. reported densities for mixtures of sub-critical propane and long chained alkanes close to the phase boundary (Aalto et al., 1996). The values of the densities are of the same order of magnitude to the densities measured in this work.

As a first attempt to correlate the density, the same linear approach was adopted as for the pressure corrections. The densities were generally found have a reasonably linear relationship with temperature. Selected values for the density correlations used for the system C3-C54 are shown in Figure 6-13:
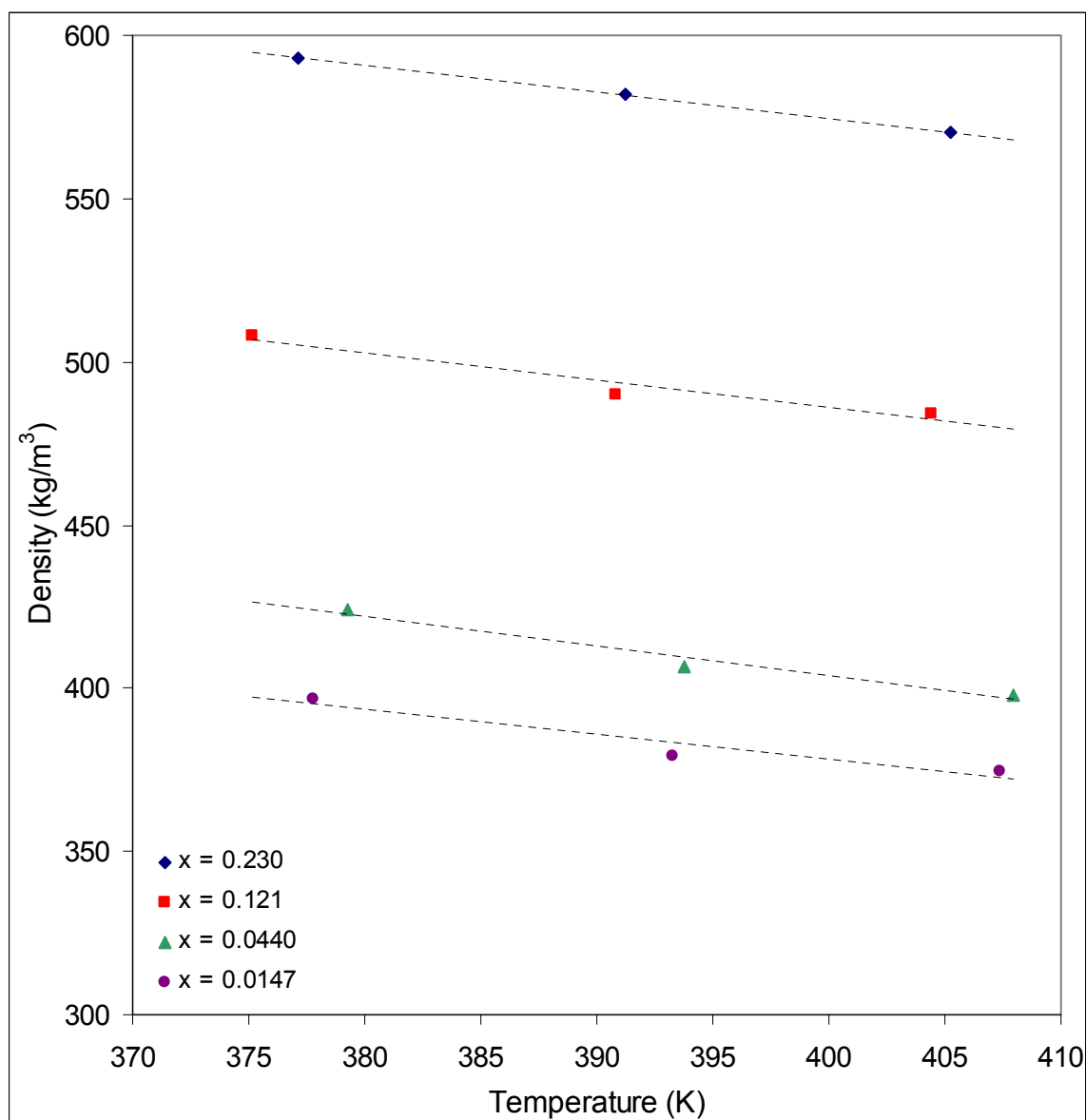
Figure 6-13: Temperature Correction of Density Data at the Phase Boundary by Linear Interpolation: Density-Temperature Plot at Constant Mass Fraction: C3-C54

Although the fit above is not perfect, it is well within the accuracy of the experimental measurements. For the density correlation, an average R^2 value of 0.9641 was found for the correlation of all the experimental data.

Accuracy of Density Data

The accuracy of the density measurements was a lot less that that of the pressure measurements. This can be attributed firstly to the fact that the volume measurements are not very accurate. The primary aim of the equipment designed was not to measure densities but rather phase equilibria.

The main errors in the density are due to small leaks that may have occurred while the cell was operational as well as inaccuracies in the calculation of the amount of solvent loaded. The effect of leaks are not seen in the pressure-composition plots as the cell was in the single phase region for most of the time. Consider a density composition plot:

- Where the cell loses mass due to a small leak, the mass fraction in the cell remains constant but the density measured is incorrect. When calculating the density the actual mass in the cell is less that the mass used for the calculations and thus the actual density will be less.

- Should the amount of solvent calculated be incorrect, both the density and the mass fraction will be incorrectly estimated. For example, if the actual amount of solvent is less that the calculated amount of solvent, the actual density is less than the calculated density and the actual mass fraction is higher then the calculated mass fraction.

These two possible errors are explained in Figure 6-14.
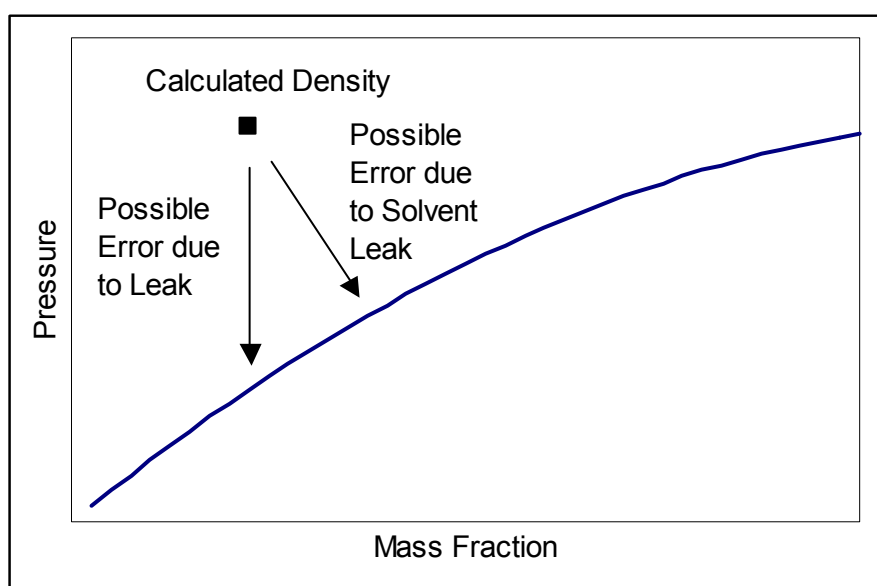
Figure 6-14: Schematic Representation of Possible Errors in density calculation.

The errors illustrated in Figure 6-14 can possible explain the scatter in the composition density plots. Taking all factors into account a maximum error of $\pm$ 40 kg/m^3 can be expected.

6.2.3. DENSITY-COMPOSITION PLOTS

In Figure 6-15 to Figure 6-23, the density is plotted as a function of mass fraction. The temperature corrected data used to generate the graphs is given in Appendix B. A second degree polynomial is plotted through the data at 408.15 K.
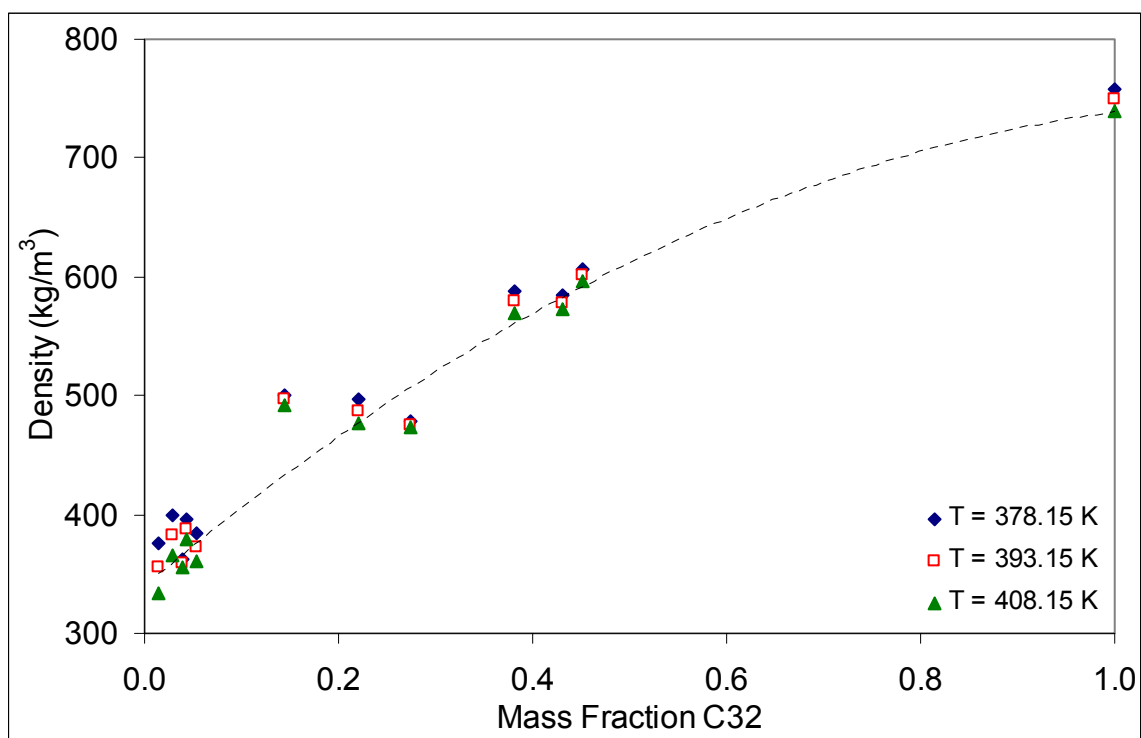
Figure 6-15: Isothermal Density – Composition Plot of Phase Boundary for Propane-Dotriacontane system
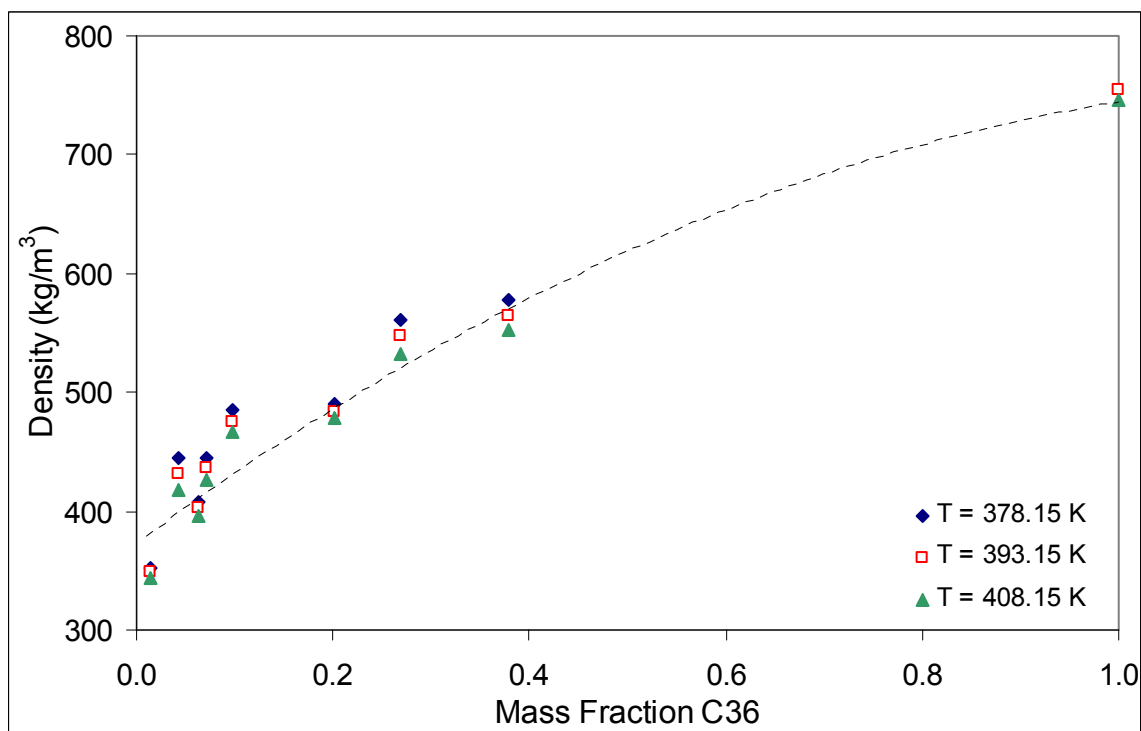
Figure 6-16: Isothermal Density – Composition Plot of Phase Boundary for Propane-Hexatriacontane system
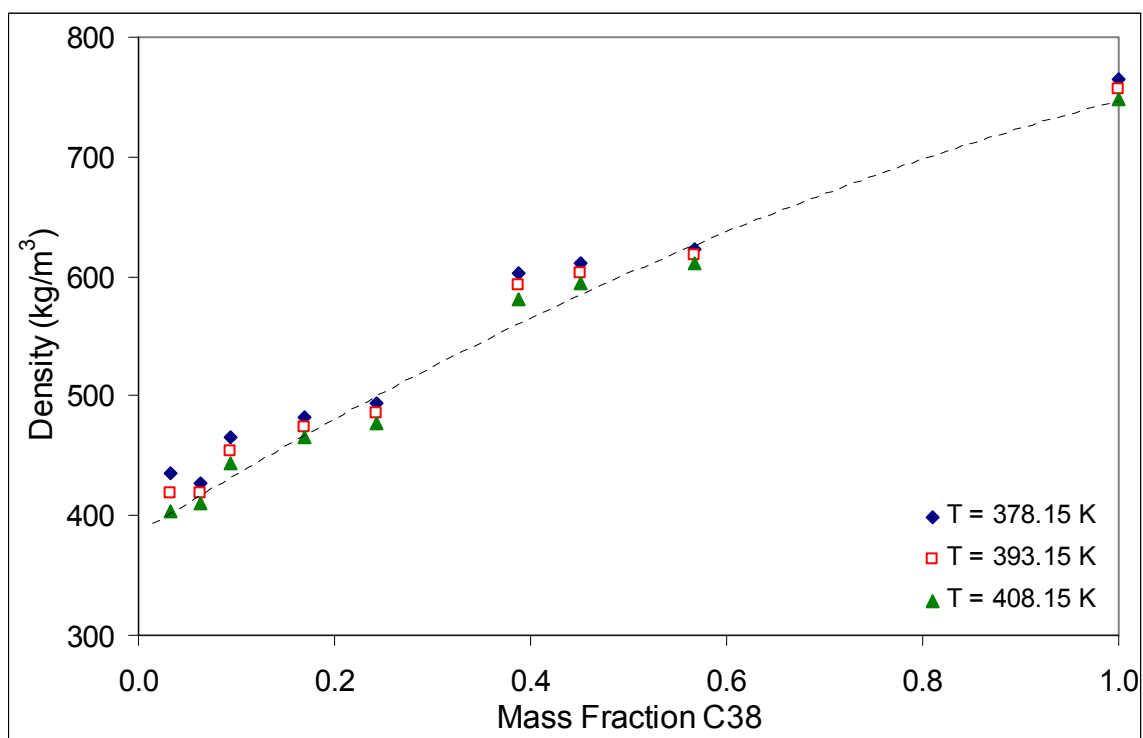
Figure 6-17: Isothermal Density – Composition Plot of Phase Boundary for Propane-Octatriacontane system
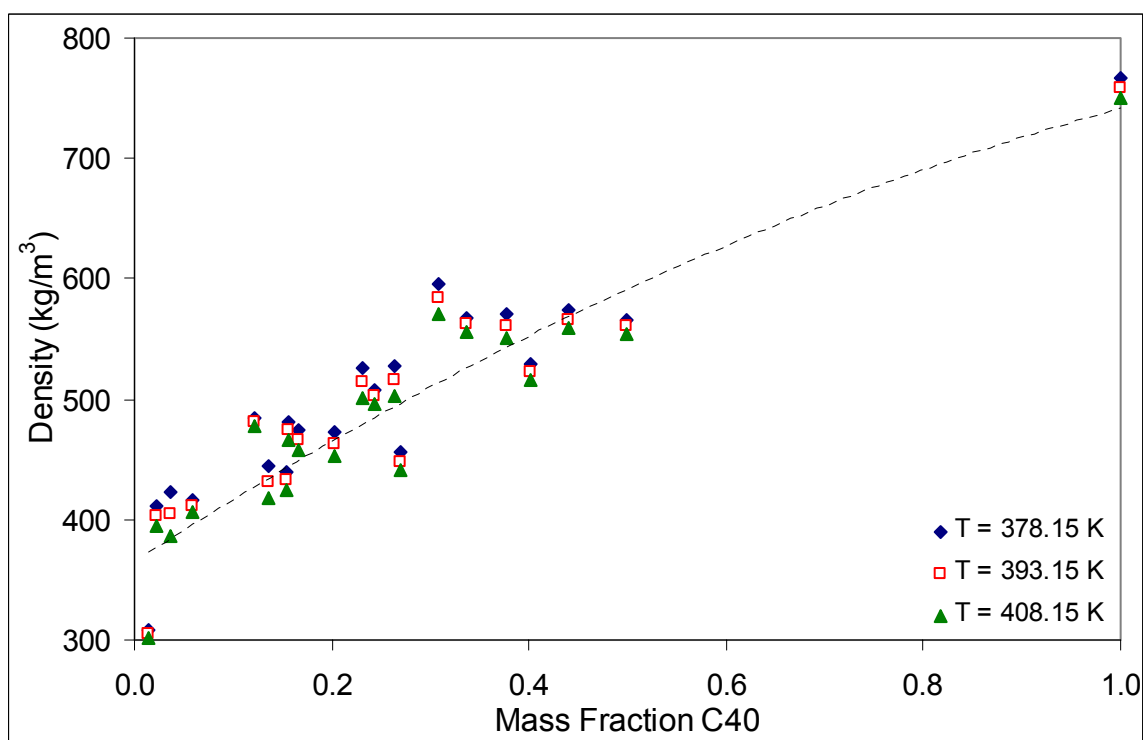
Figure 6-18: Isothermal Density – Composition Plot of Phase Boundary for Propane-Tetracontane system
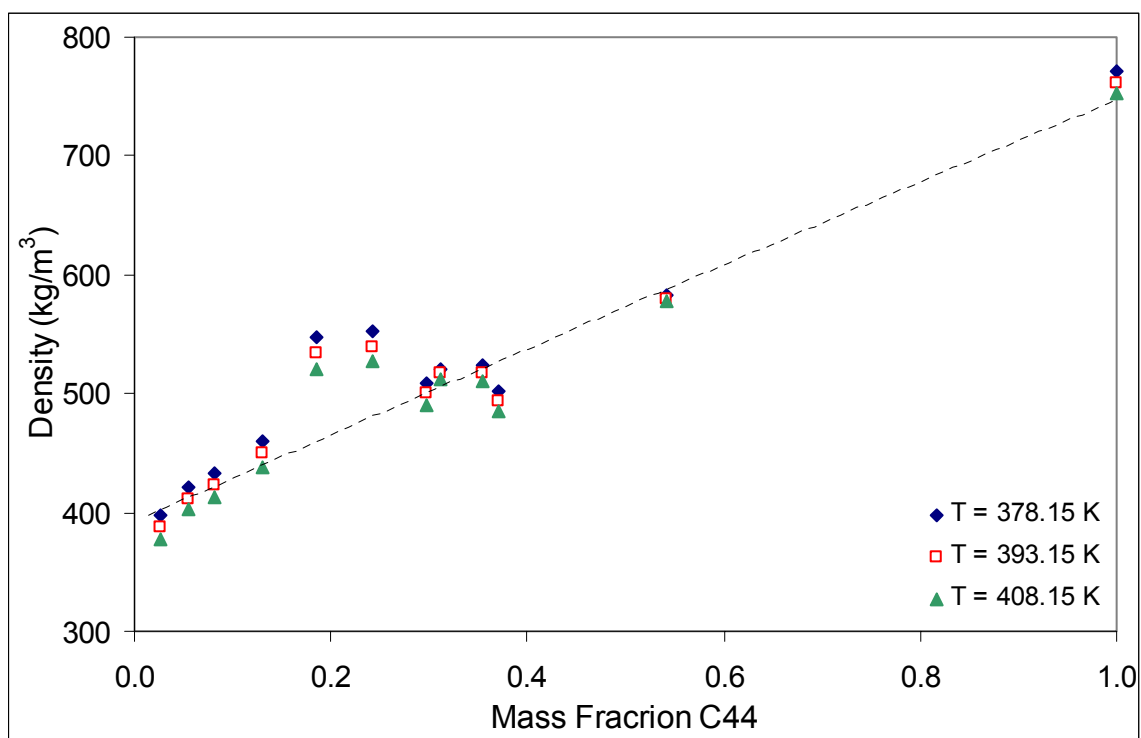
Figure 6-19: Isothermal Density – Composition Plot of Phase Boundary for Propane-Tetratetracontane system
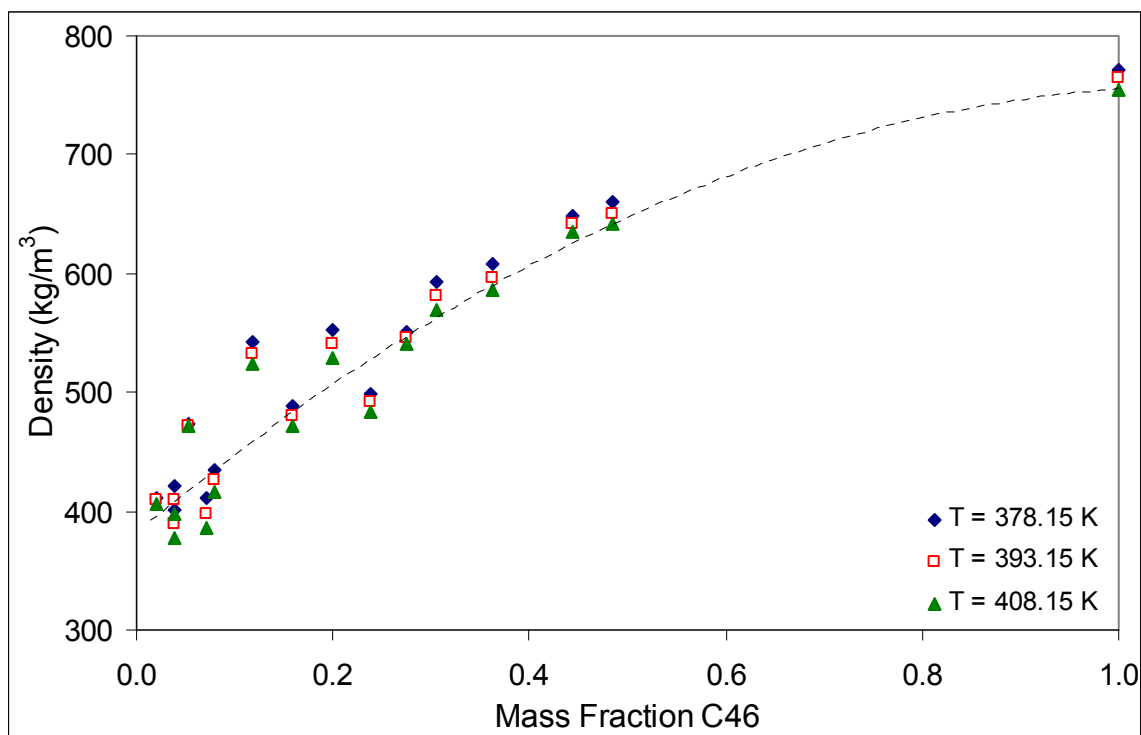
Figure 6-20: Isothermal Density – Composition Plot of Phase Boundary for Propane-Hexatetracontane system
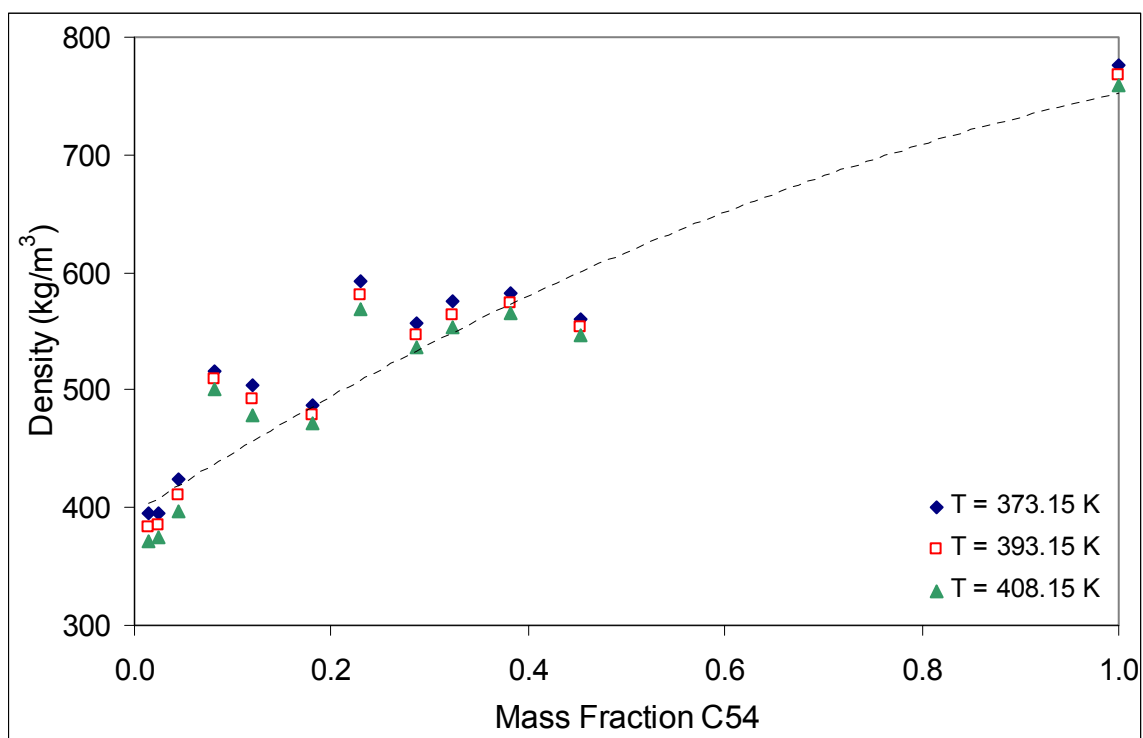
Figure 6-21: Isothermal Density – Composition Plot of Phase Boundary for Propane-Tetrapentacontane system
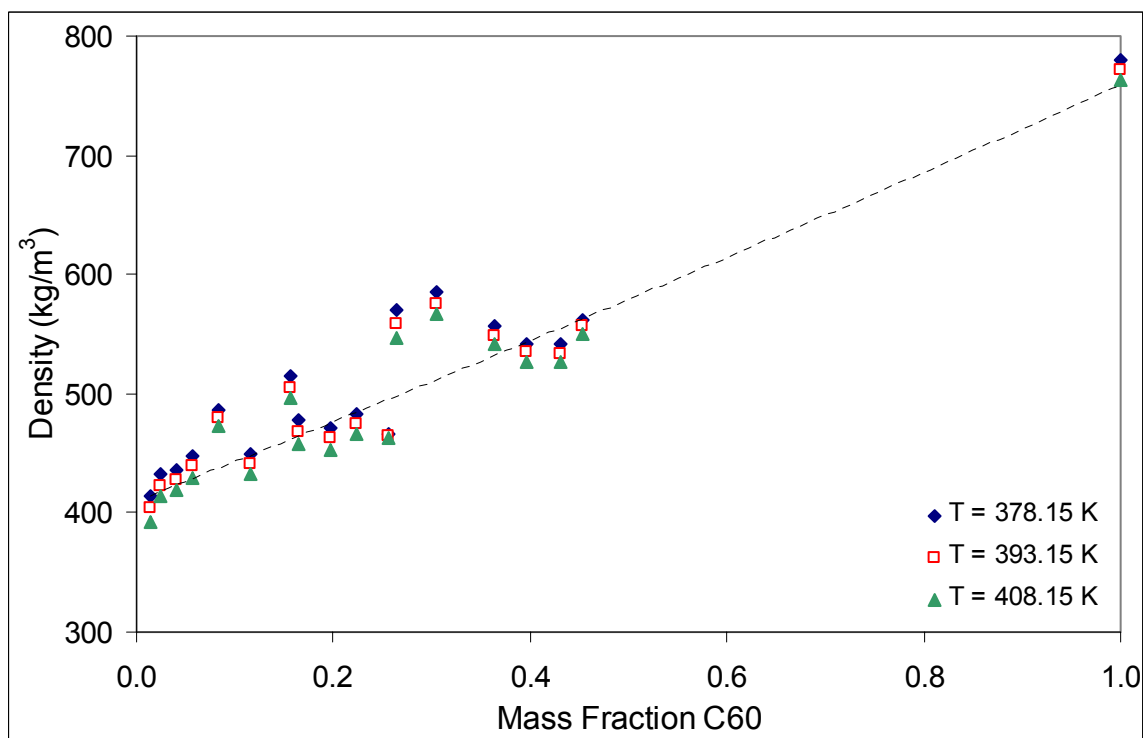
Figure 6-22: Isothermal Density – Composition Plot of Phase Boundary for Propane-Hexacontane system
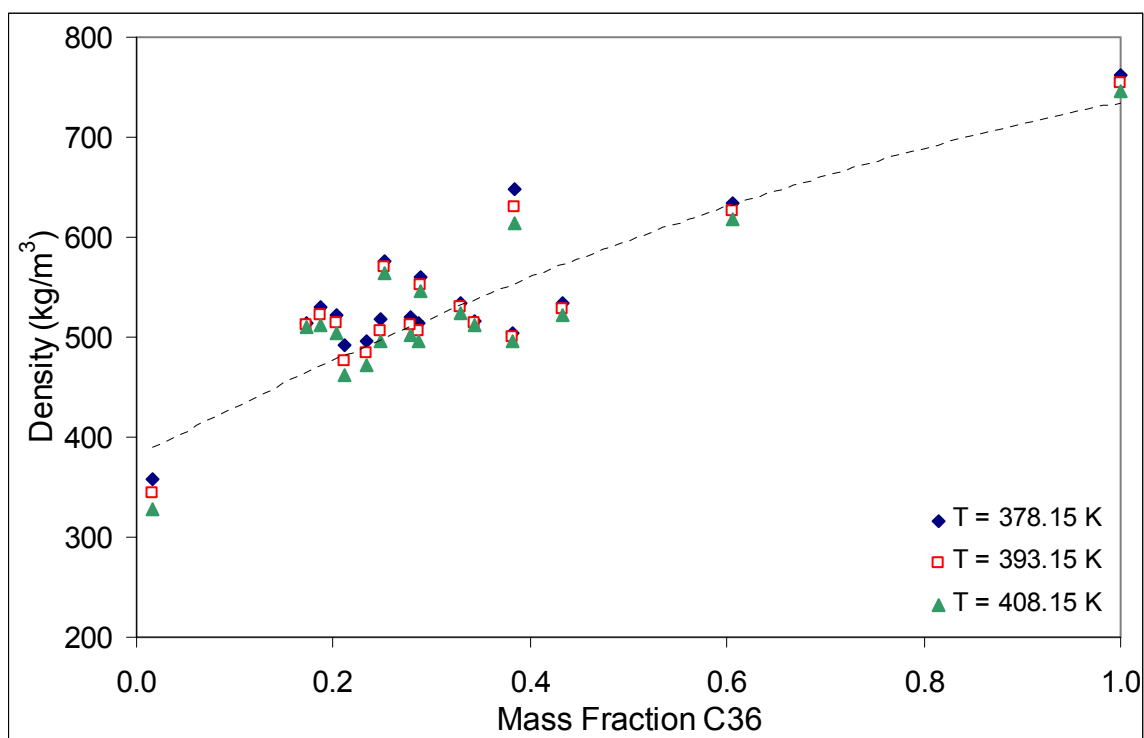
Figure 6-23: Isothermal Density – Composition Plot of Phase Boundary for LPG-Hexatriacontane system

6.2.4. PRESSURE-DENSITY PLOT

It is necessary to determine if there is a density difference between the two phases in equilibrium. A significant difference in density is a prerequisite for phase split between two phases and the larger the density difference, the easier the two phases will split.

In Figure 6-24 to Figure 6-31 the pressure is plotted as a function of the density. These plots can be used to determine if there is a significant difference in density between the two phases that are in equilibrium. A polynomial is fitted through each data set, the order depending on the best fit.
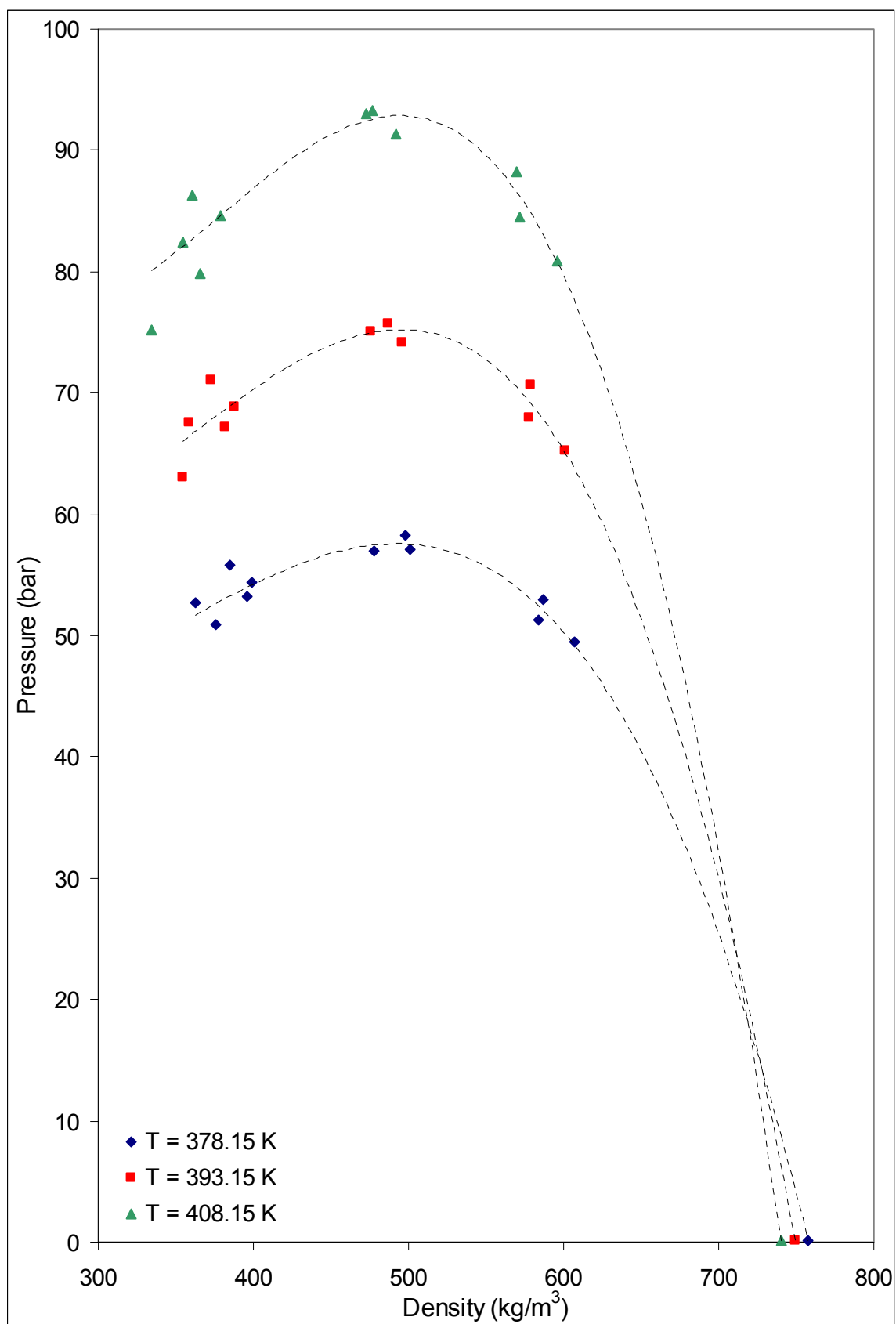
Figure 6-24: Isothermal Pressure – Density Plot of Phase Equilibrium Boundary for Propane-Dotriacontane system
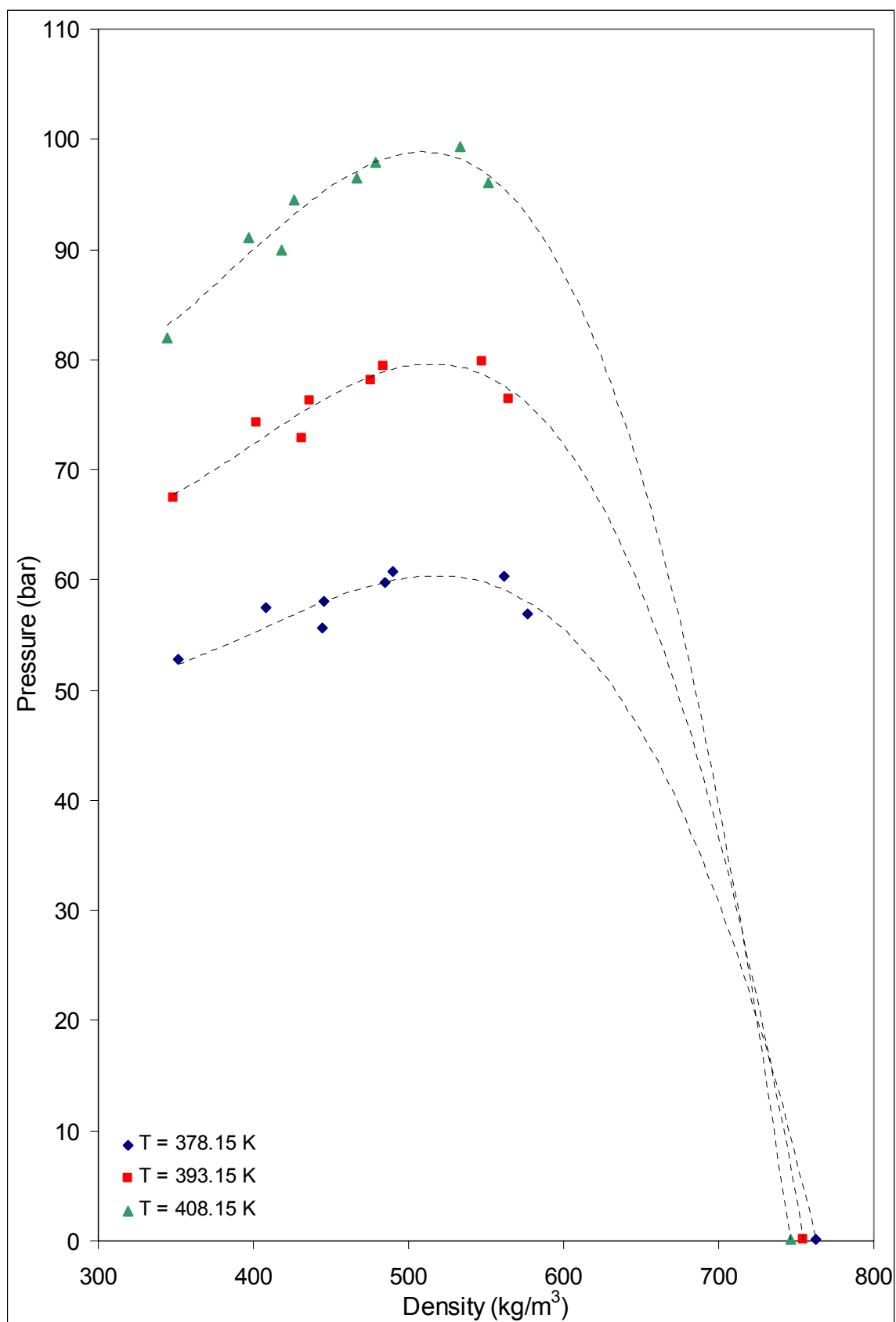
Figure 6-25: Isothermal Pressure – Density Plot of Phase Equilibrium for Propane-Hexatriacontane system
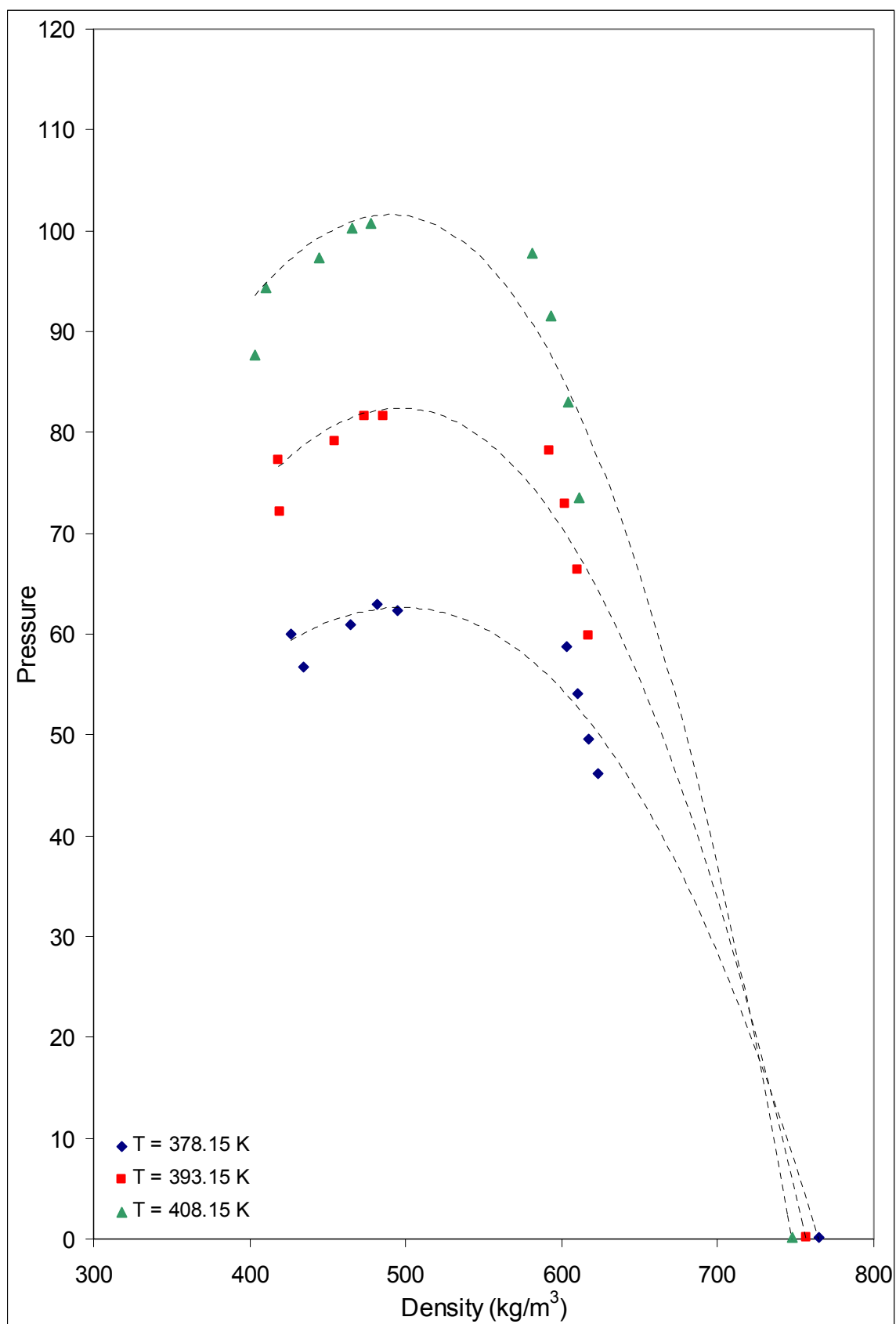
Figure 6-26: Isothermal Pressure – Density Plot of Phase Equilibrium Boundary for Propane-Octatriacontane system
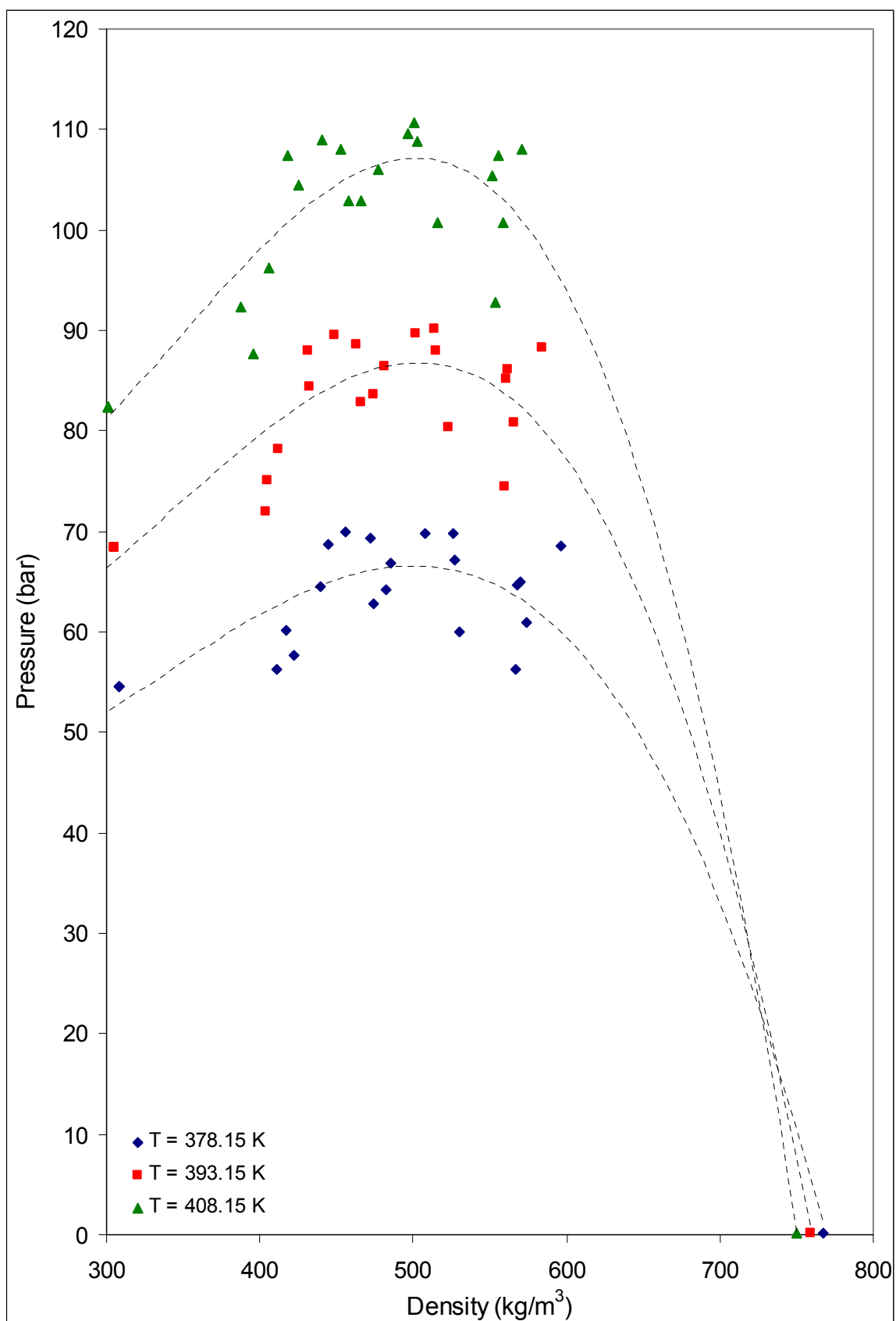
Figure 6-27: Isothermal Pressure – Density Plot of Phase Equilibrium Boundary for Propane-Tetracontane system
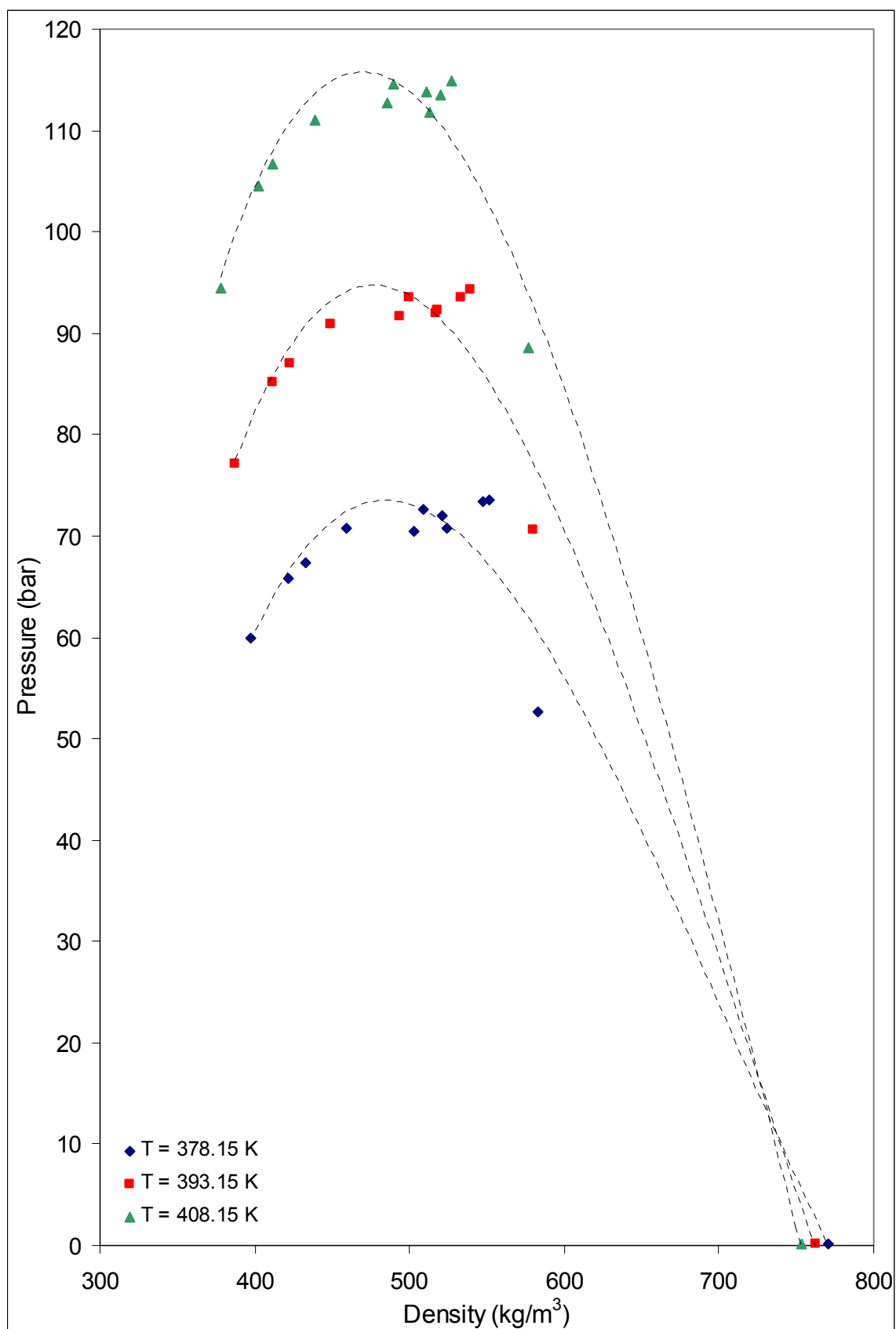
Figure 6-28: Isothermal Pressure – Density Plot of Phase Equilibrium Boundary for Propane-Tetratetracontane system
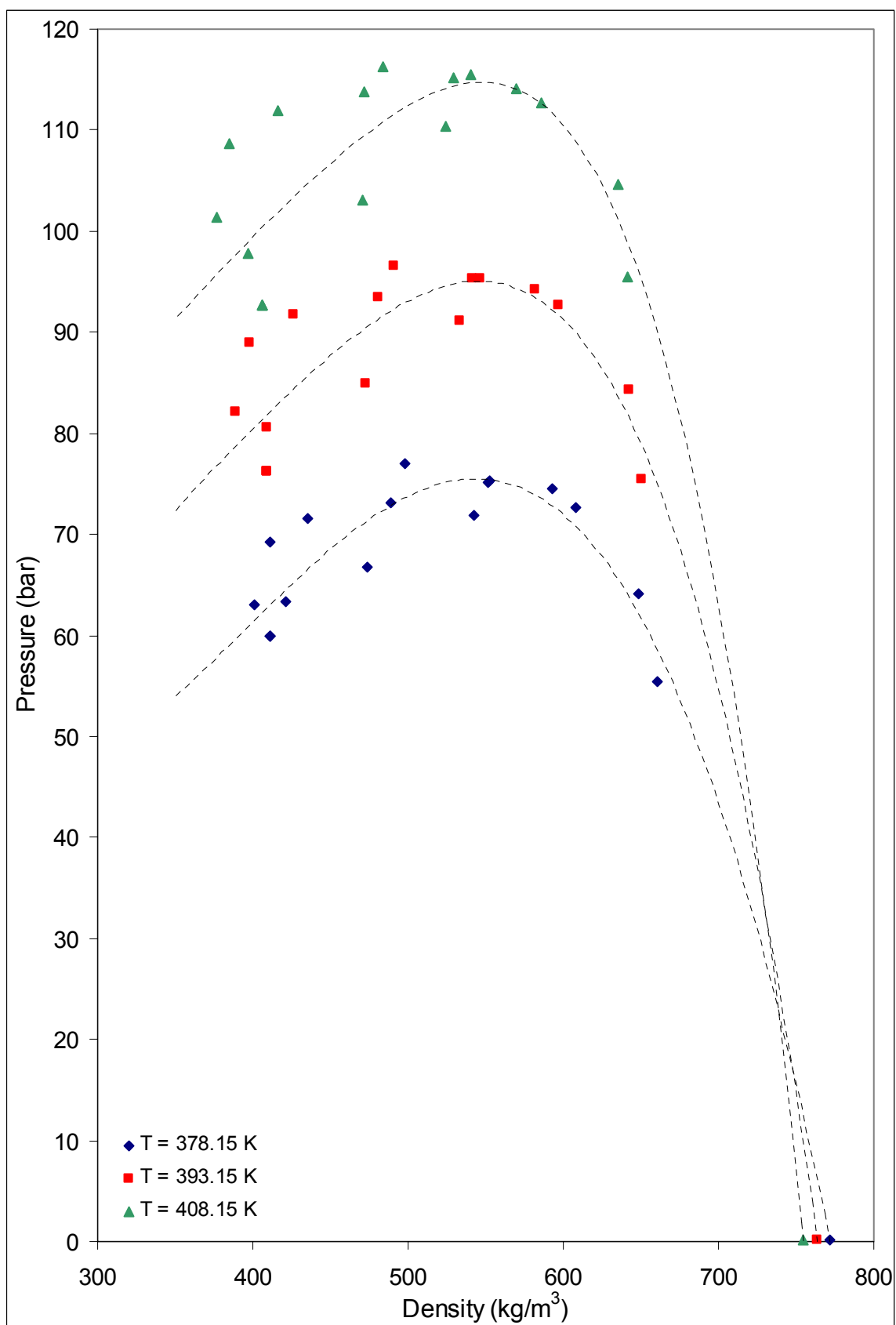
Figure 6-29: Isothermal Pressure – Density Plot of Phase Equilibrium Boundary for Propane-Hexatetracontane system
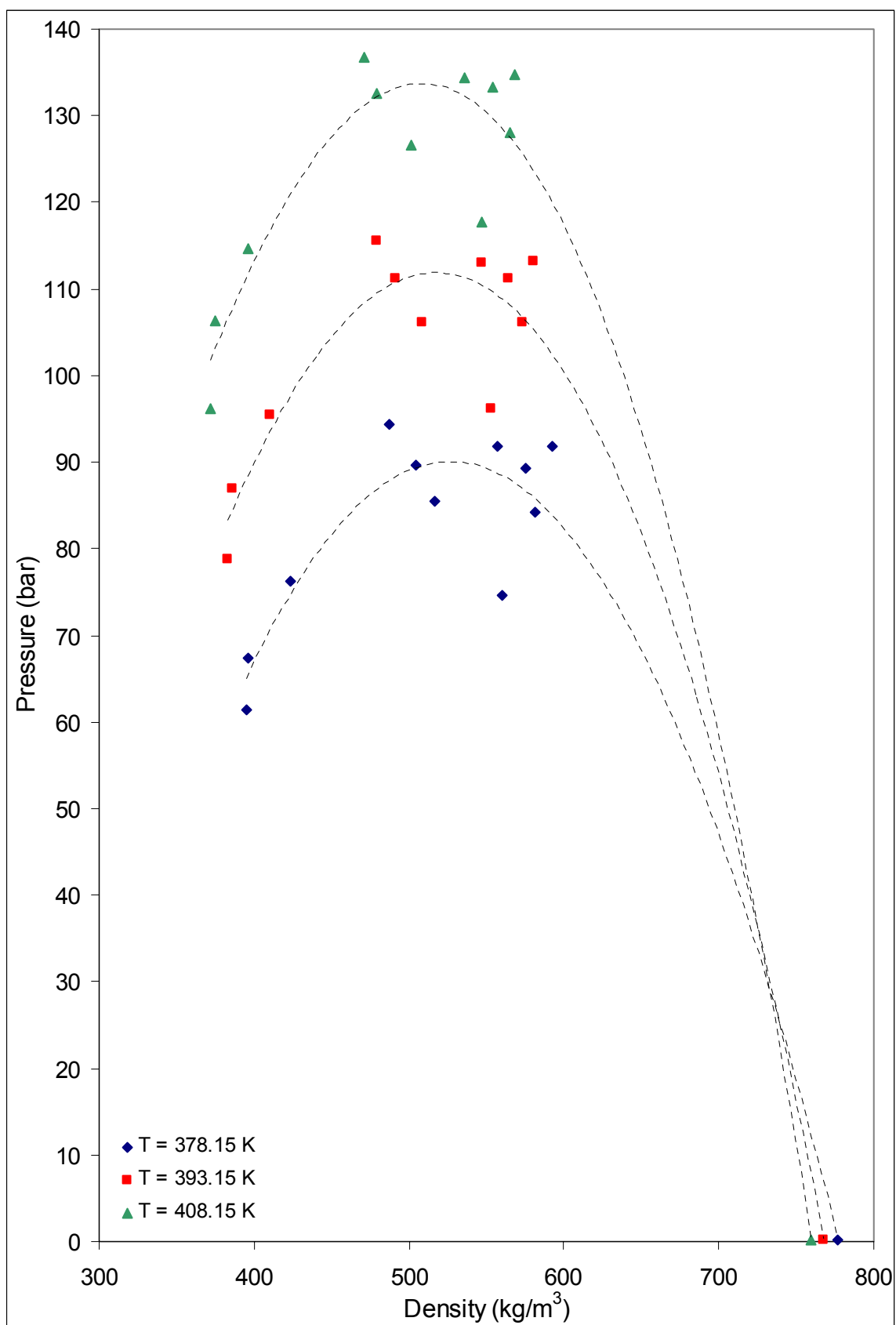
Figure 6-30: Isothermal Pressure – Density Plot of Phase Equilibrium Boundary for Propane-Tetrapentacontane system
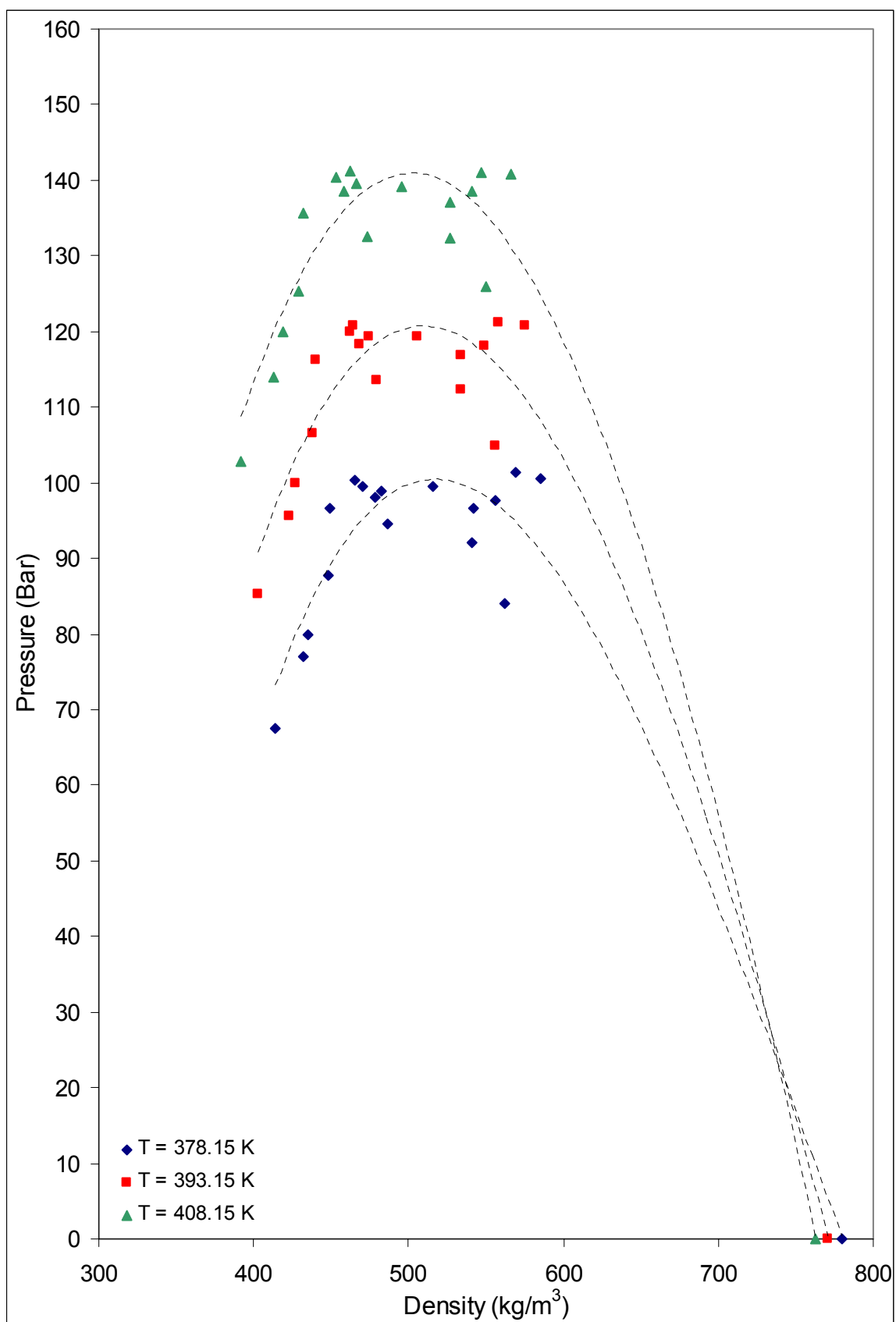
Figure 6-31: Isothermal Pressure – Density Plot of Phase Equilibrium Boundary for Propane-Hexacontane system
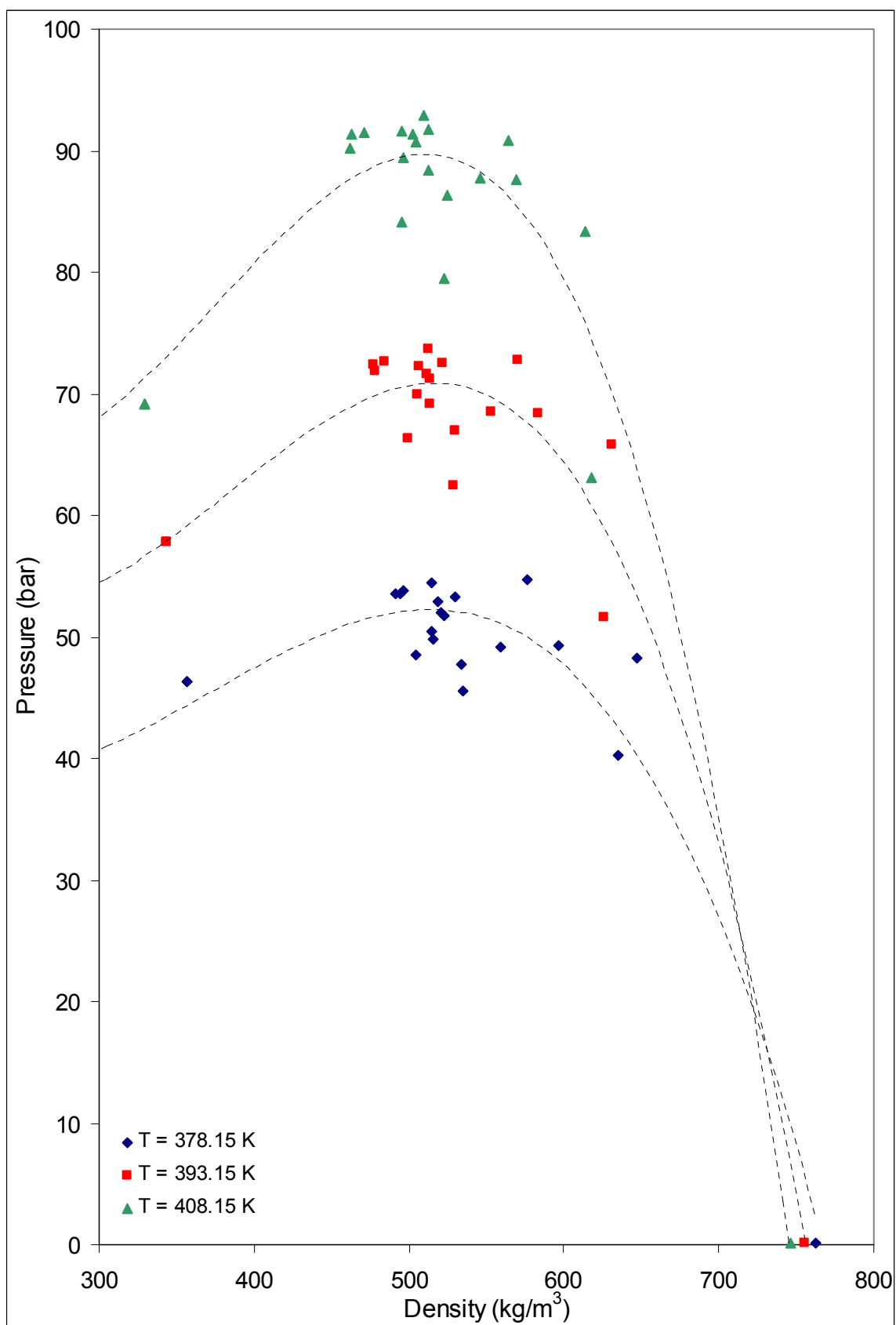
Figure 6-32: Isothermal Pressure – Density Plot of Phase Equilibrium Boundary for LPG-Hexatriacontane system

6.2.5. DISCUSSION OF DATA

The accuracy of the density measurements is discussed in paragraph 6.2.2. Due to the fact that the density measurements are not as accurate as the pressure measurements, it can be seen that the density plots are not as smooth. It must be remembered that density measurements are not the primary aim of the project.

Phase Inversions

Additionally, it can be seen that no phase inversion occurs for these systems at the temperatures studied here. The absence of phase inversions is important for the design of columns.

Effect of Temperature

As expected, an increase in temperature leads to a decrease in the phase transition density at constant composition due to the effect of thermal expansion.

Flash Considerations

For a flash to be able to separate easily into two different phases, the densities of the two phases need to differ significantly. No fixed rule exists for the magnitude of the density difference, yet a larger density difference will be conducive to a better and faster phase split. Typically a minimum density difference of about 110 kg/m^3 is required for a good phase split.
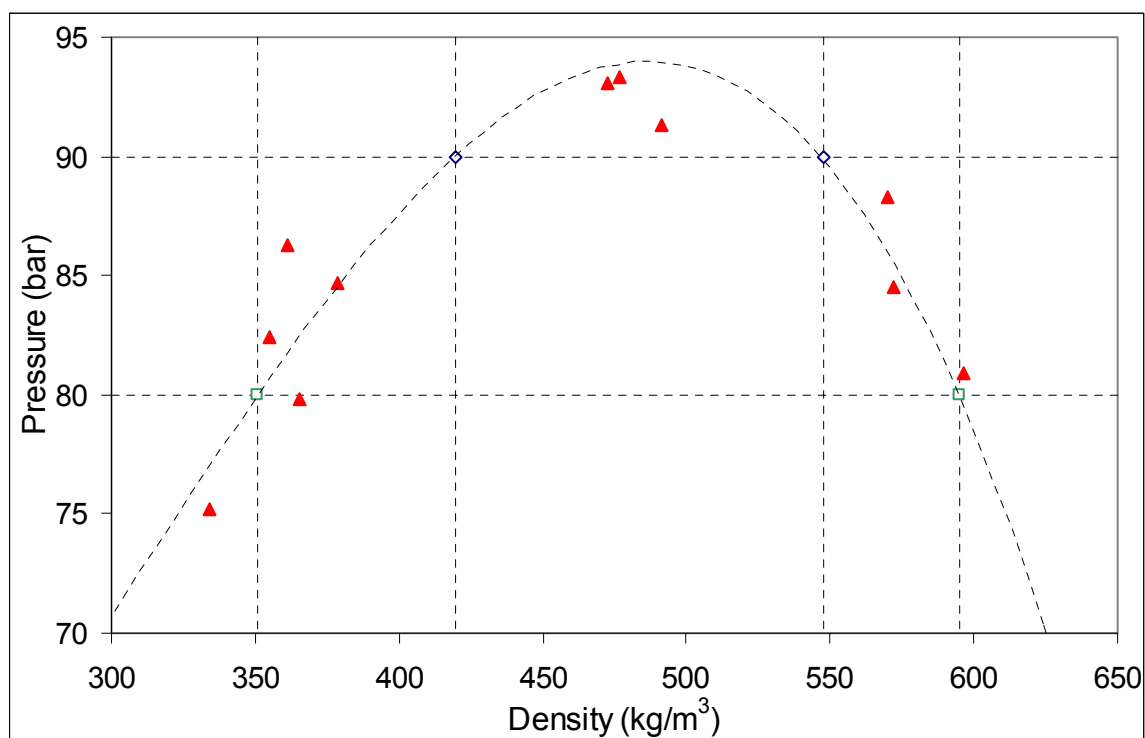
Figure 6-33: Isothermal (408.15 K) Pressure-Density Plot for Propane-Dotriacontane for use in Flash Calculations

As can be seen above, at a pressure of 90 bar and 408.15 K a bubble point flash would results in a light phase with a density of about 420 kg/m^3 and a heavy phase density of 548 kg/m^3. Similarly, a flash at 80 bar would result in densities of 351 and 595 kg/m^3. An operating pressure of 90 bar may be a little high due to the densities being quite close and 85 bar should typically be favoured for this example.

6.3.   COMPARISON OF EXPERIMENTAL AND LITERATURE DATA

Although only limited data is available in the literature where comparisons can be made, these comparisons are shown below.

6.3.1.   COMPARISON OF PROPANE-DOTRIACONTANE AND PROPANE-HEXATRIACONTANE WITH PROPANE-TETRATRIACONTANE DATA

A comparison of the propane data generated for dotriacontane and hexatriacontane with published data of tetratriacontane is compared in Figure 6-34.
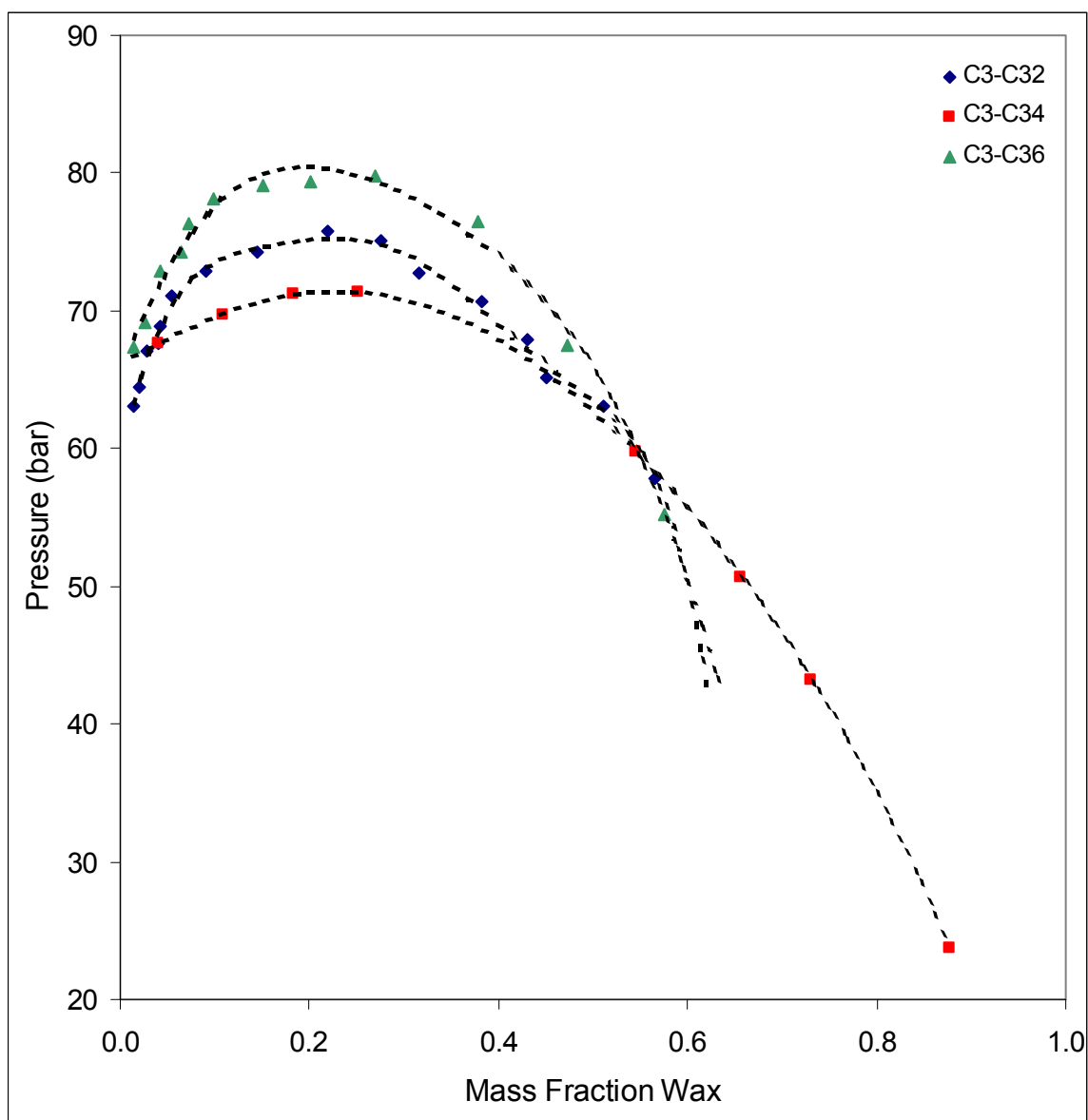
Figure 6-34: Comparison of Experimental Propane-C32 and Propane-C36 Pressure Composition Plot with Literature Data of Propane-C34 by Peters et al. at 393.15 K (Peters et al., 1992).

To compare the tetratriacontane data with the hexatriacontane and dotriacontane data, temperature correction of the data was required and the same type of linear interpolation used for the experimental data generated in this work was applied to the literature data.

It is expected that the tetratriacontane data should lie between the dotriacontane and hexatriacontane data. As can be seen above, the high mass fraction wax data points seem to correspond well, yet those in the critical region differ from those measured in this work.

The accuracy of the data from this work in the above figure can be justified through the pressure carbon number plots in paragraph 6.4.1 and the fact that the equipment was tested against other data and proved to be accurate. (Paragraph 5.5)

6.3.2. COMPARISON OF PROPANE-TETRACONTANE DATA

Chan et al. published data for propane-tetracontane (Chan et al., 2000). As stated in paragraph 5.2.3, the pressure measurement technique of Chan et al is not very accurate. These inaccuracies can be seen when their data is compared to that of this work in Figure 6-35:
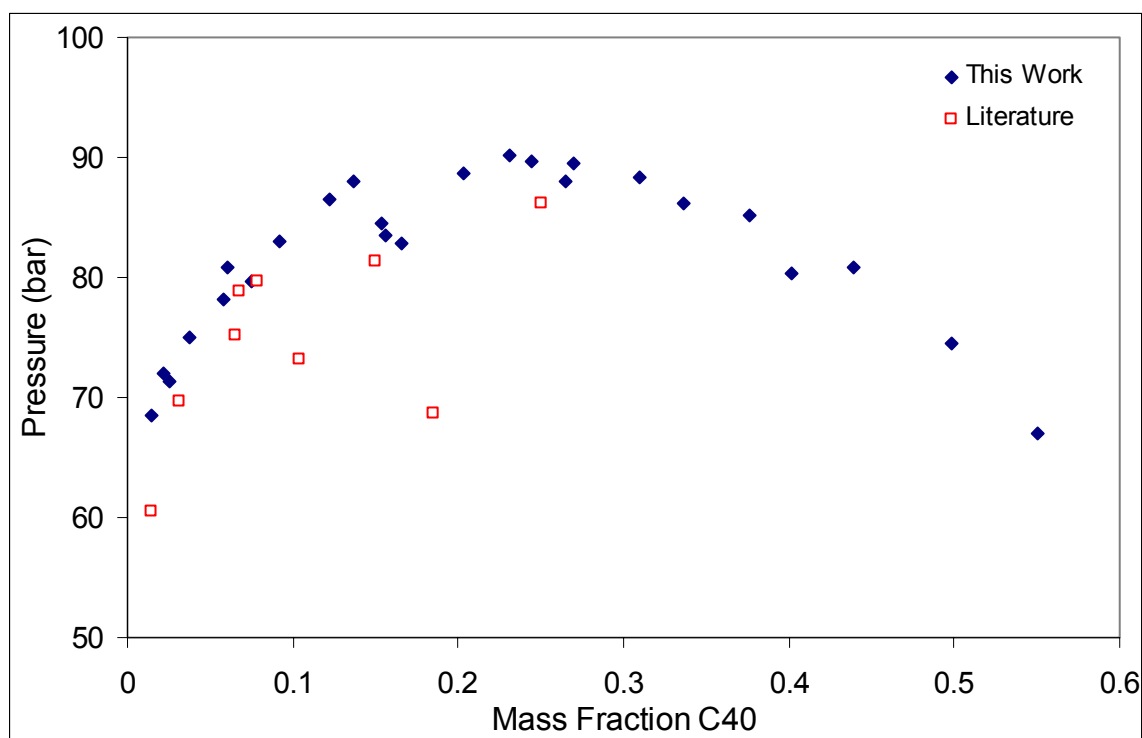
Figure 6-35: Comparison of Experimental Propane-C40 Pressure-Composition Plot with Literature Data by Chan et al. at 393.15 K (Chan et al., 2000)

In generating Figure 6-35 the same method of temperature correction was used for the literature data that was used in this work. The accuracy of the linearization for the temperature corrections of the literature data was in the same order than found in this work and resulted in R^2 values of 0.9970.

The scattered data can possibly be explained by considering the experimental set-up of Chan et al. (Chan et al., 2000). The pressure measurements were not done directly in the cell, but rather the pressure applied to generate the pressure in the cell. This method leads to inaccuracies due to inertia and friction. Additionally, no indication is given indicating if the temperature is measured directly or indirectly. These two factors could result in the scattering as shown in the data above.

The comparison thus has no real value outside confirming that the range of the experiments done in this work is in the correct order of magnitude.

6.3.3. COMPARISON OF PROPANE-HEXACONTANE DATA

Peters et al. published data for propane – hexacontane. A comparison of the data is given in Figure 6-36 (Peters et al., 1993).
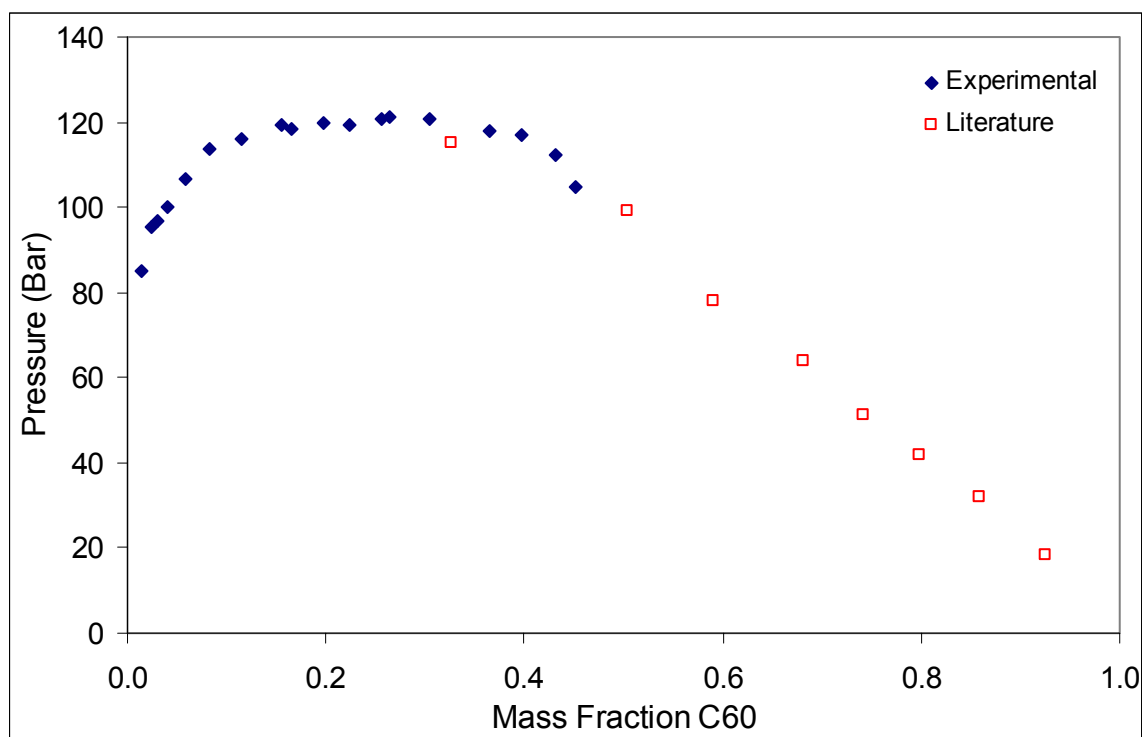
Figure 6-36: Comparison of Experimental Propane-C60 Pressure-Composition Plot with Literature Data by Peters et al. at T = 393.15 K (Peters et al., 1993)

From Figure 6-36 it can be seen that the data sets compare well and complement each other. If the lowest mass fraction data point from the literature data is omitted the data forms a continuous set that can be used well in the modelling. Omission of the data point can be justified due to the fact that the same equipment was used for the above data as was used for the propane-tetratriacontane data and the pressure measurements of the tetratriacontane data in the mixture critical region are generally lower than what should be expected.

6.3.4. COMPARISON OF DENSITY

No data was found where a direct comparison of the density measurement could be made. For the systems propane plus triacontane and squalene (2,6,10,15,19,23 Hexamethyltetracosane) Aalto et al. measured densities at 373.3 K and at pressures just above the phase boundary (Aalto et al., 1996). The values of 291.6 and 330 kg/m^3 are in the same order of magnitude than those measured in this work for dotriacontane.

6.4. COMPARISON OF DATA SETS

A comparison of the various data sets is also required to determine if fractionation between different waxes is possible. A study of the effect of the molecular weight on the phase equilibrium pressure and density, and the effect of the solvent will be presented below.

6.4.1. EFFECT OF MOLECULAR WEIGHT OF WAX ON PHASE EQUILIBRIA

To determine the effect of the molecular weight on the phase equilibrium pressure, pressure-carbon number plots at constant composition and temperature are given in Figure 6-37 to Figure 6-48. Linear interpolation was used to determine the points on the graphs and the data is given in Appendix E.4.
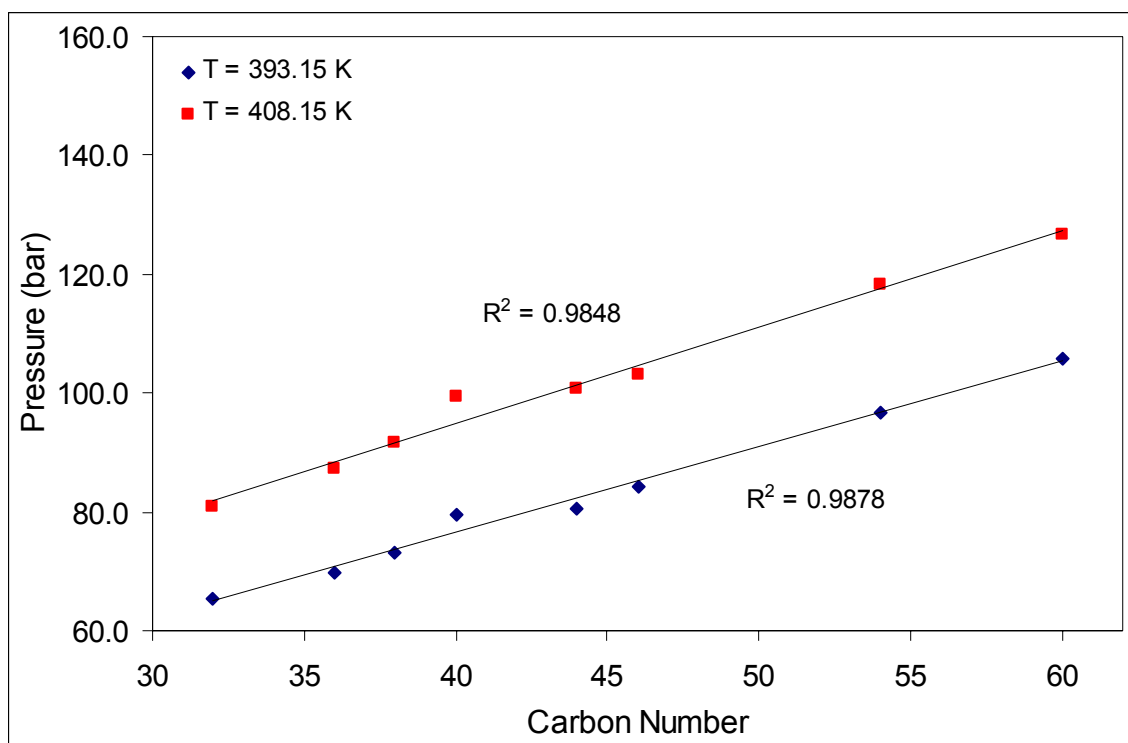
Figure 6-37: Pressure-Carbon Number Plot at mass fraction 0.45
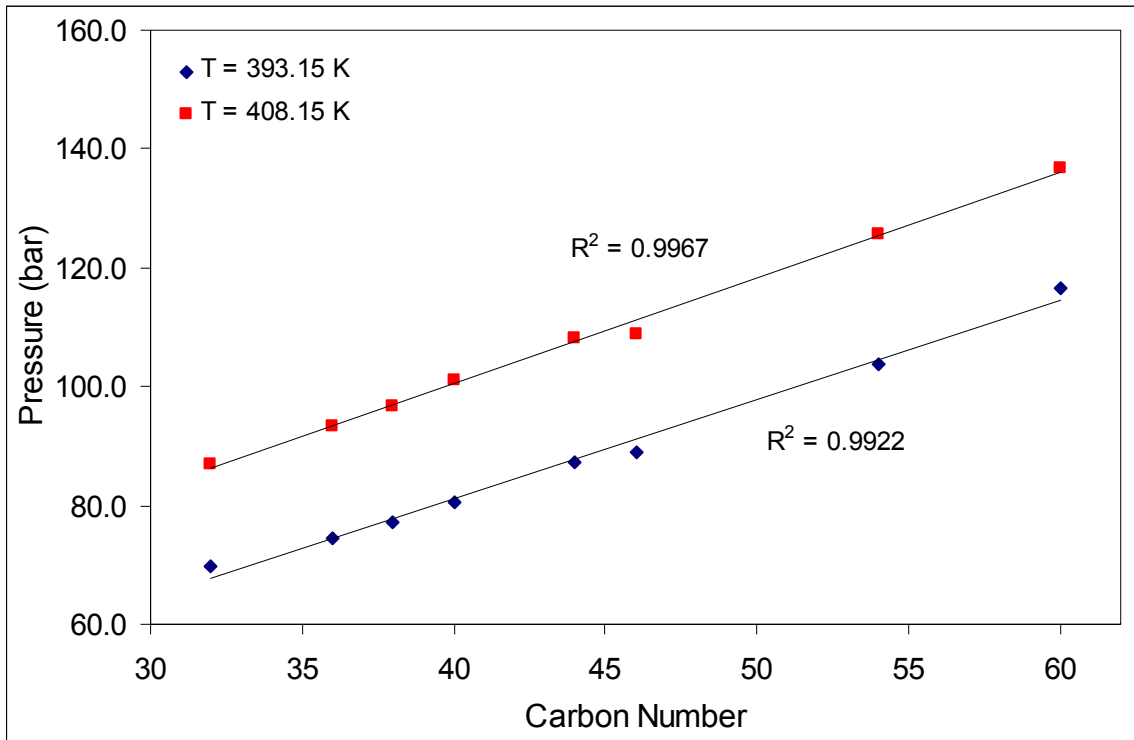
Figure 6-38: Pressure-Carbon Number Plot at mass fraction 0.40
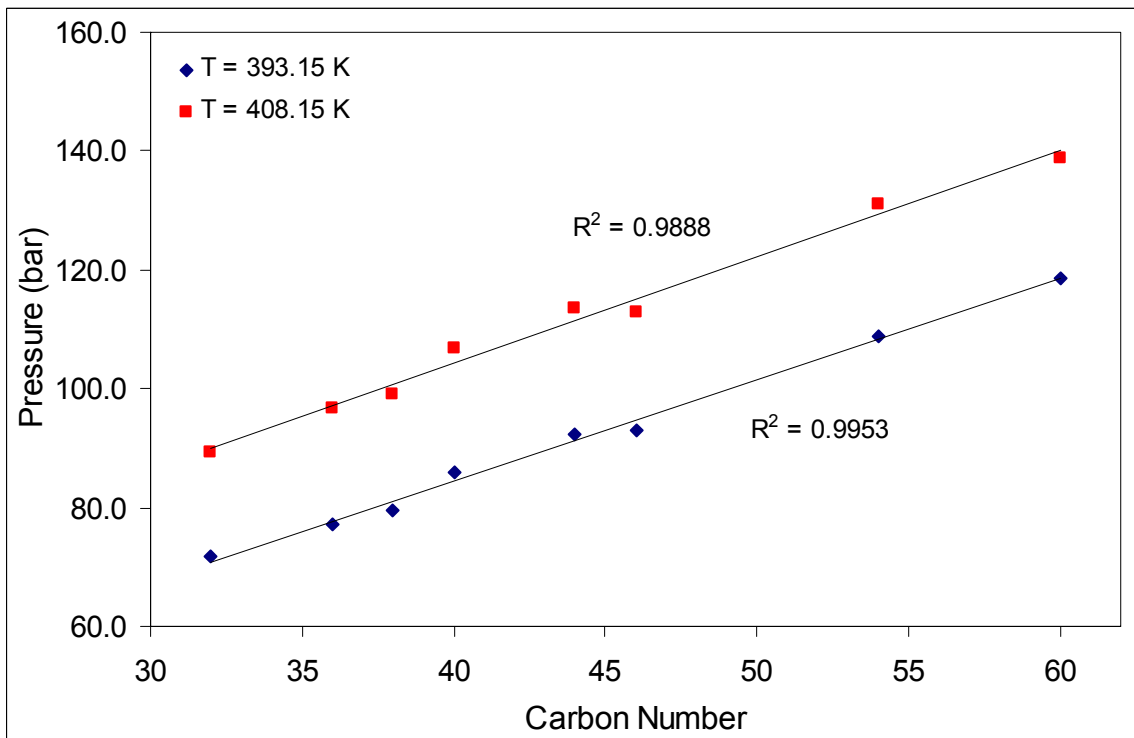
Figure 6-39: Pressure-Carbon Number Plot at mass fraction 0.35
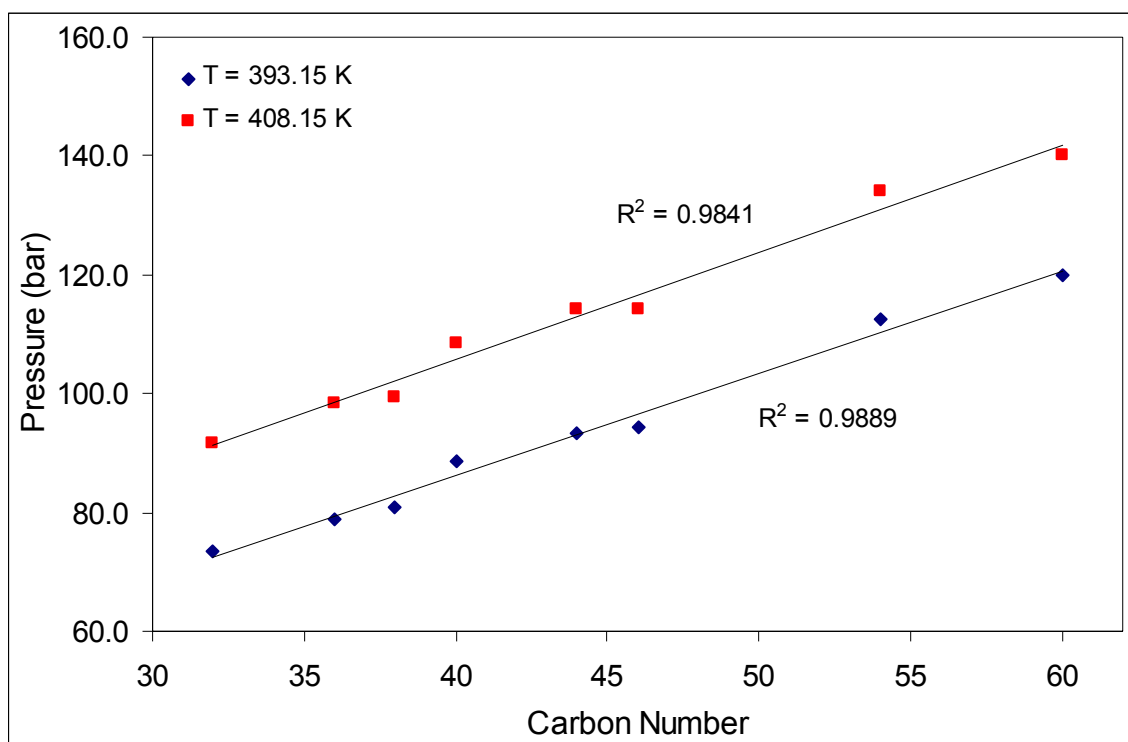
Figure 6-40: Pressure-Carbon Number Plot at mass fraction 0.30
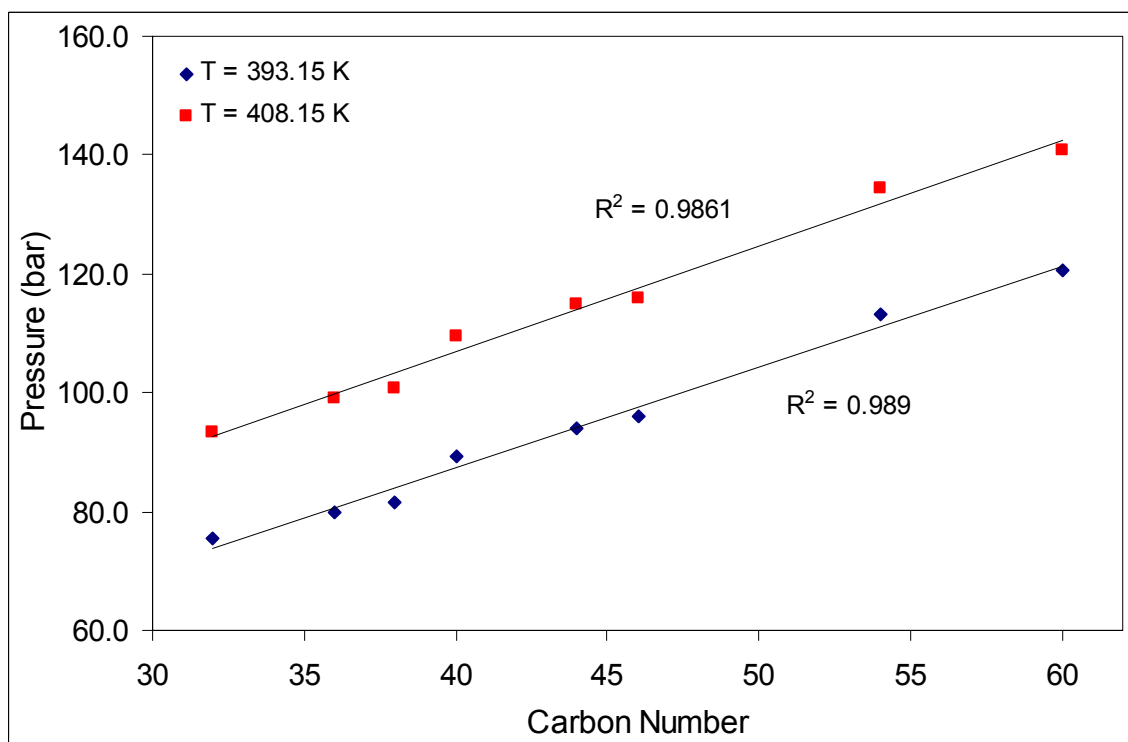
Figure 6-41: Pressure-Carbon Number Plot at mass fraction 0.25
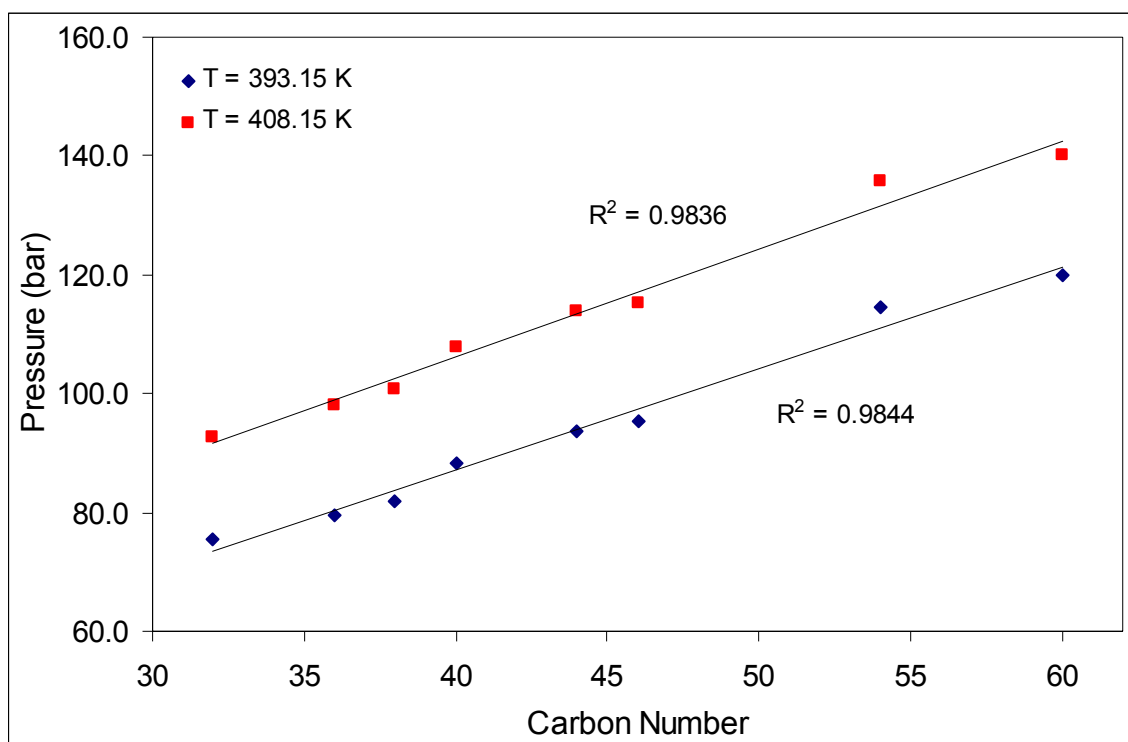
Figure 6-42: Pressure-Carbon Number Plot at mass fraction 0.20
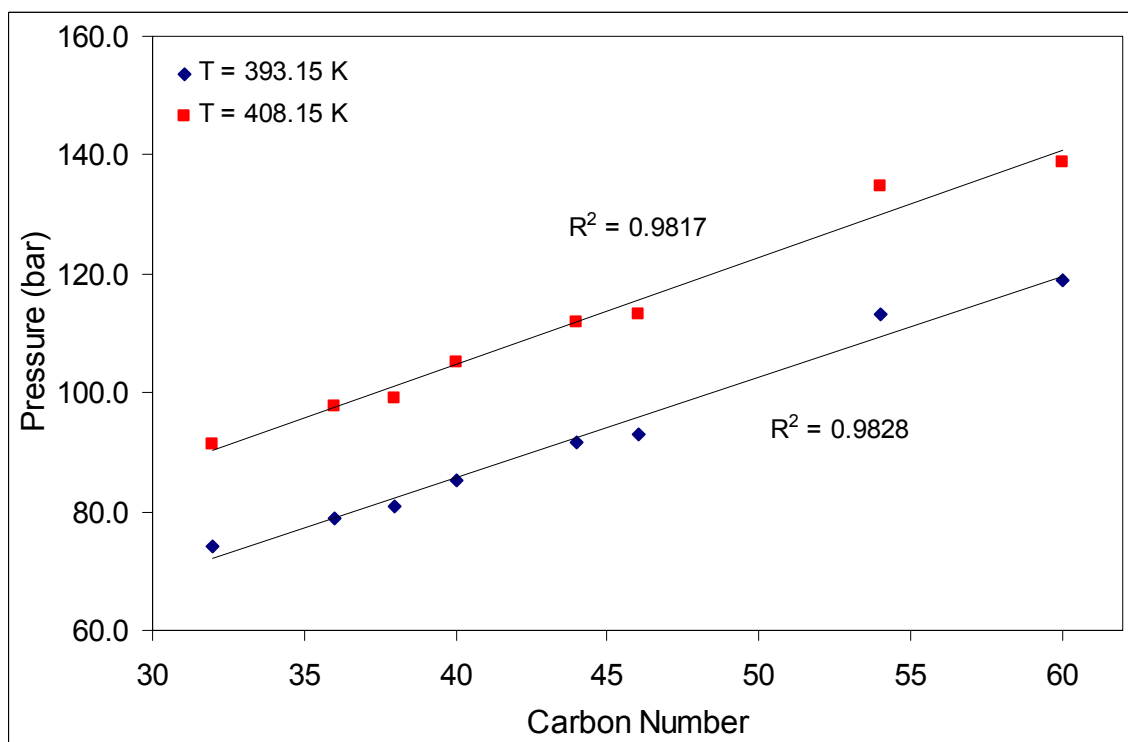
Figure 6-43: Pressure-Carbon Number Plot at mass fraction 0.15
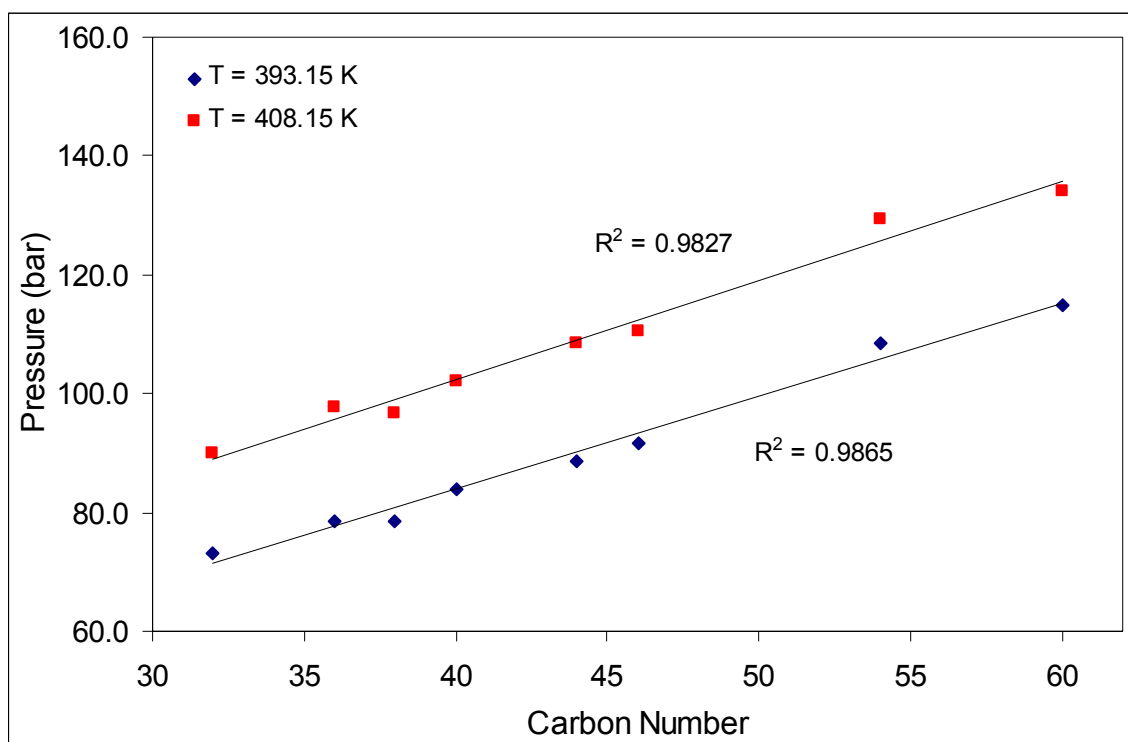
Figure 6-44: Pressure-Carbon Number Plot at mass fraction 0.10
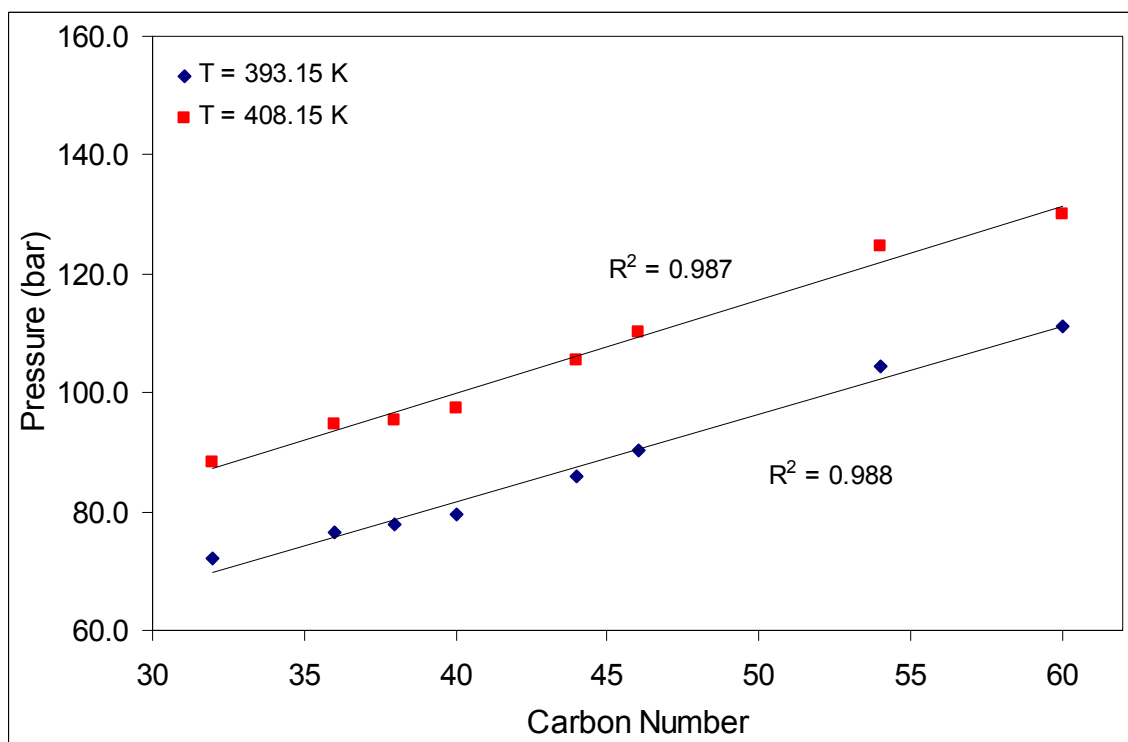
Figure 6-45: Pressure-Carbon Number Plot at mass fraction 0.075
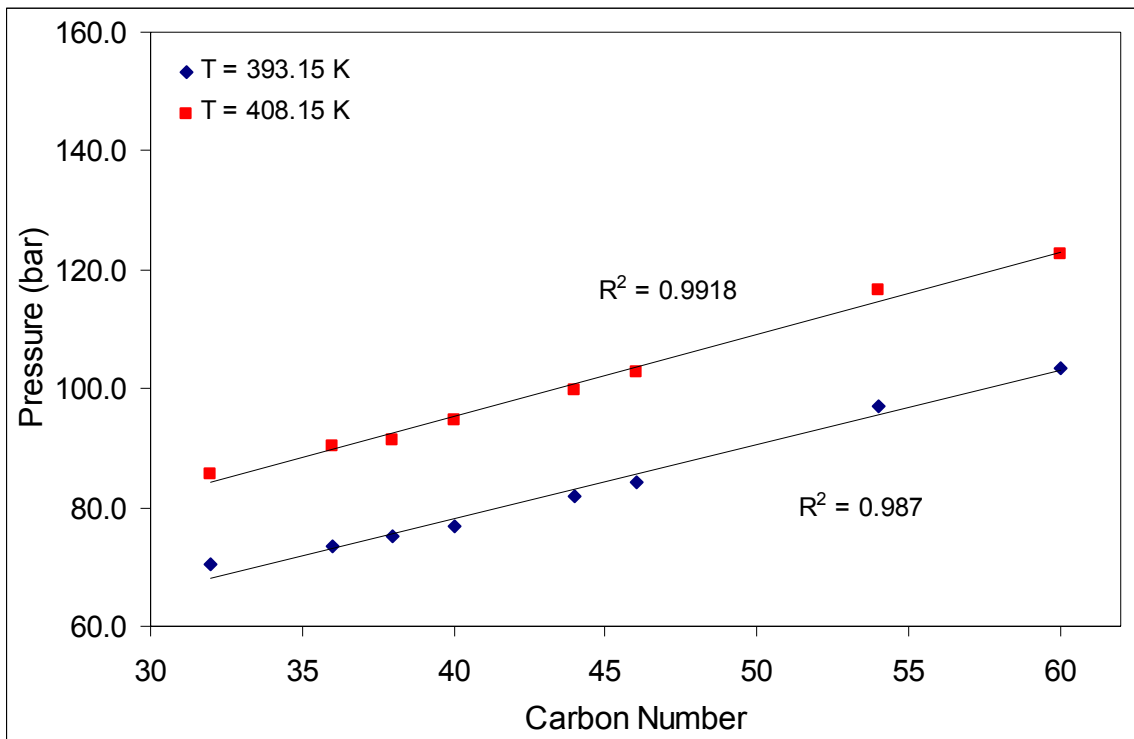
Figure 6-46: Pressure-Carbon Number Plot at mass fraction 0.05
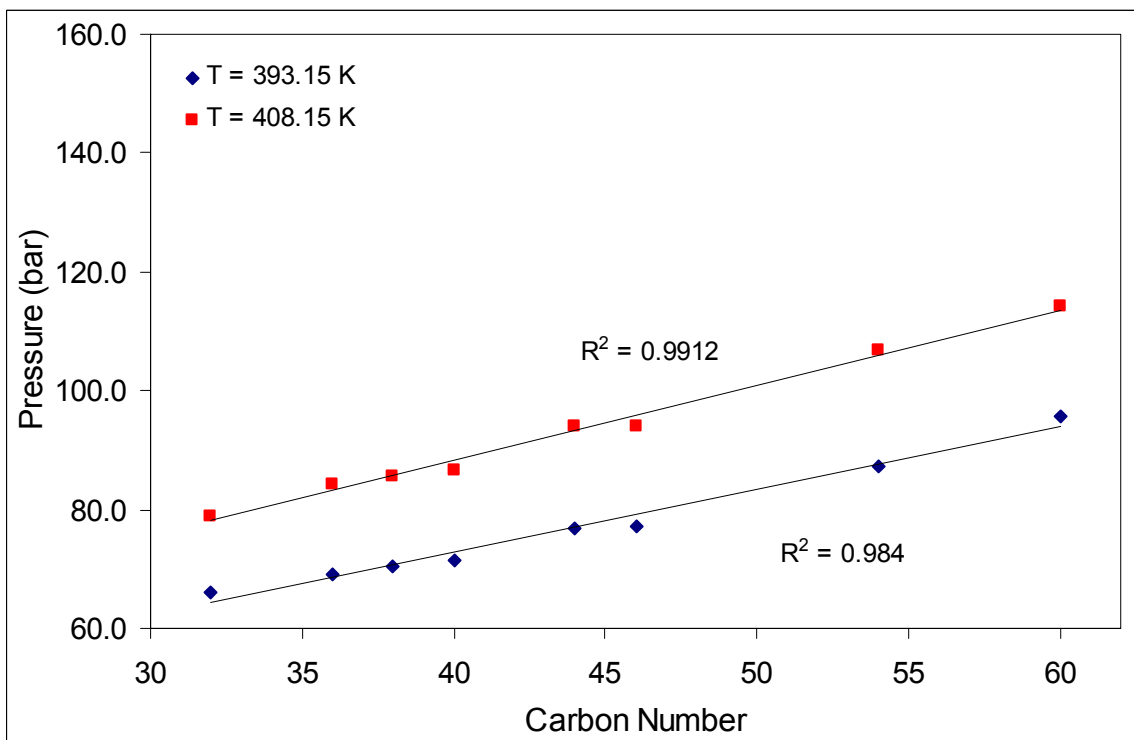
Figure 6-47: Pressure-Carbon Number Plot at mass fraction 0.025
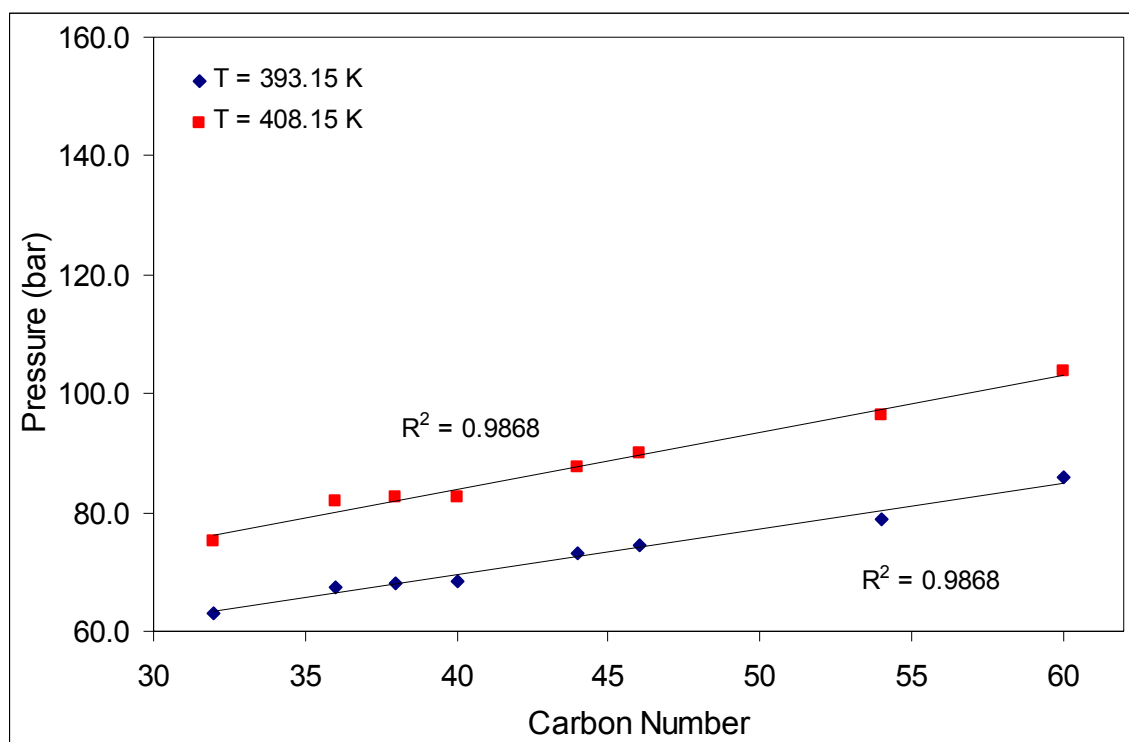
Figure 6-48: Pressure-Carbon Number Plot at mass fraction 0.015

As can be seen above, the pressure-carbon number plots reveal a linear relationship between the phase transition pressure and the carbon number. This linear relationship allows for the interpolation of the data for sets not studied here.

Table 6-3 gives the numerical values of the equations of the trend lines plotted through the data in Figure 6-37 to Figure 6-48 as well as the fit of these trend lines in terms of R^2 values.

Table 6-3: Equation and R^2 values for linear trend lines for data in Figure 6-37 to Figure 6-48.

Mass Fraction Paraffin	T = 408.15 K		T = 393.15 K	
	Correlation	R^2	Correlation	R^2
0.45	P = 1.629 CN + 30.44	0.9848	P = 1.442 CN + 18.77	0.9878
0.40	P = 1.778 CN + 29.34	0.9967	P = 1.655 CN + 15.25	0.9922
0.35	P = 1.790 CN + 32.77	0.9888	P = 1.702 CN + 16.41	0.9953
0.30	P = 1.804 CN + 33.62	0.9841	P = 1.721 CN + 17.50	0.9889
0.25	P = 1.788 CN + 35.32	0.9861	P = 1.691 CN + 19.67	0.9890
0.20	P = 1.820 CN + 33.42	0.9832	P = 1.707 CN + 18.91	0.9844
0.15	P = 1.804 CN + 32.51	0.9817	P = 1.685 CN + 18.68	0.9828
0.10	P = 1.662 CN + 35.90	0.9827	P = 1.568 CN + 21.13	0.9865
0.075	P = 1.574 CN + 36.44	0.9870	P = 1.471 CN + 23.12	0.9880
0.050	P = 1.385 CN + 39.91	0.9918	P = 1.248 CN + 28.26	0.9870
0.025	P = 1.271 CN + 37.36	0.9912	P = 1.059 CN + 30.46	0.9840
0.015	P = 0.961 CN + 45.41	0.9868	P = 0.774 CN + 38.60	0.9868
	Average R^2	0.9871	Average R^2	0.9877

From the above table, it can be seen that none of the gradients are zero. From this observation is can be deduced that separation is highly feasible. Additionally, it can be seen in Table 6-3 that an increase in temperature leads to an increase in the gradients. This indicates that better separation will occur at higher operating temperatures.

Figure 6-37 to Figure 6-48 indicates a linear relationship between the pressure and the carbon number at constant temperature. To determine if extrapolation is possible, data for propane-eicosane (C20) and propane-decane is plotted on the same scale. Propane-eicosane data was measured by Gregorowicz et al for temperatures 288 to 358 K (Gregorowicz et al., 1992). They used a third degree polynomial to describe the relationship between the pressure and the temperature at constant mass fraction and the highest five values were used in a third degree polynomial to extrapolate to the values given in Figure 6-49. For propane-decane data was obtained from the Dechema Chemistry Data Series (Knapp et al., 1982) and interpolation was used to determine the required data points. Dimitrelis et al measured the solubility of Octadecane in propane (Dimitrelis et al., 1989). The results they presented do not allow for temperature correction and the mass fractions of wax studied are lower than the lowest fractions studies here.
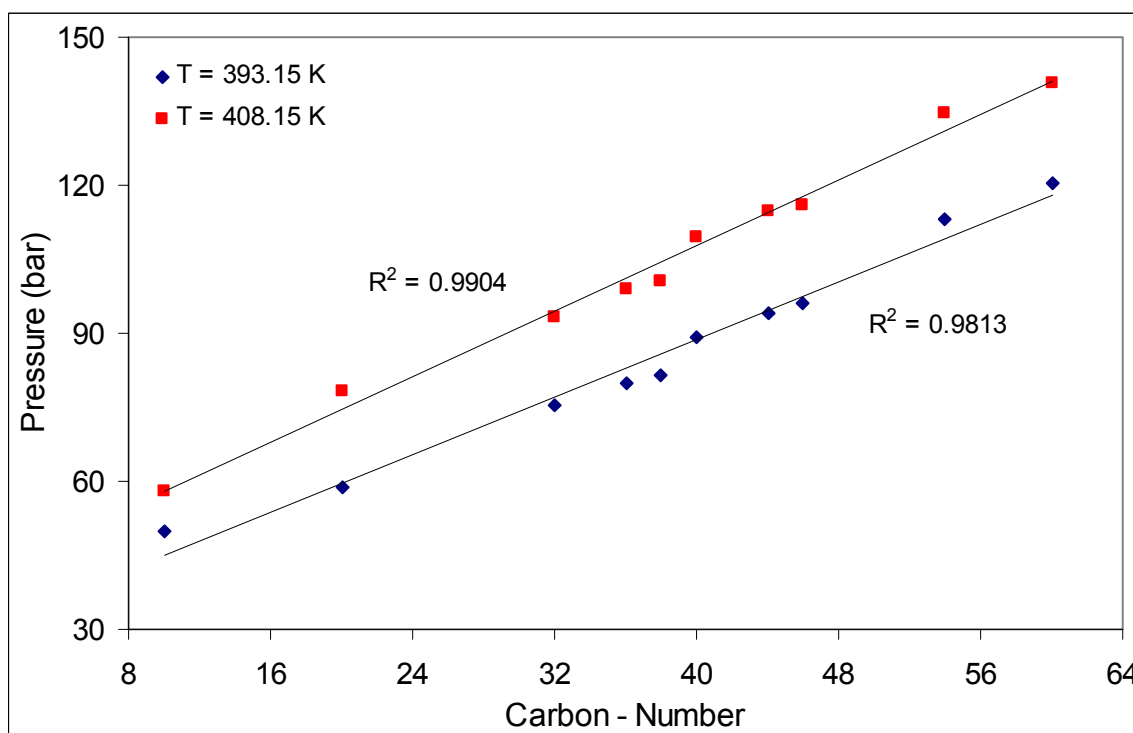
Figure 6-49: Pressure-Carbon Number Plot at x = 0.25 with experimental data and literature data.

As can be seen above, the data shows that extrapolation is possible to lower carbon number mass fractions. This also indicates that extrapolation to the other side may be possible and this needs to be confirmed experimentally.

The relationships in Table 6-3 can be used to generate smoothed pressure composition curves with paraffins in the range studied here. In Figure 6-50 the pressure – carbon number relationships are used to generate pressure composition graphs for paraffins with 30, 40, 50 and 60 carbon numbers respectively. To test the validity of the smoothed curves, a comparison of the data generated with the relationships of Table 6-3 is made with the experimental data for the propane-tetrapentacontane system and is illustrated in Figure 6-51:
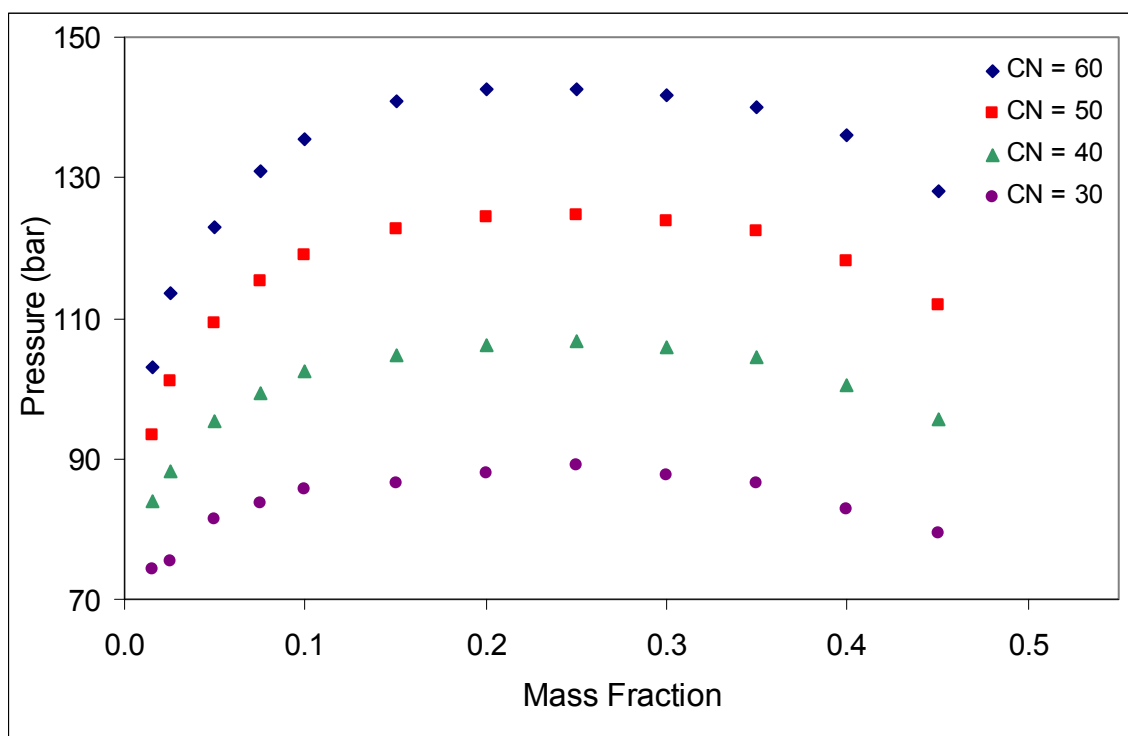
Figure 6-50: Smoothed Pressure Composition Curve at 408.15 K
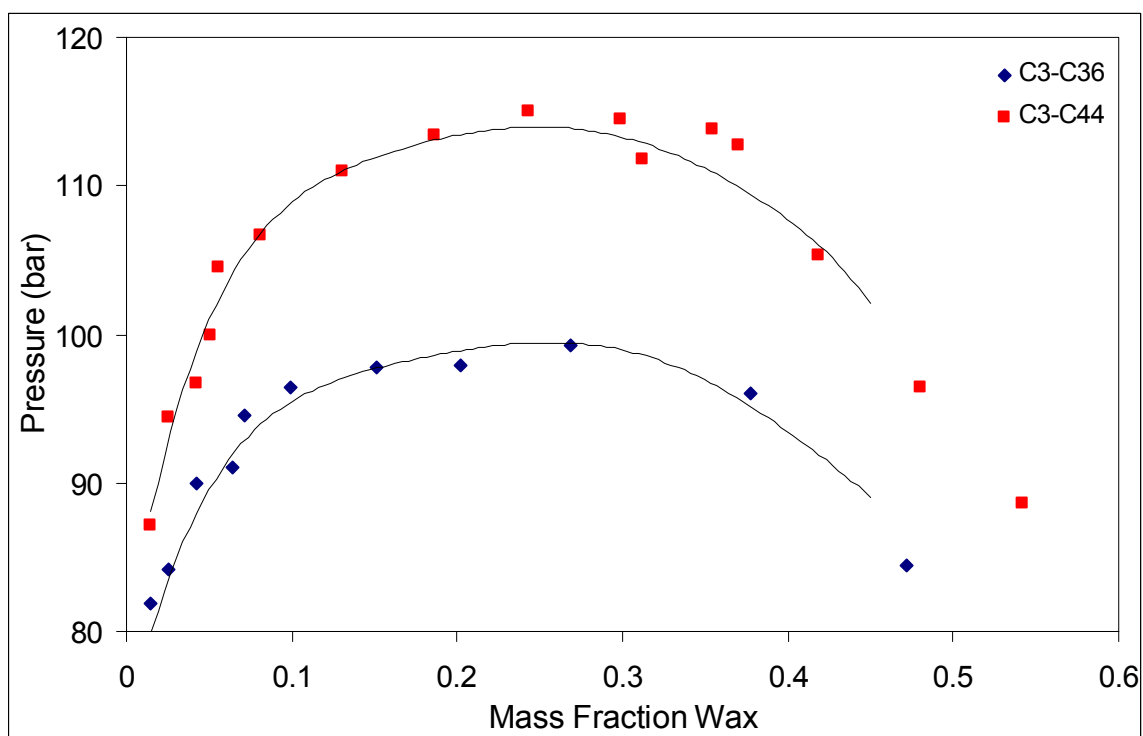
Figure 6-51: Comparison of Smoothed and Experimental Data for Propane-Hexatriacontane and Propane-Tetratetracontane Systems at 408.15 K

As can be seen above, the experimental and the smoothed data correspond well. The difference in the values is in the same order as the experimental uncertainties.

To be able to predict the phase equilibria from the highest mass fraction given above to a mass fraction of 1, it is suggested that a linear approximation is used. Thus the highest mass fraction point is combined with a mass fraction of 1 and a pressure of zero, and any point in between is predicted with this straight-line graph. The point where the mass fraction is one and the pressure is zero can be justified due to the fact that the pure component vapour pressure will be very low at the operating temperatures and can be approximated to zero for this application.

To test this method, the values measured for propane hexacontane phase equilibrium by Peters et al are predicted in this manner. The prediction is shown in Figure 6-52 (Peters et al., 1993).
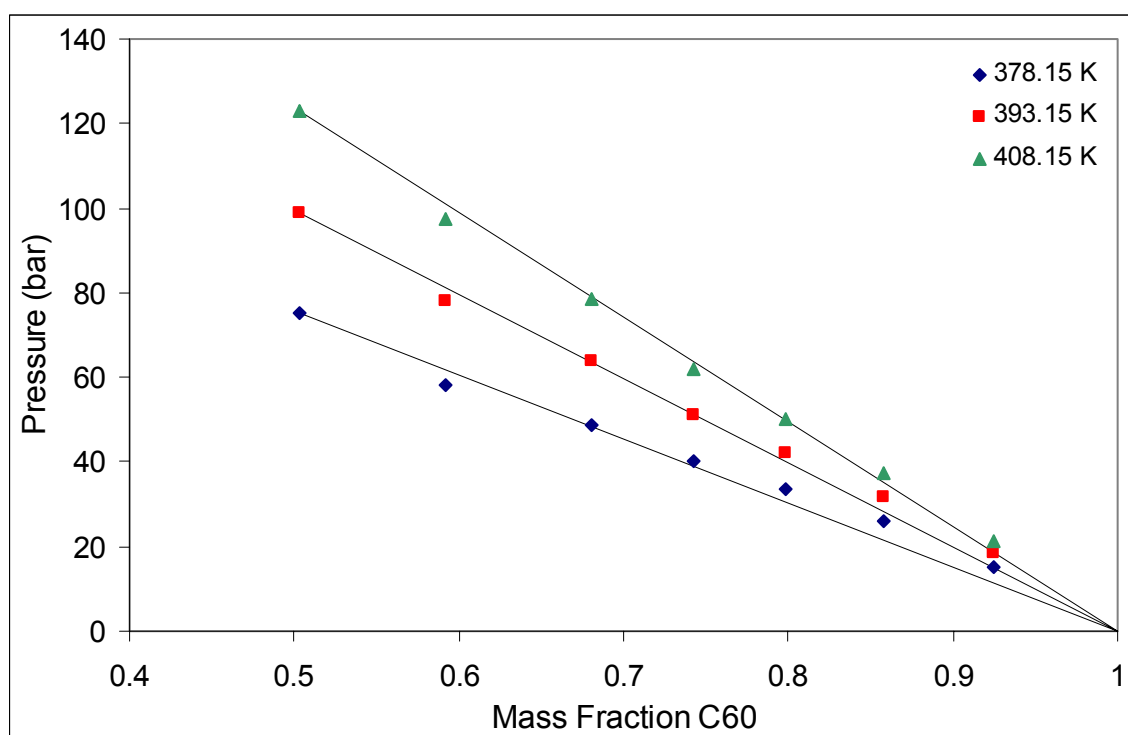
Figure 6-52: Test of prediction of higher mass fraction paraffin data points on Propane – Hexacontane system.

As can be seen above, the method works well and the average error in the calculation of the phase equilibrium pressure is 0.68 bar.

A complete prediction of the composition pressure plot at phase equilibrium can now be made. The experimental data measured in this work and the data published by Peters et al is compared with the predicted plot in Figure 6-54 (Peters et al., 1993).
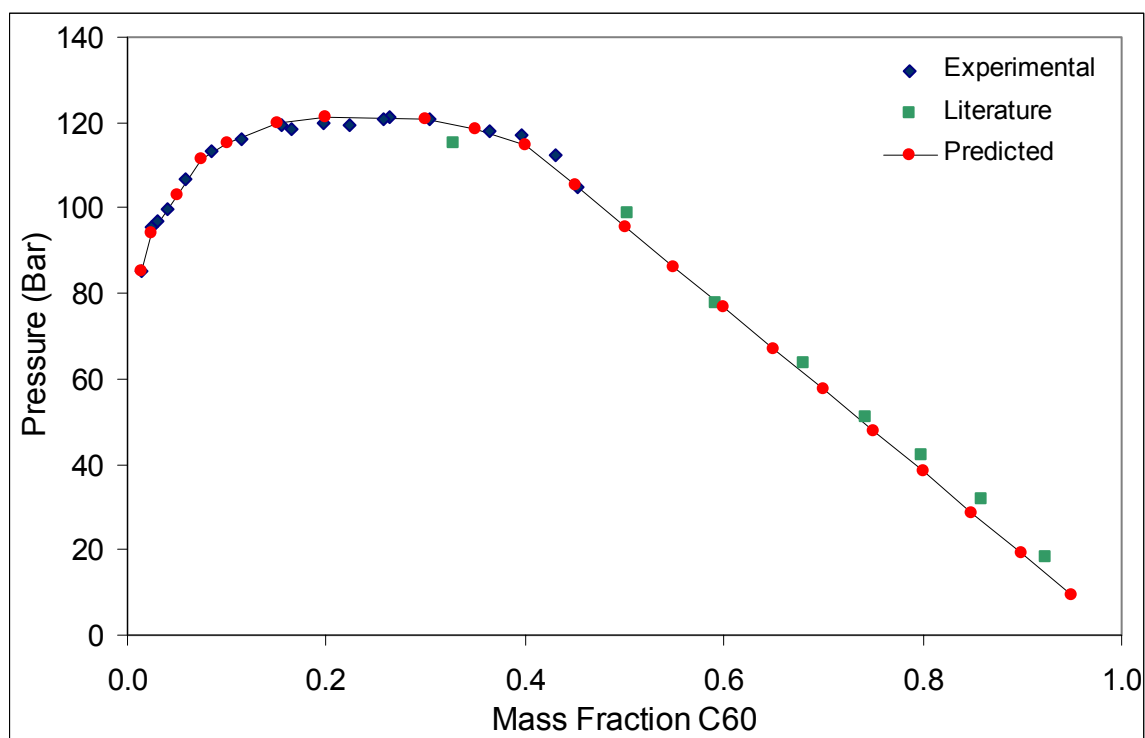
Figure 6-53: Comparison of experimental data from this work, literature data by Peters et al and predicted phase equilibrium data for propane-hexacontane at 393.15 K (Peters et al., 1993)

6.4.2. EFFECT OF SOLVENT ON PHASE EQUILIBRIA AND DENSITY

The data generated in this work was mainly done with pure propane. The pure solvent data is of interest in developing a process concept and to develop equations of state models, but might be cheaper to use LPG as a solvent. It is therefore important to consider the effect of using LPG on the phase equilibrium data.

Comparison of Propane and LPG Data for Hexatriacontane

Firstly, a comparison of the phase boundaries of propane and LPG with hexatriacontane will be investigated. As stated in paragraph 5.6, the LPG used in this study has a propane content of 87.8 % and as stated in paragraph 6.1.3, the scattering in the LPG-Hexatriacontane data can be attributed to the fact that the endoscope was not used for these measurements.
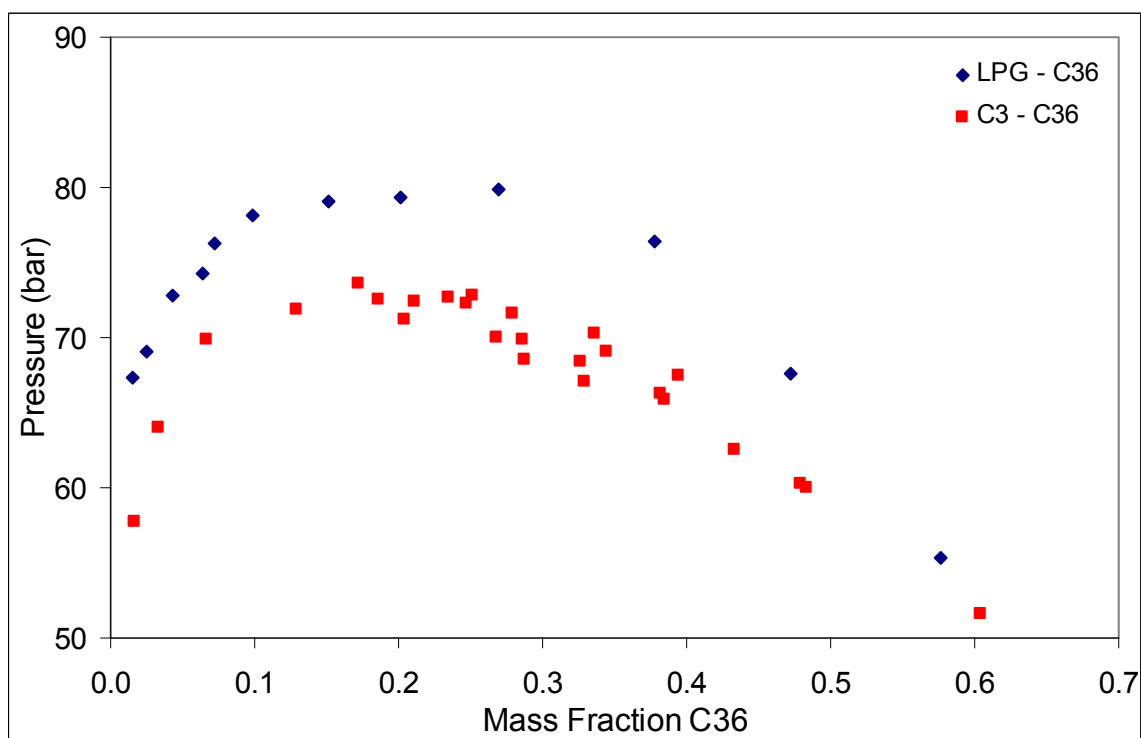
Figure 6-54: Isothermal Pressure-Composition Plot of Phase Equilibrium Boundary for comparison of Propane and LPG as solvents for Hexatriacontane at 393.15 K

The phase equilibrium pressure of the LPG data is lower than that of the propane data. This can be attributed to the presence of butanes in the LPG. Additionally, it is important to note that critical point has moved. The critical point of the LPG data is at a lower mass fraction wax and would thus result in a lower loading of the vapour phase.
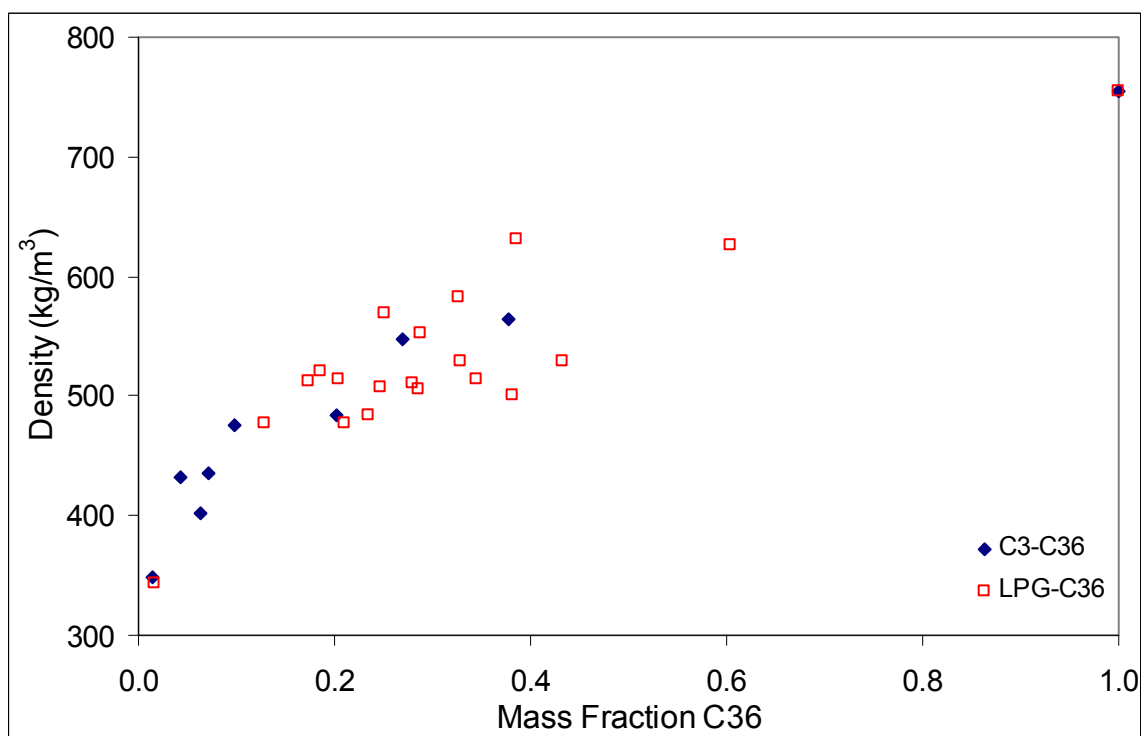
Figure 6-55: Isothermal Density-Composition Plot of Phase Equilibrium Boundary for comparison of Propane and LPG as solvents for Hexatriacontane.

The densities of the propane and LPG systems do not differ significantly. This can be attributed to the fact that propane constitutes the majority of the solvent in the LPG.

Comparison of Propane and LPG Data for Tetrapentacontane

A comparison can be made between the experimental propane-tetrapentacontane data and literature data for LPG and tetrapentacontane. The LPG gas used for this data shows the following composition:

Table 6-4: Composition of LPG used in data by Nieuwoudt (Nieuwoudt, 2001)

Component	Mass Fraction	Mole Fractions
Propane	0.931	0.947
Iso-Butane	0.039	0.030
Butane	0.021	0.016
Butene-isomers	0.009	0.007

The composition of the LPG used by Nieuwoudt has a significantly higher propane content than the LPG used in this work.
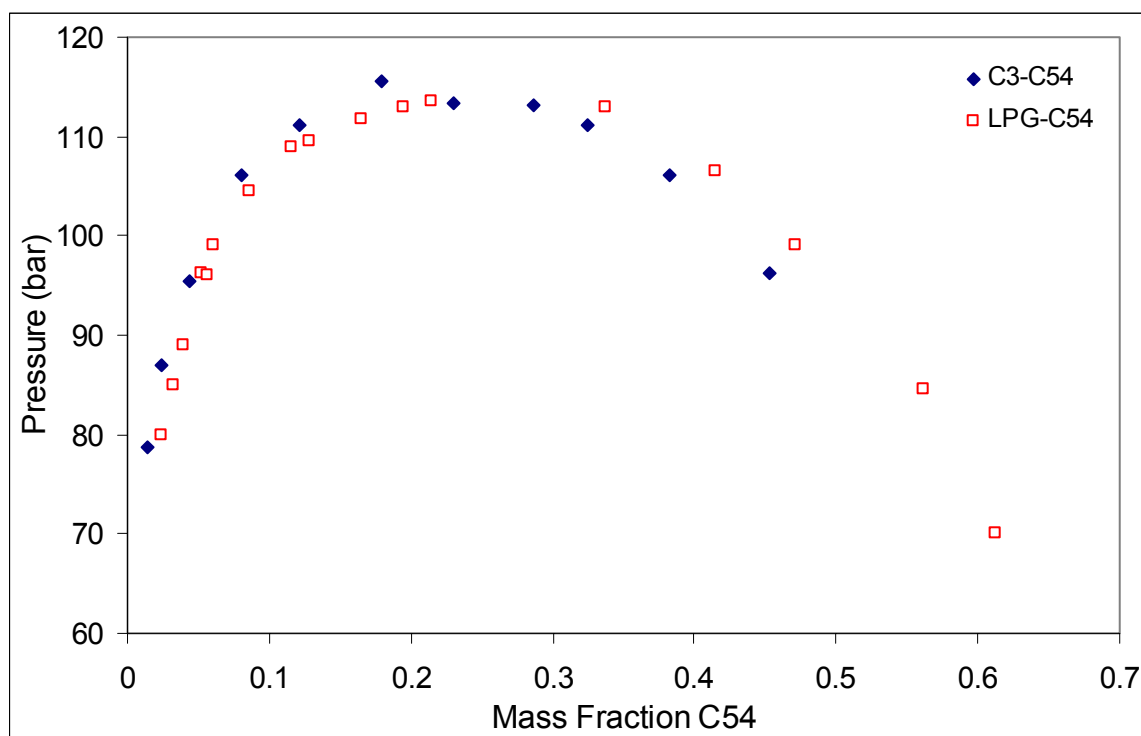
Figure 6-56: Isothermal Pressure-Composition Plot of Phase Equilibrium Boundary for comparison of Experimental Propane and Literature LPG as solvents for Tetrapentacontane at 393.15 K (Nieuwoudt, 2001).

As expected, no large difference in the phase equilibrium pressure is seen.

Comparison of Propane and Butane Data for Tetrapentacontane and Hexacontane

To compare propane and butane as solvents for fractionation, the phase equilibrium of butane and propane with tetrapentacontane and with hexacontane will be investigated. Due to the fact that the operating temperatures differ due to different critical temperatures, a comparison at the same solvent reduced temperatures will be done.
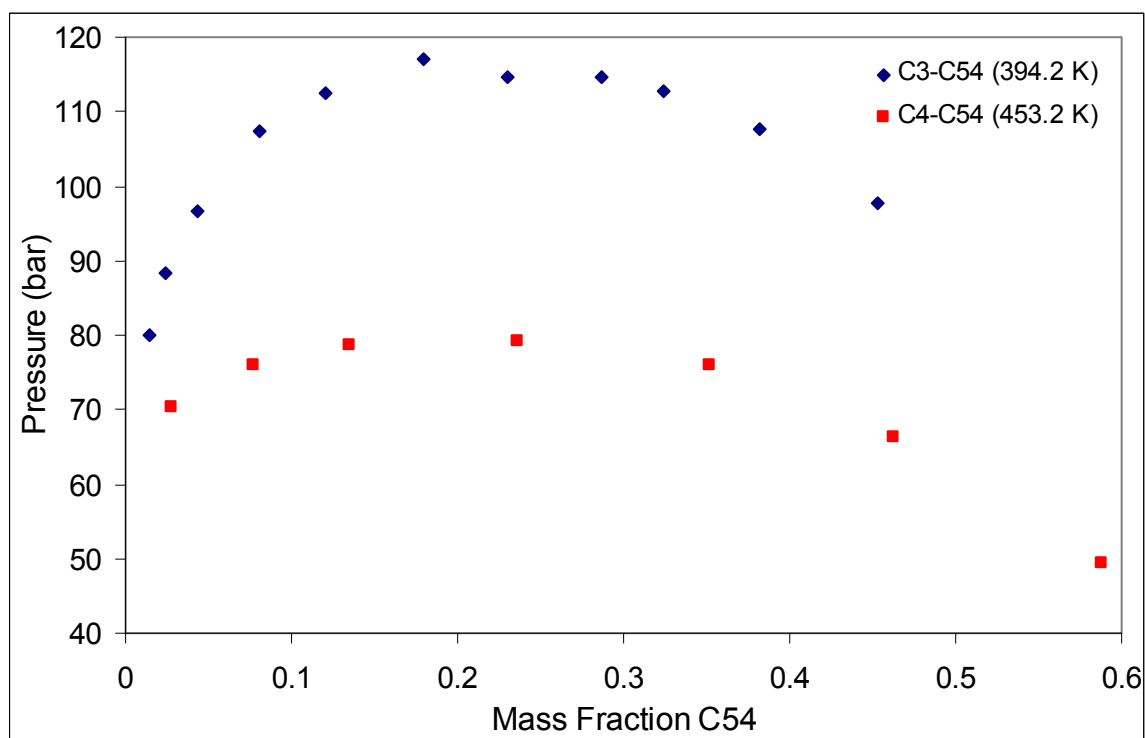
Figure 6-57: Isothermal Pressure-Composition Plot of Phase Equilibrium Boundary for comparison of Experimental Propane and Literature Butane as solvents for Tetrapentacontane at T_R = 1.066 (Nieuwoudt, 1996)
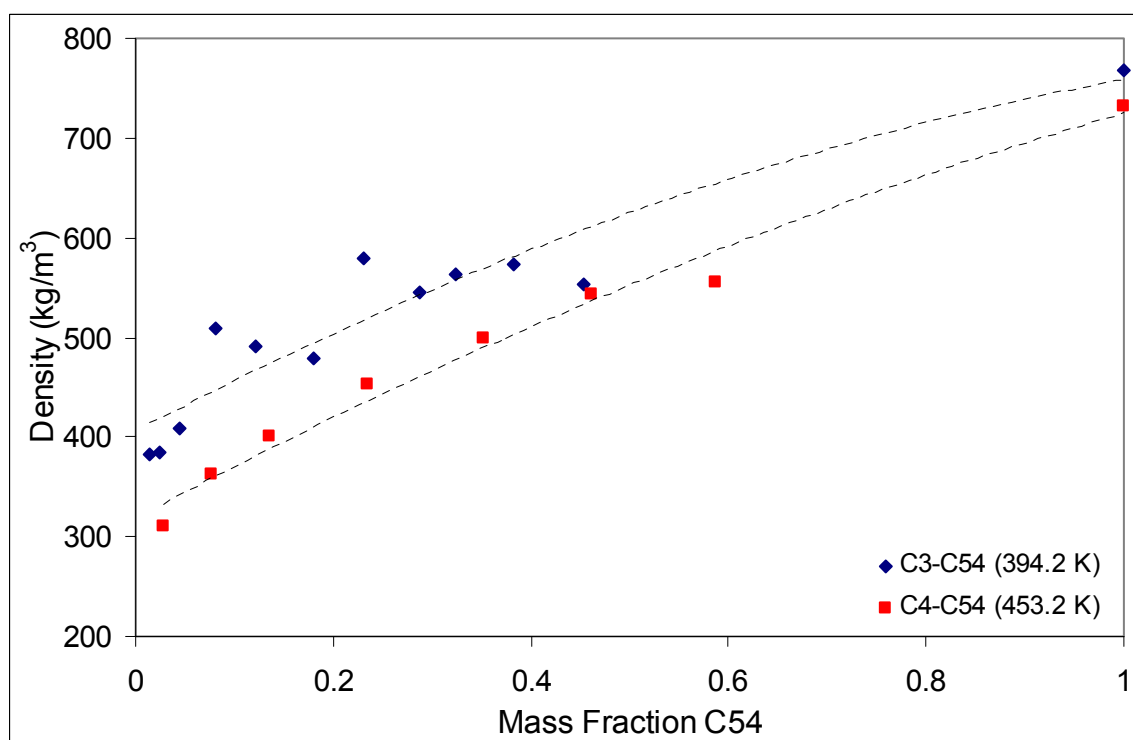
Figure 6-58: Isothermal Density-Composition Plot of Phase Equilibrium Boundary for comparison of Experimental Propane and Literature Butane as solvents for Tetrapentacontane (Nieuwoudt, 1996).
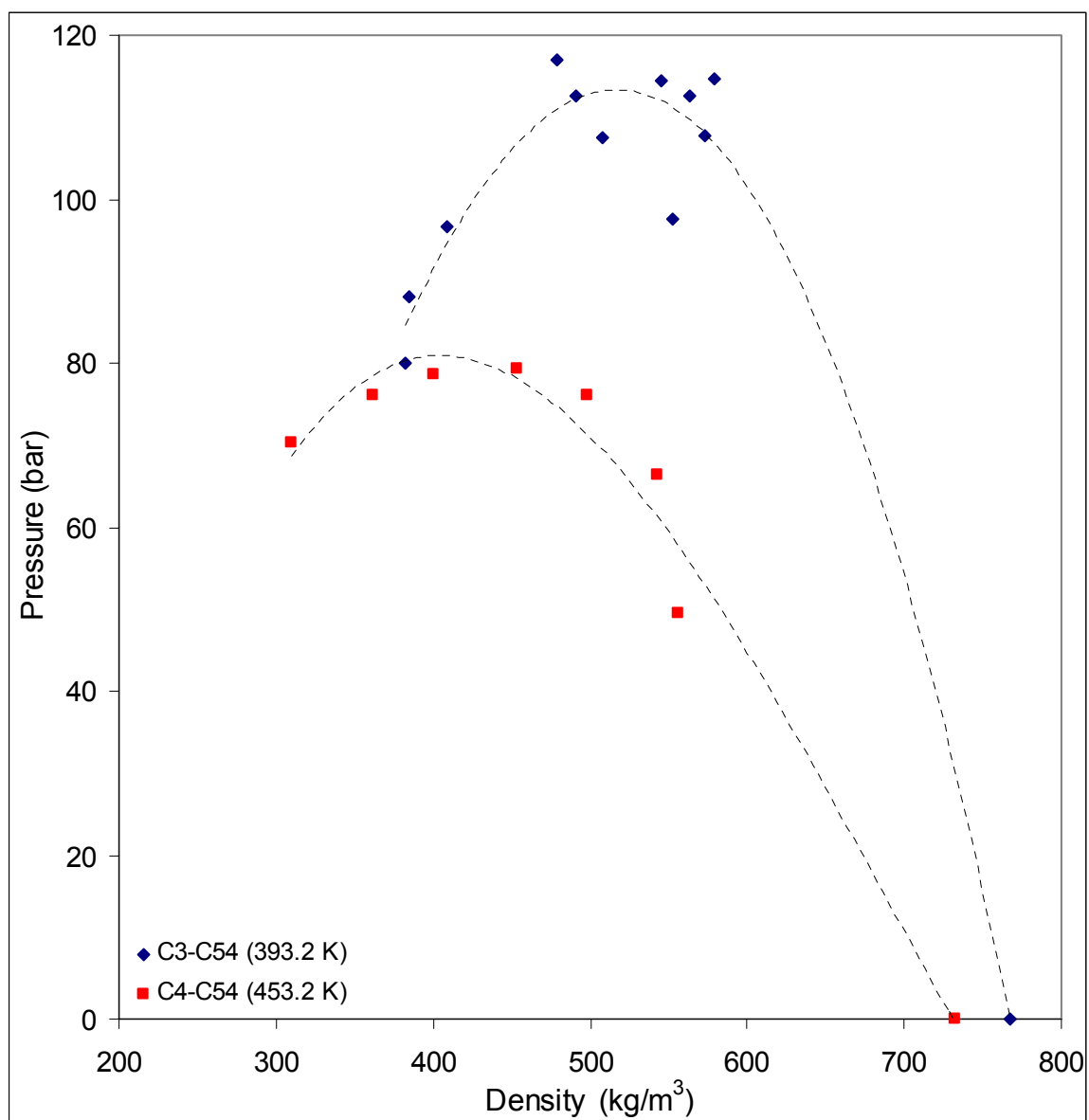
Figure 6-59: Isothermal Pressure-Density Plot of Phase Equilibrium Boundary for comparison of Experimental Propane and Literature Butane as solvents for Tetrapentacontane.
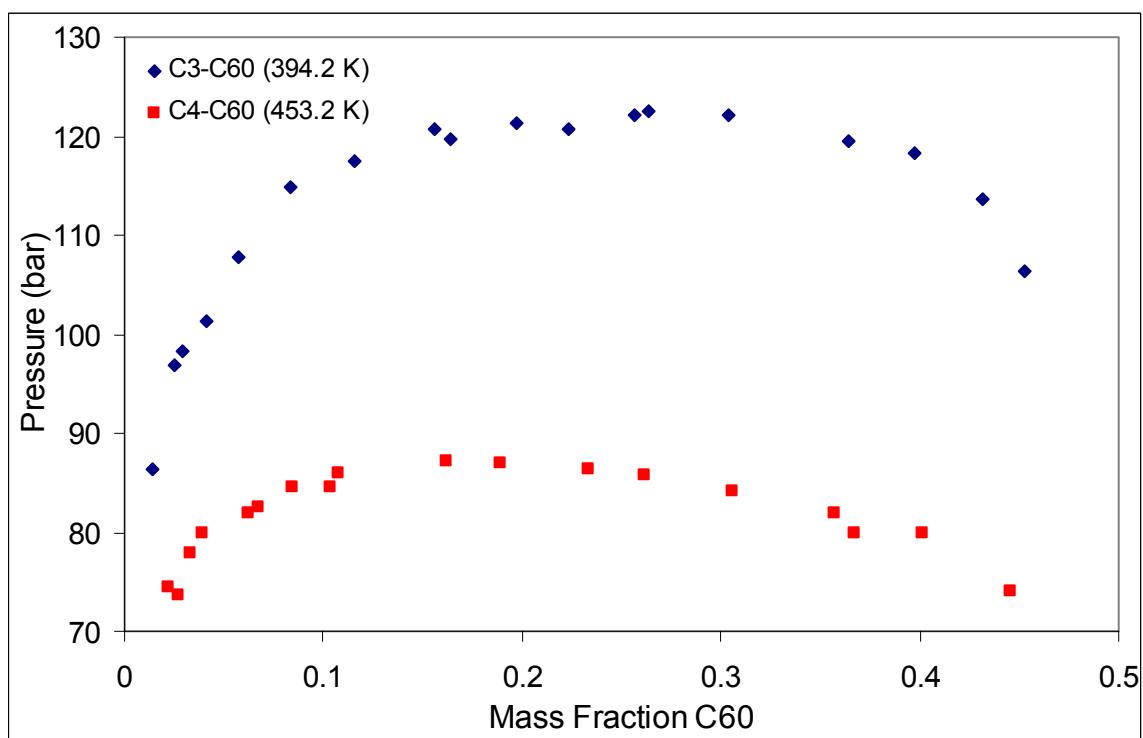
Figure 6-60: Isothermal Pressure-Composition Plot of Phase Equilibrium Boundary for comparison of Experimental Propane and Literature Butane as solvents for Hexacontane at T_R = 1.066 (Nieuwoudt, 1996)
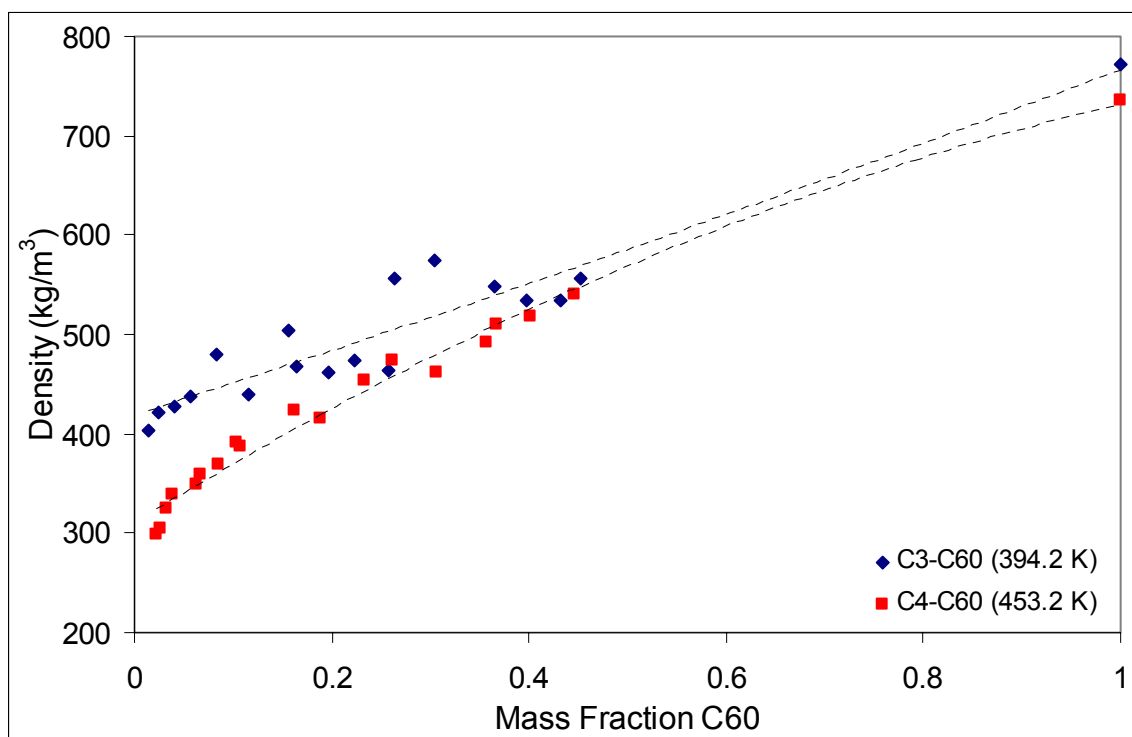
Figure 6-61: Isothermal Density-Composition Plot of Phase Equilibrium Boundary for comparison of Experimental Propane and Literature Butane as solvents for Hexacontane (Nieuwoudt, 1996).
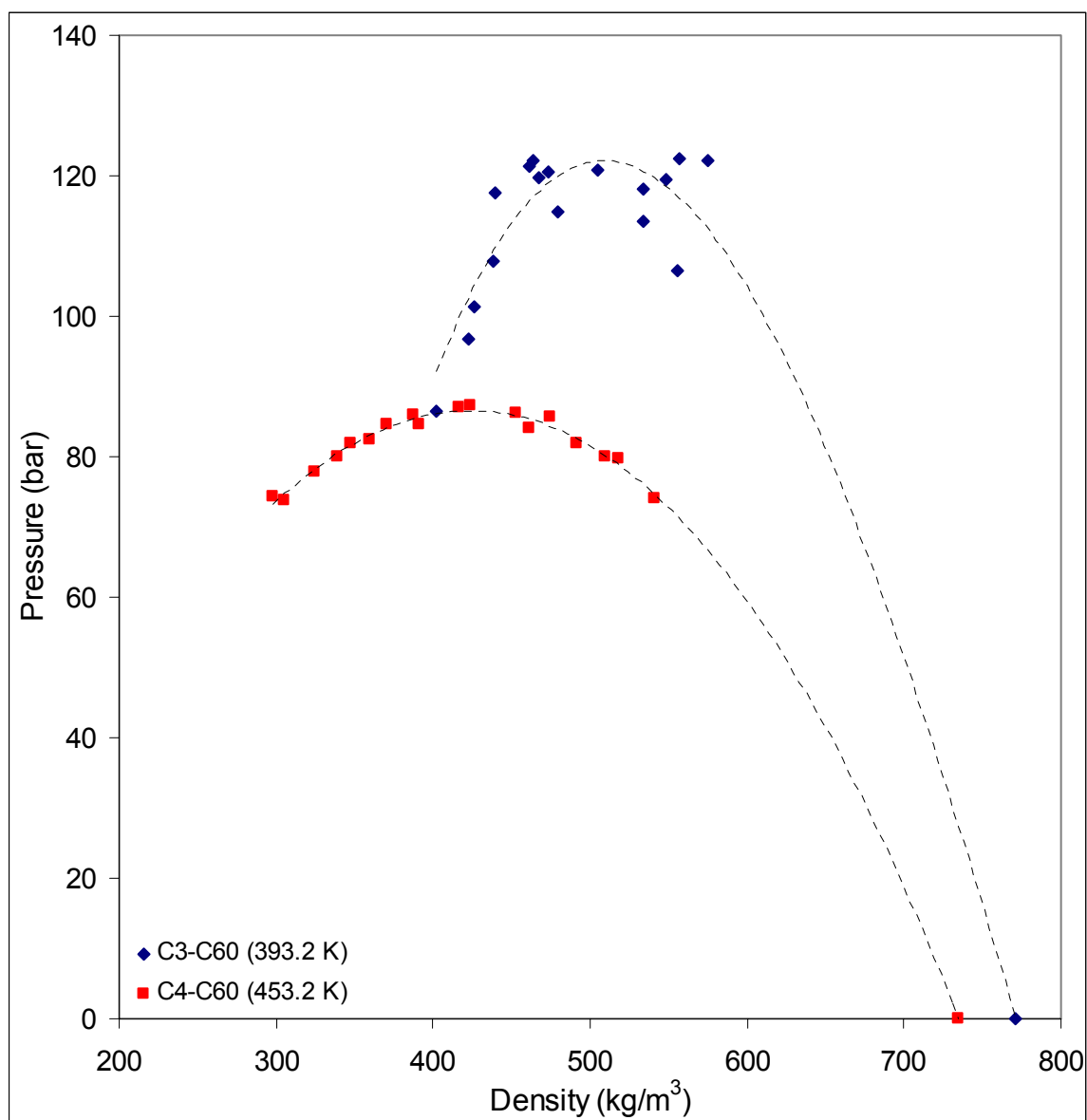
Figure 6-62: Isothermal Pressure-Density Plot of Phase Equilibrium Boundary for comparison of Experimental Propane and Literature Butane as solvents for Hexacontane.

The butane curve is at a lower density than the propane curve. This can be explained by considering the densities of the solvents. The density of butane at 453.2 K and 80 bar is 341.36 kg/m^3 while the density of propane at 394.2 K and 120 bar is 370.94 (from NIST website [165]). The propane system is thus expected to show higher density values.

As expected, a pressure-composition plot of the phase equilibrium boundary reveals that the butane phase equilibrium occurs at much lower pressures. Due to the fact that the butane is a longer molecule and the system less asymmetrical, butane has the ability to dissolve the wax better, therefore at lower pressures. As in the case of the propane LPG comparison, the mixture critical point of the butane system is at a lower mass fraction than the mixture critical point of the propane system. Propane as a solvent would thus provide a higher loading in the vapour phase.

The trend seen in the pressure density plot can be explained as a combined effect of pressure reduction due the difference is solubility of the butane and the propane as well the fact that the absolute temperatures differ.

Additionally, the phase equilibrium pressures of the butane system is much lower than that of the propane system, thus resulting in the solvent being less dense.

To be able to compare the densities of the two solvents, a vapour phase of 10 mass percent wax and the corresponding equilibrium liquid phases will be compared. As example, hexacontane, will be considered. For propane the comparison is done at 115 bar and yields a density difference of about 110 kg/m^3 while for butane the comparison is done at 85.5 bar, yielding a density difference of 70 kg/m^3. A propane system will thus allow operation closer to the mixture critical region.

Comparison of Ethane-Triacontane, Propane-Pentatetracontane and Butane-Hexacontane Data

To ascertain if a relationship exists between the ratio of the carbon numbers in the solvent to those in the wax, a plot of ethane-triacosane, propane-pentatetracontane and butane-hexacontane is given below. The aim of this plot is to determine if the principle of congruency as suggested by Peters et al (Peters et al., 1995) can be applied in this manner.

Peters et al stated: "The principle of congruence claims that certain thermodynamic and transport properties of a mixture of n-alkanes are the same as those of the pure n-alkane of the mole fraction average carbon number."

This principle can be applied to three-component phase equilibrium for the type of systems studied here, providing the two non-volatile components only differ slightly in length. To apply the principle, the mole-fraction-average carbon number of the non-volatile component needs to be equal to that of a single non-volatile component. For example, according to the principle of congruence, the phase equilibria of a mixture of 1 mole percent C44, 1 mole percent C46 and 98 mole percent propane will be the same as that of 2 mole percent C45 and 98 mole percent propane.

The propane-pentatetracontane plot is generated from the relationships in Table 6-3. The ethane-triacontane data is generated in the same manner from data generated by du Rand (du Rand, 2000). All the plots are at the same solvent reduced temperature and pressure. Both sets of generated data is given in Appendix E.5
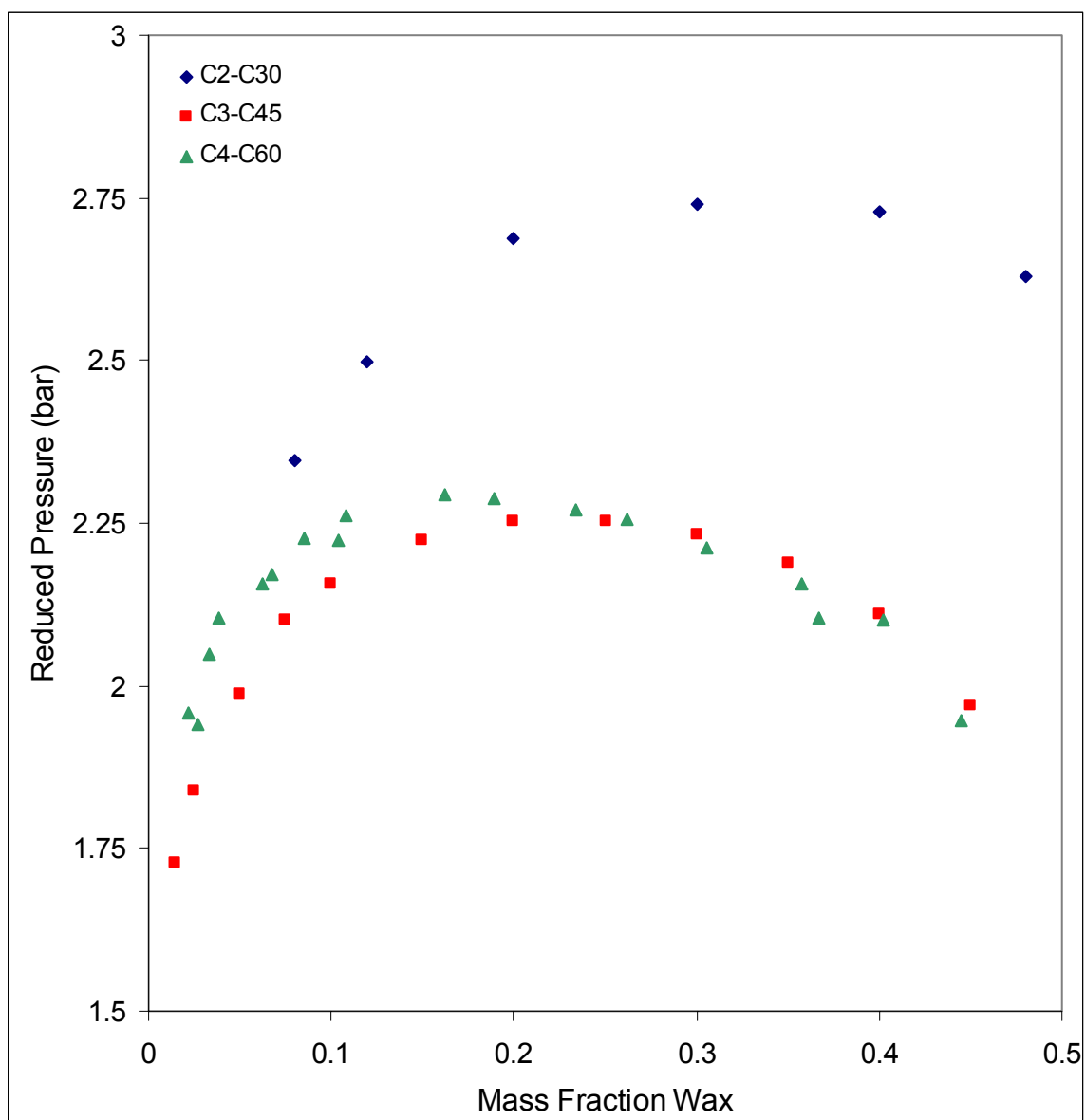
Figure 6-63: Isothermal Pressure-Composition Plot of Phase Equilibrium Boundary for comparison of generated Ethane – Triacontane, Propane – Pentatetracontane and Literature Butane – Hexacontane at T_r = 1.066 (Nieuwoudt, 1996)

In the Figure 6-63 it can be seen that the propane and butane data lies close to one another while the ethane seems to deviate. When considering the molecules of the solvent, the ethane consists of two CH_3– while the propane and butane also consist of two CH_3– groups but additionally they have one and two –CH_2– groups respectively. Although these –CH_2– groups are shielded they do influence the phase transition of the system and can possibly describe the phenomenon seen above. Additionally, it must be mentioned that the ethane data is extrapolated in both temperature and carbon number, therefore serving merely as an indication of the pressures and not as an accurate data set.

It is also noticeable that the butane data is shifted slightly to the left, the shift being more noticeable at lower mass fractions. The principle of congruency can therefore not predict

phase equilibria accurately and can only be applied in this manner as an indication of the pressure and not as a substitute for experimental measurements.

6.5. OPTICAL EFFECTS

Two main optical effects are observed, namely critical opalescence near the critical composition and light scattering at low mass fractions of wax. Both these effects are discussed below with the aid of photographic sequences.

6.5.1. CRITICAL OPALESCENCE

Critical opalescence was first observed by Travers et al in 1906 (Travers et al., 1906). Yet very little information on critical opalescence of systems similar to those studied here is available. Du Rand found critical opalescence for ethane systems with C16, C24 and C28 and the bluish colours expected were found (du Rand, 2000). Additionally Singh et al reported the presence of critical opalescence for systems with ethane and n-alkanes from pentane to decane (Singh et al., 2000). In the application of Singh et al critical opalescence was used to determine critical properties and no indication of phenomenon was given other than the fact that cloudiness occurred.

For the systems studied here, critical opalescence was found for all the components for phase transitions near the critical composition. Only one sequence is illustrated below. In Figure 6-64 critical opalescence is observed for a mixture of tetracontane and propane at a mass fraction of 0.244 and a temperature of 407.35 K and a phase transition pressure of 108.8 bar abs. The optical effects seen below occur over a pressure drop of about 10 bar.

In the first picture in Figure 6-64 the mixture is in a single phase. The start of the onset of the phase transition can be seen in the second picture and is more clearly seen in the third. In the forth picture the phase transition is about to occur while the fifth picture is as close as possible to the phase transition. In the sixth and seventh pictures the effect of the reflection of light can be seen while this effect is no longer so clear in the eighth picture. In the ninth and tenth pictures the light reflection is no longer as prominent while the second phase can be seen clearly in the eleventh and twelfth pictures. The colours seen here agree with those stated in McHugh and Krukonis (McHugh et al., 1994)
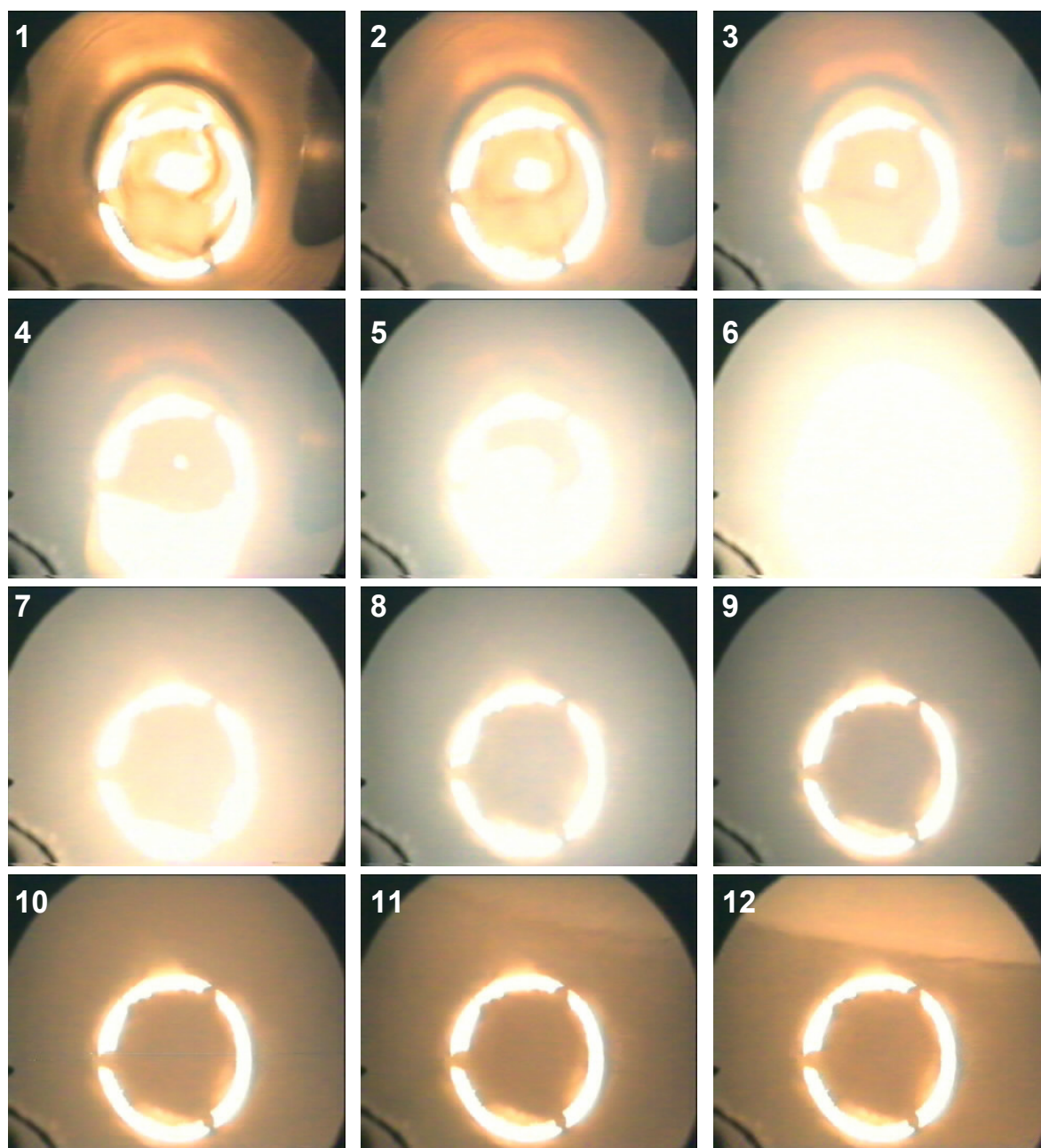
Figure 6-64: Critical Opalescence Observed during Phase Transition with Composition near Critical Point.

6.5.2. OPTICAL EFFECT AT LOW MASS FRACTIONS

An optical effect was also noticed for very low mass fraction of the wax. A example of this light scattering can be seen in Figure 6-65 for Dotriacontane and Propane at a temperature of 407.25 K and a mass fraction of 0.0152. The optical effect seen in Figure 6-65 takes place over a pressure drop of 10 bar.

In the first picture above, the mixture is in a single phase. In pictures 2 to 6 above the phase transition is observed with the light scattering around the brim caused by the light

source. These light scattering patterns are a sign of the phase transition. In the last three pictures the phase transition is completed.
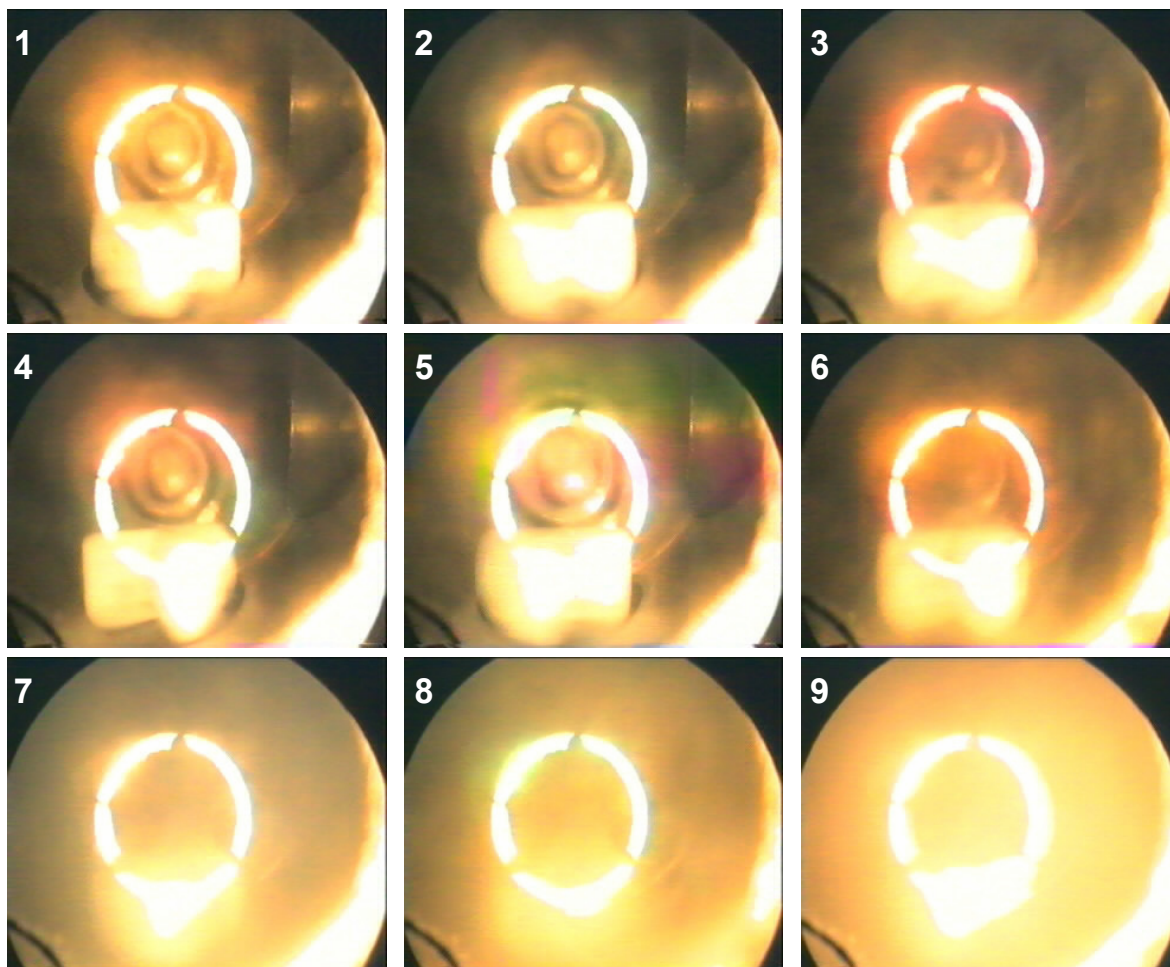
Figure 6-65: Optical Effect observed at low mass fractions.

6.6. CONCLUSIONS

The main results in this chapter can be summarised as follows:

- The phase equilibrium boundary pressures and densities were measured for the systems C3-C32, C3-C36, C3-C38, C3-C40, C3-C44, C3-C46, C3-C54, C3-C60 and LPG-C36.

- A linearization method was used to interpolate both the pressure data and the density data. This was used to generate constant temperature data.

- No region of liquid-liquid immiscibility was found at the temperatures in this study.

- Pressure-composition data found in the literature was of the same order of magnitude to that measured in this work. For propane-hexacontane the experimental and literature data complement each other well.

- The pressure-carbon number plots revealed that a linear relationship exists between the phase transition pressure and the carbon number of the wax for constant mass fraction. The pressure carbon number plots can be used to generate data for systems not measured here and, within limits, extrapolation to systems outside the region of those studied here can be applied successfully.

- The slopes of pressure – carbon number plots were all positive and thus revealed that fractionation is highly feasible. Additionally, the slopes increased with increasing temperature, thus suggesting that the fractionation will be easier at higher temperatures. This is supported by the fact that higher temperatures yield more favourable transport properties.

7. THERMODYNAMIC MODELLING OF BINARY PHASE EQUILIBRIUM DATA

To be able to predict the phase behaviour of the long-chain normal alkanes and supercritical fluids an equation of state model is required. In this chapter the thermodynamic theory required is given, followed by a discussion of various equations of state and their applicability to this type of system.

For the purpose of this project, the following will be taken into account:

The aim of the thermodynamic modelling is to investigate various equations of state available and their applicability to this type of system. The aim of this chapter is thus to do a study on the general applicability of the equations of state and not to model every system at every temperature and pressure investigated.

The system propane-dotriacontane will be used as a test system. It is assumed that if an equation of state can not predict the phase equilibrium for the system propane-dotriacontane, it will not be able to predict the phase equilibrium of the other systems, since the difference in chain length is even larger.

To be able to do the modelling, computer software is required. The equations of state to be studied will be limited to those available in software already in use. No detailed computer programming will thus be done.

The evaluation of the equations of state available will be divided into four main parts.

- Firstly, equations of state that are not applicable to the type of system studied here will be eliminated.

- Secondly, a survey will be done to predict the pure component vapour pressure of dotriacontane and equations of state that are unable to predict the vapour pressure will be eliminated.

- Thirdly, the remaining equations of state will me used to model the propane-dotriacontane data at 408.15 K. One cubic and one non-cubic equation of state will then be used to model a selection of the other systems studied.

- Finally, a discussion and comparison of the various equation of state will be given.

In this chapter a general overview of the various equations of state available will be given, including the historical development, followed by the thermodynamic theory and the software packages to be used.

7.1. GENERAL OVERVIEW OF EQUATIONS OF STATE

An equation of state can be used to evaluate many important properties of pure substances and mixtures, including the following:

- Densities of liquid and vapour phase

- Vapour pressure

- Critical properties of mixtures

- Vapour-liquid equilibrium relations

- Deviations of enthalpy from the ideal gas state.

- Deviation of entropy from the ideal gas state.

At present no single equation of state exists that can be used that is well suited for the prediction of all these properties for any large variety of substances, but many equations of state perform well for the limited component range in which they were developed.

7.1.1. HISTORICAL OVERVIEW AND DEVELOPMENT

The history of equations of state started with Boyle's experiments in 1662 where he found that the volume of a gas is inversely proportional to its pressure. The effect of temperature was first quantified by Charles and Gay-Lussac in 1802 and later Clapeyron combined these two results into the ideal gas law. (Walas, 1985)

From the beginning it was realised that the ideal gas law is often only a rough approximation. Deviations were ascribed to the finite volumes occupied by the molecules themselves and to the forces of attraction and repulsion that exist between the molecules. Both these factors were taken into account by van der Waals when he formulated his equation of state in 1873. Although not perfect, the van der Waals equation of state gave a significant improvement compared to the ideal gas law and has become the basis for many current equations of state (Van der Waals, 1873).

Equations of state were originally applied to pure components. Later the equations were applied first to non-polar and slightly polar mixtures. Equations of state have subsequently developed rapidly to be applicable to both polar and non-polar liquids.

The Van der Waals equation of state was the first equation to predict vapour-liquid coexistence. Many modifications have been made to both the attractive and repulsive terms in this equation to allow for more accurate predictions.

While the Van der Waals type equations were mainly used to model small molecules, efforts have also been made to model chain like molecules. In addition, statistical

mechanics have also been used as an alternative to the Van der Waals type equations of state.

In 1885 Thiessen proposed a purely empirical equation of state, the Viral equation of state (Thiessen, 1885). This equation of state was developed further by Onnes and later evolved naturally from a statistical mechanical analysis of the forces between molecules. (Onnes, 1912)

7.1.2. CUBIC EQUATIONS OF STATE

Cubic equations of state generally describe simple molecules quite well. They are called cubic due to the fact that the equation of state can be transformed to a cubic expression of compressibility in terms of pressure and temperature.

The first equation capable of describing liquid-vapour coexistence was the van der Waals equation of state. Although not applicable to this system it deserves mention here, as many of the subsequent equations are modification of the Van der Waals equation of state.

The van der Waals equation of state can be described according to the following equation (Wei et al., 2000):

$$Z = \underbrace{\frac{v}{v-b}}_{Repulsive\ Term} - \underbrace{\frac{a}{RTv}}_{Attractive\ Term} \dots\dots\dots\dots\dots\dots\dots\dots\dots\dots\dots\dots\dots\ 7.1$$

OR

$$P = \underbrace{\frac{RT}{v-b}}_{Repulsive\ Term} - \underbrace{\frac{a}{v^2}}_{Attractive\ Term} \dots\dots\dots\dots\dots\dots\dots\dots\dots\dots\dots\dots\dots\ 7.2$$

For consistency, in this project, where possible, all equations of state will be expressed as pressure being a function of temperature, specific volume and equation parameters, similar to the form of equation 7.2.

Modifications to equation 7.2 were made to both the attractive and the repulsive terms. These modifications are discussed below:

Modification of Attractive Term

The main disadvantage of the attractive term as given in equation 7.2 is that the influence of temperature is not taken into account.

Redlich et al. were the first to introduce the temperature dependent attractive term, resulting in a considerable improvement of the van der Waals equation. Their equation of state, known as the Redlich-Kwong equation of state, performed well for simple fluids but did not describe complex fluids with non-zero acentric factors very well. This equation of state predicts a universal critical compressibility of 0.333, which in most cases is an overestimation (Redlich et al., 1949).

Until 1972 the best available equation of state was the Redlich-Kwong (RK) equation. Although the RK equation of state is able to reproduce the pure component properties with relative accuracy, its application to mixtures gives poor results (Redlich et al., 1949).

Soave made a modification to the temperature dependence of the attractive term of the Redlich-Kwong equation of state, introducing the acentric factor. This modification allowed the equation of state to fit the experimental data well and was able to predict the phase behaviour of mixtures in the critical region. (Soave, 1972)

Peng et al. redefined the temperature term defined by Soave slightly and proposed a different volume dependence. The Peng-Robinson equation of state slightly improves the prediction of the liquid volumes and predicts a universal critical compressibility of 0.307 (Peng et al., 1976).

Both the Peng-Robinson and the Soave-Redlich-Kwong equations are widely used due to their simplicity and the fact that they only require critical properties and the acentric factor for the generation of data. Liquid specific volumes are, however, not improved and are invariably higher that experimental measurements.

Other modifications have been made and are listed below:

- Scott (Scott, 1971)

- Hederer-Peter-Wenzel (Hederer et al., 1976)

- Schimidt-Wenzel (Schmidt et al., 1980)

- Harmens-Knapp (Harmens et al., 1980)

- Kubic (Kubic, 1982)

- Patel-Teja (Patel et al., 1982)

- Adachi et al. (Adachi et al., 1983)

- Stryjek-Vera (Stryjek et al., 1986a)

- Yu and Lu (Yu et al., 1987)

- Trebble and Bishnoi (Trebble et al., 1987)

- Schwartzentruber and Renon (Schwartzentruber et al., 1989)

- Heyen (Sandler, 1994)

Modification of Repulsive Term

Modification of the repulsive term is an alternative way to improve the accuracy of an equation of state.

Guggenheim proposed a simple, yet effective equation of state which can be applied to high pressure systems. The equation was found to be useful in calculating both the liquid and the vapour properties and the general critical transition of mixtures and the repulsive terms can be expressed as follows (Guggenheim, 1965):

$$P_{Rep} = \frac{RT}{v}\left(\frac{1}{(1-\eta)^4}\right) \quad\text{..} 7.3$$

However, in equation 7.3 the cubic nature of the equation is lost. Perhaps the most widely used alternative to the van der Waals hard sphere term is that of Carnahan et al, which is an alternative to the Guggenheim equation of state. The repulsive term can be expressed as follows (Carnahan et al., 1969),(Carnahan et al., 1972):

$$P_{Rep} = \frac{RT}{v}\left(\frac{1+\eta+\eta^2-\eta^3}{(1-\eta)^3}\right) \quad\text{..} 7.4$$

In both the equations of Guggenheim and Carnahan et al, the modified term is defined in terms of the packing fraction which can be defined as follows:

$$\eta = \frac{b}{4v} \quad\text{...} 7.5$$

where b is the molecular co-volume.

The repulsive term of the van der Waals equation of state leads to an inaccurate estimation of the repulsive forces. As a consequence of this shortcoming, high pressure and high-density predictions are inaccurate. Modifications to the repulsive term, such as those made by Guggenheim and Carnahan allow the quantitative reproduction of high pressure and high-density predictions.

Modification to Attractive and Repulsive Terms

Some cubic equations of state have been formed by the combination of modifications to the attractive as well as the repulsive terms of the van der Waals equation.

Carnahan et al. combined their repulsive term with the Redlich Kwong attractive term. The resultant equation of state improves the prediction of hydrocarbon densities and supercritical phase equilibria. (Carnahan et al., 1972)

Other Modifications

Many other modifications of the van der Waals equation of state have been made. Many of these modifications have lead to complex equations of state, often resulting in non-cubic equations of state.

Of notable mention is the work of Dieterici. Two equations of state were developed by Dieterici in 1899. The second equation proposed takes into account the variation of the potential energy near the walls of containers and resulted in the following unusual form:

$$P = \frac{RT}{v-b} EXP\left(\frac{-a}{RTv}\right)$$ 7.6

7.1.3. VIRIAL EQUATION OF STATE

Thiessen proposed a empirical equation of state that was later derived from a statistical mechanical basis. This equation of state, know as the Virial equation of state, can be formulated as follows:

$$P = \frac{RT}{v}\left(1 + \frac{B}{v} + \frac{C}{v^2} + ...\right)$$ 7.7

The coefficients B and C are known as the second and third virial coefficients and in theory, for a given substance, these coefficients are functions of temperature only. The coefficients can also be determined for mixtures with the use of a single set of interaction parameters.

If assumptions are made about the mathematical form of intermolecular potentials theoretical expressions can be developed for several coefficients: The coefficient B refers to the interaction between pairs of molecules and the coefficient C to the three-body interactions.

Since the infinite series is impractical for calculation purposes, truncation usually occurs after the second or third term. Dymond et al published an exhaustive compilation of experimental second and third virial coefficients (Dymond et al., 1980).

Various equations of state have developed from the virial equation of state. The Benedict-Webb-Rubin and its modification by Starling is a non-linear equation of state that evolved from the viral equation of state. The equation of state is intended to incorporate the

representation of liquids and gasses above the critical density. The equation was superior to the cubic equations of state available at the time, yet wide application was hampered by the complexity of the equation of state. Additionally, the number of mixing rules and interaction parameters required is a drawback. The equation of state parameters are also only available for fairly small molecules (Benedict et al., 1940).

7.1.4. Chain Type Equations of State

Chain type equations of state are very much applicable to the type of systems studied here as the wax is a long chain normal alkane.

Perturbed hard sphere equations is a modern expression of the physical concepts suggested by van der Waals. They are based on the fundamental assumption that the microstructure of a fluid is determined primarily by the repulsive forces of molecules (i.e. the molecular diameter). Once the microstructure has been determined as a function of density, the effect of the attractive forces can then be calculated by assuming that the molecules are situated in a uniform average field of force (mean field approach).

In these types of equations, the translational degree of freedom has been included, which is a satisfactory assumption for small molecules. However, fluids containing large polyatomic molecules exercise, in addition to translational, also vibrational and rotational motions. These motions depend on density and thus contribute to the equation of state.

The first attempts to develop equations of state that can be applied to chain type molecules were based on the assumption of Prigogine: At high densities all density dependent degrees of freedom can be treated as equivalent to translational degrees of freedom (Prigogine, 1957). The theory of Prigogine was used successfully in developing equations of state for large molecules but was limited to high or liquid like densities.

Beret et al proposed the perturbed hard chain theory, which was a combination of the theory of Prigogine with the perturbed hard sphere theory. Their theory was based on the fact that the extent to which a molecule can vibrate or rotate depends on whether or not a molecule is alone or surrounded by other molecules, the effect of the neighbours being smaller on the vibrational than the rotational motion. The contribution of the vibrational and rotational degrees of freedom can be divided into an external and an internal part, where the internal part depends only on the temperature while the external part depends also on the density. (Beret et al., 1975)

The perturbed hard chain theory was the first attempt to model long chain molecules at a wide variety of densities. This equation of state is successful in calculating properties of fluids but due to practical limitations in the mathematical complexity, especially for mixtures, this equation of state has not been widely implemented. Simplifications of the perturbed hard chain theory have, however, allowed the implementation of chain equations of state.

7.1.5. EQUATIONS OF STATE FOR ASSOCIATING FLUIDS

Associating fluid mixtures are known to contain not only monomeric molecules but also relatively long lived (typically 1-10^3 ps) clusters of like and unlike molecules, due to the effects of hydrogen bonding and donor-acceptance. Since the effective properties of these clusters differ greatly from the monomeric molecules, the bulk fluid properties are also very different. Various attempts have been made to made to model these associating fluids. Recently, most of the attention has been to use statistical mechanics.

The model is based on a fluid of spheres where two kinds of bonds are superimposed: covalent like bonds to form chains and associating bonds for the interaction of molecules. These types of equations can thus be applied to any type of system ranging from non-associating spheres to associating non-spherical molecules.

For application to chain molecules, multisegmented chain molecules can be generated by imposing strong, covalent-like bonds on equisized segments, each of which have one or two sites for bonding (Huang et al., 1990).

These type of equations provide a useful thermodynamic basis for deriving fugacities needed for phase equilibrium simulations and allow for the separation and quantification of the effects of the molecular structure and interactions on the bulk properties of the fluid.

Although the systems investigated here are non-associating, these type of equations of state allow for the inclusion of the molecular shape into the equation of state.

7.1.6. PREVIOUS APPLICATIONS TO TYPES OF SYSTEMS STUDIED HERE

Many equations of state have been applied to systems similar to those studied here. The most important applications are mentioned below:

- Peters et al have applied the SPHSC and the PR equation of state to the C3-nC34 system. Their results show that the SPHSC should be preferred over the PR equation of state when modelling vapour-liquid equilibrium systems with a large difference in carbon chain length (Peters et al., 1992).

- Peters et al studied the ethane – nC24 system. They found that the Redlich-Kwong was incapable of representing the phase equilibria correctly (Peters et al., 1987a).

- Gregorowicz et al used the Peng Robinson equation of state to model the phase equilibria of propane with eicosane. They found that the equation of state worked well, but deviations did occur at high pressures and high propane concentrations (Gregorowicz et al., 1992).

- Chan et al. applied the SAFT equation of state to the fluid-liquid phase equilibrium of propane and tetracontane. The application of the SAFT equation of state to this system seemed successful for their limited data set (Chan et al., 2000).

- Dimitrelis et al. fitted the PHC equation of state to the propane-octadecane system. They showed that with a single interaction parameter of -0.06, the results were fitted to a 5 % rms accuracy (Dimitrelis et al., 1989).

- Nieuwoudt attempted to model phase equilibria of LPG and butane with normal alkanes and found that statistical mechanical equations are inaccurate in the mixture critical region, while an empirically modified Peng-Robinson equation was used with success (Nieuwoudt, 1994).

- Du Rand modelled ethane n-alkane systems with the Cubic Simplified Perturbed Hard Chain, Patel-Teja, Soave-Redlich-Kwong and Peng-Robinson equations of state and found that the Patel-Teja equation fitted the data the best (du Rand, 2000).

- Crause used various cubic and chain equations of state to model ethane and n-alkane phase equilibrium. The chain equations did not predict the critical region with accuracy. The Patel-Teja equation of state was modified for applications to normal alkanes and gave similar results to the Peng-Robinson and Soave-Redlich-Kwong equations of state. The modified form of the Patel-Teja equation of state was used further to model a fractionation column (Crause, 2001).

7.2. THERMODYNAMIC THEORY

For an equation of state to be applicable to a certain system, the equation of state needs to fulfil the following requirements:

- The equation of state needs to correctly predict the pure component vapour pressure of all the components in the temperature range applicable. If any components are in the supercritical state, the equation of state needs to predict the pressure-volume-temperature properties in the region of interest.

- The equation of state needs to correctly predict the phase equilibrium composition at a set temperature and phase.

Although these predictions will probably never be completely correct, a reasonable accuracy is required. This accuracy is usually set by the accuracy of the experimental measurements.

7.2.1. PREDICTION OF PURE COMPONENT VAPOUR PRESSURE

For equilibrium between two phases, the chemical potential of each of the species in the various phases needs to be the same:

$$\mu_i^\alpha = \mu_i^\beta \quad\text{..} \quad 7.8$$

From the assumption in equation 7.8 and from thermodynamics it can be proven that for a pure component the molar Gibbs energy, g, of two phases in equilibrium will be equal to one another. The molar residual Gibbs energy of the two phases is thus equal to one another. Due to the fact that neither the chemical potential nor the molar Gibbs energy can be measured, calculations are facilitated by the introduction of the fugacity of a species, f_i. The relationship between the molar Gibbs energy and fugacity can be expressed as follows (Smith et al., 1996):

$$g_i^R = RT \ln \frac{f_i}{P} \quad\text{..} \quad 7.9$$

From equation 7.9 a new property can be defined, namely the fugacity coefficient:

$$\phi_i = \frac{f_i}{P} \quad\text{...} \quad 7.10$$

It can be proven that for a constant temperature analysis the fugacity coefficient for a specific phase where the phase consists of a pure component can be expressed as follows in terms of the pressure, temperature and compressibility (Smith et al., 1996):

$$\ln(\phi_i) = (Z-1) - \ln Z + \int_\infty^v \left(\frac{1}{v} - \frac{P}{RT} \right) dv \quad\text{...} \quad 7.11$$

In Figure 7-1 the general algorithm to determine the vapour pressure of a pure component is given. The liquid and vapour compressibility can be determined from the equation of state. Cubic equations of state result in three values for the compressibility at a given pressure and temperature. The smallest positive real Z value is the liquid compressibility while the largest Z value is the vapour compressibility. If all three roots are the same or if any of the roots are imaginary, then the system is in the one phase region and a pressure correction needs to be made accordingly. For non-cubic equations of state, the same principle is used to determine the roots, only there may be more than three roots.
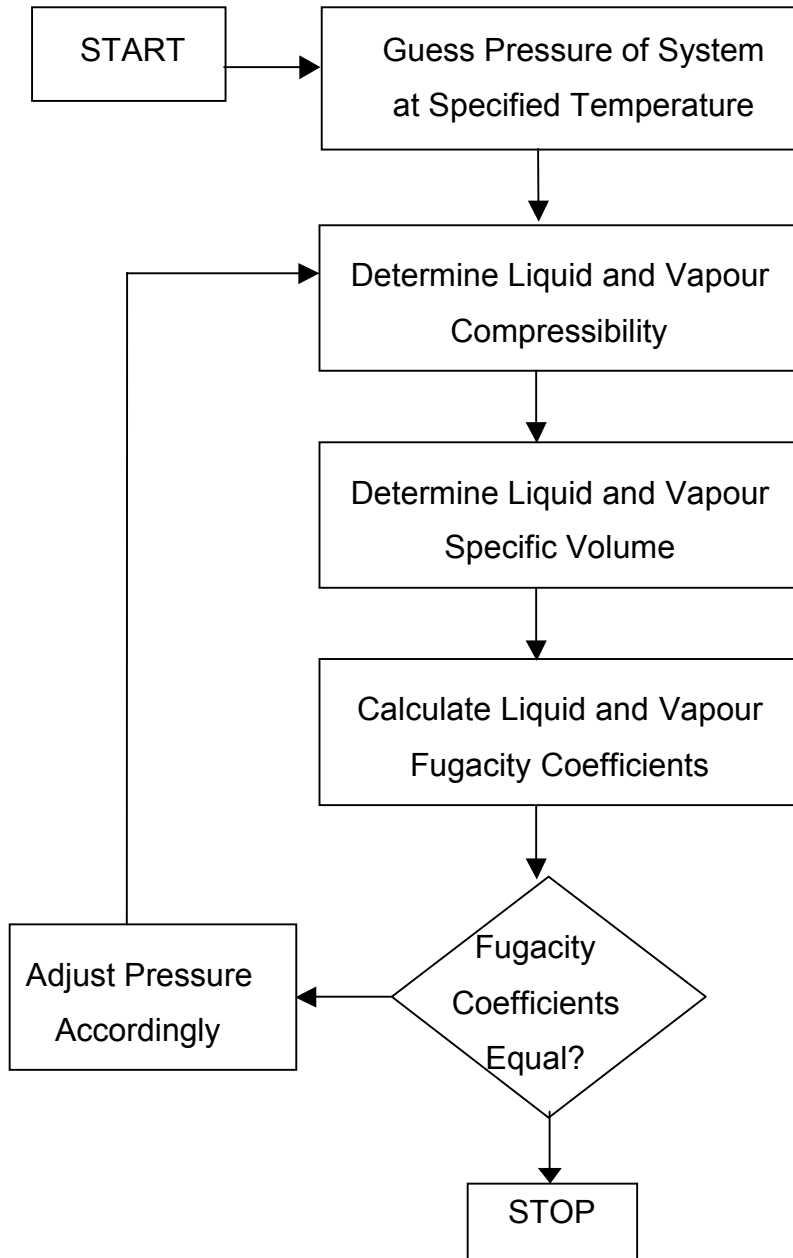
Figure 7-1: Algorithm for predictions of vapour pressure

The liquid and vapour specific volumes can be calculated from the general gas law given as follows:

$$Pv = ZRT \quad\text{..} 7.12$$

The liquid and vapour fugacity coefficients for each phase are calculated from equation 7.11.

7.2.2. PREDICTION OF COMPOSITION AT SET PRESSURE AND TEMPERATURE FOR A BINARY SYSTEM

To predict phase equilibrium data, the following constant temperature and pressure flash set-up, with a feed stream resulting in a liquid and a vapour stream in equilibrium with one another needs to be considered:
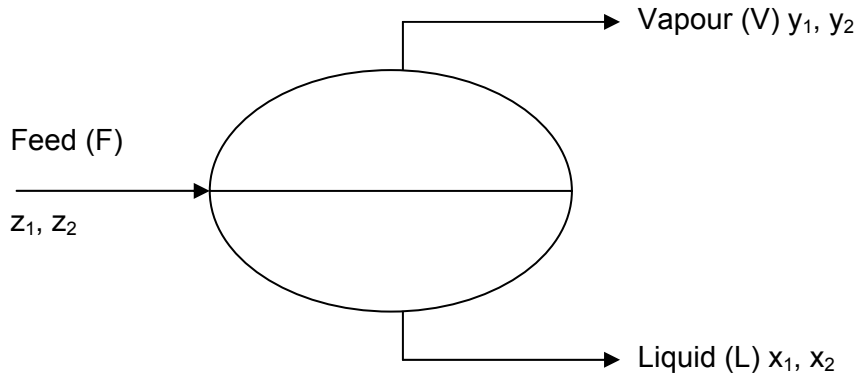
Figure 7-2: Schematic representation of flash process

The following definitions need to be made:

$$\beta = \frac{V}{L} \qquad \text{7.13}$$

$$K_i = \frac{x_i}{y_i} \qquad \text{7.14}$$

From the above definitions, together with mass balances, the following can be proven:

$$x_i = \frac{z_i}{1 + \beta(K_1 - 1)} \qquad \text{7.15}$$

$$\sum \left(\frac{(K_i - 1)z_i}{1 + \beta(K_i - 1)} \right) = 0 \qquad \text{7.16}$$

For phase equilibrium, for each component, the fugacity of the liquid and the vapour phase needs to be the same:

$$\hat{f}_i^L = \hat{f}_i^V \qquad \text{7.17}$$

For a multi-component system the liquid and vapour fugacities can be defined as follows:

$$\hat{\phi}_i^L = \frac{\hat{f}_i^L}{x_i P} \dots\dots\dots\dots\dots\dots\dots\dots\dots\dots\dots\dots\dots\dots\dots\dots\dots\dots\dots\dots\dots\dots\dots\dots\dots\dots\dots\dots 7.18$$

$$\hat{\phi}_i^V = \frac{\hat{f}_i^V}{y_i P} \dots\dots\dots\dots\dots\dots\dots\dots\dots\dots\dots\dots\dots\dots\dots\dots\dots\dots\dots\dots\dots\dots\dots\dots\dots\dots\dots\dots 7.19$$

By substituting equations 7.18 and 7.19 into equation 7.17 and by applying the definition of K_i in equation 7.14 the following expression for K_i can be found in terms of the fugacity coefficients:

$$\frac{y_i}{x_i} = K_i = \frac{\hat{\phi}_i^L}{\hat{\phi}_i^V} \dots\dots\dots\dots\dots\dots\dots\dots\dots\dots\dots\dots\dots\dots\dots\dots\dots\dots\dots\dots\dots\dots\dots\dots\dots\dots 7.20$$

The value of the fugacity coefficients can be calculated from thermodynamics. The residual chemical potential can be defined in terms of the Helmholtz energy:

$$\mu_i^R = \frac{\partial(A - A^\circ)}{\partial n_i}\bigg|_{T,V,n_j} \dots\dots\dots\dots\dots\dots\dots\dots\dots\dots\dots\dots\dots\dots\dots\dots\dots\dots\dots\dots\dots\dots 7.21$$

Equation 7.21 and the derivative at constant temperature of equation 7.9 leads to the following expression for the fugacity coefficient. This expression is only valid for a constant temperature analysis (Smith et al., 1996):

$$\ln\left(\hat{\phi}_i\right) = \frac{1}{RT}\frac{\partial(A - A^\circ)}{\partial n_i}\bigg|_{T,V,n_j} - \ln(Z) - \ln\left(\frac{v^\circ}{v}\right) \dots\dots\dots\dots\dots\dots\dots\dots\dots 7.22$$

Where the residual Helmholtz Energy can be expressed as follows, which follows from the definition of the Helmholtz Energy:

$$\left(A - A^\circ\right) = -\int_\infty^v \left(P - \frac{RTn}{V}\right)dV - nRT\ln\left(\frac{V}{V^\circ}\right) \dots\dots\dots\dots\dots\dots\dots\dots\dots 7.23$$

The solving algorithm for the calculation of the composition of the liquid and the vapour phase at a set temperature and pressure is given in Figure 7-3:
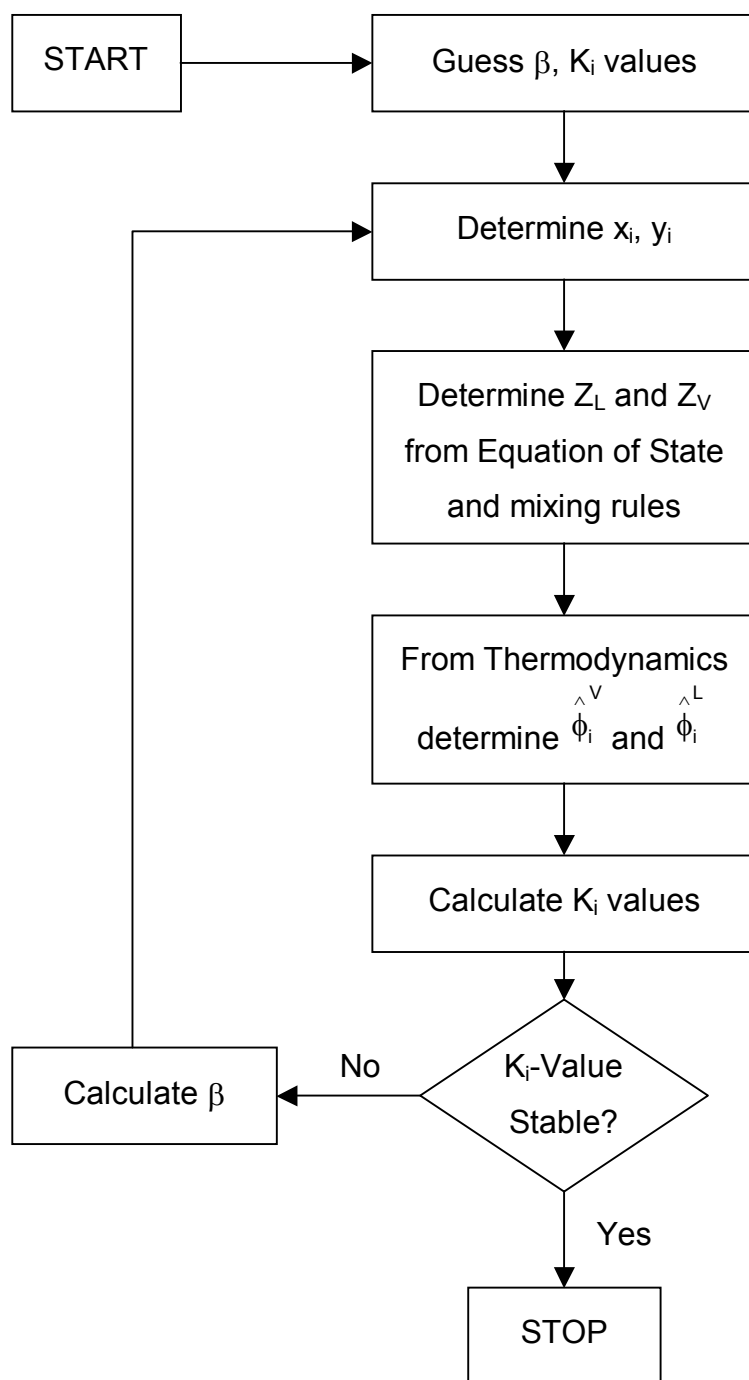
Figure 7-3: Algorithm for Prediction of Composition at set Pressure and Temperature for a Binary System

To guess the initial values for K_i and β the experimental values are used. The values of x_i and y_i can be determined from equation 7.15 and equation 7.14 respectively. The Z^L and Z^V values are determined from the equations of state, in the same manner as described in section 7.2.1. The values of the fugacity coefficients are determined from equation 7.22. The value of K_i is determined from equation 7.20.

7.2.3. THERMODYNAMIC CONSISTENCY TEST

When generating thermodynamic data, it is important to ensure that the data adheres to the basic rules of thermodynamics. Various tests exist that can be performed to ensure the system is thermodynamically consistent.

The most common tests are applicable to low pressures and based on the Gibbs/Duhem Equation with the use of an activity coefficient model (Smith et al., 1996). The Gibbs/Duhem Equation, in turn, is based on the Gibbs excess energy. An excess property can be defined as the difference between the actual property value of a solution and the value it would have in an ideal solution at the same temperature, pressure and composition. To calculate the Gibbs excess energy, an activity coefficient model is required, which, in turn required the calculation of the vapour pressure. It is here where problems arise to determine the thermodynamic consistency of supercritical phase equilibria. The vapour pressure of the solvent phase can not be calculated and thus the method can not be applied to these type of systems.

An alternative method for medium and high pressure phase equilibria has been proposed by Bertucco et al. This model uses residual properties instead of excess properties and thus an equation of state is required instead of an activity coefficient model. Since an equation of state is suppose to be thermodynamically consistent, there is no sense in applying a thermodynamic consistency test to an equation that is inherently consistent (Bertucco et al., 1997).

As stated in paragraph 5.5, data available in the literature was measured and compared well and thus it is assumed that the data generated is reliable.

7.2.4. SOFTWARE AVAILABLE

Two software programs were used for the thermodynamic modelling.

PE (Phase Equilibria) version 2.086 by Pfohl, Petkov and Brunner (Pfohl et al., 2000) was used for most of phase equilibrium modelling. Unless stated otherwise, all thermodynamic modelling was done with the aid of this program.

For the chain equations of state, as well as a few others, LMDataFit by Crause and Nieuwoudt was used. The following equations of state were modelled by LMDataFit:

- Peng Robinson for Heavy Hydrocarbons

- Stryjek Vera Modification of Peng Robinson

- Modified Patel Teja

- Simplified Perturbed Hard Chain

- Cubic Simplified Perturbed Hard Chain

7.3. CRITICAL PARAMETERS AND EXPERIMENTAL PURE COMPONENT DATA

To be able to fit an equation of state to data, the critical properties, as well as the vapour pressure data is required. Due to the fact that for the normal paraffins these properties are often not very accurate and not easily measurable, the values used in this work will be given, together with the method used to estimate these values.

7.3.1. CRITICAL PARAMETERS

In most cases equations of state require the use of the critical temperature and pressure of the components as well as the acentric factor. For the purpose of the PE phase equilibrium simulator, the critical compressibility, boiling temperature and the molecular weight are required.

For propane, these values are easily measured and also well documented in literature.

For the long hydrocarbon chains, these values cannot be measured due to the fact that the compound decomposes before the critical temperature can be reached. The critical values for the long chained hydrocarbons are thus 'pseudo' values determined by means of extrapolations.

For the purpose of this project, the values used were determined by Crause (Crause, 2001). The critical temperature, pressure and compressibility were correlated by Tsonopoulos et al (Tsonopoulos et al., 1993), the acentric factor by Magoulas et al (Magoulas et al., 1990) and the boiling point by Riazi et al (Riazi et al., 1996). The following values were used for the compounds studied in this work:

Table 7-1: Critical Values for Compound studied in this Work

Compound	T_c (K)	P_c (bar)	Omega	Z_c (-)	T_b (K)	M_R (mol/g)
Propane	369.83	42.48	0.155593	0.279	231.11	44.0965
nC32	855	7.50	1.377	0.196	739	450.876
nC36	874	6.80	1.526	0.196	770	506.984
nC38	881	6.42	1.559	0.193	784	535.037
nC40	889	6.12	1.631	0.192	797	563.091
nC44	903	5.59	1.774	0.190	820	619.199
nC46	909	5.36	1.845	0.189	831	647.252
nC54	929	4.60	2.129	0.186	868	759.467
nC60	941	4.46	2.342	0.184	891	843.629

All other parameters required will be provided together with the equation of state.

7.3.2. PURE COMPONENT VAPOUR PRESSURE FOR PARAFFINS

Very little data exists for the vapour pressures of pure paraffins. This can be attributed to the difficulty in the measurements due to the high temperatures required and the low pressures.

However, for some of the paraffins used in this work, data has been measured or estimated (Twu, 1983), (Piacente et al., 1994), (Tobler, 1998), (Morgan et al., 1994). For the purpose of this project the vapour pressures reported in these sources were plotted and the best fit through the data was used. Due to the fact that data is only available for carbon numbers up to 38, for the systems studied in this project data could only be generated for dotriacontane, hexatriacontane and octatriacontane. Data generated is given in Appendix D1.

7.3.3. PvT DATA FOR PROPANE

Pressure-volume-temperature data for propane was obtained from the NIST website [165]. The PvT and vapour pressure data is given in appendices D2 and D3 respectively, and resulted in the following pressure-volume-temperature plot:
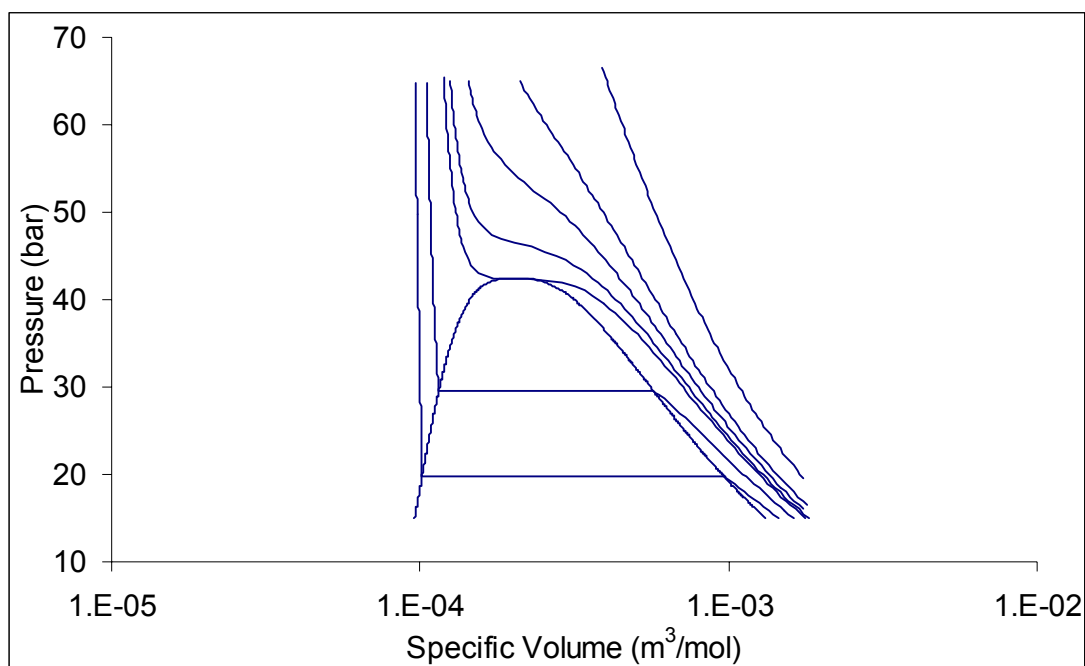
Figure 7-4: Pressure-volume-temperature plot for propane

7.4.   EQUATIONS NOT SUITABLE

Before any calculations were done, the applicability of the equations of state were investigated. The following equations of state were investigated but found not to be applicable to the type of system studied here:

Table 7-2: Equations of state not applicable to the systems studied here

Equation	Application problem
BACK (Pfohl et al., 1998)	This equation of state is only applicable to small molecules
Anderko-Linear (Anderko, 1989b), (Anderko, 1989a)	This equation of state is only applicable to associating fluids
Cubic Plus Association Equations of State (Kontogeogis et al., 1996)	These equations of state reduce to the original equations when the associating term is turned off.
Chen (Chen et al., 1996)	This equation of state was fitted to saturated data and no work was done in the critical region.

Various equations of state were investigated and the first criteria for applicability of an equation of state is the prediction of the vapour pressure curve of the pure components.

The following equations of state were considered but were not able to predict the pure component vapour pressure curve of dotriacontane. These equations of state are given below with a short description of the shortcomings. Details of the equations can be found in appendix E.7.

Table 7-3: Equations of State unable to predict the vapour pressure correctly

Equation	Problem
Van der Waals (Van der Waals, 1873)	Temperature independence of attractive term
Redlich-Kwong (Redlich et al., 1949)	Does not perform well for complex fluids with non-zero acentric factors.
Dohrn-Prausnitz (Dohrn et al., 1990)	Water was used as a reference fluid
Saku-Wu-Prausnitz (Sako et al., 1989)	Incorrect estimation of the van der Waals volume
Pfennig (Pfennig, 1988)	Inaccuracies in pure component parameters
SAFT-Pfennig-Pfohl (Pfohl et al, 2000)	Inaccuracies in pure component parameters

A comparison of the vapour pressures of dotriacontane predicted by the above mentioned equations of state with literature data is given in Figure 7-5.
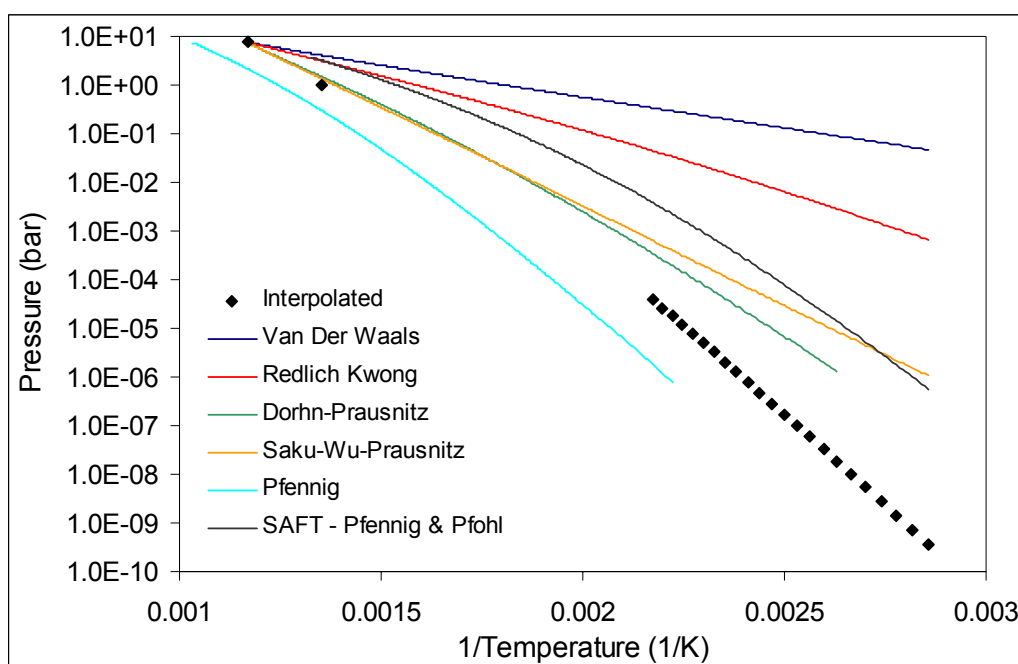
Figure 7-5: Vapour pressure prediction of dotriacontane with various equation of state that do not fit the data well.

As can be seen in Figure 7-5 the RK equation of state is a marked improvement of the VDW equation of state but nowhere near accurate enough. The curvature of both the SAFT-PP as well as the Pfennig equation of state is too large, while the DP and SWP equations of state have the correct type of shape but an incorrect slope.

Possibly detailed fitting of the parameters may result in more accurate prediction of the vapour pressure, yet, as stated above, this lies outside the scope of the modelling of the data done in this work.

7.5. CUBIC EQUATIONS OF STATE

Cubic equations of state are mathematically simple and allow for easy application in phase equilibrium calculations due to the fact that they are cubic with respect to volume. Yet, cubic equations of state have the disadvantage that they are usually unable to accurately predict the liquid densities.

7.5.1. MIXING RULES

Currently there are two main types of mixing rules, composition independent and composition dependent mixing rules. In terms of the mathematical expression the main difference between the two types is the inclusion of an additional parameter in the composition dependent mixing rules. Although the prediction with the two types of mixing rules will be compared, the mixing rules as such cannot be compared due to the fact that the mixing rules have a different number of parameters.

Composition Independent Mixing Rule

The most common mixing rule is the quadratic mixing rule. This mixing rule has two interaction parameters and is composition independent. The mixing rule can be formulated as follows:

$$a_{ij} = \sqrt{a_i a_j}\left(1 - k_{ij}\right) \text{ with } k_{ij} = k_{ji} \quad \dots\dots\dots\dots\dots\dots\dots\dots\dots\dots\dots\dots\dots\dots\dots\dots\dots\dots\dots\dots 7.24$$

$$b_{ij} = \frac{b_i + b_j}{2}\left(1 - \ell_{ij}\right) \text{ with } \ell_{ij} = \ell_{ji} \quad \dots\dots\dots\dots\dots\dots\dots\dots\dots\dots\dots\dots\dots\dots\dots\dots\dots\dots\dots 7.25$$

The cross coefficients a_{ij} and b_{ij} can now be used to determine the values of a and b according to the following combining rules:

$$a = \sum_{i=1}^{N}\sum_{j=1}^{N} x_i x_j a_{ij} \quad \dots\dots\dots\dots\dots\dots\dots\dots\dots\dots\dots\dots\dots\dots\dots\dots\dots\dots\dots\dots\dots\dots\dots\dots 7.26$$

$$b = \sum_{i=1}^{N} \sum_{j=1}^{N} x_i x_j b_{ij} \quad \text{..} \quad 7.27$$

Composition Dependent Mixing Rule

In many cases the quadratic mixing rule described above is not sufficient to fully describe the interaction of the various fluids. An additional parameter is introduced to quantify the interaction of the parameter a.

Panagiotopoulos and Reid were the first to introduce a second composition dependent interaction parameter to fine-tune the parameter a (Panagiotopoulos et al., 1985). Adachi and Sugie proposed a mixing rule slightly later than Panagiotopoulos and Reid, claiming their mixing rule is identical to that of Panagiotopoulos and Reid for binary systems, but differs for multicomponent systems (Adachi et al., 1986). However, Pfohl showed that the mixing rules were identical (Pfohl, 1998). Stryjek and Vera proposed a mixing rule that they claimed results in better correlation than the Panagiotopoulos and Reid type mixing rule (Stryjek et al., 1986a).

However, all the above mixing rules suffer from the so-called Michelsen-Kistenmacher-Syndrome (Michelsen et al., 1990). This syndrome can be defined as follows: If a binary mixture (x_1, x_2) is calculated as a ternary mixture (x_1, x_2^a, x_2^b) where $x_2 = x_2^a + x_2^b$ a different value for a for the mixture will result. This will usually lead to different total molar properties, such as enthalpy and partial molar properties such as fugacities.

Additionally, Michelsen et al described the dilution effect. The interaction parameter for b is calculated in a double summation but contains the product of three mole fractions. Thus, as the number of components increase, the effect of this term becomes smaller, eventually vanishing when an infinite number of compounds are present.

Melheim et al proposed a mixing rule that does not suffer from the dilution problem, i.e., that the concentration dependence of the mixing rule decreases as the number of components increase. (Melheim et al., 1991)

Mathias et al proposed a new mixing rule that does not suffer from this syndrome (Mathias et al., 1991). This mixing rule yield the same result if the mole fraction x_i is split into x_i^1 and x_i^2 where $x_i = x_i^1 + x_i^2$. The strong theoretical advantage of the mixing rule was proven by Mathias et al for benzene and cyclohexane and by Pfohl (Pfohl, 1998) for two cresol isomers. It must, however, be mentioned that for a binary mixture, the mixing rule proposed by Mathias et al reduces to the same mixing rule proposed by Panagiotopoulos and Reid, Adachi and Sugie and the mixing rule of Melheim.

For the purpose of this work, the mixing and combining rules of Mathias et al, known as the Mathias, Klotz and Prausnitz (MKP) mixing Rules, will be used as an example of a concentration dependent mixing rule. The mixing rule can be defined as follows:

$$a = \sum_{i=1}^{N}\sum_{j=1}^{N}\left[x_i x_j \sqrt{a_i a_j}\left(1-k_{ij}\right)\right] + \sum_{i=1}^{N} x_i \left[\sum_{j=1}^{N} x_j \left(\sqrt{a_i a_j}\,\lambda_{ji}\right)^{\frac{1}{3}}\right]^3 \quad \text{................................ 7.28}$$

with

$$k_{ji} = k_{ij} \text{ and } \lambda_{ji} = -\lambda_{ij} \quad \text{.. 7.29}$$

The value of b is determined in the same manner as for the quadratic mixing rule:

$$b = \sum_{i=1}^{N}\sum_{j=1}^{N} x_i x_j b_{ij} \quad \text{... 7.27}$$

where

$$b_{ij} = \frac{b_i + b_j}{2}\left(1-\ell_{ij}\right) \text{ with } \ell_{ij} = \ell_{ji} \quad \text{... 7.30}$$

7.5.2. SOAVE-REDLICH-KWONG (SRK)

The Redlich-Kwong equation of state can be expressed as follows:

$$P = \frac{RT}{v-b} - \frac{a/T^{0.5}}{v(v-b)} \quad \text{.. 7.31}$$

Soave recognized that the inability of the RK equation of state to predict vapour liquid equilibrium calculations for mixtures does not lie solely with the mixing rules, but in the equations lack to express the influence of temperature accurately. (Soave, 1972)

Soave modified the attractive term by replacing the $a/T^{0.5}$ term with a more general temperature dependent a (T) term

$$P = \frac{RT}{v-b} - \frac{a(T)}{v(v-b)} \quad \text{... 7.32}$$

By applying the assumption that at the critical point the first and second derivatives in terms of pressure are zero, and by fitting the PvT data to the reduced temperature and the acentric factor, the values of a and b can be expressed as follows:

$$a(T) = 0.42747\ \alpha(T)\frac{R^2 T_c^{\ 2}}{P_c} \quad \text{.. 7.33}$$

$$b = 0.08664 \frac{RT_c}{P_c} \quad \text{...} \quad 7.34$$

where:

$$\alpha(T) = \left[1 + m\left(1 - \sqrt{T_R}\right)\right]^2 \quad \text{...} \quad 7.35$$

and

$$m = 0.480 + 1.574\omega - 0.176\omega^2 \quad \text{..} \quad 7.36$$

The SRK prediction of the propane pressure-volume-temperature plot is given in Figure 7-6. As is typical for a cubic equation of state, the vapour densities are predicted well, but the equation fails in the liquid density prediction.

Figure 7-6: SRK EOS prediction of Propane Pressure-Volume-Temperature Diagram

The SRK prediction of the dotriacontane vapour pressure is given in Figure 7-7. As can been, the equation of state is able to predict the vapour pressure curve well.
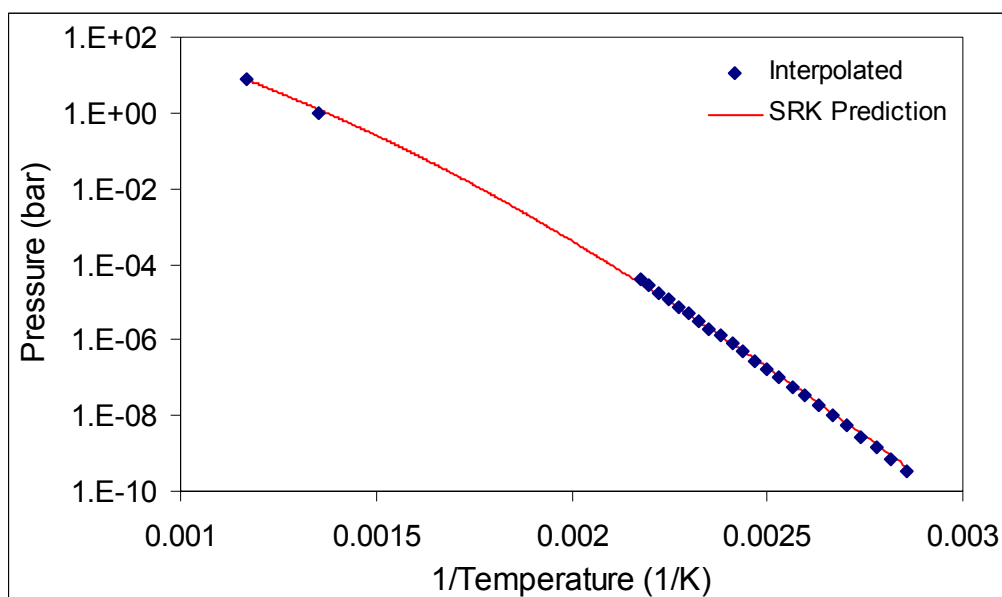
Figure 7-7: SRK EOS prediction of Dotriacontane Vapour Pressure Curve

The SRK equation of state was fitted to the experimental data and the following interaction parameters were found for a good prediction of the phase equilibrium. The equation of state predictions are given for the quadratic and MKP mixing rules in Figure 7-8 and Figure 7-9 respectively:

Table 7-4: SRK Binary Interaction Parameters for Propane-C32

Quadratic	$k_{12} = 0.02181$
	$l_{12} = 0.03713$
MKP	$k_{12} = 0.1307$
	$l_{12} = 0.06531$
	$\lambda_{12} = 0.1850$

Figure 7-8: SRK EOS with Quadratic Mixing Rules prediction of Pressure Composition Diagram for Propane-Dotriacontane at 408.15 K
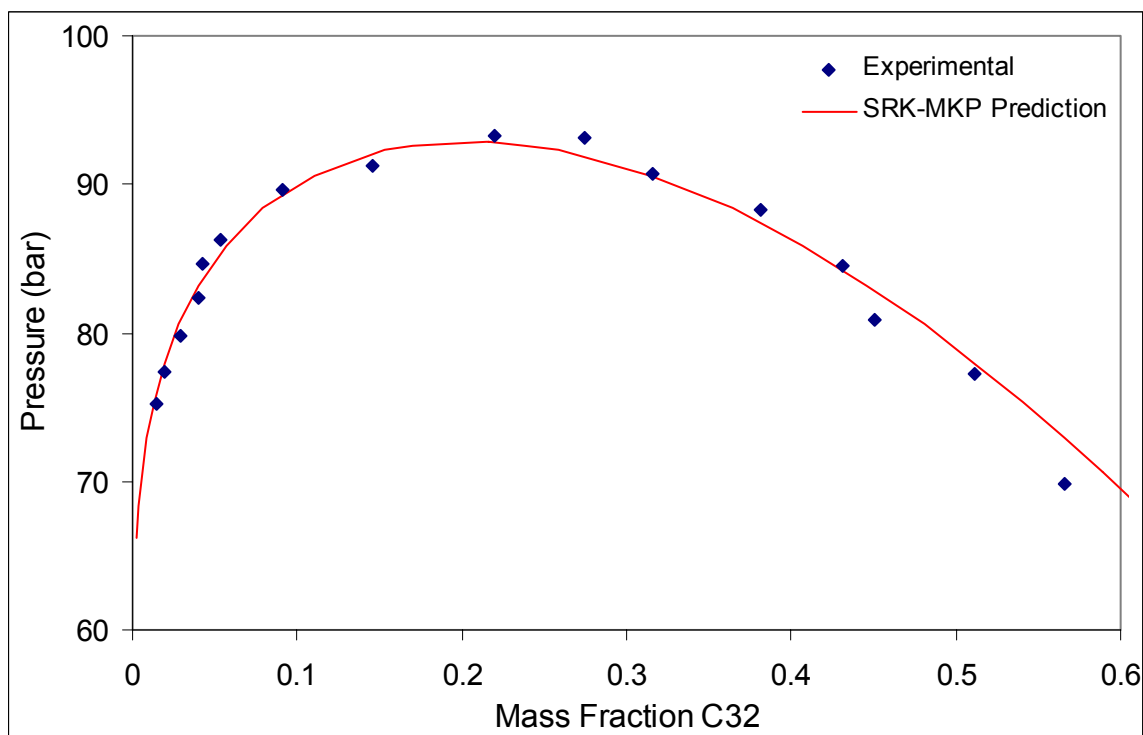
Figure 7-9: SRK EOS with MKP Mixing Rules prediction of Pressure Composition Diagram for Propane-Dotriacontane at 408.15 K

It can be seen that both the quadratic and the MKP mixing rules predict the system quite well. There is essentially no difference in the accuracy of the predictions for the binary

case, yet due to the fact that the MKP mixing rules do not suffer from the Michelsen-Kistenmacher-Syndrome, it is expected to perform better in the ternary case. It also needs to be mentioned that the MKP interaction parameters are large and thus indicate that for the SRK equation of state the MKP mixing rules do not predict the system well.

7.5.3. PENELOUX VOLUME TRANSLATED SOAVE-REDLICH-KWONG (SRK-VT-P)

As seen in Figure 7-6, the SRK equation of state is not satisfactory in the prediction of the PvT calculations due to the inaccuracies in the volume estimations. Various volume translations have been proposed to improve the volume predictions of the SRK equation of state. Peneloux et al was the first to propose a volume translation and as an example of a volume translation equation of state, this equation of state will be investigated (Peneloux et al., 1982). The equation of state has the following functional form:

$$P = \frac{RT}{(v-b)} - \frac{a}{(v+c)(v+b+2c)} \quad \text{..} 7.37$$

The values of a and b are calculated in the same manner as for the original SRK equation of state (see equations 7.35 through 7.38) while the value of c is calculated as follows:

$$c = 0.40768 \frac{RT_c}{P_c}(0.29441 - z_{RA}) \quad \text{..} 7.38$$

where z_{RA} is the Rackett compressibility factor. Peneloux et al provided values for the values of z_{RA}. For propane the value of z_{RA} was given as 0.2767 and for the waxes the following correlation was given:

$$z_{RA} = \sum_{j=0}^{5} Z_j (CN - 6)^j \quad \text{..} 7.39$$

where the values of Z_j are as follows:

$$Z_0 = 0.26461$$
$$Z_1 = -4.0597E - 3$$
$$Z_2 = 2.6801E - 4$$
$$Z_3 = -1.1970E - 5$$
$$Z_4 = 2.7563E - 7$$
$$Z_5 = -2.4443E - 9$$

For extension to mixture the same mixing rules are used for the parameter a as in the original equation of state. For the quadratic mixing rule the mixing rule is thus:

$$a = \sum_{i=1}^{N} \sum_{j=1}^{N} x_i x_j a_{ij} \quad \dotfill \quad 7.26$$

where

$$a_{ij} = \sqrt{a_i a_j} \left(1 - k_{ij}\right) \text{ with } k_{ij} = k_{ji} \quad \dotfill \quad 7.24$$

For the MKP mixing rules the following mixing rule is used for the parameter a:

$$a = \sum_{i=1}^{N} \sum_{j=1}^{N} \left[x_i x_j \sqrt{a_i a_j} \left(1 - k_{ij}\right) \right] + \sum_{i=1}^{N} x_i \left[\sum_{j=1}^{N} x_j \left(\sqrt{a_i a_j} \lambda_{ji}\right)^{\frac{1}{3}} \right]^3 \quad \dotfill \quad 7.28$$

The parameters b and c are calculated as the arithmetic mean of the pure component parameters, i.e.:

$$b = \sum_{i=1}^{N} x_i b_i \quad \dotfill \quad 7.40$$

$$c = \sum_{i=1}^{N} x_i c_i \quad \dotfill \quad 7.41$$

The PvT prediction for propane of the SRK-VT-P equation of state is given in Figure 7-10. As can be seen there is a slight increase in the accuracy of the liquid densities but there is still a marked difference between the experimental and predicted values.
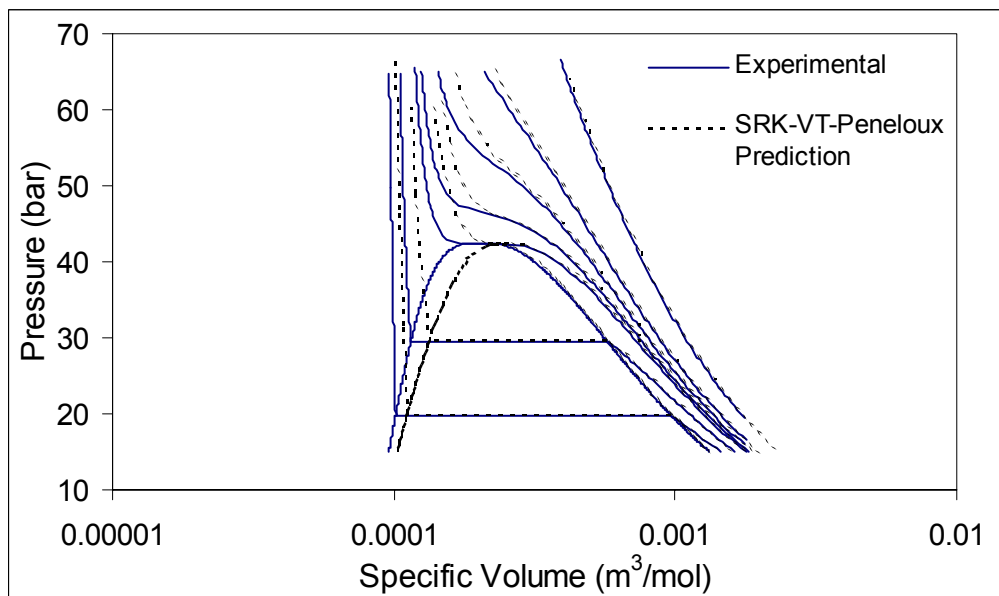
Figure 7-10: SRK-VT-P EOS prediction of Propane Pressure-Volume-Temperature Diagram

The equation of state has been formulated in such a way that the vapour pressure prediction is identical to that of the original equation of state. This was tested and confirmed with the aid of the PE simulator.

The equation of state was fitted to the phase equilibrium data and the binary interaction parameters for the system propane-dotriacontane are given in Table 7-5:

Table 7-5: SRK-VT-P Binary Interaction Parameters for Propane – C32

Quadratic	k_{12} = 0.02772
MKP	k_{12} = -0.1416
	λ_{12} = -0.2579

The equation of state predictions are given for the quadratic and MKP mixing rules in Figure 7-11.
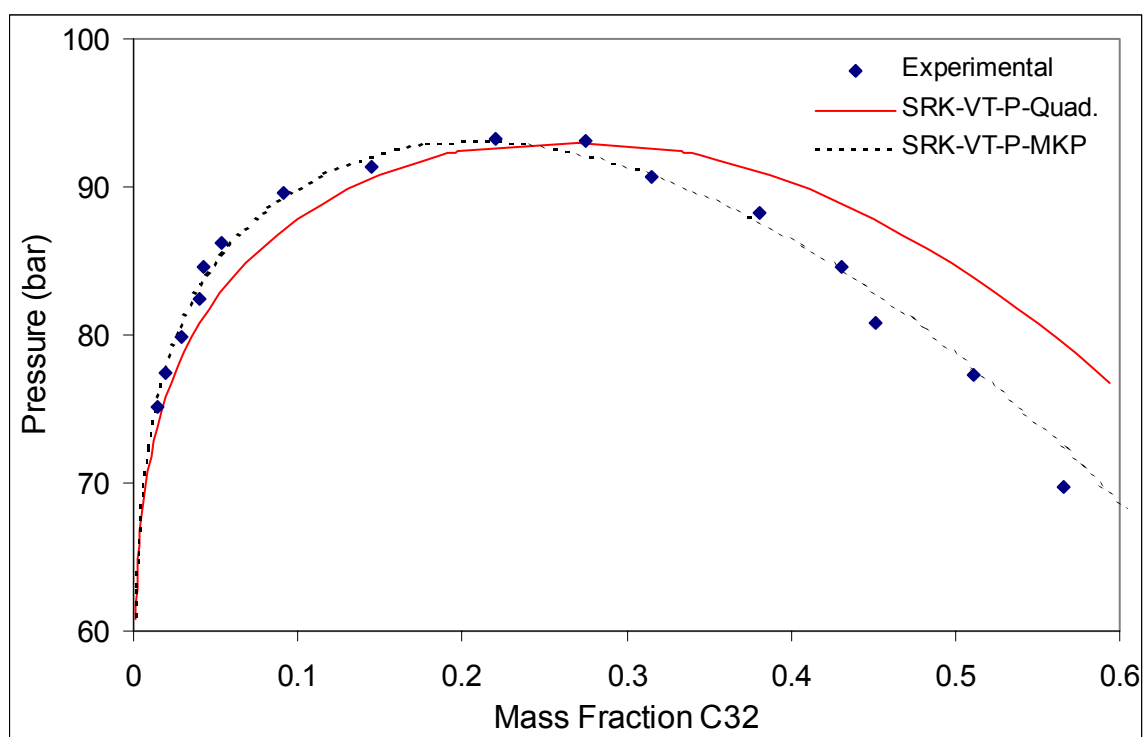
Figure 7-11: SRK-VT-P EOS with Quadratic and MKP Mixing Rules prediction of Pressure Composition Diagram for Propane-Dotriacontane at 408.15 K

As can be seen above, the MKP mixing rules gives a profoundly better prediction of the phase equilibrium data to that of the quadratic mixing rules. The difference in the prediction can be attributed to the fact that for the MKP mixing rule two interaction parameters are used while only one is used for the quadratic mixing rule. However, when considering the interaction parameter values it is noted that the parameters for the MKP

mixing rule are both quite large and negative and thus the conclusion can be made that the equation of state is not fitted to the data but rather forced through it.

7.5.4. SOAVE-REDLICH-KWONG FOR HEAVY HYDROCARBONS (SRK-HH)

The modification of the SRK equation of state for heavy hydrocarbons is a modification of the alpha function so that the alpha function fits the heavy hydrocarbons better. The alpha function was fitted to the vapour pressure data.

Equations 7.32 through 7.34 are used in the SRK-HH equation of state. However, the alpha function was modified by Soave (Soave, 1993) as follows:

$$\alpha = 1 + m(1 - T_R) + n(1 - \sqrt{T_R})^2 \dots\dots\dots\dots\dots\dots 7.42$$

where

$$m = 0.484 + 1.515\omega - 0.044\omega^2 \dots\dots\dots\dots\dots\dots 7.43$$

$$n = 2.756m - 0.700 \dots\dots\dots\dots\dots\dots 7.44$$

The PvT prediction for propane of this modification of the SRK equation of state is given in Figure 7-12. the graph obtained is virtually identical to that of the original SRK equation of state.
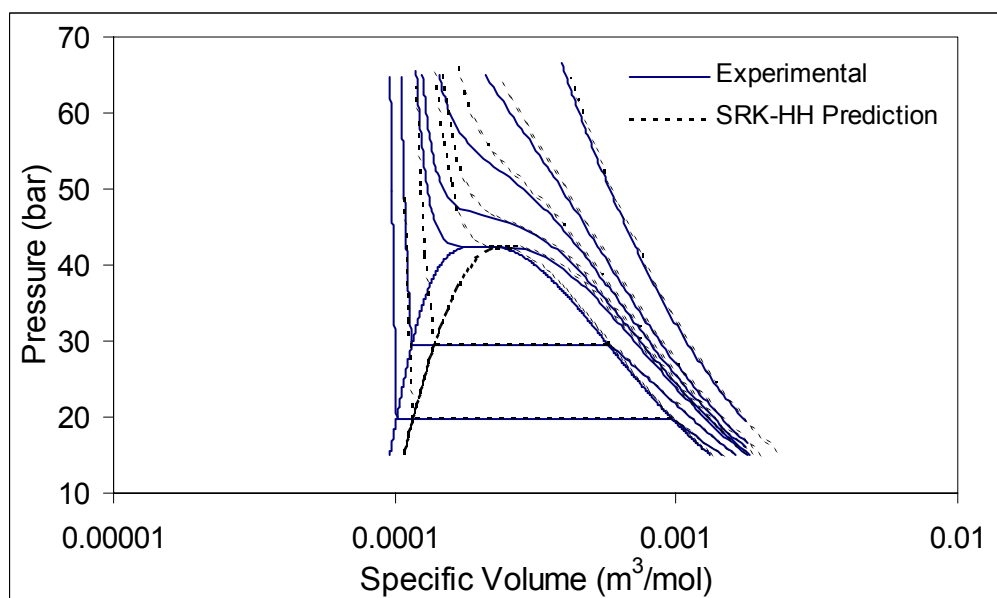
Figure 7-12: SRK-HH EOS prediction of Propane Pressure-Volume-Temperature Diagram

The vapour pressure curve for dotriacontane predicted with the SRK-HH equation of state is compared to the original SRK equation of state in Figure 7-13. As can be seen, the

modification actually produces a slightly worse fit of the vapour pressure curve compared to the original equation of state
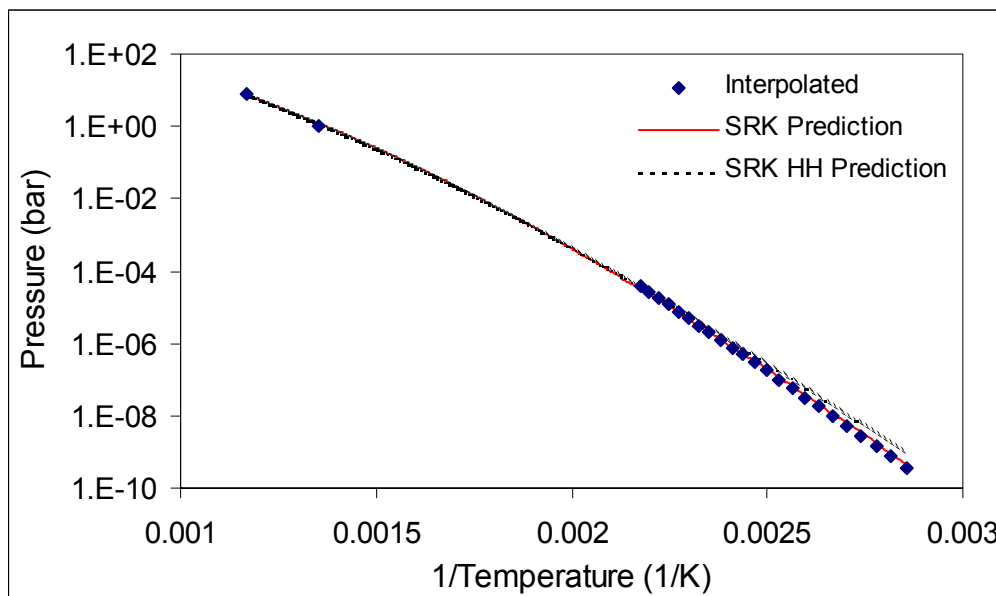
Figure 7-13: SRK-Heavy-Hydrocarbons EOS prediction of Dotriacontane Vapour Pressure Curve

This modification of the SRK equation of state was used to predict the binary phase diagram of propane with dotriacontane. The interaction parameters for the two mixing rules used are given in Table 7-6 and followed by the plots in Figure 7-14 and Figure 7-15.

Table 7-6: SRK-HH Binary Interaction Parameters for Propane – C32

Quadratic	$k_{12} = 0.02379$
	$l_{12} = 0.05035$
MKP	$k_{12} = 0.02385$
	$l_{12} = 0.05039$
	$\lambda_{12} = 0.00008463$
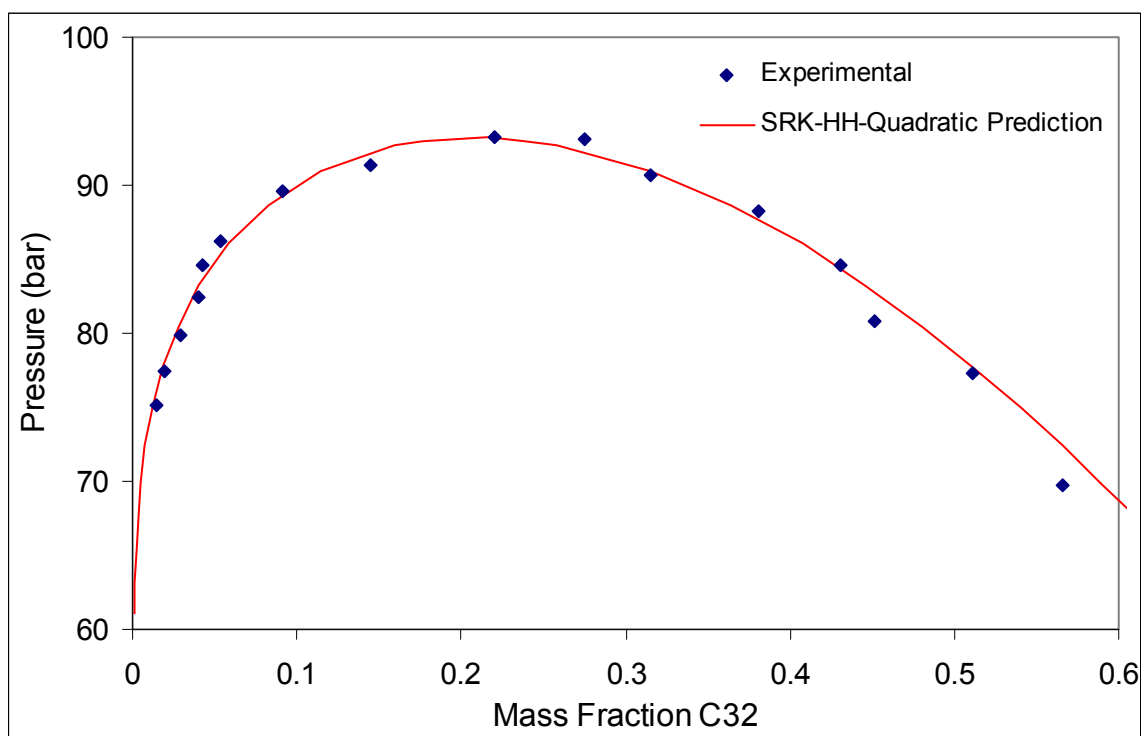
Figure 7-14: SRK-HH EOS with Quadratic Mixing Rules prediction of Pressure Composition Diagram for Propane-Dotriacontane at 408.15 K
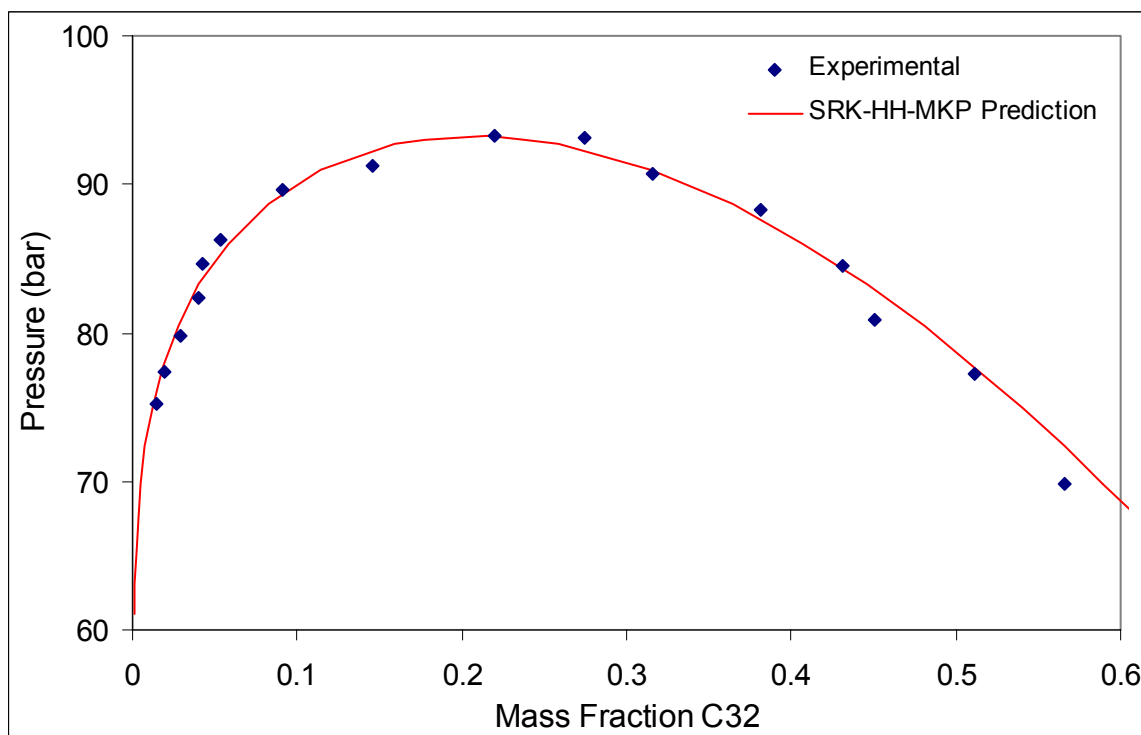
Figure 7-15: SRK-HH EOS with MKP Mixing Rules prediction of Pressure Composition Diagram for Propane-Dotriacontane at 408.15 K

Comparing Figure 7-14 and Figure 7-15 with Figure 7-8 and Figure 7-9 it can be seen that roughly the same quality of fit is obtained. When comparing the interaction parameters for

the cubic mixing rules, the values are the same. However, for the MKP mixing rules, the interaction parameters are a lot smaller for this modified SRK equation of state, to the original equation of state. This can explained by the fact that the errors in the vapour pressure simply cancel out the inaccuracies in the equation of state.

7.5.5. PENG-ROBINSON (PR)

Peng et al found that the SRK equation of state could not predict the liquid densities well, despite the fact that the vapour densities were predicted with reasonable accuracy (Peng et al., 1976). They proposed the following equation of state (PR):

$$P = \frac{RT}{v-b} - \frac{a(T)}{v(v+b)+b(v-b)}$$ 7.45

where

$$a(T) = 0.45724\,\alpha(T)\frac{R^2 T_c^{\,2}}{P_c}$$ 7.46

$$b = 0.07780\frac{RT_c}{P_c}$$ 7.47

$$\alpha(T) = \left[1 + m\left(1 - \sqrt{T_R}\right)\right]^2$$ 7.48

$$m = 0.37464 + 1.54226\omega - 0.26992\omega^2$$ 7.49

The PvT plot of propane generated with the PR equation of state is given in Figure 7-16. Comparing the PR PvT prediction with that of the SRK PvT prediction it can be seen that the PR equation of state improves the liquid side volume prediction, yet in the critical region there is no noticeable improvement.
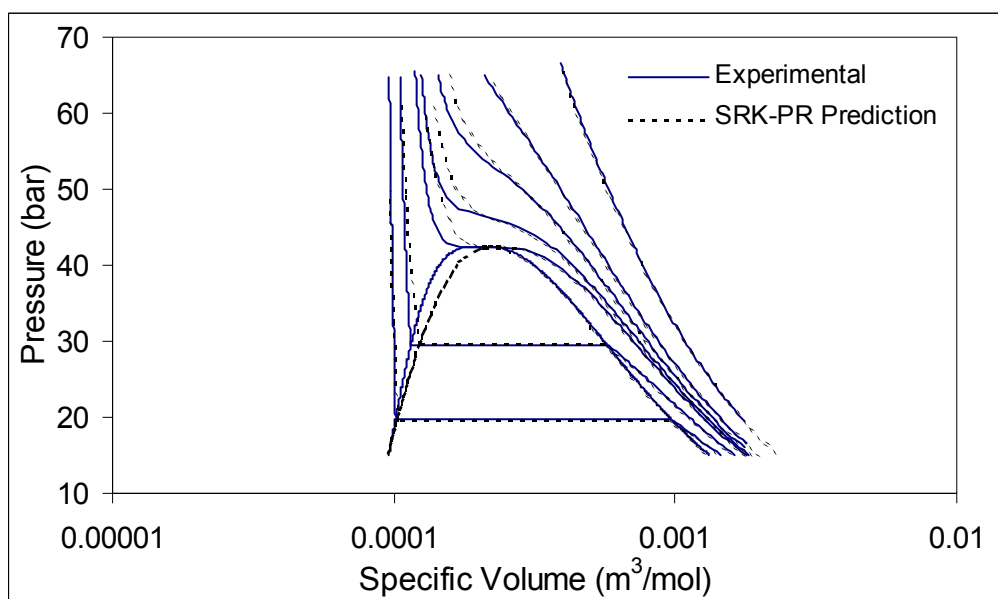
Figure 7-16: PR EOS prediction of Propane Pressure-Volume-Temperature Diagram

In Figure 7-17 the vapour pressure curve prediction for Dotriacontane with the PR equation of state is given. In contrast to the PvT diagram above, the vapour pressure curve here is not as accurate as it deviates at lower temperatures.
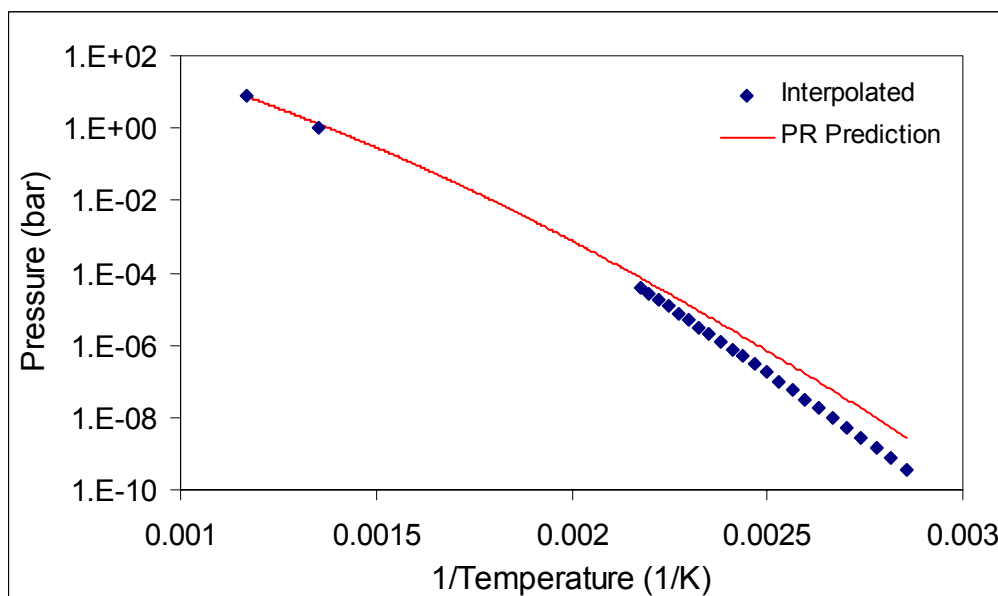
Figure 7-17: PR EOS prediction of Dotriacontane Vapour Pressure Curve

The PR equation of state was fitted to the propane-dotriacontane data. The interaction parameters required for the best fit are given in Table 7-7 while the resultant fits are shown in Figure 7-18 and Figure 7-19.

Table 7-7: PR Binary Interaction Parameters for Propane – C32

Quadratic	$k_{12} = 0.02379$
	$l_{12} = 0.05035$
MKP	$k_{12} = 0.1020$
	$l_{12} = 0.1056$
	$\lambda_{12} = 0.1394$
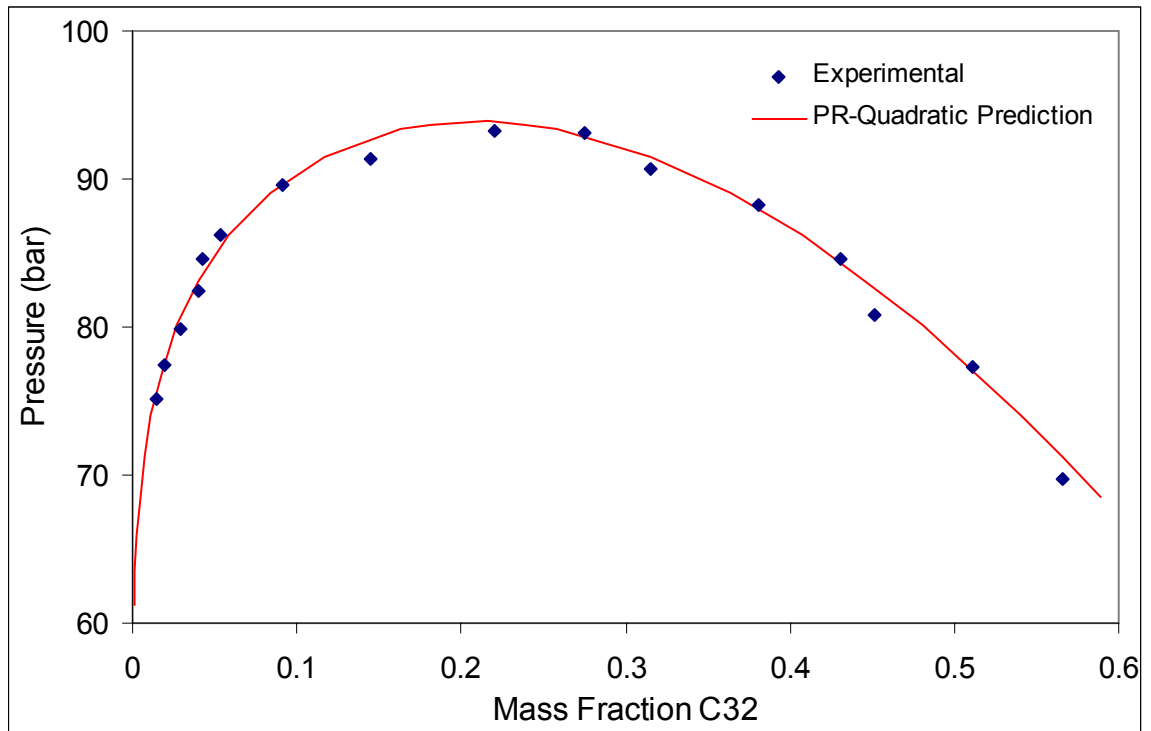
Figure 7-18: PR EOS with Quadratic Mixing Rules prediction of Pressure Composition Diagram for Propane-Dotriacontane at 408.15 K
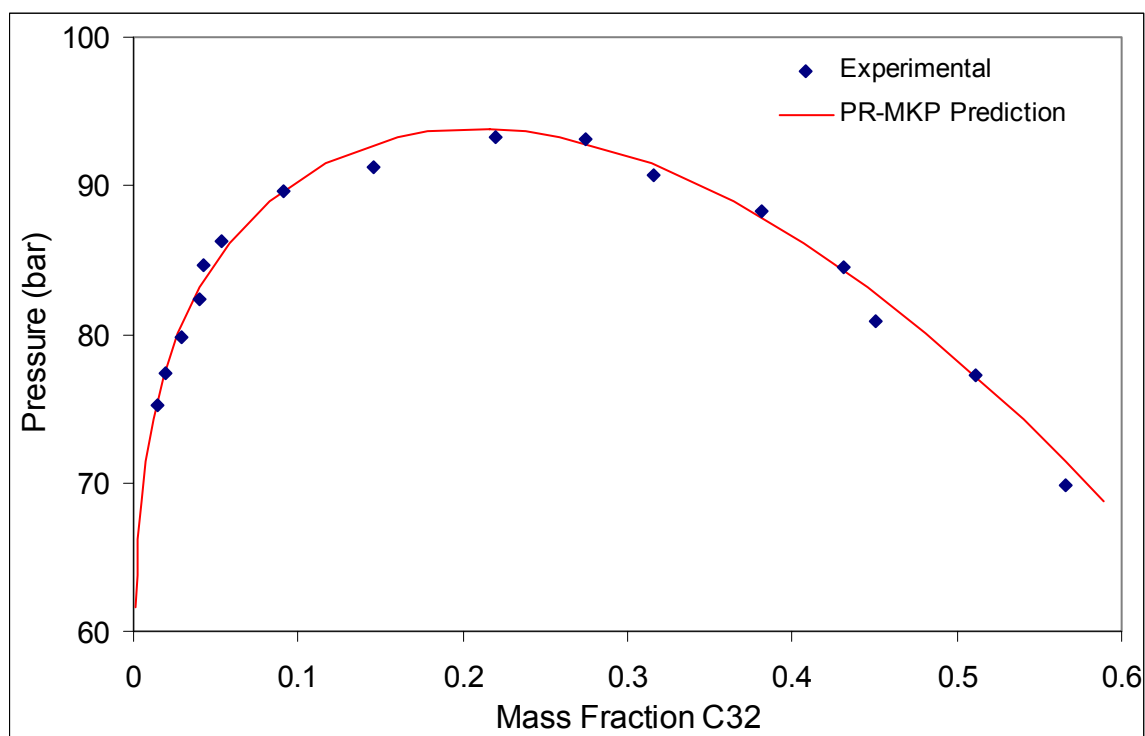
Figure 7-19: PR EOS with MKP Mixing Rules prediction of Pressure Composition Diagram for Propane-Dotriacontane at 408.15 K

The binary modelling results of the PR equation of state gives very similar results to the SRK equation of state. When comparing the PR interaction parameters with those of the SRK equation of state, it can be seen that the values do not vary in order of magnitude. It can therefore be deduced that the PR and SRK equations of state have similar ability to fit the data.

7.5.6. PENELOUX VOLUME TRANSLATED PENG-ROBINSON (PR-VT-P)

Although the PR equation of state has an improved liquid density prediction, the prediction is far from perfect. The same type of volume translations modifications of the PR equation of state was done as for the SRK equation of state. Once again the Peneloux volume translation will be illustrated here as an example of these type of modifications. The equation of state can be expressed as follows:

$$P = \frac{RT}{v-b} - \frac{a}{v^2 + 2vb + 4vc + 2c^2 - b} \quad \dots\dots\dots\dots\dots\dots\dots\dots\dots\dots\dots\dots\dots\dots\dots\dots\dots\dots\dots 7.50$$

The values of a and b are calculated in the manner same as for the original PR equation of state (see equations 7.48 to 7.50) while the value of c is calculated in the same way as for the SRK-VT-Peneloux equation of state:

$$c = 0.40768 \frac{RT_c}{P_c}\left(0.29441 - z_{RA}\right) \dotfill 7.38$$

where z_{RA} is the Rackett compressibility factor. Peneloux et al provided values for the values of z_{RA} (Peneloux et al., 1982). For propane the value of z_{RA} was given as 0.2767 and for the waxes the following correlation was given:

$$z_{RA} = \sum_{j=0}^{5} Z_j (N-6)^j \dotfill 7.39$$

where the values of Z_j are as follows:

$$Z_0 = 0.26461$$
$$Z_1 = -4.0597E-3$$
$$Z_2 = 2.6801E-4$$
$$Z_3 = -1.1970E-5$$
$$Z_4 = 2.7563E-7$$
$$Z_5 = -2.4443E-9$$

For extension to mixture the same mixing rules are used for the parameter a as in the original equation of state. For the quadratic mixing rule the mixing rule is thus:

$$a = \sum_{i=1}^{N}\sum_{j=1}^{N} x_i x_j a_{ij} \dotfill 7.26$$

where

$$a_{ij} = \sqrt{a_i a_j}\left(1 - k_{ij}\right) \text{ with } k_{ij} = k_{ji} \dotfill 7.24$$

For the MKP mixing rules the following mixing rule is used for the parameter a:

$$a = \sum_{i=1}^{N}\sum_{j=1}^{N}\left[x_i x_j \sqrt{a_i a_j}\left(1 - k_{ij}\right)\right] + \sum_{i=1}^{N} x_i \left[\sum_{j=1}^{N} x_j \left(\sqrt{a_i a_j}\,\lambda_{ji}\right)^{\frac{1}{3}}\right]^3 \dotfill 7.28$$

The parameters b and c are calculated as the arithmetic mean of the pure component parameters, i.e.:

$$b = \sum_{i=1}^{N} x_i b_i \dotfill 7.40$$

$$c = \sum_{i=1}^{N} x_i c_i \quad \text{.. 7.41}$$

The PvT diagram for propane predicted with the PR-VT-P is given in Figure 7-20. As can be seen, the prediction of the liquid volumes is significantly better than both the PR and the SRK-VT-P equation of state.
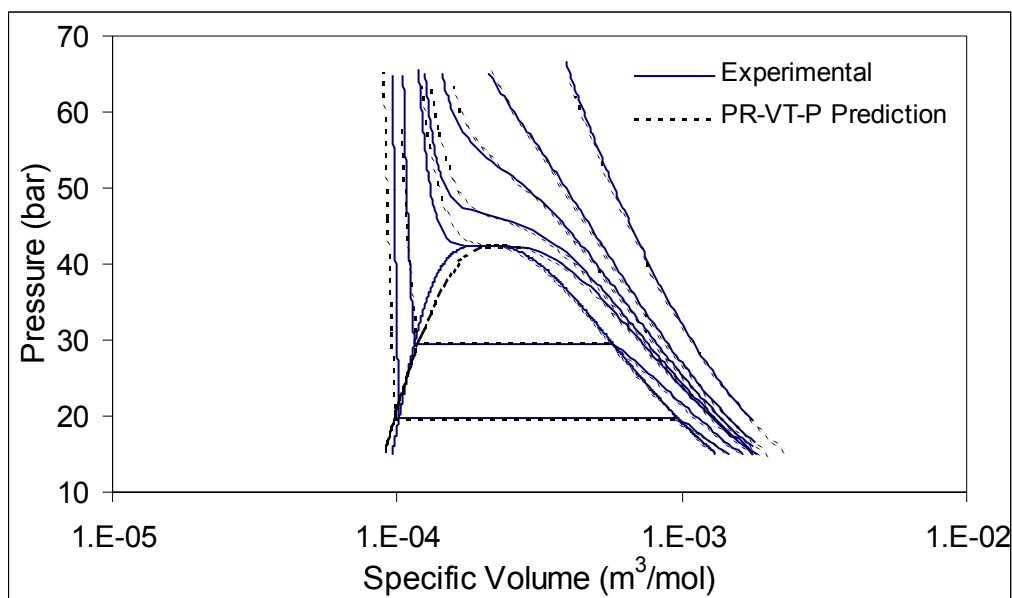
Figure 7-20: PR-VT-P EOS prediction of Propane Pressure-Volume-Temperature Diagram

As is the case with the SRK equation of state, the same vapour pressure curve is produced as for the PR equation of state. The PR-VT-P equation of state was used to predict the binary phase diagram of propane with dotriacontane. The interaction parameters are given in Table 7-8 while the resultant curves are plotted in Figure 7-21.

Table 7-8: PR-VT-P Binary Interaction Parameters for Propane – C32

Quadratic	k_{12} = 0.04967
MKP	k_{12} = -0.3110
	λ_{12} = -0.5516
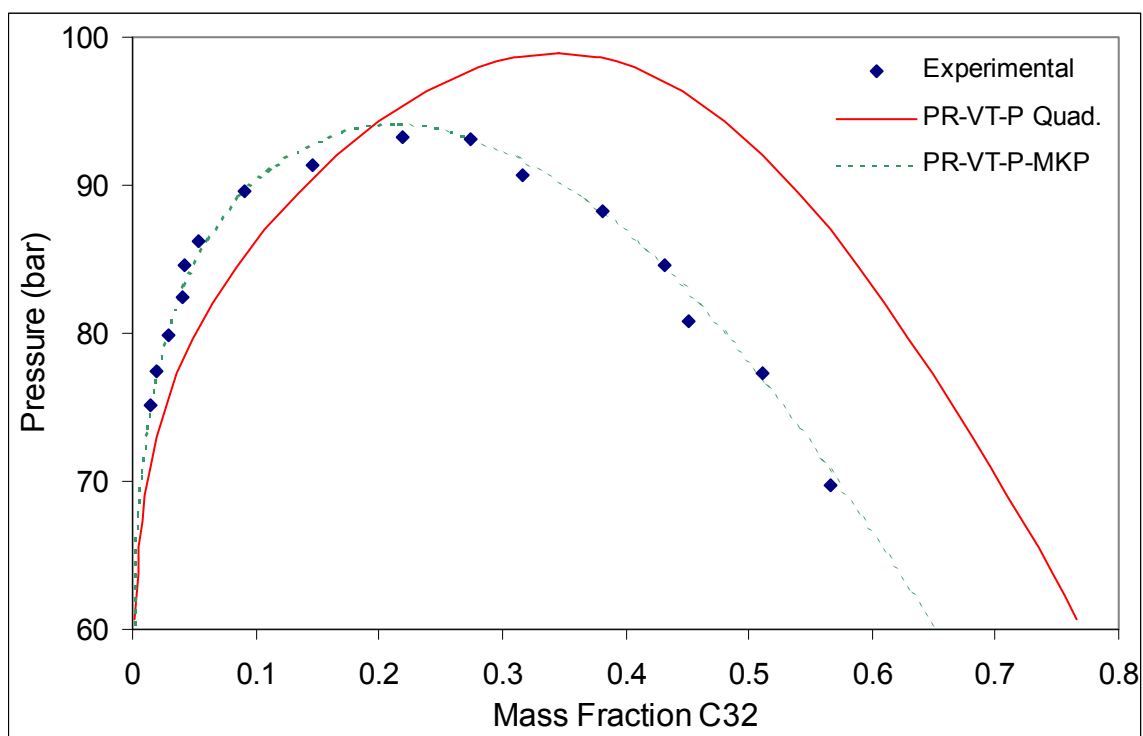
Figure 7-21: PR-VT-P EOS with Quadratic and MKP Mixing Rules prediction of Pressure Composition Diagram for Propane-Dotriacontane at 408.15 K

As was the case with the SRK-VT-P equation of state, the PR-VT-P equation of state does not perform well when quadratic mixing rules are used and for the MKP mixing rules it once again seems like the equation of state is forced through the data with relatively large but negative interaction parameters.

7.5.7. PENG-ROBINSON MATHIAS COPEMAN MODIFICATION (PR-MC)

Mathias et al made two modifications to the PR equation of state (Mathias et al., 1983). Firstly, the alpha function of the equation of state has been modified as follows:

$$\alpha = \left[1 + c_1\left(1 - \sqrt{T_R}\right) + c_2\left(1 - \sqrt{T_R}\right)^2 + c_3\left(1 - \sqrt{T_R}\right)^3\right]^2 \quad \text{.......................} 7.51$$

Equation 7.51 reduces to the original PR equation of state when $c_2 = c_3 = 0$. For low boiling non-polar substances these two parameters should be zero, yet for the purpose of this project the values of c_1, c_2 and c_3 were fitted to experimental vapour pressure data for both propane and dotriacontane. The following parameters were obtained:

Table 7-9: Parameters for PR-MC Equation of State for Propane – C32

Parameter	Propane	C32
c_1	0.595939	2.16666
c_2	0.0589221	0.0009651
c_3	-0.0276139	0.0009993

Secondly, Mathias et al modified the PR equation of state to include the concept of density dependent local composition (DDLC). The DDLC model was separately proposed by Mollerup (Mollerup, 1981) and by Whiting et al (Whiting et al., 1981). The model proposed by Mathias et al is a modification of the model proposed by Mollerup so as to improve the inaccuracies found for highly asymmetrical systems when using the Mollerup DDLC model.

The equation of state is proposed in the form of the Helmholtz energy. Only the associating term for the Helmholtz energy has been modified and thus only this term will be given. Due to the large amount of computational time required for the calculations, a truncated or approximated model was proposed. The attractive contribution to the Helmholtz energy is expressed as follows:

$$A_{Att} = -a \cdot F - \frac{a^{NC}}{RT} F^2 \dotfill 7.52$$

where a^{NC} is the non-conformal term and can be expressed as follows:

$$a^{NC} = \sum_{i=1}^{N} \left(x_i^2 a_{ci} \sum_{j=1}^{N} x_j d_{ji} \right) \dotfill 7.53$$

For the binary case equation 7.53 reduces to:

$$a^{NC} = x_1 x_2 \left(x_1 a_{c1} d_{21} + x_2 a_{c2} d_{12} \right) \dotfill 7.54$$

F is a simplification term and can be expressed as follows:

$$F = \frac{1}{2\sqrt{2}b} \ln \left[\frac{v + \left(1 + \sqrt{2}\right)b}{v + \left(1 - \sqrt{2}\right)b} \right] \dotfill 7.55$$

No interaction parameter is required for the mixing rule of parameter b:

$$b = \sum_{i=1}^{N} x_i b_i \dotfill 7.56$$

The parameter a is combined as follows:

$$a = \sum_{i=1}^{N} \sum_{j=1}^{N} x_i x_j a_{ij} \quad\dots\dots\dots\dots\dots\dots 7.26$$

where

$$a_{ij} = \sqrt{a_i a_j}\left(1 - k_{ij}\right) \text{ with } k_{ij} = k_{ji} \quad\dots\dots\dots\dots 7.27$$

In PE, the MKP mixing rules were also implemented. For the MKP mixing rules the only difference between the PR and PR-MC equation of state is the alpha function (Compare equations 7.51 and 7.48). The interaction parameters are thus the same as for the original PR EOS with MKP mixing rules.

The PvT diagram obtained for propane is given in Figure 7-22. The fit obtained is very similar to that of the traditional PR equation of state, once again the equation of state not performing well in the critical region.
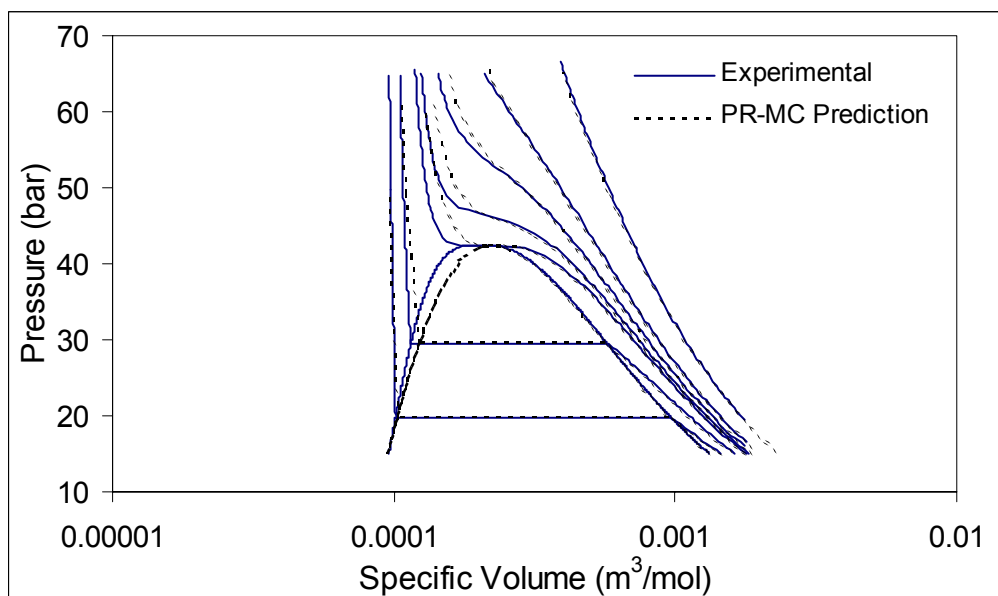
Figure 7-22: PR-MC EOS prediction of Propane Pressure-Volume-Temperature Diagram

The vapour pressure curve for dotriacontane predicted by the PR-MC equation of state is given in Figure 7-23. The prediction is a significant improvement on the PR equation of state.
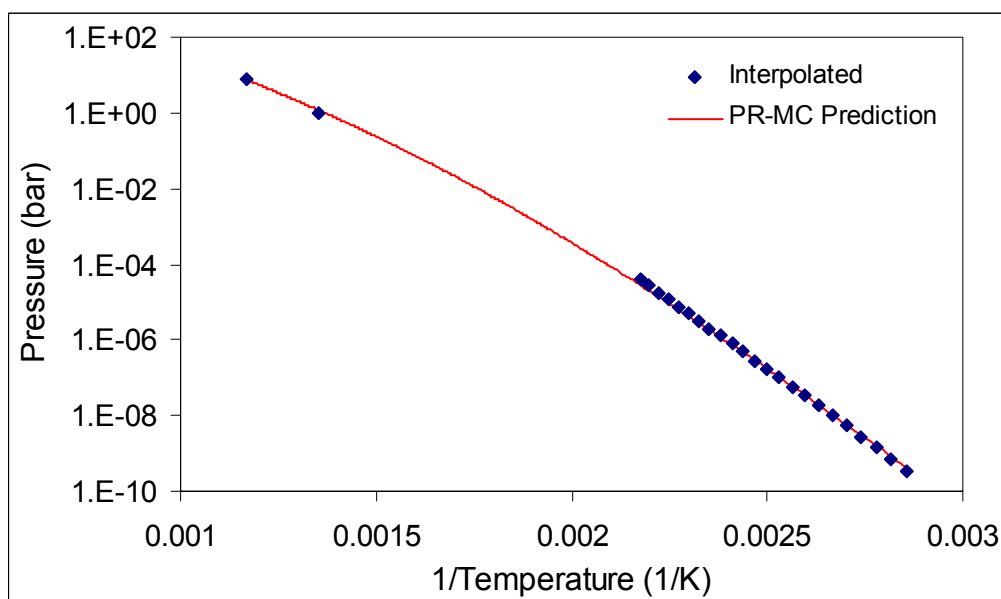
Figure 7-23: PR-MC EOS prediction of Dotriacontane Vapour Pressure Curve

The PR-MC equation of state was fitted to the experimental data with the interaction parameters in Table 7-10 and the resultant graphs are plotted in Figure 7-24 and Figure 7-25.

Table 7-10: PR-MC Binary Interaction Parameters for Propane – C32

Mathias Copeman	k_{12} = 0.01188
	d_{12} = 0.03963
	d_{21} = 0.03511
MKP	k_{12} = 0.1788
	l_{12} = 0.08347
	λ_{12} = 0.2799

Figure 7-24: PR-MC EOS with Quadratic Mixing Rules prediction of Pressure Composition Diagram for Propane-Dotriacontane at 408.15 K

Figure 7-25: PR-MC EOS with MKP Mixing Rules prediction of Pressure Composition Diagram for Propane-Dotriacontane at 408.15 K

The resultant plots are of the same accuracy as the original PR equation of state. When comparing the interaction parameters with the original PR equation of state, it can be seen

that the values for the PR-MC equation of state are generally larger. It can also be seen that the mixing rules proposed by Mathias Copeman require smaller interaction parameters to fit the data when compared to the MKP mixing rules. Larger of the interaction parameters are undesirable since generalization is lost with larger interaction parameters.

7.5.8. PENG-ROBINSON FOR HEAVY HYDROCARBONS (PR-HH)

Crause modified the PR equation of state to produce a better fit for alkanes. The modification was made by adjusting the m parameter in equation 7.49. A third degree polynomial was fitted to the data (Crause, 2001):

$$m = 0.379642 + 1.48503\omega - 0.146623\omega^2 + 0.01666\omega^3 \dots\dots\dots\dots\dots\dots\dots\ 7.57$$

Equation 7.57 is implemented for carbon numbers above 5. For all other compounds, the same m (equation 7.49) value as in the original equation of state is used.

The vapour pressure curve for Dotriacontane predicted by PR-HH is given in Figure 7-26. In comparison to the original PR equation of state, the vapour pressure prediction is not significantly improved, except at very low temperatures.
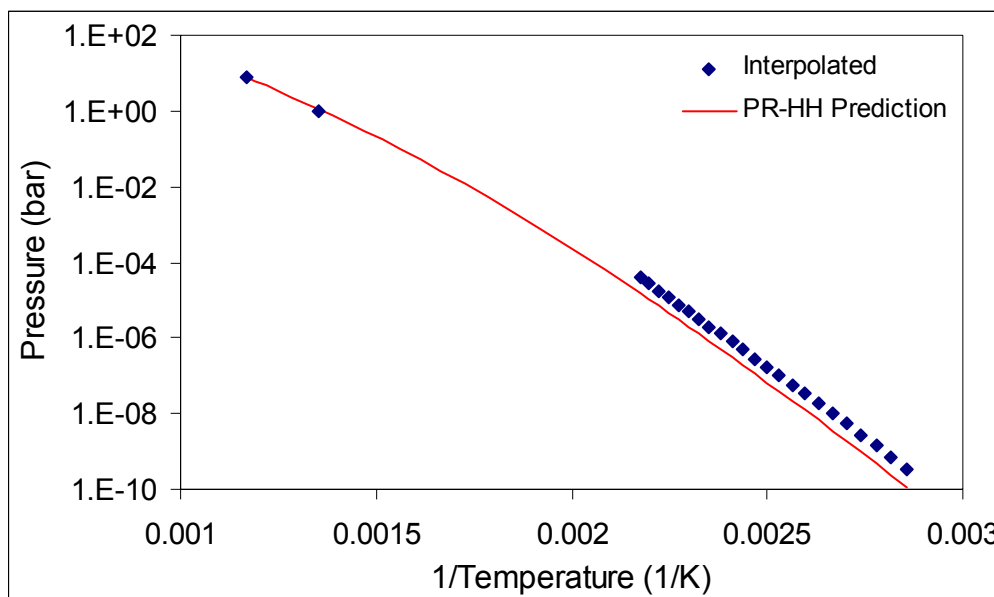
Figure 7-26: PR-HH EOS Prediction of Dotriacontane Vapour Pressure Curve

The PvT diagram for propane as predicted by the PR-HH equation of state is the same as for the original PR equation of state. Only the quadratic mixing rules are implemented in LMDataFit and the resultant plot is given in Figure 7-27. Interaction parameter values of k_{12} = 0.008148 and l_{12} = 0.04100 were found to give the optimum fit.
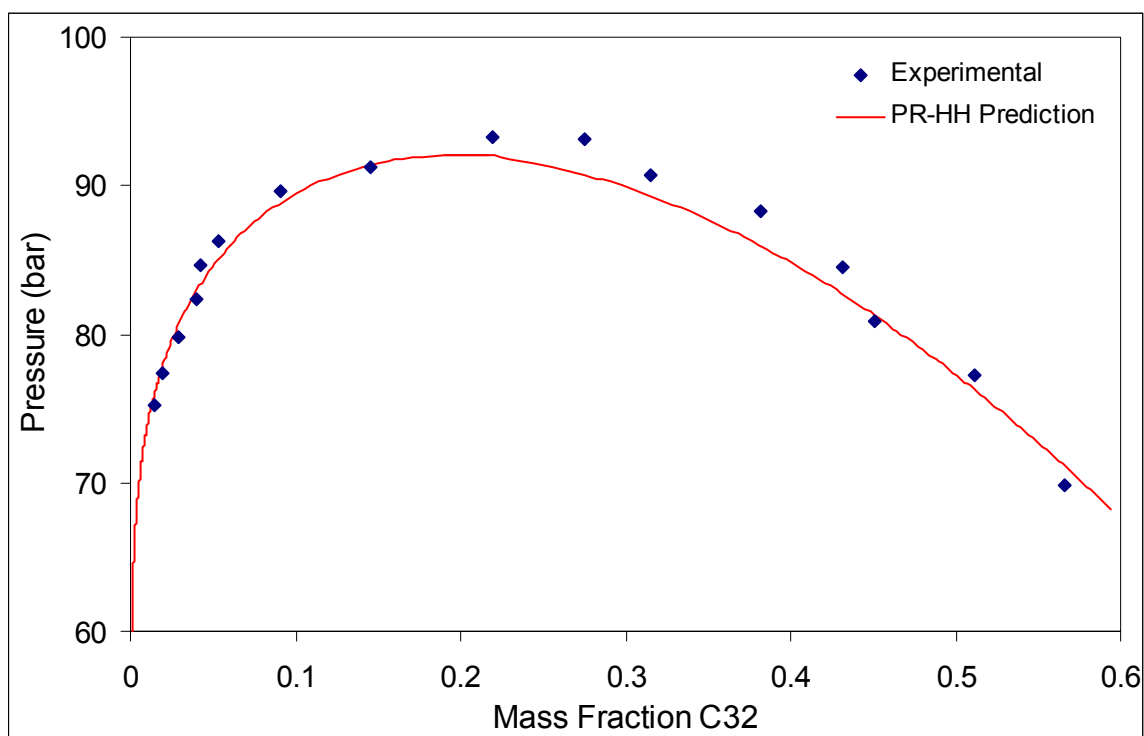
Figure 7-27: PR-HH EOS with Quadratic Mixing Rules prediction of Pressure Composition Diagram for Propane-Dotriacontane at 408.15 K

The fit obtained with this modification does not significantly improve the prediction but when comparing the interaction parameters it can be seen that the PR-HH equation of state had better predictive qualities. Additionally, at higher mass fractions of C32, the heavy hydrocarbon equation seems to fit better.

7.5.9. PENG-ROBINSON STRYJEK VERA MODIFICATION (PR-SV)

The PR equation of state considers m to be a function of only the acentric factor only. Stryjek et al found that for reduced temperatures below 0.7 different m values can be obtained, depending on the reduced temperature range used to correlate the data (Stryjek et al., 1986a), (Stryjek et al., 1986b). Additionally they found that for different compound with a large variation in critical temperature, values of m has a smooth relation with the acentric factor only when all compounds were considered in the same reduced temperature range.

Stryjek et al proposed to retain the basic structure of the PR equation of state and only modify the function for m (PR-SV equation of state). Equations 7.45 through 7.46 from the PR equation of state are therefore still used and they propose an expression for m that is a function of the reduced temperature:

$$m = m_o + m_1 \left(1 + T_R^{0.5}\right)\left(0.7 - T_R\right) \quad \text{..} \quad 7.58$$

where

$$m_o = 0.378893 + 1.4897153\omega - 0.17131848\omega^2 + 0.0196554\omega^3 \quad .... \quad 7.59$$

and m_1 is an adjustable parameter characteristic of each pure component. Stryjek et al gives values for over 90 compound (Stryjek et al., 1986a). They found that for water and alcohols equations 7.58 and 7.59 applies to temperatures up to the critical point while for all other compounds a slightly better result is obtained using m_1 = 0 for reduced temperatures above 0.7.

For the purpose of this project it will be assumed that all the m_1 values are equal to zero. The equation of state is thus reduced to the original PR equation with a different m function. When considering the solvent, this assumption can be justified by the fact that the solvent is always in the supercritical critical region. When considering the alkanes, operation occurs in the region of T_R = 0.4 – 0.5. Although according to the PR-SV equation of state, values for m_1 are required, Stryjek et al only published data up to Octadecane. When plotting these value as a function of carbon number, no clear trend can be seen and thus due to a lack of better data available, values of zero are accepted. This decision can be justified when considering the work of Nieuwoudt and du Rand (Nieuwoudt, 1994),(du Rand, 2000).

The vapour pressure curve prediction for dotriacontane is shown in Figure 7-28. As can be seen, the PR-SV prediction is a marked improvement on the original PR equation of state.
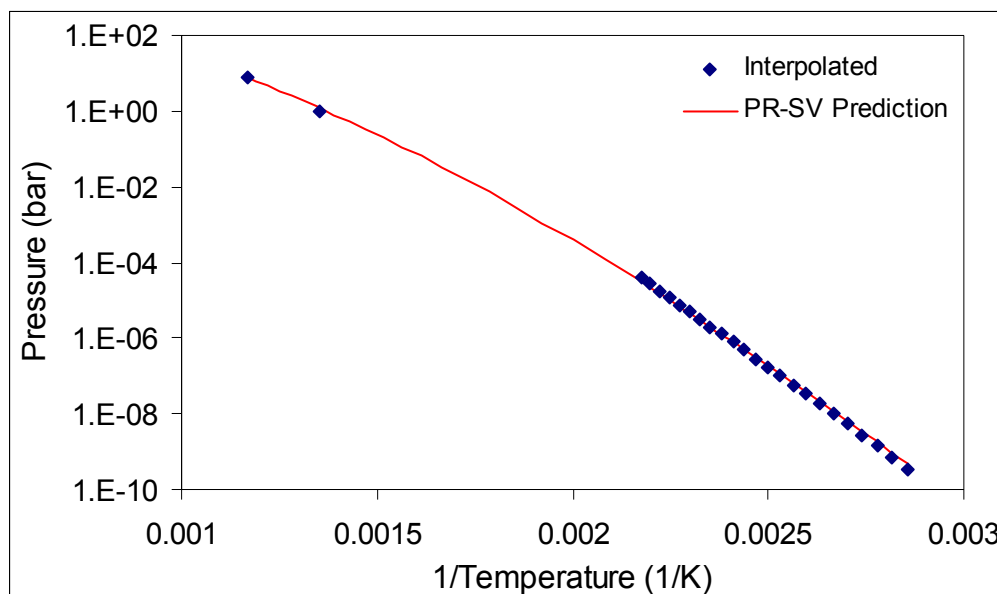
Figure 7-28: PR-SV EOS prediction of Dotriacontane Vapour Pressure Curve

The PvT diagram for Propane is given in Figure 7-29. As can be seen, this diagram is no improvement on the PR equation of state. Once again in the critical and liquid region the predictions are not as accurate as required.
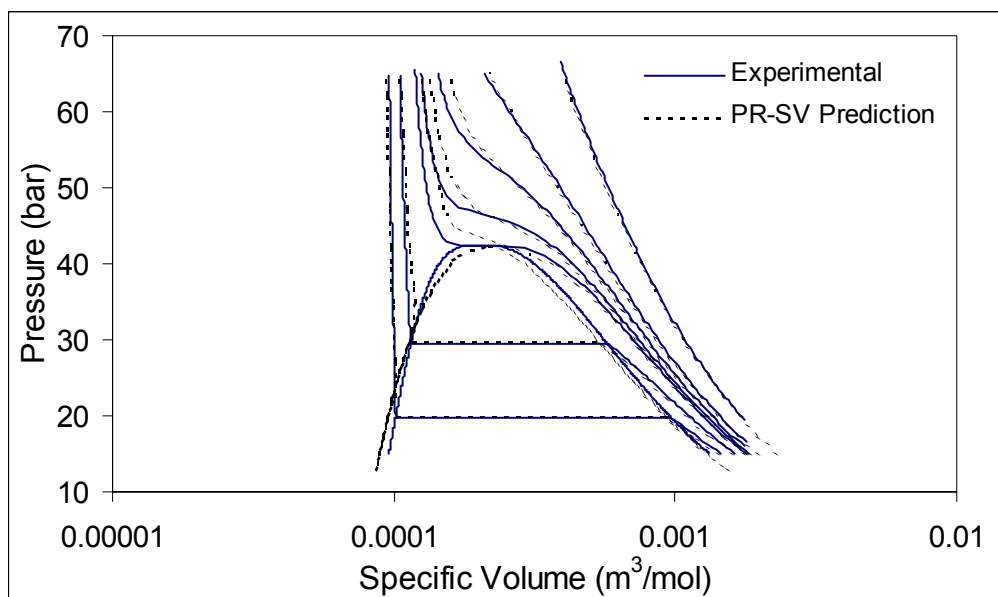
Figure 7-29: PR-SV EOS prediction of the PVT diagram for Propane

Figure 7-30: PR-SV EOS with Quadratic Mixing Rules prediction of Pressure Composition Diagram for Propane-Dotriacontane at 408.15 K

For the quadratic mixing rules implemented, the interaction parameters k_{12} = 0.005777 and l_{12} = 0.05380 were found to provide the optimum plot and the resultant plot is given in

Figure 7-30.As with the PR-HH modification, the PR-SV modification does not yield a much better plot but by decreasing the value of the interaction parameters, it can be seen that this equation of state is more predictive than the original form.

7.5.10. HEDERER-PETER-WENZEL (HPW)

The HPW equation of state is a modification of the RK equation of state to improve the temperature dependence of the attractive term (Hederer et al., 1976). The equation of state appeared at the same time as the PR equation of state and has the same expression for pressure as the SRK equation of state (Equation 7.32). The b parameter is expressed the same as for the SRK equation of state and the a function can be expressed as follows:

$$a = T_R{}^\alpha \cdot 0.42747 \frac{R^2 T_c{}^2}{P_c} \quad\text{.. 7.60}$$

In equation 7.60 α is a measure of the slope of the vapour pressure curve and for an α values of –0.5 the simple RK equation of state can be obtained.

The values of α used in this work were obtained by fitting the equation of state to the vapour pressure curve. The values of –0.5794 and –1.46 were obtained for propane and dotriacontane respectively.

The PvT diagram generated by the HPW equation of state is given in Figure 7-31. The resultant plot is typical of a cubic equation of state, the vapour side is predicted well, while the liquid side is predicted poorly.
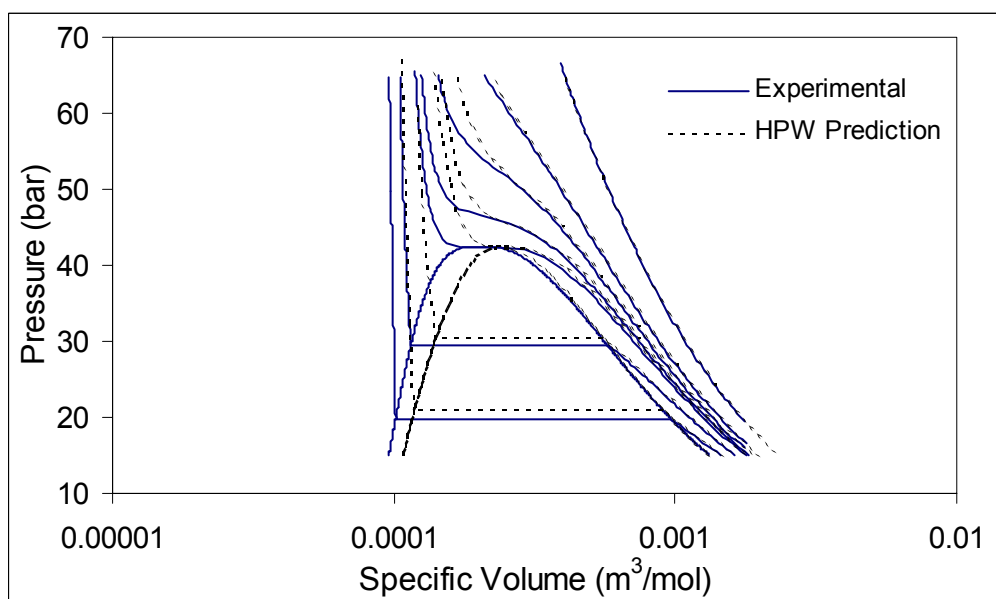
Figure 7-31: HPW EOS prediction of Propane Pressure-Volume-Temperature Diagram

The vapour pressure curve for dotriacontane is predicted in Figure 7-32. Although the fit is acceptable, it can be seen that at low temperatures the fit is not good.
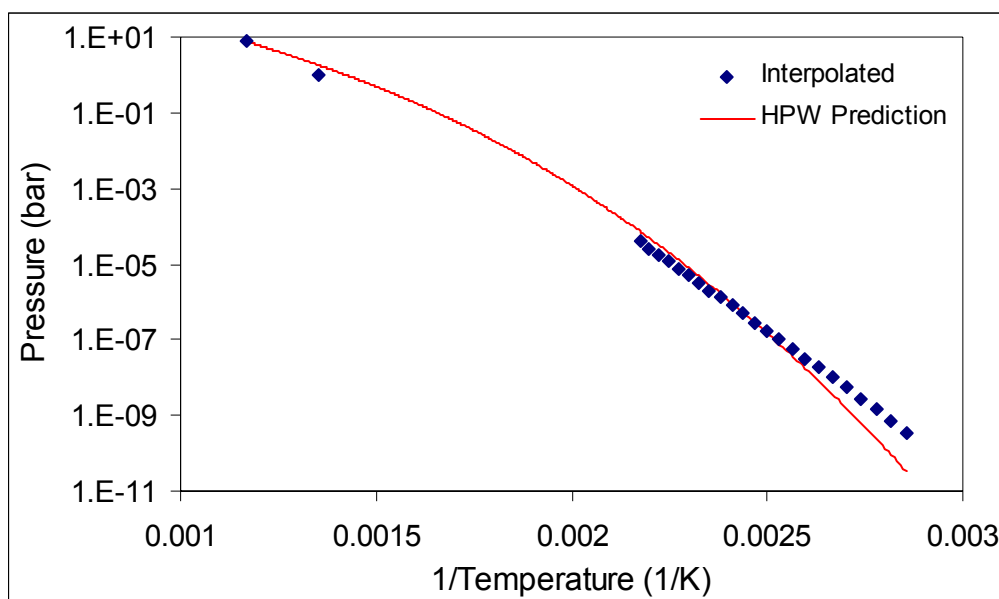
Figure 7-32: HPW EOS prediction of Dotriacontane Vapour Pressure Curve

The HPW equation of state was fitted to the experimental data with the interaction parameters in Table 7-11 and the resultant graphs are plotted in Figure 7-33 and Figure 7-34.

Table 7-11: HPW Binary Interaction Parameters for Propane – C32

Quadratic	$k_{12} = 0.02573$
	$l_{12} = 0.06727$
MKP	$k_{12} = 0.1117$
	$l_{12} = 0.08895$
	$\lambda_{12} = 0.1458$
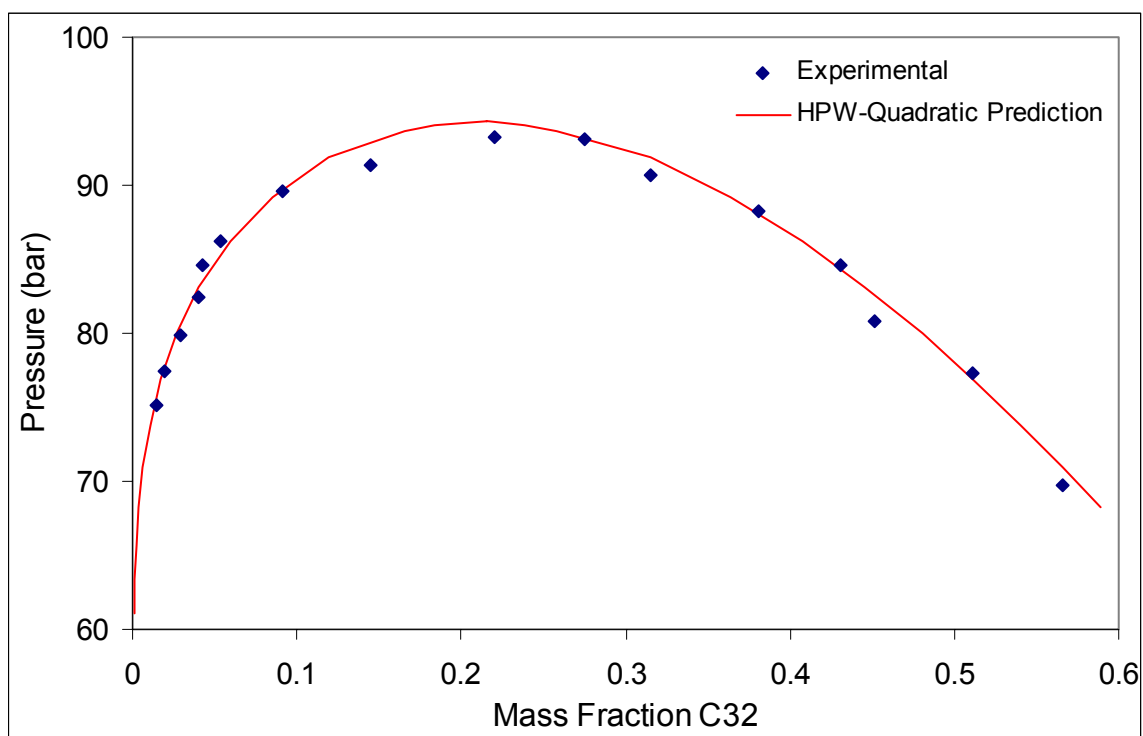
Figure 7-33: HPW EOS with Quadratic Mixing Rules prediction of Pressure Composition Diagram for Propane-Dotriacontane at 408.15 K
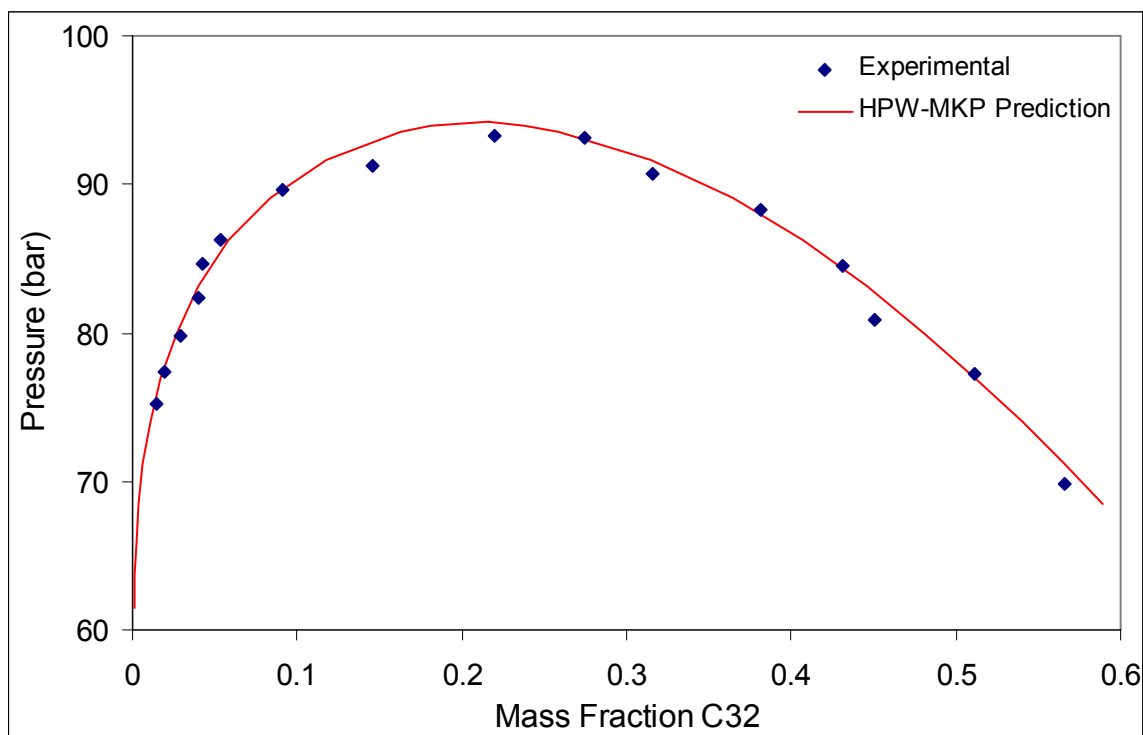
Figure 7-34: HPW EOS with MKP Mixing Rules prediction of Pressure Composition Diagram for Propane-Dotriacontane at 408.15 K

The resultant binary curves fit the data as well as the SRK and PR equations of state, and the interaction parameters are of the same order of magnitude. The difference in the

equations of state and vapour pressure curve predictions can thus be masked with the interaction parameters.

7.5.11. PATEL TEJA (PT)

Both the PR and the SRK equations of state assume fixed values for the critical compressibility factor resulting in predicted liquid densities and critical volumes that differ considerably from experimental values. Where the PR and SRK equations of state have set values for the critical compressibility, Patel et al proposed an equation of state where it is assumed that the critical compressibility is substance dependent (Patel et al., 1982).

The PT equation of state can be expressed as follows:

$$P = \frac{RT}{v-b} + \frac{a(T)}{v(v-b)+c(v-b)} \quad \text{...} \quad 7.61$$

By applying the fact that at the critical point the first and second derivative of pressure with respect to volume is zero and that the critical compressibility can be expressed by ξ_c the following relations can be derived:

$$a(T) = \Omega_a \alpha(T) \frac{R^2 T_c^2}{P_c} \quad \text{...} \quad 7.62$$

$$b = \Omega_b \frac{RT_c}{P_c} \quad \text{...} \quad 7.63$$

$$c = \Omega_c \frac{RT_c}{P_c} \quad \text{...} \quad 7.64$$

where

$$\Omega_c = 1 - 3\xi_c \quad \text{...} \quad 7.65$$

$$\Omega_a = 3\xi_c^2 + 3(1 - 2\xi_c)\Omega_b + \Omega_b^2 + 1 - 3\xi_c \quad \text{...} \quad 7.66$$

and Ω_b is the smallest positive root of the following cubic equation:

$$\Omega_b^3 + (2 - 3\xi_c)\Omega_b^2 + 3\xi_c^2\Omega_b - \xi_c^3 = 0 \quad \text{...} \quad 7.67$$

The value of $\alpha(T)$ in equation 7.62 can be expressed as follows:

$$\alpha(T) = \left[1 + m\left(1 - T_R^{0.5}\right)\right]^2 \quad \text{...} \quad 7.68$$

Patel et al correlated values for m and ξ_c in terms of the acentric factor:

$$m = 0.452413 + 1.30982\omega - 0.295937\omega^2 \dots\dots\dots\dots \quad 7.69$$

$$\xi_c = 0.329032 + 0.076799\omega - 0.0211947\omega^2 \dots\dots\dots \quad 7.70$$

The PT prediction of the PvT diagram is shown in Figure 7-35. Once again, it can be seen that the vapour side prediction is good but that of the liquid side is poor.
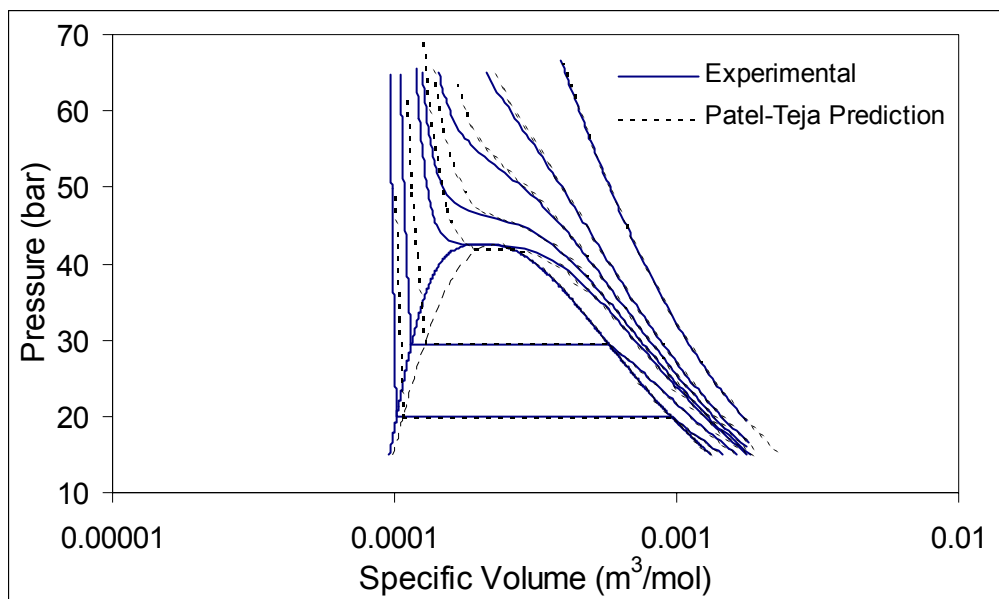
Figure 7-35: PT EOS prediction of Propane Pressure-Volume-Temperature Diagram

The vapour pressure prediction for dotriacontane with the use of the PT equation of state is given in Figure 7-36. It can be seen that the vapour pressure curve deviates slightly at low temperatures resulting in higher predicted vapour pressure values. This deviation is, although significant, not large enough to exclude the PT equation of state from further investigations, yet justifies the refitting of the acentric factor. Figure 7-36 shows that by adjusting the value of the acentric factor to 1.98585 the vapour pressure prediction can be significantly improved.
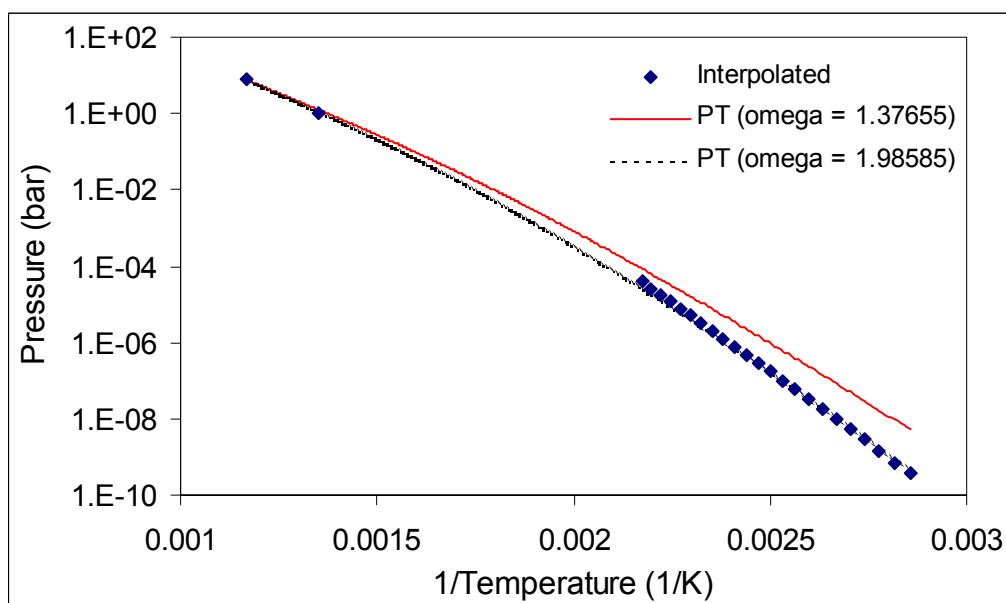
Figure 7-36: PT EOS prediction of Dotriacontane Vapour Pressure Curve

The binary modelling of the propane-dotriacontane data was done with the PT equation of state for both values of the acentric factor. The interaction parameters are given in Table 7-12 and the resultant plots are shown in Figure 7-37 and Figure 7-38.

Table 7-12: PT Binary Interaction Parameters for Propane – C32

	ω = 1.37655	ω = 1.98585
Quadratic	k_{12} = -0.07160	k_{12} = -0.07262
	l_{12} = 0.2038	l_{12} = 0.2038
MKP	k_{12} = -0.06112	k_{12} = -0.04217
	l_{12} = 0.2067	l_{12} = 0.2117
	λ_{12} = 0.01622	λ_{12} = 0.05057
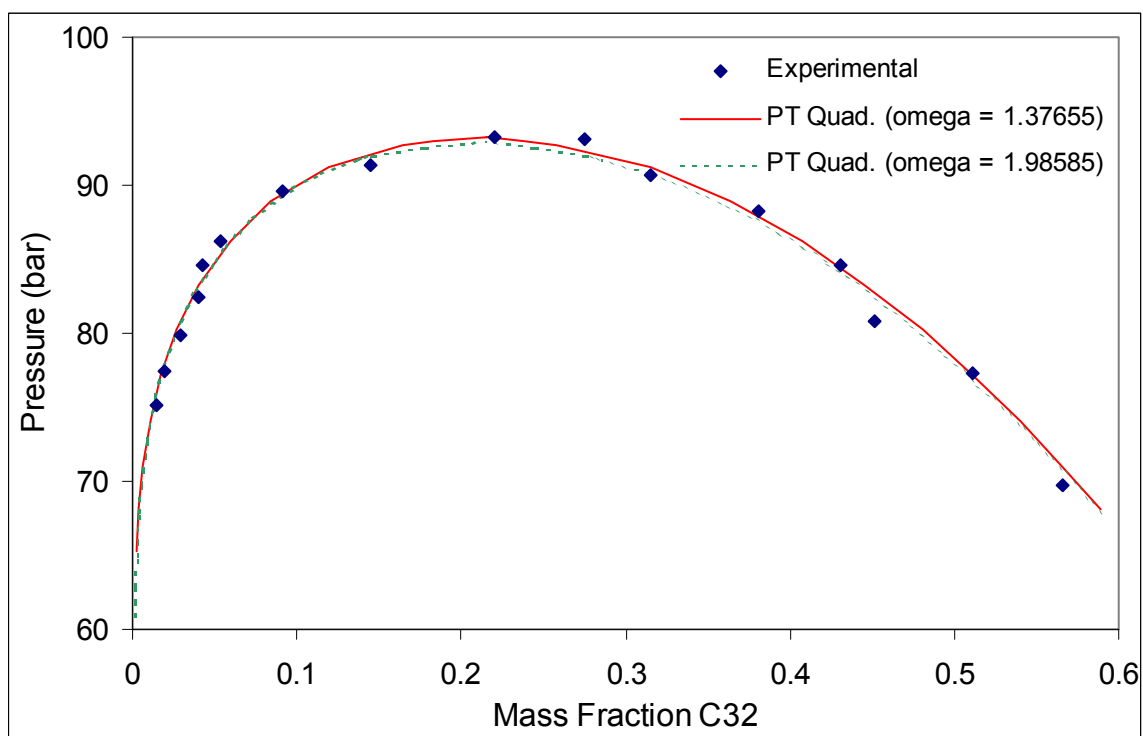
Figure 7-37: PT EOS with Quadratic Mixing Rules prediction of Pressure Composition Diagram for Propane-Dotriacontane at 408.15 K
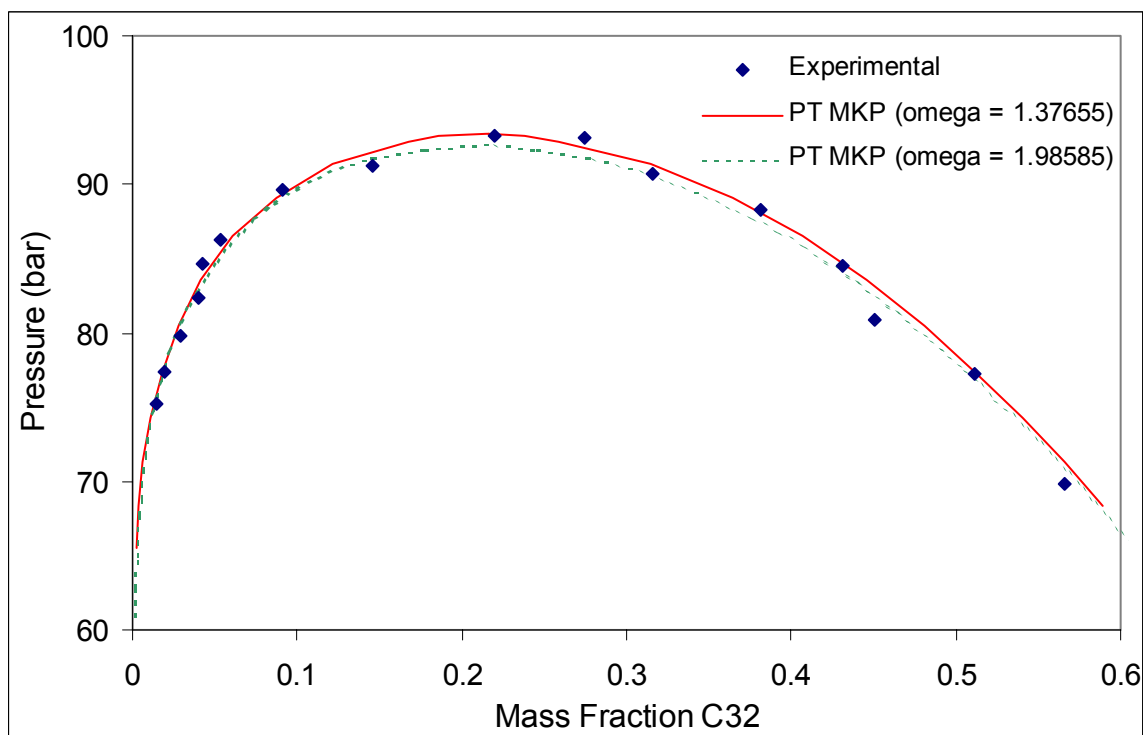
Figure 7-38: PT EOS with MKP Mixing Rules prediction of Pressure Composition Diagram for Propane-Dotriacontane at 408.15 K

The same accuracy of fit was obtained for both the values of the acentric factor. The interaction parameter size does not differ significantly and although the adjusted acentric

factor does improve the pure component prediction, the binary phase equilibrium prediction is not improved. This can be attributed to the fact that the mixing rules are not predictive and the interaction parameters thus force the equation of state through the experimental data.

7.5.12. MODIFIED PATEL TEJA (MPT)

Crause modified the PT equation of state so that the m and ξ_c factors give a better fit for alkanes (Crause, 2001). He proposed the following equations:

$$m = 0.002516 \cdot M_R + 0.70647 \quad\text{... 7.71}$$

$$\xi_c = 0.253168556 + 0.09253326 \cdot e^{-0.0048018 \cdot M_R} \quad\text{... 7.72}$$

The vapour pressure curve for the MPT equation of state is shown in Figure 7-39. As can be seen, the curve produces a much better fit than the original PT equation of state.
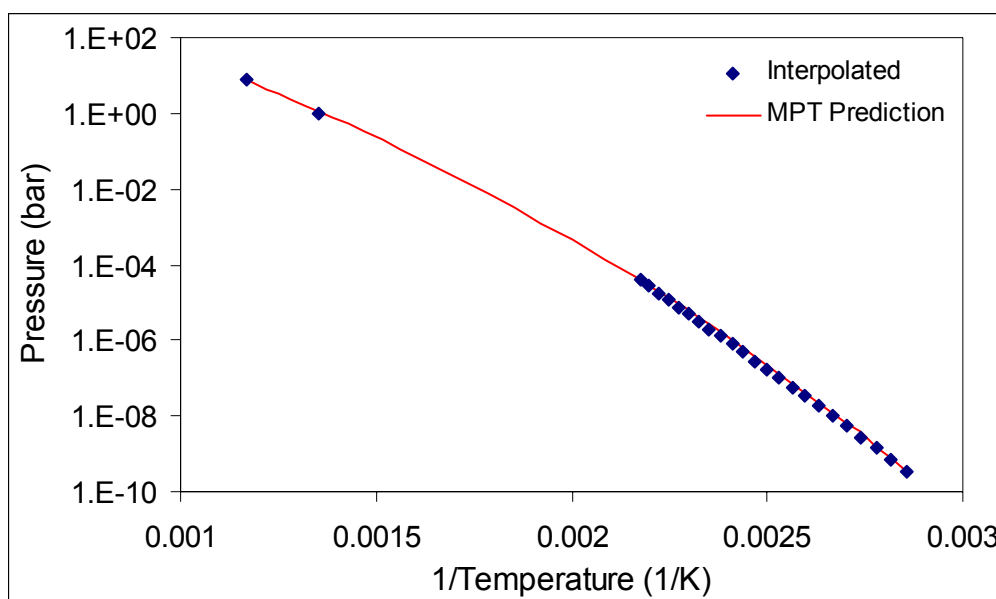
Figure 7-39: MPT EOS prediction of Dotriacontane Vapour Pressure Diagram

The modifications made for the PT equation of state was made for higher carbon numbers. The pure component PvT diagram for propane is thus identical to that of the original PR equation of state. Binary modelling of the MPT equation of state was done and the optimum interaction parameters were found to be k_{12} = -0.07014 and l_{12} = 0.1418.
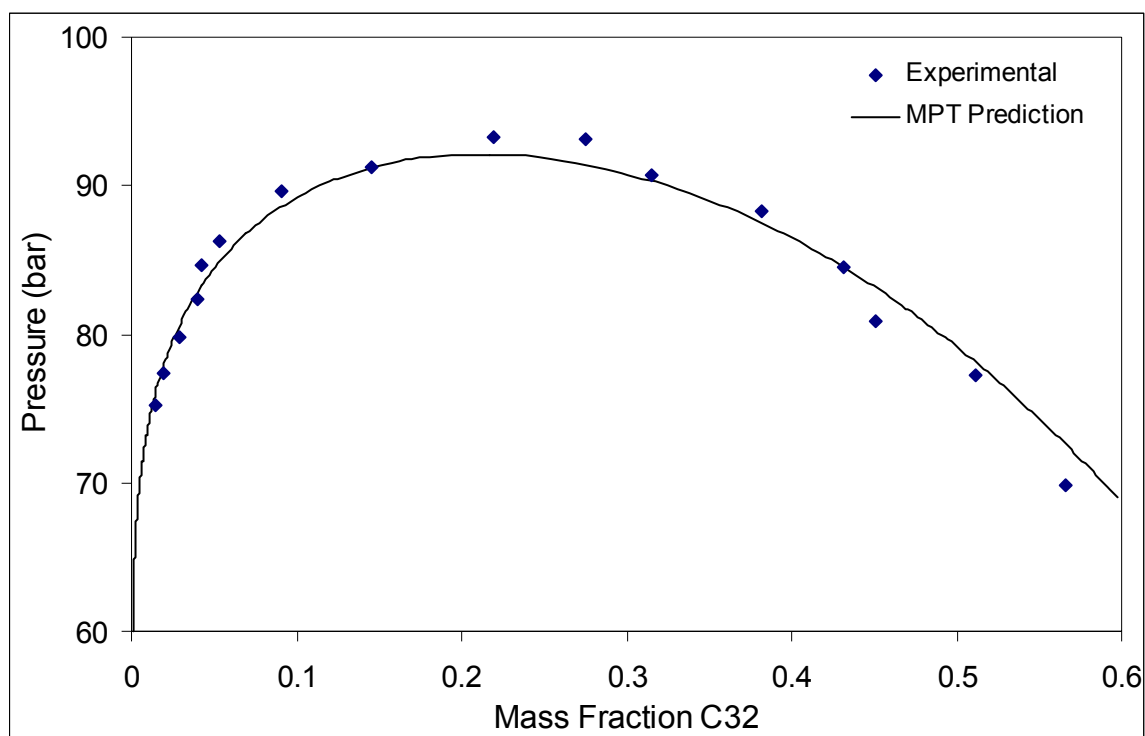
Figure 7-40: MPT EOS with Quadratic Mixing Rules prediction of Pressure Composition Diagram for Propane-Dotriacontane at 408.15 K

The MPT equation of state does not significantly improve the binary phase equilibrium prediction and when comparing the interaction parameters with that of the PT equation of state, it was found that the values have the same sign and are of similar magnitude.

7.6.   NON-CUBIC EQUATIONS OF STATE

Various non-cubic equations of state have been proposed, most of them having a statistical mechanical basis. Each equation of state will be treated separately and will also include a discussion on the mixing rules used.

7.6.1.   ELLIOT-SURESH-DONOHUE (ESD)

The ESD equation of state (Elliot et al., 1990) takes into account the non-spherity of the molecules according to the theory of Prigogine (Prigogine, 1957). The resultant equation of state is semi-empirical and can accurately represent thermodynamic properties of hydrogen bonding and non-spherical molecules.

The inclusion of the shape factor, c, in the repulsive term allows for the extension of the equation of state to polymers. Elliot et al illustrated that this form of the repulsive term significantly improves agreement with molecular simulation data for hard spheres and chains relative to the repulsive term assumed by equations of state like that of the VDW and PR equations of state.

The equation is non-cubic for associating fluids but for non-associating fluids the equation reduces to an equation of state that is cubic in volume. For non-associating fluids the equation of state is defined as follows:

$$P = \frac{RT}{v} + \frac{RT}{v}\frac{\langle 4c\eta \rangle}{1-1.9\eta} - \frac{RT}{v}\frac{9.49\langle q\eta Y \rangle}{1+1.7745\langle \eta Y \rangle} \qquad \text{.. 7.73}$$

The pure component parameters a_i, b_i, c_i and q_i are determined as follows:

$$a_i = T_c \frac{1+0.945(c_i-1)+0.134(c_i-1)^2}{1.023+2.225(c_i-1)+0.478(c_i-1)^2} \qquad \text{... 7.74}$$

$$b_i = \frac{RT_c}{P_c}\frac{0.00312+0.087(c_i-1)+0.008(c_i-1)^2}{1+2.455(c_i-1)+0.732(c_i-1)^2} \qquad \text{.. 7.75}$$

$$c_i = 1+3.535\omega+0.533\omega^2 \qquad \text{... 7.76}$$

$$q_i = 1+1.90476(c_i-1) \qquad \text{... 7.77}$$

The equation has been extended to mixtures with the aid of the following mixing rules:

$$\eta = \frac{\sum\limits_{i=1}^{N} x_i b_i}{v} \qquad \text{.. 7.78}$$

$$\langle 4c\eta \rangle = \frac{4\sum\limits_{i=1}^{N}\sum\limits_{j=1}^{N} x_i x_j \left(\frac{c_i b_j + c_j b_i}{2}(1-\ell_{12}) \right)}{v} \qquad \text{.. 7.79}$$

$$\langle q\eta Y \rangle = \frac{\sum\limits_{i=1}^{N}\sum\limits_{j=1}^{N} x_i x_j \left(\frac{q_i b_j + q_j b_i}{2}(1-\ell_{12}) \right)\left(EXP\left(\frac{\sqrt{a_i a_j}(1-k_{ij})}{T} \right) - 1.0617 \right)}{v} \qquad \text{....... 7.80}$$

$$\langle \eta Y \rangle = \frac{\langle q\eta Y \rangle}{\sum\limits_{i=1}^{N} x_i q_i} \qquad \text{... 7.81}$$

The PvT diagram for propane is shown in Figure 7-41. The resultant phase diagram is accurate in the vapour region but as is the case with the cubic equations of state, the equation is unable to predict the liquid densities accurately.
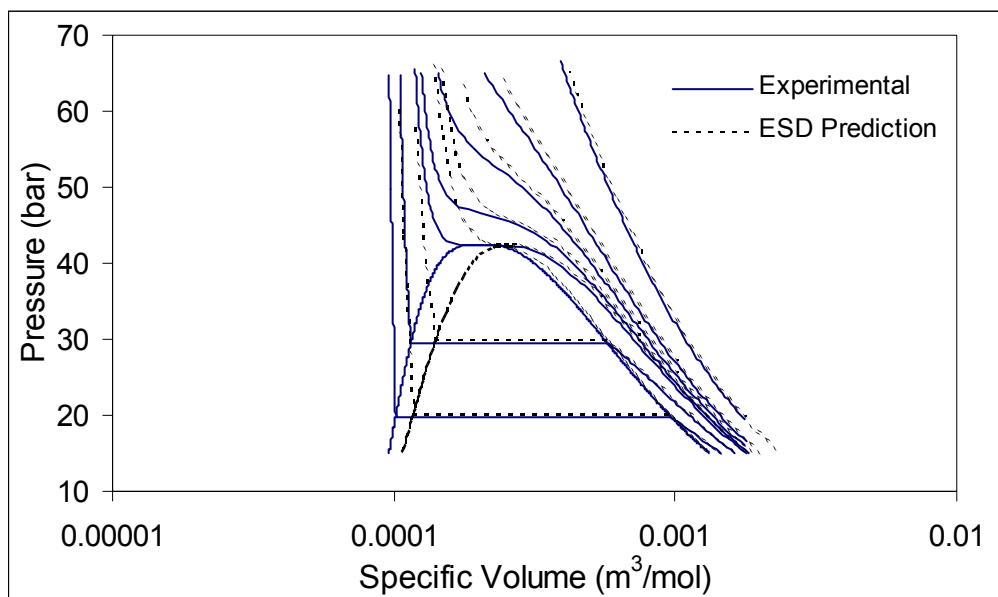
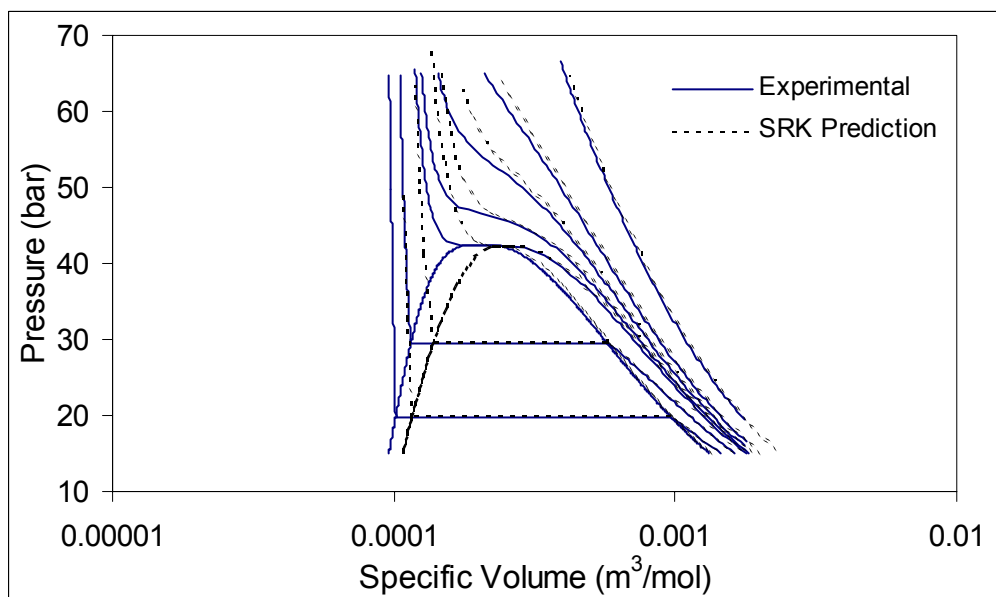*Figure 7-41: ESD EOS prediction of Propane Pressure-Volume-Temperature*

The prediction of the vapour pressure curve is given in Figure 7-42. The equation of state is able to predict the vapour pressure within the accuracy of the experimental measurements.
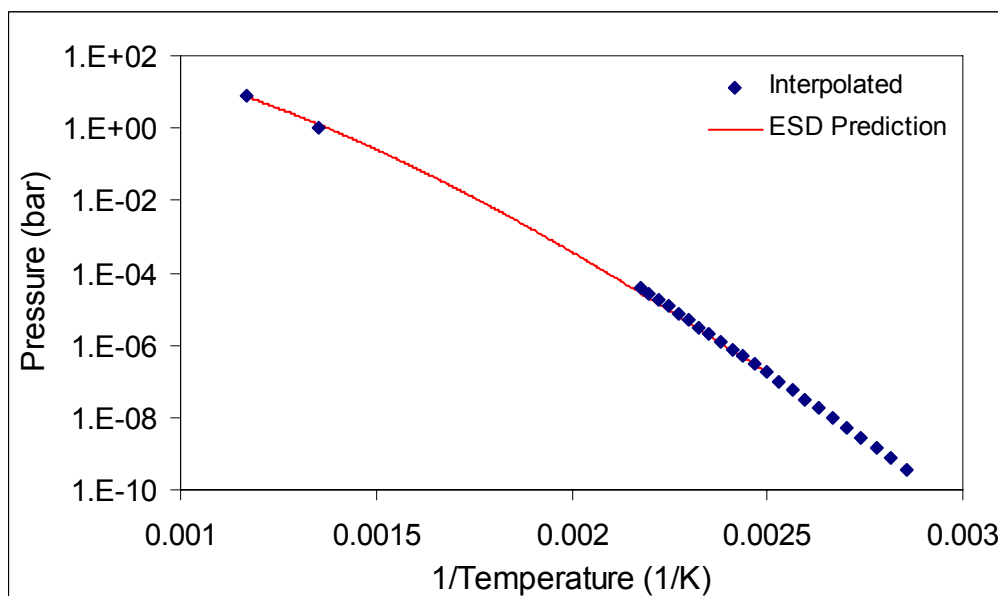
Figure 7-42: ESD EOS prediction of Dotriacontane Vapour Pressure Curve

The equation of state was applied to the binary propane-dotriacontane system. The interaction parameters are given in Table 7-13 and the resultant phase diagram is shown in Figure 7-56.

Table 7-13: EDS Binary Interaction Parameters for Propane – C32

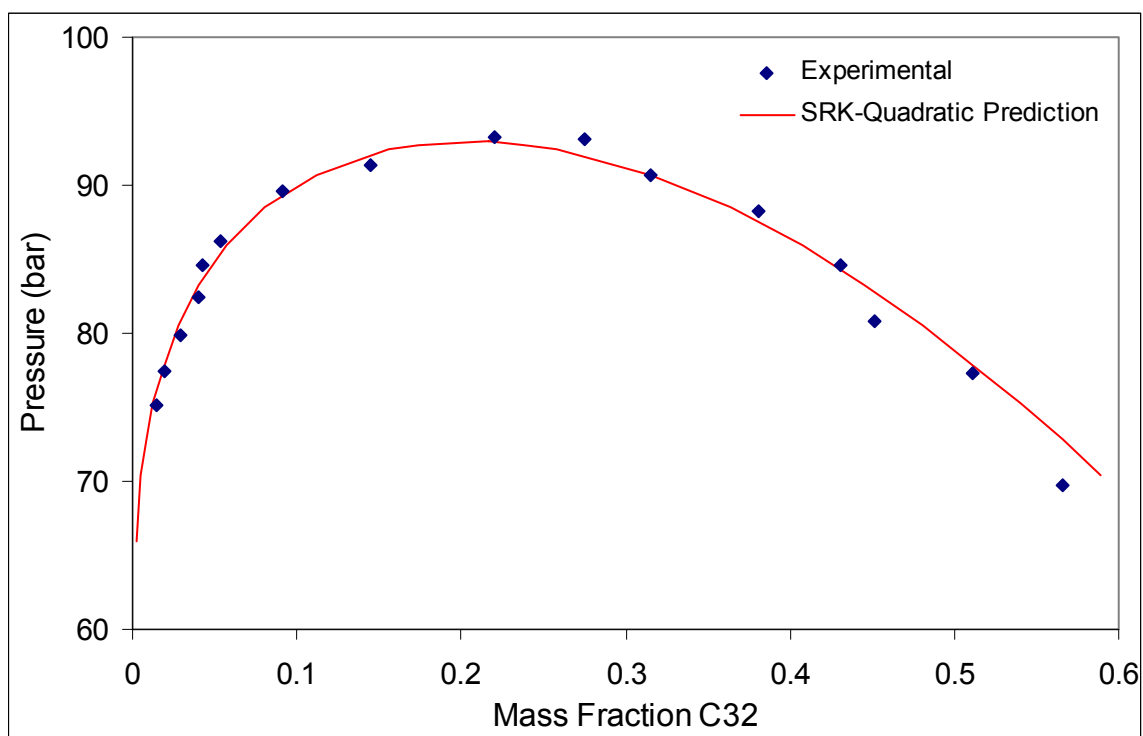| Standard	$k_{12} = 0.08662$
	$l_{12} = -0.2324$
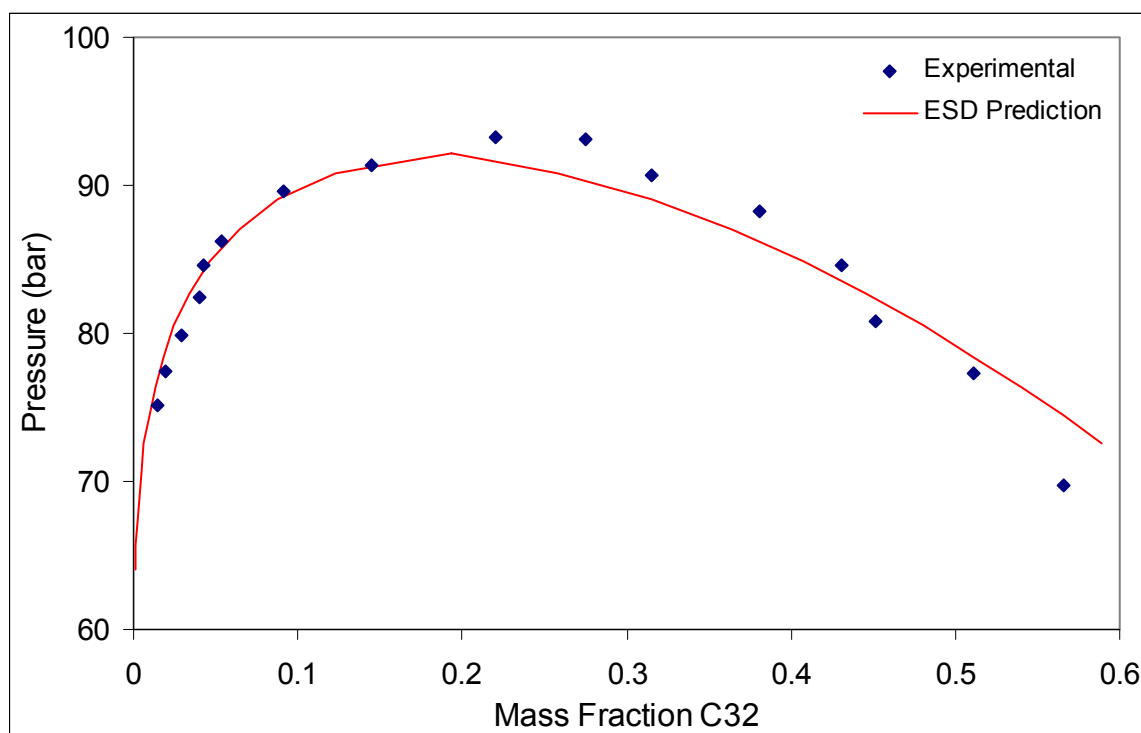
Figure 7-43: ESD EOS with Standard Mixing Rules prediction of Pressure Composition Diagram for Propane-Dotriacontane at 408.15 K

As illustrated in Figure 7-56, the vapour side prediction of the phase equilibrium is within the accuracy of the system, while the liquid side prediction is not very good.

7.6.2. PERTURBED HARD CHAIN (PHC)

Beret et al and Donohue et al did the initial development of the perturbed hard chain theory and Cotterman built further on these theories (Beret et al., 1975), (Donohue et al., 1978), (Cotterman, 1985).

Cotterman aimed to develop a molecular thermodynamic correlation that is applicable over a wide density range for fluids containing small or large molecules. The novel feature of the PHC equation of state proposed is the division of the Helmholtz energy into a low density and a high-density contribution. On application of this correlation to mixtures, separate mixing rules are applied to each of the phases.

Due to the complexity and the mathematical intricacy the correlation will not be given here. For details the reader is referred to Cotterman. Additionally, due to the complexity,

the implementation of this equation of state into a phase equilibrium simulator has not been performed.

7.6.3. SIMPLIFIED PERTURBED HARD CHAIN (SPHC)

The mathematical complexity of the PHC theory, as proposed by Beret et al, Donohue et al and Cotterman has been simplified by Kim et al (Kim et al., 1986).

Kim et al proposed a new equation of state based on the PHC theory using the theory of Prigogine to determine the partition function and thus taking into account the rotational and vibrational degrees of freedom (Prigogine, 1957). To simplify the equation, the attractive term of the perturbed hard chain theory is replaced with that proposed by Lee et al. (Lee et al., 1985). The new equation of state is thus valid for all densities for both small and large molecules.

Even though the SPHC equation of state is a lot simpler than the PHC equation, it is still mathematically complex. The pressure expression of the equation of state is given below while the reader is referred to the work of Kim et al for details of the mixing rules.

$$P = \frac{RT}{v}\left[1 + c\left(Z_{Rep} - Z_m \frac{v^* Y}{v + v^* Y}\right)\right] \quad \text{...} 7.82$$

where

$$Y = EXP\left[\frac{T^*}{2T} - 1\right] \quad \text{...} 7.83$$

$$Z_{Rep} = \frac{4\tau\tilde{\rho} - 2(\tau\tilde{\rho})^2}{(1 - \tau\tilde{\rho})^3} \quad \text{...} 7.84$$

and

$$\tilde{\rho} = \frac{v^*}{v} \quad \text{...} 7.85$$

The value of τ is 0.7405 while Z_m, the maximum coordination number is assumed to be 36. There are thus three pure component parameters, c, which is a third of the total number of density dependent degrees of freedom, v^*, the characteristic volume and T^* the characteristic temperature.

The PvT diagram for propane is shown in Figure 7-44. The vapour phase prediction at moderate temperatures is good, but the equation is not able to predict the liquid phase nor

the critical point well. Although conversion close the critical point was not obtained, phase equilibrium lines near the critical point indicate that the pressure and temperature are overpredicted.
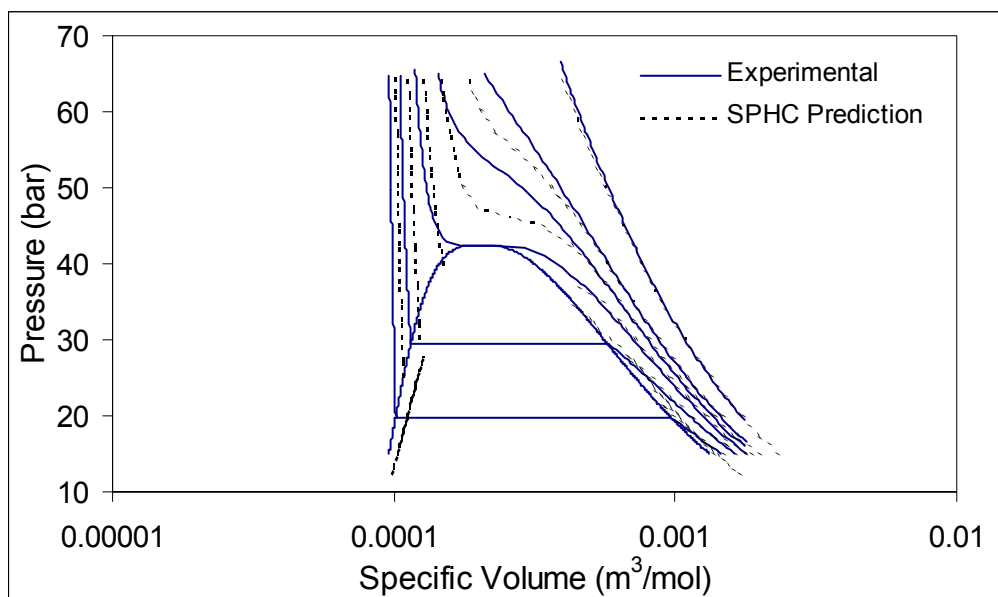
Figure 7-44: SPHC EOS prediction of Propane Pressure-Volume-Temperature

The prediction of the vapour pressure curve for dotriacontane is given in Figure 7-45 below.
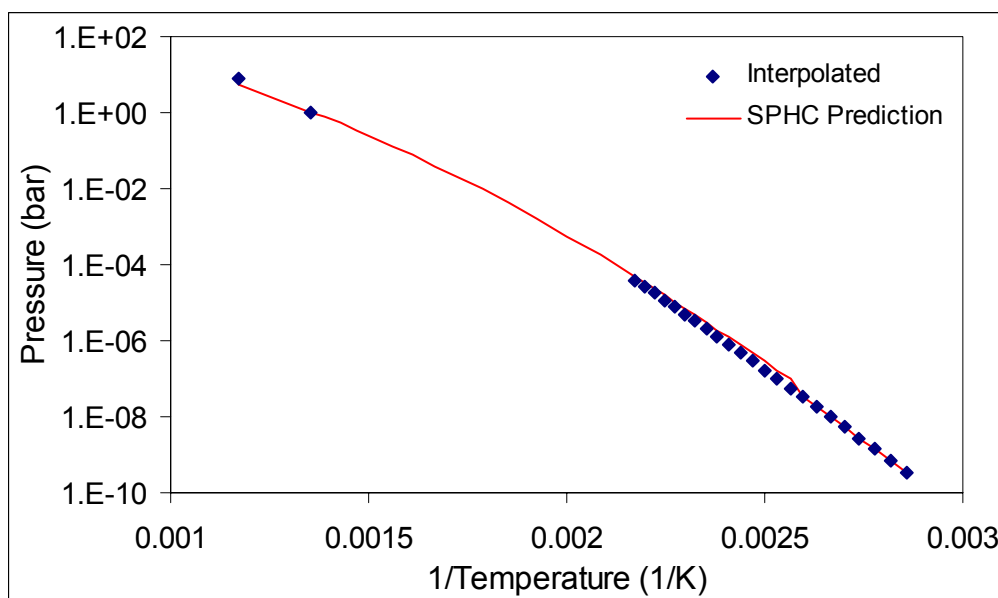
Figure 7-45: SPHC EOS prediction of Dotriacontane Vapour Pressure Curve

For the binary propane-dotriacontane system, the interaction parameters were fitted to the experimental data, resulting in k_{12} = 0.0025 and l_{12} = 0.0035.

194
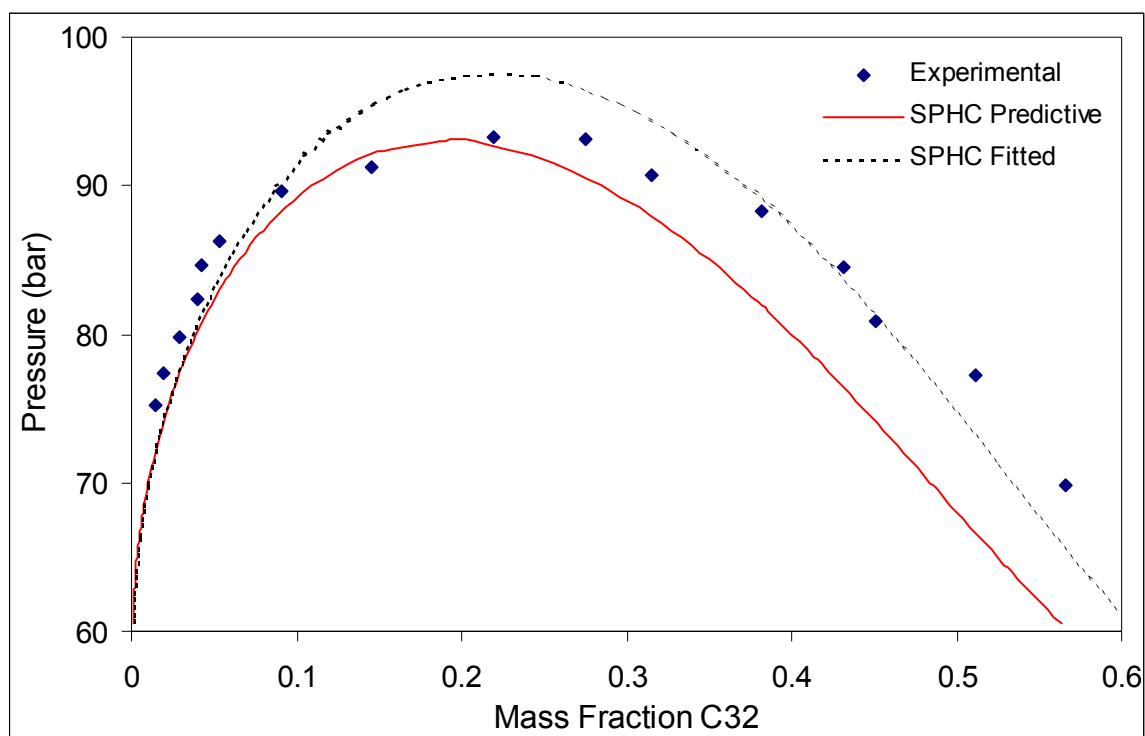
Figure 7-46: SPHC EOS prediction of Pressure Composition Diagram for Propane-Dotriacontane Diagram at 408.15 K

The fit of the data is not as good as the cubic equations of state fit, yet it does qualitatively predict the correct shape in the correct pressure range. However, the predictive fit, i.e. where the interaction parameters are zero, warrants mention. The predication when the interaction parameters are zero, is not perfect but gives a fair representation of the data and thus indicates that the equation of state can be used predictively.

7.6.4. CUBIC SIMPLIFIED PERTURBED HARD CHAIN (CSPHC)

The SPHC and the PHC theories discussed above are still computationally difficult due to the fact that the equation is not cubic with respect to the specific volume. This may result in extensive calculations, especially in the determination of the calculation of the compressibility factor.

Wang et al aimed to simplify and improve the SPHC equation of state by starting with the generalized Van der Waals partition function for mixtures, modifying the attractive portion of the SPHC equation of state and by replacing the repulsive portion with a simple simulated expression (Wang et al., 1993). The modifications were incorporated into a cubic simplified perturbed hard chain (CSPHC) equation of state and resulted in an equation that required ¼ of the CPU time. According to Wang the predictions of non-polar mixtures with the CSPHC equation of state has the same accuracy as the PHC equation of state and significantly improves prediction of the SPHC equation of state.

In terms of the mathematical expression, the CSPHC equation of state is very similar to the SPHC equation of state. Equations 7.82 and 7.83 are the same for the CSPHC and the SPHC. The value of τ and z_m are the same, as well as the three pure component parameters, c, v^* and T^*. The difference in the equations in the repulsive terms. For the CSPHC equation of state the value of z^{rep} is calculated as follows:

$$z^{rep} = \frac{d_1 b}{v - d_2 b}$$ 7.86

where d_1 = 1.11574, d_2 = 0.44744 and

$$b = 4\tau v^*$$ 7.87

Due to the repulsive term simplification the equation is cubic and can thus be solved with ease.

For extension to mixtures, the mixing rules are slightly different as the CSPHC equation of state mixing rules includes a density effect. A complete discussion of the mixing rules is given by Wang et al (Wang et al., 1993).

The PvT diagram for Propane is shown in Figure 7-47. In comparison to the SPHC equation of state, the CSPHC prediction is slightly superior. The prediction of the vapour phase is just as good and the liquid phase is of the same accuracy. However, in the region of the critical point the prediction is better. As in the case of the SPHC, the CSPHC also over predicts the critical pressure and temperature.
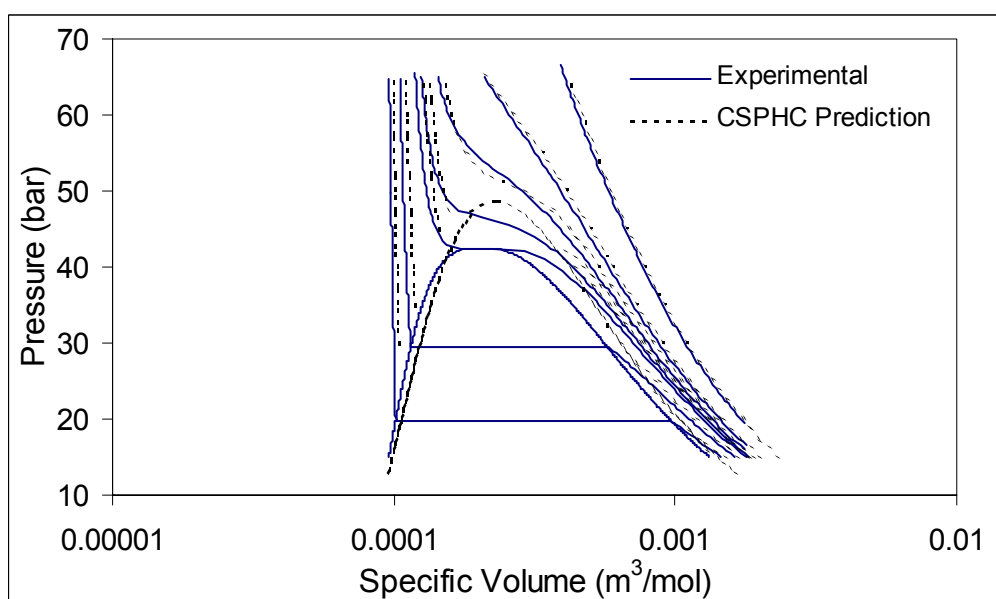
Figure 7-47:CSPHC EOS prediction of Propane Pressure-Volume-Temperature Diagram

The vapour pressure curve for dotriacontane is given in Figure 7-48. Although in the correct order of magnitude, in the moderate temperature range the equation of state does not perform as well as the SPHC equation of state.
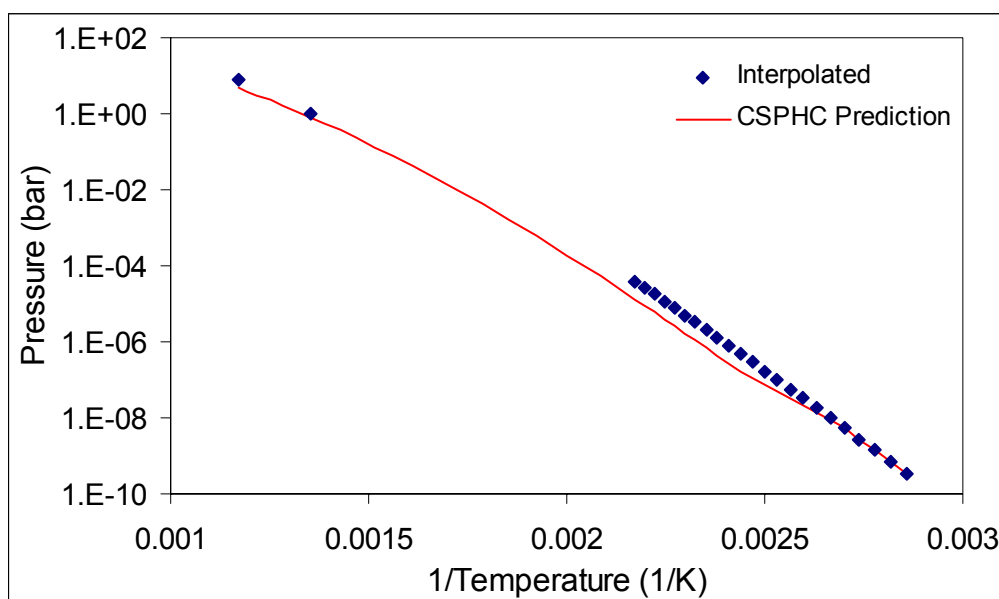
Figure 7-48: CSPHC EOS prediction of Dotriacontane Vapour Pressure Curve

The binary phase equilibrium prediction with the interaction parameters k_{12} = -0.0086 and l_{12} = 0.028 is given in Figure 7-49:
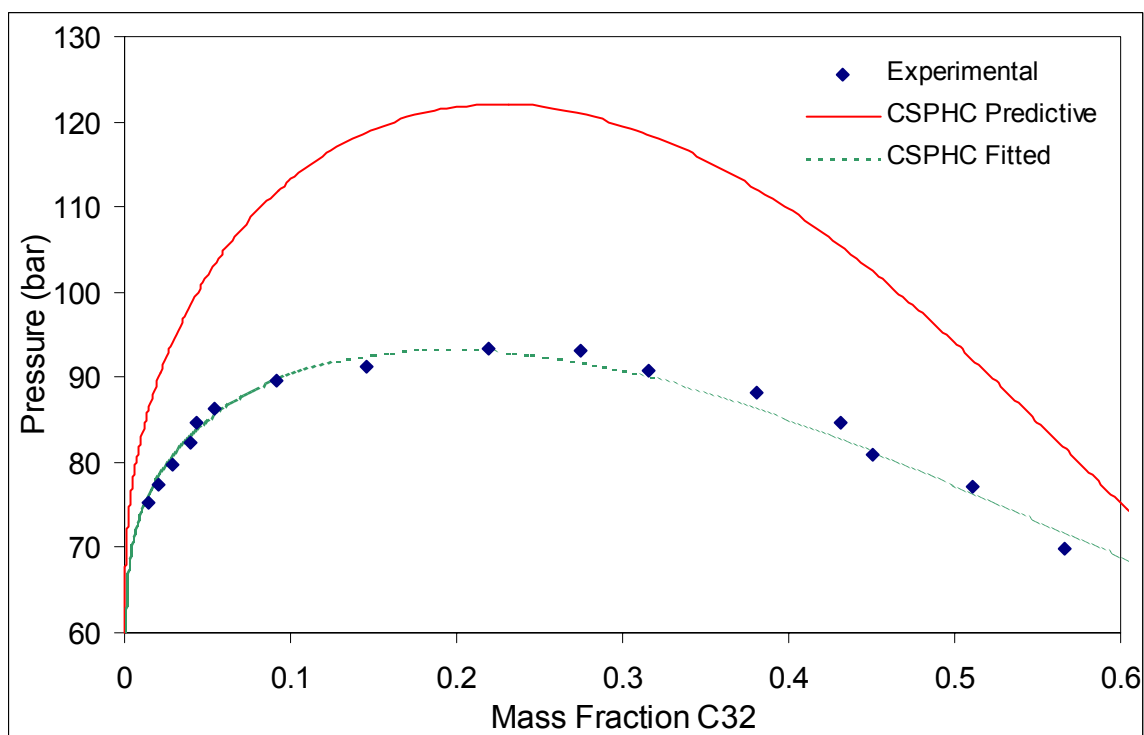
Figure 7-49: CSPHC EOS prediction of Pressure Composition Diagram for Propane-Dotriacontane at 408.15 K

The prediction of the CSPHC equation of state gives a phase equilibrium prediction that is no improvement of the SPHC equation of state. In fact, the prediction of the SPHC equation of state is better. When considering the interaction parameters, the SPHC equation of state is also superior as the interaction parameters for the CSPHC are significantly larger. Additionally, the predictive fit of the SPHC is better than the CSPHC.

7.6.5. STATISTICAL ASSOCIATING FLUID THEORY (SAFT)

The SAFT equation of state is developed to be applicable to small, large, chain and associating molecules over the whole density range. The equation of state models a fluid containing molecules of homobonded chains, i.e., chains that are composed of identical segments connected with identical bonds. The equation of state is expressed as a sum of the compressibility factors. This summation is derived from the residual Helmoltz energy. The derivation can be seen in Huang et al. (Huang et al., 1990).

$$Z - 1 = Z_{seg} + Z_{chain} + Z_{assoc}$$ 7.88

The contribution to the compressibility factor due to the segments can be expressed as follows:

$$Z_{seg} = m \left[\frac{4\eta - 2\eta^2}{(1-\eta)^3} + \sum_i \sum_j j D_{ij} \left[\frac{u}{k} \cdot \frac{1}{T} \right]^i \left[\frac{\eta}{\tau} \right]^j \right]$$ 7.89

The contribution due to the chain can be expressed as follows:

$$Z_{chain} = (1-m) \frac{\frac{2}{5}\eta - \eta^2}{(1-\eta)\left(1 - \frac{1}{2}\eta\right)}$$ 7.90

For the purpose of this project, the value of Z_{assoc} is assumed to be zero. This assumption is justified due to the fact that the components used here are non-polar hydrocarbon chains which are assumed not to associate with one another.

For each component three parameters exists:

- m, the segment number

- υ^{oo}, the segment volume

- u^o/k, the segment energy

The reduced segment density, also know as the segment packing fraction, is defined as follows:

$$\eta = \tau \rho_m m \upsilon^{\text{o}} \qquad\qquad\qquad\qquad\qquad 7.91$$

In equation 7.91 the parameter τ has the value 0.74047. The temperature dependent segment molar density can be defined as follows:

$$\upsilon^{\text{o}} = \upsilon^{\text{oo}} \left[1 - C \cdot \exp\left(\frac{-3}{T} \cdot \frac{u^{\text{o}}}{k} \right) \right]^3 \qquad\qquad\qquad 7.92$$

In equation 7.92 the parameter C is an integration constant set at 0.12 by Chen et al. (Chen et al., 1977) The temperature dependent segment energy required in equation 7.89 is defined as follows:

$$\frac{u}{k} = \frac{u^{\text{o}}}{k} \left[1 - \frac{e}{k} \cdot \frac{1}{T} \right] \qquad\qquad\qquad\qquad 7.93$$

The value of e/k is set to 10 according to Huang et al. (Huang et al., 1990). Exceptions are given by Huang et al. In equation 7.89 the parameter D_{ij} is a universal parameter given by Chen et al.

Huang et al. gave correlations according to which the three pure component parameters can be measured. The three correlations for n-alkanes are given in equations 7.94 to 7.96;

$$m = 0.70402 + 0.046647 \cdot M_R \qquad\qquad\qquad 7.94$$

$$m\upsilon^{\text{oo}} = 11.888 + 0.55187 \cdot M_R \qquad\qquad\qquad 7.95$$

$$\frac{u^{\text{o}}}{k} = 210 - 26.886 \cdot \text{EXP}\left[-0.013341 \cdot M_R \right] \qquad\qquad 7.96$$

In contrast to other equations of state, here only the dispersion term requires mixing rules. Huang et al. suggested two approaches, a van der Waals one-fluid approximation and a volume fraction approximation (Huang et al., 1991). Both mixing rules will be discussed and tested.

The mixing rule for m is the same for both mixing rules:

$$m = \sum_i \sum_j \frac{1}{2} x_i x_j \left(m_i + m_j \right) \left(1 - \ell_{12} \right) \qquad\qquad 7.97$$

For the van der Waals one fluid approximation mixing rule the following mixing rules are used:

$$\frac{u}{kT} = \frac{\sum_{i=1}^{N}\sum_{j=1}^{N} x_i x_j m_i m_j \left[\frac{u_{ij}}{kT}\right]\left(v^\circ\right)_{ij}}{\sum_{i=1}^{N}\sum_{j=1}^{N} x_i x_j m_i m_j \left(v^\circ\right)_{ij}}$$ 7.98

where

$$\left(v^\circ\right)_{ij} = \frac{1}{8}\left[\left(v^\circ\right)_i^{1/3} + \left(v^\circ\right)_j^{1/3}\right]^3$$ 7.99

$$\frac{u_{ij}}{k} = \left(1-k_{ij}\right)\sqrt{\frac{u_i}{k}\cdot\frac{u_j}{k}}$$ 7.100

For the volume fraction mixing rules the following mixing rules are applied:

$$\frac{u}{k} = \sum_i\sum_j f_i f_j \left[\frac{u_{ij}}{k}\right]$$ 7.101

$$f_i = \frac{x_i m_i \upsilon^\circ_i}{\sum_j x_j m_j \upsilon^\circ_j}$$ 7.103

$$\frac{u_{ij}}{k} = \left(1-k_{ij}\right)\left(\frac{u_i}{k}\cdot\frac{u_j}{k}\right)^{1/2}$$ 7.104

The PvT diagram for propane is given in Figure 7-50. Although the liquid and vapour volumes well away from the critical point are well predicted, the critical region is predicted rather poorly. The critical temperature and pressure are over-predicted, and this over-prediction can be attributed to the fact that the pure component parameters are independent of the critical temperature and pressure. This over-prediction is likely to have an effect on the phase equilibrium in a binary system where the propane is in the critical state, and may lead to an over-prediction of the phase transition pressure. The PvT prediction may be improved should the parameters be fitted to the experimental data.
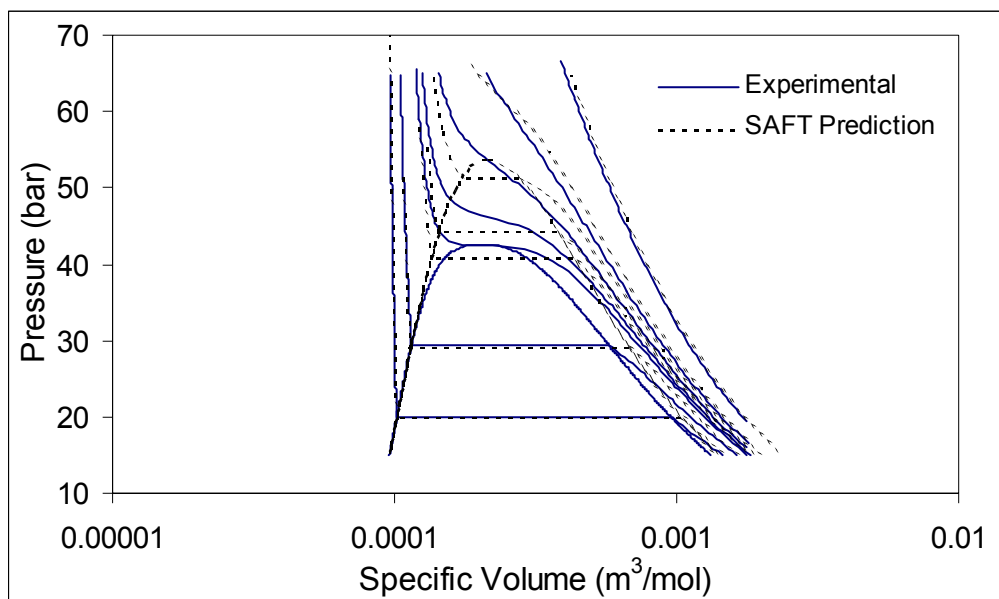
Figure 7-50: SAFT EOS prediction of Propane Pressure-Volume-Temperature Diagram

The vapour pressure curve for propane-dotriacontane is plotted in Figure 7-51. The vapour pressure curve is represented quite well. The critical temperature is over-predicted by 30 K and the critical pressure under-predicted by about half a bar. These inaccuracies for the heavy compound are not expected to have a profound effect on the phase equilibrium due to the fact that the operation will take place well away from the critical point. Additionally, it must also be remembered that the critical point for dotriacontane and the other heavy paraffins are not experimentally verified values but rather extrapolations with the possibility of errors.
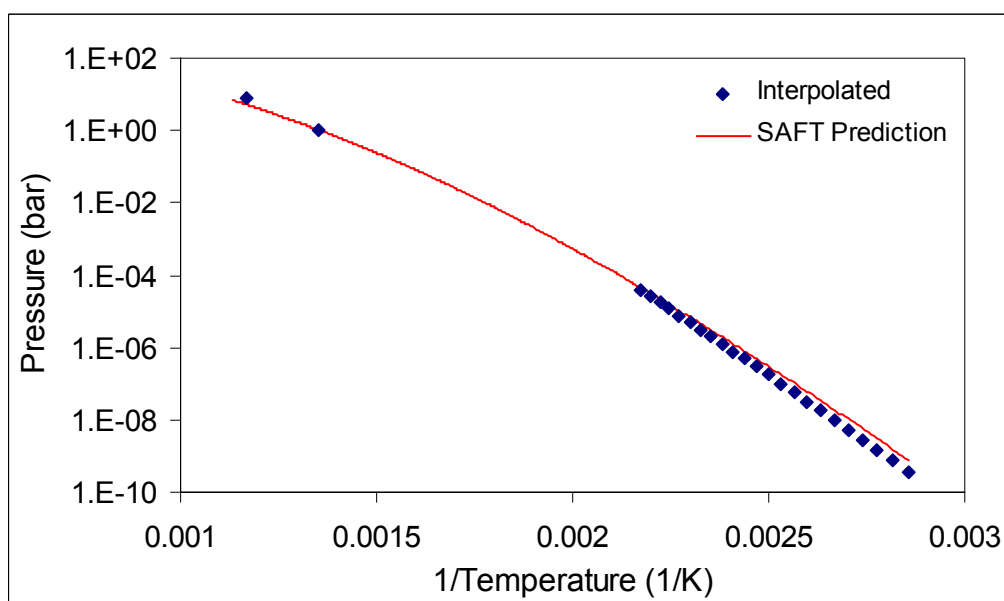
Figure 7-51: SAFT EOS prediction of Dotriacontane Vapour Pressure Curve

The SAFT equation of state was used to model the system and the interaction parameters are given in Table 7-14 while the resultant phase diagrams are shown in Figure 7-52 and Figure 7-53. In addition to the fitted curves, the influence of the volume interaction parameters, l_{12}, is seen by plotting the curves with the fitted k_{12} values and with $l_{12} = 0$.

Table 7-14: SAFT Binary Interaction Parameters for Propane – C32

Van der Waals One Fluid Approximation	$k_{12} = 0.02989$
	$l_{12} = 0.003210$
Volume Fraction	$k_{12} = 0.02846$
	$l_{12} = 0.00126$
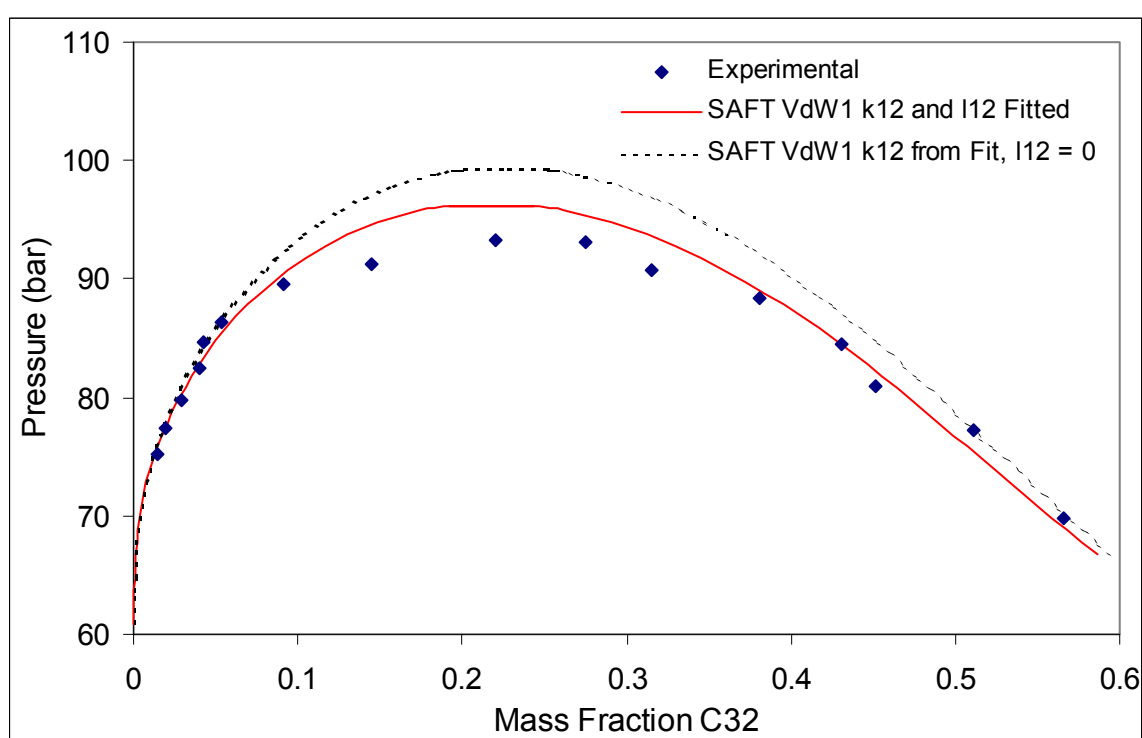
Figure 7-52: SAFT EOS with VdW1 mixing rules for prediction of Pressure Composition Diagram for Propane-Dotriacontane at 408.15 K
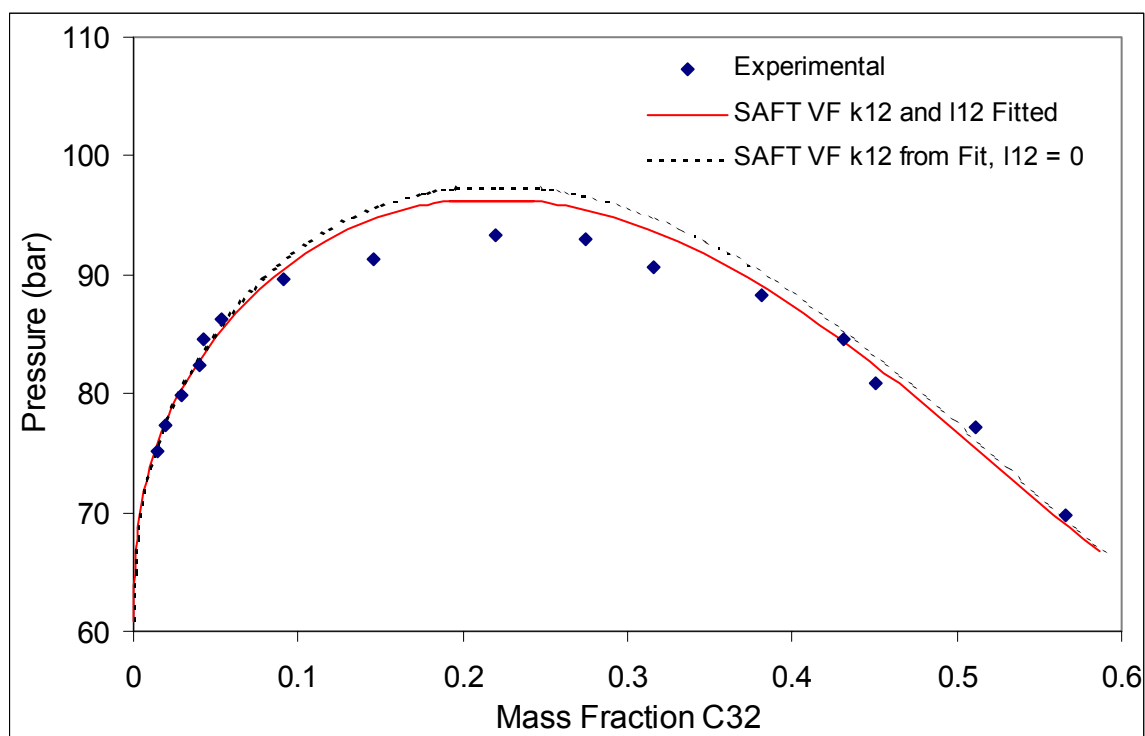
Figure 7-53: SAFT EOS with VF Mixing Rules prediction of Pressure Composition Diagram for Propane-Dotriacontane at 408.15 K

Both mixing rules tend to over-predict the phase transition pressure in the mixture critical region. The most probable cause of this over-prediction is the inaccuracies in the critical region of the pure component predictions. When comparing the two graphs there is no noticeable difference in predictions with the various mixing rules and when comparing the numerical values it can be seen that for both types of mixing rules, the values are small, with very little difference between them. However, the volume fraction mixing rules predict the phase equilibrium better with $l_{12} = 0$ than the van der Waals one fluid theory does.

7.6.6. PERTURBED-CHAIN SAFT (PC-SAFT)

In the original SAFT model the dispersion term does not take into account the chain like structure of polymer compounds since a hard sphere reference term is used. In the PC-SAFT equation of state the dispersion forces are taken into account by applying a perturbation theory of the second order using an expression for the radial pair distribution of a hard-chain reference fluid. The equation of state is mathematically complex and details can be found in the work of Gross et al (Groß et al., 1999).

Three pure component parameters are used for non-associating fluids: the segment number, the segment diameter and the attraction parameter. The values for the original SAFT equation of state were used as starting values and these values were obtain so as to obtain the best possible fit.

The PC-SAFT equation of state is applied to mixtures by using the one fluid mixing rules. These mixing rules result in a single interaction parameter applied to the attraction term.

The PvT diagram for propane is given in Figure 7-54. The PvT plot is a clear improvement of the SAFT equation of state but the critical temperature and pressure are still over-predicted. Refitting the parameters may improve the PvT prediction.
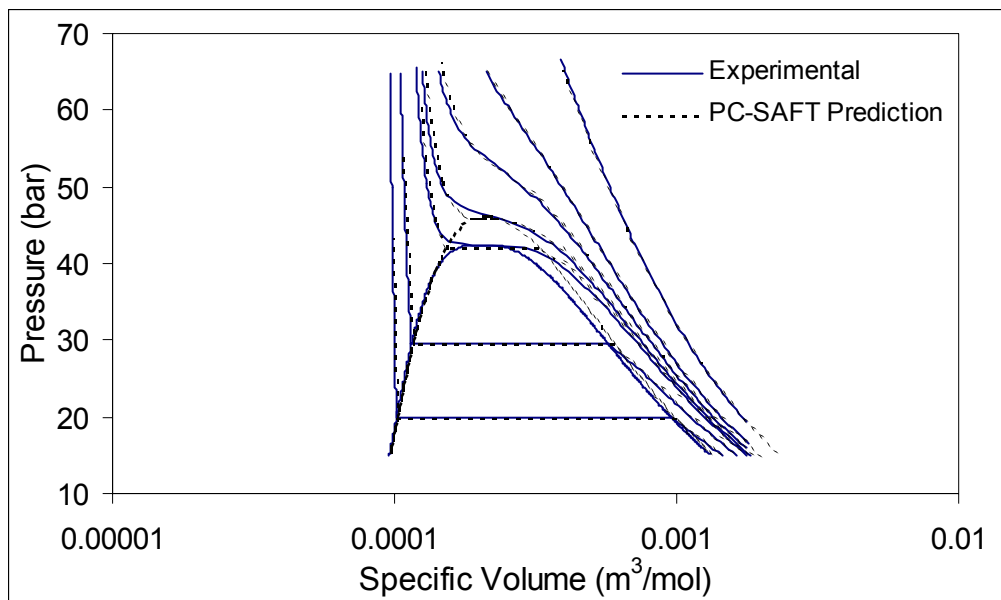
Figure 7-54: PC-SAFT EOS prediction of Propane Pressure-Volume-Temperature Diagram
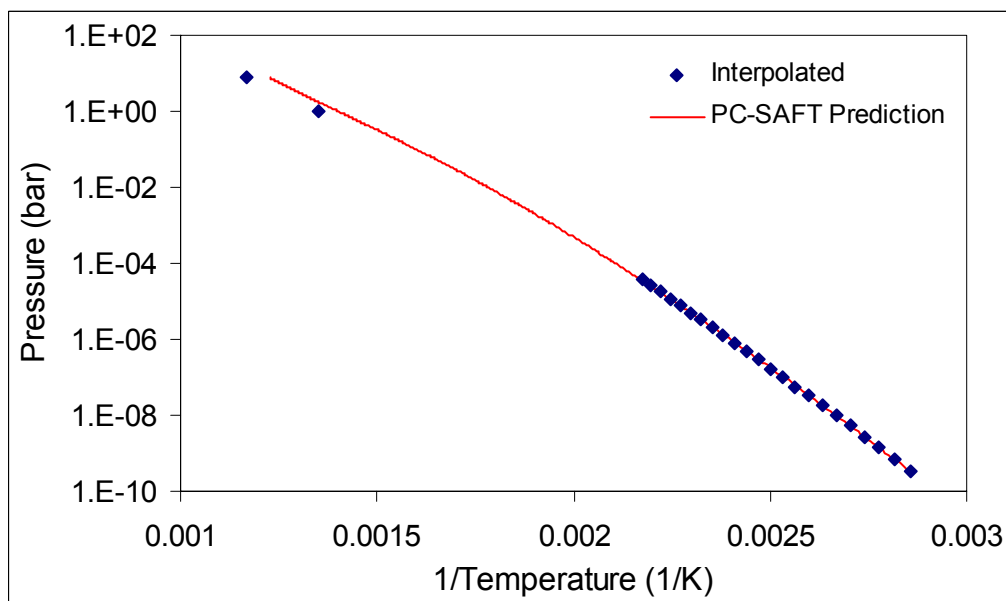
Figure 7-55: PC-SAFT EOS prediction of Dotriacontane Vapour Pressure Curve

The extension of the PC-SAFT equation of state to mixtures was done and an interaction parameter of –0.01622 gave the optimum fit, shown in Figure 7-56.
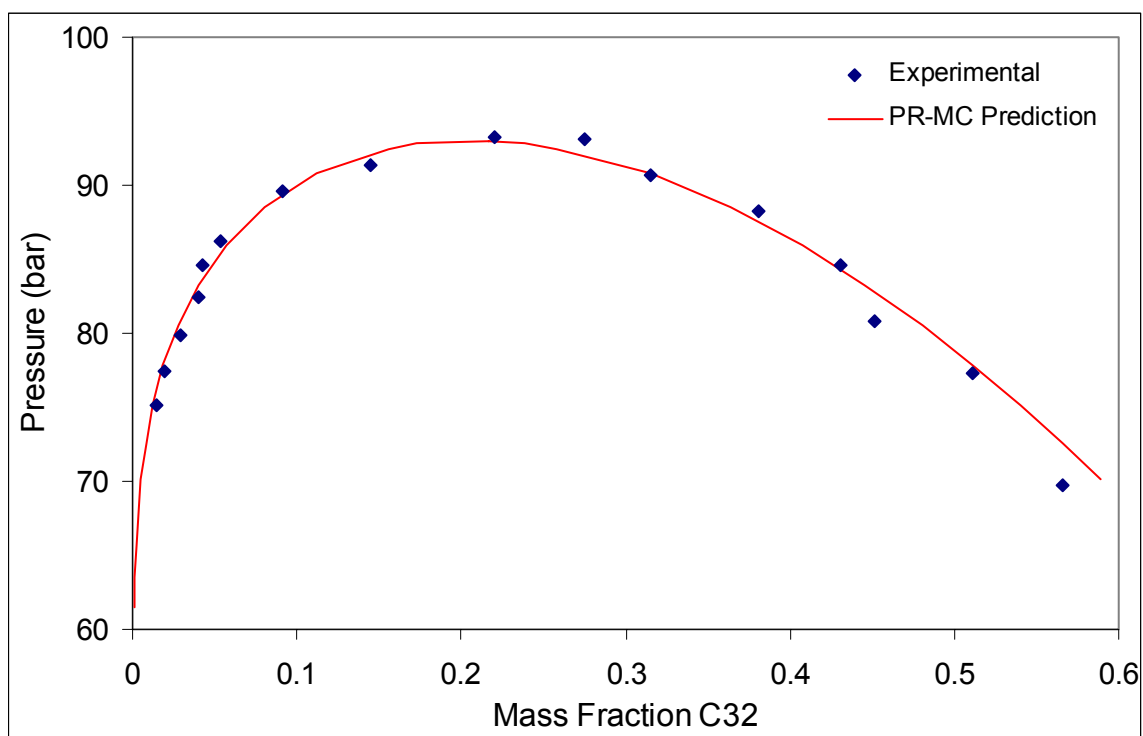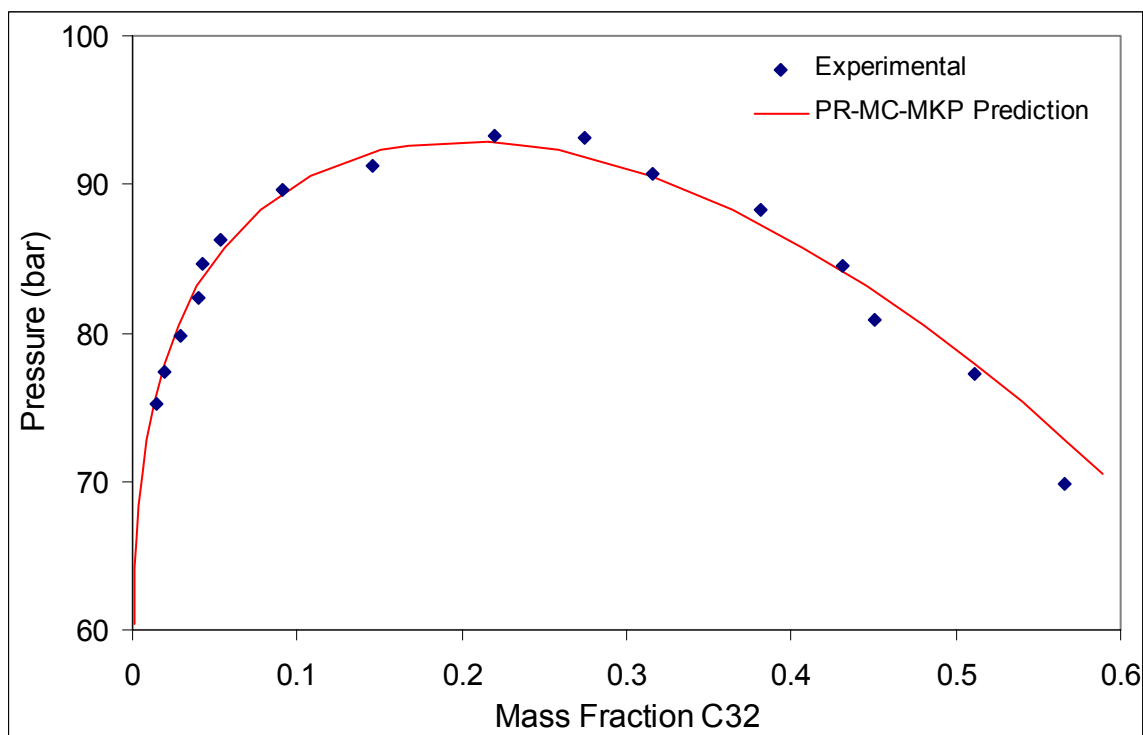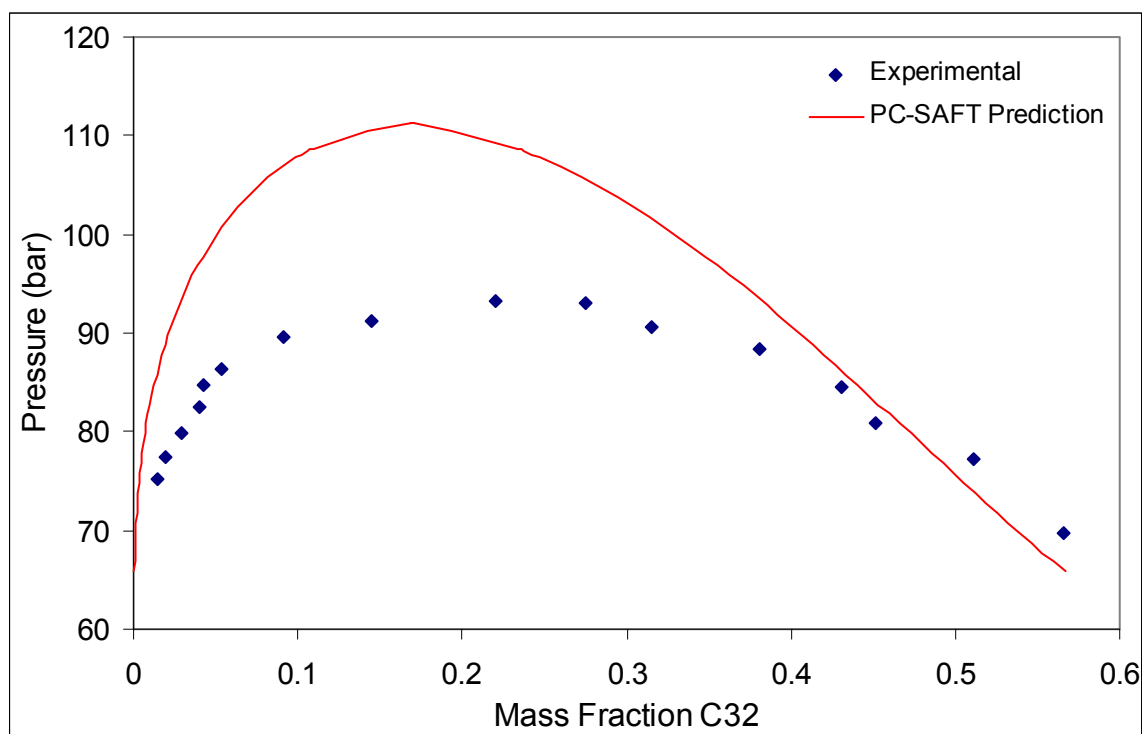

Figure 7-56: PC-SAFT EOS with Standard Mixing Rules prediction of Pressure Composition Diagram for Propane-Dotriacontane at 408.15 K

The vapour pressure curve for dotriacontane is plotted in Figure 7-55.as was the case for the SAFT equation of state, the PC-SAFT equation of state is able to predict the vapour pressure curve for dotriacontane quite well in the low temperature region. The best obtained for the PC-SAFT equation of state for a single interaction parameter is not very good. Similar types of fits were obtained for other systems where only one interaction parameter is used. The implementation of an additional interaction parameter is thus required to improve the fit.

7.7. COMPARISON OF EQUATIONS OF STATE

In order to improve clarity, not all sixteen equations of state studied in detail above can be compared at once. Firstly a comparison of the cubic equations of state followed by the non-cubic equations of state.

7.7.1. COMPARISON OF CUBIC EQUATIONS OF STATE

Eleven cubic equations of state were investigated. To be able to compare the equations of state properly, firstly the SRK equation of state and its modifications will be compared,

followed by the PR and its modifications, followed by a comparison of the remaining equations of state.

The first comparison will be made for the SRK equation of state at the modifications of this equation. The comparison will be done for the MKP mixing rules due to the fact that although in most cases the prediction is virtually identical, in the case of the volume translated equations of state, the MKP prediction is superior. The comparison can be seen in Figure 7-57:
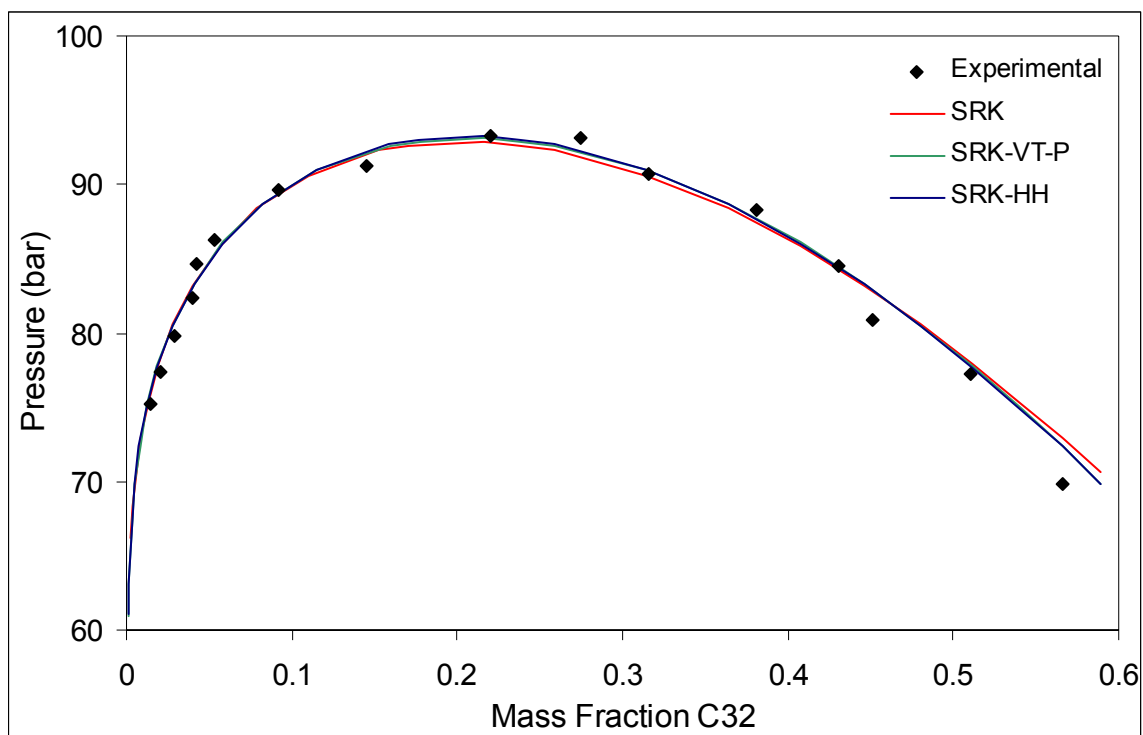
Figure 7-57: Comparison of SRK type of Equations of State with MKP mixing rules at 408.15 K

As can be seen in Figure 7-57, the modifications of the SRK equation of state show no advantage in the phase equilibrium plot. However, if the interaction parameter size is taken into account, the SRK-HH seams to be superior.

In the same manner that the various SRK equations of state have been compared, the modifications of the PR equation of state with the MKP mixing rule are compared in Figure 7-58:
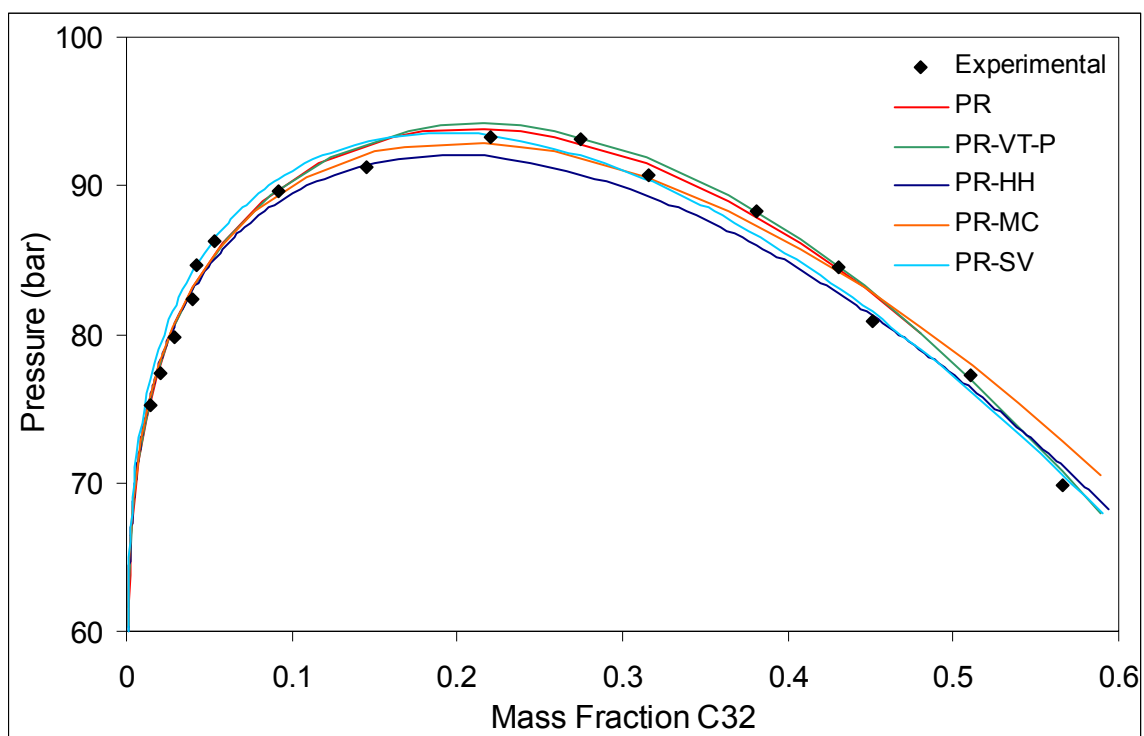
Figure 7-58: Comparison of PR type of Equations of State for MKP mixing rules at 408.15 K

From the figure above it can be seen that the various modifications provide similar phase equilibrium predictions. However the original PR seems to provide a slightly better fit than the modifications.

Lastly, the SRK and PR equations of state will be compared with the other cubic equations of state. The comparison is shown in Figure 7-59.
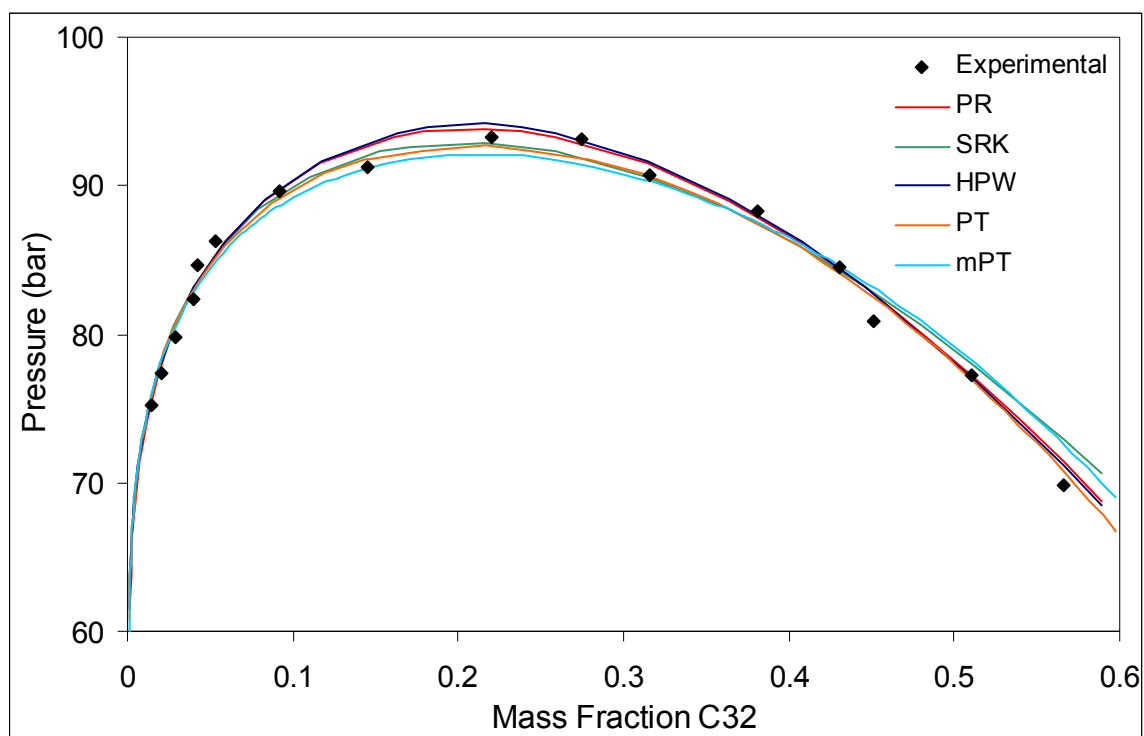
Figure 7-59: Comparison of Cubic Equations of State with MKP mixing rules at 408.15 K

From the above plot it can be seen that all the cubic equations of state predict the phase equilibrium quite well. On closer examination it can be seen that the PT and MPT equations of state seem to be superior to the others followed by the PR equation of state. The superiority of the PT and MPT equations of state can be attributed to the fact that the critical compressibility is not constant and PR equation of state has a superior temperature dependent attraction term. When comparing the MPT and PT equations of state it can be seen that there is very little difference in the binary phase prediction but when considering the pure component prediction, the MPT is superior to the PT equation of state. The MPT and PR equation of state will thus be used for the comparison of the cubic and non-cubic equations of state.

7.7.2. COMPARISON OF NON-CUBIC EQUATIONS OF STATE

The non-cubic equations studied in this work are compared in Figure 7-60. For all the equations of state, except the SAFT equation of state, only one type of mixing rule was used in this work and thus to compare the work in the best possible way, the van der Waals mixing rules were used for the SAFT equation of state.
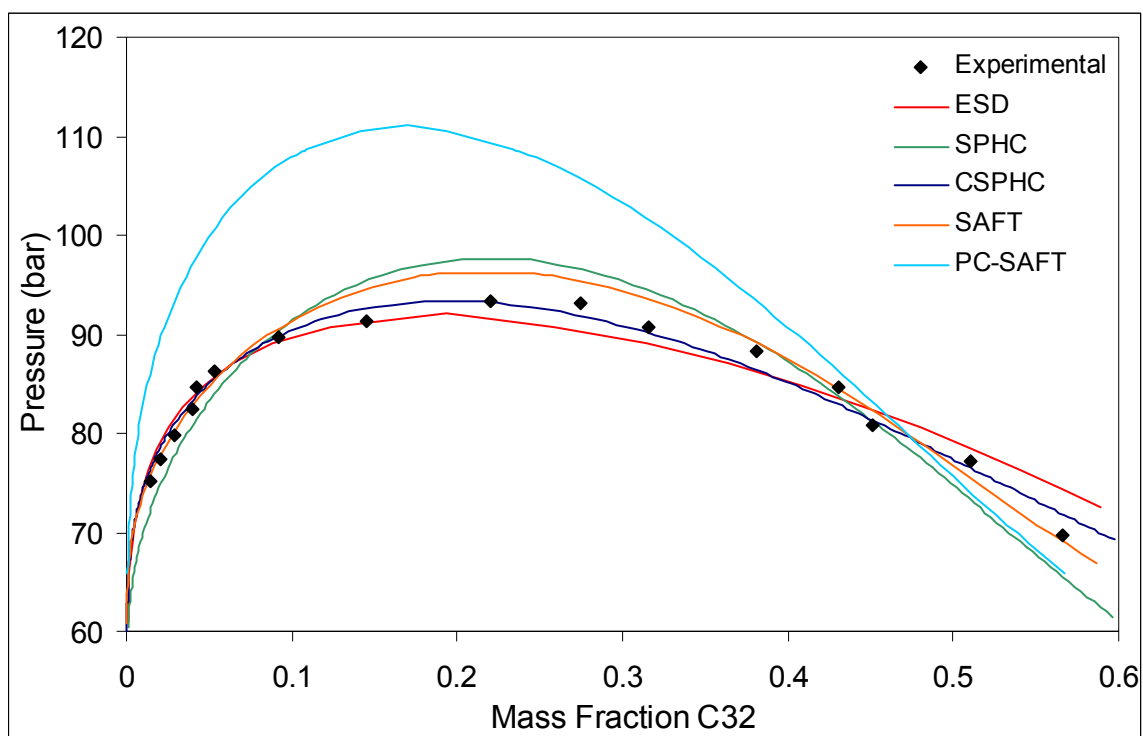
Figure 7-60: Comparison of Non-Cubic Equations of State at 408.15 K

The non-cubic equations of state are not able to predict the phase equilibrium as well as the cubic equations of state. When comparing the non-cubic equations of state it can be seen that the SAFT equation provides the best prediction followed by that of the ESD equation. These two equations of state will be used for the comparison of cubic versus non-cubic equations of state.

7.7.3. CUBIC VS NON-CUBIC EQUATIONS OF STATE

A comparison of the cubic and non-cubic equations of state will be done by comparing the best two cubic equations of state with the best two non-cubic equations of state.
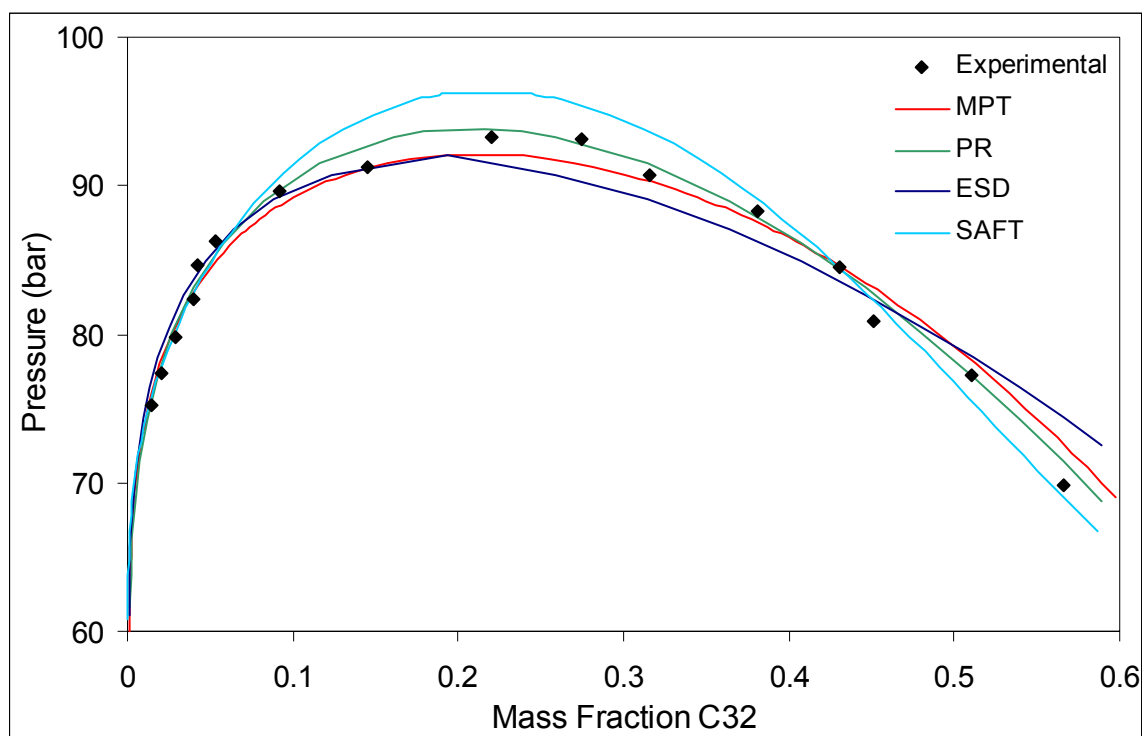
Figure 7-61: Comparison of Cubic and Non-Cubic Equations of State at 408.15 K

Figure 7-61 reveals that the cubic equations of state have a better ability to predict the phase equilibrium pressure-composition graph than the non-cubic equations. This does, however, lie with the fact that the mixing rules allow for the cubic equations of state to be forced through the data and a comparison of the values of the interaction parameters for the cubic equations with the non-cubic equations shows generally the values for the non-cubic equations are a smaller in magnitude.

For all further investigations the MPT equation of state will be used for as an example of a cubic equation of state and the SAFT equation as a non-cubic equation.

7.8. EXTENSION TO OTHER TEMPERATURES

The fitting of the equations of state done in paragraphs 7.5 and 7.6 was all done at 408.15 K. To investigate the temperature dependence of the interaction parameters other temperatures will be investigated. For the SAFT equation of state, van der Waals parameters will be investigated.

7.8.1. CUBIC EQUATION OF STATE (MODIFIED PATEL-TEJA)

In Figure 7-62 the interaction parameters fitted to the data at T = 408.15 K is used to determine the predicted phase equilibrium pressures. As can be seen, these interaction parameters do not yield the optimum predictions, but the predictions are not far off, the vapour side predictions being slightly high.
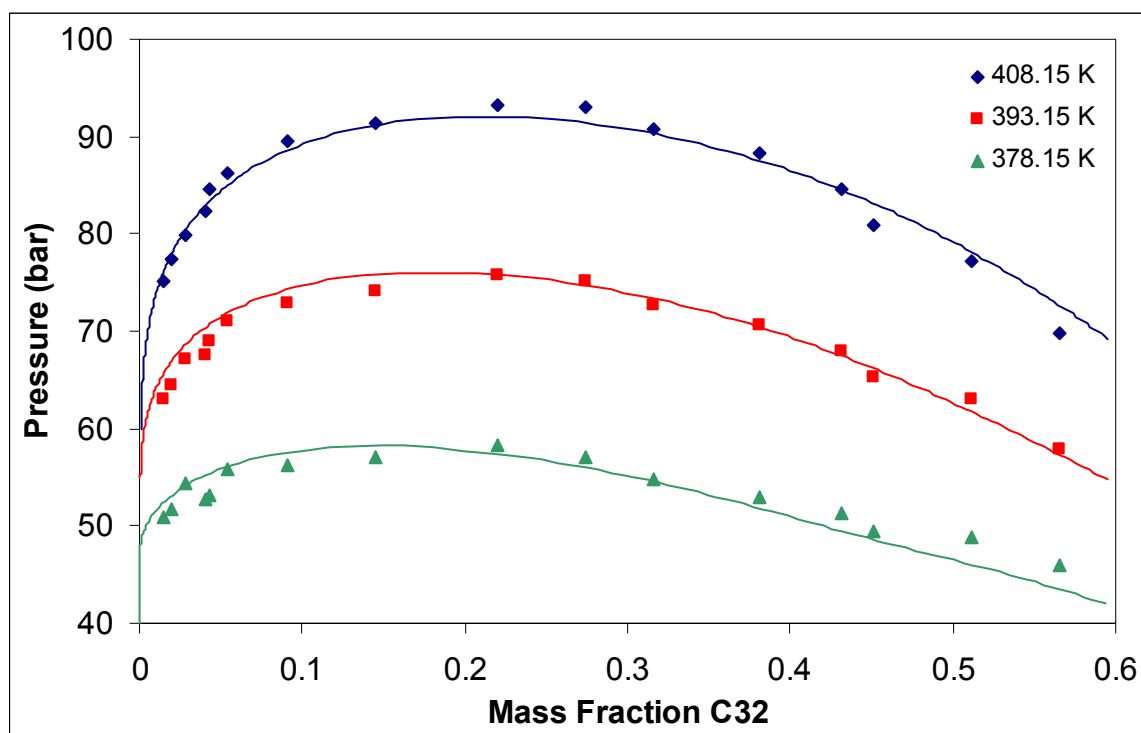
Figure 7-62: PT EOS with Quadratic Mixing Rules prediction of Pressure Composition Diagram for Propane-Dotriacontane. Interaction parameters fitted at T = 408.15 K.

The interactions parameters were now fitted to the data at the experimental temperature and the following interaction parameters were found:

Table 7-15: Interaction parameters for PT EOS with quadratic mixing rules at various temperatures

Temperature	k_{12}	l_{12}
408.15 K	-0.07014	0.1418
393.15 K	-0.06601	0.1231
378.15 K	-0.05813	0.1157

From Table 7-15 it can be seen that there is some temperature dependence of the interaction parameters. A more detailed study will have to be conducted to determine the functional dependence.

The interaction parameters given in Table 7-15 are used to generate Figure 7-63:

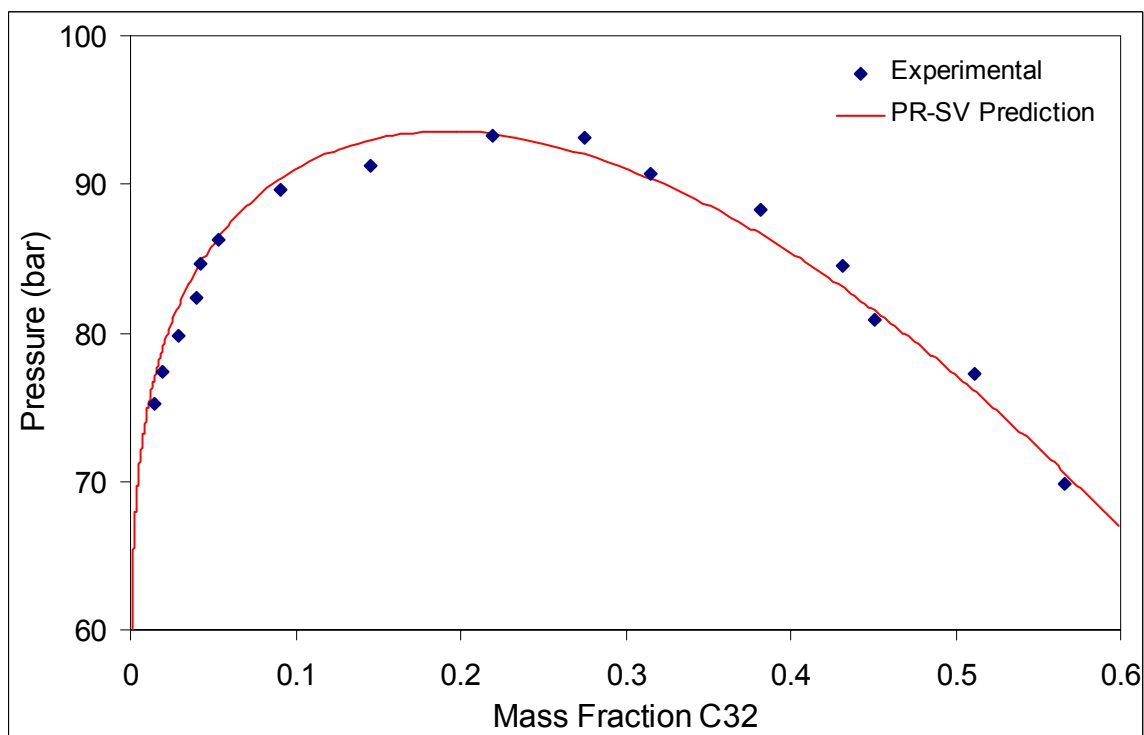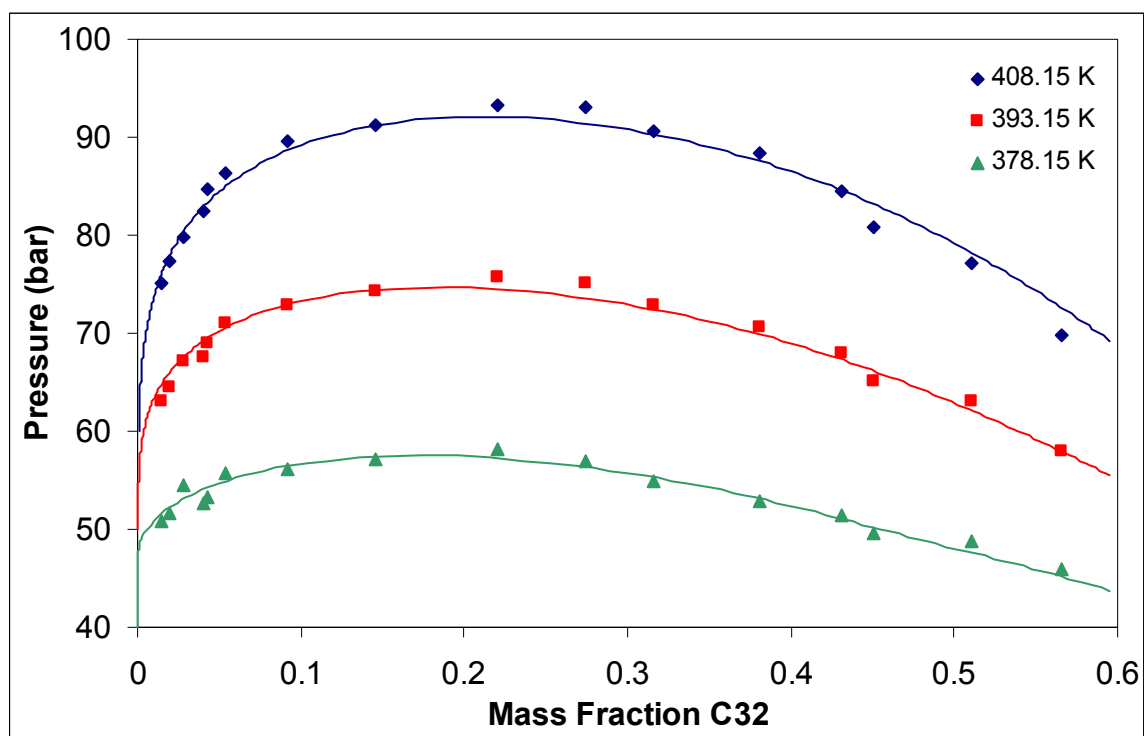*Figure 7-63: PT EOS with Quadratic Mixing Rules prediction of Pressure Composition Diagram for Propane-Dotriacontane. Interaction parameters fitted at system temperature.*

As seen, by changing the interaction parameters the data can be fitted well at other temperatures.

7.8.2. NON-CUBIC EQUATION OF STATE (SAFT)

A similar approach to that used for the PT equation of state was used for the SAFT equation of state. Firstly the phase equilibrium was calculated at the various temperatures with the interaction parameters fitted for T = 408.15 K. The resultant plot is given in Figure 7-64.
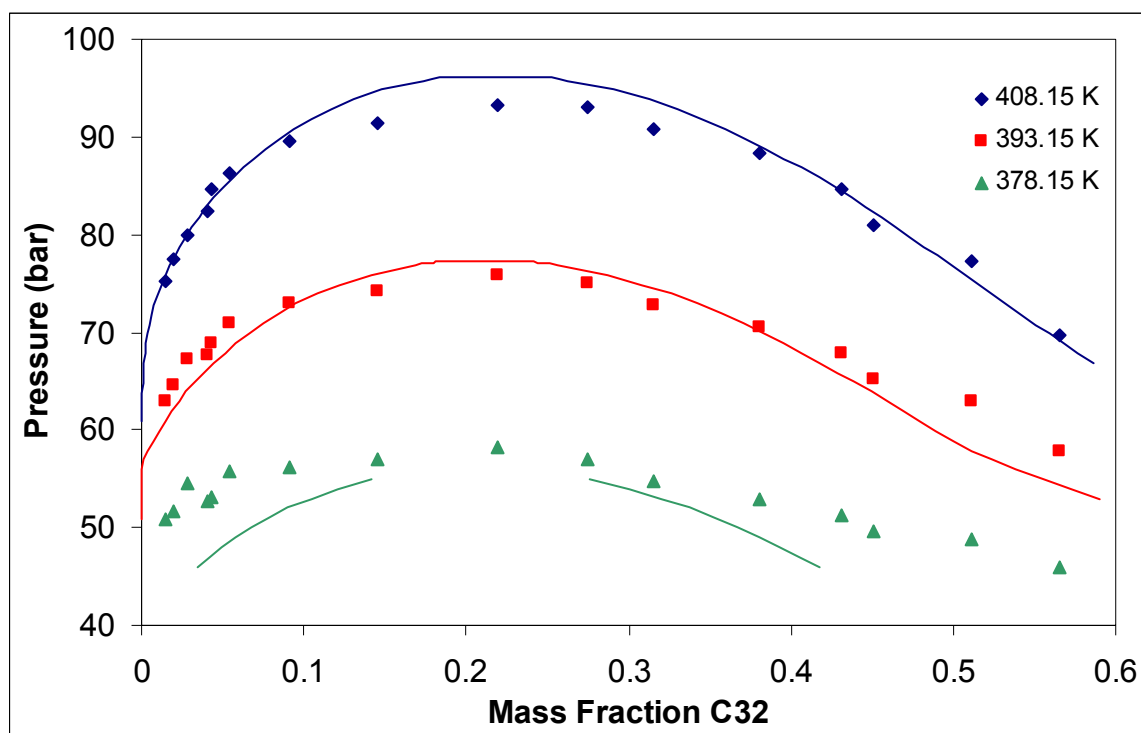
Figure 7-64: SAFT EOS with van der Waals Mixing Rule prediction of Pressure Composition Diagram for Propane-Dotriacontane. Interaction parameters fitted at T = 408.15 K.

As can be seen in Figure 7-64 these interaction parameters do not perform badly at all but do tend to under-predict the phase equilibrium pressure. It should also be note that calculations for the lowest temperature (378.15 K) were found to be very difficult to converge, especially in the critical region. It is thus necessary to fit the data at each temperature of operation. However, due to convergence problems, fitting of data at 378.15 K was not possible and the interaction parameters were determined by linear extrapolation of the interaction parameters at 408.15 and 393.15 K. The resultant plots are given in Figure 7-65 with the interaction parameters in Table 7-16

Table 7-16: Interaction parameters for SAFT EOS with van der Waals Mixing rule at various temperatures

Temperature	k_{12}	l_{12}
408.15 K	0.02989	0.003210
393.15 K	0.01918	-0.007957
378.15 K	0.00848	-0.01270
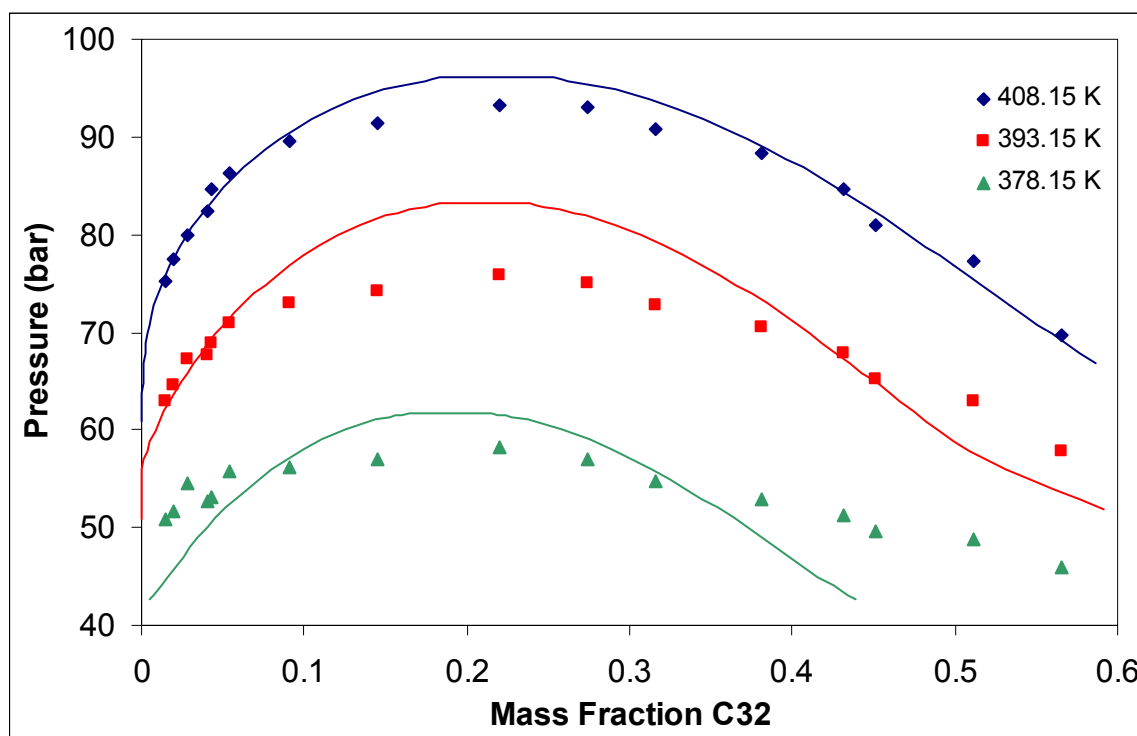
Figure 7-65: SAFT EOS with van der Waals Mixing Rule prediction of Pressure Composition Diagram for Propane-Dotriacontane. Interaction parameters fitted at system temperature.

As can be seen above, the SAFT equation of state once again over-predicts the phase transition pressure in the mixture critical region. For the calculated interaction parameters (408.15 and 393.15 K) the resultant plots describe the vapour side well and a good approximation is obtained for the liquid side. It can also be seen that linear extrapolation does not result in a good approximation of the optimum interaction parameters.

7.8.3. COMPARISON OF TEMPERATURE DEPENDENCE

Comparing the results of the graphs obtained when the interaction parameter obtained at 408.15 K is used for the two equations of state, it can be seen that the MPT equation of state seems less sensitive to temperature. To determine if this phenomenon is valid for all cubic equations of state a more detailed investigation is required.

By comparing the values of the interaction parameters, it can be seen that for both equations of state the interaction parameters are dependent on temperature, yet for neither of the equations of state is this dependence strictly linear. Once again, a more detailed study will be required to determine the exact relationship between temperature and the interaction parameter.

7.9.   EXTENSION TO OTHER SYSTEMS

To be able to predict the phase equilibrium of systems not studied in this work, the interaction parameters are required. The other systems for which experimental data was measured will be fitted with the PT and SAFT equations of state and the effect of the carbon number on the interaction parameters will be investigated.

7.9.1.   CUBIC EQUATION OF STATE (MODIFIED PATEL TEJA)

The interaction parameters for the MPT equation of state for the various systems is given in Table 7-17. The critical temperature and pressure used are given in Table 7-1.

Table 7-17: Interaction parameters for PT for various systems at 408.15 K:

System	k_{12}	l_{12}
C3-C32	-0.07014	0.1418
C3-C 36	-0.09192	0.1783
C3-C 38	-0.09675	0.1939
C3-C 40	-0.0975	0.2310
C3-C 44	-0.1127	0.2601
C3-C 46	-0.1211	0.2691
C3-C 54	-0.1145	0.2941
C3-C 60	-0.1239	0.2982

The values of the interaction parameters are plotted as a function of carbon number in Figure 7-66 and Figure 7-67:
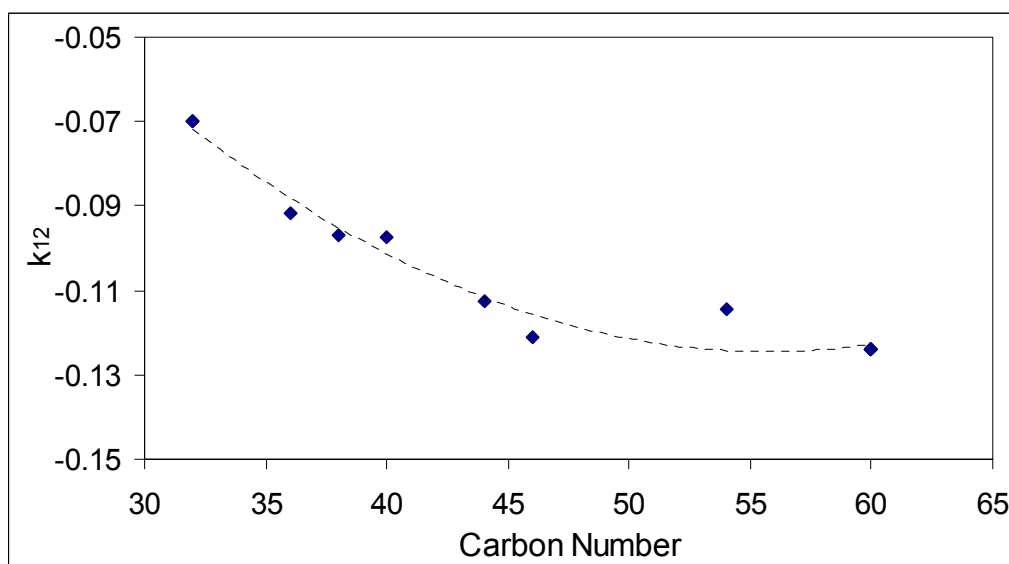
Figure 7-66: Plot of k_{12} as a function of carbon number for MPT EOS
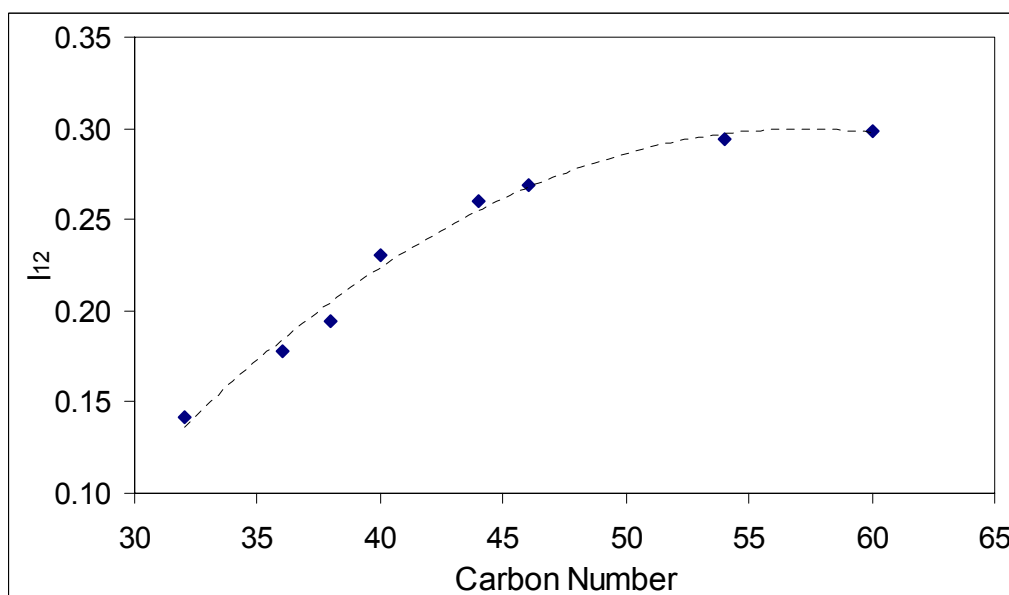
Figure 7-67: Plot of l_{12} as a function of carbon number for MPT EOS

For both k_{12} and l_{12} the interaction parameters show asymtotic behaviour towards a set value at high carbon numbers. For k_{12} this value is about –0.13 and for l_{12} the value is about –0.3. The exact numerical values would require a more detailed analysis.

7.9.2. NON-CUBIC EQUATION OF STATE (SAFT)

The SAFT equation of state was applied to the other systems at 408.15 K. The pure component parameters used are given in Table 7-18. The parameters for C36, C44 and Propane were given by Huang et al. All other parameters were estimated with the relations in equations 7.96 through 7.98.

Table 7-18: Pure Component Parameters for SAFT EOS

Component	u^o/k	v^{oo}	m
C 32	208.79	0.012	21.736
C 36	208.74	0.012	24.443
C 38	209.00	0.012	25.661
C 40	209.05	0.012	26.970
C 44	207.73	0.012	29.252
C 46	209.19	0.012	30.896
C 54	209.33	0.012	36.130
C 60	209.40	0.012	40.056
Propane	190.22	0.01307	2.7619

The interaction parameters for the SAFT equation of state are given in Table 7-19

Table 7-19: Interaction parameters for SAFT for various systems at 408.15 K:

System	k_{12}	l_{12}
C3-C 32	0.02989	0.00321
C3-C 36	0.03807	0.01029
C3-C 38	0.04091	0.01352
C3-C 40	0.04474	0.01440
C3-C 44	0.04810	0.01460
C3-C 46	0.03981	0.01598
C3-C 54	0.03343	0.00879
C3-C 60	0.04459	0.01756

The values of the interaction parameters are plotted as a function of carbon number in Figure 7-68 and Figure 7-69:
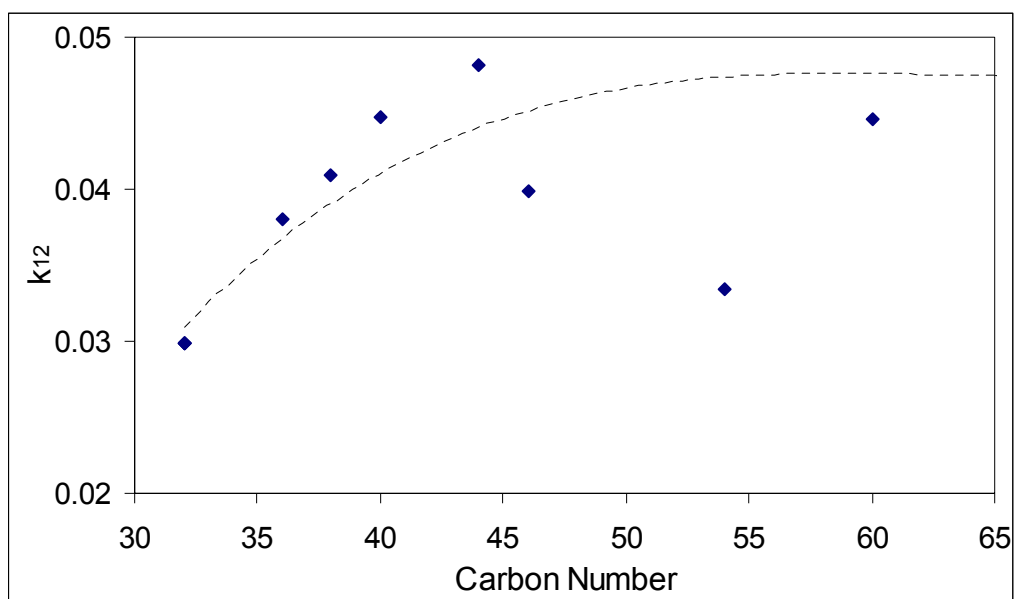
Figure 7-68: Plot of k_{12} as a function of carbon number for SAFT EOS
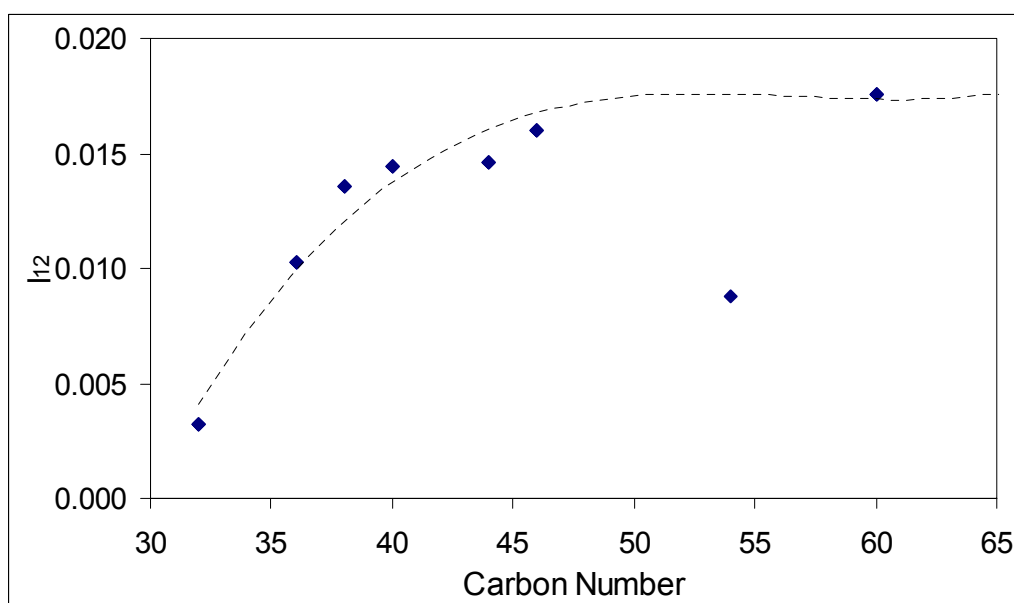
Figure 7-69: Plot of l_{12} as a function of carbon number for SAFT EOS

The same trend is seen for the SAFT equation of state that was seem for the MPT equation of state. Here the value of k_{12} tends towards 0.045 and l_{12} towards 0.0175. Once again, a more detailed analysis is required to verify these values.

7.10.   CONCLUSIONS

The following conclusions can be made for the thermodynamic modelling:

- Due to the nature of the paraffins used, the critical properties (temperature, pressure and compressibility) as well as the boiling point cannot be measured directly and must

thus be estimated. The values used can thus be regarded as pseudo values generated as extrapolations of data available for lighter paraffins.

- Due to the high boiling points of the paraffins and the low vapour pressure of the compounds, vapour pressure data exists only for paraffins up to nC38, which can be extrapolated as far as nC40. As a result, fitting pure component parameters to the experimental data becomes problematic.

- Various equations of state are unable to predict the vapour pressure data of nC32. For the early equations of state this can be attributed to the fact that the temperature dependence of the attractive term may be incorrect, while for later equations of state it may be due to the inability of may equations of state to incorporate the effect of chain molecules. Additionally, the use of the pseudo parameters may result in incorrect estimations.

- As commonly found in the literature, the cubic equations of state were unable to predict the pure component PvT diagram of propane in the liquid region and also show deviations in the critical region. Volume translated modifications did show improvements but the improved predictions were still not within experimental accuracies.

- With the aid of the mixing rules the equations of state were forced through the experimental data. Similar results were obtained for both types of mixing rules. For both types of mixing rules relatively large interaction parameters were required for a good fit.

- The non-cubic equations of state did provide an improved liquid density prediction, however the critical point was often overestimated in both temperature and pressure.

- For mixtures, the non-cubic equations of state were more difficult to force through the data and thus the predictions are not as good. Due to the fact that the non-cubic equations of state generally over predict the critical point of the pure component, the mixture critical region is usually over predicted as well. However, the interaction parameters are significantly smaller and with modifications these equations of state may thus be able to act predictively in future.

- The interaction parameters for the cubic equations of state were found to be less sensitive to temperature than the non-cubic equations of state.

- For both the cubic and the non-cubic equations of state, the interaction parameters show asymptotic behaviour at high carbon numbers.

8. CONCLUSIONS AND FURTHER WORK

The work done in this project can be divided into two main categories: Firstly, experimental work done in terms of the measurement of the phase diagrams and, secondly, phase equilibrium modelling of the experimental data.

Experimental work was done to determine the phase diagrams for propane and various paraffins with a range of 32 to 60 carbon atoms. By plotting the phase equilibrium pressure as a function of carbon number at a constant mass fraction, a straight-line relationship was obtained.

This straight-line relationship facilitated the estimation of phase equilibrium diagrams of propane with a paraffin between 32 and 60 carbon atoms. It has been proven that extrapolation of the straight line graphs to lower carbon numbers allows for the prediction of phase equilibrium of these systems. It can thus be postulated that extrapolation to higher carbon numbers will hold true as long as the paraffins do not start to do polymer folding.

Phase diagrams for systems such as propane-nC80 can thus be predicted. Currently C60 is the highest carbon number paraffin commercially available. In the future higher carbon number paraffins need to be synthesised and the experimental results need to be tested against the predicted phase diagrams. By synthesising higher carbon number paraffins it can be determined at which pressure the paraffin starts to fold and thus indicating to what extent the pressure-carbon number plots can be extrapolated.

Pure component critical properties and vapour pressure curves for the higher molecular weight paraffins can not be measured and thus require pseudo values for the critical temperature, pressure, composition, the acentric factor and the boiling point. These pseudo values, together with the inability of many cubic equations of state to incorporate the effect of a chain molecule, often result in equations of state having difficulty in the prediction of the binary phase transition.

Where the cubic equation can predict the pure component data with satisfactory results, high interaction parameters were found. This indicates that the mixing rules are not predictive and thus require revision.

In a move to incorporate the effect of chain molecules and to use pure component parameters that are not dependent on the critical point, statistical mechanical models have been suggested. However, these models have difficulty in the predicting the critical region accurately and thus often over predict the mixture critical region of the binary phase diagram.

Currently the cubic equations of state provide better predictions than the non-cubic equations of state. However, the statistical mechanical models show promise for these types of systems due to the fact that the pure component parameters can be easily extrapolated and the incorporation of the effect of the chain. By improving the prediction of the statistical mechanical models in the critical region they may be able to provide a gateway for the thermodynamic modelling of these highly non-ideal systems.

From the discussion in Chapter 1 it can be seen that a need exists for an alternative method for the fractionation of synthetic waxes. The aim of this project was to conduct a preliminary study on the use of supercritical fluids as one of these alternatives.

The first two steps in Figure 1.1 were completed in this work. The third step is to obtain an accurate thermodynamic model and in this work current models were investigated and it can be seen that more work is required in this regard.

The main aim was to determine if fractionation by supercritical fluids is technically feasible. Two main criteria are required to ensure technical feasibility of the fractionation process:

Firstly, from the binary phase diagrams it can be seen that the solvent is able to dissolve a significant amount of paraffin in the vapour phase. Secondly, from the binary phase diagrams, as well as the pressure-carbon number plots, it can be seen that propane will be able to fractionate the paraffins.

These two factors thus indicate that the fractionation process is technically feasible. To test the binary data, pilot plant scale tests need to be done to determine the exact selectivity of the solvent. In addition to the pilot plant tests, an economic evaluation of the process needs to be done to determine the economic viability of the process.

This project has thus provided the initial tools for an alternative process for synthetic wax fractionation.

9.   BIBLIOGRAPHY

1.   (**1985**). <u>UOP Processing Guide.</u>(Address: UOP Inc., Box 5017 Algonquin & Mt. Prospect Roads, Des Plaines, Illinois 60017-5017, USA. Tel: 312-391-2900, Fax: 312-391-2253)

2.   Aalto, M., Liukkonen, S. (**1996**). "Bubble Point Pressures and Densities with Triacontane, Hexatriacontane, Tetraconatane, Pentacontane and Squalene at 353 - 373 K and 4.00 - 7.00 MPa." <u>Journal of Chemical and Engineering Data</u>(41): 79-83

3.   Aalto, M.M., Liukkonen, S.S. (**1998**). "Liquid Densities of Propane + Linear Low-Density Polyethylene Systems at (354 - 378) K and (4.00 - 7.00) MPa." <u>Journal of Chemical and Engineering Data</u> 43: 29-31

4.   Adachi, Y., Lu, B.C., Suige, H. (**1983**). "Three Parameter Equation of State." <u>Fluid Phase Equilibria</u> 13: 133 et seq

5.   Adachi, Y., Sugie, H. (**1986**). "A New Mixing Rule - Modified Conventional Mixing Rule." <u>Fluid Phase Equilibria</u> 28: 103 et seq

6.   Anderko, A. (**1989a**). "Extension of the AEOS model to systems containing any number of associating and inert compounds." <u>Fluid Phase Equilibria</u> 50: 21 et seq

7.   Anderko, A. (**1989b**). "A Simple Equation of State Incorporating Association." <u>Fluid Phase Equilibria</u> 45: 39 et seq

8.   Basta, N., McQueen, S. (**1985**). "Supercritical Fluids: Still Seeking Acceptance." <u>Chemical Engineering</u> February 4: 14-17

9.   Benedict, M., Webb, G.B., Rubin, L.C. (**1940**). "An empirical equation for thermodynamic properties of light hydrocarbons and their mixtures." <u>Journal of Chemical Physics</u> 8: 334-345

10.   Beret, S., Prausnitz, J.M. (**1975**). "Perturbed Hard-Chain Theory: An Equation of State for Fluids Containing Small or Large Molecules." <u>AIChE Journal</u> 21(6): 1123-1132

11.   Bertucco, A., Barolo, M., Elvassore, N. (**1997**). "Thermodynamic Consistency of Vapour-Liquid Equilibrium Data at High Pressure." <u>AIChE Journal</u> 43(2): 547-554

12.   Breman, B.B., Beenackers, A.A.C.M., Rietjies, E.W.J., Stege, R.J.H. (**1994**). "Gas-Liquid Solubilities of Carbon Monoxide, Carbon Dioxide, Hydrogen, Water, 1-Alcohols (1 =< n =< 6), and Paraffins (2 =< n =< 6) in Hexadecane, Octacosane, 1-Hexadecanol, Phenanthrene, and Tetraethylene Glycol at Pressures up to 5.5 MPa

and Temperatures from 293 to 553 K." <u>Journal of Chemical and Engineering Data</u> 39: 647-666

13. Brennecke, J.F., Eckert, C.A. (**1989**). "Phase Equilibria for Supercritical Fluid Process Design." <u>AIChE Journal</u> 35(9): 1409 - 1427

14. Britto, L.J.D., Soares, J.B.P., Penlidis, A., Krukonis, V. (**1999**). "High-Density Polyethylene Fractionation with Supercritical Propane." <u>Journal of Polymer Science: Part B: Polymer Physics</u> 37: 553-560

15. Brunner, G. (**1990**). "Mass Separation with Supercritical Gases (Gas Extraction)." <u>International Chemical Engineering</u> 30(2): 191-205

16. Brunner, G. (**1994**). <u>Gas Extraction: An Introduction to Fundamentals of Supercritical Fluids and the Application to Separation Processes</u>. Darmstadt, Germany, Steinkopff.

17. Carnahan, N.F., Starling, K.E. (**1972**). "Intermolecular Repulsions and the Equation of State." <u>AIChE Journal</u> 18: 1184 et seq.

18. Carnahan, N.F., Startling, K.E. (**1969**). "Equation of State for Nonattracting Rigid Spheres." <u>Journal of Chemical Physics</u> 51: 635 et seq.

19. Chan, A.K.C., Hemmingsen, P.V., Radosz, M. (**2000**). "Fluid-Liquid and Fluid-Solid Transisions of Tetracontane in Propane." <u>Journal of Chemical Engineering Data</u> 45: 362-368

20. Chapman, W.G., Gubbins, K.E., Jackson, G., Radosz, M. (**1989**). <u>Fluid Phase Equilibria</u> 52: 31-38

21. Chapman, W.G., Gubbins, K.E., Jackson, G., Radosz, M. (**1990**). "New reference Equation of State for Associating Liquids." <u>Industrial and Engineering Chemistry Research</u> 29: 1709-1720

22. Chen, S.-H., Chou, Y.-L., Chen, Y.-P. (**1996**). "A New Cubic Simplified Perturbed Hard-Body Equation of State." <u>Fluid Phase Equilibria</u> 118: 201-219

23. Chen, S.S., Kreglewski, A. (**1977**). "Applications of the Augmented van der Waals Theory of Fluids. I. Pure Fluids." <u>Berichte der Bunsen-Gesellshaft, Physical Chemistry</u> 81: 1048-1052

24. Cheng, J., Fan, Y., Zhan, Y. (**1994**). "Supercritical propane Fractionation of Wax Bearing Residue." <u>Separation Science and Technology</u> 29(14): 1779-1787

25. Chou, J.S., Chao, K.-C. (**1992**). "Solubility of Sysnthesis and Product Gases in a Fischer-Tropsch SASOL Wax." <u>Industrial Engineering and Chemistry Research</u> 32: 621-623

26.   Chung, K.H., Xu, C., Hu, Y., Wang, R. (**1997**). "Supercritical Fluid Extraction Reveals Resid Properties." <u>Oil and Gas Journal</u>(20 January): 66-69

27.   Clifford, A.A., Bartle, K.D., Gélébart, I., Zhu, S. (**1998**). "Production of Narrow Fractionsof Polymers using Supercritical Fluids with a Density Program." <u>Polymer</u> 39(24): 6037 - 6040

28.   Clifford, T. (**1999**). <u>Fundamentals of Supercritical Fluids</u>. New York, Oxford University Press.

29.   Cotterman, R.L. (**1985**). <u>Phase Equilibria for Complex Fluid Mixturs at High Pressures. Development and Application of Continuous Thermodynamics</u>. Chemical Engineering. Berkeley, University of California, Berkeley

30.   Crause, J.C. (**2001**). <u>Supercritical Fluid Extraction of Paraffin Wax</u>. Chemical Engineering. Stellenbosch, University of Stellenbosch

31.   Crause, J.C., Nieuwoudt, I. (**2000**). "Fractionation of Paraffin Wax." <u>Industrial and Engineering Chemistry Research</u> 39: 4871-76

32.   de Haan, A.B. (**1991**). <u>Supercritical Fluid Extraction of Liquid Hydrocarbon Mixtures</u>. Faculty of Chemical Technology and Material Science, Delft University of Technology

33.   de Haan, A.B., de Graauw, J. (**1991**). <u>A Process for the Fractionation of Alkanes with Supercritical Carbon Dioxide</u>. 2nd International Symposium on Supercritical Fluids, Boston, Massachusetts, USA.

34.   de Podesta, M. (**1997**). <u>Understanding the Properties of Matter</u>.

35.   Dimitrelis, D., Prausnitz, J.M. (**1989**). "Solubilities of n-Octadecane, Phenanthrene, and n-Octadecane/Phenanthrene Mixtures in Supercritical Propane at 390 and 420 K and Pressures to 60 bar." <u>Journal of Chemical Engineering Data</u> 34: 286-291

36.   Dohrn, R., Brunner, G. (**1995**). "High Pressure Fluid-Phase Equilibria: Experimental Methods and Systems Invesitgated (1988 - 1993)." <u>Fluid Phase Equilibria</u> 106: 213-282

37.   Dohrn, R., Prausnitz, J.M. (**1990**). "A simple preturbation term for he Carnahan Starling equation of state." <u>Fluid Phase Equilibria</u> 61: 53 et seq

38.   Donohue, M.D., Prausnitz, J.M. (**1978**). "Perturbed Hard Chain Mixture: Thermodynamic Properties for Mixtures in Natural Gas and Petroleum Technology." <u>AIChE Journal</u> 24(5): 849 - 860

39.   du Rand, M. (**2000**). <u>High Pressure Fluid Phase Equilibria</u>. Chemical Engineering, University of Stellenbosch

40. du Rand, M., Nieuwoudt, I. (**2001**). "Measurement of Phase Equilibria of Supercritical Carbon Dioxide and Paraffins." <u>Journal of Supercritical Fluids</u> in Press

41. du Rand, M., Nieuwoudt, I. (**2001**). "Measurement of Phase Equilibria of Supercritical Ethane and Paraffins." <u>Journal of Supercritical Fluids</u> in press

42. Dymond, J.H., Smith, E.B. (**1980**). <u>The Virial Coefficients of Pure Gasses and Mixtures: A Critical Compilation</u>. Oxford, Clarendon Press.

43. Eckert, C.A., Knutson, B.L., Debenedetti, P.G. (**1996**). "Supercritical Fluids as Solvents for Chemcial and Material Processing." <u>Nature</u> 383: 313-318

44. Elliot, J.R., Suresh, S.J., Donohue, M.D. (**1990**). "A Simple Equation of State for Non-Spherical and Associating Molecules." <u>Industial and Chemical Engineering Research</u> 29: 1476

45. Fisher, C.H. (**1989**). "How to Predict n-Alkane Densities." <u>Chemical Engineering</u>: 195-196

46. Floeter, E., de Loos, T.W., de Swaan Arons, J. (**1997**). "High pressure solid-fluid and vapour-liquid equilibria in the system (methane + tetracosane)." <u>Fluid Phase Equilibria</u> 127: 129-146

47. Fornari, R.E., Alessi, P., Kikic, I. (**1990**). "High Pressure Fluid Phase Equilibria: Experimental Methods and Systems Investigated (1978 - 1987)." <u>Fluid Phase Equilbria</u> 57: 1-33

48. Fuller, G.G. (**1976**). "A Modified Redlich-Kwong Equation of State for Associating Compounds and Mixtures." <u>Industrial and Engineering Chemistry Research</u> 34: 1897 et seq.

49. Garcia, D.C., Luks, K.D. (**1999**). "Patterns of Solid-Fluid Phase Equilibria: New Possibilities." <u>Fluid Phase Equilibria</u> 161: 91-106

50. Gasem, K.A.M., Bufkin, B.A., Robinson, R.L. (**1989a**). "Solubilities of Ethane in Heavy Normal Paraffins at Pressures to 7.8 MPa and Temperatures from 348 to 423 K." <u>Journal of Chemical and Engineering Data</u> 34: 187-191

51. Gasem, K.A.M., Disckson, K.B., Dulcamara, P.B., Robinson, R.L. (**1989b**). "Equilibrium Phase Compositions, Phase Densities, and Interfacial Tensions for CO_2 + Hydrocarbon Systems. 5. CO_2 + n-Tetradecane." <u>Journal of Chemical Engineering Data</u> 34: 191-195

52. Gasem, K.A.M., Robinson, R.L. (**1990**). "Evaluation of the Simplified-Perturbed-Hard-Chain-Theory (SPHCT) for prediction of phase behaviour of n-paraffins and mixtures of n-paraffins with ethane." <u>Fluid Phase Equilibria</u> 58: 13-33

53. Gasem, K.A.M., Robinson, R.L.J. (**1985**). "Solubilities of Carbon Dioxide in Heavy Normal Paraffins (C20 - C44) at Pressures to 9.6 MPa and Temperatures from 232 - 423 K." Journal of Chemical and Engineering Data 30: 53 - 56

54. Gearhart, J.A., Garwin, L. (**1976**). "ROSE Process Improves Resid Feed." Hydrocarbon Processing 55: 125-128

55. Gregorowicz, J., de Loos, T.W., de Swaan Arons, J. (**1992**). "The System Propane and Eicosane: P, T, and x Measurements in the Temperature Range 288-358." Journal of Chemical Engineering Data 37: 356-358

56. Groß, J., Sadowski, G. (**1999**). Pertuberd-Chain SAFT: A New Equation of State for Chain Melocules. AIChE Annual Meeting, Dallas, Texas, USA.

57. Guggenheim, E.A. (**1965**). "Variations on the van der Waals Equation of State for High Densities." Molecular Physics 9: 199 et seq.

58. Harmens, A., Knapp, H. (**1980**). "Three Parameter Cubic Equation of State for Normal Substances." Industrial and Engineering Chemistry Fundamentals 19: 291 et seq.

59. Hederer, H., Peter, S., Wenzel, H. (**1976**). "Calculation of Thermodynamic Properties from a Modified Redlich-Kwong Equation of State." Chemical Engineering Journal 11: 183 et seq

60. Huang, S.H., Lin, H.-M., Chao, K.-C. (**1988b**). "Solubility of Carbon Dioxide, Methane and Ethane in Octacosane." Journal of Chemical and Engineering Data 33: 143-145

61. Huang, S.H., Lin, H.-M., Tsai, F.-N., Chao, K.-C. (**1988a**). "Solubility of Synthesis Gases in Heavy n-Paraffins and Fisher-Tropsch Wax." Industrial Engineering and Chemistry Research 27: 162-169

62. Huang, S.H., Radosz, M. (**1990**). "Equation of State for Small, Large, Polydisperse and Associating Molecules." Industrial and Engineering Chemistry Research 1990: 2284-2294

63. Huang, S.H., Radosz, M. (**1991**). "Equation of State for Small, Large, Polydisperse and Associating Molecules: Extension to Fluid Mixtures." Industrial and Chemical Engineering Research 30: 1994-2005

64. Hubert, P., Vitzthum, O.G. (**1978**). Angew. Chem. Int. Ed. 17: 731 et seq.(As cited in Williams (1981))

65. Jennings, D.W., Schucker, R.C. (**1994**). Phase Behaviour of Mixtures of Various Supercritical Fluids and Petroleum Fractions. 3rd International Symposium on Supercritical Fluids, Strassbourg, France.

66. Joyce, P.C., Gorden, J., Thies, M.C. (**2000**). "Vapour Liquid Equilibria for the Hexane + Tetracosane and Hexame + Hexatriacontane Systems at Elevated Temperatures and Pressures." <u>Journal of Chemical and Engineering Data</u> 45: 424-427

67. Kim, C.-H., Vimalchand, Donohue, M.D. (**1986**). "Local Composition Model for Chainlike Molecules: A New Simplified Version of the Perturbed Hard Chain Theory." <u>AIChE Journal</u> 32(10): 1726-1734

68. Kiran, E., Levelt Sengers, J.M.H., Eds. (**1994**). <u>Supercritical Fluids: Fundamentals for Application</u>, Kluwer Academic Publisher.

69. Knapp, H., Doering, R., Oellrich, L., Ploecker, U., Prausnitz, J.M., Eds. (**1982**). <u>Vapour-Liquid Equilibria for Mixtures of Low Boiling Substances</u>. Dechema Chemistry Data Series. Frankfurt/Main, Germany, Dechema Deutsche Gesellschaft fuer Chemiesche Apparatewesen.

70. Kohn, P.M., Savage, P.R., McQueen, S. (**1979**). "Supercritical Fluids Try for CPI Applications." <u>Chemical Engineering</u> March 12: 41-43

71. Kontogeogis, G.M., Voutsas, E.C., Yakoumis, I.V., Tassios, D.P. (**1996**). "An Equation of State for Associating Fluids." <u>Industrial and Engineering Chemistry Research</u> 35: 4310 et seq

72. Kubic, W.L. (**1982**). "A Modification of Martin Equation of State for Calculating Vapour-Liquid Equilibria." <u>Industrial and Engineering Chemistry Research</u> 9: 79 et seq

73. Leder, F., Irani, C.A., McHenry, J.A. (**1976**). "Miscibility Considerations in the System Propane-Hexatriacontane." <u>AIChE Journal</u> 22(1): 199-200

74. Lee, K.H., Lombardo, M., Sandler, S.I. (**1985**). "The Generalised Van der Waals Partition Function II: Application to Square Well Fluids." <u>AIChE Journal</u> 1986(32): 10

75. Li, Y.-H., Dillard, K.H., Robinson, R.L. (**1981**). "Vapour-Liquid Phase Equilibrium for Carbon-Dioxide-n-Hexane at 0, 80 and 120 oC." <u>Journal of Chemical and Engineering Data</u> 26: 53 et seq

76. Magoulas, K., Tassios, D. (**1990**). "Thermophysical Properties of n-alkanes from C1 to C20 and the prediction for higher ones." <u>Fluid Phase Equilibria</u> 56: 119=140

77. Marano, J.J., Holder, G.D. (**1997**). "Charaterization of Fischer-Tropsch Liquids for Vapour-Liquid Equilibria Calculations." <u>Fluid Phase Equilibria</u> 138: 1-21

78. Marr, R., Gamse, T. (**2000**). "Use of supercritical fluids for different processes including new developments - a review." <u>Chemical Engineering and Processing</u> 39: 19-28

79. Mathias, P.M., Copeman, T.W. (**1983**). "Extension of the Peng-Robinson Equation of State to Complex Mixtures: Evaluation of the Various Forms of the Local Composition Concept." <u>Fluid Phase Equilibria</u> 13: 91-108

80. Mathias, P.M., Herbert, C.K., Prausnitz, J.M. (**1991**). "Equations-of-State mixing rules for multicomponent mixtures: the problem of invariance." <u>Fluid Phase Equilibria</u> 67: 31-44

81. McHugh, M., Krukonis, V. (**1994**). <u>Supercritical Fluid Extraction</u>, Butterworth-Heinemann.

82. Meilchen, M., Hasch, B.M., McHugh, M.A. (**1990**). <u>High Pressure Phase Behaviour of Copolymer Supercritical Fluid Mixtures</u>. 2nd International Symposium on High Pressure Chemical Engineering, Erlangen, Germany.

83. Melheim, G.A., Saini, R., Leibovici, C.F. (**1991**). <u>On the application of concentration dependent mixing rules to systems containing large numbers of compounds</u>. Second International Symposium on Supercritical Fluids, Boston, MA, USA.

84. Michelsen, M.L., Kistenmacher, H. (**1990**). "On Composition-Dependent Interaction Coefficients." <u>Fluid Phase Equilibria</u> 58: 229-230

85. Mollerup, J. (**1981**). "A Note on Excess Gibbs Energy Models, Equations of State and the Local Composotion Concept." <u>Fluid Phase Equilibria</u> 7: 121-138

86. Morgan, D.L., Kobayashi, R. (**1994**). "Direct vapor pressure measurement of ten n-alkanes in the C10-C28 range." <u>Fluid Phase Equilibria</u> 97: 211-242

87. Nieuwoudt, I. (**1994**). <u>The Fractionation of High Molecular Weight Alkane Mixtures with Supercritical Fluids</u>. Chemical Engineering. Stellenbosch, Univeristy of Stellenbosch

88. Nieuwoudt, I. (**1996**). "Vapour-Liquid Equilibria and Densities for the System Butane + Hexacontane." <u>Journal of Chemical and Engineering Data</u> 41: 1024 - 1027

89. Nieuwoudt, I. (**2001**). <u>Personal Communication</u>

90. Nieuwoudt, I., Crause, M., du Rand, M. (**2001**). "Supercritical Fractionation vs. Competing Processes: An Operating Cost Comparison."

91. Onnes (**1912**). <u>Konink. Akad. Wetens</u>: 273 et seq.(as cited in Walas, 1985)

92. Panagiotopoulos, A.Z., Reid, R.C. (**1985**). "High Pressure Phase Equilibria in Ternary Fluid Mixtures with Supercritical Component." <u>ACS Division of Fuel Chemistry, Preprints</u> 30(3): 46 et seq

93. Patel, N.C., Teja, A.S. (**1982**). "A New Cubic Equation of State for Fluids and Fluid Mixtures." <u>Chemical Engineering Science</u> 37: 463 et seq

94. Peneloux, A., Rauzy, E. (**1982**). "A Consistent Correction for Redlich-Kwong-Soave Volumes." <u>Fluid Phase Equilibria</u> 8: 7-23

95. Peng, C.L., Wang, R.A., Fan, Y.H., Yang, G.H. (**1988**). <u>Phase Equilibria of the Mixture Containing Petroleum Residue and Supercritical Solvent</u>. International Syposium on Supercritical Fluids, Nice, France.

96. Peng, D.Y., Robinson, D.B. (**1976**). "A New Two-Constant Equation of State." <u>Industrial and Engineering Chemistry Fundamentals</u> 15: 59 et seq.

97. Perrut, M. (**1998**). <u>New Challenges for Supercritical Fluids</u>. 3rd Meeting of on Supercritical Fluids: Materials and Natural Products, Nice, France.

98. Perrut, M. (**2000**). "Supercritical Fluid Applications: Industrial Applications and Economic Issues." <u>Industrial and Engineering Chemistry Research</u> 39: 4531-4535

99. Peters, C.J., de Roo, J.L. (**1987b**). "Measurement and Calculations of Phase Equilibria of Binary mixtures of Ethane + Eicosane. Part 1: Vapour + Liquid Equilibira." <u>Fluid Phase Equilibria</u> 34: 287-308

100. Peters, C.J., de Roo, J.L., de Swaan Arons, J. (**1993**). "Phase Equilibria in Binary mixtures of Propane and Hexacontane." <u>Fluid Phase Equilibria</u> 85: 301-312

101. Peters, C.J., de Roo, J.L., J., d.S.A. (**1992**). "Measurement and Calculation of Phase Equilibria in Binary Mixtures of Propane and Tetratriacontane." <u>Fluid Phase Equilibria</u> 72: 251-266

102. Peters, C.J., de Swaan Arons, J., Levelt Sengers, J.M.H., Gallagher, J.S. (**1988a**). "Global phase behaviour of mixtures of short and long n-alkanes." <u>AIChE Journal</u> 34: 834-839

103. Peters, C.J., Florusse, L.j., de Roo, J.L., de Swaan Arons, J., Levelt Sengers, J.M.H. (**1995**). "The princible of congruence and its application to compressible stated." <u>Fluid Phase Equilbria</u> 105: 193-219

104. Peters, C.J., Lichtenthaler, R.N., de Swaan Arons, J. (**1986**). "Three Phase Equilibria in Binary Mixtures of Ethane and Higher n-Alkanes." <u>Fluid Phase Equilibria</u> 29: 495-504

105. Peters, C.J., Speigelaar, J., de Swaan Arons, J. (**1988b**). "Phase Equilibria in Binary Mixtures of Ethane + Docosane and Molar Volumes of Liquid Docosane." Fluid Phase Equilibria 41: 245-256

106. Peters, C.J., Van der Kooi, H.J., De Roo, J.L., De Swaan Arons, J., Gallagher, J.S., Levelt Sengers, J.M.H. (**1989**). "The Search for Tricriticality in Binary Mixtures of Near Critical Propane and Normal Paraffins." Fluid Phase Equilibria 51: 339-351

107. Peters, C.J., Van der Kooi, H.J., de Swaan Arons, J. (**1987a**). "Measurement and Calculations of Phase Equilibria for (ethane+tetracosane) and (p,Vm,T) for Liquid Tetracosane." Journal of Chemical Thermodynamics 19: 395-405

108. Pfennig, A. (**1988**). Zur Entwicklung einer Dreiparametrigen, auf der Genauen Beschreibung des Hartkugelsystems Aufbauenden Zustandsgleichung. Verfahrenstechnik. Aachen, Germany, Rheinisch-Westfälishen Technischen Hochschule Aachen**:** 159

109. Pfohl, O. (**1998**). Messung und Berechnung von Phasengleichgewichten mit nahe-unf überkritischem Kohlendioxid sowie assoziierende Komponenten in Hochdruckbereich. Termishe Verfahrenstechnik II. Hamburg-Harburg, Germany, Technishe Universität Hamburg-Harburg

110. Pfohl, O., Brunner, G. (**1998**). "Use of BACK to Modify SAFTin Order to Enable Density and Phase Equilibrium Calculations Corrected to Gas-Extraction Processes." Industrial and Engineering Chemistry Research 37: 2966 et seq

111. Pfohl, O., Petkov, S., Bunner, G. (**2000**). PE 2000 A powerful Tool to Correlate Phase Equilibria. München, Herbert Utz Verlag.

112. Piacente, V., Fontana, D., Scardala, P. (**1994**). "Enthalpies of Vaporization of a Homologous Series of n-Alkanes Determined from Vapour Pressure Measurements." Journal of Chemical and Engineering Data 39: 231-237

113. Prigogine, I. (**1957**). The Molecular Theory of Solutions. Amsterdam, North Holland Publishing Company.

114. Radosz, M. (**1987a**). "Multiphase Behaviour of Supercritical Fluid Systems: Oil Solutions in Light Hydrocarbon Solvents." Industrial and Engineering Chemistry Research 26: 2134-2139

115. Radosz, M., Cotterman, R.L., Prausnitz, J.M. (**1987b**). "Phase Equilibria in Supercritical Propane Systems for Separation of Continuous Oil Mixtures." Industrial Engineering and Chemistry Research 26: 731-737

116. Radosz, M., Huang, S.H. (**1990**). Phase Behaviour of Supercritical-Fluid Solutions of Polydisperse Oils and Polymers. 2nd Internationa Symposium on High Pressure Chemical Engineering, Erlangen, Germany.

117. Redlich, O., Kwong, J.N.S. (**1949**). "On the Termodynamics of Solutions. V: An Equation of State. Fugasities of Gaseous Solutions." <u>Chem. Rev</u> 44: 233 et seq.(as cited in Smith et al, 1996)

118. Reid, R.C., Prausnitz, J.M. (**1987**). <u>The properties of gasses and liquids</u>, New York, USA, McGraw-Hill.

119. Riazi, H., Al-Sahhaf, T.A. (**1996**). "Physical Properties of Heavy Petroleum Fractions and Crude Oils." <u>Fluid Phase Equilibria</u> 117: 217-224

120. Rowlinson, J.S., Swinton, F.L. (**1982**). <u>Liquids and Liquid Mixtures</u>. Great Brittain, Butterworth & Co.

121. Saito, M., Yamauchi, Y., Okuyama, T., Eds. (**1994**). <u>Fractionation by Packed-Column SFC and SFE: Principles and Applications</u>, VCH Publishers.

122. Sako, T., Wu, A.H., Prausnitz, J.M. (**1989**). "A Cubic Equation of State for High Pressure Phase Equilibria of Mixtures Containing Polymers and Volatile Fluids." <u>Journal of Applied Polymer Science</u> 38: 1839-1858

123. Sandler, S.I., Ed. (**1994**). <u>Models for Thermodynamic and Phase Equilibrium Calculations</u>. New York, Marcel Decker.

124. Schmidt, G., Wenzel, H. (**1980**). "A Modified van der Waals Equation of State." <u>Chemical Engineering Science</u> 35: 1503 et seq

125. Schneider, G., Alwani, Z., Heim, W., Horvath, E., Franck, E.U. (**1967**). "Phasengleichgewichte und kritische Erscheinungen in binaeren Mischsystemen bis 1500 bar. CO2 mit n-Oktan, n-Undecan, n-Tridecan unf n-Hexadecan." <u>Chem. Ing. Techn</u> 39(649 et seq)

126. Schneider, G.M. (**1988**). <u>Thermodynamics of mixtures at high pressures: Basis of supercritical fluid technology</u>. International Symposium on Supercritical Fluids, Nice, France.

127. Schneider, G.M. (**1998**). "High-Pressure Investigations of Fluid Mixtures - Review and Recent Results." <u>Journal of Supercritical Fluids</u> 13: 5-14

128. Schwartzentruber, J., Renon, H. (**1989**). "Development of a New Cubic Equation of State for Phase Equilibrium Calculations." <u>Fluid Phase Equilibria</u> 52: 127 et seq.

129. Scott, R.L. (**1971**). <u>Physical Chemistry: An Advanced Treatise, Volume 8A: Liquid State</u>, American Press, New York.

130. Shi, T.-P., Hu, Y.-X., Xu, Z.-M., Wang, R.-A. (**1997**). "Characterizing Petroleum Vacuum Risidue by Supercritical Fluid Extraction and Fractionation." <u>Industrial and Engineering Chemistry Research</u> 36: 3988-3992

131. Singh, H., Lucien, F.P., Foster, N.R. (**2000**). "Critical Properties for Binary Mixtures of Ethane Containing Low Concentrations of n-Alkanes." <u>Journal of Chemical Engineering Data</u> 45: 131-135

132. Sinnott, R.K. (**1998**). <u>Chemical Engineering Volume 6: Design</u>. Oxford, England, Butterworth-Heinemann.

133. Smith, J.M., Van Ness, H.C., Abbot, M.M. (**1996**). <u>Introductory Chemical Engineering Thermodynamics</u>. New York, USA, McGraw-Hill.

134. Soave, G. (**1972**). "Equilibrium Constans from a Modified Redlich-Kwong Equation of State." <u>Chemical Engineering Science</u> 27: 1197 et seq.

135. Soave, G. (**1993**). "Improving the Treatment of Heavy Hydrocarbons by the SRK Equation of State." <u>Fluid Phase Equilibria</u> 84: 339-342

136. Stenger, H.G., Johnson, H.E., Satterfield, C.N. (**1984**). "Molecular Weight Distribution of the Heavy Wax Fraction from Fischer-Tropsch Synthesis." <u>Journal of Catalysis</u> 86: 447-480

137. Stewart, R.B., Jacobsen, R.T., Penoncello, S.G. (**1986**). <u>Thermodynamic Properties of Refrigerants</u>, American Society of Heating, Refrigerating and Air Conditioning Engineers. Inc.

138. Stryjek, R., Vera, J.H. (**1986a**). "PRSV: An Improved Peng Robinson Equation of State for Pure Components and Mixtures." <u>Canadian Journal of Chemical Engineering</u> 64: 334 et seq.

139. Stryjek, R., Vera, J.H. (**1986b**). <u>An Improved Cubic Equation of State</u>. Equations of State: Theories and Application.

140. Suleiman, D., Eckert, C.A. (**1995a**). "Phase Equilibria of Alkanes in Natural Gas Systems. 1. Alkanes in Methane." <u>Journal of Chemical and Engineering Data</u> 40: 2 - 11

141. Suleiman, D., Eckert, C.A. (**1995b**). "Phase Equilibria of Alkanes in Natural Gas Systems. 2. Alkanes in Ethane." <u>Journal of Chemical Engineering Data</u> 40: 572-577

142. Thiessen (**1885**). <u>Ann. Phys.</u> 24: 467 et seq.(as cited in Walas, 1985)

143. Tobler, F.C. (**1998**). "Correlation of the Density of the Liquid Phase of Pure n-Alkanes with Temperature and Vapour Pressure." <u>Industrial and Engineering Chemistry Research</u> 37: 2565-2570

144. Todd, D.B., Elgin, J.C. (**1955**). "Phase Equilibria in Systems with Ethylene Abive Its Critical Temperature." <u>AIChE Journal</u> 1(1): 20 - 27

145. Travers, M.W., Usher, F.L. (**1906**). "On the Behaviour of Certain Substances at their Critical Temperatures." <u>Proc. Roy. Soc. A.</u> 78: 247-261

146. Trebble, M.A., Bishnoi, P.R. (**1987**). "Extension of the Trebble-Bishnoi Equation of State to Fluid Mixtures." <u>Fluid Phase Equilibria</u> 40: 1 et seq.

147. Tsai, F.N., Huang, S.H., Lin, H.-M., Chao, K.-C. (**1988**). "Solubility of Methane, Ethane and Carbon Dioxide in a Mobil Fischer-Tropsch Wax and in n-Paraffins." <u>The Chemical Engineering Journal</u> 38: 41-46

148. Tsonopoulos, C., Tan, Z. (**1993**). "Critical Constants of Normal Alkanes from Methane to Polyethylene II. Application of Flory Theory." <u>Fluid Phase Equilibria</u> 83: 127-138

149. Twu, C.H. (**1983**). "Prediction of Thermodynamic Properties of Normal Paraffins using only Normal Boiling Point." <u>Fluid Phase Equilibria</u> 11: 65-81

150. Van der Waals, J.D. (**1873**). <u>Over de continuiteit van den gas- en vloeistof-toestand</u>. Leiden, Niederlande, Leiden University.(As cited in Walas, 1981)

151. van Konynenburg, P.H., Scott, R.L. (**1980**). "Critical Lines and Phase Equilibria in Binary van der Waals Mixtures." <u>Phil. Trans. Roy. Soc.</u> 298: 495-540.(As cited in Brunner, 1990)

152. Via, J.C., Braue, C.L., Taylor, L.T. (**1994**). "Supercritical Fluid Fractionation of a Low Molecular Weight, High Density Polyethylene Wax using Carbon Dioxide, Propane and Propane-Modified Carbon Dioxide." <u>Analytical Chemistry</u> 66: 603-609

153. Vladimir Oliviera, J., Dariva, C., Pinto, J.C. (**2000**). "High Pressure Phase Equilibria for Polypropylene - Hydrocarbon Systems." <u>Industrial and Chemical Engineering Research</u> 39: 4627-4633

154. Walas, S.M. (**1985**). <u>Phase Equilibria in Chemical Engineering</u>, Butterworth Publishers.

155. Walsh, J.M., Gubbins, K.E. (**1990**). "A Modified Thermodynamic Perturbation Theory Equation for Molecules with Fused Hard Sphere Cores." <u>Journal of Physical Chemistry</u> 94: 5115-5120

156. Wang, L.-S., Guo, T.-M. (**1993**). "A Cubic Simplified Perturbed Hard-Chain Equation of State for Fluids with Chainlike Molecules." <u>The Canadian Journal of Chemical Engineering</u> 71: 591-604

157. Warth, A. (**1956**). <u>The Chemistry and Technology of Waxes</u>. New York, Reinhold Publishers Corp.

158. Wei, Y.S., Sadus, R.J. (**2000**). "Equations of State for the Calculation of Fluid-Phase Equilibria." <u>AIChE Journal</u> 46(1): 169-196

159. Whiting, W.B., Prausnitz, J.M. (**1981**). <u>Equations of State for Strongly Non-Ideal Mixtures: Application of The Local Composition Concept</u>. Spring National Meeting, American Institute of Chemical Engineering, Houston, Texas, USA.

160. Worthy, W. (**1981**). "Supercritical Fluids Offer Improved Separations." <u>Chemical and Engineering News</u>(August 3): 16-17

161. Yang, G., Wang, R.A. (**1999**). "The supercritical fluid extractive fractionation and the characterisation of heavy oils and petroleum residua." <u>Journal of Petroleum Science and Engineering</u> 22: 47-52

162. Younglove, B.A., Ely, J.F. (**1987**). "Thermophysical Properties of Propane." <u>Journal of Physical and Chemical Reference Data</u> 16(4): 688-721

163. Yu, J.M., Lu, B.C.-Y. (**1987**). "A Three Parameter Equation of State for Asymmetric Mixture Density Calculations." <u>Fluid Phase Equilibria</u> 34: 1 et seq.

164. Zosel, K. (**1978**). <u>Angew. Chem. Int. Ed.</u> 17: 702 et seq.(As in William, 1981)

The following websites were consulted:

165. NIST: <u>http://webbook.nist.gov/chemistry/fluid/</u>

166. Schümann-Sasol: <u>http://www.schuemann-sasol.com/</u>

A.   EXPERIMENTAL DATA

1.   EXPERIMENTAL DATA

Temperature corrections are done according to Appendix C-1. The same temperature corrections are used for all the data points.

Pressure corrections are done according to data in Appendix C-2. Subscripts next to corrected pressures indicate the pressure calibration set used.

Density calculations are done according to the equations in Appendix C-3. Subscripts next to the density indicate the equation used for calculating the density.

1.1.   PROPANE-C32

Table A-1: Experimental Data for Propane – Dotriacontane System

Wax Type				Dotriacontane (nC32)						
Solvent Type				Propane (C3)						
Wax Molar Mass (g/mol)				450.87						
Solvent Molar Mass (g/mol)				44.10						
Mass Wax	Mass Solvent	Total Mass	Mass Fraction	Molar Fraction	Pressure Reading	Piston Position	Correct Pressure	Temp	Density	Side
g	g	g	g/g	mol/mol	bar	mm	bar (abs)	^{o}C	kg/m^3	-
5.38	4.13	9.51	0.566	0.11301	45.7	19.6	47.1 ^{2}	106.2	579 ^{c}	Liq
					57.2	21.1	58.1 ^{2}	120.6	566 ^{c}	Liq
					69.6	21.0	70.0 ^{2}	135.1	567 ^{c}	Liq
5.38	5.15	10.53	0.511	0.09270	48.6	26.2	50.0 ^{2}	106.0	581 ^{c}	Liq
					62.1	26.5	63.0 ^{2}	120.5	579 ^{c}	Liq
					76.8	27.3	77.2 ^{2}	134.7	572 ^{c}	Liq

Table A-1 continued

Mass Wax	Mass Solvent	Total Mass	Mass Fraction	Molar Fraction	Pressure Reading	Piston Position	Correct Pressure	Temp	Density	Side
g	g	g	g/g	mol/mol	bar	mm	bar (abs)	°C	kg/m³	-
5.38	6.55	11.93	0.451	0.07436	49.9	32.4	51.3 [2]	106.4	605 [c]	Liq
					64.8	32.6	65.6 [2]	121.0	603 [c]	Liq
					81.3	33.7	81.6 [2]	135.4	595 [c]	Liq
5.38	7.10	12.48	0.431	0.06900	51.3	38.2	52.7 [2]	106.2	588 [c]	Liq
					67.9	38.7	68.7 [2]	120.7	585 [c]	Liq
					84.6	39.6	84.9 [2]	135.3	578 [c]	Liq
5.38	8.73	14.11	0.381	0.05685	52.5	49.2	53.9 [2]	106.0	587 [c]	Liq
					70.3	50.5	71.1 [2]	120.3	579 [c]	Liq
					87.8	51.9	88.1 [2]	135.0	570 [c]	Liq
5.38	11.66	17.04	0.316	0.04318	54.4	66.2	55.8 [2]	106.0	599 [c]	Liq
					72.6	69.0	73.4 [2]	120.2	584 [c]	Liq
					90.2	71.5	90.5 [2]	135.0	572 [c]	Liq
2.06	5.44	7.50	0.275	0.03571	56.5	16.8	57.9 [2]	105.9	478 [c]	Liq
					75.0	17.0	75.8 [2]	120.3	476 [c]	Liq
					92.1	17.5	92.4 [2]	134.6	472 [c]	Liq
2.06	7.31	9.37	0.220	0.02682	55.8	28.9	57.2 [2]	104.5	498 [c]	Liq
					74.5	30.4	75.4 [2]	118.9	488 [c]	Liq
					91.4	32.1	91.8 [2]	134.1	477 [c]	Liq
2.06	12.12	14.18	0.145	0.01635	54.9	65.4	56.3 [2]	104.6	502 [c]	Liq
					72.8	67.3	73.7 [2]	119.0	494 [c]	Vap
					89.0	67.4	89.4 [2]	133.6	493 [c]	Vap
0.972	9.65	10.62	0.0915	0.009755	55.7	49.9	57.1 [2]	106.0	438 [c]	Vap
					73.1	51.0	73.7 [2]	120.4	433 [c]	Vap
					88.9	49.8	89.2 [2]	134.8	439 [c]	Vap
0.510	9.00	9.51	0.0536	0.005512	55.3	51.9	56.7 [2]	106.2	384 [c]	Vap
					71.7	55.2	72.3 [2]	120.7	371 [c]	Vap
					85.9	58.0	86.2 [2]	135.2	361 [c]	Vap
0.340	11.53	11.87	0.0286	0.002876	50.2	70.9	52.3 [2]	103.5	400 [c]	Vap
					64.3	75.5	66.4 [2]	117.2	385 [c]	Vap
					76.9	81.9	79.0 [2]	134.8	365 [c]	Vap

Table A-1 continued

Mass Wax	Mass Solvent	Total Mass	Mass Fraction	Molar Fraction	Pressure Reading	Piston Position	Correct Pressure	Temp	Density	Side
g	g	g	g/g	mol/mol	bar	mm	bar (abs)	^{o}C	kg/m^3	-
0.377	9.02	9.40	0.0401	0.004071	57.6	56.4	53.4 [4]	105.9	363 [c]	Vap
					72.8	57.7	68.5 [4]	120.5	358 [c]	Vap
					86.7	58.5	82.2 [4]	135.0	355 [c]	Vap
0.446	9.98	10.43	0.0428	0.004352	52.2	58.2	54.3 [4]	106.2	395 [c]	Vap
					68.0	60.2	70.1 [4]	120.8	388 [c]	Vap
					81.7	62.8	83.8 [4]	134.3	378 [c]	Vap
0.196	9.62	9.82	0.0200	0.001989	56.2	70.4	52.0 [4]	105.4	333 [c]	Vap
					68.4	74.7	64.1 [4]	119.6	321 [c]	Vap
					81.3	68.0	76.9 [4]	134.4	340 [c]	Vap
0.168	11.01	11.18	0.0150	0.001490	49.3	72.3	51.4 [4]	106.3	373 [c]	Vap
					62.6	77.6	64.7 [4]	120.7	356 [c]	Vap
					72.3	86.0	74.4 [4]	134.7	333 [c]	Vap

1.2.   PROPANE-C36

Table A-2: Experimental Data for Propane – Hexatriacontane System

Wax Type				Hexatriacontane (nC36)						
Solvent Type				Propane (C3)						
Wax Molar Mass (g/mol)				506.97						
Solvent Molar Mass (g/mol)				44.10						
Mass Wax	Mass Solvent	Total Mass	Mass Fraction	Molar Fraction	Pressure Reading	Piston Position	Correct Pressure	Temp	Density	Side
g	g	g	g/g	mol/mol	bar	mm	bar (abs)	^{o}C	kg/m^3	-
8.92	6.56	15.48	0.576	0.106	41.7	34.9	43.2 [2]	103.9	781 [b]	Liq
					52.2	35.2	53.2 [2]	117.7	778 [b]	Liq
					63.9	36.6	64.4 [2]	131.8	764 [b]	Liq
8.45	9.44	17.89	0.472	0.0722	48.1	54.6	49.6 [2]	103.9	719 [b]	Liq
					64.4	55.8	65.3 [2]	118.3	709 [b]	Liq
					80.8	57.2	81.2 [2]	132.0	699 [b]	Liq

Table A-2 Continued

Mass Wax	Mass Solvent	Total Mass	Mass Fraction	Molar Fraction	Pressure Reading	Piston Position	Correct Pressure	Temp	Density	Side
g	g	g	g/g	mol/mol	bar	mm	bar (abs)	^{o}C	kg/m^3	-
					53.8	38.6	55.2 [2]	103.9	578 [b]	Liq
					73.6	40.3	74.5 [2]	118.1	566 [b]	Liq
4.54	7.47	12.01	0.378	0.0502	91.3	42.0	91.7 [2]	131.9	554 [b]	Liq
					57.8	53.8	59.2 [2]	104.1	563 [b]	Liq
					76.7	56.6	77.6 [2]	118.3	547 [b]	Liq
3.74	10.16	13.90	0.269	0.0310	95.4	58.5	95.8 [2]	132.3	536 [b]	Liq
					57.9	44.5	59.3 [2]	104.1	489 [b]	Liq
					77.4	44.5	78.3 [2]	118.5	488 [b]	Liq
2.20	8.69	10.89	0.202	0.0215	94.2	46.4	94.6 [2]	132.6	478 [b]	Liq
					65.5	40.0	61.2 [3]	106.1	452 [c]	Vap
					84.9	41.5	80.5 [3]	120.5	444 [c]	Vap
1.48	8.32	9.80	0.151	0.0152	101.9	40.0	97.4 [3]	135.0	452 [c]	Vap
					56.2	62.8	57.6 [2]	103.4	488 [b]	Vap
					74.4	66.4	75.3 [2]	117.4	472 [b]	Vap
1.30	11.88	13.18	0.0986	0.00943	91.3	66.4	91.7 [2]	131.3	472 [b]	Vap
					54.6	48.7	56.7 [2]	104.2	445 [b]	Vap
					75.2	50.1	77.3 [2]	120.1	438 [b]	Vap
0.762	9.88	10.64	0.0716	0.00666	90.7	52.8	92.8 [2]	133.9	426 [b]	Vap
					62.3	56.5	58.1 [3]	106.0	408 [c]	Vap
					80.1	57.9	75.7 [3]	120.5	402 [c]	Vap
0.676	9.90	10.58	0.0639	0.00590	95.2	54.8	90.7 [3]	135.1	415 [c]	Vap
					55.3	47.3	57.4 [4]	106.7	444 [c]	Vap
					71.9	50.1	74.0 [4]	120.6	430 [c]	Vap
0.444	10.01	10.45	0.0425	0.00384	83.3	52.0	85.4 [4]	131.2	422 [c]	Vap
					59.3	58.3	55.1 [3]	106.4	369 [c]	Vap
					74.8	60.0	70.5 [3]	120.8	363 [c]	Vap
0.248	9.49	9.74	0.0255	0.00227	88.7	59.5	84.2 [3]	135.3	365 [c]	Vap
					57.0	67.9	52.8 [3]	105.1	352 [c]	Vap
					71.4	69.1	67.1 [3]	119.4	348 [c]	Vap
0.153	10.01	10.16	0.0151	0.00133	85.3	63.9	80.8 [3]	134.0	365 [c]	Vap

1.3. PROPANE-C38

Table A-3: Experimental Data for Propane – Octatriacontane System

Wax Type				Octatriacontane (nC38)						
Solvent Type				Propane (C3)						
Wax Molar Mass (g/mol)				535.04						
Solvent Molar Mass (g/mol)				44.10						
Mass Wax	Mass Solvent	Total Mass	Mass Fraction	Molar Fraction	Pressure Reading	Piston Position	Correct Pressure	Temp	Density	Side
g	g	g	g/g	mol/mol	bar	mm	bar (abs)	^{o}C	kg/m3	-
4.86	3.71	8.57	0.567	0.09744	46.9	11.4	47.5 [2]	106.5	622 [b]	Liq
					60.4	11.9	61.2 [2]	121.3	617 [b]	Liq
					73.6	12.4	74.0 [2]	135.7	611 [b]	Liq
4.86	4.75	9.61	0.506	0.07777	49.7	18.5	51.1 [2]	106.3	616 [b]	Liq
					66.5	19.0	67.3 [2]	121.0	611 [b]	Liq
					83.6	19.8	83.9 [2]	135.7	603 [b]	Liq
4.86	5.91	10.77	0.451	0.06347	54.3	26.4	55.7 [2]	106.3	611 [b]	Liq
					73.5	27.6	74.3 [2]	121.0	600 [b]	Liq
					91.8	28.3	92.1 [2]	135.5	594 [b]	Liq
4.86	7.68	12.54	0.388	0.04957	59.6	38.8	60.9 [2]	106.9	602 [b]	Liq
					79.7	40.3	80.5 [2]	121.3	591 [b]	Liq
					98.1	41.7	98.4 [2]	135.7	581 [b]	Liq
4.86	10.21	15.07	0.322	0.03775	61.8	52.1	63.1 [2]	106.6	621 [b]	Liq
					82.0	54.2	82.8 [2]	121.1	608 [b]	Liq
					100.1	56.2	100.4 [2]	135.6	595 [b]	Liq
4.86	11.61	16.47	0.295	0.03335	62.0	55.7	63.3 [2]	106.3	654 [b]	Liq
					81.9	57.7	82.7 [2]	120.7	641 [b]	Liq
					100.2	59.5	100.5 [2]	136.3	629 [b]	Liq
1.79	5.56	7.35	0.244	0.02585	63.3	15.8	64.6 [2]	107.0	493 [b]	Liq
					83.3	16.7	84.1 [2]	121.4	486 [b]	Liq
					101.4	17.7	101.7 [2]	136.0	477 [b]	Liq
2.09	7.45	9.54	0.219	0.02257	62.5	-	64.6 [5]	106.8	-	Liq
					81.8	-	82.2 [5]	120.8	-	Liq
					100.8	-	101.7 [5]	135.8	-	Liq

Table A3 Continued

Mass Wax	Mass Solvent	Total Mass	Mass Fraction	Molar Fraction	Pressure Reading	Piston Position	Correct Pressure	Temp	Density	Side
g	g	g	g/g	mol/mol	bar	mm	bar (abs)	°C	kg/m3	-
1.81	7.17	8.98	0.202	0.02038	63.8	15.1	65.1[2]	107.1	610[b]	Liq
					83.6	16.5	84.4[2]	121.5	595[b]	Liq
					101.4	18.0	101.7[2]	136.0	580[b]	Liq
1.79	8.77	10.56	0.170	0.01654	63.3	43.1	64.6[2]	106.6	481[b]	Liq
					82.9	44.8	83.7[2]	121.1	472[b]	Liq
					100.5	45.9	100.8[2]	135.8	466[b]	Liq
0.718	6.54	7.26	0.0989	0.00897	60.4	-	62.3[5]	106.5	-	Vap
					79.9	-	80.6[5]	121.5	-	Vap
					97.9	-	98.9[5]	136.9	-	Vap
1.195	11.41	12.61	0.0948	0.008558	61.2	61.3	62.5[2]	106.6	464[c]	Vap
					80.3	63.7	81.1[2]	121.1	454[c]	Vap
					97.4	66.0	97.7[2]	135.6	444[c]	Vap
0.724	10.60	11.32	0.0639	0.005598	58.8	58.7	60.2[2]	105.5	427[c]	Vap
					77.4	61.1	78.2[2]	120.1	418[c]	Vap
					93.6	62.7	93.9[2]	135.0	411[c]	Vap
0.393	11.82	12.21	0.0322	0.002733	55.7	65.0	57.1[2]	105.5	434[c]	Vap
					71.9	68.8	72.5[2]	119.9	420[c]	Vap
					86.6	73.4	87.0[2]	134.6	403[c]	Vap
0.156	10.29	10.45	0.0149	0.001248	52.9	65.6	54.3[2]	106.0	369[c]	Vap
					68.6	63.4	69.4[2]	120.5	377[c]	Vap
					83.3	62.2	83.6[2]	136.6	381[c]	Vap

1.4. PROPANE-C40

Table A-4: Experimental Data for Propane – Tetracontane System

Wax Type				Tetracontane (nC40)						
Solvent Type				Propane (C3)						
Wax Molar Mass (g/mol)				563.08						
Solvent Molar Mass (g/mol)				44.10						
Mass Wax	Mass Solvent	Total Mass	Mass Fraction	Molar Fraction	Pressure Reading	Piston Position	Correct Pressure	Temp	Density	Side
g	g	g	g/g	mol/mol	bar	mm	bar (abs)	^{o}C	kg/m3	-
4.89	3.99	8.88	0.551	0.08027	50.8	15.5	52.2 [2]	105.1	578 [c]	Liq
					65.2	16.2	66.1 [2]	119.6	571 [c]	Liq
					81.1	17.6	81.5 [2]	134.0	558 [c]	Liq
4.89	4.91	9.80	0.499	0.06623	55.8	23.1	57.2 [2]	105.9	566 [c]	Liq
					74.4	23.7	75.2 [2]	120.4	561 [c]	Liq
					92.1	24.6	92.4 [2]	134.8	553 [c]	Liq
4.89	6.24	11.13	0.439	0.05286	61.0	31.2	62.3 [2]	106.3	573 [c]	Liq
					81.9	32.2	82.7 [2]	120.9	566 [c]	Liq
					100.2	33.2	100.5 [2]	135.1	559 [c]	Liq
3.29	4.90	8.19	0.402	0.04563	58.2	15.9	60.3 [4]	105.4	529 [c]	Liq
					78.5	16.6	80.6 [4]	119.8	523 [c]	Liq
					96.7	17.4	98.8 [4]	133.7	517 [c]	Liq
4.89	8.10	12.99	0.376	0.04122	64.3	44.3	65.6 [2]	105.8	570 [c]	Liq
					85.6	45.9	86.4 [2]	120.3	560 [c]	Liq
					104.6	47.2	104.9 [2]	134.9	552 [c]	Liq
3.29	6.49	9.78	0.336	0.03484	60.5	22.6	62.6 [4]	103.8	569 [c]	Liq
					81.1	23.4	83.2 [4]	117.4	562 [c]	Liq
					99.9	23.9	102.0 [4]	131.4	558 [c]	Liq
4.89	10.93	15.82	0.309	0.03088	67.7	58.9	69.0 [2]	105.6	596 [c]	Liq
					87.1	60.8	87.9 [2]	119.1	585 [c]	Liq
					106.8	63.3	107.1 [2]	134.5	571 [c]	Liq
2.02	5.46	7.48	0.270	0.02567	69.7	19.6	71.0 [2]	106.0	455 [c]	Liq
					90.0	20.7	90.8 [2]	120.7	448 [c]	Liq
					108.5	21.7	108.8 [2]	135.0	441 [c]	Liq

Table A-4 Continued

Mass Wax	Mass Solvent	Total Mass	Mass Fraction	Molar Fraction	Pressure Reading	Piston Position	Correct Pressure	Temp	Density	Side
g	g	g	g/g	mol/mol	bar	mm	bar (abs)	^{o}C	kg/m3	-
3.29	6.49	9.78	0.264	0.02497	64.8	47.4	66.9 [4]	105.0	527 [c]	Liq
					85.5	49.5	87.6 [4]	119.2	516 [c]	Liq
					103.8	51.5	105.9 [4]	133.1	505 [c]	Liq
2.02	6.25	8.27	0.244	0.022499	69.6	19.2	70.8 [2]	106.0	507 [c]	Liq
					90.2	19.7	90.9 [2]	120.4	503 [c]	Liq
					108.5	20.6	108.8 [2]	134.7	496 [c]	Liq
3.29	10.95	14.24	0.231	0.02095	63.5	60.0	65.6 [4]	102.5	531 [c]	Cri
					83.7	63.6	85.8 [4]	115.7	513 [c]	Cri
					100.5	64.7	102.6 [4]	129.6	508 [c]	Cri
2.02	7.93	9.95	0.203	0.01782	70.2	37.8	71.5 [2]	106.9	471 [c]	Cri
					90.2	39.6	90.9 [2]	121.4	461 [c]	Cri
					108.6	41.2	108.9 [2]	135.8	452 [c]	Cri
1.892	9.54	11.43	0.166	0.01393	61.8	49.3	63.8 [5]	105.8	475 [c]	Vap
					89.7	52.4	91.0 [5]	125.8	460 [c]	Vap
					98.0	51.9	99.1 [5]	132.4	462 [c]	Vap
1.766	9.55	11.32	0.156	0.01300	60.8	47.0	63.8 [6]	105.4	482 [c]	Vap
					74.4	48.0	77.1 [6]	113.9	477 [c]	Vap
					100.9	50.2	103.0 [6]	135.4	465 [c]	Vap
1.363	9.54	10.90	0.154	0.01276	64.1	34.3	67.1 [6]	107.0	439 [c]	Vap
					82.8	35.6	85.3 [6]	120.6	432 [c]	Vap
					98.2	36.6	100.6 [6]	132.1	426 [c]	Vap
2.02	12.81	14.83	0.136	0.01111	67.6	73.3	68.9 [2]	105.3	490 [c]	Vap
					87.1	76.7	87.9 [2]	119.5	476 [c]	Vap
					104.9	79.7	105.3 [2]	133.6	465 [c]	Vap
1.456	10.41	11.87	0.123	0.009862	63.8	50.6	65.9 [4]	104.6	486 [c]	Vap
					83.8	51.8	85.9 [4]	118.8	480 [c]	Vap
					101.2	52.0	103.3 [4]	133.2	479 [c]	Vap
1.005	9.93	10.94	0.0919	0.007156	68.6	48.8	64.4 [3]	104.3	457 [c]	Vap
					86.3	51.3	81.9 [3]	118.7	445 [c]	Vap
					103.3	49.9	98.8 [3]	133.5	451 [c]	Vap

Table A-4 Continued

Mass Wax	Mass Solvent	Total Mass	Mass Fraction	Molar Fraction	Pressure Reading	Piston Position	Correct Pressure	Temp	Density	Side
g	g	g	g/g	mol/mol	bar	mm	bar (abs)	°C	kg/m3	-
0.731	8.99	9.72	0.0752	0.005757	62.4	47.7	65.3 [6]	108.2	411 [c]	Vap
					81.1	50.0	83.6 [6]	122.6	401 [c]	Vap
					97.5	47.0	99.6 [6]	137.3	414 [c]	Vap
0.685	10.62	11.31	0.0606	0.004572	60.2	45.8	62.3 [4]	105.3	488 [c]	Vap
					79.2	46.4	81.3 [4]	119.5	485 [c]	Vap
					95.3	45.7	97.4 [4]	133.8	488 [c]	Vap
0.536	8.61	9.15	0.0586	0.004414	65.8	40.9	61.5 [3]	106.5	417 [c]	Vap
					84.4	42.5	80.0 [3]	120.9	410 [c]	Vap
					100.6	43.1	96.2 [3]	135.4	407 [c]	Vap
0.422	10.90	11.32	0.0373	0.002750	54.2	57.7	56.3 [4]	104.3	431 [c]	Vap
					74.5	61.1	76.6 [4]	120.3	417 [c]	Vap
					89.8	67.0	91.9 [4]	135.1	395 [c]	Vap
0.266	10.43	10.70	0.0249	0.001813	60.4	62.7	56.2 [3]	105.5	388 [c]	Vap
					76.3	64.9	72.0 [3]	119.8	381 [c]	Vap
					90.3	59.9	85.8 [3]	134.5	399 [c]	Vap
0.247	11.14	11.39	0.0217	0.001577	53.9	64.0	56.0 [4]	104.9	409 [c]	Vap
					69.8	64.0	71.9 [4]	119.4	409 [c]	Vap
					84.0	68.2	86.1 [4]	133.7	393 [c]	Vap
0.141	9.38	9.52	0.0148	0.001069	57.4	60.8	53.2 [3]	104.6	352 [c]	Vap
					73.6	59.3	69.3 [3]	118.9	357 [c]	Vap
					84.4	59.0	79.9 [3]	133.3	358 [c]	Vap

1.5.   PROPANE-C44

Table A-5: Experimental Data for Propane – Tetratetracontane System

Wax Type				Tetratetracontane (nC44)						
Solvent Type				Propane (C3)						
Wax Molar Mass (g/mol)				619.19						
Solvent Molar Mass (g/mol)				44.10						
Mass Wax	Mass Solvent	Total Mass	Mass Fraction	Molar Fraction	Pressure Reading	Piston Position	Correct Pressure	Temp	Density	Side
g	g	g	g/g	mol/mol	bar	mm	bar (abs)	^{o}C	kg/m3	-
5.13	4.33	9.46	0.542	0.0778	61.7	18.8	54.7 [4]	106.6	583 [c]	Liq
					78.9	19.4	71.8 [4]	121.1	578 [c]	Liq
					96.4	19.4	89.3 [4]	135.5	578 [c]	Liq
5.13	5.54	10.67	0.481	0.0619	68.1	26.5	58.0 [4]	106.5	586 [c]	Liq
					88.0	27.2	77.8 [4]	120.9	580 [c]	Liq
					107.6	26.2	97.3 [4]	135.8	589 [c]	Liq
5.13	7.13	12.26	0.418	0.0487	69.8	35.0	66.7 [4]	107.1	601 [c]	Liq
					91.0	35.9	87.8 [4]	121.7	594 [c]	Liq
					110.4	34.6	107.1 [4]	136.6	604 [c]	Liq
3.27	5.55	8.82	0.371	0.0403	67.8	24.0	69.9 [4]	104.9	502 [c]	Liq
					88.3	24.9	90.4 [4]	118.6	496 [c]	Liq
					108.4	26.3	110.5 [4]	133.6	486 [c]	Liq
3.27	5.97	9.24	0.354	0.0375	68.6	24.2	70.7 [4]	105.3	525 [c]	Liq
					89.8	25.3	91.9 [4]	119.1	516 [c]	Liq
					108.3	25.8	110.4 [4]	132.9	513 [c]	Liq
3.27	7.20	10.47	0.312	0.0313	69.4	34.0	71.5 [4]	105.2	520 [c]	Liq
					91.0	34.2	93.1 [4]	119.6	519 [c]	Liq
					109.0	35.2	111.1 [4]	135.0	512 [c]	Liq
3.27	7.69	10.96	0.298	0.0294	69.4	39.3	71.5 [4]	104.4	510 [c]	Liq
					90.2	40.9	92.3 [4]	118.6	500 [c]	Liq
					109.2	42.4	111.3 [4]	132.9	491 [c]	Liq
3.27	10.17	13.44	0.243	0.0224	71.3	50.4	73.4 [4]	105.2	552 [c]	Liq
					92.0	52.5	94.1 [4]	119.3	540 [c]	Liq
					110.7	54.6	112.8 [4]	133.7	528 [c]	Liq

Table A-5 Continued

Mass Wax	Mass Solvent	Total Mass	Mass Fraction	Molar Fraction	Pressure Reading	Piston Position	Correct Pressure	Temp	Density	Side
g	g	g	g/g	mol/mol	bar	mm	bar (abs)	^{o}C	kg/m3	-
3.27	14.29	17.56	0.186	0.0160	71.5	80.5	73.6 [4]	105.4	547 [c]	Liq
					90.9	83.4	93.0 [4]	119.0	534 [c]	Liq
					108.7	86.5	110.8 [4]	133.3	522 [c]	Vap
1.219	8.13	9.35	0.130	0.0106	69.3	34.9	71.4 [4]	105.9	459 [c]	Vap
					90.1	36.7	92.2 [4]	120.2	449 [c]	Vap
					108.1	38.5	110.2 [4]	134.8	439 [c]	Vap
0.761	8.67	9.43	0.0807	0.00621	66.4	40.5	68.5 [4]	106.2	432 [c]	Vap
					86.5	42.7	88.6 [4]	120.4	421 [c]	Vap
					104.0	44.6	106.1 [4]	134.9	412 [c]	Vap
0.509	8.69	9.20	0.0553	0.00415	63.5	40.7	65.6 [4]	105.4	421 [c]	Vap
					83.7	42.4	85.8 [4]	119.4	413 [c]	Vap
					99.8	44.4	101.9 [4]	133.5	403 [c]	Vap
0.499	9.39	9.89	0.0505	0.00377	62.5	-	65.5 [6]	106.8	-	Vap
					81.1	-	83.6 [6]	120.4	-	Vap
					98.3	-	100.4 [6]	135.8	-	Vap
0.363	8.28	8.64	0.0420	0.00311	60.5	35.8	62.6 [4]	106.3	420 [c]	Vap
					80.3	35.8	82.4 [4]	121.1	420 [c]	Vap
					100.2	35.3	102.3 [4]	139.0	422 [c]	Vap
0.235	8.97	9.21	0.0255	0.00186	58.1	45.7	60.2 [4]	105.4	398 [c]	Vap
					74.9	48.2	77.0 [4]	119.6	387 [c]	Vap
					91.2	50.2	93.3 [4]	134.1	379 [c]	Vap
0.102	6.88	6.982	0.0146	0.00105	56.1	24.5	58.2 [4]	104.9	395 [c]	Vap
					71.8	21.6	73.9 [4]	119.3	412 [c]	Vap
					83.3	16.9	85.4 [4]	133.8	444 [c]	Vap

1.6. PROPANE-C46

Table A-6: Experimental Data for Propane – Hexatetracontane System

Wax Type				Hexatetracontane (nC46)						
Solvent Type				Propane (C3)						
Wax Molar Mass (g/mol)				647.24						
Solvent Molar Mass (g/mol)				44.10						
Mass	Mass	Total	Mass	Molar	Pressure	Piston	Correct	Temp	Density	Side
Wax	Solvent	Mass	Fraction	Fraction	Reading	Position	Pressure			
g	g	g	g/g	mol/mol	bar	mm	bar (abs)	°C	kg/m³	-
					55.3	19.9	56.7 [2]	106.0	660 [b]	Liq
					75.6	21.0	76.4 [2]	120.5	649 [b]	Liq
5.10	5.44	10.54	0.484	0.0600	95.1	21.7	95.4 [2]	135.0	642 [b]	Liq
					63.9	26.7	65.2 [2]	106.0	648 [b]	Liq
					84.9	27.4	85.7 [2]	120.6	641 [b]	Liq
5.10	6.38	11.48	0.444	0.0516	104.0	28.0	104.3 [2]	135.0	636 [b]	Liq
					72.9	48.0	74.2 [2]	106.3	607 [b]	Liq
					93.6	49.4	94.3 [2]	120.9	597 [b]	Liq
5.10	8.98	14.08	0.362	0.0373	112.7	51.4	113.0 [2]	135.4	585 [b]	Liq
					74.6	67.2	75.9 [2]	106.2	593 [b]	Liq
					95.0	69.7	95.7 [2]	120.8	580 [b]	Liq
5.10	11.60	16.70	0.305	0.0291	113.8	71.5	114.1 [2]	135.2	571 [b]	Liq
					74.0	27.0	75.3 [2]	105.4	551 [b]	Liq
					95.1	27.7	95.9 [2]	119.9	546 [b]	Liq
2.69	7.12	9.81	0.274	0.0251	114.1	28.3	114.4 [2]	134.4	541 [b]	Liq
					70.5	33.7	73.7 [2]	102.6	499.7 [b]	Cri
					95.1	35.3	97.6 [2]	120.6	489.4 [b]	Cri
2.32	7.43	9.75	0.238	0.0209	109.0	35.7	111.3 [2]	131.3	486.8 [b]	Cri
					74.7	52.7	76.0 [2]	105.8	552 [b]	Cri
					95.7	54.7	96.5 [2]	120.3	541 [b]	Cri
2.69	10.79	13.48	0.200	0.0167	114.2	56.7	114.5 [2]	134.8	530 [b]	Cri
					72.3	33.3	75.3 [6]	106.9	488.3 [c]	Vap
					94.9	35.0	97.4 [6]	122.2	477.5 [c]	Vap
1.51	7.97	9.48	0.159	0.0128	113.4	35.9	115.5 [6]	136.6	472.0 [c]	Vap

Table A-6 Continued

Mass Wax g	Mass Solvent g	Total Mass g	Mass Fraction g/g	Molar Fraction mol/mol	Pressure Reading bar	Piston Position mm	Correct Pressure bar (abs)	Temp °C	Density kg/m³	Side -
					72.0	53.3	73.3 [2]	106.4	541 [b]	Vap
					92.6	54.9	93.3 [2]	121.1	532 [b]	Vap
1.56	11.74	13.30	0.117	0.00897	110.6	56.5	110.9 [2]	135.7	524 [b]	Vap
					71.8	36.4	74.8 [6]	106.9	460.4 [c]	Vap
					91.7	38.2	94.1 [6]	121.2	450.0 [c]	Vap
0.93	8.38	9.31	0.0996	0.00748	110.1	36.6	112.2 [6]	136.6	459.2 [c]	Vap
					69.0	44.9	71.1 [4]	105.0	435 [c]	Vap
					90.7	47.0	92.8 [4]	120.1	425 [c]	Vap
0.789	9.20	9.99	0.0790	0.00581	108.1	48.8	110.2 [4]	134.1	417 [c]	Vap
					68.6	38.8	70.2 [4]	105.9	412 [c]	Vap
					88.1	42.4	89.7 [4]	120.3	394 [c]	Vap
0.626	8.17	8.80	0.0712	0.00519	106.2	44.0	107.8 [4]	134.5	387 [c]	Vap
					66.3	57.7	67.6 [2]	106.0	474 [b]	Vap
					85.7	58.1	86.4 [2]	120.6	472 [b]	Vap
0.646	11.53	12.18	0.0531	0.00380	102.9	58.2	103.2 [2]	135.4	471 [b]	Vap
					62.2	54.2	64.3 [4]	106.3	399 [c]	Vap
					82.5	57.0	84.6 [4]	121.1	388 [c]	Vap
0.401	9.72	10.12	0.0396	0.00280	99.0	60.2	101.1 [4]	135.2	376 [c]	Vap
					62.3	48.1	65.3 [6]	107.0	419.8 [c]	Vap
					80.3	50.7	82.8 [6]	121.2	408.1 [c]	Vap
0.374	9.38	9.75	0.0383	0.00271	94.7	53.1	96.9 [6]	134.5	397.8 [c]	Vap
					59.2	36.3	60.5 [2]	105.9	410 [b]	Vap
					76.6	36.5	77.4 [2]	120.4	409 [b]	Vap
0.174	8.11	8.28	0.0210	0.00146	92.1	37.1	92.4 [2]	135.1	406 [b]	Vap
					58.0	54.2	59.3 [4]	106.1	392 [c]	Vap
					75.6	53.1	76.4 [4]	120.6	396 [c]	Vap
0.149	9.78	9.93	0.0150	0.00104	88.9	56.5	89.2 [4]	134.9	383 [c]	Vap

1.7.   PROPANE-C54

Table A-7: Experimental Data for Propane – Tetrapentacontane System

Wax Type					Tetrapentacontane (nC54)					
Solvent Type					Propane (C3)					
Molar Mass Wax					759.45					
Molar Mass Solvent					44.10					
Mass	Mass	Total	Mass	Molar	Pressure	Piston	Correct	Temp	Density	Side
Wax	Solvent	Mass	Fraction	Fraction	Reading	Position	Pressure			
g	g	g	g/g	mol/mol	bar	mm	bar (abs)	^{o}C	kg/m^3	-
					72.6	15.7	74.7 [4]	105.3	560 [c]	Liq
					94.2	16.4	96.3 [4]	119.5	553 [c]	Liq
3.91	4.72	8.63	0.453	0.0557	113.5	17.0	115.6 [4]	133.7	548 [c]	Liq
					81.0	24.0	83.1 [4]	104.4	583 [c]	Liq
					102.6	25.1	104.7 [4]	118.5	573 [c]	Liq
3.91	6.32	10.23	0.382	0.0422	122.8	25.9	124.8 [4]	133.0	567 [c]	Liq
					86.8	37.4	88.9 [4]	105.0	574 [c]	Liq
					107.7	38.6	109.8 [4]	118.5	566 [c]	Liq
3.91	8.16	12.07	0.324	0.0330	127.3	40.2	129.3 [4]	132.6	555 [c]	Liq
					88.6	50.6	90.7 [4]	104.4	558 [c]	Liq
					108.7	52.3	110.8 [4]	118.0	548 [c]	Liq
3.91	9.71	13.62	0.287	0.0279	128.7	54.2	130.7 [4]	132.6	537 [c]	Liq
					88.2	67.0	90.3 [4]	104.0	593 [c]	Liq
					108.9	69.1	111.0 [4]	118.1	582 [c]	Liq
3.91	13.07	16.98	0.230	0.0209	128.3	71.4	130.3 [4]	132.1	570 [c]	Liq
					88.9	28.5	91.0 [4]	102.7	488 [c]	Vap
					108.7	29.6	110.8 [4]	116.4	481 [c]	Vap
1.64	7.49	9.13	0.180	0.0154	127.4	30.7	129.4 [4]	130.0	474 [c]	Vap
					83.1	59.8	85.2 [4]	102.0	508 [c]	Vap
					106.3	63.7	108.4 [4]	117.7	490 [c]	Vap
1.64	11.97	13.61	0.121	0.00968	125.0	65.0	127.0 [4]	131.3	484 [c]	Vap
					86.0	32.3	88.1 [4]	107.2	514 [c]	Vap
					105.5	32.7	107.6 [4]	120.4	511 [c]	Vap
0.821	9.30	10.12	0.0811	0.00625	122.3	34.3	124.3 [4]	133.7	501 [c]	Vap

Table A7 Continued

Mass	Mass	Total	Mass	Molar	Pressure	Piston	Correct	Temp	Density	Side
Wax	Solvent	Mass	Fraction	Fraction	Reading	Position	Pressure			
g	g	g	g/g	mol/mol	bar	mm	bar (abs)	^{o}C	kg/m^3	-
					75.5	35.6	77.6 [4]	106.1	424 [c]	Vap
					94.3	39.0	96.4 [4]	120.6	407 [c]	Vap
0.383	8.33	8.71	0.0440	0.00326	112.2	40.8	114.3 [4]	134.8	398 [c]	Vap
					66.1	41.5	68.2 [4]	105.3	398 [c]	Vap
					83.4	45.0	85.5 [4]	119.5	382 [c]	Vap
0.214	8.56	8.77	0.0244	0.00178	102.9	45.9	105.0 [4]	133.6	378 [c]	Vap
					59.2	56.3	61.3 [4]	104.6	397 [c]	Vap
					75.9	60.9	78.0 [4]	120.1	379 [c]	Vap
0.151	10.12	10.27	0.0147	0.00106	93.7	62.3	95.8 [4]	134.2	374 [c]	Vap

1.8. PROPANE-C60

Table A-8: Experimental Data for Propane – Hexacontane System

Wax Type					Hexacontane (C60)					
Solvent Type					Propane (C3)					
Wax Molar Mass					843.6116					
Solvent Molar Mass					44.1					
Mass	Mass	Total	Mass	Molar	Pressure	Piston	Correct	Temp	Density	Side
Wax	Solvent	Mass	Fraction	Fraction	Reading	Position	Pressure			
g	g	g	g/g	mol/mol	bar	mm	bar (abs)	^{o}C	kg/m^3	-
					82.2	16.1	84.3 [4]	106.3	562 [c]	Liq
3.949	4.78	8.73	0.452	0.0556	104.7	16.9	106.8 [4]	120.9	555 [c]	Liq
					123.7	17.4	125.7 [4]	134.1	551 [c]	Liq
					89.3	21.5	91.4 [4]	106.0	542 [c]	Liq
3.949	5.21	9.16	0.431	0.0512	112.1	22.5	114.2 [4]	120.4	533 [c]	Liq
					130.8	23.4	132.8 [4]	134.8	526 [c]	Liq

Table A-8 Continued

Mass Wax	Mass Solvent	Total Mass	Mass Fraction	Molar Fraction	Pressure Reading	Piston Position	Correct Pressure	Temp	Density	Side
g	g	g	g/g	mol/mol	bar	mm	bar (abs)	°C	kg/m³	-
3.949	6.00	9.95	0.397	0.0448	93.7	27.2	95.8 [4]	105.7	541 [c]	Liq
					116.7	28.0	118.7 [4]	120.8	535 [c]	Liq
					136.0	29.3	138.0 [4]	134.9	526 [c]	Liq
3.949	6.89	10.84	0.364	0.0392	96.2	31.5	98.3 [4]	106.6	556 [c]	Liq
					118.0	32.6	120.0 [4]	120.9	548 [c]	Liq
					137.4	33.7	139.4 [4]	134.9	540 [c]	Liq
3.949	9.03	12.98	0.304	0.0302	98.0	42.0	100.1 [4]	105.9	585 [c]	Liq
					120.5	43.4	122.5 [4]	120.6	575 [c]	Liq
					135.9	44.7	137.9 [4]	132.4	567 [c]	Liq
3.949	11.03	14.98	0.264	0.0249	100.0	58.1	102.1 [4]	106.7	569 [c]	Liq
					121.4	60.1	123.4 [4]	121.1	558 [c]	Liq
					140.2	62.4	142.2 [4]	135.2	546 [c]	Liq
2.013	5.83	7.84	0.257	0.0240	98.0	21.2	100.1 [4]	106.1	466 [c]	Cri
					119.3	21.5	121.3 [4]	119.8	464 [c]	Cri
					138.4	21.7	140.4 [4]	133.8	462 [c]	Cri
1.755	6.09	7.85	0.224	0.0201	99.4	19.1	101.5 [4]	107.9	481 [c]	Cri
					120.1	20.2	122.1 [4]	121.6	473 [c]	Cri
					136.1	21.1	138.1 [4]	133.3	467 [c]	Cri
2.013	8.18	10.19	0.197	0.0172	96.7	39.9	98.8 [4]	105.7	471 [c]	Cri
					117.9	41.5	119.9 [4]	119.6	462 [c]	Cri
					137.3	43.0	139.3 [4]	133.5	454 [c]	Cri
1.755	8.92	10.68	0.164	0.0138	95.7	42.4	97.8 [4]	106.1	479 [c]	Cri
					118.6	44.5	120.6 [4]	121.0	467 [c]	Cri
					137.0	46.3	139.0 [4]	134.7	458 [c]	Cri
2.013	10.92	12.93	0.156	0.0130	96.8	53.2	98.9 [4]	105.8	516 [c]	Cri
					117.0	55.1	119.0 [4]	119.2	506 [c]	Cri
					138.4	57.3	140.4 [4]	135.2	495 [c]	Cri
1.018	7.81	8.83	0.115	0.00920	94.4	32.2	96.5 [4]	106.1	449 [c]	Vap
					115.8	33.8	117.8 [4]	120.7	440 [c]	Vap
					135.0	35.3	137.0 [4]	135.3	431 [c]	Vap

Table A-8 Continued

Mass Wax	Mass Solvent	Total Mass	Mass Fraction	Molar Fraction	Pressure Reading	Piston Position	Correct Pressure	Temp	Density	Side
g	g	g	g/g	mol/mol	bar	mm	bar (abs)	^{o}C	kg/m^{3}	-
					90.5	52.7	92.6 [4]	105.0	488 [c]	Vap
1.018	11.15	12.17	0.0837	0.00646	111.8	54.7	113.9 [4]	119.5	478 [c]	Vap
					130.5	55.4	132.5 [4]	134.4	474 [c]	Vap
					87.3	30.9	89.4 [4]	107.3	447 [c]	Vap
0.500	8.15	8.65	0.0578	0.00435	106.9	32.6	109.0 [4]	121.5	437 [c]	Vap
					125.7	34.4	127.7 [4]	136.0	427 [c]	Vap
					81.1	43.8	83.2 [4]	108.2	434 [c]	Vap
0.402	9.43	9.83	0.0409	0.00303	99.8	45.4	101.9 [4]	121.7	426 [c]	Vap
					117.2	-	119.2 [4]	133.4	-	Vap
					73.4	53.9	75.5 [4]	104.0	356 [c]	Vap
0.265	8.73	9.00	0.0295	0.00216	93.7	56.4	95.8 [4]	118.8	347 [c]	Vap
					112.1	58.5	114.2 [4]	133.1	340 [c]	Vap
					71.9	48.3	74.0 [4]	103.9	434 [c]	Vap
0.257	10.08	10.34	0.0249	0.00181	92.4	50.7	94.5 [4]	118.9	423 [c]	Vap
					110.6	52.7	112.7 [4]	133.1	414 [c]	Vap
					66.4	55.0	68.5 [4]	107.5	413 [c]	Vap
0.151	10.39	10.54	0.0143	0.00103	86.6	57.3	88.7 [4]	121.3	403 [c]	Vap
					101.7	60.6	103.8 [4]	135.4	391 [c]	Vap

1.9.　LPG-C36

Table A-9: Experimental Data for LPG – Hexatriacontane System

Wax Type				Hexatriacontane						
Solvent Type				LPG						
Wax Molar Mass (g/mol)				506.97						
Solvent Molar Mass (g/mol)				44.10						
Mass	Mass	Total	Mass	Molar	Pressure	Piston	Correct	Temp	Density	Side
Wax	Solvent	Mass	Fraction	Fraction	Reading	Position	Pressure			
g	g	g	g/g	mol/mol	bar	mm	bar (abs)	°C	kg/m³	-
					39.0	25.2	38.4 [1]	103.3	635 [a]	Liq
					51.8	26.0	50.6 [1]	117.2	629 [a]	Liq
7.498	4.9	12.4	0.605	0.121	60.9	27.1	59.5 [1]	131.0	620 [a]	Liq
					44.8	22.5	44.2 [1]	103.6	525 [a]	Liq
4.783	5.1	9.9	0.484	0.0775	72.6	20.6	71.1 [1]	131.6	539 [a]	Liq
					43.7	25.1	43.1 [1]	102.4	552 [a]	Liq
					57.9	24.9	56.7 [1]	116.9	553 [a]	Liq
5.148	5.6	10.7	0.479	0.0761	72.9	22.5	71.5 [1]	131.2	571 [a]	Liq
					44.7	18.4	44.1 [1]	103.5	536 [a]	Liq
					60.5	19.5	59.3 [1]	117.7	528 [a]	Liq
4.122	5.4	9.5	0.433	0.0640	77.7	19.9	76.2 [1]	131.8	525 [a]	Liq
					46.7	21.8	46.1 [1]	101.9	540 [a]	Liq
3.970	6.1	10.1	0.394	0.0551	80.1	21.2	78.7 [1]	129.6	545 [a]	Liq
					45.8	26.8	45.2 [1]	102.1	653 [a]	Liq
					61.9	29.5	60.7 [1]	116.1	631 [a]	Liq
5.002	8.0	13.0	0.385	0.0531	79.1	30.6	77.7 [1]	129.9	622 [a]	Liq
					46.9	12.9	46.3 [1]	103.1	505 [a]	Liq
3.153	5.1	8.3	0.382	0.0525	81.1	14.0	79.7 [1]	131.3	496 [a]	Liq
					47.1	20.6	46.5 [1]	102.4	516 [a]	Liq
3.253	6.2	9.5	0.344	0.0449	84.4	21.0	83.0 [1]	130.8	513 [a]	Liq
					47.0	28.6	46.4 [1]	101.1	532 [a]	Liq
3.640	7.2	10.8	0.336	0.0433	83.5	25.2	82.1 [1]	129.3	556 [a]	Liq
					46.5	21.9	45.9	103.7	535 [a]	Liq
					65.6	22.9	64.3 [1]	117.6	528 [a]	Liq
3.286	6.7	10.0	0.329	0.0421	83.0	23.0	81.5 [1]	131.4	527 [a]	Liq

Table A-9 Continued

Mass Wax g	Mass Solvent g	Total Mass g	Mass Fraction g/g	Molar Fraction mol/mol	Pressure Reading bar	Piston Position mm	Correct Pressure bar (abs)	Temp °C	Density kg/m³	Side -
					49.5	37.3	48.9[1]	104.7	597[a]	Liq
4.419	9.1	13.5	0.327	0.0417	80.7	40.7	79.3[1]	128.5	575[a]	Liq
					47.5	19.5	46.9[1]	103.2	560[a]	Liq
2.908	7.2	10.1	0.288	0.0349	84.8	21.1	83.3[1]	131.5	548[a]	Liq
					48.4	23.2	47.8[1]	103.0	516[a]	Liq
2.807	7.0	9.8	0.286	0.0347	85.9	25.8	84.5[1]	131.2	499[a]	Liq
					49.0	28.8	48.4[1]	102.3	522[a]	Liq
2.974	7.7	10.7	0.279	0.0335	86.7	31.5	85.3[1]	130.4	505[a]	Liq
					48.0	31.1	47.4[1]	102.3	571[a]	Liq
					67.3	32.4	68.6[1]	117.0	562[a]	Liq
3.218	8.8	12.0	0.268	0.0317	84.8	32.1	83.3[1]	131.8	564[a]	Liq
					48.0	50.7	47.5[1]	99.0	578[a]	Liq
3.790	11.3	15.1	0.251	0.0292	85.7	52.9	84.3[1]	129.6	566[a]	Liq
					50.2	32.7	49.6[1]	102.4	521[a]	Liq
2.766	8.4	11.2	0.248	0.0287	86.8	36.3	85.4[1]	130.2	499[a]	Liq
					50.7	33.8	50.1[1]	102.1	499[a]	Liq
2.545	8.3	10.8	0.235	0.0267	86.6	38.0	85.2[1]	130.0	475[a]	Liq
					52.0	47.3	51.4[1]	103.3	493[a]	Liq
2.619	9.8	12.4	0.211	0.0234	88.4	52.9	86.9[1]	131.5	466[a]	Liq
					48.1	48.0	47.5[1]	102.0	524[a]	Liq
					67.9	49.6	66.6[1]	116.0	516[a]	Liq
2.717	10.6	13.3	0.204	0.0225	85.2	51.2	83.8[1]	129.9	508[a]	Liq
					49.5	27.5	48.9[1]	101.8	532[a]	Liq
					68.5	28.8	67.2[1]	115.5	523[a]	Liq
1.988	8.7	10.7	0.186	0.0201	85.7	29.8	84.3[1]	129.4	516[a]	Liq
					50.9	45.9	50.3[1]	101.8	516[a]	Liq
2.212	10.6	12.8	0.173	0.0184	87.0	46.9	85.6[1]	129.3	510[a]	Liq
					52.1	72.5	51.5[1]	103.3	496[a]	Vap
2.031	13.7	15.7	0.129	0.0131	86.5	80.4	85.1[1]	130.8	466[a]	Vap

Table A-9 Continued

Mass Wax	Mass Solvent	Total Mass	Mass Fraction	Molar Fraction	Pressure Reading	Piston Position	Correct Pressure	Temp	Density	Side
g	g	g	g/g	mol/mol	bar	mm	bar (abs)	°C	kg/m³	-
					47.0	68.5	46.5 [1]	100.9	514 [a]	Vap
					64.3	71.2	63.1 [1]	114.5	502 [a]	Vap
1.059	14.7	15.8	0.0672	0.00641	79.8	67.5	78.4 [1]	127.0	518 [a]	Vap
					46.0	-	45.5 [1]	100.9	-	Vap
					60.7	-	59.5 [1]	115.4	-	Vap
0.539	15.5	16.0	0.0336	0.00311	74.6	-	73.2 [1]	129.4	-	Vap
					44.5	50.4	43.9 [1]	102.2	360 [a]	Vap
					56.8	54.3	55.6 [1]	116.2	346 [a]	Vap
0.159	9.2	9.4	0.0170	0.00155	66.4	58.3	65.0 [1]	130.0	334 [a]	Vap

2. TEST DATA

Pressure corrections and density calculation references are the same as above. No temperature correction is required as the temperatures are below 95 °C.

Table A-10: Experimental Test Data for Ethane – Tetracosane System

Wax Type				Tetracosane						
Solvent Type				Ethane						
Wax Molar Mass (g/mol)				338.65						
Solvent Molar Mass (g/mol)				30.07						
Mass Wax	Mass Solvent	Total Mass	Mass Fraction	Molar Fraction	Pressure Reading	Piston Position	Correct Pressure	Temp	Density	Side
G	g	g	g/g	mol/mol	bar	mm	bar (abs)	°C	kg/m³	-
5.41	6.55	11.96	0.452	0.0683	123.7	37.8	125.0 [2]	67.2	582 [b]	Liq
0.783	11.19	11.97	0.0654	0.00617	115.5	67.1	116.8 [2]	67.8	377 [b]	Vap

B.   TEMPERATURE CORRECTED PHASE EQUILIBRIUM AND DENSITY DATA

The following data was used to generate the phase equilibrium and density graphs in chapter 6.

1.   PROPANE-C32

Table B-1: Temperature Corrected Pressure at Phase Equilibrium for Propane – Dotriacontane

Mass Fraction Wax	Parameters for Temperature Correction of Pressure P = A * T + B			Temperature		
				105.0 °C	120 °C	135 °C
				Pressure	Pressure	Pressure
(g/g)	A	B	R^2	(bar)	(bar)	(bar)
0.566	0.792	-37.19	0.9996	46.0	57.9	69.8
0.511	0.948	-50.69	0.9990	48.8	63.0	77.2
0.451	1.045	-60.17	0.9987	49.5	65.2	80.9
0.431	1.107	-64.83	1.0000	51.4	68.0	84.5
0.381	1.179	-70.89	0.9999	52.9	70.6	88.3
0.316	1.196	-70.80	0.9996	54.8	72.8	90.7
0.275	1.202	-69.21	0.9996	57.0	75.0	93.1
0.220	1.168	-64.40	0.9979	58.3	75.8	93.3
0.145	1.141	-62.75	0.9989	57.1	74.2	91.3
0.092	1.115	-60.86	0.9996	56.2	72.9	89.6
0.054	1.017	-51.05	0.9989	55.8	71.0	86.3
0.043	1.050	-57.05	0.9997	53.2	68.9	84.7
0.040	0.990	-51.20	0.9993	52.7	67.6	82.4
0.029	0.846	-34.40	0.9892	54.4	67.1	79.8
0.020	0.859	-38.54	1.0000	51.6	64.5	77.4
0.015	0.810	-34.18	0.9933	50.9	63.0	75.2

Table B-2: Temperature Corrected Density at Phase Equilibrium for Propane –
Dotriacontane

Mass Fraction Wax (g/g)	Parameters for Temperature Correction of Density $\rho = A * T + B$			Temperature		
				105.0 $^{\circ}$C	120 $^{\circ}$C	135 $^{\circ}$C
				Density	Density	Density
	A	B	R^2	(kg/m^3)	(kg/m^3)	(kg/m^3)
0.451	-0.3480	643.1	0.8610	607	601	596
0.431	-0.3882	624.6	0.9755	584	578	572
0.381	-0.5690	647.0	1.0000	587	579	570
0.275	-0.1891	498.1	0.9426	478	475	473
0.220	-0.7065	571.8	0.9999	498	487	476
0.145	-0.3100	533.4	0.7835	501	496	492
0.054	-0.7916	467.9	0.9958	385	373	361
0.043	-0.6042	459.9	0.9927	396	387	378
0.040	-0.2552	389.4	0.9805	363	359	355
0.029	-1.1165	515.9	1.0000	399	382	365
0.015	-1.3800	520.4	0.9885	376	355	334

2.   PROPANE-C36

Table B-3: Temperature Corrected Pressure at Phase Equilibrium for Propane –
Hexatriacontane

Mass Fraction Wax (g/g)	Parameters for Temperature Correlation of Pressure $P = A * T + B$			Temperature		
				105 $^{\circ}$C	120 $^{\circ}$C	135 $^{\circ}$C
				Pressure	Pressure	Pressure
	A	B	R^2	(bar)	(bar)	(bar)
0.576	0.760	-35.93	0.9993	43.9	55.3	66.7
0.472	1.124	-67.37	0.9997	50.7	67.5	84.4
0.378	1.304	-80.01	0.9994	56.9	76.4	96.0
0.269	1.298	-75.92	1.0000	60.4	79.8	99.3
0.202	1.239	-69.28	0.9986	60.8	79.4	98.0
0.151	1.253	-71.27	0.9984	60.2	79.0	97.8
0.0986	1.222	-68.59	0.9996	59.8	78.1	96.4

Table B-3 Continued

Mass Fraction Wax	Parameters for Temperature Correlation of Pressure P = A * T + B			Temperature		
				105 °C	120 °C	135 °C
				Pressure	Pressure	Pressure
(g/g)	A	B	R ^{2}	(bar)	(bar)	(bar)
0.0716	1.217	-69.73	0.9984	58.0	76.3	94.6
0.0639	1.120	-60.18	0.9977	57.4	74.2	91.0
0.0425	1.145	-64.58	0.9991	55.6	72.8	90.0
0.0255	1.007	-51.73	0.9987	54.0	69.1	84.2
0.0151	0.969	-48.87	0.9997	52.9	67.4	81.9

Table B-4: Temperature Corrected Density at Phase Equilibrium for Propane – Hexatriacontane

Mass Fraction Wax	Parameters for Temperature Correlation of Density ρ = A * T + B			Temperature		
				105 °C	120 °C	135 °C
				Density	Density	Density
(g/g)	A	B	R ^{2}	(kg/m^3)	(kg/m^3)	(kg/m^3)
0.378	-0.8468	666.1	0.9999	577	564	552
0.269	-0.9466	660.7	0.9844	561	547	533
0.202	-0.3771	529.5	0.7652	490	484	479
0.0986	-0.5934	546.7	0.7518	484	476	467
0.0716	-0.6282	511.4	0.9562	445	436	427
0.0639	-0.3860	448.7	-	408	402	397
0.0425	-0.8888	538.3	0.9979	445	432	418
0.0151	-0.2609	379.4	-	352	348	344

3.   PROPANE-C38

Table B-5: Temperature Corrected Pressure at Phase Equilibrium for Propane – Octatriacontane

Mass Fraction Wax	Parameters for Temperature Correction of Pressure $P = A * T + B$			Temperature		
				150 $^{\circ}$C	120 $^{\circ}$C	135 $^{\circ}$C
				Pressure	Pressure	Pressure
(g/g)	A	B	R^2	(bar)	(bar)	(bar)
0.567	0.908	-49.07	1.000	46.2	59.8	73.5
0.506	1.116	-67.56	1.000	49.6	66.3	83.0
0.451	1.247	-76.72	1.000	54.2	72.9	91.6
0.388	1.302	-78.01	0.999	58.7	78.2	97.8
0.322	1.286	-73.66	0.999	61.4	80.7	100.0
0.295	1.239	-67.83	0.998	62.2	80.8	99.4
0.244	1.279	-71.91	0.999	62.4	81.6	100.8
0.219	1.280	-72.16	1.000	62.2	81.4	100.6
0.202	1.266	-70.17	0.999	62.8	81.8	100.8
0.170	1.240	-67.16	0.999	63.0	81.6	100.2
0.099	1.204	-65.83	1.000	60.6	78.6	96.7
0.0948	1.214	-66.56	0.999	60.9	79.1	97.3
0.0639	1.142	-59.84	0.998	60.1	77.2	94.3
0.0322	1.027	-51.08	1.000	56.8	72.2	87.6
0.0149	0.956	-46.62	0.998	53.8	68.1	82.4

Table B-6: Temperature Corrected Density at Phase Equilibrium for Propane – Octatriacontane

Mass Fraction Wax	Parameters for Temperature Correction of Density $\rho = A * T + B$			Temperature		
				105 $^{\circ}$C	120 $^{\circ}$C	135 $^{\circ}$C
				Density	Density	Density
(g/g)	A	B	R^2	(kg/m^3)	(kg/m^3)	(kg/m^3)
0.567	-0.3916	664.0	1.0000	623	617	611
0.506	-0.4406	663.3	0.9840	617	610	604
0.451	-0.5654	670.0	0.9765	611	602	594

Table B-6 Continued

Mass Fraction Wax (g/g)	Parameters for Temperature Correction of Density $\rho = A * T + B$			Temperature		
				105 °C Density (kg/m^3)	120 °C Density (kg/m^3)	135 °C Density (kg/m^3)
	A	B	R^2			
0.388	-0.7239	679.1	0.9991	603	592	581
0.244	-0.5410	551.1	0.9997	494	486	478
0.170	-0.5246	536.6	0.9817	481	474	466
0.0948	-0.6829	536.5	0.9994	465	455	444
0.0639	-0.5421	483.9	0.9829	427	419	411
0.0322	-1.0669	547.0	0.9992	435	419	403

4. PROPANE-C40

Table B-7: Temperature Corrected Pressure at Phase Equilibrium for Propane – Tetracontane

Mass Fraction Wax (g/g)	Parameters for Temperature Correction of Pressure $P = A * T + B$			Temperature		
				105 °C Pressure (bar)	120 °C Pressure (bar)	135 °C Pressure (bar)
	A	B	R^2			
0.551	1.014	-54.61	0.9990	51.8	67.0	82.2
0.499	1.218	-71.68	0.9999	56.2	74.5	92.8
0.439	1.327	-78.39	0.9990	60.9	80.8	100.7
0.402	1.360	-82.84	0.9995	60.0	80.4	100.8
0.376	1.350	-76.87	0.9987	64.9	85.2	105.4
0.336	1.426	-85.08	0.9988	64.7	86.1	107.5
0.309	1.317	-69.65	0.9989	68.6	88.4	108.1
0.270	1.304	-66.98	0.9996	69.9	89.5	109.0
0.264	1.388	-78.48	0.9991	67.2	88.0	108.8
0.244	1.324	-69.21	0.9990	69.8	89.7	109.5
0.231	1.363	-73.41	0.9954	69.7	90.2	110.6
0.203	1.294	-66.64	0.9996	69.3	88.7	108.1
0.166	1.335	-77.31	0.9996	62.8	82.9	102.9

Table B-7 Continued

Mass Fraction Wax	Parameters for Temperature Correction of Pressure P = A * T + B			Temperature		
				105 ^{o}C	120 ^{o}C	135 ^{o}C
				Pressure	Pressure	Pressure
(g/g)	A	B	R ^{2}	(bar)	(bar)	(bar)
0.156	1.287	-70.84	0.9962	64.3	83.6	102.9
0.154	1.335	-75.71	1.0000	64.4	84.5	104.5
0.136	1.286	-66.30	0.9995	68.8	88.1	107.3
0.123	1.307	-70.34	0.9981	66.9	86.5	106.1
0.092	1.178	-58.28	0.9997	65.4	83.1	100.7
0.075	1.178	-61.75	0.9980	62.0	79.7	97.3
0.061	1.231	-66.83	0.9975	62.4	80.9	99.3
0.059	1.201	-65.96	0.9984	60.1	78.1	96.2
0.037	1.157	-63.80	0.9966	57.7	75.0	92.4
0.025	1.020	-51.04	0.9978	56.1	71.4	86.7
0.022	1.045	-53.37	0.9992	56.3	72.0	87.7
0.015	0.930	-43.15	0.9856	54.5	68.5	82.4

Table B-8: Temperature Corrected Density at Phase Equilibrium for Propane – Tetracontane

Mass Fraction Wax	Parameters for Temperature Correction of Density ρ = A * T + B			Temperature		
				105 ^{o}C	120 ^{o}C	135 ^{o}C
				Density	Density	Density
(g/g)	A	B	R ^{2}	(kg/m^{3})	(kg/m^{3})	(kg/m^{3})
0.499	-0.4273	611.3	0.9878	566	560	554
0.439	-0.5151	628.1	1.0000	574	566	559
0.402	-0.4561	577.7	0.9983	530	523	516
0.376	-0.6221	635.4	0.9950	570	561	551
0.336	-0.3935	609.1	0.9788	568	562	556
0.309	-0.8455	685.3	0.9992	597	584	571
0.270	-0.5014	508.5	0.9992	456	448	441
0.264	-0.8050	611.8	0.9996	527	515	503
0.244	-0.3820	547.8	0.9747	508	502	496
0.231	-0.8416	614.6	0.9004	526	514	501

Table B-8 Continued

Mass Fraction Wax (g/g)	Parameters for Temperature Correction of Density ρ = A * T + B			Temperature		
				105 °C	120 °C	135 °C
				Density	Density	Density
	A	B	R²	(kg/m³)	(kg/m³)	(kg/m³)
0.203	-0.6500	540.5	0.9981	472	463	453
0.166	-0.5484	532.0	0.8576	474	466	458
0.156	-0.5396	538.4	0.9984	482	474	466
0.154	-0.4993	492.3	0.9988	440	432	425
0.136	-0.8952	538.9	0.9976	445	431	418
0.123	-0.2472	511.0	0.8505	485	481	478
0.059	-0.3642	455.3	0.9319	417	412	406
0.037	-1.1684	544.8	0.9767	422	405	387
0.022	-0.5274	466.7	0.7465	411	403	395
0.015	-0.2140	330.4	0.8713	308	305	301

5. PROPANE-C44

Table B-9: Temperature Corrected Pressure at Phase Equilibrium for Propane – Tetratetracontane

Mass Fraction Wax (g/g)	Parameters for Temperature Correction of Pressure P = A * T + B			Temperature		
				105 °C	120 °C	135 °C
				Pressure	Pressure	Pressure
	A	B	R²	(bar)	(bar)	(bar)
0.542	1.197	-73.01	0.9999	52.7	70.7	88.6
0.481	1.341	-84.66	0.9998	56.2	76.3	96.4
0.418	1.369	-79.57	0.9990	64.2	84.7	105.3
0.371	1.413	-77.94	0.9990	70.4	91.6	112.8
0.354	1.438	-80.27	0.9985	70.7	92.3	113.8
0.312	1.326	-67.21	0.9949	72.1	91.9	111.8
0.298	1.396	-73.92	0.9992	72.6	93.6	114.5
0.243	1.382	-71.55	0.9987	73.5	94.2	114.9
0.186	1.332	-66.38	0.9985	73.5	93.4	113.4

Table B-9 Continued

Mass	Parameters for Temperature			Temperature		
Fraction	Correction of Pressure			105 ^{o}C	120 ^{o}C	135 ^{o}C
Wax	P = A * T + B			Pressure	Pressure	Pressure
(g/g)	A	B	R ^{2}	(bar)	(bar)	(bar)
0.130	1.342	-70.15	0.9977	70.7	90.8	110.9
0.0807	1.309	-70.05	0.9979	67.4	87.0	106.7
0.0553	1.291	-69.79	0.9955	65.8	85.1	104.5
0.0505	1.201	-62.15	0.9967	64.0	82.0	100.0
0.0420	1.201	-65.37	0.9972	60.7	78.7	96.7
0.0255	1.153	-61.17	0.9998	59.9	77.1	94.4
0.0146	0.941	-39.77	0.9918	59.0	73.1	87.2

Table B-10: Temperature Corrected Density at Phase Equilibrium for Propane – Tetratetracontane

Mass	Parameters for Temperature			Temperature		
Fraction	Correction of Density			105 ^{o}C	120 ^{o}C	135 ^{o}C
Wax	ρ = A * T + B			Density	Density	Density
(g/g)	A	B	R ^{2}	(kg/m^3)	(kg/m^3)	(kg/m^3)
0.542	-0.1910	602.8	0.7517	583	580	577
0.371	-0.5732	563.0	0.9920	503	494	486
0.354	-0.4352	569.8	0.9526	524	518	511
0.312	-0.2659	548.8	0.8850	521	517	513
0.298	-0.6410	576.5	0.9990	509	500	490
0.243	-0.8236	638.2	0.9997	552	539	527
0.186	-0.9001	641.5	0.9999	547	533	520
0.130	-0.6922	532.2	0.9996	460	449	439
0.0807	-0.6962	506.0	0.9962	433	422	412
0.0553	-0.6261	486.9	0.9989	421	412	402
0.0255	-0.6608	466.8	0.9930	397	388	378

6.   PROPANE-C46

*Table B-11: Temperature Corrected Pressure at Phase Equilibrium for Propane –
Hexatetracontane*

Mass Fraction Wax	Parameters for Temperature Correction of Pressure P = A * T + B			Temperature		
				105 ^{o}C	120 ^{o}C	135 ^{o}C
				Pressure	Pressure	Pressure
(g/g)	A	B	R^2	(bar)	(bar)	(bar)
0.556	1.253	-69.29	0.9922	62.1	82.8	98.2
0.540	0.602	-22.91	0.9996	41.1	50.2	58.8
0.484	1.335	-84.64	0.9999	56.7	76.4	95.4
0.444	1.348	-77.46	0.9994	65.2	85.7	104.3
0.362	1.333	-67.33	0.9996	74.2	94.3	113.0
0.305	1.317	-63.81	0.9997	75.9	95.7	114.1
0.274	1.348	-66.46	0.9990	75.3	95.9	114.4
0.238	1.312	-60.83	0.9999	73.7	97.6	111.3
0.200	1.328	-64.04	0.9986	76.0	96.5	114.5
0.159	1.355	-69.05	0.9984	75.3	97.4	115.5
0.117	1.283	-62.87	0.9988	73.3	93.3	110.9
0.100	1.258	-59.25	0.9984	74.8	94.1	112.2
0.079	1.344	-69.62	0.9983	71.1	92.8	110.2
0.071	1.314	-68.81	0.9997	70.2	89.7	107.8
0.053	1.211	-60.36	0.9987	67.6	86.4	103.2
0.040	1.274	-70.63	0.9979	64.3	84.6	101.1
0.038	1.150	-57.37	0.9981	65.3	82.8	96.9
0.021	1.092	-54.82	0.9985	60.5	77.4	92.4
0.015	1.039	-50.21	0.9938	59.3	76.4	89.2

Table B-12: Temperature Corrected Density at Phase Equilibrium for Propane –
Hexatetracontane

Mass Fraction Wax (g/g)	Parameters for Temperature Correction of Density $\rho = A * T + B$			Temperature		
				105 °C	120 °C	135 °C
				Density	Density	Density
	A	B	R^2	(kg/m³)	(kg/m³)	(kg/m³)
0.484	-0.6432	727.8	0.9818	660	651	641
0.444	-0.4150	691.9	0.9979	648	642	636
0.362	-0.7587	688.0	0.9913	608	597	586
0.305	-0.7750	674.8	0.9899	593	582	570
0.274	-0.3515	588.3	0.9975	551	546	541
0.238	-0.4612	546.5	0.9636	498	491	484
0.200	-0.7713	633.6	0.9999	553	541	529
0.159	-0.5502	546.3	0.9724	489	480	472
0.117	-0.6000	605.1	0.9999	542	533	524
0.079	-0.6285	501.2	0.9988	435	426	416
0.071	-0.8502	500.0	0.9487	411	398	385
0.053	-0.0803	481.9	0.8899	473	472	471
0.040	-0.7946	484.1	0.9989	401	389	377
0.038	-0.8028	505.6	0.9996	421	409	397
0.021	-0.1422	425.7	0.9262	411	409	407

7. PROPANE-C54

Table B-13: Temperature Corrected Pressure at Phase Equilibrium for Propane – Tetrapentacontane

Mass Fraction Wax	Parameters for Temperature Correction of Pressure P = A * T + B			Temperature		
				105 ^{o}C	120 ^{o}C	135 ^{o}C
				Pressure	Pressure	Pressure
(g/g)	A	B	R ^{2}	(bar)	(bar)	(bar)
0.453	1.439	-76.52	0.9989	74.6	96.2	117.8
0.382	1.461	-69.07	0.9992	84.3	106.2	128.1
0.324	1.466	-64.70	0.9990	89.2	111.2	133.2
0.287	1.421	-57.39	0.9995	91.8	113.1	134.4
0.230	1.426	-57.89	0.9997	91.9	113.3	134.7
0.180	1.410	-53.64	0.9998	94.4	115.5	136.7
0.121	1.431	-60.52	0.9996	89.7	111.1	132.6
0.0811	1.369	-58.22	0.9980	85.5	106.1	126.6
0.0440	1.278	-57.96	0.9999	76.3	95.4	114.6
0.0244	1.300	-69.06	0.9987	67.4	86.9	106.4
0.0147	1.164	-60.86	0.9979	61.3	78.8	96.2

Table B-14: Temperature Corrected Density at Phase Equilibrium for Propane – Tetrapentacontane

Mass Fraction Wax	Parameters for Temperature Correction of Density ρ = A * T + B			Temperature		
				105 ^{o}C	120 ^{o}C	135 ^{o}C
				Density	Density	Density
(g/g)	A	B	R ^{2}	(kg/m^3)	(kg/m^3)	(kg/m^3)
0.453	-0.4194	603.8	0.9974	560	553	547
0.382	-0.5525	639.9	0.9887	582	574	565
0.324	-0.6919	647.5	0.9964	575	564	554
0.287	-0.7245	633.5	1.0000	557	547	536
0.230	-0.8037	676.5	0.9997	592	580	568
0.180	-0.5257	541.9	1.0000	487	479	471
0.121	-0.8355	591.8	0.9391	504	492	479

Table B-14 Continued

Mass Fraction Wax	Parameters for Temperature Correction of Density $\rho = A * T + B$			Temperature		
				105 °C	120 °C	135 °C
				Density	Density	Density
(g/g)	A	B	R^2	(kg/m^3)	(kg/m^3)	(kg/m^3)
0.0811	-0.4950	568.2	0.8968	516	509	501
0.0440	-0.9060	518.8	0.9660	424	410	396
0.0244	-0.6873	468.0	0.8919	396	386	375
0.0147	-0.7620	474.7	0.9225	395	383	372

8.   PROPANE-C60

Table B-15: Temperature Corrected Pressure at Phase Equilibrium for Propane – Hexacontane

Mass Fraction Wax	Parameters for Temperature Correction of Pressure $P = A * T + B$			Temperature		
				105 °C	120 °C	135 °C
				Pressure	Pressure	Pressure
(g/g)	A	B	R^2	(bar)	(bar)	(bar)
0.452	1.493	-74.21	0.9996	84.0	104.9	125.8
0.431	1.440	-60.62	0.9968	92.1	112.2	132.4
0.397	1.449	-57.01	0.9991	96.6	116.8	137.1
0.364	1.455	-56.56	0.9992	97.7	118.1	138.5
0.304	1.434	-51.32	0.9980	100.6	120.7	140.8
0.264	1.410	-48.04	0.9990	101.4	121.2	140.9
0.257	1.457	-54.13	0.9986	100.4	120.8	141.2
0.224	1.446	-54.29	0.9992	99.0	119.2	139.5
0.197	1.460	-55.23	0.9993	99.5	119.9	140.4
0.164	1.445	-55.08	0.9985	98.1	118.3	138.5
0.156	1.412	-50.06	0.9988	99.6	119.4	139.1
0.115	1.390	-50.62	0.9990	96.7	116.1	135.6
0.0837	1.359	-49.64	0.9979	94.5	113.5	132.5
0.0578	1.337	-53.91	0.9997	87.8	106.6	125.3
0.0409	1.431	-71.82	0.9996	79.8	99.8	119.9

Table B-15 Continued

Mass	Parameters for Temperature			Temperature		
Fraction	Correction of Pressure			105 °C	120 °C	135 °C
Wax	P = A * T + B			Pressure	Pressure	Pressure
(g/g)	A	B	R ^{2}	(bar)	(bar)	(bar)
0.0295	1.330	-62.59	0.9997	78.3	96.9	115.6
0.0249	1.325	-63.50	0.9997	77.0	95.5	114.1
0.0143	1.264	-66.47	0.9920	67.5	85.2	102.9

Table B-16: Temperature Corrected Density at Phase Equilibrium for Propane – Hexacontane

Mass	Parameters for Temperature			Temperature		
Fraction	Correction of Density			105 °C	120 °C	135 °C
Wax	ρ = A * T + B			Density	Density	Density
(g/g)	A	B	R ^{2}	(kg/m^3)	(kg/m^3)	(kg/m^3)
0.431	-0.5293	597.5	0.9985	541.4	534.0	526.6
0.397	-0.5288	597.8	0.9781	541.7	534.3	526.9
0.364	-0.5557	615.4	1.0000	556.5	548.7	540.9
0.304	-0.6695	655.8	0.9989	584.8	575.4	566.1
0.264	-0.8053	654.7	0.9988	569.3	558.0	546.8
0.257	-0.1277	479.3	0.9849	465.8	464.0	462.2
0.224	-0.5820	544.2	0.9996	482.5	474.4	466.2
0.197	-0.6026	534.3	0.9992	470.4	461.9	453.5
0.164	-0.7227	555.2	0.9989	478.6	468.5	458.3
0.156	-0.7083	590.4	0.9996	515.3	505.4	495.5
0.115	-0.6001	512.3	0.9991	448.7	440.3	431.9
0.084	-0.4490	533.6	0.9212	486.0	479.7	473.4
0.058	-0.6950	521.9	1.0000	448.3	438.5	428.8
0.041	-0.5740	496.1	-	435.2	427.2	419.1
0.025	-0.6760	503.9	0.9975	432.3	422.8	413.3
0.014	-0.7914	498.2	0.9934	414.3	403.2	392.1

9.   LPG-C36

Table B-17: Temperature Corrected Pressure at Phase Equilibrium for LPG – Hexatriacontane

Mass	Parameters for Temperature			Temperature		
Fraction	Correction of Pressure			105 ^{o}C	120 ^{o}C	135 ^{o}C
Wax	P = A * T + B			Pressure	Pressure	Pressure
(g/g)	A	B	R^2	(bar)	(bar)	(bar)
0.605	0.762	-39.77	0.9923	40.2	51.7	63.1
0.484	0.961	-55.33		45.5	60.0	74.4
0.479	0.986	-58.10	0.9992	45.4	60.2	75.0
0.433	1.134	-73.59	0.9989	45.5	62.5	79.5
0.394	1.177	-73.83		49.7	67.4	85.1
0.382	1.184	-75.81		48.6	66.3	84.1
0.344	1.285	-85.11		49.8	69.1	88.4
0.336	1.266	-81.59		51.3	70.3	89.3
0.329	1.285	-87.20	0.9997	47.7	67.0	86.3
0.327	1.277	-84.83		49.3	68.4	87.6
0.288	1.286	-85.84		49.2	68.5	87.8
0.286	1.301	-86.25		50.4	69.9	89.4
0.279	1.313	-85.94		51.9	71.6	91.3
0.268	1.217	-75.96	0.9888	51.8	70.0	88.3
0.251	1.203	-71.56		54.7	72.8	90.8
0.248	1.288	-82.27		52.9	72.3	91.6
0.235	1.258	-78.35		53.7	72.6	91.5
0.211	1.259	-78.64		53.5	72.4	91.3
0.204	1.301	-84.92	0.9992	51.7	71.2	90.7
0.186	1.283	-81.41	0.9994	53.3	72.5	91.7
0.173	1.284	-80.37		54.4	73.7	92.9
0.129	1.222	-74.71		53.6	71.9	90.2
0.067	1.222	-76.83	1.0000	51.5	69.8	88.2
0.034	0.972	-52.59	1.0000	49.5	64.0	78.6
0.017	0.759	-33.33	0.9966	46.4	57.8	69.2

Table B-18: Temperature Corrected Density at Phase Equilibrium for LPG – Hexatriacontane System

Mass	Parameters for Temperature			Temperature		
Fraction	Correction of Density			105 °C	120 °C	135 °C
Wax	ρ = A * T + B			Density	Density	Density
(g/g)	A	B	R^2	(kg/m^3)	(kg/m^3)	(kg/m^3)
0.605	-0.5616	693.8	0.9926	635	626	618
0.433	-0.4040	577.1	0.9311	535	529	523
0.385	-1.1011	762.8	0.9414	647	631	614
0.382	-0.3055	536.5		504	500	495
0.344	-0.1016	526.2		516	514	512
0.329	-0.2894	564.0	0.8183	534	529	525
0.327	-0.9358	695.3		597	583	569
0.288	-0.4424	605.9		559	553	546
0.286	-0.6239	580.5		515	506	496
0.279	-0.6120	584.8		521	511	502
0.251	-0.4023	618.3		576	570	564
0.248	-0.7769	600.2		519	507	495
0.235	-0.8491	585.8		497	484	471
0.211	-0.9462	590.4		491	477	463
0.204	-0.5916	584.8	0.9999	523	514	505
0.186	-0.5516	587.4	0.9924	529	521	513
0.173	-0.1925	535.2		515	512	509
0.129	-1.0889	608.6		494	478	462
0.017	-0.9400	455.8	0.9999	357	343	329

C. PRESSURE GAUGE CALIBRATIONS AND DENSITY CORRELATIONS

1. THERMOCOUPLE CALIBRATIONS

The thermocouple was calibrated by the Cape Metrology Centre (Pty) Ltd in Epping Industria 1, Cape Town, South Africa. In the range of operation used here the following calibration was found:

Table C-1: Temperature Calibrations for the Thermocouple:

Actual (^{o}C)	Measured (^{o}C)	Error (^{o}C)
99.1	99.1	0.0
180.4	179.3	1.1

Linear interpolation was used between the two points and corrections were made in 0.1 ^{o}C increments.

2. PRESSURE GAUGE CALIBRATIONS

Various sets of calibrations were done for the pressure gauge. Subscripts next to corrected pressures in Appendix A indicate which of the pressure calibration sets were used.

Calibrations were done with the aid of a dead weight tester. A set pressure was applied to the cell with the dead weight tester and the gauge pressure was measured. The pressure difference is then used for pressure corrections. For each set the pressure difference was then plotted as a function of pressure and a linear trend line was applied. The trend lines were then used to determine the deviation temperatures above and below the operating temperature at the system pressure. Linear interpolation was used between to determine the deviation at the correct temperature.

Table C-2: Data for Pressure Calibration Set 1

Dead Weight Pressure	T = 108.1°C		T = 126.6 °C	
	Pressure Reading	Pressure Deviation	Pressure Reading	Pressure Deviation
20	21.2	-1.2	21.7	-1.7
35	36.2	-1.2	36.6	-1.6
50	51.2	-1.2	51.6	-1.6
65	66.2	-1.2	66.6	-1.6
80	81.2	-1.2	81.5	-1.5
95	96.2	-1.2	96.4	-1.4
110	111.1	-1.1	111.4	-1.4
125	126.1	-1.1	126.4	-1.4
140	141.1	-1.1	141.4	-1.4
155	156.1	-1.1	156.4	-1.4
170	171.1	-1.1	171.3	-1.3
185	186.1	-1.1	186.3	-1.3
200	201.1	-1.1	201.3	-1.3

The following equations were formulated for Calibration Set 1:

At T = 108.1 °C: Correction = 7.69E-4 P – 1.23 (bar).......................................C.1

At T = 126.6 °C: Correction = 2.16E-3 P – 1.69 (bar).......................................C.2

Table C-3: Data for Pressure Calibration Set 2

Dead Weight Pressure	T = 99.7 °C		T = 115.4 °C		T = 130.6 °C	
	Pressure Reading	Pressure Deviation	Pressure Reading	Pressure Deviation	Pressure Reading	Pressure Deviation
20.0	19.4	0.6	19.9	0.1	20.4	-0.4
35.0	34.4	0.6	34.9	0.1	35.4	-0.4
50.0	49.4	0.6	49.9	0.1	50.4	-0.4
65.0	64.5	0.5	65.0	0.0	65.5	-0.5
80.0	79.5	0.5	80.0	0.0	80.5	-0.5
95.0	94.6	0.4	95.1	-0.1	95.6	-0.6
110.0	109.6	0.4	110.1	-0.1	110.6	-0.6
125.0	124.7	0.3	125.2	-0.2	125.6	-0.6
140.0	139.7	0.3	140.2	-0.2	140.7	-0.7
155.0	154.8	0.2	155.3	-0.3	155.7	-0.7
170.0	169.9	0.1	170.4	-0.4	170.8	-0.8
185.0	184.9	0.1	185.5	-0.5	185.8	-0.8
200.0	200.0	0.0	200.5	-0.5	200.8	-0.8

The following equations were formulated for Calibration Set 2:

At T = 99.7 °C: Correction = -3.48E-3 P + 0.737 (bar) C.3

At T = 115.4 °C: Correction = -3.66E-3 P + 0.249 (bar) C.4

At T = 130.6 °C: Correction = -2.59E-3 P – 0.318 (bar) C.5

Table C-4: Data for Pressure Calibration Set 3

Dead Weight Pressure	T = 99.4 °C		T = 111.5 °C		T = 124.5 °C		T = 136.7 °C	
	Pressure Reading	Pressure Deviation	Pressure Reading	Pressure Deviation	Pressure Reading	Pressure Deviation	Pressure Reading	Pressure Deviation
20.0	25.0	-5.0	25.2	-5.2	25.2	-5.2	-	-
35.0	40.1	-5.1	40.3	-5.3	40.3	-5.3	40.3	-5.3
50.0	55.1	-5.1	55.3	-5.3	55.3	-5.3	55.4	-5.4
65.0	70.2	-5.2	70.3	-5.3	70.4	-5.4	70.4	-5.4
80.0	85.2	-5.2	85.4	-5.4	85.4	-5.4	85.5	-5.5
95.0	100.3	-5.3	100.4	-5.4	100.5	-5.5	100.5	-5.5
110.0	115.3	-5.3	115.4	-5.4	115.5	-5.5	115.5	-5.5
125.0	130.4	-5.4	130.5	-5.5	130.6	-5.6	130.6	-5.6
140.0	145.4	-5.4	145.6	-5.6	145.6	-5.6	145.6	-5.6
155.0	160.5	-5.5	160.6	-5.6	160.7	-5.7	160.7	-5.7
170.0	175.6	-5.6	175.7	-5.7	175.7	-5.7	175.7	-5.7
185.0	190.6	-5.6	190.8	-5.8	190.8	-5.8	190.8	-5.8
200.0	205.7	-5.7	205.8	-5.8	205.8	-5.8	205.8	-5.8

The following equations were formulated for Calibration Set 3:

At T = 99.4 °C: Correction = -3.68E-3 P – 4.93 (bar) C.6

At T = 111.5 °C: Correction = -3.38E-3 P – 5.11 (bar) C.7

At T = 124.5 °C: Correction = -3.26E-3 P – 5.17 (bar) C.8

At T = 136.7 °C: Correction = -2.94E-3 P – 5.22 (bar) C.9

Table C-5: Data for Pressure Calibration Set 4

Dead Weight Pressure	Pressure Reading				Average Pressure Deviation
	Temperature				
	94.5 °C	111.9 °C	125.1 °C	144.1°C	
20.0	18.8	19.2	19.1	18.9	1.0
35.0	33.9	34.3	34.1	34.0	0.9
50.0	48.9	49.4	49.2	49.0	0.9
65.0	64.0	64.5	64.3	64.1	0.8
80.0	79.0	79.6	79.4	79.1	0.7
95.0	94.1	94.7	94.4	94.2	0.6
110.0	109.2	109.8	109.5	109.3	0.6
125.0	124.3	124.8	124.6	124.3	0.5
140.0	139.4	139.9	139.7	139.4	0.4
155.0	154.5	155.0	154.8	154.4	0.3
170.0	169.6	170.1	169.9	169.5	0.2
185.0	184.6	185.2	184.9	184.5	0.2
200.0	199.7	200.3	200.1	199.5	0.1

For this correlation set, the effect of the temperature was less than the accuracy of the thermocouple. The average deviation will therefore be used and the pressure correction is thus just a function of the applied pressure. The following equation was formulated for Calibration Set 4

For all temperatures: Correction = -5.505E-3 P + 1.11 (bar)............................C.10

Table C-6: Data for Pressure Calibration Set 5

Dead Weight Pressure	T = 98.9 $^{\circ}$C		T = 112.8 $^{\circ}$C		T = 126.2 $^{\circ}$C		T = 140.5 $^{\circ}$C	
	Pressure Reading	Pressure Deviation	Pressure Reading	Pressure Deviation	Pressure Reading	Pressure Deviation	Pressure Reading	Pressure Deviation
20.0	18.7	-1.3	19.4	-0.6	19.8	-0.2	20.3	0.3
35.0	33.7	-1.3	34.4	-0.6	34.8	-0.2	35.3	0.3
50.0	48.6	-1.4	49.4	-0.6	49.8	-0.2	50.2	0.2
65.0	63.6	-1.4	64.4	-0.6	64.7	-0.3	65.2	0.2
80.0	78.6	-1.4	79.3	-0.7	79.7	-0.3	80.2	0.2
95.0	93.6	-1.4	94.3	-0.7	94.7	-0.3	95.1	0.1
110.0	108.6	-1.4	109.3	-0.7	109.7	-0.3	110.1	0.1
125.0	123.5	-1.5	124.2	-0.8	124.7	-0.3	125.1	0.1
140.0	138.5	-1.5	139.2	-0.8	139.6	-0.4	140.1	0.1
155.0	153.5	-1.5	152.1	-2.9	154.6	-0.4	155.0	0.0
170.0	168.5	-1.5	169.1	-0.9	169.6	-0.4	169.9	-0.1

The following equations were formulated for Data Set 5:

At T = 98.9 $^{\circ}$C: Correction = -1.39E-3 P – 1.29 (bar) C.11

At T = 112.8 $^{\circ}$C: Correction = -2.24E-3 P – 0.505 (bar) C.12

At T = 126.2 $^{\circ}$C: Correction = -1.45E-3 P – 0.162 (bar) C.13

At T = 136.7 $^{\circ}$C: Correction = -2.30E-3 P + 0.355 (bar) C.14

Table C-7: Data for Pressure Calibration Set 6

Dead	T = 102.6 °C		T = 111.8 °C		T = 129.4 °C		T = 143.0 °C	
Weight	Pressure	Pressure	Pressure	Pressure	Pressure	Pressure	Pressure	Pressure
Pressure	Reading	Deviation	Reading	Deviation	Reading	Deviation	Reading	Deviation
20.0	17.9	-2.1	18.4	-1.6	18.8	-1.2	19.3	-0.7
35.0	32.9	-2.1	33.3	-1.7	33.8	-1.2	34.3	-0.7
50.0	47.9	-2.1	48.3	-1.7	48.8	-1.2	49.3	-0.7
65.0	62.8	-2.2	63.3	-1.7	63.8	-1.2	64.2	-0.8
80.0	77.8	-2.2	78.3	-1.7	78.7	-1.3	79.2	-0.8
95.0	92.8	-2.2	93.3	-1.7	93.7	-1.3	94.1	-0.9
110.0	107.7	-2.3	108.3	-1.7	108.7	-1.3	109.1	-0.9
125.0	122.7	-2.3	123.3	-1.7	123.6	-1.4	124.1	-0.9
140.0	137.7	-2.3	138.2	-1.8	138.6	-1.4	139.0	-1.0
155.0	152.7	-2.3	153.2	-1.8	153.6	-1.4	154.0	-1.0
170.0	167.7	-2.3	168.2	-1.8	168.5	-1.5	168.9	-1.1

The following equations were formulated for Calibration Set 5:

At T = 102.6 °C: Correction = -1.46E-3 P – 2.06 (bar) C.15

At T = 111.8 °C: Correction = -1.03E-3 P – 1.62 (bar) C.16

At T = 129.4 °C: Correction = -2.00E-3 P – 1.12 (bar) C.17

At T = 143.0 °C: Correction = -2.67E-3 P – 0.610 (bar) C.18

3.   DENSITY CORRELATIONS

The density of the fluid in the cell is calculated from the volume of the cell. Three equations are required for the calculation of the volume due to the fact that corrections were constantly made to the cell. Superscripts next to corrected pressures in Appendix A indicate which of the pressure calibration sets were used.

To determine the relationship between the piston position and the density, a known amount of propane was loaded into the cell. At various temperatures and piston positions, the cell was allowed to reach equilibrium and the pressure was measured. From the temperature and pressure data the density was obtained from the NIST website [165] and the required correlation obtained graphically.

The calibration was conducted for the third data set and the changes required for the first and second sets were determined mathematically.

Table C-8: Data for correlation between Volume and Piston Position

Corrected Temperature	Corrected Pressure	Piston Position	Calculated Density	Estimated Volume
^{o}C	bar	mm	kg/m^3	cm^3
108.7	51.0	54.6	241	23.3
108.7	53.2	43.1	269	20.9
108.8	56.5	32.1	294	19.1
108.8	63.4	23.8	322	17.5
108.9	73.1	19.8	345	16.3
108.9	82.6	17.6	360	15.6
108.9	93.1	16.1	372	15.1
109.0	100.5	15.3	380	14.8
109.0	108.1	14.8	386	14.6
117.1	55.9	55.3	215	26.2
117.5	63.4	35.1	274	20.5
118.0	69.7	27.6	300	18.7
118.2	78.4	22.8	324	17.4
118.3	91.7	19.1	349	16.1
118.4	101.2	17.4	359	15.7
118.4	110.8	16.2	369	15.3
118.5	122.4	14.9	379	14.9
127.8	61.7	58.1	197	28.6
127.9	71.3	38.7	258	21.8
128.0	82.9	26.6	300	18.8
128.1	92.2	23.3	320	17.6
128.1	102.5	20.3	337	16.7
128.1	119.5	17.4	357	15.8

Table C-8 continued

Corrected Temperature °C	Corrected Pressure bar	Piston Position mm	Calculated Density kg/m³	Estimated Volume cm³
137.2	71.7	48.0	258	21.8
137.4	81.6	35.4	260	21.7
137.4	91.7	27.4	273	20.6
137.5	103.5	23.3	314	17.9
137.5	112.4	21.0	328	17.2
137.5	129.0	17.9	348	16.2
137.5	143.0	16.2	361	15.6

In Figure C-1 the above data is plotted.
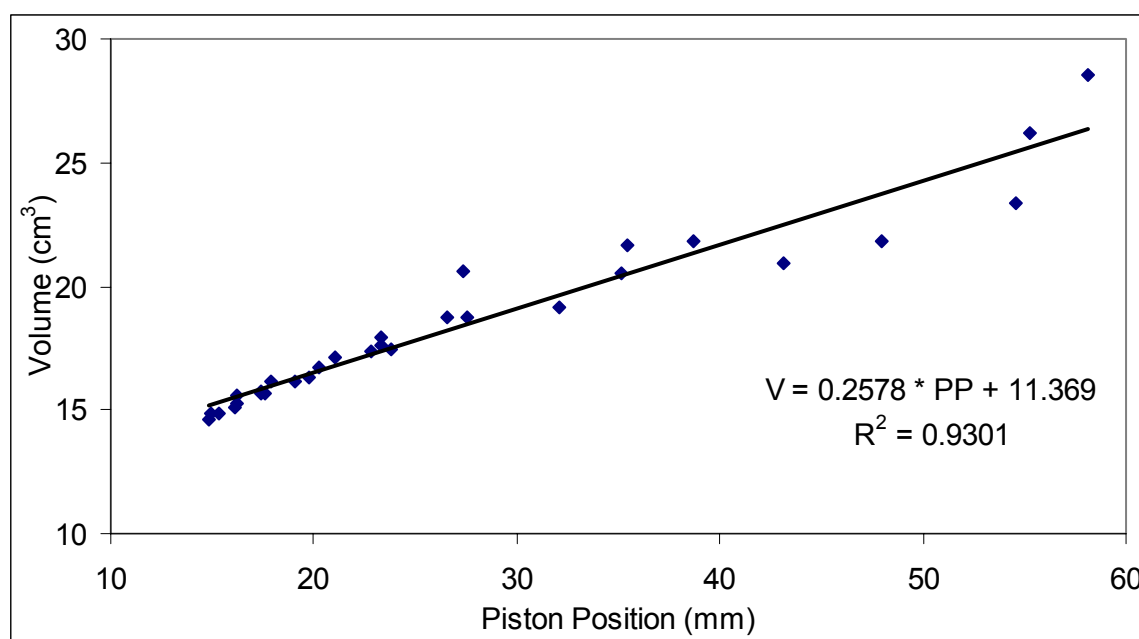
Figure C-1: Plot of Volume as a function of Piston Position

From the above graphs and mathematical calculations the following relationships can be made between the volume (V) and the Piston Position (PP) with the piston position in mm:

Correlation A:

$$V = 0.2578 * PP + 13.016 \ (cm^3) \dotfill C19$$

Correlation B:

$$V = 0.2578 * PP + 10.832 \ (cm^3) \dotfill C20$$

Correlation C:

$$V = 0.2578 * PP + 11.369 \ (cm^3) \dotfill C21$$

D.   PURE COMPONENT DATA

1.   DOTRIACONTANE VAPOUR PRESSURE DATA

Table D-1: nC32 Vapour Pressure Data

Temperature	Pressure	Liquid Density	Vapour Density
K	Bar	mol/m^3	mol/m^3
350	3.55E-10	1.72E+03	1.22E-08
355	7.23E-10	1.72E+03	2.45E-08
360	1.44E-09	1.71E+03	4.80E-08
365	2.80E-09	1.70E+03	9.21E-08
370	5.32E-09	1.69E+03	1.73E-07
375	9.94E-09	1.69E+03	3.19E-07
380	1.82E-08	1.68E+03	5.76E-07
385	3.27E-08	1.67E+03	1.02E-06
390	5.79E-08	1.67E+03	1.79E-06
395	1.01E-07	1.66E+03	3.06E-06
400	1.72E-07	1.65E+03	5.18E-06
405	2.90E-07	1.65E+03	8.61E-06
410	4.82E-07	1.64E+03	1.41E-05
415	7.89E-07	1.63E+03	2.29E-05
420	1.27E-06	1.62E+03	3.65E-05
425	2.03E-06	1.62E+03	5.75E-05
430	3.20E-06	1.61E+03	8.96E-05
435	4.99E-06	1.60E+03	1.38E-04
440	7.67E-06	1.60E+03	2.10E-04
445	1.17E-05	1.59E+03	3.16E-04
450	1.76E-05	1.58E+03	4.70E-04
455	2.62E-05	1.58E+03	6.94E-04
460	3.87E-05	1.57E+03	1.01E-03

2.   HEXATRIACONTANE VAPOUR PRESSURE DATA

Table D-2: nC36 Vapour Pressure Data

Temperature	Pressure	Liquid Density	Vapour Density
K	Bar	mol/m^3	mol/m^3
355	3.46E-11	1.54E+03	1.17E-09
360	7.46E-11	1.53E+03	2.49E-09
365	1.57E-10	1.52E+03	5.17E-09
370	3.23E-10	1.52E+03	1.05E-08
375	6.50E-10	1.51E+03	2.08E-08
380	1.28E-09	1.50E+03	4.05E-08
385	2.47E-09	1.50E+03	7.72E-08
390	4.69E-09	1.49E+03	1.44E-07
395	8.72E-09	1.49E+03	2.65E-07
400	1.59E-08	1.48E+03	4.79E-07
405	2.86E-08	1.47E+03	8.51E-07
410	5.07E-08	1.47E+03	1.49E-06
415	8.83E-08	1.46E+03	2.56E-06
420	1.52E-07	1.45E+03	4.34E-06
425	2.56E-07	1.45E+03	7.26E-06
430	4.28E-07	1.44E+03	1.20E-05
435	7.05E-07	1.44E+03	1.95E-05
440	1.15E-06	1.43E+03	3.14E-05
445	1.84E-06	1.42E+03	4.98E-05
450	2.93E-06	1.42E+03	7.82E-05
455	4.60E-06	1.41E+03	1.22E-04
460	7.14E-06	1.41E+03	1.87E-04

3. OCTATRIACONTANE VAPOUR PRESSURE DATA

Table D-3: nC38 Vapour Pressure Data

Temperature	Pressure	Liquid Density	Vapour Density
K	Bar	mol/m^3	mol/m^3
365	3.86E-11	1.45E+03	1.27E-09
370	8.25E-11	1.44E+03	2.68E-09
375	1.72E-10	1.44E+03	5.53E-09
380	3.52E-10	1.43E+03	1.11E-08
385	7.05E-10	1.42E+03	2.20E-08
390	1.38E-09	1.42E+03	4.26E-08
395	2.66E-09	1.41E+03	8.10E-08
400	5.03E-09	1.41E+03	1.51E-07
405	9.34E-09	1.40E+03	2.77E-07
410	1.70E-08	1.39E+03	5.00E-07
415	3.06E-08	1.39E+03	8.88E-07
420	5.42E-08	1.38E+03	1.55E-06
425	9.45E-08	1.38E+03	2.67E-06
430	1.62E-07	1.37E+03	4.54E-06
435	2.75E-07	1.37E+03	7.61E-06
440	4.60E-07	1.36E+03	1.26E-05
445	7.60E-07	1.35E+03	2.05E-05
450	1.24E-06	1.35E+03	3.31E-05
455	2.00E-06	1.34E+03	5.28E-05
460	3.18E-06	1.34E+03	8.32E-05
465	5.02E-06	1.33E+03	1.30E-04
470	7.82E-06	1.32E+03	2.00E-04
475	1.21E-05	1.32E+03	3.06E-04

Table D-5: Propane PvT Data

Pressure	Specific Volume (m^3/mol)						
(bar)	T = 330 K	T = 350 K	T = 370 K	T = 375 K	T = 385 K	T = 400 K	T = 450 K
16	1.33E-03	1.50E-03	1.65E-03	1.69E-03	1.76E-03		
18	1.12E-03	1.29E-03	1.43E-03	1.47E-03	1.53E-03	1.63E-03	
20	1.01E-04	1.12E-03	1.26E-03	1.29E-03	1.35E-03	1.44E-03	1.71E-03
22	1.01E-04	9.76E-04	1.11E-03	1.14E-03	1.20E-03	1.29E-03	1.54E-03
24	1.01E-04	8.53E-04	9.88E-04	1.02E-03	1.08E-03	1.16E-03	1.40E-03
26	1.01E-04	7.45E-04	8.83E-04	9.14E-04	9.70E-04	1.05E-03	1.28E-03
28	1.00E-04	6.45E-04	7.92E-04	8.23E-04	8.78E-04	9.54E-04	1.17E-03
30	1.00E-04	1.15E-04	7.10E-04	7.42E-04	7.97E-04	8.72E-04	1.08E-03
32	9.97E-05	1.14E-04	6.37E-04	6.70E-04	7.26E-04	8.00E-04	1.00E-03
34	9.94E-05	1.13E-04	5.69E-04	6.04E-04	6.62E-04	7.36E-04	9.35E-04
36	9.92E-05	1.12E-04	5.06E-04	5.44E-04	6.04E-04	6.78E-04	8.73E-04
38	9.89E-05	1.11E-04	4.44E-04	4.87E-04	5.50E-04	6.26E-04	8.18E-04
40	9.87E-05	1.11E-04	3.79E-04	4.32E-04	5.01E-04	5.79E-04	7.68E-04
42	9.85E-05	1.10E-04	2.90E-04	3.76E-04	4.55E-04	5.36E-04	7.23E-04
44	9.83E-05	1.09E-04	1.46E-04	3.15E-04	4.11E-04	4.96E-04	6.82E-04
46	9.80E-05	1.09E-04	1.38E-04	2.29E-04	3.69E-04	4.58E-04	6.45E-04
48	9.78E-05	1.08E-04	1.34E-04	1.63E-04	3.27E-04	4.24E-04	6.10E-04
50	9.76E-05	1.08E-04	1.31E-04	1.48E-04	2.85E-04	3.92E-04	5.79E-04
52	9.74E-05	1.07E-04	1.28E-04	1.42E-04	2.44E-04	3.61E-04	5.49E-04
54	9.72E-05	1.07E-04	1.26E-04	1.37E-04	2.07E-04	3.32E-04	5.22E-04
56	9.70E-05	1.07E-04	1.25E-04	1.34E-04	1.82E-04	3.05E-04	4.97E-04
58	9.68E-05	1.06E-04	1.23E-04	1.31E-04	1.67E-04	2.80E-04	4.74E-04
60	9.66E-05	1.06E-04	1.22E-04	1.29E-04	1.57E-04	2.57E-04	4.52E-04
62	9.65E-05	1.05E-04	1.21E-04	1.28E-04	1.50E-04	2.37E-04	4.32E-04
64	9.63E-05	1.05E-04	1.20E-04	1.26E-04	1.45E-04	2.19E-04	4.13E-04

E.   CALCULATIONS, DATA TABLES AND ADDITIONAL INFORMATION

1.   DESIGN CALCULATIONS

The following calculations were done during the design process of the experimental equipment.

1.1.   DESIGN SPECIFICATIONS:

Figure E.1: Design Specifications

Inner Diameter of Piston	22 mm
Volume Variation in Cell	20 to 40 cm^3
Max Pressure Required in Cell	500 bar
Max Pressure Supplied by Nitrogen Gas	15 bar

1.2.   SHAFT LENGTH

The total shaft length can be calculated as the sum of the following:

- To ensure that the piston can move freely in the cell twice the length required to make allowance for volume changes is needed (80 mm).

- A safety factor to ensure shaft remains in cylinder (30 mm)

- The piston disc thickness (18 mm)

- The upper disc thickness (34.6 mm)

- An additional 12 mm is required so that at the minimum position the piston is not completely inside the cell.

The total shaft length is thus 254.6 mm $\approx$ 255 mm.

1.3. DIAMETER OF PISTON DISC

Assume pressure is applied to a piston with a diameter of 21.5 mm. Subscript a refers to the piston disc and the head end while subscript b refers to the piston and the inner cell.

$$\frac{P_b}{P_a} = \frac{A_a}{A_b} = \frac{\pi/4\left(d_a^{\,2} - d_b^{\,2}\right)}{\pi/4\,d_b^{\,2}}$$

$$d_a = d_b\sqrt{\left(\frac{P_b}{P_a} - 1\right)}$$

$$= 21.5\sqrt{\left(\frac{500}{15} - 1\right)}$$

$$= 125.97 \approx 126\,\text{mm}$$

1.4. PISTON THICKNESS

The following correlation is given by Sinnott (Sinnott, 1998) for t, the thickness of a disc subjected to pressure:

$$t = C \cdot D\sqrt{\frac{P}{f}}$$

Where t is the piston thickness, C a constant between 0.43 (rigid) and 0.56 (free to rotate), D is the effective diameter, P the maximum pressure and f the maximum allowable stress.

$$t = 0.56 \cdot 127\sqrt{\frac{15}{95}}$$

$$= 8.94\,\text{mm}$$

Allow for a safety factor of 1.25 and therefore the thickness is 11.35 ≈ 12 mm. To be able to accommodate the o-rings required, the piston thickness needs to be increases to 18 mm.

1.5. UPPER DISC THICKNESS

The upper disc is thickness is calculated in the same manner as above but to ensure that enough screw thread is used and to accommodate the o-rings required, 28.6 mm is required. Additionally, so that the disc can be gripped, around the shaft the thickness is 34.6 mm.

1.6. CELL WALL THICKNESS

The following correlation is given by Sinnott (Sinnott, 1998) to calculate the wall thickness in a pressure vessel:

1.7. HEAD WALL THICKNESS

The head wall thickness is calculated in the same manner as for the pressure cell. The value is calculated at 1.46 mm but to allow construction of the cell and the use of screw thread, the thickness is set at 6 mm.

1.8. AIR HOLES SIZE

The maximum volume required to be released:

$$V = \frac{\pi}{4}h \cdot \left(OD^2 - ID^2\right)$$
$$= \frac{\pi}{4}0.08 \cdot \left(0.126^2 - 0.0215^2\right)$$
$$= 9.6847E-4\,m^3$$

Assume that the air is required to be released within two seconds. The volumetric flow rate is thus 4.8424E-4 m³/s. For a gas velocity of 10 m/s the cross sectional area of the air holes should therefore be 4.8424E-5 m². Assuming there are 4 air holes, each air hole has a cross sectional area of 1.211E-5 m². The diameter of the holes are thus 3.93 mm $\approx$ 4 mm.

2. ESTIMATION OF AIR IN CELL

2.1. ASSUMPTIONS

The following assumptions are made in this estimation:

- The air obeys the ideal gas law. This assumption is justified due to the fact that the pressure is low and the temperature well above the critical point of the components.

- The cell is at its maximum volume (41.4 cm³) and the volume allowed for the inlet and evacuator is 5.6 cm³.

- An ambient temperature of 20 °C is assumed.

- It is assumed that the air and the solvent in the cell mix totally in each flush and that the amount of solvent used in each flush is the same.

- After each flush it is assumed that the density of the gas in the cell can be approximated as the propane density and that the propane density can be calculated with the aid of the ideal gas law.

- It is assumed that the pressure in the cell after each flush (once the propane is released) is 1.5 Bar.

2.2.   CALCULATION METHOD

The calculations were done as follows:

- The density and then the mass of the air in the cell before the flush was calculated from the ideal gas law.

- The density of the solvent in the cell after each flush was calculated with the aid of the ideal gas law.

- Under the assumption that the propane and the air mix completely, the mass of propane and air in the cell is calculated after each flush.

- From the ideal gas law the density and the mass of air in the inlet before the load is calculated.

- Under the assumption that the air and the propane mix completely, the mass of air in the cell and in the inlet is calculated and therefore the percentage air in the cell is estimated.

2.3   RESULTS

The calculations were done for numerous experiments, randomly chosen, over the entire composition range.

The average mass of air in the cell was found to be 4.5 E-6 grams and the mass ranged from 1.7 E-6 grams to 1.0 E-5. The average percentage of air in the cell was found to be 4.6 E-5 percent and the mass ranged from 1.4 E-5 percent to 1.1 E-4 percent.

The results are shown in Table E.2:

Table E.2.:Estimation of percentage air in cell

Solvent	Flush			Load			Air in Run	
	Solvent (grams)	No.	Press (mbar)	Solvent (grams)	Wax (grams)	Press (mbar)	Mass (grams)	%
nC32	26.14	5	3	9.65	0.972	1	6.8E-06	6.3E-05
nC32	41.13	5	3	9	0.51	1.5	1.0E-05	1.1E-04
nC32	26.57	5	3	7.3	0.191	1	6.7E-06	8.9E-05
nC32	22.58	5	1.75	7.76	0.12	0.7	4.7E-06	6.0E-05
nC32	26.97	5	1	9.02	0.377	0.7	4.7E-06	5.0E-05
nC40	25.7	5	1.5	8.1	4.89	0.55	3.7E-06	2.8E-05
nC40	25.25	5	1.5	12.81	2.02	0.5	3.4E-06	2.3E-05
nC40	26.73	5	1.5	9.93	1.005	0.6	4.1E-06	3.7E-05
nC40	29.33	5	2	8.61	0.536	0.9	6.1E-06	6.6E-05
nC40	27.43	5	1.5	10.43	0.266	0.7	4.7E-06	4.4E-05
nC40	21.55	5	0.75	9.38	0.141	0.8	5.4E-06	5.6E-05
nC40	29.22	5	1.5	3.99	4.89	0.55	3.7E-06	4.1E-05
nC40	31.23	5	1	4.91	4.89	0.6	4.0E-06	4.1E-05
nC40	25.56	5	2	5.86	4.89	0.6	4.0E-06	3.7E-05
nC40	30.1	5	3	6.24	4.89	0.4	2.7E-06	2.4E-05
nC40	25.03	5	2	10.93	4.89	0.5	3.4E-06	2.1E-05
nC40	28.54	5	0.75	6.25	2.02	0.6	4.0E-06	4.9E-05
nC40	22.6	5	1.5	5.46	2.02	0.45	3.0E-06	4.0E-05
nC40	27.26	5	2	7.93	2.02	0.7	4.7E-06	4.7E-05
Test 1	19.2	4	0.3	6.55	5.41	0.25	1.7E-06	1.4E-05
Test 2	14.69	4	0.7	11.19	0.783	0.4	2.7E-06	2.3E-05

## 3.	PHASE TRANSITION BY DENSITY

The comparison was done for both the liquid and vapour side and four comparisons were done for each the low, the medium and the high temperature.

Table E-3: Liquid Side Comparison of Calculated (by Density Measurement) and Experimental Phase Transition Point

	Piston Position			Pressure		
	Calculated	Experiment	% Difference	Calculated	Experiment	% Difference
Temperature	mm	mm	-	bar	bar	-
	24.5	24.6	0.224%	92.1	92.1	-0.017%
	51.4	51.5	0.158%	103.9	103.8	-0.050%
	47.0	47.2	0.376%	105.3	104.6	-0.623%
	63.2	63.3	0.151%	106.8	106.8	-0.032%
	41.4	41.2	-0.419%	108.1	108.6	0.469%
High	40.1	40.2	0.265%	127.7	127.3	-0.283%
	23.5	23.7	0.757%	74.5	74.4	-0.142%
	49.5	49.5	-0.093%	85.3	85.5	0.211%
	45.9	45.9	0.027%	85.4	85.6	0.192%
	60.8	60.8	-0.042%	87.0	87.1	0.119%
	38.7	38.6	-0.237%	107.2	107.7	0.481%
Med	52.2	52.3	0.135%	108.8	108.7	-0.060%
	23.0	23.1	0.394%	55.6	55.8	0.435%
	44.4	44.3	-0.146%	64.1	64.3	0.380%
	47.4	47.4	0.037%	64.6	64.8	0.346%
	59.0	58.9	-0.142%	67.5	67.7	0.359%
	37.7	37.8	0.191%	70.2	70.2	-0.026%
Low	37.3	37.4	0.295%	87.8	86.8	-1.207%
	Average		0.107%	Average		0.031%

Table E-4: Liquid Side Comparison of Calculated (by Density Measurement) and Experimental Phase Transition Point

Temperature	Piston Position			Pressure		
	Calculated	Experiment	% Difference	Calculated	Experiment	% Difference
	mm	mm	-	bar	bar	-
	40.5	40.8	0.826%	113.5	112.2	-1.160%
	67.1	68.0	1.293%	81.7	81.3	-0.486%
	79.4	79.7	0.351%	105.4	104.9	-0.456%
	57.8	58.0	0.357%	86.0	85.9	-0.142%
	54.9	54.8	-0.142%	94.9	95.2	0.315%
High	59.3	58.8	-0.922%	73.4	73.7	0.405%
	54.4	55.2	1.558%	72.2	71.7	-0.648%
	42.2	42.5	0.632%	84.9	84.4	-0.554%
	39.8	40.2	1.050%	68.9	68.6	-0.408%
	41.4	41.5	0.145%	85.0	84.9	-0.106%
	76.5	76.7	0.197%	87.2	87.1	-0.095%
Med	51.1	51.3	0.360%	86.3	86.3	-0.028%
	57.3	58.7	2.429%	61.6	58.8	-4.679%
	60.1	60.8	1.104%	57.6	57.4	-0.335%
	61.2	61.3	0.115%	61.1	61.2	0.113%
	62.6	62.7	0.205%	60.2	60.4	0.275%
	40.1	40.0	-0.292%	65.3	65.5	0.322%
Low	73.5	73.3	-0.321%	66.9	67.6	0.998%
	Average		0.497%	Average		-0.371%

4. DATA TABLES FOR PRESSURE-CARBON NUMBER PLOT AT CONSTANT MASS FRACTION

Table E-5: Data for generation of Pressure-Carbon Number Plot for x = 0.45

Carbon Number	x1	x2	T = 393.15 K		T = 408.15 K		Interpolated Values	
			P1	P2	P1	P2	T = 393.15 K	T = 408.15 K
C32	0.451	0.431	65.2	68.0	80.9	84.5	65.3	81.0
C36	0.472	0.378	67.5	76.4	84.4	96.0	69.7	87.2
C38	0.451	0.388	72.9	78.2	91.6	97.8	73.0	91.7
C40	0.499	0.439	74.5	80.8	92.8	100.7	79.7	99.3
C44	0.481	0.418	76.3	84.7	96.4	105.3	80.4	100.8
C46	0.484	0.444	84.3	84.3	95.5	104.6	84.3	103.3
C54	0.453	0.382	96.2	106.2	117.8	128.1	96.6	118.2
C60	0.452	0.431	104.9	112.2	125.8	132.4	105.8	126.6

Table E-6: Data for generation of Pressure-Carbon Number Plot for x = 0.40

Carbon Number	x 1	x 2	T = 393.15 K		T = 408.15 K		Interpolated Values	
			P1	P2	P1	P 2	T = 393.15 K	T = 408.15 K
C32	0.431	0.381	68.0	70.6	84.5	88.3	69.6	86.9
C36	0.472	0.378	67.5	76.4	84.4	96.0	74.4	93.3
C38	0.451	0.388	72.9	78.2	91.6	97.8	77.2	96.6
C40	0.402	0.376	80.4	85.2	100.8	105.4	80.7	101.1
C44	0.418	0.371	84.7	91.6	105.3	112.8	87.4	108.2
C46	0.444	0.362	84.3	92.7	104.6	112.7	88.8	108.9
C54	0.453	0.382	96.2	106.2	117.8	128.1	103.7	125.5
C60	0.431	0.397	112.2	116.8	132.4	137.1	116.4	136.7

Table E-7: Data for generation of Pressure-Carbon Number Plot for x = 0.35

Carbon Number	x1	x2	T = 393.15 K		T = 408.15 K		Interpolated Values	
			P1	P2	P1	P2	T = 393.15 K	T = 408.15 K
C32	0.381	0.316	70.6	72.8	88.3	90.7	71.6	89.4
C36	0.378	0.269	76.4	79.8	96.0	99.3	77.3	96.9
C38	0.388	0.322	78.2	80.7	97.8	100.0	79.7	99.0
C40	0.376	0.336	85.2	86.1	105.4	107.5	85.8	106.8
C44	0.354	0.312	92.3	91.9	113.8	111.8	92.2	113.6
C46	0.362	0.305	92.7	94.3	112.7	114.0	93.0	113.0
C54	0.382	0.324	106.2	111.2	128.1	133.2	109.0	130.9
C60	0.364	0.264	118.1	121.2	138.5	140.9	118.5	138.8

Table E-8: Data for generation of Pressure-Carbon Number Plot for x = 0.30

Carbon Number	x1	x2	T = 393.15 K		T = 408.15 K		Interpolated Values	
			P1	P2	P1	P2	T = 393.15 K	T = 408.15 K
C32	0.316	0.275	72.8	75.0	90.7	93.1	73.6	91.6
C36	0.378	0.269	76.4	79.8	96.0	99.3	78.9	98.4
C38	0.322	0.295	80.7	80.8	100.0	99.4	80.8	99.5
C40	0.309	0.270	88.4	89.5	108.1	109.0	88.6	108.3
C44	0.312	0.298	91.9	93.6	111.8	114.5	93.4	114.2
C46	0.305	0.274	94.3	95.3	114.0	115.6	94.4	114.3
C54	0.324	0.287	111.2	113.1	133.2	134.4	112.4	134.0
C60	0.364	0.264	118.1	121.2	138.5	140.9	120.1	140.0

Table E-9: Data for generation of Pressure-Carbon Number Plot for x = 0.25

Carbon Number	x1	x 2	T = 393.15 K		T = 408.15 K		Interpolated Values	
			P1	P2	P1	P 2	T = 393.15 K	T = 408.15 K
C32	0.275	0.220	75.0	75.8	93.1	93.3	75.4	93.2
C36	0.269	0.202	79.8	79.4	99.3	98.0	79.7	98.9
C38	0.295	0.244	80.8	81.6	99.4	100.8	81.5	100.6
C40	0.264	0.244	88.0	89.7	108.8	109.5	89.2	109.3
C44	0.298	0.243	93.6	94.2	114.5	114.9	94.1	114.9
C46	0.274	0.238	95.3	96.6	115.6	116.3	96.2	116.0
C54	0.287	0.230	113.1	113.3	134.4	134.7	113.2	134.6
C60	0.257	0.224	120.8	119.2	141.2	139.5	120.4	140.8

Table E-10: Data for generation of Pressure-Carbon Number Plot for x = 0.20

Carbon Number	x1	x2	T = 393.15 K		T = 408.15 K		Interpolated Values	
			P1	P2	P1	P2	T = 393.15 K	T = 408.15 K
C32	0.220	0.145	75.8	74.2	93.3	91.3	75.4	92.8
C36	0.202	0.151	79.4	79.0	98.0	97.8	79.4	98.0
C38	0.202	0.170	81.8	81.6	100.8	100.2	81.8	100.8
C40	0.203	0.166	88.7	82.9	108.1	102.9	88.2	107.7
C44	0.243	0.186	94.2	93.4	114.9	113.4	93.6	113.8
C46	0.200	-	95.3	-	115.2	-	95.3	115.2
C54	0.230	0.180	113.3	115.5	134.7	136.7	114.6	135.9
C60	0.224	0.197	119.2	119.9	139.5	140.4	119.9	140.3

Table E-11: Data for generation of Pressure-Carbon Number Plot for x = 0.15

Carbon Number	x1	x2	T = 393.15 K		T = 408.15 K		Interpolated Values	
			P1	P2	P1	P2	T = 393.15 K	T = 408.15 K
C32	0.220	0.145	75.8	74.2	93.3	91.3	74.3	91.4
C36	0.151	0.099	79.0	78.1	97.8	96.4	79.0	97.8
C38	0.170	0.099	81.6	78.6	100.2	96.7	80.8	99.2
C40	0.154	0.136	84.5	88.1	104.5	107.3	85.2	105.1
C44	0.186	0.130	93.4	90.8	113.4	110.9	91.7	111.8
C46	0.159	0.117	93.5	91.1	113.8	110.4	93.0	113.0
C54	0.180	0.121	115.5	111.1	136.7	132.6	113.3	134.6
C60	0.156	0.115	119.4	116.1	139.1	135.6	118.9	138.6

Table E-12: Data for generation of Pressure-Carbon Number Plot for x = 0.10

Carbon Number	x1	x2	T = 393.15 K		T = 408.15 K		Interpolated Values	
			P1	P2	P1	P2	T = 393.15 K	T = 408.15 K
C32	0.145	0.0915	74.2	72.9	91.3	89.6	73.1	89.9
C36	0.202	0.1510	79.4	79.0	98.0	97.8	78.7	97.7
C38	0.170	0.0989	81.6	78.6	100.2	96.7	78.7	96.7
C40	0.123	0.0919	86.5	83.1	106.1	100.7	84.0	102.1
C44	0.130	0.0807	90.8	87.0	110.9	106.7	88.5	108.3
C46	0.117	0.0996	91.1	91.7	110.4	110.6	91.7	110.6
C54	0.121	0.0811	111.1	106.1	132.6	126.6	108.5	129.5
C60	0.115	0.0837	116.1	113.5	135.6	132.5	114.9	134.1

Table E-13: Data for generation of Pressure-Carbon Number Plot for x = 0.075

Carbon Number	x1	x2	T = 393.15 K		T = 408.15 K		Interpolated Values	
			P1	P2	P1	P2	T = 393.15 K	T = 408.15 K
C32	0.0915	0.0536	72.9	71.016	89.6	86.274	72.1	88.2
C36	0.0986	0.0716	78.1	76.3	96.4	94.6	76.5	94.8
C38	0.0948	0.0989	79.1	77.2	97.3	94.3	88.2	111.6
C40	0.0752	0.0606	79.7	80.9	97.3	99.3	79.7	97.4
C44	0.0807	0.0505	87.0	82.0	106.7	100.0	86.1	105.4
C46	0.0790	0.0712	91.7	88.9	111.9	108.6	90.3	110.2
C54	0.0811	0.0440	106.1	95.4	126.6	114.6	104.3	124.6
C60	0.0837	0.0578	113.5	106.6	132.5	125.3	111.2	130.1

Table E-14: Data for generation of Pressure-Carbon Number Plot for x = 0.05

Carbon Number	x1	x2	T = 393.15 K		T = 408.15 K		Interpolated Values	
			P1	P2	P1	P2	T = 393.15 K	T = 408.15 K
C32	0.054	0.043	71.0	68.9	86.3	84.7	70.3	85.7
C36	0.064	0.042	74.2	72.8	91.0	90.0	73.3	90.4
C38	0.064	0.032	77.2	72.2	94.3	87.6	75.0	91.4
C40	0.059	0.037	78.1	75.0	96.2	92.4	76.9	94.6
C44	0.055	0.042	85.1	78.7	104.5	96.7	82.6	101.4
C46	0.053	0.040	84.9	82.2	103.1	101.3	84.3	102.7
C54	0.081	0.044	106.1	95.4	126.6	114.6	97.2	116.5
C60	0.058	0.041	106.6	99.8	125.3	119.9	103.5	122.8

Table E-15: Data for generation of Pressure-Carbon Number Plot for x = 0.025

Carbon Number	x1	x2	T = 393.15 K		T = 408.15 K		Interpolated Values	
			P1	P2	P1	P2	T = 393.15 K	T = 408.15 K
C32	0.0286	0.0200	67.1	64.5	79.8	77.4	66.0	78.8
C36	0.0255	0.0151	69.1	67.4	84.2	81.9	69.0	84.1
C38	0.0322	0.0149	72.2	68.1	87.6	82.4	70.5	85.5
C40	0.0373	0.0249	75.0	71.4	92.4	86.7	71.4	86.8
C44	0.0255	0.0146	77.1	73.1	94.4	87.2	76.9	94.1
C46	0.0383	0.0210	80.6	76.3	97.9	92.6	77.3	93.8
C54	0.0440	0.0244	95.4	86.9	114.6	106.4	87.2	106.6
C60	0.0295	0.0249	96.9	95.5	115.6	114.1	95.6	114.1

Table E-16: Data for generation of Pressure-Carbon Number Plot for x = 0.015

Carbon Number	x1	x2	T = 393.15 K		T = 408.15 K		Interpolated Values	
			P1	P2	P1	P2	T = 393.15 K	T = 408.15 K
C32	0.015	-	63.0	-	75.2	-	63.0	75.2
C36	0.025	0.015	69.1	67.4	84.2	81.9	67.4	81.9
C38	0.032	0.015	72.2	68.1	87.6	82.4	68.1	82.5
C40	0.022	0.015	72.0	68.5	87.7	82.4	68.6	82.6
C44	0.026	0.015	77.1	73.1	94.4	87.2	73.2	87.5
C46	0.015	-	74.4	-	90.0	-	74.4	90.0
C54	0.024	0.015	86.9	78.8	106.4	96.2	79.0	96.5
C60	0.025	0.014	95.5	85.2	114.1	102.9	85.9	103.6

5.   DATA FOR GENERATION OF C2-C30

Table E-17: Data for Linearization of C2-C24 Data.

Mass Fraction	Pressure			Regression Values		Pressure
	T=332.8 K	T=342.7K	T=352.7K	A	B	T=325.37K
0.046	93.7	106.4	118.1	1.226	-314.1	84.8
0.075	101.1	115.7	128.2	1.362	-351.7	91.4
0.125	108.3	123.6	137.0	1.442	-371.3	97.9
0.189	111.1	126.8	140.8	1.492	-385.2	100.3
0.268	113.4	129.3	143.7	1.523	-393.0	102.4
0.315	113.3	129.4	143.8	1.533	-396.4	102.2
0.351	113.1	129.2	144.0	1.553	-403.4	101.8
0.431	110.5	127.1	142.0	1.583	-415.9	99.1
0.515	102.5	118.7	133.9	1.578	-422.4	91.0
0.550	96.9	113.4	129.1	1.618	-441.4	85.0

Table E-18: Data for Linearization of C2-C28 Data.

Mass Fraction	Pressure			Regression Values		Pressure
	T=337.8K	T=342.8K	T=352.6K	A	B	T=325.37
0.056	117.7	125.3	137.7	1.339	-334.4	101.4
0.103	130.2	137.8	151.7	1.448	-358.8	112.4
0.209	140.5	148.5	163.1	1.522	-373.4	121.8
0.307	142.2	150.1	164.8	1.523	-372.3	123.4
0.413	-	148.6	163.6	1.531	-376.1	121.9
0.492	134.1	142.1	157.3	1.565	-394.6	114.7
0.582	117.7	126.1	141.7	1.618	-428.6	97.7

Table E-19: Data for generation of C2-C30 data.

Mass Fraction	Pressure		
	nC24	nC28	nC30
0.08	92.0	107.0	114.5
0.12	97.7	113.9	121.9
0.20	100.6	121.0	131.1
0.30	102.3	123.3	133.8
0.40	100.1	122.1	133.1
0.48	94.3	117.0	128.3

6.   DATA FOR GENERATION OF C3-C45 DATA

Table E-20: Data for generation of C3-C45 data.

Mass Fraction	Regression Values: P = A * CN + B		Pressure (bar)
Wax (g/g)	A	B	for CN = 45
0.45	1.412	20.49	84.0
0.40	1.693	13.70	89.9
0.35	1.710	16.49	93.5
0.30	1.740	17.15	95.5
0.25	1.698	19.70	96.1
0.20	1.685	20.10	95.9
0.15	1.653	20.30	94.7
0.10	1.563	21.36	91.7
0.050	1.198	31.17	85.1
0.025	0.941	35.30	77.6
0.015	0.770	39.31	74.0

7.   INFORMATION ON EQUATIONS OF STATE UNABLE TO PREDICT VAPOUR PRESSURE OF PARAFFIN

The following equations of state were considered but were not able to predict the pure component vapour pressure curve of dotriacontane. These equations of state are given below with a short description of the shortcomings.

7.1.   VAN DER WAALS (VDW)

The VDW's equation of state (Van der Waals, 1873) is given in equation 7.2. This equation was the first equation of state capable of predicting liquid-vapour coexistence. The only parameters required for the calculation of a and b is the critical temperature and pressure.

As can be seen in Figure 7-5, although the VDW equation of state can qualitatively predict liquid-vapour coexistence, quantitative errors are large. The errors can mainly be attributed to the temperature independence of the attractive term.

7.2.   REDLICH KWONG (RK)

The RK equation of state (Redlich et al., 1949) is the first modification of the VDW equation of state to incorporate temperature in the attractive form and can be formulated as follows:

$$P = \frac{RT}{v-b} - \frac{a/T^{0.5}}{v(v-b)}$$ E-1

Parameters a and b were determined from the assumption that at the critical point, the first and second derivatives of pressure with respect to volume are zero. The only parameters required for the calculation of a and b is the critical temperature and pressure.

The RK equation performed well for simple fluids, but as can be seen in Figure 7-5 the equation could not describe complex fluids with non-zero acentric factors.

7.3.   DOHRN-PRAUSNITZ (DP)

The DP equation of state is based on a repulsive term of hard spheres and an attractive term similar to that of the Carnahan-Starling-van der Waals (Carnahan et al., 1972) equation of state. Dohrn and Prausnitz (Dohrn et al., 1990) formulated the equation of state and a detailed description of the equation of state is published by Dohrn and Prausnitz (Dohrn et al., 1990) as well as by Pfohl et al (Pfohl et al., 2000). The inability of this equation to predict these type of fluids can be attributed to the fact that water was used as a reference fluid, and the fluids used in this work and water differ too much.

7.4.   SAKO-WU-PRAUSNITZ (SWP)

Sako et al (Sako et al., 1989) proposed an equation of state that is useful for both small and large molecules and required the minimum amount of experimental information. The equation of state was used to correlate volumetric data for n-alkanes and was tested on the system ethylene-polyethylene.

The SWP equation of state is formulated as follows:

$$P = \frac{RT(v-b+bc)}{v(v-b)} - \frac{a(T)}{v(v-b)}$$ E-2

As in the above equations of state, the parameters a, b and c are determined from the critical conditions, i.e., at the critical point the first and second derivative of pressure with respect to volume is zero. Additionally, the van der Waals volume was used in the correlation of the a parameter.

The equation of state proposed here has 4 parameters, the critical temperature, the critical pressure, the van der Waals volume and the parameter c. The van der Waals volumes were determined by Crause (Crause, 2001) while Sako et al (Sako et al., 1989) gave values for the parameter c for normal alkanes up to a carbon number of 15. These values were correlated with the molar mass and the following relationship can be used for normal alkanes:

$$c = 0.8041 + 0.0122 \cdot M_R \text{ .... E-3}$$

For nC32 a value of 6.305 was used for the parameter c and the van der Waals volume was estimated to be 0.3342 l/mol. The inability of this equation to describe the phase behaviour can possibly be attributed to the estimation of the van der Waals volume and the parameter c. However, the aim of this work was not to refit the parameters this equation of state.

7.5. PFENNIG

The Pfennig equation of state (Pfennig, 1988) is a modification of the PHCT equation of state. The equation of state is mathematically complex and details can be found in the work of Pfennig.

Three parameters are used for this equation of state, namely the core volume, the potential depth and the parameter c. Values for the parameters till eicosane were published by Pfennig and to estimate values for the higher carbon number paraffins, extrapolation was conducted. The core volume and the parameter c were found to have a linear relationship with carbon number, while the potential depth has a logarithmic relationship. The following parameters were estimated by Phennig (Pfennig, 1988):

Table E-21: Parameters for Pfennig Equation of State for nC32

Parameter	Value
Core Volume	0.2416 l/mol
Potential Depth	569.7 K
Parameter c	6.871

The inability of this equation of state to predict the vapour pressure may be attributed to inaccuracies in the values of the parameters.

7.6.   SAFT – Phennig and Pfohl (SAFT-PP)

Pfohl et al (Pfohl et al., 2000) modified the SAFT equation of state by applying the attractive interactions between spheres from the Pfennig equations of state. (Pfennig, 1988).

The equation of state required three parameters, the depth of the potential, the volume of one sphere and the number of spheres in one molecule. The parameter values are the same as for SAFT.
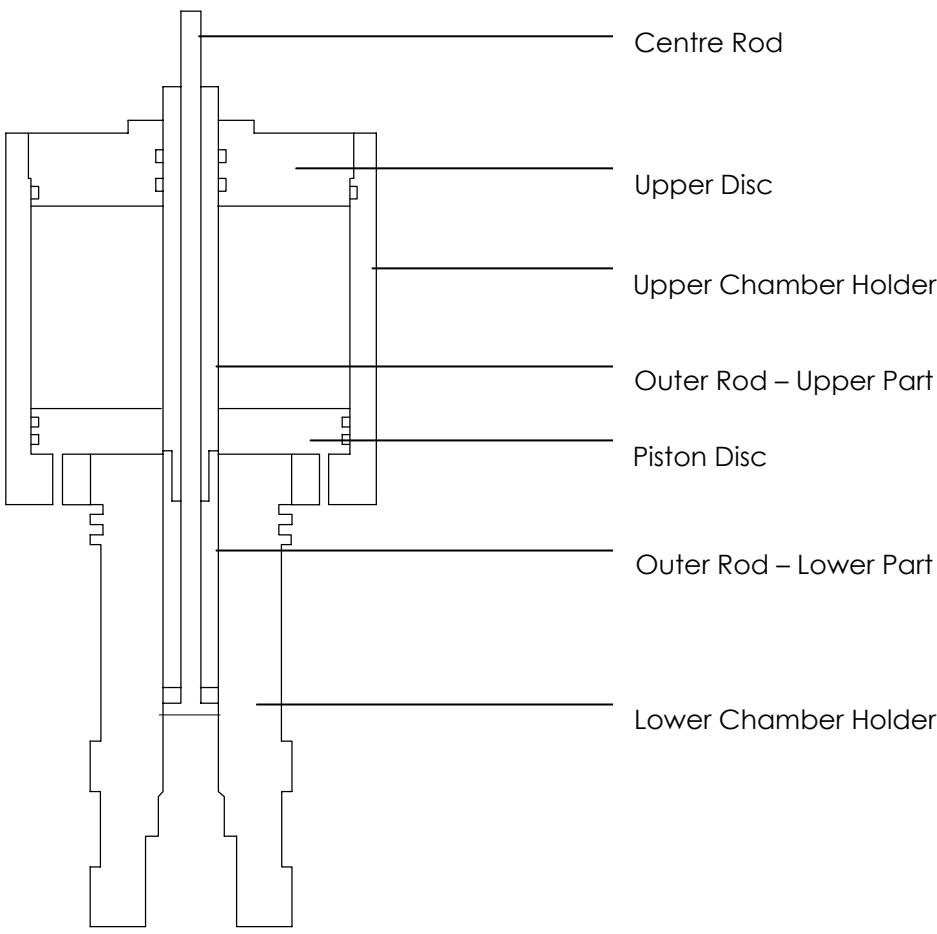
Table E-22: Parameters for SAFT-PP Equation of State for nC32

Parameter	Value
The depth of potential	208.8 K
The volume of one sphere	0.012 l/mol
The number of spheres in one molecule	21.34

This equation of state has not been thoroughly tested yet and Pfohl et al (Pfohl et al., 2000) claim that to date the equation has no real advantage compared to the original SAFT equations
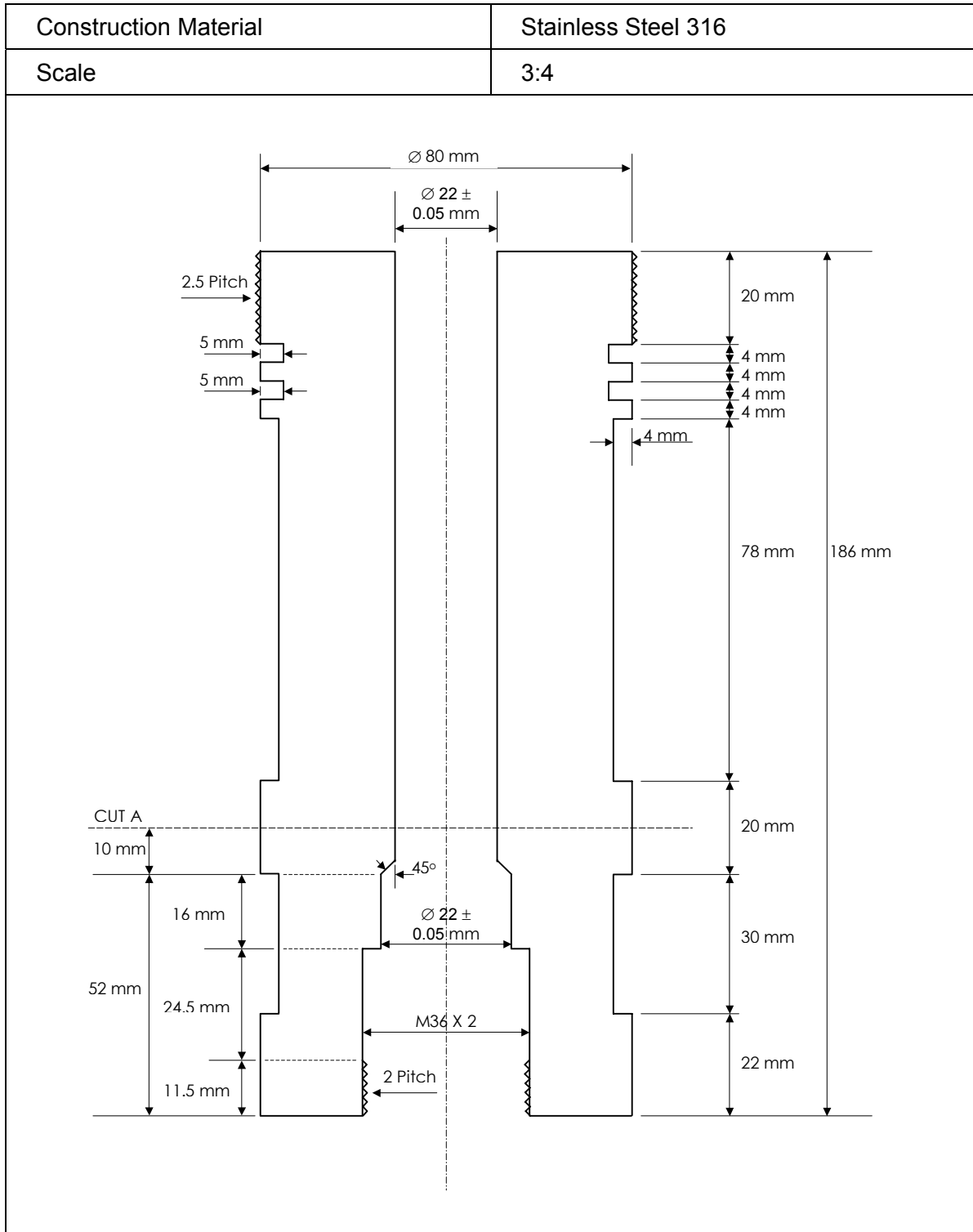
F.   MECHANICAL DRAWINGS AND AUXILIARY EQUIPMENT DATA

1.   GENERAL VIEW OF CELL

Construction Material	Stainless Steel 316
Scale	1:3

Centre Rod

Upper Disc

Upper Chamber Holder

Outer Rod – Upper Part

Piston Disc

Outer Rod – Lower Part

Lower Chamber Holder

2. LOWER CHAMBER HOLDER

2.1. TOP VIEW

Construction Material	Stainless Steel 316
Scale	3:4

2.2.   SIDE VIEW

Construction Material	Stainless Steel 316
Scale	3:4

Top   Bottom

2.3. Cᴜᴛ A

Construction Material	Stainless Steel 316
Scale	3:4

3.   CENTRE ROD

Construction Material	Stainless Steel 316
Scale	2:3

4.   OUTER ROD – LOWER PART

Construction Material	Stainless Steel 304
Scale	3:4

∅ 21.82 ± 0.05 mm

∅ 14.9 mm

1.5 pitch

20 mm

94 mm   74 mm

∅ 8.1mm

5.   OUTER ROD – UPPER PART

Construction Material	Stainless Steel 304
Scale	3:4

∅ 12 mm

∅ 8.1 mm

4 mm

123 mm   166 mm

1.5 Pitch

23 mm

1.5 Pitch

20 mm

∅ 14.9 mm

∅ 21.82 ± 0.05 mm

6.   PISTON DISC

Construction Material	Stainless Steel 304
Scale	3:4

See Detail A

1.5 Pitch

18 mm

Diameter to Match Rod

$\varnothing$ 127 $\pm$ 0.05 mm

Detail A

3.1 mm

4.4 $\pm$ 0.1 mm

3.0 mm

4.4 $\pm$ 0.1 mm

3.1 mm

7. UPPER CHAMBER HOLDER

7.1. SIDE VIEW

Construction Material	Stainless Steel 304
Scale	3:4
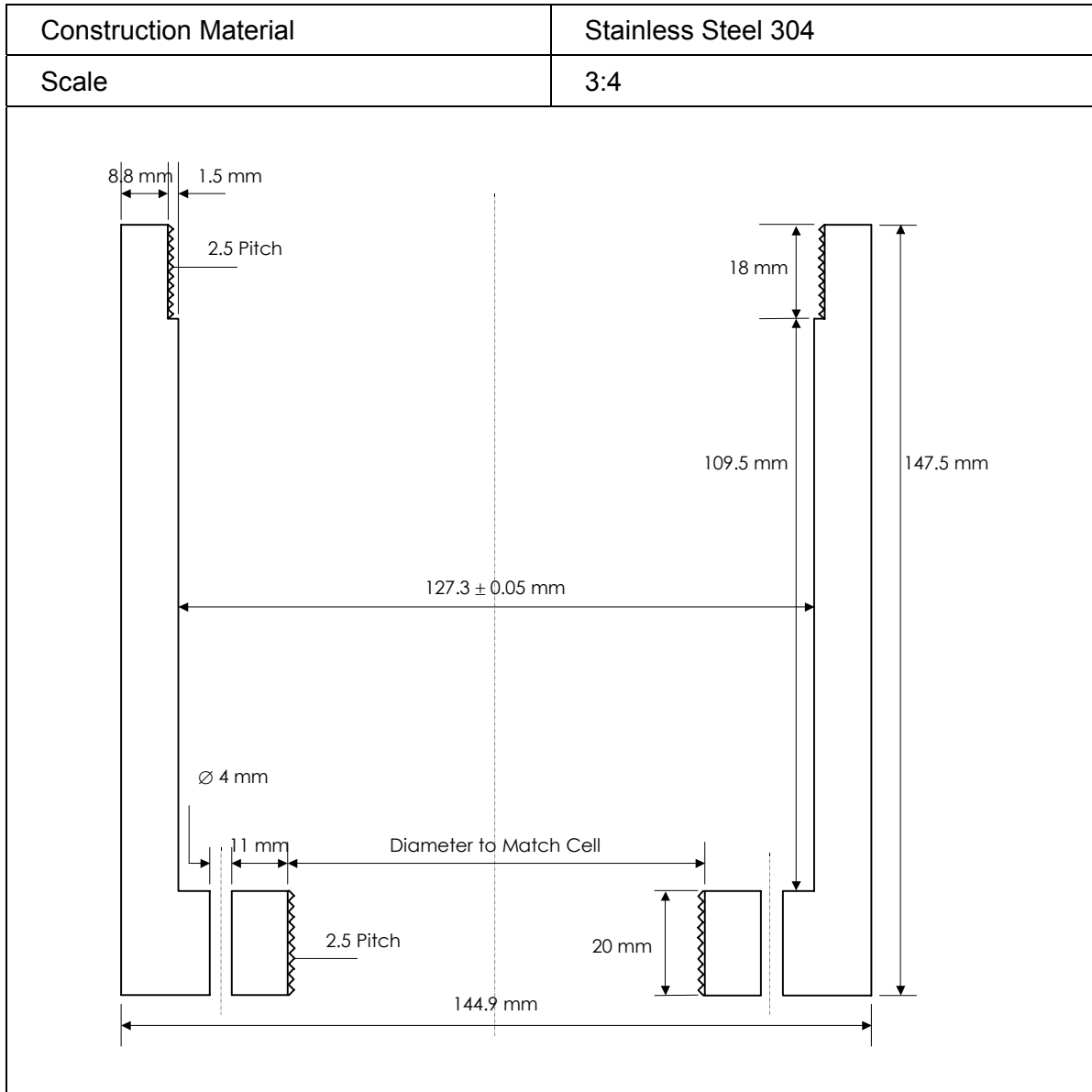
7.2.   BOTTOM VIEW
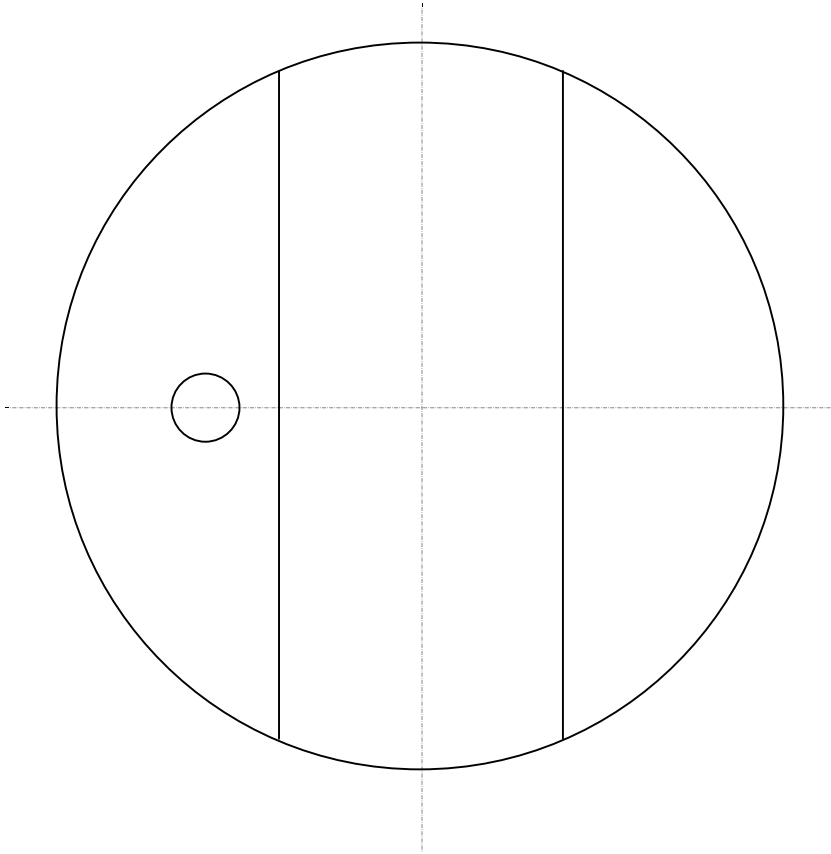
Construction Material	Stainless Steel 304
Scale	3:4

8. UPPER DISC

8.1. SIDE VIEW

Construction Material	Stainless Steel 316
Scale	3:4

8.2.   TOP VIEW

Construction Material	Stainless Steel 304
Scale	3:4

9.   SIGHT GLASS

The sight glass was obtained from SITEC. The sight glass seals with a Bridgman type seal, has an optical diameter of 18 mm, a maximum pressure of 500 bar and a maximum temperature of 200 $^{\circ}$C. (SITEC Part Number 742.0106)

10.   SEAL RINGS

Table F-1: O-Ring and Seals Dimensions and Material of Construction

Location	Inner Diameter	Thickness	Material
Upper Disc and Upper Chamber	120.4 mm	3.53 mm	Viton
Piston Disc and Upper Chamber	120.4 mm	3.53 mm	Viton
Upper Disc and Outer Rod – Upper Part	21.82 mm	3.53 mm	Viton
Piston Disc and Outer Rod – Upper Part	18 mm	2.5 mm	Viton
Seal Cell Chamber from Environment at Piston	Made to Fit		Teflon
Seal Cell Chamber from Environment at Sight Glass	Made to Fit		Teflon

G. EXPERIMENTAL PROCEDURES, MAINTENANCE AND SAFETY PLAN

1. EXPERIMENTAL PROCEDURE

1.1. LOADING PROCEDURE

A schematic representation of the set-up for flushing and loading the cell is given in Figure G-1. This set-up is used to load the solvent and is thus used for both types of loading procedures.
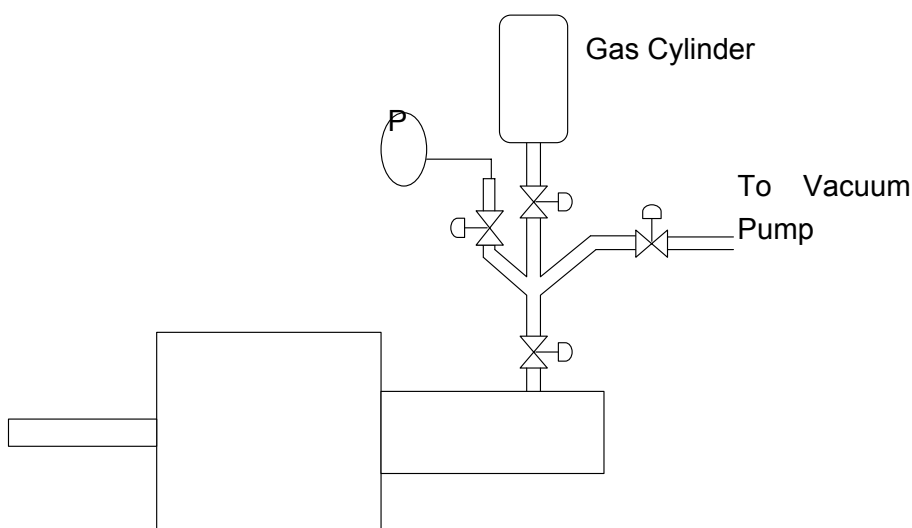
Figure G-1: Schematic Representation of Solvent Loading Set-up

Loading Solvent and Wax

The following process was used to load the cell with both solvent and wax.

1. The piston is removed from the cell so that wax can be loaded.

2. The cell is loaded with a known amount of wax. The amount of wax required is calculated from the mass fraction desired and the expected density. The wax is weighed of in grams accurate to 0.01g. In cases where less than one and a half grams of wax is required, the wax is weighed off accurate to 0.001g.

3. The cell, now containing the wax and a magnetic stirrer bar, is closed and securely fastened.

4. The next step is the evacuation of the cell to remove as much air as possible from the cell. An evacuation set-up is used for this purpose and the cell is evacuated to at least 1 mBar (100 Pa).

5. To remove even more of the air in the cell, the cell is flushed 4 to 6 times with the solvent. For this process, the solvent is introduced into the cell and bled through the valve on the gas cylinder. For each subsequent flush, the solvent is bled until only gas remains in the cell but the pressure in the cell remains above that of the environment. In addition, care needs to be taken that all the liquid solvent used in the last flush is evaporated and the pressure in the cell is only slightly above atmospheric pressure. This is required to ensure that the least amount of solvent possible remains in the cell without allowing any air in. On completion of the flushing process, the inlet valve to the cylinder is closed and the gas cylinder is removed.

6. The gas cylinder, containing the liquefied solvent, is now weighed accurate to 0.01g. To simplify the loading process and prevent the process from being repeated, some of the solvent in the gas cylinder is vented so that all the solvent in the gas cylinder can be loaded and the resultant amount of solvent in the cell provides the correct total mass and mass fraction.

7. The cylinder is re-attached to the cell and the section between the cell valve and the gas cylinder is evacuated to 1 mBar again.

8. On completion of the evacuation process, the cell valve is opened for the loading of the solvent.

9. The gas cylinder is heated up, opened and the solvent is now loaded.

10. Once all the solvent is loaded the gas cylinder is closed from the equilibrium cell.

11. Before the valve can be closed, the section between the cell valve and the gas cylinder is heated up to allow any solvent in this section to evaporate, therefore minimizing the error in the calculation of the amount of solvent added. With the aid of the camera and the pressure sensor it can be determined when the solvent in the section outside the cell is evaporated. The pressure will first remain constant while the liquid solvent in the section enters the cell and will then start to rise as the temperature increases. With the aid of the camera, the liquid solvent in the section can be seen flow into the cell while there is still solvent in the section between the valve and the gas cylinder.

12. Before the cell is heated for the experimental measurements, the composition needs to be calculated to ensure that there is not too much or too little material in the cell. This can be seen from a density estimate or from previous runs. Should there be too much or too little solvent in the cell, a new batch of solvent needs to be loaded into

the cell. The gas cylinder, of known weight, is reattached to the cell and the section between the valve and the gas cylinder is evacuated. The valve is now opened and the content of the cell is now bled until the pressure of the cell is just above the environmental pressure. The procedure can now be repeated from the solvent loading step. This process needs to be repeated until the desired amount of solvent is added.

13. The cell is now completely loaded and ready for heating and experimental measurements.

In paragraph E.1 the amount of air left in the cell for a couple of runs has been estimated. The average amount of air is 4.5 E-6 grams, which is negligible when compared to the mass of the wax and the propane, which is in the order of a couple of grams.

It has been claimed that the solidified wax used here may contain as much as 5 volume percent air. To determine the effect of the air in the wax, steps 3 and 4 are omitted and replaced with the following:

• The closed cell is heated with the valve open so that the wax can melt at atmospheric pressure.

• The cell is flushed 4 to 6 times with propane gas to remove as much of the air as possible. During the last flush, the propane is bled so that the pressure inside the cell is only slightly above atmospheric pressure, thus preventing excess propane in the cell. The valve is closed and the cell is cooled down thus allowing the wax to solidify under a propane atmosphere. However, enough propane needs to be left in the cell so that even at the lower temperatures the pressure in the cell is above atmospheric pressure. This step is also used as the flushing step and once the cell has cooled down completely, the loading process can be repeated from step 6 onwards.

The above process was compared experimentally with the normal process and it was found that the results were the same. The amount of air in the solid wax is thus negligible.

Loading only solvent

The process used here is virtually identical to the above process and is conducted as follows:

1. Steps one and two are not required and the above process is followed from step three onwards.

2. Care is required in the solvent flushing process. Due to the fact that the wax is solidified while the solvent is in the cell, it becomes a spongy mass when the solvent is released. During the flushing process, care thus needs to be taken that all the liquid solvent is removed from the pores in the spongy mass. To ensure that all the liquid solvent is removed from the cell, the cell should be vented a few times during the last flush. This can be achieved by venting the cell to just above atmospheric pressure and leaving it for about five minuets between each vent. The venting process needs to be repeated until the pressure in the cell after the five minuets is below the vapour pressure of the solvent.

1.2. PROCEDURE TO OBTAIN DATA

The following process was followed to obtain the experimental data:

1. After the cell is loaded, the heating oil is set to 110 °C.

2. Once all the wax has melted the magnetic stirrer is switched on and the pressure can be increased. While the cell reaches thermal equilibrium, the pressure inside the cell is kept high enough that the fluid is in the one phase region. This will ensure that in the event of a small leak, the composition in the cell remains constant and the pressure data from the run can still be used.

3. Once it has been established that the cell is at thermal equilibrium the phase transition point can be determined. Thermal equilibrium usually takes about 45 minuits to reach for the first data point and 30 minuits for the subsequent points. Thermal equilibrium takes longer for the first data point due to the fact that the temperature needs to rise about 80 K for the first data point and only 15 K for the subsequent data points.

4. To determine the phase transition point the pressure in the cell is adjusted. The pressure in the cell is adjusted by adjusting the pressure of the nitrogen gas in the head end of the cell. The pressure, temperature, piston position and number of phases present are logged. This is repeated at various points and with the aid of a bisection method, the transition point is measured. The transition point is measured accurate to 0.2 Bar and the highest pressure where two phases occur is taken as the transition pressure.

5. Once the transition pressure is determined at a heating oil temperature of 110 °C, the temperature of the heating oil is adjusted to 125 °C and the process is repeated. The process is once again repeated at a heating oil temperature of 140 °C. When the set point of the heating oil is changed, the pressure in the cell needs to be increased by about 30 bar therefore ensuring that the contents is in the single phase while thermal equilibrium is attained.

1.3. UNLOADING PROCEDURE

Two unloading procedures are required. The procedure selected depends on if the wax and the solvent are removed from the cell or if only the solvent is removed and the wax is left behind to be used again.

Removing Solvent and Wax

The following process was followed to unload both the wax and solvent from the cell and to clean the cell from all possible wax.

1. To unload the solvent as well as the wax from the cell, the wax in the cell needs to be a liquid. The temperature inside the cell as well as in the nozzle should therefore be above the melting point of the wax. However, for safety reasons the unloading temperature and pressure should be kept as low as possible. To take both these factors into account, the cell will therefore be unloaded with the heating oil set at about 25 to 30 $^{\circ}$C above the melting temperature of the wax. For systems where the wax is of lower molecular weight, the cell may be needed to be cooled down.

2. In addition the pressure on the piston needs to be released. This will allow the cell to be unloaded at the lowest possible pressure.

3. The cell is now ready to be unloaded. To protect the operator, safety glasses and thermal gloves need to be worn for this step. The first step in unloading the cell is to remove the cap from the nozzle. This needs to be done with care as a pressure build-up due to small leakages through the valve may occur as well as thermal expansion.

4. Before unloading the contents of the cell, the cell is turned upside down. This allows the liquid phase to be unloaded first therefore unloading the most of the wax before the solvent is unloaded.

5. The cell needs to be set up as shown in Figure G-1 with an erlenmeyer flask below the outlet pipe to catch the contents of the cell.
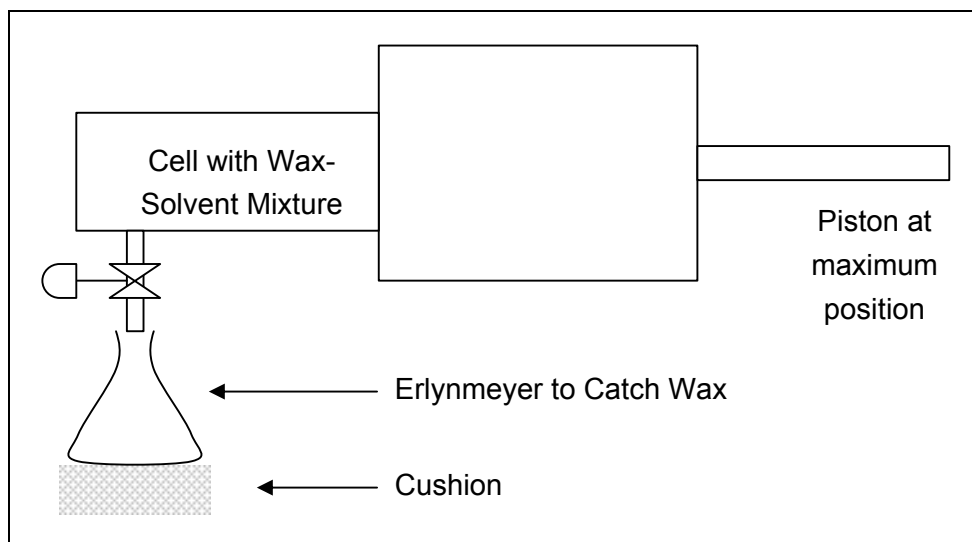
Figure G-2: Set-up for unloading the cell.

6. The valve is opened very slowly in small increments to allow the wax and the solvent to escape. The cell should not be unloaded too slowly as this allows the wax to solidify in the nozzle resulting in a blockage and a loss of wax. In addition, it has been noticed that the faster the release rate, the finer the wax. An optimum release rate is therefore required. This rate is determined experimentally as more and more runs were conducted.

7. Once all the wax and solvent are removed, the cell is positioned upright and the head is removed with care. As the cell is still hot, thermal gloves are recommended. Care is required to ensure the inside of the cell is not scratched in this process. The unloading procedure is now complete and the cell is now ready to be cleaned.

Removing Solvent Only

The following steps are used when only the solvent is removed:

1. To ensure only the solvent is unloaded, the wax needs to be in a solid form. To ensure that the wax is not entrained with the solvent, it should be in as large crystals as possible. On completion of the run the cell is allowed too cool down. In addition the, the magnetic stirrer is turned off to allow the wax to solidify in as large pieces as possible. The cell is positioned in the normal operating position to prevent the solid wax from clogging the inlet valve.

2. Once the cell is at about 25 $^{\circ}$C, the solvent can be removed. Although thermal gloves are not required, safety glasses are recommended to protect the user. Firstly the cap is removed with care as there might be a pressure build-up under the cap.

3. The solvent can now be removed. Once again the solvent is removed slowly to prevent any loose wax from escaping.

4. Once all the solvent is removed, the cell should be left open for about 15 to 30 minuets to allow any free solvent in the wax to escape. The cell is now ready to be loaded with solvent again.

1.4.   CLEANING PROCEDURE

Cleaning Procedure Between Consecutive Runs

The cleaning procedure is only required if the wax is removed.

1. The first washing cycle is done with xylene at about 110 ^{o}C. Xylene is a solvent that, at temperatures close to its boiling point, dissolves the wax quite well. The cell is first washed with xylene until the xylene is relatively free of wax. To test the wax content, a little methanol is added and should wax be present, the wax will precipitate.

2. Once most of the wax is removed the cell is positioned upright and the valve is closed. The cell is filled with xylene and the magnetic stirrer is switched on to allow the xylene to move as freely as possible and to obtain the highest temperature possible. The cell, with the magnetic stirrer on, is left standing for about 30 minuets to allow the wax in the crevices to dissolve in the xylene.

3. The xylene is removed and the process is repeated, but the xylene is left stirring for an hour.

4. The cell is now rinsed with xylene until the xylene is relatively free of wax. Testing is once again done with methanol.

5. The next step in the process is to wash the cell with toluene which will remove any excess wax and the xylene in the cell. The cell needs to be cooled down below the boiling point of toluene and the oil bath is set at 80 ^{o}C. The cell is positioned at 45 degrees to the horizontal with the open end facing downwards. Air is blown into the cell while toluene is sprayed into the cell through the cylinder. This allows for the toluene to enter the crevices and remove any excess wax. The process is repeated until the toluene is free of wax, once again tested with methanol.

6. On completion of the toluene washing process, the cell is cooled down to about 50 ^{o}C where the cell is washed with methanol. Methanol is used to remove the toluene from the cell.

7. The process is repeated until the methanol that exits the cylinder is free of tiny pieces of wax. The cell is now regarded to be free of wax and any remaining methanol can be removed by blowing air into the cell.

8. The final step in the process is to remove any remaining oils or other substances in the cell. This can be done by rinsing the cell with pentane once the cell is below 30 $^{\circ}$C and using paper to wipe the inside if the cell. On completion of this step the remaining pentane can once again be removed by drying the cell with air.

Cleaning Procedure Between Consecutive Sets of Data

Between consecutive data sets extra care is required to ensure that the cell is free of wax. To ensure that all possible wax is removed and, in the event that any wax remains behind the experiments are scheduled so that the high mass fractions of wax runs are done first and the low fractions last.

In addition to the xylene wash is repeated three times and the if possible, the xylene is left in the cell overnight for the third run.

2.   MAINTENANCE REQUIRED ON EQUIPMENT

To allow the equipment to last longer the following needs to be done periodically:

1. The Teflon seal on the piston needs to be checked after every run to ensure that the creep is kept to a minimum.

2. The piston shaft needs to be tightened after the loading procedure in every run to ensure that the cell is fully leakproof.

3. The piston shaft needs to be checked to ensure that no major scratches have occurred and that the shaft is sufficiently lubricated.

4. The cylinder needs to be checked regularly to ensure that the cylinder is not scratched. Scratches will allow for leaks and thus cause inaccuracies in the measurement.

5. The screw thread between the cylinder and the head needs to be checked to ensure that it is well lubricated as failure of lubrication may result in the head and the cylinder becoming locked.

6. The optical lens needs to be checked regularly to ensure that no scratching has occurred.

7. The pressure gauge needs to be calibrated frequently.

3.   SAFETY PROCEDURES

It is of utmost importance that the operator is safe when using the equipment. The following were taken into account to ensure safety:

- The chemicals used in operation and for cleaning.

- The pressure of the system.

- The temperature of the system.

3.1.   SAFETY IN DESIGN

During design the equipment needs to be designed so that the cell will be able to withstand the high pressures required. Large safety factors were included in the design and the system was tested well above the operation pressures envisaged.

In addition, the pressure regulator used on this cell has been chosen so that the maximum pressure applied by the regulator can not exceed the maximum pressure of the cell.

3.2.   SAFETY IN OPERATION

Three main factors, namely the chemicals, the temperature and the pressure of the system dictates the safety procedures required.

Chemicals Used

Before operation the operator should take note of the safety precautions with regard to the chemicals and the international safety cards should be consulted. The main safety precautions are discussed below.

The waxes used here do not pose a serious hazard to the operator or the environment.

The following precautions are required when handling the supercritical solvent and during operation:

- The solvents are highly flammable and therefore no open flames, sparks or smoking is permitted near the equipment, both during set-up and during the run.

- In addition, the laboratory needs to be well ventilated to prevent a build-up of the solvents.

- Propane and LP gas are heavier than air and may travel along the ground. Precaution should be taken due to the fact that the gas can travel and distant ignition may occur.

Although nitrogen is not combustible and occurs freely in air, the inhalation of excess nitrogen may result in weakness and unconsciousness due to the lowering of the concentration of oxygen in the air. Should loss of containment occur, the room should be evacuated.

Xylene, toluene, methanol and pentane are used to clean the cell after operation. The following precautions are required for safe operation:

- All the solvents are highly flammable and thus no open flames, sparks or smoking is allowed. In addition, no strong oxidants are permitted when using solvents as these may result in fire and explosion hazard.

- Explosive vapour/air mixtures can be formed for all components. The laboratory should thus be well ventilated.

- The solvents may cause the skin to dry out and methanol can be absorbed through the skin. Protective clothing is thus required. Long-term exposure results in defatting of the skin and dermatitis.

- All the components are hazardous when inhaled and thus the solvents should only be used below their boiling temperature. In addition, special care should be taken when working with methanol and pentane because these substances are volatile at room temperature.

- Safety goggles are required during the cleaning process to protect the eyes.

- Vapours produced by the liquids are heavier than air and may travel along the ground. Precaution should be taken due to the fact that the gas can travel and distant ignition may occur.

Temperature

Although the temperatures used here are not excessively high, they are still able to cause injury.

All equipment around the cell and the heating bath needs to be treated as if it is hot.

During the unloading process, the solvent wax mixture needs to be unloaded while hot. To protect the operator, safety goggles and thermal gloves need to be worn.

During cleaning with xylene and toluene, the operator is also required to treat the entire equipment as if hot and safety goggles are required.

Pressure

The cell contains fluids at high pressures. The hazard associated with the high pressures is the possible rupture of the cell. This was taken into account in the design of the cell. In addition, the operator is not allowed to look directly into the cell and the camera system must be used.

To prevent the cell from containing so much of the wax-solvent mixture that the pressure of the cell at the maximum piston position is excessively high, the operator needs to log loadings made and with the aid of these loadings and the phase transition piston positions ensure that not too much wax or solvent is loaded. Additionally, before heating up the cell, the mass of the contents needs to be determined and the resultant pressure estimated. As an additional precaution, the cell pressure increase needs to be monitored at regular intervals while the cell is heating up. The last two requirements are especially important during the first few runs and when a new system will be studied.

H. NOMENCLATURE

1. LIST OF SYMBOLS

Symbol	Description	Unit
$\hat{f}$	Fugacity of Species in Solution	Pa or Bar
ℓ_{12}	Second Interaction Parameter	-
A	Area	m^2 or mm^2
A	Helmholtz Energy	J
a	Parameter in Equation of State	-
a	Specific Helmholtz Energy	J/mol
a_c	Parameter a evaluated at critical point	-
a^{NC}	Non-Conformal Term of Specific Helmholtz Energy	J/mol
b	Molecular Co-volume	m^3/kmol
b	Parameter in Equation of State	-
B	Second Virial Coefficient	
C	Interaction Constant	-
c	Parameter in Chain EOS with value of a third of the total number of density dependent degrees of freedom	-
c	Parameter in Equation of State	-
C	Third Virial Coefficient	
c_1	Acentric Factor Function in Equation of State	-
c_2	Acentric Factor Function in Equation of State	-
c_3	Acentric Factor Function in Equation of State	-
CN	Carbon Number	-
d	Actual Diameter	m or mm
D	Effective Diameter	m or mm
d_{12}	Equation of State Parameter	-
d_{12}	MC Equation of State Interaction Parameter	-
d_{21}	Equation of State Parameter	-
d_{21}	MC Equation of State Interaction Parameter	-
D_{ij}	Universal Parameter	-
D_o	Constant in Equation of State	-
e/k	SAFT Parameter	-
f	Fugacity	Pa or Bar
f	Maximum Allowable Stress	Bar
F	Simplification term in MC equation of State	-
F	Degrees of Freedom	-

f_i	Volume Fraction of Component I	-
G	Gibbs Energy	J
g	Specific Gibbs Energy	J/mol
h	Height	m
ID	Inner Diameter	m
K	Vapour-Liquid-Equilibrium Constant	-
k_{ij}	First Interaction Parameter	-
L	Liquid Stream Flow Rate	kmol/s
m	Acentric Factor Function in Equation of State	-
m	Segment Number	-
m_1	Pure Component Acentric Factor Function	-
m_o	Acentric Factor Function in Equation of State	-
M_R	Molar Mass	g/mol
n	Acentric Factor Function on Equation of State	-
N	Number of Compounds in System	-
n	Number of Moles	Mol
OD	Outer Diameter	m
P	Pressure	Pa or bar
q	Parameter accounting for effect of shape	-
R	Universal Gas Constant	J/mol.K
t	Piston Thickness	mm
T	Temperature	K
T^{*}	Characteristic Temperature of a Compound	K
u/k	Temperature Dependent Segment Energy	K
u^o/k	Temperature Independent Segment Energy	K
V	Molar Volume	Mol
V	Number of Variable in Phase Rule	-
v	Specific Molar Volume	m^3/kmol
V	Vapour Stream Flow Rate	kmol/s
V	Volume	m^3
v^{*}	Characteristic Volume of a Compound	m^3/kmol
V_m	Van der Waals Volume	cm3/mol
v^o	Temperature Dependent Molar Volume	m^3/kmol
v^{oo}	Temperature Independent Molar Volume	m^3/kmol
x	Mole Fraction Liquid Phase	-
Y	Equation of State Temperature Function	-
y	Mole Fraction Vapour Phase	-
Y	Effect of Shape in ESD Equation of State	-
Z	Compressibility	-
Z	Feed Flow Rate	kmol/s
z	Mole fraction in feed	-
z	Parameter in Equation of State	-
Z_m	Maximum Coordination Number	-

| Z_{RA} | Racket Compressibility Factor | - |

2. GREEK SYMBOLS

Symbol	Description	Unit
α	Measure of Slope of Vapour Pressure Curve	-
α	Temperature dependent function in Cubic Equation of State	-
β	Splitting coefficient	-
ϕ	Fugacity Coefficient	-
$\hat{\phi}$	Fugacity Coefficient for species in Solution	
η	Dynamic Viscosity	Pa.s
λ_{12}	Third Interaction Parameter used in MKP mixing Rules	-
μ	Chemical Potential	-
η	Packing Fraction	-
μ	Kinematic Viscosity	kg/m.s
ν	Dynamic Viscosity	m^2/s
Π	Number of Phases in Phase Rule	-
ρ	Density	kg/m^3
$\tilde{\rho}$	Reduced Density	-
τ	Constant in Chain and SAFT Equations of State	-
Ω	Constant in Patel Teja Equation of State	-
ω	Acentric Factor	-
ξ_c	Critical Compressibility	-

3. SUPERSCRIPTS

Symbol	Description
α	Refers to phase α
β	Refers to phase β
L	Refers to Liquid Phase
O	Refers to Ideal Phase
R	Residual Property
V	Refers to Vapour Phase

4. SUBSCRIPTS

Symbol	Description
a	Refers to Equation of State Parameter a
a	Refers to Part a
b	Refers to Equation of State Parameter b
b	Refers to Part b
c	Refers to Equation of State Parameter c
c	Property evaluated at critical point
i	For Phase i (Phase currently being considered)
i	Summation index for components
i	Applicable to component I
ij	Interaction between components i and j
j	For Phase j (Phase not currently being considered)
j	Summation index for components
Rep	Refers to Repulsive Term
b	Property at Normal Boiling Point
R	Refers to Reduced Property
seg	Refers to Segment Contribution
chain	Refers to Chain Contribution
assoc	Refers to Associating Contribution

5. VALUE OF CONSTANTS

Constant	Description	Value
R	Universal Gas Constant	8.314 J/mol.K
τ	EOS Parameter	0.7401

(Aalto et al., 1998)

(Chapman et al., 1989)

(Chapman et al., 1990)

(Clifford, 1999)

(de Haan et al., 1991)

(Eckert et al., 1996)

(Fuller, 1976)

(Gasem et al., 1990)

(Marr et al., 2000)

(Peters et al., 1988a)

(Schneider, 1988)

(Schneider, 1998)

(Walsh et al., 1990)

(Warth, 1956)